

# THE JOURNAL OF PHYSICAL CHEMISTRY

---

Volume 74, Number 11 May 28, 1970

Unavailability Factor in Catalytic Reactions. Isolation and Steric Hindrance . . . . .	Marshall M. Lih	2245
Catalysis in Liquid Phase Autoxidation. II. Kinetics of the Poly(tetrafluoroethylene)-Catalyzed Oxidation of Tetralin . . . . .	William F. Taylor	2250
Negative Ion Formation by Boron Trifluoride and Phosphorus Trifluoride . . . . .	K. A. G. MacNeil and J. C. J. Thynne	2257
Electron Spin Resonance Study of Deamination of Amino Acids by Hydrated Electrons . . . . .	P. Neta and Richard W. Fessenden	2263
A Mass Spectrometric Study of the Mercury-Photosensitized Reactions of Silane and Methylsilane with Nitric Oxide . . . . .	E. Kamaratos and F. W. Lampe	2267
The Radiolysis of Liquid <i>n</i> -Pentane . . . . .	William P. Bishop and Richard F. Firestone	2274
Photolysis of 3-Pentanone-2,2,4,4- <i>d</i> <sub>4</sub> . . . . .	Charles I. Barta and Alvin S. Gordon	2285
The Laser Flash Photolysis of Solutions of Naphthalene and 1,2-Benzanthracene . . . . .	R. McNeil, J. T. Richards, and J. K. Thomas	2290
Line Width Effects on the Lower Field Electron Spin Resonance Signal in the Titanium(III)-Hydrogen Peroxide System . . . . .	R. E. James and F. Sicilio	2294
Fluorescence Study of 2-( <i>N,N</i> -Dimethylamino)pyridine and Related Molecules . . . . .	A. Weisstuch and A. C. Testa	2299
Reactions of Adsorbed Organic Molecules. I. Bromination of Diethyl Fumarate on a Silica Surface . . . . .	M. J. Rosen and C. Eden	2303
Confirmation of Spontaneous Spreading by Water on Pure Gold . . . . .	Marianne K. Bennett and W. A. Zisman	2309
Ultrahigh-Vacuum Techniques in the Measurement of Contact Angles. II. Water on Gold . . . . .	Malcolm E. Schrader	2313
The Effects of Common Gases on the Flotation of the Water Boule . . . . .	Peter J. Harris	2317
On the Ultrasonic Cavitation Intensity of Aqueous Sodium Lauryl Sulfate Solutions . . . . .	Kenneth Beard, Michael Rios, Douglas Currell, and Richard Reis	2324
Sorption Isotherms of Polar-Nopolar Systems on Liquid-Coated Adsorbents . . . . .	Paul Urone, Yoshihiro Takahashi, and George H. Kennedy	2326
Some Thermodynamic Properties of Liquid-Coated Adsorbents . . . . .	Yoshihiro Takahashi, Paul Urone, and George H. Kennedy	2333
The Thermodynamics of Absorption of Xexon by Myoglobin . . . . .	Gordon J. Ewing and Sigfredo Maestas	2341
Gas-Liquid Partition Chromatographic Determination and Theoretical Interpretation of Activity Coefficients for Hydrocarbon Solutes in Alkane Solvents . . . . .	Y. B. Tewari, D. E. Martire, and J. P. Sheridan	2345
Solvation Enthalpies of Various Ions in Water and Heavy Water . . . . .	C. V. Krishnan and H. L. Friedman	2356
Tunnel Effect, Infrared Continuum, and Solvate Structure in Aqueous and Anhydrous Acid Solutions . . . . .	Ilse Karpschulte-Scheuing and G. Zundel	2363
Hydrogen Bonding in Primary Alkylammonium-Vermiculite Complexes . . . . .	R. H. Laby and G. F. Walker	2369
The Hindered Rotation of the Cyanide Ion in Its Compounds . . . . .	David Smith	2373
Averaged Potential and the Viscosity of Some Polar Organic Vapors . . . . .	I. Crivelli and F. Danon	2376

Designed for  
the potential  
scientist  
in your  
family . . .



**Chemistry** magazine—for the high school or college student whose curiosity of chemistry extends *beyond* required course work.

Eleven issues a year, including a special Summer issue, bring the reader

- experimental projects and investigations
- news items on recent research developments
- feature articles on theoretical and applied science
- book reviews
- chemical puzzles
- reader's column.

All adding up to an exciting opportunity to see chemistry in *action*—out of the textbook and in the real laboratory!

Each issue of *Chemistry* is as broad as the science itself. It delves into the past . . . reports the present . . . relates to the future.

Below is a sample of the interesting and timely articles offered in *Chemistry* . . .

"Anti-matter" . . . "Ionic Bonding" . . . "Drugs and the Student" . . . "Benjamin Rush" . . . "Anomalous Water" . . . "How to Become a Scientist" . . . "Plutonium" . . . "Record Papers and Their Preservation" . . . " $pH$ ,  $pOH$  and  $K_w$ ".

Each issue of *Chemistry* is unusual in its attractiveness and diversity of subject matter. The student can enter through many doors with a choice of reading from the rather general to the relatively technical, all informative . . . entertaining . . . useful in academic work.

Order *Chemistry* now and start an exciting adventure for a young member in your family!

**American Chemical Society  
Publications  
1155 Sixteenth Street, N.W.  
Washington, D.C. 20036**

Yes—start a subscription to *Chemistry* at the low yearly rate of \$4.  
 Canada, PUAS \$7.00\*  Foreign \$7.50\*

Payment must be made in U.S. currency, by international money order, UNESCO coupons, or U.S. bank draft; or order through your book dealer.

Send *Chemistry* to:

Name \_\_\_\_\_

Address \_\_\_\_\_

City \_\_\_\_\_ State \_\_\_\_\_ Zip \_\_\_\_\_

Recipient is a  student.  teacher.

other \_\_\_\_\_

Check enclosed (payable to American Chemical Society)

Send bill to:

Name \_\_\_\_\_

Address \_\_\_\_\_

State \_\_\_\_\_ City \_\_\_\_\_ Zip \_\_\_\_\_

Dielectric Studies. XXVIII. Consideration of Weight Factor Anomalies in Hydroxylic Compounds . . . . .	<b>M. D. Magee and S. Walker</b>	2378
Evaluation of Some Interactions in Permselective Membranes. . . . .	<b>N. Lakshminarayanaiah</b>	2385
Correlation of Fluorescence Quenching and Photopolymerizability of N-Vinylcarbazole in the Presence of Electron Acceptors . . . . .	<b>Shigeo Tazuke</b>	2390
Stretching Vibration of Nitro and N-Oxide Groups of the Anion Radicals of 4-Nitropyridine N-Oxide and Related Nitro Compounds . . . . .	<b>Kiyoshi Ezumi, Hiroshi Miyazaki, and Tanekazu Kubota</b>	2397

**NOTES**

Photochromism of Metal Carbonyls. . . . .	<b>James A. McIntyre</b>	2403
Fluorescence of Liquid Benzene under Proton and Electron Impact . . . . .	<b>M. L. West and L. L. Nichols</b>	2404
Mutual Diffusion Coefficients of Aqueous Copper(II) Sulfate Solutions at 25° . . . . .	<b>L. A. Woolf and A. W. Hoveling</b>	2406
Thin Layer Direct Current Conductivity of Benzene Solutions of Quaternary Ammonium Salts . . . . .	<b>Alfred Prock and William A. LaVallee</b>	2408

**COMMUNICATIONS TO THE EDITOR**

Fluorescence of <i>p</i> -Dioxane . . . . .	<b>Fumio Hirayama, Craig W. Lawson, and Sanford Lipsky</b>	2411
Fluorescence of <i>p</i> -Dioxane. Lifetime and Oxygen Quenching . . . . .	<b>Arthur M. Halpern and William R. Ware</b>	2413

## AUTHOR INDEX

- |                        |                                |                              |                           |                        |
|------------------------|--------------------------------|------------------------------|---------------------------|------------------------|
| Barta, C. I., 2285     | Gordon, A. S., 2285            | Laby, R. H., 2369            | Neta, P., 2263            | Taylor, W. F., 2250    |
| Beard, K., 2324        |                                | Lakshminarayanaiah, N., 2385 | Nichols, L. L., 2404      | Tazuke, S., 2390       |
| Bernett, M. K., 2309   | Halpern, A. M., 2413           | Lampe, F. W., 2267           | Prock, A., 2408           | Testa, A. C., 2299     |
| Bishop, W. P., 2274    | Harris, P. J., 2317            | LaVallee, W. A., 2408        | Reis, R., 2324            | Tewari, Y. B., 2345    |
| Crivelli, I., 2376     | Hirayama, F., 2411             | Lawson, C. W., 2411          | Richards, J. T., 2290     | Thomas, J. K., 2290    |
| Currell, D., 2324      | Hoveling, A. W., 2406          | Lih, M. M., 2245             | Rios, M., 2324            | Thynne, J. C. J., 2257 |
| Danon, F., 2376        | James, R. E., 2294             | Lipsky, S., 2411             | Rosen, M. J., 2303        | Urone, P., 2326, 2333  |
| Eden, C., 2303         | Kamaratos, E., 2267            | MacNeil, K. A. G., 2257      | Schrader, M. E., 2313     | Walker, G. F., 2369    |
| Ewing, G. J., 2341     | Kampschulte-Scheuing, I., 2363 | Maestas, S., 2341            | Sheridan, J. P., 2345     | Walker, S., 2378       |
| Ezumi, K., 2397        | Kennedy, G. H., 2326, 2333     | Magee, M. D., 2378           | Sicilio, F., 2294         | Ware, W. R., 2413      |
| Fessenden, R. W., 2263 | Krishnan, C. V., 2356          | Martire, D. E., 2345         | Smith, D., 2373           | Weisstuch, A., 2299    |
| Firestone, R. F., 2274 | Kubota, T., 2397               | McIntyre, J. A., 2403        | Takahashi, Y., 2326, 2333 | West, M. L., 2404      |
| Friedman, H. L., 2356  |                                | McNeil, R., 2290             |                           | Woolf, L. A., 2406     |
|                        |                                | Miyazaki, H., 2397           |                           | Zisman, W. A., 2309    |
|                        |                                |                              |                           | Zundel, G., 2363       |

## ANNOUNCEMENT

### Catalog of Physicochemical Standard Substances

For the past fifty years, the Commission I.4 on Physicochemical Measurement and Standards of the International Union of Pure and Applied Chemistry has concerned itself with standardized substances of a physicochemical nature. Over this period, world trade has grown rapidly, and the machine age has spawned automation. Continued growth demands the development of additional standards to meet these world needs.

During the past two years, Commission I.4 has polled standardizing agencies throughout the world to establish the availability of materials standardized for given properties. A standard substance is interpreted as one which produces a certified value of a physical property within a given accuracy and can be applied to the following type of measurements: (1) the calibration and standardization of a measuring mechanism; (2) the proof of measurement accuracy by a given method; (3) the transfer of measured quantities from one place to another; and (4) the comparison of measurements made in different locations.

Approximately 140 standardized substances from nine countries have been assembled into Information Bulletin Number 2, a "CATALOG OF PHYSICOCHEMICAL STANDARD SUBSTANCES." The physical properties represented include the following types: Acidimetric Standards; Calorimetric Standards (A) Heat Capacity, (B) Heat of Transition and Fusion, (C) Heat of Combustion, (D) Solution Calorimetry; Color Standards for Spectrophotometry; Density Standards; Dielectric Constants; Molar Conductance; Molecular Weight Polymers; Mossbauer Differential Chemical Shift; Permittivity Standards; pH Standards; pD Standards; Redox Standards; Refractive Index Standards; Saccharimetric (Polarimetric) Standards; Thermal Conductivity Standards; Thermometric Fixed Points; Vapor Pressure Standard; and Viscosity Standards.

Information Bulletin Number 2 has been published in tentative form and is believed to be incomplete. Comments or details about additional standard substances are earnestly solicited until the end of August, 1970, when the catalog will be reviewed by the Commission and submitted to the IUPAC Division of Physical Chemistry for final approval and publication.

Copies of Information Bulletin Number 2, Catalog of Physicochemical Standard Substances, may be obtained gratis upon application to

IUPAC Secretariat  
Bank Court Chambers, 2/3 Pound Way  
Cowley Center, Oxford OX4 3YF, England

Comments on the catalog should be sent to the Chairman of IUPAC Commission I.4

Dr. Daniel R. Stull  
The Dow Chemical Company  
1707 Building  
Midland, Michigan 48640

Also available from the IUPAC Secretariat:

Information Bulletin No. 3: "Manual of Definitions, Terminology and Symbols in Colloid and Surface Chemistry"

Information Bulletin No. 4: "Recommendations for the Presentation of NMR Data for Publication in Chemical Journals"

# THE JOURNAL OF PHYSICAL CHEMISTRY

Registered in U. S. Patent Office © Copyright, 1970, by the American Chemical Society

VOLUME 74, NUMBER 11 MAY 28, 1970

## Unavailability Factor in Catalytic Reactions. Isolation and Steric Hindrance

by Marshall M. Lih<sup>1</sup>

Department of Chemical Engineering, The University of Wisconsin, Madison, Wisconsin (Received April 1, 1969)

Differential reaction rate data from hydrogenation of isobutylene over platinum catalyst are correlated using a modified Hougen-Watson type initial rate equation based on Langmuir adsorption

$$r = \frac{(1 - F_U)K_A K_B p_A p_B}{(1 + K_A p_A)(1 + K_A p_A + K_B p_B)} \left[ 1 - \frac{(1 - F_U)K_B p_B}{1 + K_A p_A + K_B p_B} \right]$$

where the additional factor  $F_U$  accounts for the active sites not available for the adsorption of one of the reacting species because of steric hindrance and/or isolation of sites. The temperature behavior of this factor is examined and compared with that for the hydrogenation of propylene over the same catalyst. Their difference is discussed and plausible explanations proposed.

### Introduction

Of the major steps involved in a catalytic reaction, three—adsorption of reactant(s), surface reaction, and desorption of product(s)—are chemical ones. Based on the assumption that only one of these is rate-controlling, Hougen and Watson<sup>2a</sup> developed a set of reaction-rate equations which were subsequently organized in systematic and tabulated form.<sup>2b</sup> The mathematical expressions for these various mechanisms were derived based on the fundamental adsorption isotherm according to Langmuir.<sup>3</sup>

An implicit assumption in the development is that when two or more reactants are involved, they compete for the same type of adsorption sites. While this is true for a good number of reactions, these rate equations have failed to correlate data taken from reactions in which one of the reactants is preferably adsorbed on some of the sites over the other.

One obvious, possible reason for this occurrence is that the molecular size of one of the reactants is very large compared with the other and with the lattice spacing of the catalyst so that it blocks part of the sites neighboring the one on which it is adsorbed. This

would prevent some of the neighboring sites, even though vacant, from adsorbing any other large molecule but does not affect the smaller ones which do not require a "full share" of the area per site. This we call the steric hindrance effect.

Another possibility, though not as obvious, occurs when one of the reactants requires two adjacent sites for its adsorption (the dual-site mechanism). If at a certain moment there is a single isolated site surrounded by adsorbed molecules, then it is not available to the reactant with a dual-site adsorption mechanism. However, it will still be open to the other reactant which needs only one site to be adsorbed. We may call this the isolation effect.

Regardless of the reason, we can consider the catalytic surface as comprised of two kinds of sites, one of which is not available to one of the reactants. In this paper,

(1) (a) Address inquiries to Department of Chemical Engineering, The Catholic University of America, Washington, D. C. 20017.

(2) O. A. Hougen and K. M. Watson, *Ind. Eng. Chem.*, **35**, 529 (1943); (b) K. H. Yang and O. A. Hougen, *Chem. Eng. Progr.*, **46**, 146 (1950).

(3) I. Langmuir, *Trans. Faraday Soc.*, **17**, 621 (1922).

we will introduce an "unavailability factor" to represent these unavailable sites. We will show how this has improved the agreement between the mathematical model and data obtained from the hydrogenation of isobutylene over platinum. Comparison will be made of the values of the unavailability factor obtained from this reaction and that from propylene hydrogenation over the same catalyst. The difference in their temperature behavior will also be discussed.

### Historical Development

The idea of noncompetitive or "preferred" adsorption is not an entirely new one. In 1935, Roberts<sup>4</sup> performed a statistical experiment in which a face-center crystal face was simulated by a block of numbered points. Then, by drawing from a deck of shuffled, numbered cards corresponding to these sites, he selected at random vacant pairs of sites on a  $20 \times 20$  array of points. At the end of the experiment when the ultimate surface coverage was reached, he found that 16 out of 196 (to avoid edge effect, he cut off three rows of points from each side) sites, or approximately 8%, were left as isolated single sites which would be unavailable for dual-site adsorption provided that the adsorbed layer was immobile and that no surface rearrangement took place. It has been found<sup>5</sup> that associative adsorption of ethylene, for example, requires two sites.

Langmuir<sup>6</sup> performed a similar experiment in which he used spherical molecules whose diameter was 1.25 times the distance between the closest neighboring atoms,  $d_s$ . In a cubic-lattice structure where there were four adsorption sites at equal distance  $d_s$  from any one site, this means that parts of these four sites would be blocked by an adsorbed molecule, in addition to the full occupation of its own site. However, any molecule with a diameter smaller than  $0.75d_s$  would not be affected. If, on the other hand, the diameter of this over-size molecule were larger than  $\sqrt{2}d_s$ , four additional sites would be at least partially blocked.

Langmuir thus found that only 83 out of 225, or roughly 37%, of the sites were covered by the molecules with diameter equal to  $1.25d_s$ . If the adsorption layer were mobile and surface rearrangement allowed, the closer packing would lead to an ultimate coverage of 50%. He then proceeded to derive some theoretical expressions to modify his famed *isotherm*.

However, not until recently<sup>7-9</sup> did researchers begin to include this effect in deriving *rate equations*. Rogers, *et al.*,<sup>10</sup> treating this as a reaction involving partially noncompetitive adsorption, presented the following initial rate equation

$$r = r_c + r_{nc} = \frac{\alpha_c K_A K_B p_A p_B}{(1 + K_A p_A + K_B p_B)^2} + \frac{\alpha_{nc} K_A K_B p_A p_B}{(1 + K_A p_A)(1 + K_A p_A + K_B p_B)} \quad (1)$$

where the first and second terms represent the rates due to the competitive and noncompetitive parts of the reaction, respectively. This equation has been found to reproduce very well experimental data from hydrogenation of propylene and isobutylene over platinum.

Kolboe<sup>11</sup> further introduced the concept that, in addition to the partially noncompetitive nature, the adsorption proceeds according to a dissociative mechanism. On the basis of slightly improved goodness of fit, he suggested that this should be the correct model for this reaction.<sup>12</sup>

### Theoretical Derivation

Presently we will concern ourselves with the introduction of an unavailability factor,  $F_U$ , to account for the part of surface which adsorbs only one of the two reacting species because of the isolation and/or steric hindrance effects. For the reaction  $A + B \rightleftharpoons R$ , we can write, for the adsorption of species A

$$\theta_A = K_A p_A \theta_1 \quad (2)$$

where  $\theta$  denotes fractional surface coverage,  $K$  adsorption equilibrium constant,  $p$  partial pressure, and subscript 1 vacant sites. With the restriction that

$$\theta_A + \theta_B + \theta_1 = 1^{13}$$

we can show easily that

$$\theta_A = \frac{K_A p_A}{1 + K_A p_A} (1 - \theta_B) \quad (3)$$

If surface reaction is the rate-controlling step, the overall forward reaction is expressed by

$$r = \alpha \theta_A \theta_B \quad (4)$$

where  $\alpha$  is the surface-reaction rate constant which includes  $k$ , the true rate constant;  $s$ , the number of equidistant sites adjacent to each other; and  $L$ , the molal concentration of active sites. When eq 3 is introduced into eq 4, we obtain the rate equation for this reaction when A is adsorbed according to the Langmuir mechanism while the type of adsorption

(4) J. K. Roberts, *Proc. Roy. Soc., Ser. A*, **152**, 445 (1935).

(5) R. P. Eischens and W. A. Pliskin in *Advan. Catal. Relat. Subj.*, **10**, 1 (1958).

(6) I. Langmuir, *J. Chem. Soc.*, 551 (1940).

(7) G. B. Rogers, Ph.D. Thesis, University of Wisconsin, Madison, Wis., 1961.

(8) M. M. Lih, Ph.D. Thesis, University of Wisconsin, Madison, Wis., 1962.

(9) J. H. Sinfelt, *J. Phys. Chem.*, **68**, 856 (1964).

(10) G. B. Rogers, M. M. Lih, and O. A. Hougen, *AIChE J.*, **12**, 369 (1966).

(11) S. Kolboe, *Ind. Eng. Chem., Fundam.*, **6**, 169 (1967).

(12) S. Kolboe, to be published.

(13) This implies the assumption that product R is desorbed so quickly or its adsorption equilibrium constant is so small that its concentration on the surface is negligible. This condition is met in the case discussed in this paper.

for B is unspecified. If we further specified that the latter also followed the Langmuir mechanism, *i.e.*

$$\theta_B = \frac{K_B p_B}{1 + K_A p_A + K_B p_B} \quad (5)$$

its substitution into eq 3 would give

$$r = \frac{\alpha K_A K_B p_A p_B}{(1 + K_A p_A + K_B p_B)^2} \quad (6)$$

which is one of the Hougen-Watson equations for forward rate or initial rate.

However, since we know that the second species, say, B, is kept from being adsorbed to part of the surface, although it does follow the Langmuir mechanism when being adsorbed to the accessible sites, we can modify eq 5 by a factor  $(1 - F_U)$ , where  $F_U$  is defined as the fraction of the surface unavailable to species B. By combining the resulting expression

$$\theta_B = \frac{K_B p_B (1 - F_U)}{1 + K_A p_A + K_B p_B} \quad (7)$$

with eq 3 and 4 the rate equation becomes

$$r = \frac{(1 - F_U) \alpha K_A K_B p_A p_B}{(1 + K_A p_A)(1 + K_A p_A + K_B p_B)} \times \left[ 1 - \frac{(1 - F_U) K_B p_B}{1 + K_A p_A + K_B p_B} \right] \quad (8)$$

Note that we have neglected the reverse reaction here; thus this equation is valid only for initial rate or extremely small reverse reaction constant.

It should also be pointed out that if we let  $F_U$  approach zero, eq 8 will become one of the Hougen-Watson rate equations, eq 6.

### Correlation with Experimental Data

To test the suitability of eq 8, the initial reaction rate data from isobutylene hydrogenation<sup>8</sup> were used. The experiments were conducted with extreme care to eliminate such physical effects as external and internal diffusion. Adjustments were made to ensure that catalyst activity decline was accounted for. The data have been elsewhere reported graphically<sup>10</sup> and documented.<sup>14a</sup>

A nonlinear least-squares method<sup>14b</sup> was used to estimate the set of parameters which gave the best fit. The program was executed on a CDC 1604 computer at the Numerical Analysis Laboratory of the University. An example of the fit between experimental data and the computed curve is shown in Figures 1 and 2.

The following sets of parameters were obtained for the various temperatures at which the experiments had been conducted.

These parameters are presented graphically in Figure 3. As expected, the first three follow the well-known linear relationship when their logarithms are

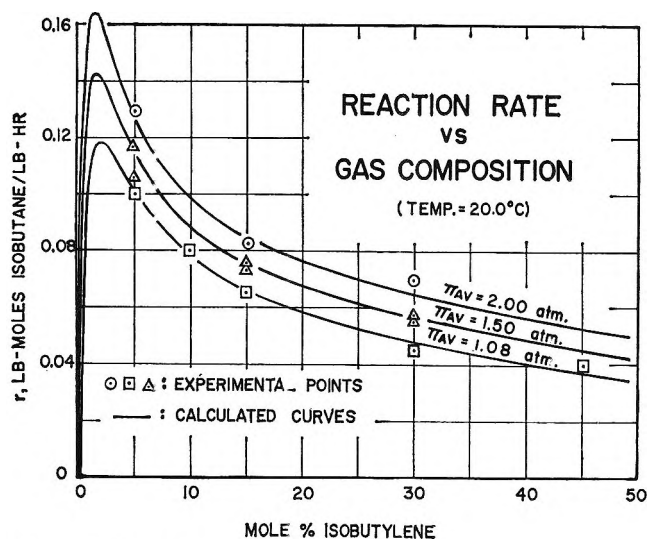


Figure 1. Reaction rate vs. gas composition.

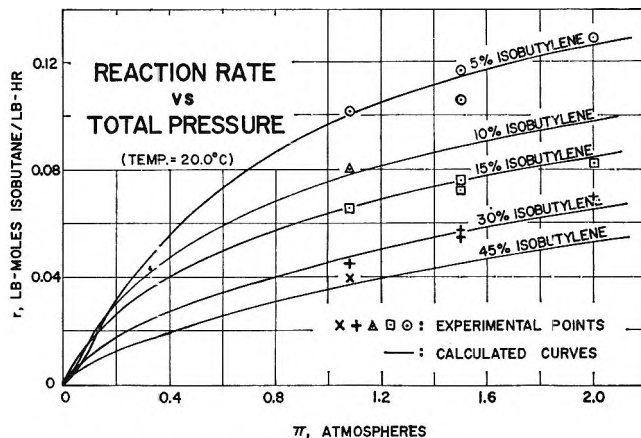


Figure 2. Reaction rate vs. total pressure.

Table I

	20.0°	35.0°	50.0°
$\alpha$	1.191	3.483	9.385
$K_A$ (hydrogen)	0.6218	0.5177	0.4663
$K_B$ (isobutylene)	100.3	89.81	55.82
$F_U$	0.1083	0.1906	0.2864
Average deviation	2.78%	4.02%	3.83%
Maximum deviation	7.52%	9.79%	10.00%

plotted against the reciprocal of the absolute temperature. Thus we further find

$$\ln \alpha = - \frac{12,952}{RT} + \frac{44.53}{R} \quad (\text{fitted to } 0.4\%)$$

$$\ln K_A = \frac{1812}{RT} - \frac{7.146}{R} \quad (\text{fitted to } 1.4\%)$$

$$\ln K_B = \frac{3639}{RT} - \frac{3.131}{R} \quad (\text{fitted to } 8.9\%)$$

(14) (a) American Documentation Institute, Document 8703, Library of Congress, Washington, D. C. 20025; (b) T. I. Peterson, *Chem. Eng. Sci.* 17, 203 (1962).

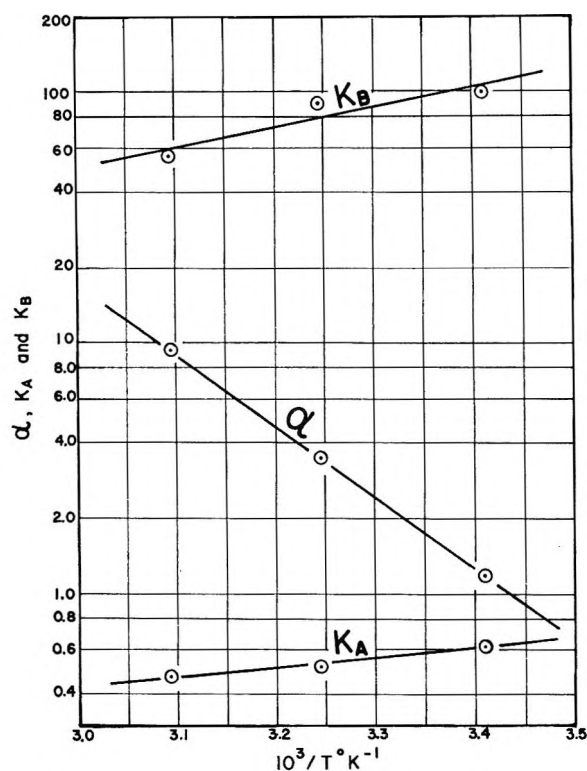


Figure 3. Temperature dependence of  $\alpha$ ,  $K_A$ , and  $K_B$ .

It may appear that the unavailability factor  $F_U$  follows a linear relationship with temperature. But obviously this cannot be true since its value must have asymptotic values between 0 and 1. Various trial functions such as

$$F_U = A(1 + B^{-C/T})$$

and

$$F_U = \frac{A}{1 + B^{C/T}}$$

which fit such criteria have been found to be unsatisfactory. We will simply present it graphically (Figure 4) with a postulated curve showing how the quantity should vary, at least qualitatively.

### Discussion

The presently proposed model is a definite improvement over any previous model without the unavailability factor. The best we have been able to achieve with any of them is an average deviation of approximately 16%, with eq 6. The improvement is so marked that it cannot be simply attributed to the additional parameter, but the parameter put in the right place. Also, the reasonable values and trends of the estimated parameters show that it is more than an accident.

The adsorption equilibrium and rate constants appear quite reasonable, as do the heats and entropies of adsorption. Therefore we will turn our attention to discussing the behavior of this new quantity  $F_U$ .

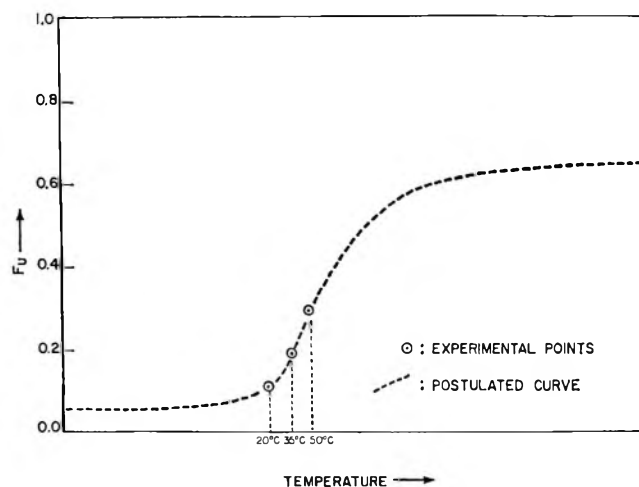


Figure 4. Temperature dependence of  $F_U$ .

The increasing unavailability factor  $F_U$  with increasing temperature clearly shows that this is a steric hindrance effect. At elevated temperatures, the motion of the large, adsorbed isobutylene molecule becomes more vigorous, thus increasing its tendency of blocking oncoming molecules from becoming its neighbors. This hardly needs profound explanation.

However, one apparent difficulty arises when we compare this behavior with that of propylene hydrogenation over the same platinum catalyst.<sup>7</sup> There the values of  $F_U$  are 0.1407, 0.1225, and 0.09061 at 1.4, 21, and 34.3°, respectively. This opposite trend has puzzled some investigators<sup>16</sup> and appears to have cast some doubt as to the validity of the mathematical model and/or experimental data. While a definite proof awaits further experimentation, preferably adsorption studies, we intend to show here that it is entirely plausible on physicochemical grounds. Unfortunately, the experiments of Sinfelt<sup>9</sup> on ethylene were performed only at one temperature. Thus we have no reliable way to extrapolate the temperature behavior and have to resort to theoretical considerations.

The decreasing  $F_U$  for propylene with increasing temperature suggests that increasing mobility of adsorbed molecules causes surface rearrangement which in turn results in freeing of isolated sites, making them available for dual-site adsorption of propylene. At least this indicates that with propylene this deisolation effect outweighs steric hindrance while for isobutylene the opposite is true because of single site adsorption which can explain the absence of isolation effect. Moreover, the larger size of isobutylene also suggests more severe steric hindrance.

Then the question becomes whether it is possible to have different adsorption mechanisms for two different members of the same chemical family. Comparison of the electron distributions in the two carbon atoms

(15) P. Kehoe and J. B. Butt, *A.I.Ch.E. J.*, **13**, 1018 (1967).



joined by the olefinic double bond suggests that it is. Take the case of ethylene at one extreme, where electrons are evenly distributed between the two carbon atoms. It is easy to see that both will be adsorbed with the same bond strength on two neighboring active sites. On the other hand, the carbon atom with the two methyl groups attached to it in isobutylene is more electron-poor than the other,<sup>16</sup> thus making it preferentially attracted to an active site. Propylene lies between the two cases, apparently with a strong enough dual-site tendency to outweigh the weak steric hindrance.

This explanation pays extra dividends in that the weaker bond resulting from dual-site adsorption suggests higher reaction rate. This is certainly true in the ethylene-propylene-isobutylene series. Let us further consider butene-2 which, despite being an isomer of isobutylene, apparently is adsorbed in the dual-site fashion because of the even distribution of electrons. Again this gives a weaker bond, and thus a higher reaction rate, compared with isobutylene. This is certainly in line with the data of Turkevich, Schissler, and Irsa<sup>17</sup> who found the rate of hydrogenation on nickel (nickel is expected to behave similarly to platinum; both are electron donors although nickel has two electrons in its outermost O shell while platinum has one in its outermost P shell) decreased over the series ethylene > propylene > butene-2 > isobutylene.

### Conclusions

A new mathematical model has been developed to account for the inaccessibility of vacant active sites to some molecules ready to be adsorbed. It reproduces extremely well experimental data of isobutylene hydrogenation on platinum. Estimated parameters have been found to be reasonable.

To account for the opposite temperature trends of this unavailability factor for isobutylene and propylene,

a plausible explanation is advanced using the electronegativity consideration. This difference in the electronic distributions, or tendencies thereof, leads to the difference in the weights of the isolation and steric hindrance effects in the two different molecules. These effects have opposite temperature dependence. Hence the unavailability factors of the two species exhibit different temperature trends.

*Acknowledgment.* The basic work in this study was carried out under financial support of the Wisconsin Alumni Research Foundation. The manuscript was prepared under National Science Foundation support (GU-2141). The author wishes to acknowledge assistance and guidance from Professor O. A. Hougen and Dr. G. B. Rogers.

### Notation

$A$	Empirical constant
$B$	Empirical constant
$C$	Empirical constant
$d_a$	Distance between two closest neighboring atoms on catalytic surface
$F_U$	Unavailability factor
$K$	Adsorption equilibrium constant
$k$	Surface reaction rate constant
$L$	Molal concentration of adsorption sites
$p$	Partial pressure
$r$	Reaction rate (initial)
$s$	Number of equidistant sites adjacent to each other
$\alpha$	$ksL$
$\theta$	Fractional surface coverage
Subscripts	
A	Reactant A
B	Reactant B
c	Competitive
l	Vacant sites
nc	Noncompetitive

(16) C. R. Noller, "Textbook of Organic Chemistry," W. B. Saunders Co., Philadelphia, Pa., 1951.

(17) J. Turkevich, D. O. Schissler, and P. Irsa, *J. Phys. Colloid Chem.*, **55**, 1078 (1951).

# Catalysis in Liquid Phase Autoxidation. II. Kinetics of the Poly(tetrafluoroethylene)-Catalyzed Oxidation of Tetralin

by William F. Taylor

*Esso Research and Engineering Company, Government Research Laboratory, Linden, New Jersey  
(Received September 25, 1969)*

A study was made of the kinetics of the poly(tetrafluoroethylene)-catalyzed oxidation of tetralin at 65–115°. The catalyzed decomposition of tetralin hydroperoxide was also studied. The initial rate of the catalyzed oxidation of tetralin was second order in tetralin, zero order in oxygen pressure, half-order in catalyst weight and exhibited an apparent activation energy of 17.0 kcal/mol. Poly(tetrafluoroethylene) catalyzed the decomposition of tetralin hydroperoxide (II). This decomposition exhibited a 16.3-kcal/mol apparent activation energy and was first order in concentration and catalyst weight. The catalyzed oxidation of tetralin involves a sequence of reactions in which tetralin hydroperoxide (II) is first formed, followed by decomposition of II to produce equal molar quantities of the ketone (III) and the alcohol (IV); and ultimately a conversion of the alcohol (IV), first into 1,2-dihydronaphthalene (V) and then into naphthalene (VI). Independent experiments indicated that the intermediate compounds IV, V, and VI exerted no measurable influence on the catalyzed oxidation of tetralin; whereas the ketone (III) accelerated this rate. The results suggest that the principal function of the catalyst is to initiate the conventional oxidation of tetralin by generating free radicals from the hydroperoxide. The observed kinetics are discussed in terms of a proposed mechanism.

## Introduction

It is well known from extensive studies that homogeneous metals can catalyze the liquid phase oxidation of a compound such as tetralin. Less extensive studies have shown that heterogeneous metal oxides are also capable of catalyzing liquid phase hydrocarbon autoxidation reactions<sup>1–5</sup> including the oxidation of tetralin.<sup>4,5</sup> More recently,<sup>6,7</sup> it has been shown that polymeric surfaces also influence liquid phase autoxidation reactions. Although no detailed kinetics were reported, it was found that low-surface energy solids such as poly(tetrafluoroethylene) and polypropylene are surprisingly active catalysts for the oxidation of tetralin.<sup>6</sup> In order to further elucidate the effect of polymeric surfaces in autoxidation reactions, the kinetics of the poly(tetrafluoroethylene)-catalyzed oxidation of tetralin have been studied in detail. Reported in the present work are studies of both the catalyzed oxidation of tetralin in chlorobenzene over the range of 65–115° and also the catalyzed decomposition of tetralin hydroperoxide in chlorobenzene under a N<sub>2</sub> atmosphere. Because of the importance of specific activity in studies of this nature,<sup>8–10</sup> the influence of poly(tetrafluoroethylene) surface in the reaction system was studied by varying the weight of catalyst in the reactor at otherwise constant conditions. In addition, particular emphasis was placed on following the secondary reactions which occur in the oxidation of tetralin and the decomposition of tetralin hydroperoxide as a function of reaction time, which previously has not been done.

## Experimental Section

*Apparatus and Procedure.* A conventional liquid phase autoxidation apparatus was used.<sup>11</sup> The rate of oxidation was measured at atmospheric pressure. The reactor was immersed in a temperature bath controlled to 0.5°. Mass transfer limitations were minimized by vibrating the reactor at a speed of 800 cpm. Experiments demonstrated that the rate of oxidation was independent of vibration speed at this level. In each run the tetralin, chlorobenzene, and a fresh charge of catalyst were added to the reactor and hooked into the reaction system; the reactants were degassed by repeated vacuum freeze-thaw cycles using liquid N<sub>2</sub>. The reactor was then filled with O<sub>2</sub> and immersed in the temperature-controlled bath. Aliquot samples for analy-

(1) J. Burger, C. Meyer, and J. C. Balaceanu, *C. R. Acad. Sci.*, **252**, 2235 (1961).

(2) I. I. Ioffe, N. V. Klimova, and I. Ya. Mokrovsova, *Dokl. Acad. Nauk. SSSR*, **169**, 389 (1966).

(3) N. V. Klimova and I. I. Ioffe, *Kinet. Katal.*, **8**, 565 (1967).

(4) A. Mukherjee and W. F. Graydon, *J. Phys. Chem.*, **71**, 4232 (1967).

(5) P. George, *Trans. Faraday Soc.*, **42**, 210 (1946).

(6) W. F. Taylor, *J. Catal.*, **16**, 20 (1970).

(7) N. M. Emanuel, "Present State of the Theory of Chain Reactions in the Liquid Phase Oxidation of Hydrocarbons," Preprints, 7th World Petroleum Congress, Mexico City, 1967.

(8) W. F. Taylor, J. H. Sinfelt, and D. J. C. Yates, *J. Phys. Chem.*, **69**, 3857 (1965).

(9) W. F. Taylor and H. K. Staffin, *ibid.*, **71**, 3314 (1967).

(10) D. J. C. Yates, W. F. Taylor, and J. H. Sinfelt, *J. Amer. Chem. Soc.*, **86**, 2996 (1964).

(11) J. L. Bolland, *Proc. Roy. Soc., Ser. A*, **186**, 220 (1946).

sis during the run were removed *via* a syringe through a septum cap attached to a side arm on the reactor. Analyses were made using an F & M Model 500 temperature-programmed gas chromatograph with a 2-ft column containing 10% QF-1 (fluorinated silicone oil) on 45/60 mesh Chromosorb W. The column was programmed from 50 to 175° at 7.9°/min. A Perkin-Elmer Model 154 gas chromatograph was used for gas analyses with a 5-ft column containing 13X molecular sieve at 35°. Infrared analyses of liquid samples were obtained on a Perkin-Elmer Model 137 NaCl spectrophotometer. Mass spectrometric analysis was carried out in a CEC Model 21-103 mass spectrometer.<sup>12</sup> The tetralin hydroperoxide content was determined chemically by the method of Wagner, *et al.*<sup>13</sup>

**Reagents.** Tetralin (Matheson Coleman and Bell, practical grade) was purified by washing with concentrated sulfuric acid until the washings were colorless, followed by washing with distilled water to remove residual acidity and drying with anhydrous MgSO<sub>4</sub>.<sup>4</sup> The resulting tetralin was then repeatedly distilled in a spinning band column until a fraction was obtained which showed no impurities by glpc analyses. Chemical analyses confirmed the tetralin was free of hydroperoxide.<sup>13</sup> Tetralin hydroperoxide was prepared by the method of Woodward and Mesrobian<sup>14</sup> using purified tetralin and dry air. Product purity was verified by chemical titration. Glpc pure chlorobenzene (Matheson Coleman and Bell) was employed. Naphthalene was obtained from Eastman Organic Chemicals Dept., Eastman Kodak Co., Rochester, N. Y. Glpc analyses showed no detectable impurities. The 1,2-dihydronaphthalene was obtained from Aldrich Chemical Co., Milwaukee, Wis. Glpc analyses indicated it contained 5% 1,4-dihydronaphthalene. Glpc pure 1,2,3,4-tetrahydro-1-naphthol and 3,4-dihydro-1(2H)-naphthalenone were obtained from Aldrich Chemical Co.

The poly(tetrafluoroethylene) was obtained from the E. I. du Pont de Nemours & Co. Wilmington, Del., and prepared as a 60/80 mesh powder using the method previously described.<sup>6</sup> The catalyst had a BET surface area of 0.69 m<sup>2</sup>/g.

## Results

A study was first made of the effect of various kinetic parameters on the oxidation of tetralin in the presence of poly(tetrafluoroethylene). Higher temperatures both increased the initial oxidation rate and reduced the length of the induction period. An Arrhenius plot of the initial reaction rate, which is shown in Figure 1, yielded an apparent activation energy of 17.0 kcal/mol. A similar plot of the reciprocal of the induction period yielded a temperature dependence equivalent to 16.7 kcal/mol.<sup>6</sup> The effect of tetralin concentration, oxygen pressure, and catalyst weight in the reaction system was next studied. Results are summarized in Table I. An examination of these re-

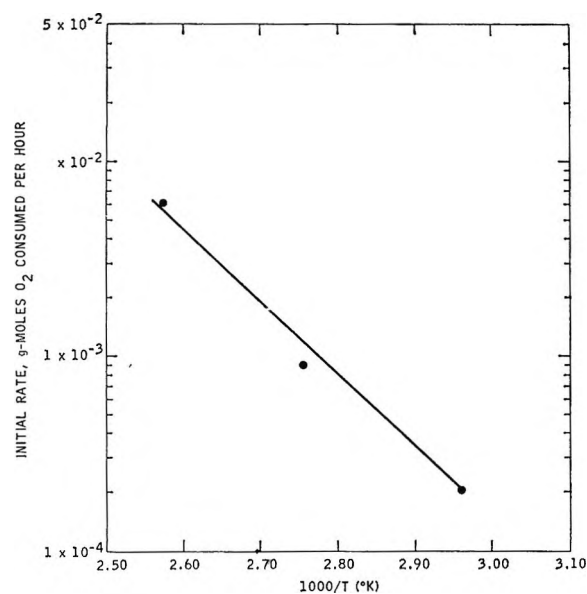


Figure 1. The effect of temperature on the initial rate of the catalyzed oxidation of tetralin. Other conditions: 2 ml of tetralin, 2 ml of chlorobenzene, 0.30 g of catalyst, and 1 atm pressure.

Table I: Relative Rates of Tetralin Oxidation As a Function of Tetralin Concentration, Oxygen Pressure, and Catalyst Loading

[Tetralin], M	Oxygen press., Torr	Catalyst loading, g	Relative initial rate of oxidn., $r/r_0^a$
3.68	660	0.30	1.1
3.68	710	0.30	1.0
3.68	760	0.30	1.00 (base) <sup>b</sup>
3.68	810	0.30	1.0
3.68	760	0.15	0.68
3.68	760	0.30	1.00 (base) <sup>c</sup>
3.68	760	0.60	1.34
2.45	760	0.30	0.44
3.68	760	0.30	1.00 (base) <sup>d</sup>
4.91	760	0.30	1.86

<sup>a</sup> Initial rate of oxidation in terms of moles per hour of tetralin converted at given conditions relative to initial rate at standard conditions as shown. <sup>b</sup> Study conducted at 65° with 2 ml of tetralin in 2 ml of chlorobenzene. <sup>c</sup> Study conducted at 90° with 2 ml of tetralin in 2 ml of chlorobenzene. <sup>d</sup> Study conducted at 90° with, respectively, 1, 2, and 4 ml of tetralin in 2 ml of chlorobenzene.

sults indicated that the initial rate of reaction is second order in tetralin concentration, zero order in oxygen pressure, and approximately half-order in catalyst

(12) W. F. Taylor, J. M. Kelliher, and T. J. Wallace, *Chem. Ind. (London)*, 651 (1968).

(13) C. D. Wagner, R. H. Smith, and E. D. Peters, *Anal. Chem.*, **19**, 976 (1947).

(14) A. E. Woodward and R. B. Mesrobian, *J. Amer. Chem. Soc.*, **75**, 6189 (1953).

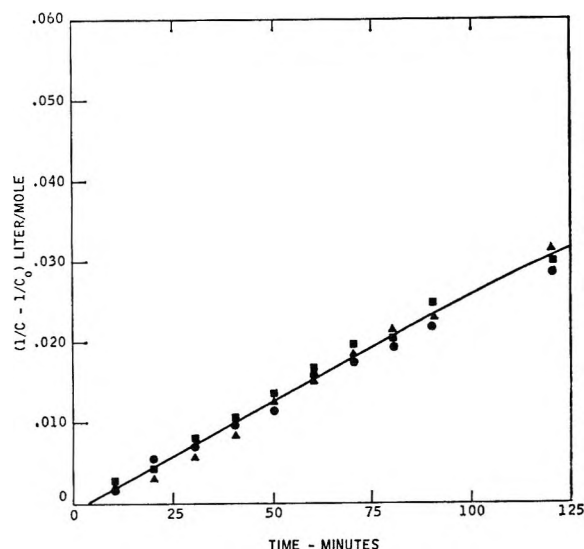


Figure 2. Second-order rate plot for the catalyzed oxidation of tetralin in chlorobenzene at 90° and 1 atm pressure using 0.30 g of catalyst: ■, 2.45 *M* tetralin; ●, 3.68 *M*; ▲, 4.91 *M*.

level. To confirm the second-order dependence on tetralin concentration, an integral second-order rate plot ( $1/C - 1/C_0$  vs. time where  $C$  is the concentration of tetralin in  $M$  at time  $t$  and  $C_0$  is the initial concentration) was prepared, which is shown in Figure 2. As can be seen, it confirms the conclusion reached from an examination of the initial rate data.

A study was also made of the poly(tetrafluoroethylene)-catalyzed decomposition of tetralin hydroperoxide in chlorobenzene under nitrogen over the range of 90–115° at atmospheric pressure. The effect of tetralin hydroperoxide concentration and catalyst weight was also studied. Results are summarized in Table II. An examination of these results indicated that the catalyzed decomposition is a first-order process, in

Table II: Relative Rates of Tetralin Hydroperoxide Decomposition As a Function of Tetralin Hydroperoxide Concentration and Catalyst Loading<sup>a</sup>

Tetralin hydroperoxide concn, wt %	Catalyst loading, g	Relative rate of decompn, $\tau/\tau_0$
4.37	0.30	0.58 <sup>b</sup>
8.30	0.30	1.00 (base) <sup>b</sup>
15.3	0.30	1.92 <sup>b</sup>
8.30	0.15	0.47 <sup>c</sup>
8.30	0.30	1.00 (base) <sup>c</sup>
8.30	0.60	2.21 <sup>c</sup>

<sup>a</sup> Conditions: 105°, tetralin hydroperoxide added to 4 cm<sup>3</sup> of chlorobenzene solvent, 1 atm N<sub>2</sub>. <sup>b</sup> Relative rates calculated from initial rate of tetralin hydroperoxide conversion in moles per hour. <sup>c</sup> Relative rates calculated from the initial observed first-order rate constants corrected for the thermal (noncatalytic) contribution at the same conditions.

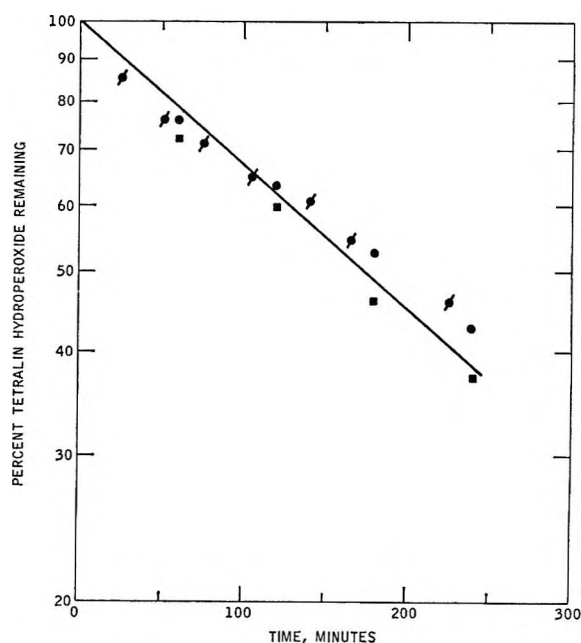


Figure 3. First-order rate plot for the catalyzed decomposition of tetralin hydroperoxide in 4 cm<sup>3</sup> of chlorobenzene under 1 atm N<sub>2</sub> using 0.30 g of catalyst at 105°: ■, 4.37 wt %; ●, 8.30 wt %; ▲, 15.3 wt % tetralin hydroperoxide.

concentration, as has been reported for the uncatalyzed decomposition.<sup>15,16</sup> An integral first-order rate plot is shown in Figure 3, which confirms the conclusion reached from the initial rate data. The catalyzed decomposition of tetralin hydroperoxide was also found to be first order in catalyst weight. An Arrhenius plot of the first-order rate constants for the poly(tetrafluoroethylene)-catalyzed decomposition of tetralin hydroperoxide is shown in Figure 4. This plot yielded an apparent activation energy of 16.3 kcal/mol. The rate of the uncatalyzed decomposition of tetralin hydroperoxide was measured at 115° at the identical conditions employed in the catalyzed decomposition measurements. The uncatalyzed decomposition was slower than the catalyzed decomposition and yielded a first-order decomposition rate constant which was only 61% of the catalyzed value.

Aliquot liquid and gas samples were taken during both the catalyzed oxidation of tetralin studies and the catalyzed tetralin hydroperoxide decomposition studies so as to quantitatively determine the major reaction products. Analytical techniques included quantitative chemical titration for tetralin hydroperoxide content, gas chromatographic, infrared and mass spectrometer analyses of liquid samples and gas chromatographic analyses of gas samples. Details are given in the Experimental Section. In Figure 5 are shown the change in reactants and liquid products in-

(15) A. Robertson and W. A. Waters, *J. Chem. Soc.*, 1578 (1948).

(16) J. R. Thomas, *J. Amer. Chem. Soc.*, 77, 246 (1955).

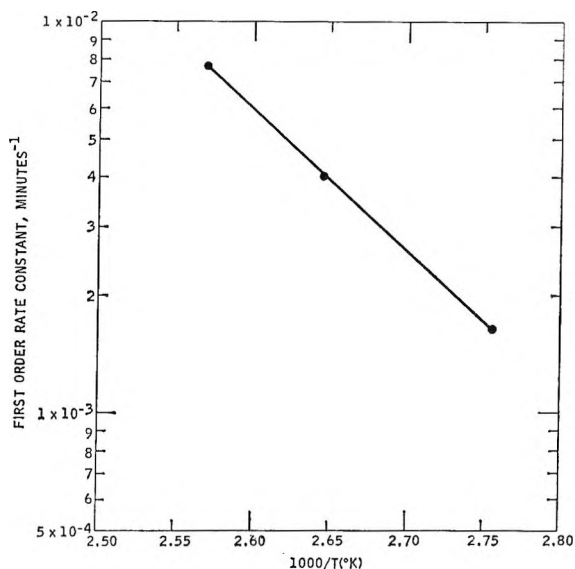


Figure 4. Arrhenius plot of the first-order rate constants for the catalyzed decomposition of tetralin hydroperoxide. Conditions: 0.40 g of tetralin hydroperoxide in 4 ml of chlorobenzene under 1 atm  $N_2$  using 0.30 g of catalyst.

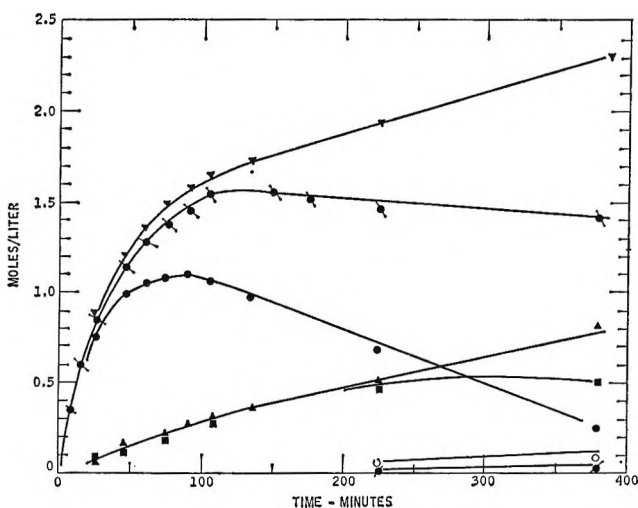
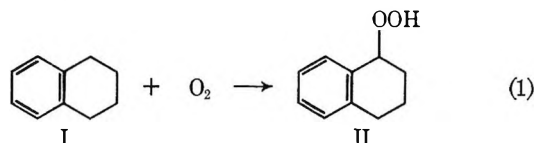


Figure 5. Reactants and liquid product changes during the catalyzed oxidation of tetralin at  $115^\circ$ . Other conditions: 4 ml of tetralin in 2 ml of chlorobenzene, 0.30 g of catalyst, and 1 atm pressure.  $\nabla$ , tetralin consumed;  $\bullet$ , oxygen consumed (by volumetric change);  $\circ$ , tetralin hydroperoxide (II) content;  $\blacktriangle$ , ketone (III) content;  $\blacksquare$ , alcohol (IV) content;  $\circ$ , 1,2-dihydronaphthalene content;  $\blacklozenge$ , naphthalene content.

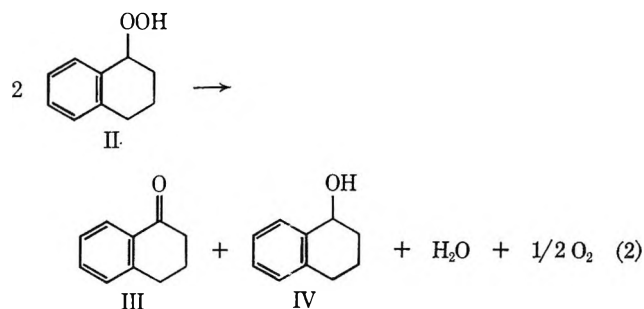
involved in the poly(tetrafluoroethylene)-catalyzed oxidation of tetralin at  $115^\circ$  as a function of reaction time. A comparison of tetralin conversion, oxygen uptake, and tetralin hydroperoxide content confirms that the initial reaction product is tetralin hydroperoxide. As the reaction progresses, however, the tetralin hydroperoxide is converted into other products. In addition to the liquid products shown in Figure 5,  $H_2O$  and  $H_2$  were also detected in samples of the gas phase. At

this point it should be noted that the oxygen uptake data obtained from volumetric changes no longer can be used as a measure of the forward progress of the reaction, *i.e.*, tetralin conversion, as light gases are being produced which make the measured volumetric change difficult to interpret. Thus, autoxidation studies dependent solely on oxygen uptake data for a measurement of the rate of progress of the reaction may be subject to some error if extensive secondary reactions have taken place. Similar analyses were made of the products of catalyzed decomposition of tetralin hydroperoxide. Results of the analyses of the liquid samples are shown in Figure 6. Analyses of samples of the gas phase indicated the presence of  $H_2O$ ,  $O_2$ , and  $H_2$ .

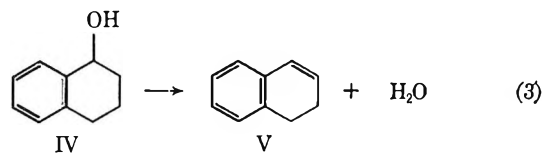
A consideration of all the product analyses indicates that the poly(tetrafluoroethylene)-catalyzed oxidation of tetralin consists of a series of sequential reactions. In analyzing these results, the light gases detected were assigned to a reaction step as dictated by the stoichiometry required by the changes in liquid constituents. As has been well established, tetralin (I) is first oxidized to tetralin hydroperoxide (II). Fol-



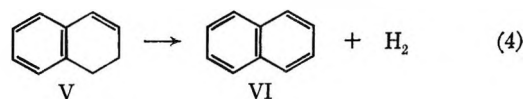
lowing this, the tetralin hydroperoxide (II) decomposes to produce equal molar quantities of the ketone, 1-tetralone (III), and the alcohol, 1,2,3,4-tetrahydro-1-naphthol (IV). The ketone (III) is essentially stable



in the reaction system. However, the alcohol (IV) undergoes further reaction to the olefin 1,2-dihydronaphthalene (V). This olefin (V) then undergoes fur-



ther reaction to produce naphthalene (VI). Reactions



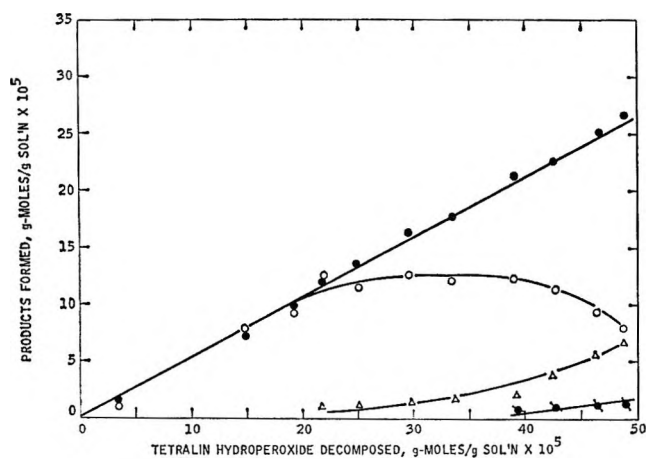


Figure 6. Liquid products present during the catalyzed decomposition of tetralin hydroperoxide in chlorobenzene under  $N_2$  at  $115^\circ$ : ●, ketone (III); ○, alcohol (IV); △, 1,2-dihydronaphthalene; ●, naphthalene.

1 through 4 represent the main routes for the poly-(tetrafluoroethylene)-catalyzed oxidation of tetralin for the conditions and reaction times studied. There is a possibility that other products were made at the end of the run at  $115^\circ$  (Figure 5) as material balances showed a tendency to fall below their normal 100% level.

A study was next made of the effect of the various products from the decomposition of tetralin hydroperoxide on the catalyzed rate of oxidation of tetralin. Included in this study was the effect of the ketone (III), the alcohol (IV), 1,2-dihydronaphthalene (V), and naphthalene (VI). In general, these studies were carried out by sequentially injecting the compound in question into the reaction mixture after the run was in progress and observing its effect on the subsequent portion of the run. This was done in order to assure that the catalyzed oxidation was proceeding in a normal manner before the effect of the added component was assessed. Studies were made at both  $65^\circ$  and  $115^\circ$ . Results of the effect of the addition of the alcohol (IV) and the ketone (III) at  $65^\circ$  are shown in Figure 7. At these conditions, data obtained from oxygen uptake and tetralin conversion are equivalent. It can be seen that the presence of the alcohol (IV) had no significant effect on the course of the reaction, whereas the addition of the ketone (III) accelerated the rate of oxidation. The results obtained at  $115^\circ$  are summarized in Table III. The presence of the alcohol (IV), dihydronaphthalene (V), and naphthalene (VI) had no significant effect on the rate of oxidation. However, the presence of the ketone (III), again increased the catalyzed rate of oxidation of tetralin.

### Discussion

The initial rate of oxidation of tetralin was found to be second order in hydrocarbon and zero order in oxygen pressure. Similar orders have been reported pre-

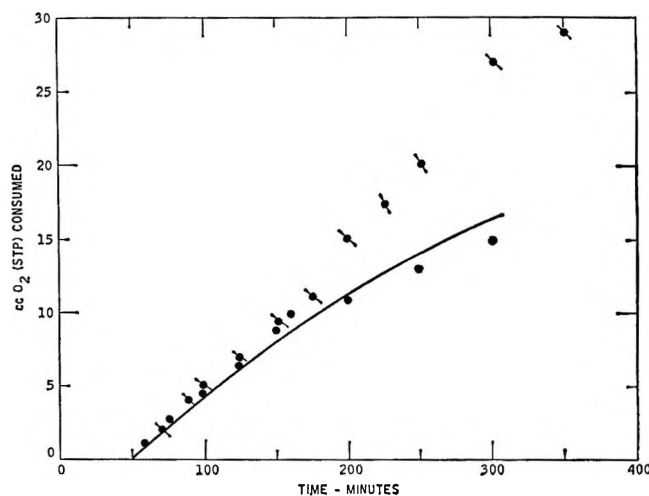


Figure 7. Effect of intermediate products on the catalyzed oxidation of tetralin at  $65^\circ$ . Line shown for run with no product addition. ●, ketone (III) addition at 90, 120, 150, and 180 min; ○, alcohol (IV) addition at 90, 120, 150, and 180 min.

Table III: Effect of Secondary Products on the Rate of Tetralin Oxidation at  $115^\circ$

Added compd	Cumulative tetralin conversion, after addition of indicated compd relative to conversion obtained with no addition <sup>a,b</sup>
None	1.00 (base)
1-Tetralone (III)	1.2 <sup>c</sup>
1,2,3,4-Tetrahydro-1-naphthol (IV)	1.0
1,2-Dihydronaphthalene (V)	1.0
Naphthalene (VI)	1.0

<sup>a</sup> Other conditions: 2 cm<sup>3</sup> of tetralin, 2 cm<sup>3</sup> of chlorobenzene, 0.30 g of catalyst, 1 atm O<sub>2</sub> pressure. <sup>b</sup> Reaction mixture injected with 0.05 g of added compound in 0.125 cm<sup>3</sup> of chlorobenzene at 25, 65, and 120 min. <sup>c</sup> Conversions compared at 150 min.

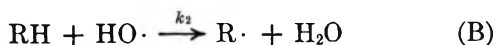
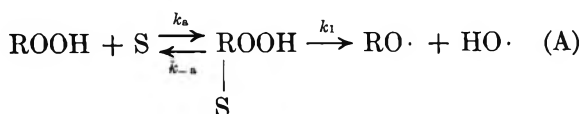
viously for the uncatalyzed oxidation of tetralin,<sup>17</sup> and in the early study of George<sup>5</sup> for the heterogeneously catalyzed oxidation. A more recent study of the catalytic effect of various metal oxides surfaces reports a zero-order dependence on oxygen pressure and a tetralin order varying between approximately one and two.<sup>4</sup> Poly(tetrafluoroethylene) was found to exhibit an apparent activation energy for the initial rate of oxidation of tetralin of 17.0 kcal/mol. Studies of the metal oxide catalyzed oxidation of tetralin showed apparent activation energies ranging from 9 to 10 kcal/mol.<sup>4</sup> The higher apparent activation energy of poly(tetrafluoroethylene) relative to metal oxide surfaces may simply reflect a weaker bonding between the surface and the reactive species, which could occur with

(17) P. George and A. Robertson, *Proc. Roy. Soc., Ser. A*, **185**, 309 (1946).

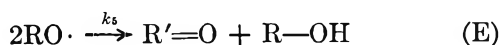
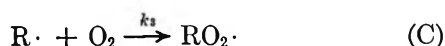
such a low-surface energy solid. In this respect, it should be noted that an interrelation between apparent activation energy and strength of the surface to reactant intermediate bond has been postulated for other catalytic reaction systems.<sup>18,19</sup>

A comparison with both the literature<sup>15</sup> and data obtained in the present work indicates that poly(tetrafluoroethylene) increases the rate of decomposition of tetralin hydroperoxide in chlorobenzene. Robertson and Waters<sup>15</sup> report a first-order decomposition of tetralin hydroperoxide in tetralin and chlorobenzene and a 24.4 kcal/mol apparent activation energy (in tetralin under N<sub>2</sub>). Thomas<sup>16</sup> reports a first-order decomposition of tetralin hydroperoxide and an apparent activation energy of 28.5 to 29 kcal/mol (in *n*-octadecane and white oil under N<sub>2</sub> in the presence of an inhibitor). It has been previously reported that poly(tetrafluoroethylene) markedly reduced the length of the induction period when oxidizing tetralin, and that an Arrhenius plot of the reciprocal of the induction period yielded a temperature dependence equivalent to 16.7 kcal/mol.<sup>6</sup> Thus, there is close agreement between the temperature dependence for tetralin hydroperoxide decomposition (*i.e.*, 16.3 kcal/mol) and the temperature dependence of the induction period. All this suggests that a major role of the poly(tetrafluoroethylene) surface is to accelerate radical production *via* the decomposition of tetralin hydroperoxide. Similar observations have been made in regard to the role of homogeneous metals in the catalyzed autoxidation of alkanes and alkylbenzenes.<sup>20</sup>

Thus, during the early portion of the oxidation in the presence of an inert solvent, the catalyzed initiation step should involve adsorption on the catalyst surface, S, followed by decomposition as follows



Well-established propagation steps and a termination reaction between peroxy radicals should also take place. Equal molar production of the alcohol and the ketone suggest a rapid termination reaction involving alkoxy radicals. Thus



The noncatalytic decomposition of tetralin hydroperoxide has been reported to be first order.<sup>16</sup> Ingold and coworkers have reported that the homogeneously

catalyzed decomposition of this hydroperoxide is also pseudo first order.<sup>21-24</sup> Present results corroborate these findings. Increasing the weight of catalyst would directly increase the surface available to catalyze the decomposition of tetralin hydroperoxide. This is presumably reflected in the observed pseudo-first-order dependence of the amount of catalyst on the catalyzed decomposition of the hydroperoxide. Studies of both the homogeneously catalyzed<sup>22-24</sup> and heterogeneously catalyzed<sup>4</sup> oxidation of tetralin in chlorobenzene indicate the reaction is quite complex. It is generally agreed that the reaction is zero order in oxygen concentration as was found in the present study. Studies of the effect of tetralin concentration and amount of catalyst on the rate of oxidation in chlorobenzene in both the homogeneously<sup>23,24</sup> and heterogeneously<sup>4</sup> catalyzed reaction indicate a complex but similar phenomena. As the catalyst amount increases at a fixed tetralin concentration, the rate increases until a critical concentration is reached above which the oxidation is inhibited and suffers a catastrophic decline. This critical catalyst concentration is a function of tetralin concentration<sup>24</sup> and at a given catalyst concentration the rate of oxidation will drop to zero if the tetralin concentration is decreased sufficiently (*i.e.*, at a given catalyst concentration there is a critical-tetralin concentration and at a given tetralin concentration there is a critical-catalyst concentration). Different kinetic schemes are postulated to account for this complex concentration-catalyst interaction on the homogeneously<sup>24</sup> and heterogeneously<sup>4</sup> catalyzed reaction system. The heterogeneously catalyzed studies<sup>4</sup> indicate an order in tetralin varying between one and two and an order in catalyst ranging from approximately one-half to one. The homogeneously catalyzed oxidation<sup>21-24</sup> indicates a second-order dependence of the maximum rate of oxidation on tetralin concentration, which is postulated to reflect a steady-state hydroperoxide concentration.

For the catalyzed decomposition of hydroperoxide in the present work, application of a steady-state treatment to the fraction of the catalyst surface covered with hydroperoxide,  $\theta$ , yields

$$\frac{d\theta}{dt} = k_a[\text{ROOH}](1 - \theta) - k_{-a}\theta - k_1\theta = 0 \quad (\text{G})$$

From which it follows

(18) V. Völter, *J. Catal.*, **3**, 287 (1964).

(19) D. Shopov and A. Andreev, *ibid.*, **6**, 316 (1966).

(20) F. R. Mayo, *Accounts Chem. Res.*, **1**, 193 (1968).

(21) Y. Kamiya, S. Beaton, A. Lafortune, and K. U. Ingold, *Can. J. Chem.*, **41**, 2020 (1963).

(22) Y. Kamiya, S. Beaton, A. Lafortune, and K. U. Ingold, *ibid.*, **41**, 2034 (1963).

(23) Y. Kamiya and K. U. Ingold, *ibid.*, **42**, 1027 (1964).

(24) Y. Kamiya and K. U. Ingold, *ibid.*, **42**, 2424 (1964).

$$K[\text{ROOH}] = \frac{\theta}{1 - \theta} \quad (\text{H})$$

where  $K = k_a/(k_{-a} + k_1)$ . The first-order dependence of the catalyzed decomposition of hydroperoxide on hydroperoxide concentration suggests that the fraction of the surface covered with hydroperoxide is low and that  $(\theta/1 - \theta) \simeq \theta$ . An application of the conventional steady-state treatment yields the following equation for the initial oxidation rate

$$\frac{-d(\text{O}_2)}{dt} = k_4[\text{RH}] \left( \frac{k_1 \theta \omega}{k_3} \right)^{1/2} \quad (\text{I})$$

where  $\omega$  is the weight of the catalyst and  $k_1$  has appropriate units. Substituting for  $\theta$  yields an equation of the form

$$\frac{-d(\text{O}_2)}{dt} \propto [\text{RH}]([\text{ROOH}]_\omega)^{1/2} \quad (\text{J})$$

In previous homogeneous studies<sup>21-24</sup> the observed second-order dependence on tetralin concentration was explained by invoking a steady-state treatment of the hydroperoxide concentration. A steady-state hydroperoxide concentration, however, was not experimentally observed for the oxidation of tetralin in chlorobenzene solvent.<sup>22</sup> It was reported that for the homogeneously catalyzed oxidation of tetralin in chlorobenzene solvent that the measured hydroperoxide concentration was proportional to the square of the tetralin concentration at low catalyst levels.<sup>22</sup> Substituting such a relationship into eq J would yield the following

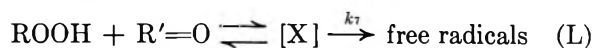
$$\frac{-d(\text{O}_2)}{dt} \propto [\text{RH}]^2 \omega^{1/2} \quad (\text{K})$$

However, in view of the obvious complexity of the catalyzed oxidation of tetralin in chlorobenzene, such a treatment must be viewed with reservation. In this respect, Ingold and coworkers<sup>21</sup> pointed out following their derivation of a rate expression showing a second-order hydrocarbon dependence, that similar rate forms could be obtained using different kinetic treatments.

In the presence of poly(tetrafluoroethylene) the initial reaction products of the decomposition of tetralin hydroperoxide are the ketone (III) and the alcohol (IV). Robertson and Waters,<sup>15</sup> in a study of the uncatalyzed decomposition of tetralin hydroperoxide, found the ketone (III) and to a lesser extent the alcohol (IV) were major decomposition products and that water and oxygen (in chlorobenzene solvent) are also formed. This work, however, did not report the formation of

dihydronaphthalene and naphthalene. Thus, it would appear that the presence of the poly(tetrafluoroethylene) catalyst exerts a major influence on the direction of these secondary reactions. In the study of the heterogeneously metal oxide catalyzed oxidation of tetralin no secondary products were identified other than the ketone and alcohol.<sup>4</sup> Ketone to alcohol ratios varying from approximately 2 to 4 were reported. However, the mechanism proposed to explain these results<sup>4</sup> does not postulate an initial equal molar production of ketone and alcohol followed by a sequential conversion of the alcohol into other products, as was found in the present study. In this work<sup>4</sup> no data are presented showing the reaction products as a function of the forward progress of the reaction, so it is not clear whether the varying ketone to alcohol ratio observed with metal oxides catalysts also reflects a secondary conversion of the alcohol or whether it reflects a different reaction sequence as postulated.

In the present study the ketone (III) was found to accelerate the rate of oxidation, whereas the alcohol (IV) and other products (V, VI) exerted no significant effect on the reaction. Robertson and Waters<sup>25</sup> also observed no significant effect of alcohols on the oxidation of tetralin. However, it has been found that ketones such as cyclohexanone can accelerate the decomposition of hydroperoxide.<sup>26</sup> Following the treatment of Emanuel,<sup>26</sup> this acceleration presumably reflects the formation of a complex between the hydroperoxide and the ketone



Initiation involves both direct hydroperoxide decomposition (reaction A) and reaction L. The complex [X] is assumed to decompose more rapidly than the hydroperoxide itself, so that at the latter stages of the reaction when the ketone concentration rises, reaction L would dominate the initiation process.

*Acknowledgment.* This work was sponsored by the Air Force Aero Propulsion Laboratory, Air Force Systems Command, United States Air Force, Wright-Patterson Air Force Base, Ohio, under Contract No. AF-33(615)-3575. Helpful discussions with H. R. Lander, Jr., J. C. Ford<sub>2</sub> and Professor Michel Boudart are gratefully acknowledged.

(25) A. Robertson and W. A. Waters, *Trans. Faraday Soc.*, **42**, 201 (1946).

(26) N. M. Emanuel, E. T. Denisov, and Z. K. Maizus, "Liquid Phase Oxidation of Hydrocarbons," Plenum Publishing Corp., New York, N. Y., 1967, p 84.



## Negative Ion Formation by Boron Trifluoride and Phosphorus Trifluoride

by K. A. G. MacNeil and J. C. J. Thynne<sup>1</sup>

Chemistry Department, Edinburgh University, Edinburgh, Scotland (Received October 1, 1969)

Negative ion formation as a result of the electron bombardment of boron trifluoride and phosphorus trifluoride has been studied as a function of the electron energy. Vertical onset behavior is a feature of the ionization processes for several ions. A value of  $1.9 \times 10^{-9}$  molecule<sup>-1</sup> cm<sup>3</sup> sec<sup>-1</sup> has been estimated for the rate constant of the ion-molecule reaction  $\text{F}_2^- + \text{BF}_3 \rightarrow \text{BF}_4^- + \text{F}$ , and a value of  $\leq -15.5$  eV has been estimated for the heat of formation of the  $\text{BF}_4^-$  ion.

As part of a continuing program<sup>2</sup> concerned with negative ion formation as the result of electron bombardment of molecules, we have studied boron trifluoride and phosphorus trifluoride. Boron trifluoride has been studied previously<sup>3</sup> but only the  $\text{F}^-$  ion was identified. Preliminary studies of  $\text{BF}_3$  and  $\text{PF}_3$  suggested that the ionization efficiency curves for several of the negative ions formed showed near-vertical onsets, the ion currents rising almost to a maximum value at the threshold. Such behavior has been noted for the  $\text{O}^-$  ion formed by CO but not for ions formed by polyatomic molecules.<sup>4</sup>

In electron impact studies, when the electrons are emitted from a heated filament, because of the energy spread of the electron beam uncertainties arise in the determination of the appearance potentials of ions. This is in part due to the smearing-out effect of the high-energy tail of the electron energy distribution. Analytical methods have been developed to reduce this effect for positive<sup>5,6</sup> and negative<sup>7</sup> ions, and we have applied this technique to the ions formed in this study.

### Experimental Section

The experiments were performed using a Bendix time-of-flight mass spectrometer, Model 3015. The pressure in the ion source was usually maintained below  $5 \times 10^{-6}$  mm except when secondary ion formation was studied, in which case pressures of up to  $8 \times 10^{-5}$  mm were used. The energy of the ionizing electrons was read on a digital voltmeter, and the spectra were recorded on two 1-mV potentiometric recorders.

The electron current was maintained constant by automatic regulation over the whole energy range studied. Ionization curves were usually measured five times, the appearance potentials being reproducible to  $\pm 0.1$  eV. The appearance potential of the  $\text{O}^-$  ion from CO was used as the reference for energy scale calibration since it has an appearance potential<sup>4</sup> (9.65 eV) which is close to the values obtained in this work for several ions.

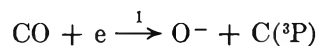
The experimental data were treated by the deconvolution method described previously;<sup>7</sup> the electron energy distribution (which was required to be known

for this procedure) was measured using the  $\text{SF}_6^-$  ion formed by sulfur hexafluoride.<sup>8,9</sup> It was found that performing 15 smoothing and 20 unfolding iterations upon the basic experimental data enabled satisfactory determination of appearance potentials, resonance peak maxima, and peak widths (at half-height) to be made.

Boron trifluoride and phosphorus trifluoride were obtained from cylinders (Cambrian Chemicals Ltd., and I.C.I. Ltd., respectively) and were used with no further purification.

### Results and Discussion

(a) *Carbon Monoxide.* The  $\text{O}^-$  ion formed by carbon monoxide has received considerable attention,<sup>4,10,11</sup> and it has been shown<sup>4</sup> that the cross section for the reaction



rises vertically to a maximum at threshold. The onset of ionization at  $9.7 \pm 0.1$  eV agrees well with the energy (9.65 eV) required to produce  $\text{C} + \text{O}^-$  from CO in the ground state, and this ion has been used as an energy scale calibrant.

Our basic experimental data for the  $\text{O}^-$  ion are shown in Figure 1a. Because of the energy spread of the electrons, a smearing-out of the appearance of the ion is noted, thereby masking the vertical onset behavior. Deconvolution of these data with the measured electron

- (1) To whom communications should be addressed.
- (2) (a) K. A. G. MacNeil and J. C. J. Thynne, *Int. J. Mass Spectrom. Ion Phys.*, **2**, 1 (1969); (b) J. C. J. Thynne, *J. Phys. Chem.*, **73**, 1586 (1969).
- (3) J. Marriott and J. D. Craggs, *J. Electron. Contr.*, **3**, 194 (1957).
- (4) P. J. Chantry, *Phys. Rev.*, **172**, 125 (1968).
- (5) J. D. Morrison, *J. Chem. Phys.*, **39**, 200 (1963).
- (6) J. H. D. Eland, P. J. Shepherd, and G. C. J. Danby, *Z. Naturforsch., A*, **21**, 1580 (1966).
- (7) K. A. G. MacNeil and J. C. J. Thynne, *Int. J. Mass Spectrom. Ion Phys.*, **3**, 35 (1969).
- (8) W. M. Hickam and R. E. Fox, *J. Chem. Phys.*, **25**, 642 (1956).
- (9) G. J. Schulz, *J. Appl. Phys.*, **31**, 1134 (1960).
- (10) H. D. Hagstrum, *Rev. Mod. Phys.*, **23**, 185 (1951).
- (11) G. G. Cloutier and H. I. Schiff, *J. Chem. Phys.*, **31**, 793 (1959).

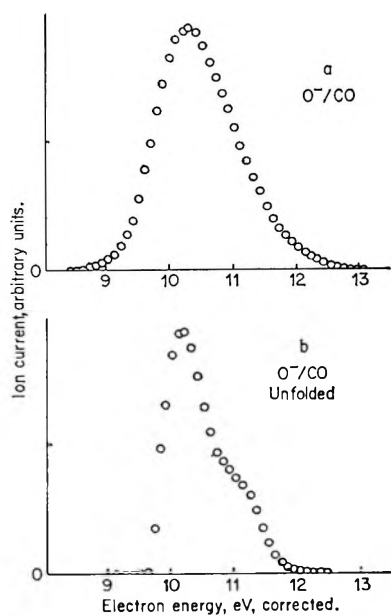
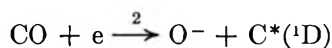


Figure 1.(a) Ionization efficiency curve for  $O^-$  ion formation by carbon monoxide. (b) Deconvoluted results for  $O^-/CO$  obtained using 15 smoothing and 20 unfolding iterations.

energy distribution yields the results shown in Figure 1b. It is clear that a vertical onset is observed for ion formation; this energy is assumed to be 9.65 eV for energy scale calibration purposes.<sup>4</sup>

A second ionization process is suggested at about 11 eV by the "bump" in the  $O^-$  deconvoluted curve. This is in agreement with the observations of Chantry,<sup>4</sup> who suggested that this second dissociative attachment process corresponded to the formation of  $C^*(^1D)$ , *i.e.*



which would have a minimum appearance potential of 10.88 eV.

If the first resonance peak is assumed to tail off steadily to 12 eV, we may make a rough estimate that the second process is about 0.05 times as intense as the first. Chantry<sup>4</sup> reports that  $\sigma_1/\sigma_2 = 21$ , where  $\sigma_1$  and  $\sigma_2$  are the cross sections for reactions 1 and 2.

(b) *Boron Trifluoride.* The following negative ions were observed:  $F^-$ ,  $F_2^-$ ,  $BF_2^-$ , and  $BF_4^-$ . Examination of the dependence of ion current upon ion source pressure showed that  $BF_4^-$  was a secondary ion and the other ions were primary. At their capture peak maxima the primary ions have the following relative intensities

$$F^- : F_2^- : BF_2^- = 1000 : 27 : <1$$

An interesting feature of ion formation in this system is that although ion formation is possible at energies  $> \sim 3.3$  eV, no ions are observed until  $\sim 10$  eV. Also, the ionization curves for  $F^-$  and  $F_2^-$  rise sharply from their thresholds. Near-vertical onset behavior has been noted for the  $O^-$  ions formed by  $CO^4$  and  $NO^{11}$

but not, so far as we are aware, for more complex molecules. Because of the energy spread of the ionizing electrons there is a distortion of the apparent cross section for ion formation; it can be shown however that a vertical threshold does obtain for an ion by comparing the data for  $O^-/CO$  and the ion in question. We have done this by normalization of the ionization curves to the same height at maximum and making an appropriate shift on the energy scale. If the leading edges of the two ionization curves may be superimposed then, clearly, the rise of the cross section of the ion from apparent onset to peak maximum is as sharp as that for  $O^-/CO$  which itself shows the vertical onset effect.

In Figure 2 we have compared ionization efficiency curves for  $F_2^-/BF_3$  and  $F^-/BF_3$  with that for  $O^-/CO$ .

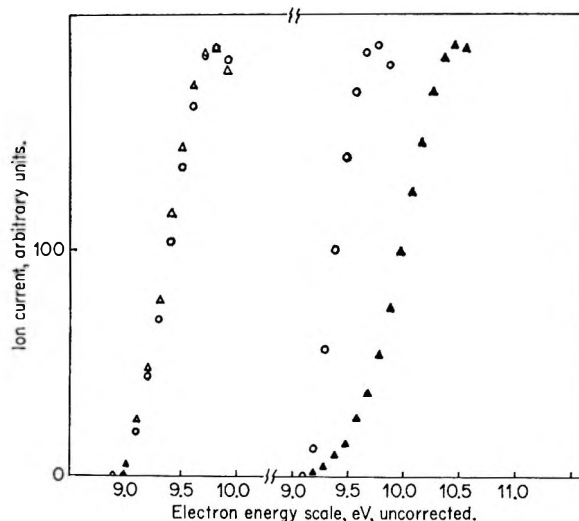


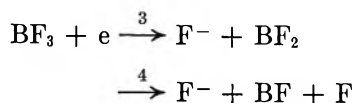
Figure 2. Comparison of the initial portions of the ionization efficiency curves for  $O^-/CO$  (open circles) and  $F_2^-/BF_3$  (open triangles) and for  $F^-/BF_3$  (full triangles). Energy scales for  $F_2^-$  and  $F^-$  shifted by  $-0.85$  and  $-1.05$  eV, respectively, to permit overlap of appearance potentials.

It is apparent that, for the  $F_2^-$  and  $O^-$  ions, complete overlap of the energy profiles for both ions is obtained when the energy scale is shifted slightly ( $\sim 1$  eV). The  $F^-$  ion curve however, although it rises quite rapidly from onset to a maximum value, does so rather slower than the corresponding rise for the  $O^-$  ion (1.3 eV *cf.* 0.7 eV), and there is no close overlap of the ionization curves. We therefore consider it likely that the ionization curve for  $F_2^-$ , but probably not for  $F^-$ , has a vertical onset edge.

(1)  $F^-$ . A typical ionization efficiency curve for this ion before and after performing 15 smoothing and 20 unfolding iterations is shown in Figures 3a and b.

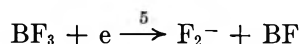
A value of  $10.7 \pm 0.1$  eV is obtained for the appearance potential of the ion; this may be compared with the value of  $11.4 \pm 0.2$  eV reported for  $A(F^-)$  by Marriott and Craggs.<sup>3</sup>

Possible reactions to explain ion formation are



Using known thermochemical data (see section d), together with a value of 3.45 eV for the electron affinity of fluorine,  $E(\text{F})$ ,<sup>12</sup> then the minimum enthalpy requirements for reactions 3 and 4 are  $3.3 \pm 0.2$  and  $7.9 \pm 0.2$  eV, respectively. It is therefore apparent that reactions 3 and 4 would have  $7.4 \pm 0.3$  and  $2.8 \pm 0.3$  eV, respectively, of kinetic and/or excitation energy distributed among the fragments. In view of these excess energies it would seem more reasonable (since  $D(\text{BF}-\text{F}) < 7.4$  eV) to suggest that  $\text{F}^-$  ion formation occurs *via* reaction 4 but, for reasons to be mentioned in the section below on  $\text{F}_2^-$  ion formation, reaction 3 is not completely ruled out.

(2)  $\text{F}_2^-$ . Typical data for this ion are shown in Figures 3a and b. A vertical threshold is obtained at  $10.5 \pm 0.1$  eV, and ion formation is assigned to the reaction



If a value of 3.0 eV is used for  $E(\text{F}_2)$ ,<sup>13</sup> then the minimum appearance potential for reaction 5 is  $6.7 \pm 0.2$  eV; this suggests that about  $3.8 \pm 0.3$  eV of excess energy is associated with reaction 5 although we are not able to assign it to kinetic or excitation energy.

In Figure 3b, the unfolded  $\text{F}_2^-$  ionization curve shows

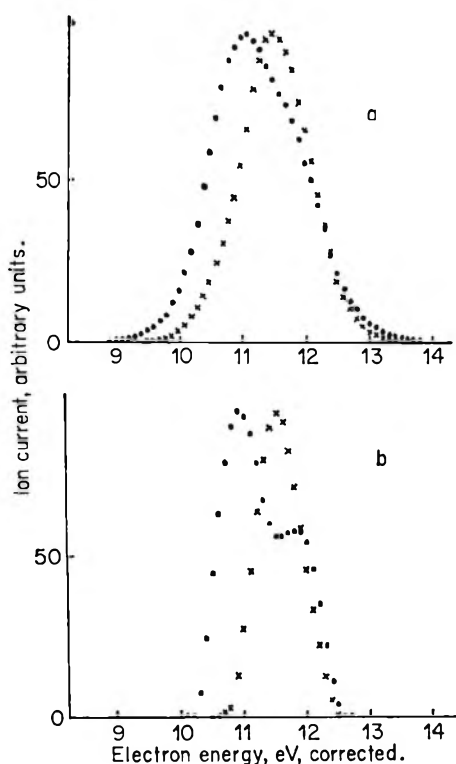
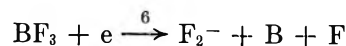
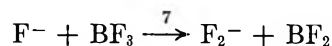


Figure 3. (a) Ionization efficiency curves for  $\text{BF}_3$ . (b) Deconvoluted curves for  $\text{BF}_3$ ;  $\text{F}^-$  (crosses),  $\text{F}_2^-$  (full circles).

an indication of a second ionization process on the tail of the first; this process has a maximum value at about 11.5 eV. It is unlikely that reaction 6 is responsible since this would require an appearance potential of  $\sim 15$  eV.



Examination of the pressure dependence of  $\text{F}_2^-$  ion formation indicated that at the first peak maximum (10.5 eV) the ion was formed by a primary process. At 11.5 eV however the pressure exponent was  $1.7 \pm 0.1$ , suggesting that a secondary process was contributing towards ion formation in the region of the second peak. This, together with the similarity of the peak maximum energies for  $\text{F}^-$  and the second  $\text{F}_2^-$  peak, suggested the possibility of an ion-molecule reaction with  $\text{F}^-$  as the reactant ion, *e.g.*



Reaction 7 is endothermic by  $5.6 \pm 0.2$  eV; if reaction 3 is responsible for  $\text{F}^-$  ion formation and the  $7.4 \pm 0.3$ -eV excess energy is all in the form of kinetic energy, then  $5.4 \pm 0.2$  eV of this energy may be partitioned to the  $\text{F}^-$  ion. It therefore appears that reaction 7 is possible; however, it is still an unlikely reaction since, in actual fact, about 2 eV more energy is required in the center-of-mass for the reaction to become thermo-neutral. We are therefore unable to suggest a likely process for the  $\text{F}_2^-$  ion formation observed at 11.5 eV.

(3)  $\text{BF}_2^-$ . Basic and deconvoluted data for this ion are shown in Figures 4a and b; the quality of the data are not good because of the extremely low ion intensity and the structure on the leading edge of the curve was not consistently reproducible. It is apparent that ion formation occurs at  $\sim 7.6$  eV, the ion current increasing slowly to reach a maximum at 11.5 eV; beyond this energy the decrease in ion current is very sharp being almost vertical.

Thermochemical calculations show that the minimum energy for reaction 8, *i.e.*, where the electron is not captured but causes dissociation of the molecule, to be



$11.4 \pm 0.2$  eV. We have not observed such a sharp decrease in ion formation in any other system we have studied. We tentatively suggest that, at 11.5 eV, the potential energy curves corresponding to reactions 7 and 8 cross and, above this energy, transitions on to the surface leading to decomposition of the molecule and not ion formation are favored.

(4)  $\text{BF}_4^-$ . This ion is a secondary species. In Figure 5 we have compared the normalized ionization

(12) R. S. Berry and C. W. Riemann, *J. Chem. Phys.*, **38**, 1540 (1963).

(13) R. M. Reese, V. H. Dibeler, and J. L. Franklin, *ibid.*, **29**, 880 (1958).

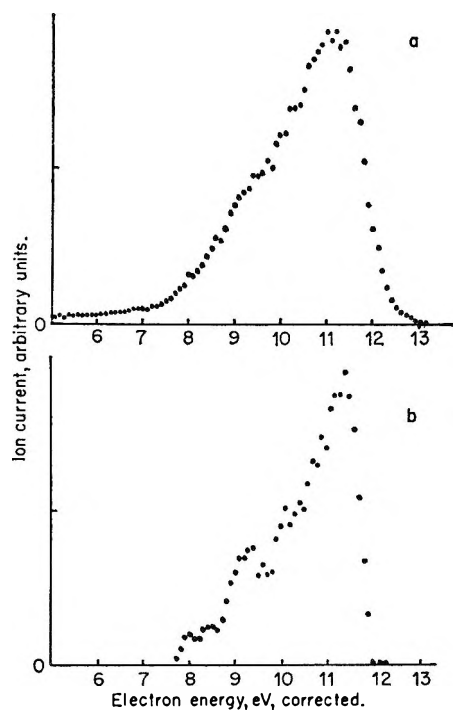
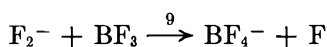
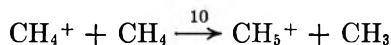


Figure 4. (a) Ionization efficiency curve for  $\text{BF}_2^-/\text{BF}_3^-$ . (b) Deconvoluted curve.

curves for  $\text{F}_2^-$  and  $\text{BF}_4^-$ . The similarity of their electron energy dependence illustrates clearly that the  $\text{F}_2^-$  ion is the precursor to  $\text{BF}_4^-$  formation so that the latter ion is formed by the ion-molecule reaction



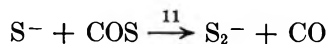
We have estimated the rate constant for reaction 9 by comparing the primary and secondary ion current ratios,  $I_{\text{sec}}/I_{\text{prim}}$ , for reactions 9 and 10, when similar pressures of  $\text{BF}_3$  and  $\text{CH}_4$  ( $7.4 \times 10^{-5}$  Torr) are maintained in the ion source. Assuming, under these con-



ditions, that

$$\frac{I_{\text{BF}_4^-}/I_{\text{F}_2^-}}{I_{\text{CH}_5^+}/I_{\text{CH}_4^+}} = \frac{k_9}{k_{10}}$$

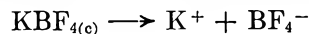
then, using a value of  $1.2 \times 10^{-9}$  molecule $^{-1}$  cm $^3$  sec $^{-1}$  for the rate constant for reaction 10 at near-thermal energies,<sup>14</sup> our data yield a value of  $1.9 \times 10^{-9}$  molecules $^{-1}$  cm $^3$  sec $^{-1}$  for  $k_9$ . This may be compared with the value of  $3 \times 10^{-10}$  molecule $^{-1}$  cm $^3$  sec $^{-1}$  reported<sup>15</sup> for the velocity constant of the negative ion-molecule reaction. Both reactions 9 and 11 were studied using



time-of-flight mass spectrometers, and the average reactant ion kinetic energy in both cases was probably  $\sim 0.3$  eV.

The requirement that an ion-molecule reaction must

not be endothermic to be observed enables an upper limit to be placed on the heat of formation of the fluoroborate ion,  $\Delta H_f^\circ(\text{BF}_4^-)$ . Since  $\Delta H_9 \leq 0$  then we find  $\Delta H_f^\circ(\text{BF}_4^-) \leq -15.5$  eV. Altschuller<sup>16</sup> has calculated a value of 6.6 eV for the lattice energy of potassium fluoroborate, *i.e.*, for the enthalpy of the reaction



Bills and Cotton<sup>17</sup> have reported the enthalpy of formation of crystalline potassium fluoroborate to be  $-19.6$  eV; using a value in conjunction with  $\Delta H_f^\circ(\text{K}^+) = 5.3$  eV we obtain a value of  $-18.3$  eV for  $\Delta H_f^\circ(\text{BF}_4^-)$  which may be compared with the upper limit calculated above.

Table I: Appearance Potentials ( $A$ ) and Half-Widths of Resonance Peaks ( $PW$ ) for Negative Ions Formed by  $\text{BF}_3$  and  $\text{PF}_3$

Ion-molecule	$A^a$	$PW^a$
$\text{F}^- - \text{BF}_3$	$10.7 \pm 0.1$	$0.9 \pm 0.1$
$\text{F}_2^- - \text{BF}_3$	$10.5 \pm 0.1$	$1.0 \pm 0.1$
$\text{BF}_2^- - \text{BF}_3$	$\sim 7.6$	$\sim 2.5$
$\text{F}_2^- - \text{PF}_3$	$10.9 \pm 0.1$	$1.2 \pm 0.1$
$\text{PF}^- - \text{PF}_3$	$11.4 \pm 0.1$	$1.3 \pm 0.1$
$\text{PF}_2^- - \text{PF}_3$	$10.3 \pm 0.1$	$1.3 \pm 0.1$

<sup>a</sup> All values in electron volts.

(c) *Phosphorus Trifluoride*. In  $\text{PF}_3$  negative ion formation by dissociative electron capture occurred with a very low probability, ion formation being much less extensive than for  $\text{BF}_3$  under similar ion source conditions. The following primary ions were observed,  $\text{F}^-$ ,  $\text{F}_2^-$ ,  $\text{PF}^-$ , and  $\text{PF}_2^-$ . Formation of the  $\text{F}^-$  ion is unusual in this case since, unlike the other ions, it is not formed by a clearly defined resonance process. The relative intensities of the ions are (a) at their respective resonance peak maxima

$$1000 (\text{PF}_2^-) : 590 (\text{PF}^-) : 485 (\text{F}_2^-)$$

and (b) at 70 eV

$$1000 (\text{F}^-) : <1 (\text{PF}_2^-) : <1 (\text{PF}^-) : 6 (\text{F}_2^-)$$

As with boron trifluoride, negative ion formation occurred only at relatively high electron energies ( $>9$  eV) and, for the ions  $\text{F}_2^-$ ,  $\text{PF}^-$ , and  $\text{PF}_2^-$ , their formation by a process involving a vertical rise to maximum at the ionization threshold was established by comparing the ion curves with that of  $\text{O}^- - \text{CO}$ .

Ionization curves for  $\text{F}_2^-$ ,  $\text{PF}^-$ , and  $\text{PF}_2^-$  are shown in Figure 6a and the deconvoluted data in Figure 6b.

(14) S. K. Gupta, E. G. Jones, A. G. Harrison, and J. J. Myher, *Can. J. Chem.*, **45**, 3107 (1967).

(15) J. G. Dillard and J. L. Franklin, *J. Chem. Phys.*, **48**, 2349 (1968).

(16) A. P. Altschuller, *J. Amer. Chem. Soc.*, **77**, 6187 (1955).

(17) J. L. Bills and F. A. Cotton, *J. Phys. Chem.*, **64**, 1477 (1960).

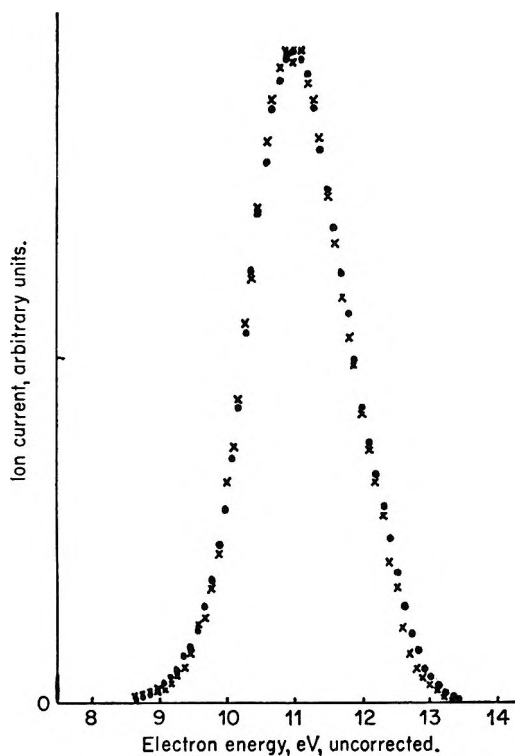
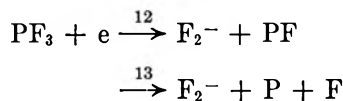


Figure 5. Normalized ionization efficiency curves for  $\text{F}_2^-$  (open circles) and  $\text{BF}_4^-$  (crosses).

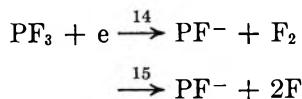
(1)  $\text{F}_2^-$ . An appearance potential of  $10.9 \pm 0.1$  eV is noted for this ion, the peak width at half-height being  $1.2 \pm 0.1$  eV. Possible rearrangement reactions to explain ion formation are given. Reactions 12 and



13 have minimum energy requirements of  $8.8 \pm 0.4$  and  $10.9 \pm 0.1$  eV, respectively. We are unable to assign the reaction leading to ion formation, but if the vertical threshold is characteristic of a process of zero excess energy (as  $\text{O}^-$  from  $\text{CO}$ ) then it is probable that reaction 13 is responsible.

In Figure 6a it may be observed that the  $\text{F}_2^-$  ion current does not fall completely to zero above 14 eV; this is due to the appearance of an unresolved non-resonance process.

(2)  $\text{PF}^-$ . Typical data for this ion are shown in Figure 6, and it is apparent that the vertical ionization threshold is at  $11.4 \pm 0.1$  eV. Reactions 14 and 15



will have minimum appearance potentials of  $8.9 \pm 0.4 - E(\text{PF})$  and  $10.5 \pm 0.4 - E(\text{PF})$  eV, respectively. We cannot identify the reaction responsible for ion formation, but it must involve a process with an excess energy  $> 0.9 \pm 0.5$  eV.

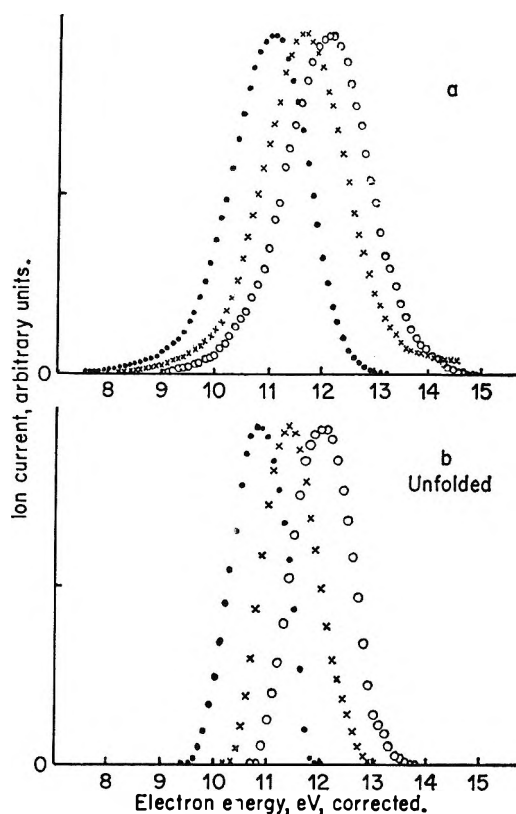


Figure 6. (a) Ionization efficiency curves for  $\text{PF}_3$ . (b) Deconvoluted data;  $\text{PF}^-$  (open circles),  $\text{F}_2^-$  (crosses),  $\text{PF}_2^-$  (full circles).

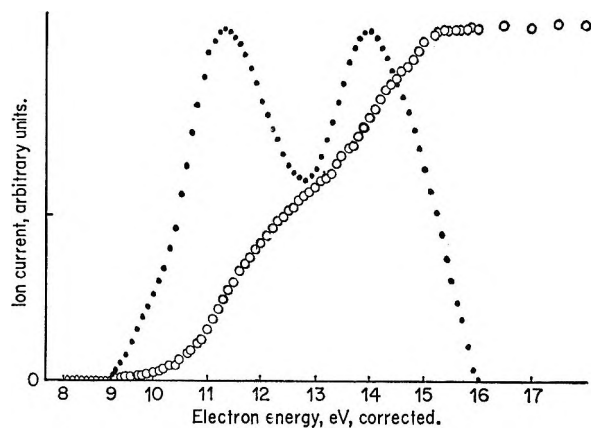
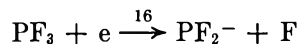


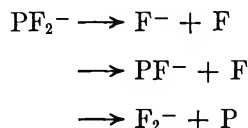
Figure 7. Ionization efficiency curve for  $\text{F}^-/\text{PF}_3$ ; full circles show the first differential.

(3)  $\text{PF}_2^-$ . This ion is formed with a vertical rise to the maximum cross section at  $10.3 \pm 0.1$  eV, the resonance peak having a width of  $1.3 \pm 0.1$  eV at half-



height. Reaction 16 will have a minimum appearance potential of  $5.6 \pm 1.0 - E(\text{PF}_2)$  eV; therefore the appearance potential of the ion at 10.3 eV implies that more than  $4.7 \pm 1.1$  eV of excess energy must be distributed among the fragments. If the observed vertical onset implies zero relative kinetic of the products

(cf.  $O^-/CO$ ), then the excess energy must be ascribed to excitation of the  $PF_2^-$  ion. This excess energy apparently does not cause rapid decomposition of the  $PF_2^-$  ion indicating that it is stable with respect to the reactions



since both  $F^-$ ,  $F_2^-$ , and  $PF^-$  have higher appearance potentials.

Little is known regarding the possibility of excited states of polyatomic negative ions. It would be of considerable interest to determine if the ions formed with a vertical onset by polyatomic molecules (*e.g.*,  $F_2^-$ - $BF_3$ ,  $PF^-$ - $PF_3$ , and  $PF_2^-$ - $PF_3$ ) have zero kinetic energy, since its absence would reveal information regarding possible excitation states of the ions mentioned.

(4)  $F^-$ .  $F^-$  ion formation by this molecule is unusual for fluorinated molecules in that no clearly defined dissociative resonance capture peak is observed. A typical ionization efficiency curve for this ion together with the first differential of the data is shown in Figure

7. The results are not unequivocal but suggest there are two ion formation processes, one process with a maximum  $\sim 11.3$  eV, the second rising to a maximum at 14 eV. It is likely that the second process is due to a nonresonance ion-pair process, but examination of the positive ion spectrum at this energy revealed no ion such as  $PF^+$  or  $PF_2^+$  which might have been a co-product. The identity of the first process is similarly unresolvable, it may be a low cross-section dissociative process such as



which would have a lower energy requirement of  $10.3 \pm 0.4$  eV.

(d) *Thermochemical Data.* The following heats of formation at 298°K have been used in calculations (all values in eV): F(0.8); B(5.8); BF(-2.0);  $BF_2^-$ (-5.9);  $BF_3$ (-11.7); P(3.5); PF(-0.7);  $PF_2^-$ (-4.7);  $PF_3$ (-9.6); O(2.6); CO(-1.1); C(7.4). All values have been taken from ref 18.

*Acknowledgment.* We thank the Science Research Council for a grant in support of this work.

(18) JANAF Thermochemical Tables, Dow Chemical Co., Midland, Mich.

# Electron Spin Resonance Study of Deamination of Amino Acids by Hydrated Electrons<sup>1</sup>

by P. Neta and Richard W. Fessenden

Radiation Research Laboratories, Mellon Institute, Carnegie-Mellon University, Pittsburgh, Pennsylvania 15213  
(Received December 12, 1969)

Esr spectroscopy has been used to observe the radicals produced by the reaction of hydrated electrons with amino acids in aqueous solutions. Irradiation with high energy electrons was carried out directly in the esr cavity; the sample container was a flat cell of high-purity silica through which solutions were driven continuously. Either formate or methanol was used as an OH radical scavenger to eliminate reactions of OH with amino acids. In neutral solutions glycine,  $\alpha$ -alanine,  $\alpha$ -aminoisobutyric acid, iminodiacetic acid, nitrilotriacetic acid, betaine, glycylglycine, and benzylamine were found to undergo deamination, *i.e.*, elimination of the  $\text{NR}_3^+$  group, and the corresponding residual radicals were observed. Deamination was found to take place to a smaller extent in alkaline solutions, where the amino group is deprotonated. No deamination could be detected with  $\beta$ -alanine, acetylglycine, acetylalanine, acetamide, and allylamine.

## Introduction

The major product in the  $\gamma$  radiolysis of glycine and alanine in aqueous solutions is ammonia ( $G = 4.3$ ), formed by both oxidative and reductive deamination of amino acids. These chemical studies have been recently reviewed by Garrison.<sup>2a</sup> Oxidative deamination is a result of a secondary reaction in the radiolysis mechanism, whereas the reductive deamination has been suggested to take place directly *via* the reaction of hydrated electrons with amino acids. This reaction, recently confirmed in alkaline glasses,<sup>2b</sup> also lead to the formation of carboxyalkyl radicals. An attempt was recently made to observe some of these radicals by pulse radiolysis.<sup>3</sup> Solutions of glycine and of alanine were pulse irradiated in the presence of *t*-butyl alcohol as OH radical scavenger, and after correcting for the *t*-butyl alcohol transient absorption and for the absorption due to partial reaction of OH with the amino acids, the spectra of  $\cdot\text{CH}_2\text{COO}^-$  and  $\text{CH}_3\dot{\text{C}}\text{HCOO}^-$  could be observed, respectively. With other compounds the corrections become so large that the method cannot be used and some other approach is necessary. ESR spectroscopy has been used very effectively for the identification of radicals during continuous *in situ* radiolysis of aqueous nitroalkane solutions,<sup>4</sup> and a recent improvement in sensitivity has been achieved.<sup>5</sup> It seemed, therefore, that esr spectroscopy during irradiation of amino acid solutions could help in the identification of the radicals produced by deamination.

The spectra of the radicals produced by hydrogen abstraction from the amino acids by OH are relatively rich in lines and complicate the overall spectrum. To simplify the esr spectra it was necessary to find a scavenger for OH radicals which would not give rise to a spectrum overlapping that of the radical from the

deamination. Formate ions and methanol were successfully used for this purpose.

## Experimental Section

Solutions of amino acids (Grade A Calbiochem or Cyclo Chemical Co.) or other amino compounds (Eastman Kodak) were prepared in doubly distilled water<sup>4</sup> at concentrations of 0.005 to 0.1 *M*. Sodium formate or methanol (both Baker Analyzed reagents) were added at concentrations high enough to scavenge most of the OH radicals. The pH was adjusted using potassium hydroxide, perchloric acid, sodium phosphates, and sodium tetraborate (all Baker Analyzed reagents). Solutions were deoxygenated by bubbling nitrogen through them. The irradiation was carried out in the esr cavity as previously described.<sup>4,5</sup> A flat silica cell of 0.5-mm internal spacing was used, and during irradiation the solution was driven through the cell at a flow rate of 1  $\text{cm}^3/\text{sec}$ . No effect of the flow rate on the spectrum could be observed between 0.5 and 3  $\text{cm}^3/\text{sec}$ . The solution was cooled slightly before entering the cell to compensate for the temperature rise during irradiation so that all measurements pertain to about room temperature. The total electron beam current was  $\sim 8 \mu\text{A}$  and that collected at an electrode in the solution was  $\sim 1 \mu\text{A}$ . Second-derivative spectra were recorded by use of two modulation frequencies. This method helps to minimize the interference by the signal from

(1) Supported in part by the U. S. Atomic Energy Commission.

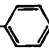

(2) (a) W. M. Garrison, in "Current Topics in Radiation Research," Vol. IV, M. Ebert and A. Howard, Ed., North-Holland Publishing Co., Amsterdam, 1968, p 43; (b) M.D. Sevilla, *J. Phys. Chem.*, **74**, in press.

(3) P. Neta, M. Simic, and E. Hayon, *ibid.*, **74**, 1214 (1970).

(4) K. Eiben and R. W. Fessenden, *ibid.*, **72**, 3387 (1968).

(5) K. Eiben and R. W. Fessenden, to be published.

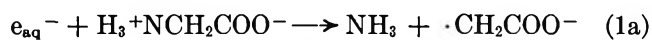
**Table I:** Structure and Coupling Constants of the Radicals Resulting from Deamination

Compound	Radical	$g$ factor	Coupling const, G ( $\pm 0.03$ G)
$H_3^+NCH_2COO^-$	$\cdot CH_2COO^-$	2.0032	$a_{\alpha^H} = 21.18$
$H_2^+N$   $CH_2COO^-$	$\cdot CH_2COO^-$	2.0032	$a_{\alpha^H} = 21.18$
$H^+N$   $CH_2COO^-$	$\cdot CH_2COO^-$	2.0032	$a_{\alpha^H} = 21.17$
$(CH_3)_3^+N$   $CH_2COO^-$	$\cdot CH_2COO^-$	2.0032	$a_{\alpha^H} = 21.17$
$H_3^+NCHCOO^-$	$\cdot CHCOO^-$	2.0032	$a_{\alpha^H} = 20.38$
$CH_3$   $CH_3$	$CH_3$   $CH_3$		$a_{\beta^H} = 24.92$
$H_3^+NCCOO^-$	$\cdot CCOO^-$	2.0032	$a_{\beta^H} = 21.73$
$CH_3$ 	$CH_3$ 		
$H_3^+NCH_2CONHCH_2COO^-$	$\cdot CH_2CONHCH_2COO^-$	2.0030	$a_{\alpha^H} = 21.15$ $a_N = 2.45$ $a_{NH^H} = 2.71$ $a_{CH_2^H} = 2.95$ $a_{\alpha^H} = 16.35$ $a_o^H = 5.13$ $a_m^H = 1.76$ $a_p^H = 6.19$
$H_3^+NCH_2$ - 	$\cdot CH_2$ - 	2.0026	

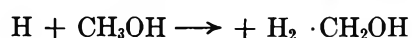
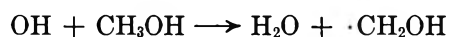
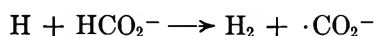
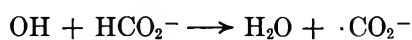
the silica cell (seen in both figures) so that only the region from 3 to 10 G above the center of the radical spectrum is obscured.

### Results and Discussion

Hydrated electrons in irradiated aqueous solutions containing the glycine zwitterion react *via* reactions 1a and b at similar rates.<sup>2a,3</sup> In order to study reactions



tion 1a without complications caused by the reaction of H and OH with glycine, either formate ion or methanol was used as a scavenger. Different concentrations of



solutes were used to ascertain that full scavenging occurred through these reactions. The radicals derived from these scavengers do not have spectra which seriously interfere with those from the amino acids. The spectrum of  $\cdot CH_2OH$  is a triplet of  $\sim 1$  G doublets or in basic solution a triplet only (for  $\cdot CH_2O^-$ ). The single line of  $\cdot CO_2^-$  cannot be seen in our experiments be-

cause it presumably is under the signal from the cell ( $g \cong 2.0000$ ).

The spectrum observed from an irradiated solution of glycine + methanol at pH 6.5 is presented in Figure 1. The lines of the  $\cdot CH_2COO^-$  and  $\cdot CH_2OH$  radicals are easily distinguishable. A recording at a lower field scan rate was used to determine the coupling constants and  $g$  factors. The values found for  $\cdot CH_2COO^-$  are given in Table I and are in good agreement with previous measurements<sup>5-8</sup> for the same radical produced by other reactions.

A solution containing glycine + formate gave an identical spectrum for the  $\cdot CH_2COO^-$  radical but also showed an additional line near the center  $g = 2.0041$ . This signal was found to be stronger in pure formate solutions containing no amino acid; it was much stronger when oxalate was initially added to the solution and sharply decreased in the presence of an efficient electron scavenger as chloroacetate or  $N_2O$ . It is most probably  $(O_2C-CO_2)^{3-}$  formed from oxalate, the product of dimerization of  $\cdot CO_2^-$ , by reaction with  $e_{aq}^-$ . An acid form of this species has been reported.<sup>5,9</sup>

(6) A. L. J. Beckwith and R. O. C. Norman, *J. Chem. Soc., B*, 400 (1969).

(7) W. T. Dixon, R. O. C. Norman, and A. L. Buley, *J. Chem. Soc.*, 3625 (1964).

(8) H. Taniguchi, K. Fukui, S. Ohnishi, H. Hatano, H. Hasegawa, and T. Maruyama, *J. Phys. Chem.*, **72**, 1926 (1968).

(9) R. O. C. Norman and P. R. West, *J. Chem. Soc., B*, 389 (1969).



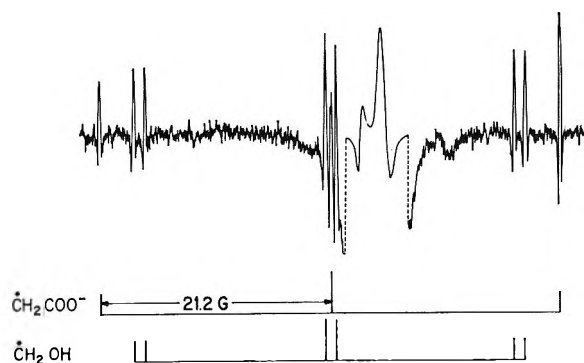
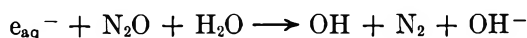


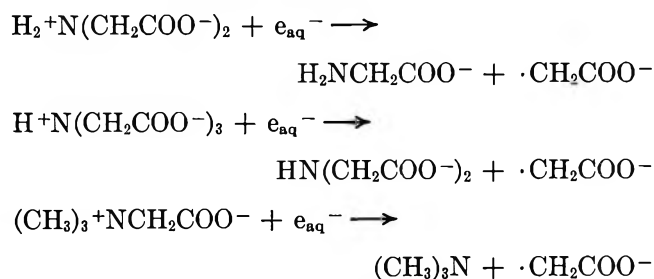
Figure 1. ESR spectrum of an aqueous solution of  $\text{H}_3^+\text{NCH}_2\text{COO}^-$  ( $4 \times 10^{-2} M$ ) +  $\text{CH}_3\text{OH}$  ( $0.5 M$ ) at pH 6.5 during irradiation with 2.8-MeV electrons. Magnetic field increases to the right. The large signal from the silica cell is seen just above the center of the spectrum and is recorded at a gain about 100 times less than the other portions. The second-order splitting of the central line of  $\cdot\text{CH}_2\text{COO}^-$  is just visible but can be fully resolved at slower field scan rates.

Because the radicals  $\cdot\text{CH}_2\text{OH}$  and  $\cdot\text{CO}_2^-$  are known to transfer electrons to a number of compounds,<sup>6,10-12</sup> it was necessary to show whether such a reaction was occurring with the amino acids. After a spectrum had been recorded  $\text{N}_2\text{O}$  was added to the remaining solution



to scavenge the electrons and the spectrum was again taken. In all cases the spectra of the radicals produced by deamination disappear showing that reactions of  $\cdot\text{CO}_2^-$  or  $\cdot\text{CH}_2\text{OH}$  do not lead to such a reaction.

The spectrum of the  $\cdot\text{CH}_2\text{COO}^-$  radical was also observed from irradiated solutions of iminodiacetate, nitrilotriacetate, and betaine containing formate ions, the deamination reactions being



Solutions of  $\alpha$ -alanine irradiated in the presence of either formate or methanol gave rise to the spectrum of the  $\text{CH}_3\dot{\text{C}}\text{HCOO}^-$  radical (Figure 2). The second-order splittings are well resolved, and the method described previously<sup>13</sup> has been applied to calculate the coupling constants and  $g$  factors. The results (Table I) are in very good agreement with those obtained<sup>6</sup> for the same radical produced by the reaction  $\text{CH}_3\text{CHBrCOO}^- + \cdot\text{CO}_2^- \rightarrow \text{CH}_3\dot{\text{C}}\text{HCOO}^- + \text{Br}^- + \text{CO}_2$ . Deamination of  $\alpha$ -aminoisobutyrate ion by hydrated electrons produces the  $(\text{CH}_3)_2\dot{\text{C}}\text{COO}^-$  radical. The five central

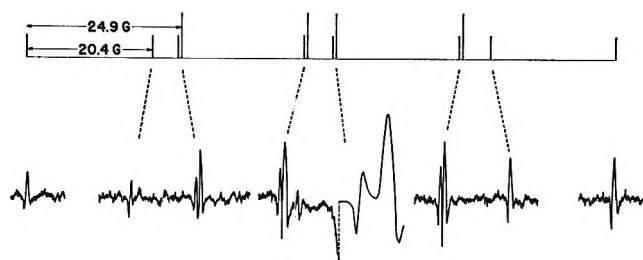


Figure 2. ESR spectrum of an aqueous solution of  $\text{H}_3^+\text{NCH}(\text{CH}_3)\text{COO}^-$  ( $4 \times 10^{-2} M$ ) +  $\text{HCO}_2^-$  ( $0.1 M$ ) at pH 6.5 during irradiation. A continuous scan of this spectrum was not reproducible because a long time constant and a very slow field scan were necessary to detect these lines. Segments of the spectrum are shown which include all of the lines detected. The stick spectrum shows the relationship of the lines and has been drawn with the second-order splitting exaggerated.

lines of its septet could be observed, and all of them showed the second-order splittings as outlined previously.<sup>13</sup> The coupling constant (Table I) was found to be in good agreement with previously published values.<sup>6,8</sup>

The reaction of hydrated electrons with glycylglycine is expected to form the  $\cdot\text{CH}_2\text{CONHCH}_2\text{COO}^-$  radical by cleavage of the terminal C-N bond. The spectrum of this radical could be observed in irradiated solutions of glycylglycine + formate, and coupling constants for all magnetic nuclei could be determined (Table I). The 18 lines in the high-field region were clearly separated and could be accurately measured. However, the equivalent lines in the center and the low-field regions were weaker and could not all be observed. The lines of the  $\cdot\text{CH}_2\text{COO}^-$  radical were absent from this spectrum, suggesting that deamination takes place at the terminal group only.

Results have been presented<sup>14</sup> which suggest that certain other amines can undergo similar deamination reactions. To show this we irradiated a solution containing benzylamine + formate or methanol and observed the ESR spectrum of the benzyl radical. The coupling constants are summarized in Table I and are in very good agreement with those previously reported<sup>15,16</sup> for benzyl radicals obtained by other methods. No evidence for allyl radical was obtained in experiments with allylamine.

All the compounds shown so far (summarized in Table I) to undergo deamination by reaction with hy-

(10) G. E. Adams, B. D. Michael, and R. L. Willson, *Advan. Chem. Ser.*, **81**, 289 (1968).

(11) M. Anbar and P. Neta, *J. Chem. Soc., A*, 837 (1967).

(12) K.-D. Asmus, A. Wiggen, and A. Henglein, *Ber. Bunsenges. Phys. Chem.*, **70**, 862 (1966).

(13) R. W. Fessenden, *J. Chem. Phys.*, **37**, 747 (1962).

(14) P. G. Clay and A. Kabi, *Chem. Ind.*, (London), 226 (1965).

(15) H. Fischer, *Z. Naturforsch. A*, **20**, 488 (1965).

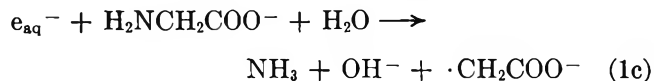
(16) W. T. Dixon and R. O. C. Norman, *J. Chem. Soc.*, 4857 (1964).

drated electrons can be generalized by the formula  $R_3^+N-CR_2-X$  where R is a hydrogen or an alkyl group and X is an electron-attracting group like carbonyl or phenyl. This generalization is essentially that given by Garrison,<sup>2a</sup> who concluded that the mechanism of reductive deamination involves an electron addition to the X group followed by dissociation or hydrolysis. Recent pulse radiolysis results<sup>3</sup> suggested that if this electron adduct is indeed formed, it has a lifetime considerably shorter than 1  $\mu$ sec. It is also possible that the  $e_{aq}^-$  reacts directly with the amino group (similarly to the dehalogenation reaction mechanism), while the X group only affects the ratio between reactions 1a and b and the overall rate constant.

To test the importance of the several parts of the structure,  $R_3^+N-CR_2-X$ , experiments were performed to determine if deamination takes place when the amino group is in its neutral or deprotonated form and when the X group is positioned differently in relation to the amino group. The latter problem could be investigated by irradiating solutions of  $\beta$ -alanine, acetamide, acetylglycine, and acetylalanine in the presence of formate or methanol. In none of these solutions could any indication of deamination be observed. The reaction of  $e_{aq}^-$  with  $H_3^+NCH_2CH_2COO^-$  does not produce  $\cdot CH_2CH_2COO^-$ , but most probably forms H atoms and  $H_2NCH_2CH_2COO^-$  (reaction 1b) as it does partially in the case of glycine and alanine. The reaction of  $e_{aq}^-$  with acetamide did not give rise to acetyl radicals at a concentration high enough to be observed under our experimental conditions. Furthermore, if the acetyl radicals had been formed they would most probably have recombined to form biacetyl, which would then react with  $e_{aq}^-$  very efficiently to give the strong esr absorption of the biacetyl anion radical. No spectrum of the biacetyl anion radical was observed in our experiments, suggesting that acetamide does not undergo a direct deamination. Similarly in irradiated solutions of acetylglycine and acetylalanine no spectra could be observed which would correspond either to  $\cdot CH_2COO^-$  or  $CH_3\dot{C}HCOO^-$ , respectively, or to  $CH_3\dot{C}O$ .

The deamination of amino acids in irradiated alkaline solutions has not previously been investigated. Although the reaction rate constants of simple amino acids

with hydrated electrons have been found to be faster in acid solution than in neutral solution,<sup>2a</sup> few measurements have been reported for alkaline solutions. The rates in alkaline solutions are expected to be even lower as the amino group becomes uncharged and reaction 1b cannot take place. There is evidence<sup>2b</sup> that a reaction 1c comparable to 1a takes place in alkaline glasses where the amino group is in the  $NH_2$  form. We irradi-



ated alkaline solutions of glycine,  $\alpha$ -alanine, and benzylamine at pH >13 in the presence of either formate ions or methanol and observed the esr spectra. In both glycine and alanine it was obvious that the deamination products were produced at an appreciable yield, although less efficiently than in neutral solutions. In benzylamine solutions the signals were too weak to demonstrate clearly the formation of the benzyl radical, but nevertheless, it seemed that very low concentrations were present. These radicals in alkaline solutions were shown to be due to the reaction of  $e_{aq}^-$  and not  $\cdot CO_2^-$  or  $\cdot CH_2O^-$  radicals as was done in neutral solutions. It may therefore be concluded that although the rate constants of the hydrated electron reactions are pH dependent and although reaction 1b takes place only with the  $-NH_3^+$  group, nevertheless the deamination reaction can occur with both  $NH_3^+$  and  $NH_2$  groups as long as these are connected to the  $-CH_2X$  grouping.

The results presented here demonstrate that esr spectroscopy can be used very effectively to study in a detailed fashion the mechanism of radiolytic reactions in aqueous solutions. We have intentionally applied this esr method to a system which could only be studied with difficulty and in a limited way by conventional pulse radiolysis with optical detection. The advantages of the specific nature and well-resolved structure of esr spectra are apparent. Radiolytic generation of radicals has the advantages relative to other chemical and photochemical methods of permitting the study of reactions of  $e_{aq}^-$  and of applicability over the full pH range. The latter advantage is currently being exploited in studies of OH reactions with amino acids.

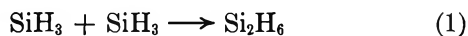
# A Mass Spectrometric Study of the Mercury-Photosensitized Reactions of Silane and Methylsilane with Nitric Oxide<sup>1a,b</sup>

by E. Kamaratos<sup>1c</sup> and F. W. Lampe

Department of Chemistry, Whitmore Laboratory, The Pennsylvania State University, University Park, Pennsylvania 16802  
(Received September 26, 1969)

Silyl radicals and methylsilyl radicals formed by Hg(<sup>6</sup>P<sub>1</sub>)-photosensitized decomposition of silane and methylsilane, respectively, react efficiently with nitric oxide to produce siloxanes and nitrous oxide as the principal products. The reaction is a chain reaction at room temperature which, from the evidence at hand, is proposed to involve SiH<sub>3</sub>O(SiH<sub>2</sub>O)<sub>n</sub> and CH<sub>3</sub>SiH<sub>2</sub>O(CH<sub>3</sub>SiHO)<sub>n</sub> radicals, (n = 0, 1, 2, . . .), as well as the primary radicals SiH<sub>3</sub> and CH<sub>3</sub>SiH<sub>2</sub>.

It has previously been reported from this laboratory that, when nitric oxide at low concentration is employed at room temperature as a scavenger of methyl radicals, trimethylhydroxylamine is the stable product of the radical-scavenging process and is formed by the successive addition of methyl radicals to nitric oxide.<sup>2,3</sup> Recent studies of the mercury-photosensitized decomposition of monosilane<sup>4,5</sup> have suggested that the formation of the predominant silicon-containing product, disilane, may occur *via* the combination of silyl radicals, *viz.*



and, in this respect, at least, may resemble mechanistically the analogous ethane formation in systems containing methyl radicals. However, despite this similarity, the analyses of products in the mercury-photosensitized reactions of monosilane-nitric oxide mixtures indicate that the scavenging reactions are quite different in the carbon and silicon systems and the same conclusions apply, in general, to the methylsilanes.<sup>5</sup>

We have applied mass spectrometric techniques, used previously in our studies of methyl radical<sup>2,3</sup> and hydrogen atom<sup>3,6</sup> scavenging by nitric oxide, to attempt to clarify the nitric oxide scavenging mechanism for silyl radicals, and the results of this investigation are reported herewith.

## Experimental Section

Silyl radicals and methylsilyl radicals were generated by the Hg (<sup>6</sup>P<sub>1</sub>)-photosensitized decomposition of SiH<sub>4</sub> (or SiD<sub>4</sub>) and CH<sub>3</sub>SiH<sub>3</sub>, respectively. All photolyses were carried out in a cell containing a pinhole leak (~0.0003-in. diameter) leading directly into the ionization region of a Bendix Model 14-101 time-of-flight mass spectrometer. Total pressures employed in the photolysis ranged from 5 to 20 Torr, with NO concentrations usually in the range of 1-9 mol % although in a few experiments NO concentrations as high as 50% were used.

*Photolysis Cell and Flow System.* The photolysis cell was 8.35 cm in length with an inner diameter of 2.10 cm. The cell volume, in which the photolysis products could accumulate and from which they could leak into the mass spectrometer, was 29.1 cm<sup>3</sup>. The cell was connected by 0.125-in. stainless steel and 6-mm Pyrex glass tubing to a 5- or 10-l. reactant reservoir. With the leak size and pumping rates employed, the silane concentration in the photolysis cell was satisfactorily constant over the course of a run; nitric oxide, which was initially present at concentrations 10-100 times less than the silane, was found to decrease to values that have been shown previously (with methyl radicals) to be undetectable.<sup>2</sup> The concentrations of all reaction products in this flow system at first increase but then approach a steady state. The time dependence of the approach of a product concentration towards the steady state is a function of the rates of the chemical reactions that produce and destroy it and of the rate of leakage from the cell; a study of the time dependencies of the various products has been shown to be a powerful diagnostic tool for the elucidation of the reaction mechanism and, in favorable circumstances, for the evaluation of specific reaction rates of chemical transients.<sup>2,3,6,7</sup>

A product of the reaction that is chemically stable in

(1) (a) AEC Document NYO-3570-15. (b) Based on a thesis submitted by E. Kamaratos to The Pennsylvania State University in partial fulfillment of the requirements for the Ph.D. degree. (c) Department of Chemistry, York University, Toronto, Canada.

(2) (a) A. Maschke, B. S. Shapiro, and F. W. Lampe, *J. Amer. Chem. Soc.*, **85**, 1876 (1963); (b) A. Maschke, B. S. Shapiro, and F. W. Lampe, *ibid.*, **86**, 1929 (1964).

(3) F. C. Kohout, A. Maschke, and F. W. Lampe, "The Chemistry of Ionization and Excitation," G. R. A. Johnson and G. Scholes, Ed., Taylor and Francis, Ltd., London, 1967, pp 51-59.

(4) H. Niki and G. J. Mains, *J. Phys. Chem.*, **68**, 304 (1964).

(5) M. A. Nay, G. N. C. Woodall, O. P. Strausz, and H. E. Gunning, *J. Amer. Chem. Soc.*, **87**, 179 (1965).

(6) F. C. Kohout and F. W. Lampe, *J. Chem. Phys.*, **46**, 4075 (1967).

(7) J. Heicklen and H. S. Johnston, *J. Amer. Chem. Soc.*, **84**, 4394 (1962).

this system will be depleted by leakage through the pinhole into the mass spectrometer, and its rate of loss will be first order in product concentration. This depletion can therefore be described by a first-order leak-rate constant,  $\lambda$ ; for the leak diameter and pressures employed in this work the flow may be taken as approximately molecular,<sup>8</sup> so that  $\lambda$  is given approximately by the relation

$$\lambda = \frac{d^2}{16V} \left( \frac{8\pi kT}{m} \right)^{1/2} \quad (I)$$

where  $d$  is the diameter of the leak,  $V$  is the cell volume,  $k$  is Boltzmann's constant,  $m$  is the mass of the product, and  $T$  is the absolute temperature. Equation I was verified as applicable (within about 20%) by a study of the decay from the cell of  $n$ -C<sub>4</sub>H<sub>10</sub> (mass = 58) and N<sub>2</sub>O (mass = 44).

**Photolysis Lamp.** The low-pressure mercury resonance lamp used in these experiments was a General Electric G4T4/1 "germicidal" lamp with a lamp envelope that does not transmit radiation below  $\lambda$  2000 Å.<sup>9</sup> The lamp was operated at ac currents of 70–100 mA by means of a shunted General Electric ballast (Cat. 58G827). It was positioned approximately 11 cm from the quartz window of the photolysis cell and was situated in a shielded housing equipped with a shutter and cooled continuously by a flow of air.

The detailed spectral characteristics of this lamp have been described previously.<sup>6</sup> It suffices to state here that over 90% of the emitted radiation was at 2537 Å and that 80–90% of this radiation was absorbed in the photolysis cell. As previously,<sup>6</sup> we assume that optical excitation of nitric oxide plays only a minor role, if any. In addition, after consideration of the relative quenching cross sections of silane<sup>5</sup> and nitric oxide<sup>10</sup> for Hg(<sup>3</sup>P<sub>1</sub>) atoms and the relative concentrations employed in these studies, it is apparent that reaction of the excited mercury with nitric oxide occurs only to a minor extent.

All photolyses were conducted at room temperature (~25°).

**Chemicals.** Monosilane and monosilane-*d*<sub>4</sub> were prepared by the reduction of silicon tetrachloride (Peninsular Chemical Research, Inc.) with lithium aluminum hydride and deuteride, respectively, in anhydrous diethyl ether solution according to the procedure of Finholt, Bond, Wilzbach, and Schlesinger.<sup>11</sup> The gases evolved from this reaction mixture were first passed through traps held at -95 and -130° and the final monosilane product collected in a third trap held at -195°.

Methylsilane was obtained from Peninsular Chemical Research, Inc. It was purified by slow distillation at -130° after thorough degassing at -195°. No significant impurities were detectable by mass spectrometric analysis.

Nitric oxide, having a stated purity of 98.5 mol %, was purchased from the Matheson Co. It was distilled from silica gel by first freezing onto the gel at -195° followed by allowing a slow temperature increase of the condensed gas to occur. The initial and final 5% of evolved gas were discarded, and the process was repeated twice more. No impurities were detectable. N<sup>15</sup>O samples prepared previously in this laboratory<sup>6</sup> were purified in the same way.

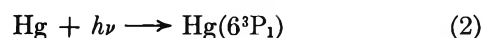
Nitrous oxide, with a stated minimum purity of 98%, was obtained from the Matheson Co., was thoroughly degassed at -195°, and was distilled at -130°. Mass spectrometric analysis indicated the purity of the gas to be in excess of 99%.

Disilane, for calibration purposes, was prepared as described previously.<sup>12</sup>

**Spectrometer Conditions.** The relationship between ion currents and partial pressures of the parent compounds were determined, insofar as possible, by admitting the pure gases to the photolysis cell and measuring the ion current of the pertinent  $m/e$  value as a function of pressure. Ion currents were measured at 50-eV ionizing energy and 0.25- $\mu$ A current of electrons.

## Results and Discussion

**Monosilane.** When pure monosilane is irradiated the only observable product is disilane, as evidenced by the time dependence and intensity pattern of the peaks at  $m/e$  56–62.<sup>12</sup> Hydrogen must also have been formed,<sup>4,5</sup> but we were unable to detect this product in our system because the contribution of the reactant monosilane to  $m/e$  2 always obscured any contribution of molecular hydrogen to this ion current. It is pertinent to point out here that in our flow system the *maximum* partial pressure attainable by a product (and this in about 2 hr) is about 1 Torr, which is smaller than the partial pressure of the reactant silane by a factor of 5–20. Hence mass interference is very serious at the  $m/e$  values characteristic of the mass spectrum of the silane and kinetic information cannot be obtained from these ion currents. At our total conversion we were not able to identify the trisilane and higher silanes reported in static experiments.<sup>4,5</sup> We conclude, then, that in the case of pure monosilane we may (within our detection sensitivity) write for the photolysis<sup>4,5</sup>



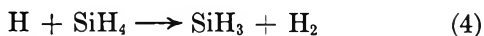
(8) H. Steinberg, "Handbook of Vacuum Engineering," Reinhold Publishing Corp., New York, N. Y., 1963.

(9) General Electric Lamp Bulletin (LD-1), Jan 1956, pp 50–52.

(10) J. G. Calvert and J. N. Pitts, Jr., "Photochemistry," John Wiley & Sons, Inc., New York, N. Y., 1966, p 74.

(11) A. E. Finholt, A. C. Bond, Jr., K. E. Wilzbach, and H. I. Schlesinger, *J. Amer. Chem. Soc.*, **69**, 2692 (1947).

(12) P. Potzinger and F. W. Lampe, *J. Phys. Chem.*, **73**, 3912 (1969).



Reaction 4 has been shown to be very fast,<sup>4</sup> so we may conclude that this is the sole fate of the H atom produced in reaction 3. Other primary processes, in addition to (3), have been indicated,<sup>4,5</sup> but (3) is the major one and, for our purposes, (1)–(4) represent adequately the photosensitization system in pure silane. From mass spectral calibrations for disilane and the initial formation rate of  $m/e$  60 ( $\text{Si}_2\text{H}_4^+$ ) on photolysis, coupled with the assumption that (1) and (4) are the sole fates of  $\text{SiH}_3$  radicals and H atoms, respectively, we can calculate the rate of formation of  $\text{SiH}_3$  radicals in our system. This was always constant for a given set of runs and depended on the lamp current used and the position of the lamp. The range of measured radical formation rates employed in this work was  $5.0\text{--}9.0 \times 10^{12}$  silyl radicals per cubic centimeter per second, with a reproducibility of  $\pm 10\%$ .

When nitric oxide is added to the monosilane–mercury mixture, at concentration levels of 1–9%, and the system irradiated, no disilane formation is observed in the initial stages; disilane is observed, as indicated by the characteristic pattern of mass peaks from 56–62, after an induction period whose duration depends on the initial concentration of nitric oxide. This observation, depicted in Figure 1, in which is shown the intensity of  $m/e$  60 ( $\text{Si}_2\text{H}_4^+$ ) as a function of photolysis time for several initial nitric oxide concentrations, demonstrates the inhibition<sup>5</sup> of disilane formation by nitric oxide. However, during the induction period of disilane formation, no ion produced by ionization of the expected adduct of  $\text{SiH}_3$  and NO was observed, as was dramatically so when the analogous  $\text{CH}_3\text{--NO}$  and  $\text{H--NO}$  systems were studied with the same technique.<sup>2,3,6</sup> The major ions whose intensities were observed to increase during the induction period of disilane formation and, therefore, in view of reaction 1, represent ions derived from products of the reaction of silyl radicals with nitric oxide, were  $m/e$  44, 47, 77, 93, 123, and 137. Although the intensities of all these ions increase with photolysis time during the disilane induction period, the explicit form of these increases is quite varied and, in fact, is diagnostic of some interesting features of the reaction mechanism.

In Figure 2 are shown the intensities of  $m/e$  44, 47, 77, 93, and 123 as a function of time during the photolysis of a mixture containing 6% nitric oxide. Substitution of  $\text{N}^{15}\text{O}$  for natural NO does not affect  $m/e$  47, but the behavior of the intensity of  $m/e$  44 in Figure 2 is then observed at  $m/e$  46. Hence, the ion with  $m/e$  47 contains no nitrogen and must be  $\text{SiH}_3\text{O}^+$ , while the ion with  $m/e$  44 must be  $\text{N}_2\text{O}^+$ . The use of  $\text{N}^{15}\text{O}$  and  $\text{SiD}_4$ , instead of  $\text{SiH}_4$ , confirmed this fact and, in addition, enabled us to conclude that the ions at  $m/e$  77, 93, and 123 in Figure 2 are, respectively,  $\text{Si}_2\text{H}_5\text{O}^+$ ,  $\text{Si}_2\text{H}_5\text{O}_2^+$ , and

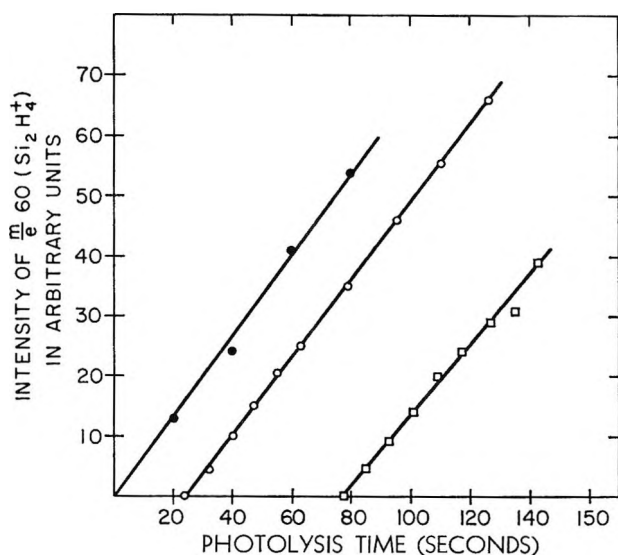


Figure 1. Inhibition of disilane formation by nitric oxide: ●,  $[\text{NO}]_0 = 0$ ; ○,  $[\text{NO}]_0 = 1\%$ ; □,  $[\text{NO}]_0 = 3.9\%$ ; total pressure  $\infty 15$  Torr; high radical formation rate.

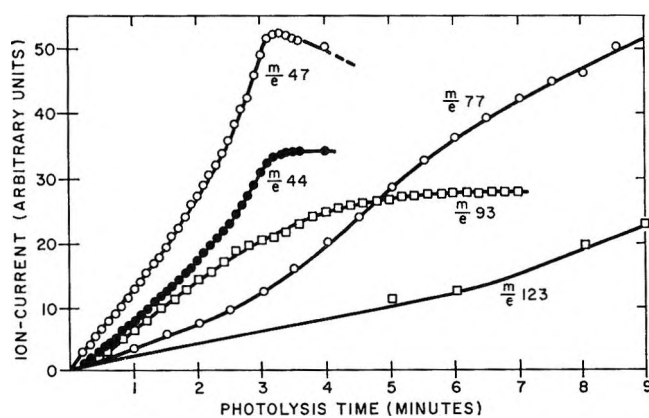


Figure 2. Product formation during photolysis of monosilane–nitric oxide mixture: total pressure  $\sim 15$  Torr;  $[\text{NO}]_0 = 6\%$ , low radical formation rate.

$\text{Si}_3\text{H}_7\text{O}_2^+$ ; the ion with  $m/e$  137 was shown in this way to be  $\text{Si}_3\text{H}_5\text{O}_3^+$ .

Now in this flow system, for an infinite supply of reactant, a stable product of the reaction—that is, a product which disappears from the photolysis cell only by leakage into the mass spectrometer—will reach within  $1/e$  of its steady-state concentration in about 2 hr. The very rapid increases of the intensities of  $m/e$  44, 47, and 93 to maximal (or steady-state) values, as shown in Figure 2, indicate that these ions arise not from stable products but from reaction intermediates whose depletion is governed predominantly by chemical reaction. On the other hand, as shown also in Figure 2,  $m/e$  77 and 123 exhibit the behavior expected of stable products, as does also  $m/e$  137 which is not shown. By comparison of the relative intensities of  $m/e$  75–78 (all of which exhibit a time dependence identical with that

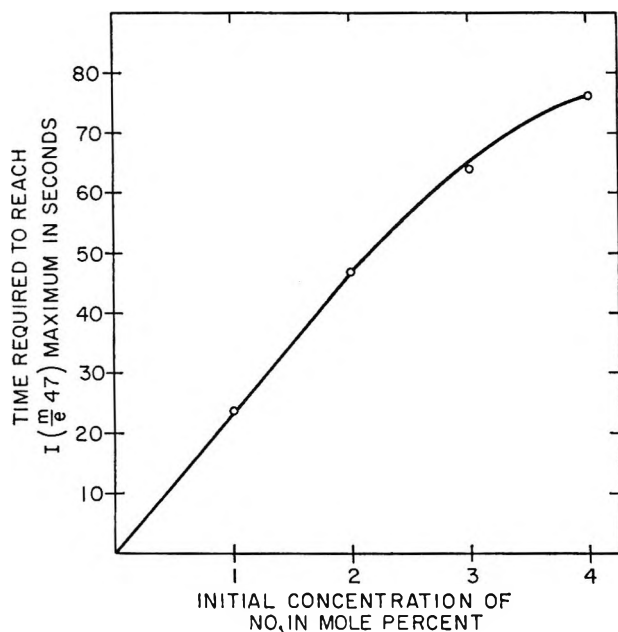


Figure 3. Attainment time of the maximum in  $I(m/e 47)$  as a function of initial nitric oxide concentration; same radical formation rate as in Figure 1.

of  $m/e 77$ ) with the mass spectrum of pure  $\text{SiH}_3\text{OSiH}_3$ ,<sup>13</sup> we have concluded that  $m/e 77$  arises from, and reflects the concentration dependence in the photolysis cell of, disiloxane. From similar comparisons with mass spectral data of pure siloxanes,<sup>13</sup> we have concluded that the intensities of  $m/e 123$  and  $137$  depict the concentration of the stable products trisiloxane ( $\text{SiH}_3\text{OSiH}_2\text{OSiH}_3$ ) and tetrasiloxane ( $\text{SiH}_3\text{OSiH}_2\text{OSiH}_2\text{OSiH}_3$ ), respectively.

In experiments in which  $m/e 47$  and  $60$  are monitored simultaneously, it is found that the time at which  $m/e 47$  ( $\text{SiH}_3\text{O}^+$ ) reaches a maximum is, within experimental error, identical with the onset time of  $m/e 60$  and, therefore, equal to the induction period of disilane formation. At low concentrations of nitric oxide this induction period increases linearly with the initial nitric oxide concentration (Figure 3) and the height of the maximum of  $m/e 47$  is approximately proportional to the initial concentration of nitric oxide. We conclude, therefore, that the maximum in the intensity of  $m/e 47$  ( $\text{SiH}_3\text{O}^+$ ) and the onset of  $m/e 60$  ( $\text{Si}_2\text{H}_4^+$ ) correspond to the essential depletion of nitric oxide in the photolysis cell. Such behavior was also observed in the  $\text{CH}_3\text{-NO}$  system.<sup>2,3</sup> It is of interest, at this point, to note in Figure 2 that the maximum formation rate of  $\text{SiH}_3\text{OSiH}_3$  ( $m/e 77$ ) corresponds closely to the maximum intensity of  $\text{SiH}_3\text{O}^+$  ( $m/e 47$ ) and that the same relationship appears to be fulfilled between  $\text{SiH}_3\text{-OSiH}_2\text{OSiH}_3$  ( $m/e 123$ ) and  $\text{SiH}_3\text{OSiH}_2\text{O}^+$  ( $m/e 93$ ), respectively; such behavior was observed for all nitric oxide concentrations studied. Thus, disiloxane formation depends on the prior formation of an intermediate that upon electron impact yields  $\text{SiH}_3\text{O}^+$  ( $m/e 47$ )

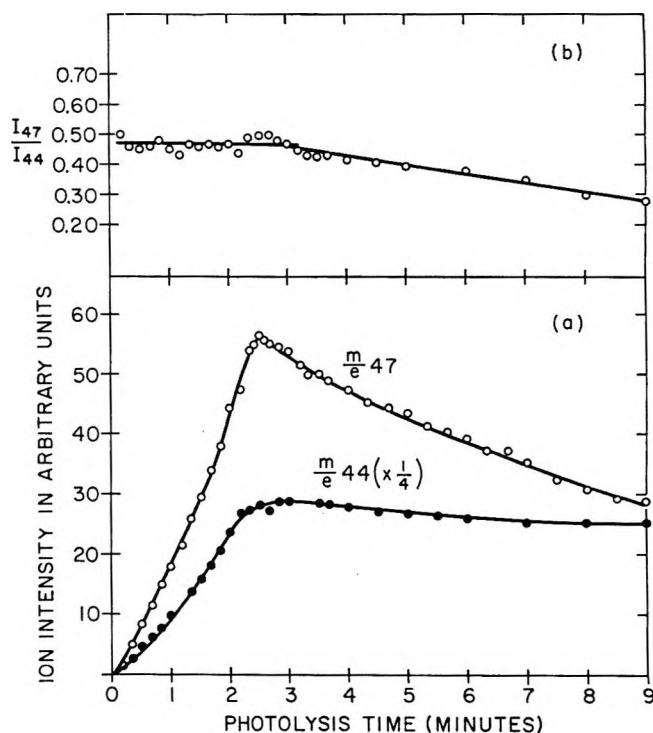


Figure 4. Formation and decay of  $I(m/e 44)$  and  $I(m/e 47)$  as a function of photolysis time; total pressure  $\sim 15$  Torr;  $[\text{NO}]_0 = 4\%$ ; same radical formation rate as in Figure 2.

and trisiloxane formation depends on the prior formation of an intermediate that forms  $\text{SiH}_3\text{OSiH}_2\text{O}^+$  ( $m/e 93$ ) in the ion source. It should be pointed out that disiloxane and trisiloxane do not yield significant intensities of  $m/e 47$  and  $93$ , respectively, on electron impact.

It is also apparent from Figure 2 and more clearly from Figure 4, that for photolysis times equal to or less than that corresponding to the maximum of  $\text{SiH}_3\text{O}^+$  ( $m/e 47$ )—or, equivalently, to the disilane induction period—the ratio of intensities  $I(m/e 47)/I(m/e 44)$  is within experimental error, quite constant; subsequent to the maximum of the  $\text{SiH}_3\text{O}^+$  ( $m/e 47$ ) intensity the ratio decreases. This indicates that until the onset of the decrease in the ratio  $I(m/e 47)/I(m/e 44)$  the ions  $\text{N}_2\text{O}^+$  and  $\text{SiH}_3\text{O}^+$  are produced by electron impact ionization of the same molecule. Nitrous oxide has been reported to be a stable product of this reaction,<sup>5</sup> a fact we have verified by adding  $\text{N}_2\text{O}$  to the system, and this fact, combined with the dependence of  $\text{N}_2\text{O}^+$  ( $m/e 44$ ), allows us to conclude that until the maximum in  $m/e 47$  is reached ( $\text{NO}$  is consumed) the amount of  $\text{N}_2\text{O}^+$  formed from  $\text{N}_2\text{O}$  is negligible compared with the amount formed from a reactive intermediate that also produces simultaneously  $\text{SiH}_3\text{O}^+$  in the ion source.

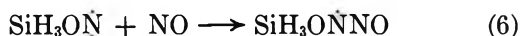
We note also from Figures 2 and 4 that the concentration of this reactive intermediate, as reflected by the intensities of  $m/e 44$  and  $47$ , increases at an increasing

(13) T. Yoshioka, Ph.D. Thesis, University of Pennsylvania, Philadelphia, Pa., 1967.

rate as long as nitric oxide is still present. This means either that the intermediate is formed in a branching chain reaction,<sup>14</sup> which is highly unlikely, or that it is formed as the second (at least) product of a consecutive reaction. We have mentioned that we are not able to detect any ions arising from the adduct of SiH<sub>3</sub> radicals and NO, yet this adduct must be the first product. We require for our intermediate a species that contains two nitrogen atoms since, on electron impact, N<sub>2</sub>O<sup>+</sup> is formed. It is thus very probable that the initial adduct of SiH<sub>3</sub> and NO reacts further with NO to produce an intermediate that yields both N<sub>2</sub>O<sup>+</sup> and SiH<sub>3</sub>O<sup>+</sup> by electron impact ionization. Such a sequence is easily shown to result in the upward curvature of *m/e* 44 and 47 shown in Figures 2 and 4.

Our failure to observe any ions from the initial adduct of SiH<sub>3</sub> and NO is most probably due to its very rapid further reaction, which results in its failure to attain concentrations that are within our detection sensitivity. Yet in the CH<sub>3</sub>-NO and H-NO systems the compounds CH<sub>3</sub>NO and HNO not only reached concentrations easily detectable<sup>2,3,6</sup> but were stable mass spectrometrically. We therefore adopt the suggestion of Nay, Woodall, Strausz, and Gunning<sup>5</sup> that, in the first step, the silyl radicals add to the oxygen atom of nitric oxide producing a diradical. This diradical is probably a triplet because it apparently associates so fast with nitric oxide that we are unable to detect its presence; however, the reaction with nitric oxide produces an intermediate that will easily yield N<sub>2</sub>O<sup>+</sup> and SiH<sub>3</sub>O<sup>+</sup> by electron impact in the ion source.

Our results, typified by Figures 1-4, are consistent with reactions 2-4 being followed in the initial stages by (5) and (6), *viz.*

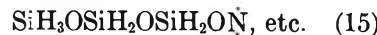
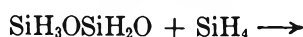
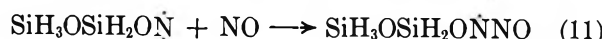
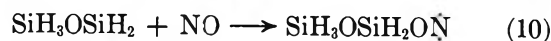
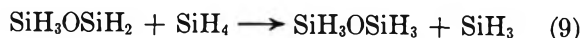


The proposed reactive intermediate, SiH<sub>3</sub>O $\dot{\text{N}}\text{NO}$ , will exhibit the correct time dependence and would be expected on mass spectral grounds to yield, as major ions, both N<sub>2</sub>O<sup>+</sup> and SiH<sub>3</sub>O<sup>+</sup>.

Thermochemical data with which to test the energetic feasibility of (5) and (6) do not exist. However, taking the Si-O bond energy as 113 kcal/mol<sup>15</sup> we estimate that the sequence (5)-(7) is 77 kcal exothermic overall. The sequence (5)-(7) is thus not precluded on thermochemical grounds and since reactions 5 and 6 are both associations it is probable that they are both energetically feasible processes.

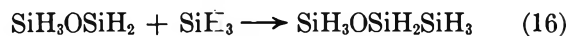
It has been reported<sup>5</sup> that the reaction is a chain reaction, and our data confirm this. For example, accepting our conclusions that at the onset of disilane formation (or maximum in *m/e* 47) the nitric oxide has been essentially completely consumed, we find that the rate of consumption of nitric oxide is *ten times greater* than the formation rate of silyl radicals. Thus, to com-

plete our mechanism we must write a chain reaction that produces *simultaneously* nitrous oxide, disiloxane, trisiloxane, and tetrasiloxane. After examining many possibilities, the mechanism most in accord with our results is the condensation chain in (7)-(15), which produces siloxanes, nitrous oxide, and hydrogen.



In this scheme, the intermediate produced in (11) yields SiH<sub>3</sub>OSiH<sub>2</sub>O<sup>+</sup> and N<sub>2</sub>O<sup>+</sup> on electron impact and accounts for the transient at *m/e* 93 (Figure 2) which is a precursor to the stable trisiloxane (*m/e* 123).

Reactions 8 and 13 are somewhat speculative and, as mentioned previously, we are unable to measure the hydrogen produced in this system. We have, however, by the use of N<sup>16</sup>O and SiD<sub>4</sub>, identified a series of ions at *m/e* 104-109, formed by ionization of a stable product, as most probably arising from SiH<sub>3</sub>SiH<sub>2</sub>OSiH<sub>3</sub>. The simplest mode of formation of this product in our system would seem to be (16), *viz.*



and, hence, the observation is at least consistent with the presence of SiH<sub>3</sub>OSiH<sub>2</sub> in the reaction.

Recent work<sup>16,17</sup> has shown that CH<sub>3</sub> radicals abstract H atoms from SiH<sub>4</sub> with an activation energy of 6.9-7.0 kcal/mol. Such a low activation energy suggests that hydrogen abstraction from SiH<sub>4</sub> by other radicals might be important in our system. In particular, consider the abstraction of hydrogen by SiH<sub>3</sub>O as in (8'), *viz.*



(14) F. S. Dainton, "Chain Reactions. An Introduction," Methuen and Co., Ltd., London, 1956, Chapter V.

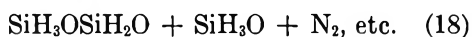
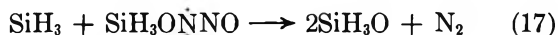
(15) C. T. Mortimer, "Reaction Heats and Bond Strengths," Pergamon Press, London, 1962, p 185.

(16) O. P. Strausz, E. Jakubowski, H. S. Sandu, and H. E. Gunning, *J. Chem. Phys.*, **51**, 552 (1969).

(17) E. R. Morris and J. C. J. Thynne, *J. Phys. Chem.*, **73**, 3294 (1969).

which would compete with (8). The silanol produced in (8') has not been isolated as yet, although it has been proposed as an intermediate that produces disiloxane and water by disproportionation.<sup>18</sup> We believe that (8') is not occurring to any great extent in our system because (1) we have sought but not observed the expected disproportionation product of silanol formation, namely water, and (2) our results require a chain mechanism that accounts for the simultaneous formation of di-, tri-, and tetrasiloxanes. Reaction 8' and the known further reactions of its products do not account for these observations.

The above mechanism is incomplete in that the reported formation of nitrogen<sup>5</sup> is not accounted for. We were unable to observe N<sub>2</sub> formation because of mass interference at  $m/e$  28 and 29 from the reactant SiH<sub>4</sub>. However, we have observed, as shown in Figure 5, that the depletion of the intermediate, SiH<sub>3</sub>O $\dot{N}$ NO, is first order in [SiH<sub>3</sub>O $\dot{N}$ NO] whether or not the photolysis is continued after the maximum or stopped at the maximum. The first-order rate constant in the presence of the radiation is greater than in the absence. This means that, when the photolysis is continued past the maximum, some entity at essentially constant concentration and not present in the absence of the radiation is reacting with the intermediate SiH<sub>3</sub>O $\dot{N}$ NO. Such an entity is most probably SiH<sub>3</sub> radicals, at a steady-state concentration during photolysis and becoming nonexistent rapidly in the absence of the radiation. Thus to account for this fact and the formation of nitrogen we suggest (17) and (18), *viz.*



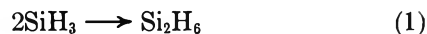
From the sum total of our data, such as in Figure 5, we conclude that at 25°,  $k_7 = 4.7 \pm 0.2 \times 10^{-4} \text{ sec}^{-1}$ . Such a rate constant is certainly consistent with the suggestion<sup>5</sup> that long-lived intermediates play a role in this reaction.

Finally, when the nitric oxide concentration is essentially completely depleted, not only does disilane form as in (1), but most likely dimerization of the adduct SiH<sub>3</sub>O $\dot{\text{N}}$  occurs,<sup>5</sup> *viz.*



However, our results indicate that reactions 1, 19, and 20 are not of importance until the nitric oxide is consumed.

It is pertinent to discuss at this point the nature of our evidence concerning the formation of disilane by reaction 1, *viz.*



since this reaction has been proposed by Niki and Mains,<sup>4</sup> but some doubt on its importance has been expressed, implicitly, at least, by Nay, Woodall, Strausz, and Gunning.<sup>5</sup> The following are apparent from our results. (a) Disilane formation is inhibited by the addition of nitric oxide to the Hg(6<sup>3</sup>P<sub>1</sub>)-sensitized decomposition of monosilane, and it remains inhibited until the nitric oxide is consumed. (b) During this

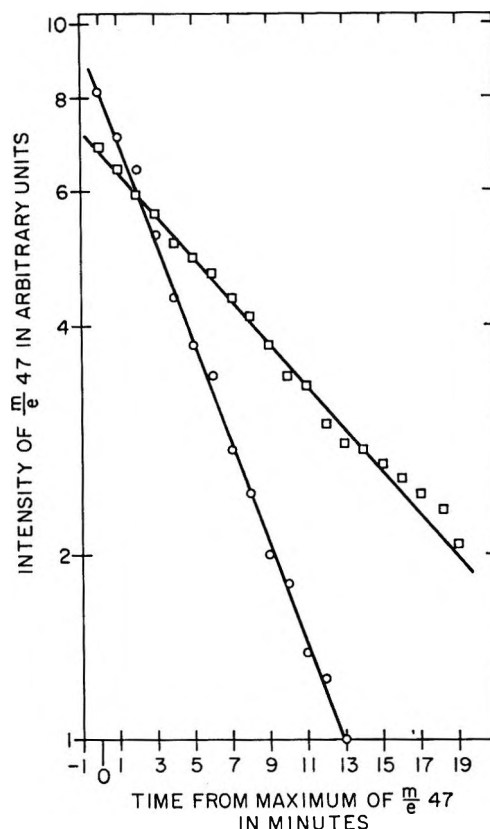


Figure 5. First-order semilog plot of decay of  $m/e$  47: O, with radiation; □, without radiation; total pressure  $\sim 15$  Torr;  $[\text{NO}]_0 = 4\%$ ; same light intensity as in Figure 4.

inhibition a product is formed from a reaction involving nitric oxide and monosilane that contains 3 hydrogen atoms, and this product forms only until the nitric oxide is consumed and disilane begins to be produced. (c) The stable products of the reaction with nitric oxide are siloxanes containing SiH<sub>3</sub> groups. (d) If ethylene is added to the silane-mercury system no evidence of SiH<sub>2</sub> addition to ethylene (formation of vinylsilane, for example) was found, the only products found being alkylsilanes. The simplest explanation by far of these facts is, we believe, that disilane is formed by reaction 1 in the absence of nitric oxide; however, in the presence of nitric oxide, its formation

(18) E. A. V. Ebsworth, "Volatile Silicon Compounds," Pergamon Press, London, 1963, pp 122-128.



is inhibited by the rapid occurrence of (5) and (6), and it can only begin to be formed when the nitric oxide is almost completely depleted.

Reaction 1 probably requires a third body to stabilize the energy-rich  $\text{Si}_2\text{H}_6$  initially formed. However, if the third-body requirement is similar to that obtaining in the combination of  $\text{CH}_3$  radicals, our pressure (10–15 Torr) is sufficiently high for (1) to be bimolecular.<sup>19</sup> Since (1) is exothermic by 83 kcal<sup>12,20,21</sup> and the combination of  $\text{CH}_3$  radicals is exothermic by 85 kcal,<sup>22</sup> we conclude that the third-body requirements of the two association reactions are most likely quite similar. Some recent work of Mazac and Simons<sup>23</sup> indicates that energy-rich dimethylsilane and ethylsilane require pressures in excess of 2000 Torr before third-body stabilization becomes essentially their exclusive fate. Since these results are contradictory to our conclusion above concerning the third-body requirement for (1), some discussion is warranted.

In the work of Mazac and Simons<sup>23</sup> energy-rich dimethylsilane and ethylsilane are formed, respectively, by the Si–H and C–H bond insertion reactions of  $\text{CH}_2$  radicals. According to the available thermochemistry,<sup>22,24</sup> the resulting species are energy rich to the extent of 102 and 99 kcal/mol, respectively. This excitation is considerably in excess of the lowest energy dissociation channel, namely the scission of a C–Si bond; this bond appears to have a dissociation energy of about 80 kcal/mol.<sup>20,21,24</sup> It is not surprising, therefore, that these energy-rich species should require such high pressures to make stabilization very probable. On the other hand, the energy-rich  $\text{Si}_2\text{H}_6$  and  $\text{C}_2\text{H}_6$  molecules formed in (1) and in methyl radical combination contain *no* energy in excess of the lowest energy dissociation path and, therefore, require much lower pressures for essentially complete stabilization.

*Methylsilane.* Using the same techniques, we have examined the mercury-photosensitized reaction of methylsilane with nitric oxide. Our results for this system are not as extensive as for the monosilane system, partly because of considerably greater interference by mass spectral overlapping of the reactant and various products. The general nature of the reaction, however, seems to be very similar to the corresponding case with monosilane.

With natural NO we were unable to detect any products containing nitrogen, since even  $\text{N}_2\text{O}^+$  at  $m/e$  44 is obscured by the contribution of  $\text{CSiH}_4^+$  from the methylsilane. We believe that  $\text{N}_2\text{O}^+$  is formed, however, both from electron impact ionization of intermediates analogous to those proposed in the silane case and of nitrous oxide itself, because of the time variation found for  $m/e$  46 when  $\text{N}^{15}\text{O}$  was employed. Even at this  $m/e$  value, however, interference from  $\text{CH}_3\text{Si}^{29}\text{H}_2^+$  was a serious problem and prevented quantitative study of this ion.

The stable products formed yielded the largest mass

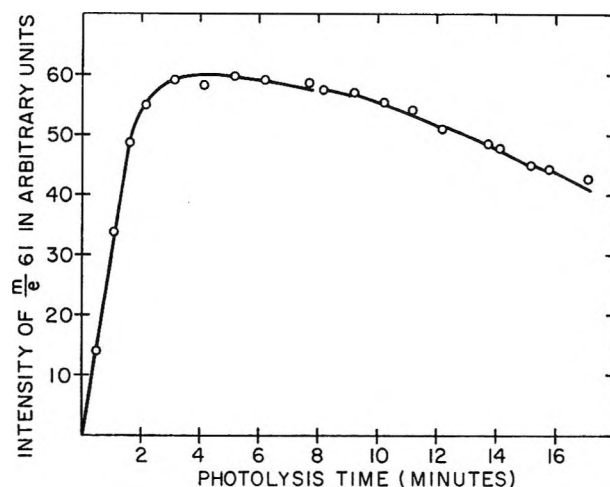


Figure 6. Time dependence of  $I(m/e$  61) in methylsilane–nitric oxide system; total pressure  $\sim$ 10 Torr;  $[\text{NO}]_0 \approx 5\%$ .

peaks at  $m/e$  59, 89, 91, and 105. From the general nature of siloxane and alkylsilane mass spectra, we believe (although we cannot prove) that  $m/e$  59 and 89 arise from electron impact on the dimer,  $\text{CH}_3\text{SiH}_2\text{SiH}_2\text{CH}_3$ , formed after nitric oxide is consumed, and that  $m/e$  105 (which is the largest stable product peak) and  $m/e$  91 arise from dimethyldisiloxane,  $\text{CH}_3\text{SiH}_2\text{OSiH}_2\text{CH}_3$ . Many other peaks corresponding to stable products of the reaction were found, namely at  $m/e$  119, 135–137, 149–150, 163–165, 177–179, 194, 208–210, 220–223, and 238. We are not able to assign this complex set of mass peaks to specific products, but we can say from our studies with  $\text{N}^{15}\text{O}$  that they contain no nitrogen. They probably, therefore, result from electron impact ionization of higher methylsiloxanes formed in a similar chain condensation to that proposed for monosilane and nitric oxide. We can also report that no methane, ethylene, or ethane is formed in this system.

In support of our proposed analogy of this reaction to that of monosilane–nitric oxide, we found that in the mercury-photosensitized reaction of methylsilane with nitric oxide a transient ion appears at  $m/e$  61. This ion behaves similarly to  $m/e$  47 (in the monosilane case), as shown in Figure 6, contains no nitrogen as evidenced by experiments with  $\text{N}^{15}\text{O}$ , and must, therefore, be  $\text{CH}_3\text{SiH}_2\text{O}^+$ , the ion analogous to  $\text{SiH}_3\text{O}^+$  in the monosilane reaction. We suggest, therefore,

(19) E. W. R. Steacie, "Atomic and Free Radical Reactions," 2nd ed, Reinhold Publishing Corp., New York, N. Y., 1954.

(20) W. C. Steele and F. G. A. Stone, *J. Amer. Chem. Soc.*, **84**, 3599 (1962).

(21) W. C. Steele, L. D. Nichols, and F. G. A. Stone, *ibid.*, **84**, 4441 (1962).

(22) D. D. Wagman, W. H. Evans, V. B. Packer, I. Halow, S. M. Bailey, and R. H. Schumm, NBS Technical Note 270-3, U. S. Government Printing Office, Washington, D. C., 1968.

(23) C. J. Mazac and J. W. Simons, *J. Amer. Chem. Soc.*, **90**, 2484 (1968).

(24) P. Potzinger and F. W. Lampe, *J. Phys. Chem.*, **74**, 719 (1970).

that the mechanism of the mercury-photosensitized reaction of methylsilane with nitric oxide is analogous to (1)–(19) if methylsilane is substituted for monosilane and if in the initiative process, reaction 3, an Si–H bond is always ruptured.<sup>5</sup>

*Acknowledgment.* This work was supported by the U. S. Atomic Energy Commission under Contract No. AT(30-1)-3570. We also wish to thank the National Science Foundation for providing funds to assist in the original purchase of the mass spectrometer.

## The Radiolysis of Liquid *n*-Pentane<sup>1</sup>

by William P. Bishop and Richard F. Firestone

Department of Chemistry, The Ohio State University, Columbus, Ohio 43210 (Received July 17, 1969)

Effects of irradiation temperature, I<sub>2</sub> concentration, and dose in the presence and absence of I<sub>2</sub> on the 100-eV yields of the forty more abundant radiolysis products ( $G \geq 0.001$ ) have been determined quantitatively and are interpreted in detail. Dose dependency is absent for all products of initially pure pentane, except ethylene, below  $3 \times 10^{20}$  eV/g. Homogeneous free-radical reactions account for 53% of pentane consumed at 25°. Abstraction steps consumed 12%, and combination and disproportionation steps account for 41% of pentane consumed at 25°. The 100-eV yields of homogeneous 1-pentyl, 2-pentyl, 3-pentyl, butyl, propyl, ethyl, and methyl radicals have been determined at 25° and –78° from measured decrements in hydrocarbon product yields caused by the presence of I<sub>2</sub> and by variation of irradiation temperature. Excellent agreement has been observed for yields of all except 1-pentyl radicals with those determined by the <sup>14</sup>C<sub>2</sub>H<sub>5</sub> radical sampling method. The C<sub>6</sub>–C<sub>10</sub> alkene products appear to be formed by thermal pentenyl radicals, whose primary radiolytic yield is 0.06 radical/100 eV.  $G(\text{H}_2)$  equals 4.2 molecules/100 eV at 25° and is independent of dose below  $10^{21}$  eV/g. The 100-eV yield of thermal H atoms is estimated to be  $0.7 \pm 0.2$  atom/100 eV from effects of temperature on  $G(\text{H}_2)$ . It is also shown that inhibition of “molecular” H<sub>2</sub> by I<sub>2</sub> is not accompanied by inhibition of the yields of pentenes or other hydrocarbon products.

### Introduction

The radiolytic decomposition of liquid hydrocarbons has been of interest to chemical kineticists for many years; essentially fragmentary information from investigations performed prior to 1962 has been partially summarized and reviewed,<sup>2,3</sup> and a review of more recent progress is available.<sup>4</sup> Results of early studies of the formation of selected products<sup>5–8</sup> and several more comprehensive investigations<sup>9–11</sup> have established the importance of free-radical reactions and of much faster reactions in a variety of liquid hydrocarbons. Scavenger techniques<sup>12–19</sup> and esr spectrometry<sup>20,21</sup> have led to identification of some free-radical intermediates in several irradiated liquid alkanes. Only relatively recently has analysis of a majority of the many products of a liquid hydrocarbon been accomplished.<sup>22,23</sup>

Koch, Houtman, and Cramer have recently reported<sup>23</sup> 100-eV yields of a majority of products of initially pure liquid *n*-pentane at several temperatures between –116 and 100° with emphasis on dose dependence and effects of temperature. The present article reports 100-eV yields of the complete set of identifiable ( $G \geq 0.001$  molecule/100 eV) hydrocarbon products of the

radiolysis of initially pure liquid pentane at 25 and –78° and of *n*-pentane containing I<sub>2</sub> (0.5 mM to 4 mM) at 25°—all at conversions in the vicinity of 0.1%

- (1) Based for the most part upon a dissertation submitted in partial fulfillment of requirements for the Ph.D. degree at The Ohio State University by W. P. B., 1967.
- (2) A. J. Swallow, “Radiation Chemistry of Organic Compounds,” Pergamon Press, Inc., Elmsford, N. Y., 1960.
- (3) A. V. Topchiev, “Radiolysis of Hydrocarbons,” American Elsevier Publishing Co., New York, N. Y., 1964.
- (4) R. A. Holroyd in “Fundamental Processes in Radiation Chemistry,” P. Ausloos, Ed., Interscience Publishers, New York, N. Y., 1968, Chapter 7.
- (5) C. S. Schoepfle and C. H. Fellows, *Ind. Eng. Chem.*, **23**, 1396 (1931).
- (6) L. H. Gevantman and R. R. Williams, *J. Phys. Chem.*, **56**, 569 (1952).
- (7) H. A. Dewhurst, *ibid.*, **61**, 1466 (1957).
- (8) H. A. Dewhurst, *ibid.*, **62**, 15 (1958).
- (9) T. J. Hardwick, *ibid.*, **64**, 1632 (1960).
- (10) C. D. Wagner, *ibid.*, **64**, 231 (1960).
- (11) A. E. DeVries and A. O. Allen, *ibid.*, **63**, 879 (1959).
- (12) E. N. Weber, P. F. Forsythe, and R. H. Schuler, *Radiat. Res.*, **3**, 68 (1955).
- (13) H. A. Dewhurst, *J. Amer. Chem. Soc.*, **80**, 5607 (1958).
- (14) T. J. Hardwick, *J. Phys. Chem.*, **65**, 101 (1961).
- (15) P. R. Geissler and J. E. Willard, *J. Amer. Chem. Soc.*, **84**, 4627 (1962).

( $1.4 \times 10^{20}$  eV/g), *i.e.*, below the region of product yield dose dependency. Products have been identified by combination of gas chromatography and fast-scan mass spectrometry.<sup>22</sup> Every identifiable product of the radiolysis of liquid pentane is shown to be formed by both fast reactions and free-radical reactions. Evidence is presented which demonstrates that  $I_2$  at 0.5 mM to 4 mM inhibits free-radical reactions but does not alter contributions of fast reactions to the 100-eV yields of hydrocarbon products. It is shown how measured decrements in the yields of hydrocarbon products caused by the presence of  $I_2$  or by irradiation at low temperature ( $-78^\circ$ ) can be used to calculate 100-eV yields of homogeneous free radicals at 25 and  $-78^\circ$ .

### Experimental Section

Phillips Research Grade *n*-pentane (99.97 mol per cent) was purified by gas chromatography to a detectable impurity level of the order  $10^{-6}$  mol per cent. Prior treatment with concentrated sulfuric acid reduced pentene-1, *trans*-pentene-2, and *cis*-pentene-2 below the level of detectability but did not provide purer final material. Iodine was prepared by vacuum sublimation of Baker Reagent Grade material. Sample materials were transferred into annular Pyrex irradiation vessels of 5 ml volume by vacuum distillation from anhydrous BaO following outgassing by repetitive freezing-pumping-thawing cycles. Irradiations were performed with a nominally 150-Ci  $^{60}\text{Co}$  cylindrical  $\gamma$ -ray source.

Dosimetry measurements were made with Fricke dosimeter solutions. Ferric ion concentrations were measured spectrophotometrically at 304 nm and ambient temperatures, assuming a molar absorptivity of  $2196 \text{ M}^{-1} \text{ cm}^{-1}$  at  $25^\circ$  and a fractional increase of 0.0069/deg.  $G(\text{ferric})$  was assumed equal to 15.6 ions/100 eV, and dose rates in *n*-pentane liquid were assumed to be equal to those in the dosimeter solution multiplied by the ratio of electron densities of *n*-pentane and 0.8 *N* sulfuric acid solution. Dose rates employed were in the range  $10^{17}$  to  $10^{18}$  eV/g min.

Irradiated samples were separated into liquid and gaseous fractions by means of a low-temperature still. Hydrogen was measured in a gas buret. The gaseous fraction of each sample was analyzed for organic constituents using a 10-ft,  $1/8$ -in. copper column packed with 60–70 mesh silica gel with a linear temperature program of  $18^\circ/\text{min}$  from 30 to  $300^\circ$ . Liquid fractions were analyzed for all products except *cis*- and *trans*-pentene-2 with a 20-ft,  $1/8$ -in. copper column packed with 70–80 mesh Anakrom ABS solid support coated with 8 wt % silicone gum rubber employing a linear temperature program of  $4^\circ/\text{min}$  from  $-50$  to  $130^\circ$ . Yields of *cis*- and *trans*-pentene-2 were determined with a 40-ft,  $1/4$ -in. copper column packed with 70–80 mesh Anakrom ABS solid support coated with 25 wt % Ucon (water insoluble) and operated at  $23^\circ$ .

Radiolysis products were identified by a combination of gas chromatography and fast-scan mass spectrometry, employing an Aerograph A-600-B gas chromatograph and a Bendix Model 14 time-of-flight mass spectrometer for "on-the-fly" mass spectrometric identification.<sup>22</sup> Carrier gas (He) was partially removed from the effluent by rapid pumping on the glass envelope of a fritted glass enrichment device. Mass spectral patterns were recorded by a Robot automatic 35 mm camera mounted on the screen face of the oscilloscope of the mass spectrometer; exposures were actuated by signals from an electronic integrator described below at times corresponding to peak maxima on the chromatograms. Identification of products was made by comparison of mass spectral patterns with those of known compounds whenever possible. Comparison of time-of-flight spectra of a selection of available compounds with tabulated (ASTM Index of Mass Spectral Data) spectral patterns obtained with conventional magnetic focussing instruments showed that the orders of intensity of ion current peaks were identical and that in most instances relative intensities were similar. Product identities were determined for some products by means of such comparisons. Neither known samples nor tabulated spectra were available for the branched chain nonanes and decanes. Identities of these products were determined partly on the basis of retention volumes corresponding to the known boiling points of the possible isomers. Cracking patterns for the branched chain nonanes and decanes were in every instance consistent with the assigned structure. All of the column effluent was diverted to the flame ionization detector for quantitative analyses. Signals from this detector were directed to a recording potentiometer and to an Infotronics Model CRS-10HB electronic integrator. The sensitivity of the flame detector for each product was determined in most instances by integration of chromatographic peaks of known solutions at several concentrations in each of the ranges of interest. Detector sensitivities were observed to be characteristic linear functions of molecular weight for the branched and straight chain alkanes and alkenes. When necessary, detector sensitivities were assigned on the basis of compound class and molecular weight.

(16) J. Dauphin, *J. Chim. Phys.*, **59**, 1223 (1962).

(17) R. A. Holroyd and G. W. Klein, *J. Amer. Chem. Soc.*, **84**, 4000 (1962).

(18) R. A. Holroyd and G. W. Klein, *Int. J. Appl. Radiat. Isotop.*, **15**, 633 (1964).

(19) H. A. Holroyd, *J. Phys. Chem.*, **70**, 1341 (1966).

(20) T. J. Hardwick, *ibid.*, **66**, 1611 (1962).

(21) R. W. Fessenden and R. H. Schuler, *J. Chem. Phys.*, **39**, 2147 (1963).

(22) H. Widmer and T. Gaumann, *Helv. Chim. Acta*, **46**, 944 (1963).

(23) R. O. Koch, J. P. W. Houtman, and W. A. Cramer, *J. Amer. Chem. Soc.*, **90**, 3326 (1968).

Table I: 100-eV Product Yields at 25°, at -78°, and in the Presence of I<sub>2</sub><sup>a</sup>

Product <sup>b</sup>	25°	-78°	In presence of I <sub>2</sub>	$\Delta G(i)_T$ <sup>c</sup>	$\Delta G(i)_{I_2^{25^\circ}}$ <sup>d</sup>	$\Delta G(i)_{I_2^{-78^\circ}}$ <sup>e</sup>
Methane	0.261	0.162	0.132	0.10	0.129	0.030
Ethane	0.417	0.31	0.234	0.11	0.183	0.08
Ethylene	0.219	0.15	0.11	0.07	0.11	0.04
Propane	0.442	0.324	0.239	0.118	0.203	0.085
Propylene	0.24	0.15	0.16	0.09	0.08	-0.01
(C <sub>4</sub> product)	0.0076	0.003	0.004	0.004	0.003	0.00
n-Butane	0.072	0.0753	0.048	-0.003	0.024	0.027
Butene-1	0.051	0.031	0.039	0.020	0.012	-0.008
(C <sub>4</sub> product)	0.0072	0.004	0.005	0.003	0.002	0.00
(C <sub>4</sub> product)	0.003	0.000	0.003	0.003	0.000	0.00
2-Methylbutane	0.0615	0.0507	0.049	0.011	0.012	0.00
Pentene-1	0.738	0.675	0.383	0.063	0.355	0.292
trans-Pentene-2	1.22	1.22	0.91	0.00	0.31	0.31
cis-Pentene-2	0.54	0.54	0.50	0.00	0.04	0.04
2-Methylpentane	0.016	0.024	0.0052	-0.008	0.011	0.019
3-Methylpentane	0.0072	0.0110	0.0048	-0.0038	0.002	0.006
n-Hexane	0.025	0.037	0.015	-0.012	0.010	0.022
3-Ethylpentene-1	0.0047	0.0095	0.000	-0.0048	0.005	0.010
4-Methylhexene-1	0.0042	0.0095	0.000	-0.0053	0.004	0.010
3-Methylhexane	0.119	0.116	0.028	0.003	0.091	0.088
3-Ethylpentane	0.0573	0.060	0.013	-0.003	0.044	0.047
n-Heptane	0.0505	0.086	0.012	-0.035	0.038	0.074
Heptene or octene	0.0015	0.0043	0.000	-0.0028	0.002	0.004
2,3-Dimethylhexane	0.011	} 0.034	0.000	} -0.010	0.011	} 0.034
2-Methyl-3-ethylpentane	0.014		0.000		0.014	
4-Methylheptane	0.0917	0.105	0.025	-0.013	0.066	0.080
3-Ethylhexane	0.040	0.0490	0.0091	-0.009	0.031	0.039
(An octene)	0.003	0.000	0.000	0.003	0.003	0.000
n-Octane	0.041	0.069	0.009	-0.028	0.032	0.060
(3,4-Dimethylheptane + 3-methyl-4-ethylhexane)	0.003	0.000	0.000	0.003	0.003	0.000
(4-Methyloctane + 3- ethylheptane)	0.029	0.024	0.000	-0.005	0.029	0.024
3-Methyloctane	0.010	0.0086	0.000	0.001	0.010	0.009
n-Nonane	0.0047	0.0064	0.000	-0.0017	0.005	0.006
(A decene)	0.014	0.0133	0.000	0.001	0.014	0.013
A decene	0.0475	0.0478	0.000	0.000	0.048	0.048
4,5-Dimethyloctane	0.751	0.390	0.052	0.361	0.699	0.338
4-Methyl-3-ethylheptane + 3,4-diethylhexane	0.183	0.205	0.042	-0.022	0.141	0.163
3-Ethylheptane + 4- methylnonane	0.0734	0.0895	0.022	-0.0161	0.051	0.068
(A decene)	0.001	0.002	0.000	-0.001	0.001	0.002
n-Decane	0.0344	0.0671	0.0270	-0.0327	0.0074	0.040
Hydrogen	4.20	4.18 <sup>f</sup>	2.40	0.64 <sup>i</sup>	2.85 <sup>j</sup>	1.55
- Pentane	6.40	5.60	3.0 <sup>f</sup>	0.80	3.4	2.7
C-C Rupture	1.16	0.96	(1.15) <sup>g</sup>	0.2	0.0	...
Ethyl iodide			0.43			
1-Propyl iodide			0.39			
1-Butyl iodide			0.067 <sup>h</sup>			
2-Pentyl iodide			1.21 <sup>h</sup>			
3-Pentyl iodide			0.65			
1-Pentyl iodide			0.52			
Hydrogen iodide			2.21 <sup>k</sup>			

<sup>a</sup> In molecules/100 eV at  $1.42 \times 10^{20}$  eV/g. <sup>b</sup> Product identities enclosed in parentheses are assigned solely on basis of parent ion mass numbers, column retention volumes, and boiling points. <sup>c</sup>  $\Delta G(i)_T$  equals the difference between 100-eV yield at 25° and that at -78°. <sup>d</sup>  $\Delta G(i)_{I_2^{25^\circ}}$  equals the difference between 100-eV yield at 25° and that in presence of I<sub>2</sub> at 25°. <sup>e</sup>  $\Delta G(i)_{I_2^{-78^\circ}}$  equals the difference between the 100-eV yield at -78° and that in presence of I<sub>2</sub> at 25°. <sup>f</sup> Excluding iodides. <sup>g</sup> Includes homogeneous radical yields from Table II. <sup>h</sup> At 4 mM iodine concentration. <sup>i</sup>  $\Delta G(H_2)_T$  is computed from the difference in yields (mol/g) at -78° and 25° measured at  $1.42 \times 10^{20}$  eV/g. The instantaneous 100-eV yield at 25° equals 4.20 molecules/100 eV at this dose. <sup>j</sup>  $\Delta G(H_2)_{I_2^{25^\circ}}$  equals  $\bar{G}(H_2)$  minus the integrated average yield of H<sub>2</sub> in presence of 4 mM I<sub>2</sub> at  $1.42 \times 10^{20}$  eV/g. <sup>k</sup> From material balance among all products at 4 mM I<sub>2</sub>.

## Results

The 100-eV yields of the forty more abundant products of irradiated, carefully purified, air-free normal pentane which are reported in columns 2 and 3 of Table I are independent of dose between  $7 \times 10^{19}$  and  $3 \times 10^{20}$  eV/g except that of ethylene, which begins to exhibit dose dependence within this range. The 100-eV yields reported in Table I are averaged results of replicate experiments at  $1.42 \times 10^{20}$  eV/g (0.1% conversion), except that of  $H_2$  at  $25^\circ$  which has been calculated from the slope of the yield *vs.* dose plot, because of a small extrapolated apparent yield of  $H_2$  at zero dose. Each of the tabulated values is an average of three or more independent determinations. Yield values have been determined with averaged precisions (average deviation from mean) as indicated for the following ranges of yield values:  $>1$  ( $\pm 2\%$ ),  $0.3-1$  ( $\pm 3\%$ ),  $0.1-0.3$  ( $\pm 4\%$ ),  $0.01-0.1$  ( $\pm 6\%$ ),  $0.001-0.01$  ( $\pm 25\%$ ).

The 100-eV yields of products formed by irradiation of pure, air-free *n*-pentane at  $-78^\circ$  and by irradiation of *n*-pentane containing iodine at  $25^\circ$  are reported in columns 3 and 4 of Table I, respectively. The 100-eV yields of products of the radiolysis of iodine solutions have been observed to be independent of iodine concentration between 0.5 mM and 4 mM, except those of  $H_2$ , 1-butyl iodide, and 2-pentyl iodide as shown in Figures 1 and 2. Yield decrements reported in columns 5, 6, and 7 of Table I are differences between pairs of 100-eV yields measured as indicated in the footnotes of Table I. Agreement between values of  $G(-\text{pentane})$  based on the H-atom sum over product yields and those based on the C-atom sum is within 0.2% for data from initially pure *n*-pentane and within 2% for data from iodine solutions.

All  $C_1$  through  $C_{10}$  normal and branched chain alkanes which may be formed by combinations of free-radicals created by C-C and by C-H scission are detectable products. Alkane products which may be formed by combination of secondary propyl and secondary butyl radicals with normal radicals have also been observed. All possible 1-alkene products containing less than six carbon atoms have also been observed. The only 2-alkene products found were *cis*- and *trans*-pentene-2. The major products are  $H_2$ , methane, ethane, propane, the pentenes, and 4,5-dimethyloctane. The yields of  $C_6$ - $C_{10}$  alkenes are small. Dienes are absent and appear to be formed only at much higher conversions than those employed in this work.<sup>3</sup> Acetylene has been identified among the radiolysis products of gaseous pentane<sup>24</sup> and liquid pentane;<sup>11</sup> we estimate 0.04 molecule/100 eV as an upper limit at  $25^\circ$  in agreement with Allen and DeVries<sup>11</sup> and an order of magnitude lower than the gas phase value.<sup>24</sup>

Comparison of 100-eV yield data of Table I with those reported previously<sup>23</sup> for conversions less than 0.5% at room temperature shows that agreement is reason-

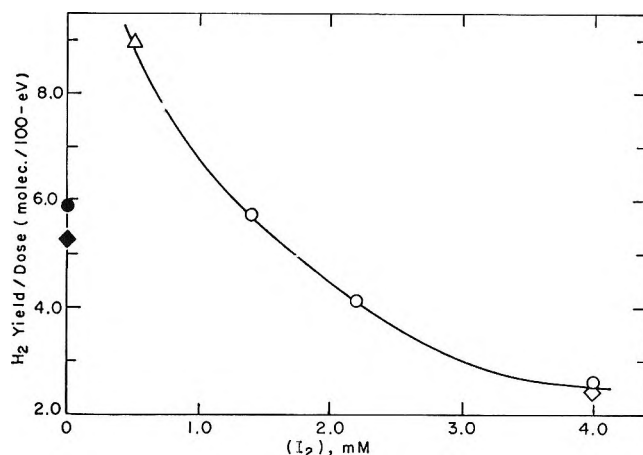


Figure 1. Effects of iodine concentration and dose on the integrated average yield of hydrogen,  $\bar{G}(H_2)$ , at  $25^\circ$ . Open symbols refer to values in the presence of  $I_2$ . Filled symbols refer to values in initially pure pentane:  $\circ$ , at  $4.3 \times 10^{19}$  eV/g;  $\Delta$ , at  $1.04 \times 10^{19}$  eV/g;  $\diamond$ , at  $14.2 \times 10^{19}$  eV/g.

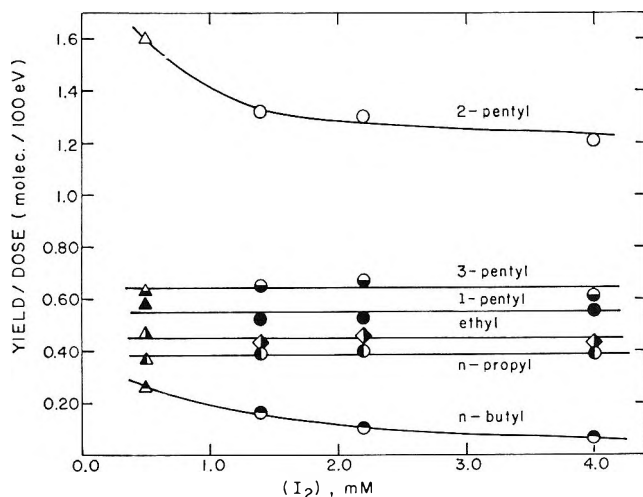


Figure 2. Effects of iodine concentration and dose on the integrated average yields of alkyl iodides,  $\bar{G}(RI)$ , at  $25^\circ$ . Each of the several triangular symbols represents values as of  $1.04 \times 10^{19}$  eV/g. All other symbols represent values at  $4.3 \times 10^{19}$  eV/g.

ably satisfactory for  $CH_4$ , the  $C_4$ - $C_9$  products, and the pentenes. A substantial discrepancy exists among the yields of the isodecenes which cannot be attributed to a dependence on dose in the vicinity of  $0.5 \times 10^{20}$  eV/g; our yield data extrapolate directly to the origin from the  $(0.7 \text{ to } 3.5) \times 10^{20}$  eV/g region. The discrepancy among  $C_2$  and  $C_3$  yields is also difficult to attribute to dose dependence, because we have found that the sums of the yields of the  $C_2$  and  $C_3$  products, respectively, are strictly linear with dose, and our values for these sums are 40-50% lower than those of Koch, Houtman, and Cramer.<sup>23</sup>

(24) J. H. Futrell, *J. Phys. Chem.*, **64**, 1634 (1960).

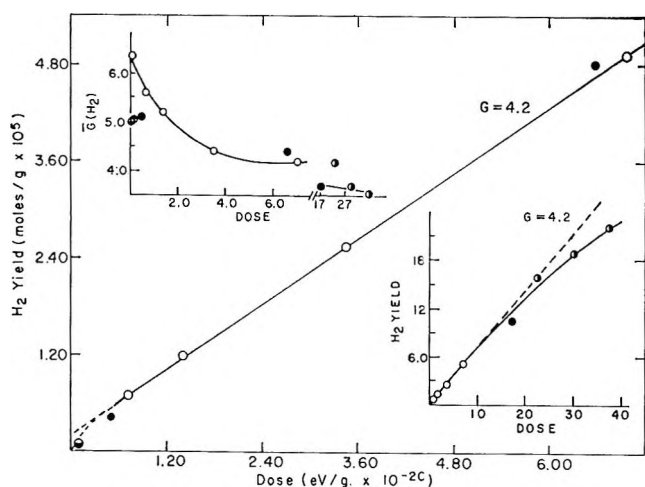


Figure 3. Upper left: integrated average 100-eV yield of hydrogen,  $\bar{G}(\text{H}_2)$ , as a function of dose. Center and lower right: hydrogen yield (mol/g of pentane), as a function of dose:  $\circ$ , this work;  $\bullet$ , ref 23;  $\ominus$ , ref 25;  $\diamond$ , J. W. Sutherland and A. O. Allen, *J. Amer. Chem. Soc.*, **83**, 1040 (1961);  $\ominus$ , ref 25;  $\diamond$ , ref 20.

## Discussion

**Hydrogen Formation.** Self-consistent sets of yield data for *n*-alkanes from which instantaneous 100-eV yields,  $G(\text{H}_2)$ , at low conversions may be determined are not available in the published literature. Values of reported integrated average 100-eV yields,  $\bar{G}(\text{H}_2)$ , from liquid *n*-pentane in the vicinity of 25° vary widely (5.0 to 6.3 molecules/100 eV) at doses below  $10^{20}$  eV/g<sup>11,20,23,25,26</sup> and suggest, as shown in the upper left of Figure 3, a strong negative dose dependence in this region and a less pronounced negative dependence beyond  $10^{21}$  eV/g. The larger scale center plot of Figure 3 shows that the instantaneous value,  $G(\text{H}_2)$ , remains constant at  $4.2 \pm 0.2$  molecules/100 eV between  $7 \times 10^{19}$  and  $7 \times 10^{20}$  eV/g. Thus, it appears, at least superficially, that a dose-independent region is preceded and followed by regions in which  $\text{H}_2$  formation is inhibited by radiolysis products.

The lower right section of Figure 3 shows that the high-range dose dependence sets in at approximately  $1 \times 10^{21}$  eV/g. This is consistent with the effect on  $G(\text{H}_2)$  of the analogous mixture of alkene products of hexane which has been attributed to H-atom scavenging.<sup>27</sup> Recent work<sup>28,29</sup> demonstrates that reactions of alkenes with ionic precursors of  $\text{H}_2$  also diminish  $G(\text{H}_2)$  in this region.

It is commonly held that neutralization of positive ions is a major source of  $\text{H}_2$  in irradiated hydrocarbons.<sup>4</sup> Positive ions which are accessible to solutes readily transfer  $\text{H}_2$  and H to alkenes.<sup>28,29</sup> Approximately 10% of positive ions in irradiated liquid isopentane are, for example, scavenged by 0.03 *M* perdeuteriocyclopropane,<sup>29</sup> and *trans*-hexene-2 is at least as efficient a reactant with hexane positive ions.<sup>28</sup> Thus, beyond  $10^{21}$  eV/g, *i.e.*, at alkene product concentrations exceeding

0.03 *M*, alkenes have been shown to significantly inhibit in-spur neutralization steps. At low concentrations competition with in-spur neutralization is negligible in the absence of high concentrations of electron attaching solutes (*ca.* 0.1 *M*).<sup>28,29</sup> Thus, in initially pure *n*-pentane at low doses only the so-called "free ions" are accessible to alkene products,<sup>28</sup> and the initial instantaneous  $\text{H}_2$  yield cannot for this cause exceed that in the dose-independent region by more than approximately 0.1 molecule/100 eV. It can be simply demonstrated with the aid of Hardwick's rate constant values<sup>27</sup> and alkene yields of Table I that H-atom scavenging is also incapable of altering  $G(\text{H}_2)$  below  $7 \times 10^{19}$  eV/g. Thus, intimations of dose dependence in this region are very probably attributable to small systematic errors in our yield measurements. Absence of dose dependence for products other than hydrogen tends to support this conclusion.

Effects of temperature and of the presence of  $\text{I}_2$  at 25° indicate that  $\text{I}_2$  alters the fate of more than one precursor of  $\text{H}_2$ . Figure 1 shows that the presence of  $\text{I}_2$  at concentrations below 1 *mM* increases the average rate of  $\text{H}_2$  formation,  $\bar{G}(\text{H}_2)$ , but data in this form can be misleading and we have no measured values for initially pure pentane in this dose region for comparison. At higher concentrations the decrement in  $\bar{G}(\text{H}_2)$  caused by  $\text{I}_2$  is substantially greater than the contribution of abstraction by thermal H atoms indicating that  $\text{I}_2$  inhibits a portion of the so-called molecular yield. Although  $\bar{G}(\text{H}_2)$ ,  $\bar{G}(\text{2-pentyl iodide})$ , and  $\bar{G}(\textit{n-butyl iodide})$  decrease as  $(\text{I}_2)$  increases beyond 0.5 *mM*, as shown in Figures 1 and 2, the 100-eV yields of hydrocarbon products become independent of  $(\text{I}_2)$  at or below this value. Thus, it is apparent that 0.5 *mM* is sufficient to scavenge all organic radicals at the dose rate employed. Material balance requires that most of the hydrogen missing at 4 *mM* be in the form of hydrogen iodide, but since HI was not measured we cannot otherwise demonstrate that this is a fact. One must in any event conclude that interactions of  $\text{I}_2$  with excited and ionic precursors of  $\text{H}_2$  occur in the 0.5–4 *mM* range but that they do not change the yields or identities of hydrocarbon products. Thus, for example, if the precursor normally produces  $\text{H}_2$  and an organic radical,  $\text{I}_2$  shall have scavenged the radical whether or not it inhibits  $\text{H}_2$  formation. If the precursor normally produces hydrogen and a stable molecule, the latter must be formed in the same yield in the presence or absence of  $\text{I}_2$ . Speculation concerning possible identities of such precursors does not appear to be warranted

(25) R. H. Schuler and R. R. Kuntz, *J. Phys. Chem.*, **67**, 1004 (1963).

(26) A. Horowitz and L. A. Rajbenbach, *J. Chem. Phys.*, **48**, 4278 (1968).

(27) T. J. Hardwick, *J. Phys. Chem.*, **66**, 291 (1962).

(28) S. J. Rzed and R. H. Schuler, *ibid.*, **72**, 228 (1968).

(29) A. A. Scala, S. G. Lias, and P. Ausloos, *J. Amer. Chem. Soc.*, **88**, 5701 (1966).

at this time. Implications concerning effects of  $I_2$  on possible precursors of the pentenes, in particular, are considered below in discussion of pentyl radical yields.

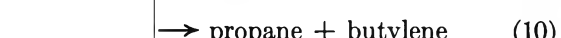
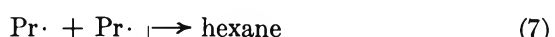
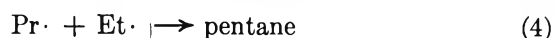
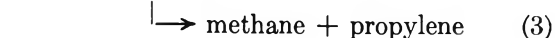
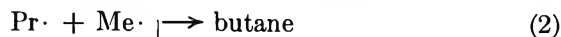
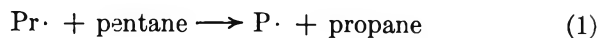
*Other Products.* The effect of lowering the irradiation temperature appears simply to be inhibition of thermal radical-solvent reactions. Inhibition of abstraction is reflected by substantial decreases in the yields of two major products,  $H_2$  and 4,5-dimethylcane. Yields of  $C_1$ - $C_4$  products, except *n*-butane, also decrease. The yields of all products which may be formed by combination of pentyl- with  $C_1$ - $C_4$  radicals increase relative to those of  $H_2$  and 4,5-dimethylcane; the majority increase in absolute magnitude. These observations suggest that effects of temperature are caused principally by inhibition of the abstraction of secondary hydrogen atoms from pentane by thermal H atoms and  $C_1$ - $C_3$  radicals.

The presence of  $I_2$  reduces the yields of all hydrocarbon products. Invariance of the yield decrements  $\Delta G(i)_{I_2}$  with respect to  $I_2$  concentration indicates that the presence of  $I_2$  provides a clean distinction between scavengable and unscavengable precursors of all hydrocarbon products.

*100-eV Yields of Homogeneous Radicals.* The alkyl iodide yields of Table I may be tentatively equated with those of radicals which are formed in the presence of  $I_2$  and are subsequently scavenged. Qualification of this assumption is necessary and will be made later in the discussion. It will be shown that free-radical yields can be determined more reliably from measured hydrocarbon product yield decrements,  $\Delta G(i)_{I_2}$ , each of which comprises contributions to the yield of product *i* by radical-radical steps which are precluded by the presence of  $I_2$ . Yields of a majority of the radical species can be computed from  $\Delta G(i)_{I_2}$  values in total ignorance of radical combination to disproportionation ratios. Those of the remaining few can be determined quite precisely with the aid of order of magnitude estimates of these ratios. The computational method is based on the assumption that the presence of  $I_2$  (0.5-4 mM) prevents homogeneous formation of radical-radical products and that it does not alter hydrocarbon product yields of other kinds of reactions, including fast reactions (*e.g.*, ion-molecule, molecular detachment, and neutralization reactions). The validity of this assumption depends on the observation that  $\Delta G(i)_{I_2}$  values are independent of ( $I_2$ ) above 0.5 mM and is discussed below in the section concerning yields of pentyl radicals. An additional assumption is necessary for computation of radical yields at  $-78^\circ$  because the required decrements,  $\Delta G(i)_{I_2}^{-78^\circ}$ , cannot be measured. It is assumed that contributions of processes other than homogeneous radical-radical and abstraction steps are unaffected by irradiation temperature between 25 and  $-78^\circ$ . Values of hydrocarbon yield decrements,  $\Delta G(i)_{I_2}^{-78^\circ}$ , in column 7 of Table I are,

accordingly, equated with the differences,  $G(i)_{-78^\circ} - G(i)_{I_2}^{25^\circ}$ . The general procedure is illustrated below by computation of the 100-eV yields of homogeneous propyl and butyl radicals at 25 and  $-78^\circ$ .

*Propyl and Butyl Radicals.* At  $25^\circ$  each free radical must either abstract an H atom from pentane or react with another radical in the absence of iodine and at very low doses. The complete list (where P = pentyl) of possible relevant steps for propyl radicals is



Propane and octane may also be formed by steps 15 and 16, respectively.



Clearly,  $G(\text{propyl radicals}) = \Delta G(\text{propane})_{I_2} + \Delta G(\text{propylene})_{I_2}^{25^\circ} + \Delta G(\text{cctane})_{I_2}^{25^\circ} + \Delta G_2 + \Delta G_4 + 2\Delta G_7 + \Delta G_9 - \Delta G_{15} - \Delta G_{16}$ . The yield of pentyl iodides is sufficiently great that when the additional yield of pentyl radicals formed by abstraction steps in initially pure pentane is taken into account it is clear that the concentration of pentyl radicals must be 10 times that of either ethyl or propyl radicals and 50 times that of butyl radicals at  $25^\circ$ . Thus, pentyl radicals are precursors of essentially all scavengable heptanes, octanes, nonanes, and decanes. Reaction 16 may, accordingly, be neglected at  $25^\circ$ . The contribution of pentyl radicals to the hexanes at  $25^\circ$  should be small, because methyl radicals can be expected to be removed largely by abstraction steps. In any event this contribution is estimable, if we assume that the proportions of secondary and primary radicals of a kind appearing in the heptanes, octanes, and hexanes are approximately equal. We note that 70% of pentyl radicals appearing in both scavengable heptanes and scavengable octanes are secondary radi-

cals and that 28% of propyl radicals appearing in scavengable octanes are secondary radicals. Thus, since the total yield of scavengable radicals appearing in the hexanes is 0.046 radical/100 eV and the yield of secondary radicals in hexanes is 0.013 radical/100 eV, it is apparent that essentially none of the hexanes has pentyl or methyl radical precursors. Thus, scavengable hexanes must be formed from propyl radicals, and it follows that  $\Delta G_7 = 0.02$  molecule/100 eV. Since homogeneous pentyl radicals in their great relative abundance do not sample methyl radicals,  $G_2$  and  $G_{15}$  must also be negligible. Thus, methyl radicals must be removed completely by abstraction steps at 25°.  $\Delta G_4$  and  $\Delta G_9$  may be estimated with the aid of the fact that the cross-combination ratio,  $k_{ab}/(k_{aa}k_{bb})^{1/2}$  for alkyl radicals in the gas phase is equal to  $2.0 \pm 0.1$  (extreme deviation) for all pairs whose values have been measured.<sup>30,31</sup> For  $\Delta G_4$  we may, therefore, write  $\Delta G(\text{octanes})\Delta G(\text{heptanes})/2\Delta G(\text{decane}) = 0.02$  radical/100 eV. Similarly,  $\Delta G_9 = \Delta G(\text{octanes})\Delta G(\text{nonanes})/2\Delta G(\text{decane}) = 0.01$  radical/100 eV. Thus, the yield of homogeneous propyl radicals in the absence of  $I_2$  is equal to 0.44 radical/100 eV at 25°, including both normal and secondary propyl radicals.

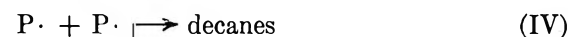
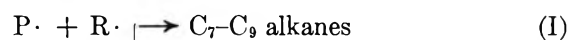
As stated above, we assume that the unscavengable yields of all products would be found to be identical at 25° and -78°, were it possible to employ the scavenger with equal efficiencies at both temperatures. Proceeding as before, we include step 17, but steps 3, 5,



8, 11, and 13 may be deleted because of the absence of propylene among homogeneous radical products at -78°. Thus,  $G(\text{propyl radicals}) = \Delta G(\text{propane})_{I_2^{-78^\circ}} + \Delta G(\text{octanes})_{I_2^{-78^\circ}} + \Delta G_2 + \Delta G_4 + 2\Delta G_7 + \Delta G_9 - \Delta G_{15} - \Delta G_{16}$  at -78°. The observed distribution of secondary and primary pentyl and propyl radicals among the "scavengable" octanes at -78° indicates that the hexanes are formed by combination of pentyl and methyl radicals as well as by reaction 7. The pentyl-methyl contribution equals 0.03 molecule/100 eV, and it follows that  $\Delta G_7 = 0.04$  molecule/100 eV.  $\Delta G_4$ ,  $\Delta G_9$ , and  $\Delta G_{15}$  equal 0.04, 0.008, and 0.008 molecule/100 eV, respectively. Since 25% of butyl radicals appearing in "scavengable" nonanes are secondary radicals, and since neither 3-methylheptane nor 3,4-dimethylhexane is formed at either temperature, reaction 16 may again be neglected. Since the pentyl-methyl contribution comprises 60% of the "scavengable" hexanes,  $\Delta G_2 = (0.6)\Delta G(\text{hexanes})\Delta G(\text{octanes})/2\Delta G(\text{decane}) = 0.004$  molecule/100 eV. The total yield of homogeneous propyl radicals at -78° appears, therefore, to be 0.42 radical/100 eV—a value identical within experimental error with that at 25°. Since there is no evidence that these values may or should differ, it may be concluded that the yield decrements,  $\Delta G(i)_{I_2^{-78^\circ}}$ , do in fact comprise homogeneous radical-radical con-

tributions at -78°. Computation of homogeneous butyl radical yields is equally straightforward.

*Homogeneous Pentyl Radicals.* The total 100-eV yield of scavengable pentyl radicals at 25° is computed by observing that pentyl radicals form only scavengable  $C_7$ - $C_9$  alkanes, decanes, and pentenes by processes I-V at low dose.



$\Delta G_{II}$ ,  $\Delta G_{III}$ , and  $\Delta G_V$  cannot be evaluated separately. Disproportionation steps II and III are, however, of roughly equal probability,<sup>30</sup> *i.e.*,  $2\Delta G_{II} \simeq \Delta G_{II} + \Delta G_{III}$ . Thus, since the yields of processes II and III are necessarily small we have, to a good approximation,  $G(\text{pentyl radicals}) = \Delta G(\text{C}_7\text{-C}_9 \text{ alkanes}) + 2\Delta G(\text{decane}) + 2\Delta G(\text{pentene}) = 3.6$  radical/100 eV at 25°, including pentyl radicals formed by abstraction reactions. Indications that  $I_2$  quenches molecular detachment of  $H_2$  in irradiated liquid cyclohexane<sup>32</sup> and decreases  $G(H_2)$  to an extent beyond that attributable to scavenging of thermal H atoms in pentane suggest that the assumption that  $I_2$  does not interfere with "molecular" processes and other fast reactions may be particularly questionable as a basis for computing yields of pentyl radicals. This follows from the reasonable expectation that "molecular"  $H_2$  and the pentenes may have a common scavengable precursor. We have observed, however, that although  $G(H_2)$  for *n*-pentane decreases steadily with  $I_2$  concentration up to 4 mM, the yields of hydrocarbon products, including each of the pentenes, do not. It is clear that the observed decrease of  $G(H_2)$  in this concentration range is not caused by inhibition of molecular detachment steps. These observations also demonstrate either the absence of interference with nonradical reactions or complete inhibition of one or more nonradical steps below 0.5 mM. The latter possibility would require occurrence of reactions with efficiencies exceeding that of a diffusion-controlled reaction of  $I_2$  with affected nonradical precursors.<sup>33</sup> Clearly, quenching of neutral

(30) S. W. Benson and W. B. DeMore, *Ann. Rev. Phys. Chem.*, **16**, 413 (1965).

(31) J. O. Terry and J. H. Futrell, private communication of results taken in part from the M.S. dissertation of J. O. T., Air Force Institute of Technology, 1964.

(32) P. J. Dyne and W. M. Jenkinson, *Can. J. Chem.*, **39**, 2163 (1961).

(33) The reaction of  $I_2$  with H atoms appears to be diffusion controlled in liquid alkanes at room temperature [*cf.*, *e.g.*, D. Perner and R. H. Schuler, *J. Phys. Chem.*, **70**, 317 (1966), and I. Mani and R. J. Hanrahan, *ibid.*, **70**, 2233 (1966)].  $(k_{H+I_2})/(k_{H+RH})$  may be roughly estimated to be of the order  $10^3$  with the aid of values for  $(k_{H+H}/k_{H+I_2})$  and  $(k_{T+T}/k_{T+RH})$  reported by these authors, and  $k_{H+I_2}$  is of the order  $10^{10} M^{-1} \text{sec}^{-1}$ .



precursors by  $I_2$  does not occur in *n*-pentane. However, "superdiffusional" processes similar to those observed in solutions of aromatic molecules in halogenated alkanes,<sup>34,35</sup> such as charge or proton transfer from alkane cations to  $I_2$ , cannot be summarily ruled out. Even in the unusually efficient transfer of charge from  $RCI^+$  ions to neutral aromatics, however, the range of concentration in which the aromatic solute competes significantly<sup>34,35</sup> lies an order of magnitude above the range in which such hypothetical reactions of  $I_2$  must go to completion in *n*-pentane. Recent work also appears to demonstrate that  $I_2$  is incapable of scavenging electrons other than, possibly, the "free-ion" yield in hydrocarbons<sup>36</sup> below 1 mM, suggesting that significant direct or indirect interference with neutralization steps is also unlikely.

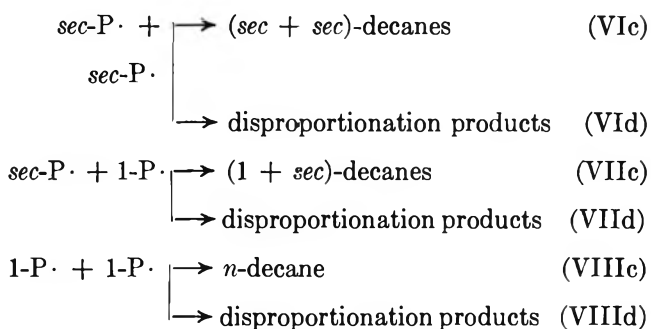
At  $-78^\circ$   $G(\text{pentyl radicals})$  equals the  $25^\circ$  yield minus the contribution of abstraction steps at  $25^\circ$ . The contribution of abstraction to  $G(\text{pentyl radicals})$  equals the sum over  $\Delta G(i)_T$  values for  $H_2$ ,  $CH_4$ ,  $C_2H_6$ , and  $C_3H_8$  (0.93 radical/100 eV). Thus,  $G(\text{pentyl radicals})_{-78^\circ} = 3.6 - 0.93 = 2.7$  radical/100 eV.

Relative yields of homogeneous 2-pentyl and 3-pentyl radicals may be determined from measured yields of scavengable heptane isomers (3-methylhexane, 3-ethylpentane) and octane isomers (4-methylheptane, 3-ethylhexane) and yields of homogeneous ethyl and *n*-propyl radicals. The ratio of rate constants for combination of 2-pentyl radicals with ethyl and *n*-propyl radicals, respectively, is given by  $(k_{c,2PEt}/k_{c,2PPr}) = [G(n\text{-Pr})/G(Et)][\Delta G(3\text{-methylhexane})_{I_2^T}/\Delta G(4\text{-methylheptane})_{I_2^T}]$  and is equal to 1.1 at  $25^\circ$  and 1.2 at  $-78^\circ$ , assuming the same relative yields of normal and secondary propyl radicals at  $25^\circ$  and  $-78^\circ$ . Similarly,  $(k_{c,3PEt}/k_{c,3PPr}) = [G(n\text{-Pr})/G(Et)][\Delta G(3\text{-ethylpentane})_{I_2^T}/\Delta G(3\text{-ethylhexane})_{I_2^T}]$ , and is equal to 1.1 at  $25^\circ$  and 1.3 at  $-78^\circ$ . It follows that the ratio of steady-state concentrations, (2-P)/(3-P), is given by either of the expressions,  $(k_{c,3PEt}/k_{c,2PEt})[\Delta G(3\text{-methylhexane})_{I_2^T}/\Delta G(3\text{-ethylpentane})_{I_2^T}]$  or  $(k_{3c,PPr}/k_{c,2PPr})[\Delta G(4\text{-methylheptane})_{I_2^T}/\Delta G(3\text{-ethylhexane})_{I_2^T}]$ . Thus, (2P)/(3P) equals  $2.1 \pm 0.05$  at  $25^\circ$  and  $2.0 \pm 0.2$  at  $-78^\circ$ , assuming, of course, that 100-eV yields are proportional to the corresponding steady-state radical concentrations in each instance.

Neither the absolute yields nor the ratio of yields of primary and secondary pentyl radicals can be determined without estimates of  $k_d/k_c$  ratios for pentyl radical reactions. The required value for that mixture of pentyl radicals present in irradiated pentane is simply the ratio,  $G_V/G_{IV}$ .  $G_{IV} = 0.90$  molecule/100 eV.  $G_V$  equals the scavengable yield of pentenes less  $G_{II}$ .  $G_{II}$  is not measurable, but may be estimated with sufficient accuracy as follows. The distribution weighted average value of the disproportionation to combination ratio for homogeneous reactions of pentyl radicals with other radicals (ethyl, propyl, butyl) is assumed to lie within

the range of observed values of a variety of primary and secondary alkyl radical-radical reactions in the gaseous phase, *i.e.*, 0.10–1.0.<sup>35–42</sup> Since  $G_I$  equals 0.48 molecule/100 eV,  $G_{II}$  must lie between 0.048 and 0.48 molecule/100 eV. Thus, the needed weighted average  $k_d/k_c$  value for pentyl + pentyl radical reactions must lie between 0.74 and 1.2. Now  $k_d/k_c$  values for secondary radicals in the gaseous phase are consistently greater than those for primary radicals by factors ranging from 6 to 10.<sup>35–43</sup> Thus, the ratio of secondary to primary pentyl radicals appearing among scavengable combination products probably does not exceed the ratio,  $G(\text{sec-P})G/(1\text{-P})$ . Values of the former ratio are 13.5/1.00 at  $25^\circ$  and 4.53/1.00 at  $-78^\circ$ . It is, therefore, apparent that the estimated range of  $k_d/k_c$  values pertains to a population consisting predominantly of secondary pentyl radicals at both temperatures.<sup>44</sup>

Processes VIc through VIIId include all homogeneous pentyl + pentyl radical reactions at low conver-



sions. Defining each 100-eV yield as  $G(\text{scavengable product})$  we have, as before

$$G_{VII} = 2(G_{VI}G_{VIII})^{1/2}$$

and it follows that

$$\frac{G(\text{sec-P}\cdot)}{G(1\text{-P}\cdot)} = \frac{G_{VIc}(1 + k_{VIId}/k_{VIc}) + [G_{VIc}G_{VIIc}]}{(1 + k_{VIc}/k_{VIc})(1 + k_{VIIId}/k_{VIIc})^{1/2}} \frac{G_{VIIc}(1 + k_{VIIId}/k_{VIIc}) + [G_{VIc}G_{VIIc}]}{(1 + k_{VIId}/k_{VIc})(1 + k_{VIIId}/k_{VIIc})^{1/2}}$$

where  $G_{VIc}$  and  $G_{VIIc}$  are measured quantities.

(34) R. Cooper and J. K. Thomas, *Advances in Chemistry Series*, No. 82, American Chemical Society, Washington, D. C., 1968, p 351.

(35) S. Arai, H. Ueda, R. F. Firestone, and L. M. Dorfman, *J. Chem. Phys.*, **50**, 1072 (1969).

(36) R. H. Schuler, private communication with W. P. B.

(37) J. G. Calvert, *Ann. Rev. Phys. Chem.*, **11**, 41 (1960).

(38) J. A. Garcia Dominguez, J. A. Kerr, and A. F. Trotman-Dickinson, *J. Chem. Soc.*, 3557 (1962).

(39) R. A. Holroyd and G. W. Klein, *J. Phys. Chem.*, **67**, 2273 (1963).

(40) R. A. Holroyd and T. C. Pierce, *ibid.*, **68**, 1392 (1964).

(41) W. E. Morganroth and J. G. Calvert, *J. Amer. Chem. Soc.*, **88**, 5387 (1966).

(42) D. H. Slater and J. G. Calvert, *ibid.*, **90**, 268 (1968).

(43) M. H. J. Wijnen, *ibid.*, **83**, 3752 (1961).

(44) Wijnen<sup>43</sup> has estimated consistently that  $k_d/k_c$  is about 0.2 for 1-pentyl radicals in the gaseous phase.

$G(\text{sec-P}\cdot)/G(\text{1-P}\cdot)$  is thus found to lie between 13 and 14 at 25° and between 3.9 and 4.2 at -78°, and is fortunately quite insensitive to the choice of  $k_d/k_c$  values. The 100-eV yields of 1-pentyl, 2-pentyl, and 3-pentyl radicals may, therefore, be evaluated to two significant figures with reasonable certainty.

**Homogeneous Ethyl and Methyl Radical Yields.** The contribution of ethyl radicals to butane at 25° is estimated by observing that, since no isobutane is formed, the only significant source of scavengable butane alternative to ethyl + ethyl is the disproportionation reaction of butyl and pentyl radicals. The other disproportionation path of butyl and pentyl radicals forms butylene, and we assume that  $k_d/k_c$  for both disproportionation steps is equal to  $\Delta G(\text{butylene})/\Delta G(\text{nonanes})$ . Thus, the 100-eV yield of butane attributable to scavengable ethyl radicals is 0.02 molecule/100 eV. Proceeding otherwise as before we find that the 100-eV yield of homogeneous ethyl radicals at 25° is 0.50 radical/100 eV. At -78° the contribution of ethyl radicals to butane appears to be insignificant, because  $\Delta G(\text{butane})$  from combination of propyl and methyl radicals is equal to  $(0.6)\Delta G(\text{hexanes})\Delta G(\text{octanes})/2\Delta G(\text{decane}) = 0.013$  molecule/100 eV, and  $\Delta G(\text{butane})$  formed by disproportionation of butyl radicals is 0.010 molecule/100 eV, which limits the ethyl contribution to about 0.004. The latter estimate assumes the value of  $k_d/k_c$  measured for ethyl radicals in isooctane at -78°. <sup>45</sup>

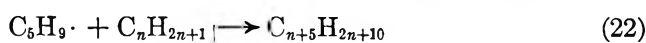
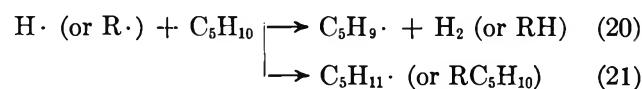
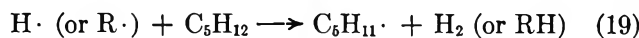
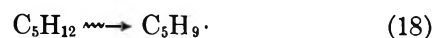
The 100-eV yield of homogeneous methyl radicals at -78° is found by means of the appropriate procedure illustrated previously for propyl radicals to equal 0.18 radical/100 eV less the contribution of disproportionation steps to the ethane yield, <sup>45</sup> *i.e.*,  $0.18 - (0.087)G(\text{ethyl radical}) = 0.15$  radical/100 eV. The value for  $G(\text{methyl radical})$  at 25° must be  $> \Delta G(\text{CH}_4)_T$  and  $< \Delta G(\text{CH}_4)_I$ , <sup>25°</sup>, or 0.12 radical/100 eV at 25°.

**Homogeneous Thermal H Atoms.** Estimates of the 100-eV yield of thermal H atoms include:  $G(\text{H}) = G(\text{HI}) = 0.33$  atom/100 eV in the presence of  $\text{I}_2$ , <sup>16</sup> 4.25 atoms/100 eV, the scavengable yield of  $\text{H}_2$  in the presence of methyl methacrylate; <sup>20</sup> and 1.3 atoms/100 eV, by means of a radical-sampling technique employing  $^{14}\text{CH}_3\text{I}$  and ethylene as reactive solutes. <sup>19</sup> Experiments with solutes which react readily with H atoms have not provided a clean distinction between the so-called molecular and atomic hydrogen yields, because of interference with precursors of both forms. <sup>46,47</sup>  $G(\text{HI})$  is clearly an unreliable measure of  $G(\text{H})$  in pentane as well as in liquid cycloalkanes. <sup>48</sup> It is clear from this and other <sup>23</sup> work that electron attaching solutes profoundly alter several  $\text{H}_2$  forming mechanisms in pentane. Other investigators <sup>15,49</sup> have found that the presence of alkyl iodides disturbs radical-forming mechanisms in general.

In the present work the observation that  $G(\text{H}_2)$  is independent of dose within a few per cent in the

vicinity of  $1.42 \times 10^{20}$  eV/g suggests that the abstraction reaction consumes more than 90% of thermal H atoms formed as of that dose at 25°, if we assume reasonably that  $G(\text{H})$  lies between 0.5 and 1.5 atoms/100 eV. Furthermore, it can be shown that about 95% of thermal H atoms shall have abstracted hydrogen from pentane at this dose. <sup>50</sup> Thus,  $G(\text{H}) \simeq \Delta G(\text{H}_2)_T/0.95 = 0.7 \pm 0.2$  atom/100 eV. <sup>51</sup>

**Homogeneous Pentenyl Radicals.** The 100-eV yields of  $\text{C}_6$ - $\text{C}_{10}$  alkenes begin to increase with dose at 0.2% conversion. Absence of products of more than ten C atoms precludes the possibility that these alkenes are radical disproportionation products, and the observation that they are not formed in the presence of  $\text{I}_2$  suggests that their precursors are homogeneous free radicals. The suggestion that the higher alkenes are formed by alkyl + alkenyl radicals in irradiated liquid *n*-hexane, <sup>27</sup> the identification of pentenyl radicals in irradiated liquid *n*-pentane, <sup>17</sup> and our observations suggest that the  $\text{C}_6$ - $\text{C}_{10}$  alkenes are formed by the following homogeneous free-radical mechanism.



Reaction 23 may be disregarded at doses below  $10^{21}$  eV/g because of the absence of diene products. Thus,

(45) M. Matsuoka, P. S. Dixon, A. P. Stefani, and M. Szwarc, *Proc. Chem. Soc.*, 304 (1962).

(46) C. E. Klots, Y. Raef, and R. H. Johnsen, *J. Phys. Chem.*, **68**, 2040 (1964).

(47) P. J. Dyne, J. Denhartog, and D. R. Smith, *Discuss. Faraday Soc.*, **36**, 135 (1963).

(48) S. Z. Toma and W. H. Hamill, *J. Amer. Chem. Soc.*, **86**, 1478 (1964).

(49) W. G. Burns, R. A. Holroyd, and G. W. Klein, *J. Phys. Chem.*, **70**, 921 (1966).

(50) Let  $f$  = the instantaneous fraction of thermal H atoms reacting with alkenes at dose  $D$ . Since the concentration of each alkene product is a linear function of dose in the range of immediate interest,  $f = (bD)/(bD + a)$ , and  $\bar{f} = \int_0^D [bD/(bD + a)] dD/D$ . The constant  $b$  is equal to a sum of terms,  $(10G_i\rho/A)(k_i/k_a)$ , including one such term for each alkene product, where  $G_i$  is the 100-eV yield of alkene  $i$ ,  $\rho$  is the density of *n*-pentane,  $A$  is Avogadro's number,  $k_i/k_a$  is the ratio of rate constants for addition of H atoms to alkene  $i$  and abstraction from pentane (Hardwick's values were measured in *n*-hexane at 23°, and Holroyd's value for ethylene <sup>19</sup> was measured in *n*-pentane at 23°; the value for ethylene has been assumed for all  $\text{C}_2$ - $\text{C}_4$  alkenes and that for decene-1 is assumed for all  $\text{C}_5$ - $\text{C}_{10}$  alkenes), and  $a$  is the molar concentration of pentane at 25°. The value of  $b$  is  $8.56 \times 10^{-21}$  eV  $M/g$ . The rate constant values employed are based on the assumption <sup>27</sup> that effects of alkenes on  $G(\text{H}_2)$  may be attributed entirely to H atom scavenging, and the values of  $f$  so computed must be considered an upper limit.

(51) Koch, Houtman, and Cramer <sup>23</sup> report that  $\bar{G}(\text{H}_2)$  increases about 0.7 molecule/100 eV (*cf.* Figure 1, ref 23) between -78° and 100°. The higher upper temperature required for quantitative abstraction in their experiments may have been caused by working to higher conversions.

Table II: 100-eV Yields of Homogeneous Free Radicals

	Hydrocarbon yield decrement <sup>a</sup>			Method		Alkyl iodide yields		<sup>14</sup> C <sub>2</sub> H <sub>5</sub> sampling <sup>b</sup>	
				Additive					
	I <sub>2</sub>			[Additive], mM				<sup>14</sup> C <sub>2</sub> H <sub>5</sub>	
	0.5-4	0.5-4	0.5-1.0 <sup>c</sup>	22 <sup>d</sup>	Temp, °C	5 <sup>e</sup>	0.5-4 <sup>e</sup>	~1	~1
25	-78	RT <sup>h</sup>	RT		20	25	10	-70	
Methyl	0.12	0.15	0.14	0.50	0.43	...	0.10	...	
Ethyl	0.50	0.34	...	1.16	0.49	0.43	0.51	0.56	
<i>n</i> -Propyl	} 0.44	} 0.42	...	0.84	0.41	0.39	0.36	(0.36) <sup>f</sup>	
<i>sec</i> -Propyl			...	0.06	...	...	0.04	...	
<i>n</i> -Butyl	0.06	} 0.09	...	0.08	0.065	0.26-0.07	0.07	...	
<i>sec</i> -Butyl	0.03		...	...	0.04	...	...	...	
1-Pentyl	0.25	0.53	...	1.4	...	0.52	0.98	1.04	
2-Pentyl	2.3	1.5	...	2.8	0.83	1.6-1.2	2.21	1.47	
3-Pentyl	1.1	0.73	...	1.4	...	0.65	1.10	0.77	
Pentenyl	0.06	...	...	...	...	...	~0.05 <sup>g</sup>	...	

<sup>a</sup> <sup>60</sup>Co  $\gamma$  rays,  $1.42 \times 10^{20}$  eV/g at  $7.0 \times 10^{18}$  eV/g min (this work). <sup>b</sup> 2-MeV electrons,  $1.9 \times 10^{21}$  eV/g min, dose not reported (ref 17). <sup>c</sup> <sup>60</sup>Co  $\gamma$  rays,  $2.6 \times 10^{16}$  eV/g min, dose not reported (ref 25). <sup>d</sup> <sup>60</sup>Co  $\gamma$  rays, (2 to 8)  $\times 10^{19}$  eV/g at (1.0 to 1.5)  $\times 10^{18}$  eV/g min (ref 15). <sup>e</sup> Radiation quality, dose, and dose rate not reported (ref 16). <sup>f</sup> Values in this column are relative values normalized to an assumed value of 0.36 for  $G(n\text{-propyl})$  at  $-70^\circ$  (ref 17). <sup>g</sup> Estimated as approximately 1% of  $G(\text{total radicals})$  (ref 17). <sup>h</sup> Room temperature.

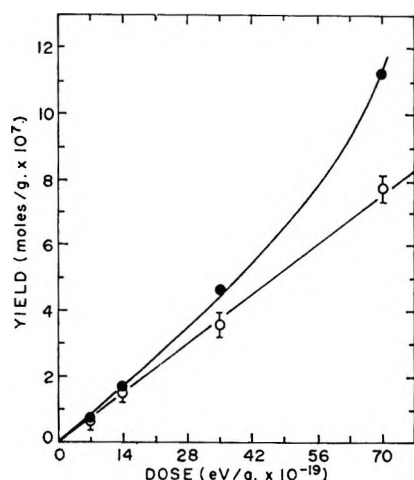


Figure 4. Total yield of higher (C<sub>6</sub>-C<sub>10</sub>) alkenes (upper curve) and a computed primary radiolytic yield of pentenyl radicals (lower curve) as functions of dose.

the yield of C<sub>5</sub>H<sub>9</sub> radicals equals the sum of yields of the C<sub>6</sub>-C<sub>10</sub> alkenes. The fraction of H atoms which shall have abstracted from pentene-1, for example, as of dose  $D$  is given by the expression  $[k_{20}/k_{19}(\text{pentane})] \int_0^D (\text{pentene-1}) dD$ , since  $k_{19}(\text{pentane}) \gg (k_{20} + k_{21})$  (pentene-1) at all dose values of interest. Similar expressions represent the fractions of H atoms consumed by abstraction from the pentene-2 isomers and the fractions of C<sub>1</sub>-C<sub>3</sub> radicals which shall have abstracted from the several pentenes as of dose  $D$ . The sum of all such terms has been estimated by assuming values for  $k_{20}/k_{19}$  assigned<sup>27</sup> to H atom reactions with *n*-hexane and corresponding hexenes at 23° and by

graphical integration of plots of the pentene concentrations as functions of dose. The product of the resulting sum and the number of moles of H atoms formed per gram of pentane as of dose  $D$  differs from the measured sum of C<sub>6</sub>-C<sub>10</sub> alkene yields (mol/g) shown as a function of dose in the upper curve of Figure 4 by an amount equal to the integrated primary radiolytic yield of pentenyl radicals at dose,  $D$ . The slope of the plot of this difference shown in the lower curve of Figure 4 is constant and corresponds to an instantaneous primary radiolytic yield equal to  $0.06 \pm 0.02$  pentenyl radical/100 eV,  $G_{18}$ .

Table II is a summary of 100-eV radical yields in pure *n*-pentane at 25° and -78° from this investigation (columns 2 and 3), in the presence of ethylene at 10° and -70° from Hclroyd and Klein,<sup>17</sup> (columns 8 and 9) and of alkyl iodide yields in the presence of I<sub>2</sub> from this work (column 7; see also Figure 2) and from earlier work (columns 4, 5, and 6). Comparison provides a measure of the dependability of the three methods of estimating homogeneous radical yields in liquid alkanes, *i.e.*, the <sup>14</sup>C<sub>2</sub>H<sub>5</sub> radical-sampling method,<sup>17</sup> the alkyl iodide method, and the present method which is referred to as the hydrocarbon yield decrement method. Agreement between results of the radical sampling and hydrocarbon yield decrement methods is excellent with a major exception in the case of 1-pentyl radicals and a minor one for ethyl radicals at low temperature. At first glance agreement among secondary pentyl radical yields might seem surprising, because the presence of ethylene must preferentially lower the yields of secondary pentyl radicals by H atom scavenging in the radical sampling experiments. The discrepancy should not and does not, however, exceed approximately

0.1–0.2 radical/100 eV, at the lowest ethylene concentrations employed.<sup>52,53</sup>

The relatively large discrepancies among 1-pentyl radical yields from the radical-sampling and hydrocarbon yield decrement experiments are difficult to understand. There is no apparent reason why the former method should overestimate nor why the latter should underestimate  $G(1\text{-pentyl})$ . If the pentyl iodide yields at 25° are well behaved with respect to  $(I_2)$ , one expects them to agree with corresponding pentyl radical yields at –78° in the absence of  $I_2$ . Figure 2 and the observed coincidence of these values may indicate that the  $G(1\text{-pentyl})$  values of columns 2 and 3 should be taken more seriously than those measured by  $^{14}C_2H_5$  radical sampling. The apparent decrease in  $G(1\text{-pentyl})$  with increasing temperature (column 3) must then be tentatively attributed to hydrogen abstraction from pentane by 1-pentyl radicals, thereby accounting for 0.3 additional *sec*-pentyl radical/100 eV and leaving 0.9 additional *sec*-pentyl radical/100 eV to be formed by H atom and  $C_1$ – $C_3$  radical abstraction of hydrogen at 25°. ( $\Delta G(H_2)_T + \Delta G(CH_4)_T + \Delta G(C_2H_6)_T + \Delta G(C_3H_8)_T$ ).

Comparison of values reported in Table II for each of the  $C_1$ – $C_4$  alkyl iodide yields indicates, consistent with advice given over a decade ago,<sup>54</sup> that alkyl iodide yields cannot as a rule be equated with yields of the corresponding radicals at  $I_2$  concentrations exceeding approximately 1 mM. Thus,  $G(\text{methyl iodide})$  coincides with  $G(\text{methyl})$  in the range 0.5–1 mM but greatly exceeds it at higher concentrations. The ethyl iodide yield exceeds that of ethyl radicals by a factor

of 2 at 22 mM, is equal to it at 5 mM, and appears to be 14–20% low between 0.5 and 4 mM. Similarly,  $G(n\text{-propyl iodide})$  exceeds  $G(n\text{-propyl})$  by a factor of 2 at 22 mM, but is equal to  $G(n\text{-propyl})$  at 0.5–4 mM. On the other hand, data illustrated in Figure 2 and summarized in Table II indicate that alkyl iodide yields may not always be equated with radical yields even at low  $I_2$  concentrations. The discrepancy is most pronounced with *n*-butyl iodide at  $(I_2)$  less than 1 mM, for which  $G(n\text{-butyl iodide})$  exceeds  $G(n\text{-butyl})$  by a factor of 4. Unexpectedly,  $G(n\text{-butyl iodide})$  approaches  $G(n\text{-butyl})$  as  $(I_2)$  increases beyond 1 mM, and the two quantities appear to coincide only at  $I_2$  concentrations exceeding 4 mM. It is, therefore, apparent that there is no  $I_2$  concentration range in *n*-pentane within which the alkyl iodide method is reliable with reasonable consistency.

*Acknowledgments.* The authors thank Ludwig Sprandel for help in measurement of the pentene-2 yields. W. P. B. is also grateful to The Chrysler Corp. and to The U. S. Department of Health, Education, and Welfare for fellowship support (NDEA, Title IV). This work has been partially supported by The U. S. Atomic Energy Commission (Contract AT-(11-1)-1116).

(52) R. A. Holroyd and G. W. Klein, *Int. J. Appl. Radiat. Isotop.*, **13**, 493 (1962).

(53) Note that  $G(^{14}C_2H_5\cdot)$  cannot literally be as large as 0.1, as stated in ref 52; this value must be the total number of H atoms which have added to ethylene/100 eV which equals  $G(^{14}C_2H_5\cdot)$  only in presence of carrier-free  $^{14}C_2H_4$ .

(54) R. H. Schuler, *J. Phys. Chem.*, **62**, 37 (1958).

## Photolysis of 3-Pentanone-2,2,4,4-*d*<sub>4</sub>

by Charles I. Barta<sup>1</sup> and Alvin S. Gordon

Research Department, Chemistry Division, Naval Weapons Center, China Lake, California 93555  
(Received August 22, 1969)

The photolysis of CH<sub>3</sub>CD<sub>2</sub>COCD<sub>2</sub>CH<sub>3</sub> has been studied over the temperature range from 20 to 407°. The ethyl-*d*<sub>2</sub> radicals produced in the primary-primary process can combine, disproportionate, and/or abstract an α-D or a β-H from the starting ketone. The disproportionation combination ratio was studied in the range 20–150° and a small negative temperature coefficient was noted for the ratio, confirming the observations of other workers and extending the effect to higher temperatures. The abstraction processes were studied in the range 150–407°. The specific rate constants for the abstraction of an α-D and β-H by ethyl radical were

$$k_{\alpha D} = 10^{8.5 \pm 0.05} 10^{-10,300 \pm 170/4.58T} M^{-1} \text{ sec}^{-1}$$

$$k_{\beta H} = 10^{8.7 \pm 0.40} 10^{-12,400 \pm 1,500/4.57T} M^{-1} \text{ sec}^{-1}$$

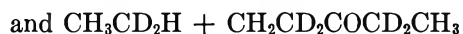
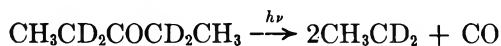
The two pentanonyl radicals formed in the abstraction reactions, CH<sub>2</sub>CD<sub>2</sub>COCD<sub>2</sub>CH<sub>3</sub> and CH<sub>3</sub>CDCOCD<sub>2</sub>CH<sub>3</sub>, can decompose to give ethene-*d*<sub>2</sub> and -*d*<sub>1</sub>, respectively, and ethyl-*d*<sub>2</sub> radicals. By studying the rates of formation of the ethenes, it was concluded that the radical CH<sub>3</sub>CDCOCD<sub>2</sub>CH<sub>3</sub> undergoes an internal rearrangement in competition with its decomposition at temperatures above 300°. This rearrangement product decomposes to give ethene-*d*<sub>2</sub> and ethyl-*d*<sub>1</sub> radicals. A possible rearrangement mechanism is discussed.

### Introduction

The photolysis of 3-pentanone-2,2,4,4-*d*<sub>4</sub> provides a convenient source of partially deuterated ethyl radicals for studying the kinetics of ethyl radical reactions with molecules R-H. For this purpose, however, one must know the kinetics of the reactions of the radical with the parent molecule.

The only previous study of this system was reported by Wijnen and Steacie.<sup>2</sup> Due to relatively low experimental accuracy available with analytical techniques and purity of deuterated compounds at that time, the parameters they report for the ethyl radical abstraction reactions are questionable. We therefore decided to reinvestigate the system.

The following are important elementary reactions in this system.

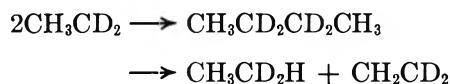


The interesting chain propagation steps involving the reactions of the pentanonyl radicals are studied in lesser detail in this work.

### Results and Discussion

The disproportionation-combination rates for the ethyl-*d*<sub>2</sub> radicals were determined from the relative rates of formation of butane-*d*<sub>4</sub>, ethane-*d*<sub>2</sub>, and ethene-

*d*<sub>2</sub> in the photolysis of 3-pentanone-2,2,4,4-*d*<sub>2</sub> (DEK) at temperatures from 20 to 150°. The reactions involved are



Between 20 and 88° inclusive, pure ethane-*d*<sub>2</sub> with an equal amount of ethene-*d*<sub>2</sub> is formed. Since ethane-*d*<sub>3</sub> would be the predominant product from ethyl radical abstraction, abstraction reactions are not important for our experimental conditions; the disproportionation-combination ratio was calculated from the ratio of the amounts of ethane-*d*<sub>2</sub> and butane-*d*<sub>4</sub> formed. When the temperature range is extended to 150°, ethane-*d*<sub>3</sub> is found in the products, and ethene-*d*<sub>2</sub> rather than ethane-*d*<sub>2</sub> must be used as the monitor for disproportionation reaction of the ethyl radicals.

A plot of the disproportionation combination ratios as a function of temperature is shown in Figure 1. A slight inverse temperature effect on the ratio is noted.<sup>3</sup> This may be interpreted as a negative temperature coefficient for the disproportionation rate constant. An explanation involving activation barriers is not suitable because if any barrier exists, the disproportionation barrier involving H atom transfer is almost certainly higher than the combination barrier and would result in a temperature effect opposite to that observed.

To determine the abstraction reactions above 150°, it

(1) National Research Council Postdoctoral Research Associate.

(2) M. H. J. Wijnen and E. W. R. Steacie, *Can. J. Chem.*, **29**, 1092 (1951).

(3) P. S. Dixon, A. P. Stefani, and M. Szwarc, *J. Amer. Chem. Soc.*, **85**, 2551 (1963), observe the same effect.

**Table I:** The Rates of Formation of Products and Product Isotope Composition in the Photolysis of 3-Pentanone-2,2,4,4- $d_4$ 

Temp, °C	Time, min	(DEK) $M \times 10^4$	Rates of formation ( $M \text{ sec}^{-1} \times 10^6$ )			Isotope composition (%)							
			Ethene	Ethane	Butane	$d_2$	Ethene $d_1$	$d_3$	Ethane $d_2$	$d_1^a$	$d_4$	Butane $d_3$	$d_2^a$
150	3.0	7.9	0.70	0.94	5.8	100	...	24.2	75.8	...	100	...	...
153	15.0	7.9	0.73	0.97	6.9	100	...	26.0	74.0	...	100	...	...
153	3.3	7.9	0.68	1.03	6.5	100	...	25.9	74.1	...	100	...	...
153	5.0	7.9	0.71	1.00	6.3	100	...	29.0	71.0	...	100	...	...
180	3.3	7.4	n.m.	0.96	4.5	100	...	37.6	62.4	...	100	...	...
183	13.5	7.4	0.57	0.99	4.8	100	...	42.5	57.5	...	100	...	...
207	16.1	7.0	0.71	1.51	6.3	100	...	53.6	46.4	...	100	...	...
209	10.0	7.0	0.65	1.51	5.9	100	...	51.7	48.3	...	100	...	...
234	10.5	6.7	0.83	2.04	5.2	100	...	64.8	35.2	...	100	...	...
234	2.0	6.7	0.75	1.92	4.9	100	...	64.0	36.0	...	100	...	...
269	15.0	6.2	0.81	2.96	4.2	96.7	3.3	72.8	27.2	...	100	...	...
274	2.0	6.2	1.02	2.35	3.7	96.5	3.5	76.0	24.0	...	100	...	...
307	15.0	5.8	1.16	4.44	3.1	89.0	11.0	76.9	23.1	...	100	...	...
314	5.0	5.8	1.25	4.20	3.1	...	...	74.4	25.6	...	100	...	...
357	3.3	5.3	2.39	4.88	1.4	81.7	18.3	70.8	27.0	2.2	80.6	18.3	1.1
357	6.3	5.3	4.07	6.17	2.1	78.9	21.1	70.3	26.9	2.8	75.5	22.8	1.7
406	6.3	5.0	9.10	10.91	2.5	80.6	19.4	57.0	38.0	5.0	63.8	32.2	4.0
405	2.0	5.0	12.58	15.24	2.8	82.0	18.0	51.0	41.1	7.9	44.6	44.2	11.2

<sup>a</sup> As calculated.

was necessary to correct for the contribution of ethane- $d_2$  formed by disproportionation. The amount of disproportionation ethane- $d_2$  was calculated from the  $k_{dis}/k_{comb}$  ratio taken as 0.10. At temperatures above 300°, the situation is further complicated by the fact that ethyl- $d_1$  radicals are present in the system and disproportionate to form ethane- $d_1$ . Fortunately, at the temperatures where ethyl- $d_1$  reactions are important, the rate of ethane formed by disproportionation is negligible compared to that by abstraction and can be ignored.

**Ethyl Radical Abstraction Reactions.** The rate constants for ethyl abstraction reactions in the range 150–407° were determined using the rates of formation of the various ethanes and butanes. The rates of formation of total ethane, ethene, and butane are reported in Table I. The rates at any one temperature depend on the light flux through the reaction vessel but the calculated rate constants are intensity independent, as was shown by Wijnen and Steacie.<sup>2</sup>

The deuterium contents of the ethene, ethane, and butane products were determined for the photolyses from 150 to 406°. At temperatures up to 314°, the butane product consisted entirely of butane- $d_4$ . At 357° and above, butane- $d_3$  was observed. This product is formed by the combination ethyl- $d_2$  and ethyl- $d_1$  radicals. The presence of ethyl- $d_1$  radicals predicts butane- $d_2$  to be a product of the photolysis. The direct mass spectral quantitative determination of this product is not feasible because the butane- $d_2$  parent peak ( $m/e$  60) is contaminated by the fragment peaks of butane- $d_3$  and - $d_4$ . Even if a butane- $d_3$  mass spectral standard had been available, the parent of butane- $d_2$  accounts for only a very small percentage of the total  $m/e$  60 peak

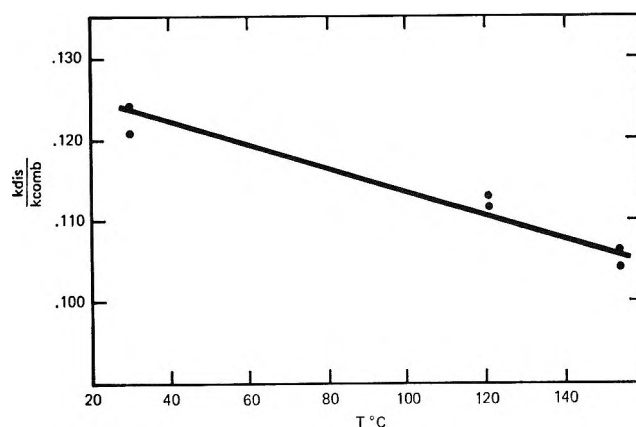


Figure 1. Plot of the ratio of ethyl- $d_2$  radical disproportionation to combination vs. temperature.

and small measurement errors would result in a very large relative error in the butane- $d_2$  determination. For similar reasons, the amount of ethane- $d_1$  could not be accurately determined.

We found it expedient to calculate the amounts of butane- $d_2$  and ethane- $d_1$  from the easily measured values of butane- $d_4$  and - $d_3$  and ethane- $d_3$  and - $d_2$  as determined by mass spectrometry.

From the rate expressions for the formation of butane- $d_4$ , - $d_3$ , and - $d_2$

$$R_{-d_4} = k_{d_4}(\text{ethyl-}d_2)^2$$

$$R_{-d_3} = k_{d_3}(\text{ethyl-}d_2)(\text{ethyl-}d_1)$$

$$R_{-d_2} = k_{d_2}(\text{ethyl-}d_1)^2$$

we can determine  $R_{-d_2}$  in terms of  $R_{-d_1}$  and  $R_{-d_3}$ , since it has been shown<sup>4</sup> that  $k_4 = k_2 = 1/2k_3$

$$R_{-d_2} = (1/4)(R_{-d_3}^2/R_{-d_4})$$

If the rates of formation of butane-*d*<sub>4</sub> and -*d*<sub>3</sub> are expressed in mass spectral peak heights/cm<sup>3</sup> sec, then the peak height/cm<sup>3</sup> sec of butane-*d*<sub>2</sub> is easily calculated.

The rate of formation of ethane-*d*<sub>1</sub> can now be calculated from the relative concentrations of the two ethyl radicals ( $2R_{-d_4}/R_{-d_3}$ ) and the measured values of the rates of formation of ethane-*d*<sub>3</sub> and -*d*<sub>2</sub> in mass spectral units/cm<sup>3</sup> sec as outline below.

Ethane-*d*<sub>3</sub> is formed only by an ethyl-*d*<sub>2</sub> abstracting an α-D atom from DEK. Ethane-*d*<sub>2</sub>, however, is formed in two abstraction processes; the abstraction of a β-H atom from DEK by ethyl-*d*<sub>2</sub> and the abstraction of an α-D atom by ethyl-*d*<sub>1</sub>. The ratio of α to β abstraction rates should be the same for ethyl-*d*<sub>2</sub> and ethyl-*d*<sub>1</sub>. The following relationship then exists

$$\frac{R_{\text{CH}_3\text{CD}_3}}{R_{\text{CH}_3\text{CD}_2\text{H}} - X} = \frac{X}{Y} = \frac{k_{\text{D abstraction}}}{k_{\text{H abstraction}}}$$

where *X* is the rate of formation, in mass spectral units, of ethane-*d*<sub>2</sub> formed by an α-D atom abstraction by an ethyl-*d*<sub>1</sub> and *Y* is the rate of ethane-*d*<sub>1</sub> formation. Another relation between *X* and *Y* may be determined from the ratio of the sum of the rate of products arising from ethyl-*d*<sub>2</sub> abstraction,  $R_{\text{CH}_3\text{CD}_3} + R_{\text{CH}_3\text{CD}_2\text{H}} - X$ , to the sum of the rates of formation of ethyl-*d*<sub>1</sub> products,  $X + Y$ . With the reasonable assumption that *k*<sub>H</sub> and *k*<sub>D</sub> are the same for the two kinds of ethyl radicals, the above ratio is seen to be equal to the ratio of the two radicals. Thus

$$\frac{R_{\text{CH}_3\text{CD}_3} + R_{\text{CH}_3\text{CD}_2\text{H}} - X}{X + Y} = \frac{(\text{CH}_3\text{CD}_2)}{(\text{CH}_3\text{CDH})} = \frac{X}{Y}$$

From the two expressions in *X* and *Y*, both quantities may be calculated. Since the total ethane and butane are known in conventional units from the measured areas of the calibrated gas chromatograph, the consistent arbitrary units of the various ethanes and butanes permit an easy conversion to conventional units.

The deuterium content of the ethene product was measured directly by mass spectrometry. The label contents for all products are given in Table I.

At temperatures up to 314°,  $R_{\text{butane-}d_4} = R_{\text{butane total}}$ , and from the relationships between the rate of formation of ethane-*d*<sub>3</sub> =  $k_{\text{D}}(\text{ethyl-}d_2)$  (DEK) and the rate of formation of butane =  $k_{\alpha}(\text{ethyl-}d_2)^2$ , the rate constant for α-D abstraction may be formulated

$$k_{\text{D}} = \frac{R_{\text{CH}_3\text{CD}_3}k_{\alpha}^{1/2}}{R_{d_4}^{1/2}(\text{DEK})}$$

The rate constant for the combination of two ethyl-*d*<sub>2</sub> radicals was taken to be the same as that for two ethyl radicals,<sup>5</sup>  $2 \times 10^{10} \text{ M}^{-1} \text{ sec}^{-1}$ . Similarly, the rate constant for β-H abstraction is

$$k_{\text{H}} = \frac{R_{\text{CH}_3\text{CD}_2\text{H}}k_{\alpha}^{1/2}}{R_{d_4}(\text{DEK})}$$

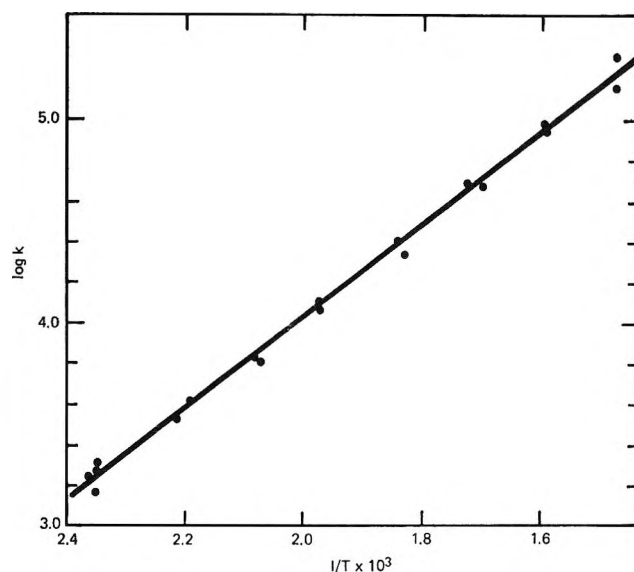


Figure 2. Arrhenius plot of the rate constants for α-D abstraction from 3-pentanone-2,2,4,4-*d*<sub>4</sub> by ethyl-*d*<sub>2</sub> radicals (in l. mol<sup>-1</sup> sec<sup>-1</sup>).

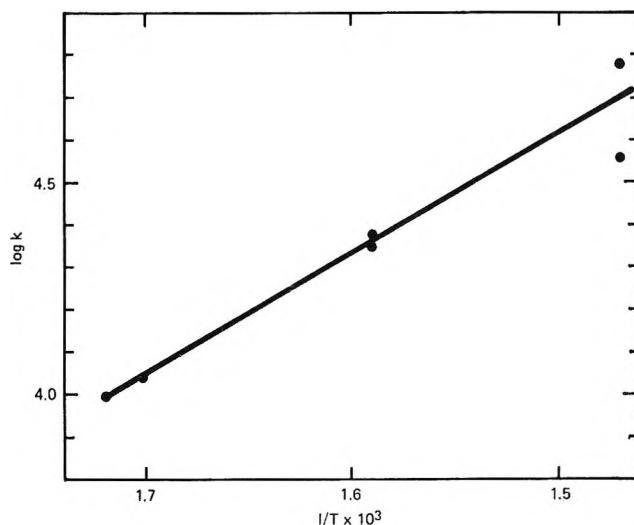


Figure 3. Arrhenius plot for the rate constants for β-H abstraction from 3-pentanone-2,2,4,4-*d*<sub>4</sub> by ethyl-*d*<sub>2</sub> radicals (in l. mol<sup>-1</sup> sec<sup>-1</sup>).

At temperatures of 357° and above, it was necessary to separate the ethane-*d*<sub>2</sub> into that formed by β-H abstraction by ethyl-*d*<sub>2</sub> and ethane-*d*<sub>2</sub> formed by α-D abstraction by an ethyl-*d*<sub>1</sub>. This is readily done using the relationship we had derived before

$$\frac{R_{\text{CH}_3\text{CD}_3}}{R_{\text{CH}_3\text{CD}_2\text{H}} - X} = \frac{X}{R_{\text{CH}_3\text{CD}_2\text{H}}}$$

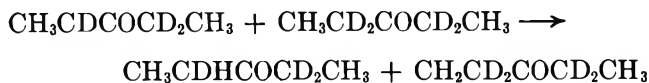
Arrhenius plots (Figures 2 and 3) and kinetic parameters for the rate constants *k*<sub>H</sub> and *k*<sub>D</sub> were obtained

(4) J. A. Kerr and A. F. Trotman-Dickenson, *Progr. React. Kinet.*, **1**, 105 (1961).

(5) A. Shepp and K. O. Kutschke, *J. Chem. Phys.*, **26**, 1020 (1957).

using a least-squares program on a UNIVAC 1108, leading to  $k_D = 10^{8.5 \pm 0.05} 10^{-(10,300 \pm 170)/4.58T} M^{-1} \text{ sec}^{-1}$  and  $k_H = 10^{8.7 \pm 0.4} 10^{-(12,400 \pm 1,500)/4.58T} M^{-1} \text{ sec}^{-1}$ , where the reported error is for one standard deviation.

Ethyl- $d_1$  radicals could conceivably be formed by a secondary reaction



As the  $d_3$  ketone builds up during the course of reaction, it photolyzes to give ethyl- $d_1$  radical. Examination of the ketone marking after 6.3 min of the experiment at  $357^\circ$  showed that the  $d_3$  ketone concentration increased by 2% over the original. That is an average over the time of reaction of 1%, and since half the ethyl radicals formed by the photolysis of  $d_3$  ketone are ethyl- $d_3$ , the ethyl- $d_1$  to ethyl- $d_2$  radical content increases by 0.5%. This extraneous source of ethyl- $d_1$  will account for butane- $d_3$  in the product being present as 1% the butane- $d_4$ . The original 2.4% ketone  $d_3$  impurity will not appear as butane- $d_3$  because of the butane- $d_4$  standard, as explained below. Since there are 4  $\alpha$  atoms, the 2.4%  $d_3$  ketone impurity results in  $(1/4)2.4 = 0.6\%$  of the  $\alpha$  positions marked H. Taking the  $\Delta E_{\text{act}}$  for abstraction as 1.5 kcal/mol less for H than D and equal preexponential factors, in the temperature range of abstraction,  $307\text{--}405^\circ$ , the ethane- $d_2$  formed from this source would be 5–8% of the ethane- $d_3$ . Since the effect on the temperature coefficient for the ethane- $d_3$ :ethane- $d_2$  ratio is quite small, the correction would have a negligible effect on the  $E_{\text{act}}$  and would appear mostly in the  $A$  factor, lowering it something over 5%. The correction was not made since the spread of the data was so much greater than the correction.

All of our rate constant calculations were corrected for the change in DEK concentration during the photolysis (always less than 10%).

*The Decomposition and Rearrangements of Pentanonyl Radicals.* Although the primary purpose of this work has been to determine the abstraction parameters for ethyl radicals from DEK, the results do allow us to make some qualitative statements about the reactions of the pentanonyl radicals formed in the abstraction processes.

Ethene produced in the photolyses to  $209^\circ$  can be accounted for by ethyl radical disproportionation. Above this temperature, there is more ethene than can be accounted for by disproportionation. In the photolysis at  $234^\circ$ , all the excess ethene formed is  $-d_2$ . Two possibilities for its formation are the decomposition of an ethyl radical or the decomposition of a pentanonyl radical. Simple kinetic calculations show clearly that ethyl radical decomposition cannot be an important source of ethene. The alternative explanation is that pentanonyl radicals decompose to give ethene.

Two pentanonyl radicals are formed when ethyl radical abstracts from the ketone parent



The rates of formation of these radicals are simply the rates of  $\alpha$  and  $\beta$  abstractions, respectively.

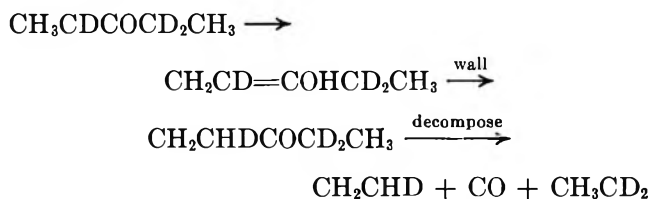
Radical I, which has some resonance stabilization, should be fairly stable to decomposition at these temperatures by analogy with the acetyl radical.<sup>6</sup>

The radical formed by  $\beta$  abstraction, II, would decompose more readily to give ethene- $d_2$  and ethyl- $d_2$  radicals. No intraradical isomerization seems to occur since no ethene- $d_3$  or ethane- $d_4$  are found in the products



If we compare the rates of formation of ethene- $d_2$  (by nondisproportionation) to that of formation of ethane- $d_2$  by nondisproportionation at  $234^\circ$ , we find they are very similar. This would suggest that the predominant fate of radical II is decomposition. As radical I concentration cannot be determined from our data, no conclusions can be drawn about the energetics of this process.

At temperatures from  $269$  to  $314^\circ$ , ethene- $d_1$  in addition to ethene- $d_2$  is formed. By examining the rates involved, we find again that the ethene- $d_2$  can be rationalized as arising from the decomposition of II. Ethene- $d_1$  cannot be explained by this process nor conveniently by a direct decomposition of radical I. A possible explanation is the isomerization of radical I by intraradical H(D) abstraction,  $\text{CH}_3\text{CDCOCD}_2\text{CH}_3 \rightarrow \text{CH}_2\text{CHDCOCD}_2\text{CH}_3$ . The radical formed by this path is analogous to radical II and would decompose to give ethene- $d_1$  and ethyl- $d_2$  radicals. The path we believe to be most reasonable<sup>7</sup> for this isomerization is



The ketonization of the enol intermediate probably takes place on a wall because of orientation requirements for the process. In experiments with undeuterated 3-pentanone, in which the vessel walls were pretreated with  $\text{D}_2\text{O}$ , we determined that exchange does

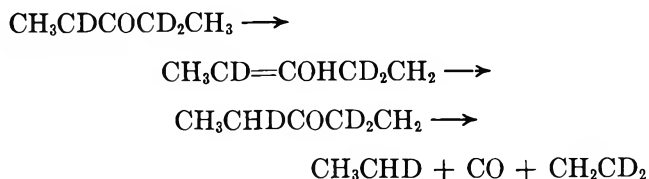
(6) J. R. McNesby and A. S. Gordon, *J. Amer. Chem. Soc.*, **76**, 1416 (1954).

(7) The formation of ethyl- $d_1$  radicals can be explained either by a path involving the carbonyl group and the hydrogen of the other methyl group or by a simple hydrogen abstraction for radical isomerization  $\text{CH}_3\text{CDCOCD}_2\text{CH}_3 \rightarrow \text{CH}_3\text{CHDCOCD}_2\text{CH}_2 \rightarrow \text{CH}_3\text{CHD} + \text{CO} + \text{CH}_2\text{CD}_2$ . However, to form ethene- $d_1$  by a hydrogen atom migration on the carbon skeleton is needed.  $\text{CH}_3\text{CDCOCD}_2\text{CH}_3 \rightarrow \text{CH}_2\text{CHDCOCD}_2\text{CH}_3 \rightarrow \text{CH}_2\text{CHD} + \text{CO} + \text{CD}_2\text{CH}_3$  and such a 1,2 gas-phase shift is not very probable.



not take place with surface deuterium atoms in the ethene forming process. While we *a priori* might have expected the enol intermediate to exchange with  $D_2O$  on the surface, the lack of such exchange does not rule out the above mechanism, since exchange would depend on the OD content of the silica and competitive rates of exchange and ketonization at this temperature ( $300^\circ$ ).

The formation of ethyl- $d_1$  radicals<sup>8</sup> in the experiments at  $357$  and  $405^\circ$  can also be explained by the rearrangement of I. A possible path for such a process would be



Any mechanism involving the formation of ethyl- $d_1$  from radical I predicts that an amount of ethene- $d_2$  equal to ethyl- $d_1$  is also formed. By subtracting the ethene- $d_2$  rate formed by disproportionation and by the decomposition of II from the total rate of formation of ethene- $d_2$ , the remainder corresponds very closely to the rate of ethane products formed by the reactions of ethyl- $d_1$ .

### Experimental Section

**Materials.** The 3-pentanone-2,2,4,4- $d_4$  was prepared in an acid-catalyzed exchange of 3-pentanone (Aldrich Chemical) with  $D_2O$  following the procedure of Siebl and Gausmann.<sup>9</sup> The isotope composition of the ketone after three exchanges was determined by mass spectrometry to be 97.6% $-d_4$ , 2.4% $-d_3$ . The label was found by nmr to be exclusively in the 2 and 4 positions.

The ethane- $d_3$  used as a mass spectral standard was research grade obtained from Merck Sharpe and Dohm of Canada, Ltd. It was used without further purification. The ethene- $d_2$  and butane- $d_4$  used as mass spectral standards were prepared by photolyzing the DEK at room temperature and collecting the ethene and butane fractions. At room temperature the ethene and butane are formed only by recombination and disproportionation. The butane actually contains about 2% butane- $d_3$  due to the starting material impurity. However, if we used this material as our butane- $d_4$  standard, we are still able to determine if the butane deuterium content has changed in any photolysis. Thus, in all the runs in Table I which show 100% butane- $d_4$  the butane label content was identical with that of the room temperature photolysis; *i.e.*, our results are effectively corrected for the starting material isotope

impurity. Similarly, the isotopic impurity in the ethene- $d_2$  is corrected by the mass spectrometer standard.

**Analysis.** Product yields were determined by gas chromatography using an 8 ft  $\times$  1/4 in. o.d. Porapak Q (Waters Associates) dual copper column operated with temperature programming from  $-196$  to  $+230^\circ$ . Samples were introduced onto the column at  $-196^\circ$  using a stainless steel flask inserted in the helium carrier stream ahead of the column. One-third of the effluent from the column was passed through a Carle thermal conductivity detector maintained at  $60^\circ$ . The remaining effluent was passed through a collection system containing packed glass U-traps cooled to liquid nitrogen temperature. Individual components were diverted through such traps which were then evacuated and sealed.

Samples obtained for label analysis were introduced from the U traps into the mass spectrometer with a CEC gas sampling system. A Hitachi-Perkin-Elmer RMU-6D double-focussing mass spectrometer was used. The isotopic composition of the ethene, ethane, and butane products were determined. Label analysis of the recovered ketone could not be accomplished by collecting it from the gas chromatograph because Porapak Q is an efficient exchange surface for deuterated ketones.<sup>10</sup> Ketone analyses were performed by introducing the photolysate directly into the mass spectrometer.

**Photolysis.** The 3-pentanone-2,2,4,4- $d_4$  was photolyzed in a quartz vessel at a pressure of 21 Torr with the full arc of a medium pressure Hanovia SC-100 mercury lamp. The photolysis temperature was varied from  $20$  to  $406^\circ$  using a furnace. The volume of the sample vessel was  $88\text{ cm}^3$ . The time of photolysis was varied but always kept short enough to ensure that less than 10% of the ketone was reacted.

In a control experiment to determine surface effects, the photolysis vessel was thoroughly rinsed with  $D_2O$  and evacuated. A sample of undeuterated 3-pentanone was photolyzed at  $300^\circ$  for a long period of time and the ethane and butane products analyzed for deuterium content.

(8) The possibility that  $\text{CH}_3\text{CDCOCD}_2\text{CH}_3$  could cause the parent purity to be changed by abstraction on H from the parent to give  $\text{CH}_3\text{CHDCOCD}_2\text{CH}_3$ , which would become a source of ethyl- $d_1$  by subsequent photolysis was eliminated by examining the purity of the ketone before and after reaction at  $357^\circ$ . At the end of 6.3 minutes, the ketone- $d_3$  had changed from 2.4%  $d_3$  to at most 6.4%  $d_3$ . The average increase of 1% increase in  $d_3$  content would only contribute 0.5% increase in ethyl  $d_1$  content, since the ketone- $d_3$  photodecomposes equally to ethyl- $d_2$  and ethyl- $d_1$  radicals.

(9) J. Siebl and H. Gausmann, *Helv. Chim. Acta*, **46**, 2858 (1963).

(10) C. I. Barta and A. S. Gordon, accepted by *J. Chromatogr. Sci.*

# The Laser Flash Photolysis of Solutions of Naphthalene and 1,2-Benzanthracene<sup>1a</sup>

by R. McNeil, J. T. Richards, and J. K. Thomas

Chemistry Division, Argonne National Laboratory, Argonne, Illinois 60439 (Received September 22, 1969)

Solutions of naphthalene and 1,2-benzanthracene have been flash photolyzed with nanosecond pulses of 2650- and 3472-Å light from a quadrupled neodymium and doubled ruby laser, respectively. Short-lived nanosecond spectra are observed which by lifetime and by heavy atom spin-orbit coupling studies are assigned to excited singlet states. Long-lived microsecond spectra are also observed and are attributed to the triplet state of these molecules. The absorption spectra of the singlet states decay, giving rise to the absorption spectra of the triplet state. The excited singlet and triplet spectra are quite similar, and this detail is discussed with regard to previous pulse-radiolysis data on these systems.

## Introduction

The initial development of flash photolysis<sup>2</sup> provided a direct method of observing species with lifetimes of only a few microseconds. The time region has been extended to nanoseconds by observing fluorescence from excited species produced either photochemically<sup>3</sup> or by ionizing radiation.<sup>4</sup> Recently the development of powerful sources of excitation, such as lasers and high-current accelerators, has enabled the chemist to observe short-lived species by absorption spectroscopy. Several aromatic molecules have been excited by the 3472-Å line from a doubled ruby laser<sup>5,6</sup> and quadrupled neodymium laser,<sup>7</sup> and the spectra of excited singlet states have been recorded. The pulse radiolysis of aromatic molecules also produces excited singlet and triplet states,<sup>8,9</sup> the data indicating that the predominant mode of formation is *via* ion recombination. The accepted mechanism of decay of an excited singlet state is fluorescence, radiationless transitions, and intersystem crossing to the triplet state. For many molecules the total rate of decay of the singlet by the above three processes has been measured by fluorescence techniques, and it remains to consolidate the measurements by direct observations on the triplet state by absorption spectroscopy. Initial data in the pulse radiolysis of anthracene, 1,2-benzanthracene, and naphthalene<sup>8-10</sup> in cyclohexane and benzene illustrate that the absorption spectrum of the triplet state shows only a small increase over the time period of decay of the excited singlet state. For naphthalene it was shown that this is due primarily to the fact that the spectra of the excited singlet and triplet state are very similar, leading to only a small spectral change associated with the intersystem crossing process. This effect is compounded in aromatic solvents due to a significant solvent effect on the excited singlet and triplet spectra which tends to broaden the spectra and produce even more similarity between the spectra. This aromatic solvent effect has also been noted in the pulse radiolysis of naphthalene in polystyrene and polymethyl methacrylate.<sup>11</sup>

It is a little disturbing that the above effects have been noted in systems excited by ionizing radiation in a situation which is more complicated than direct photochemical excitation. However, it has been recently shown that there is a close similarity between the absorption spectra of the excited singlet and triplet states of anthracene,<sup>12</sup> in agreement with the trend shown in the radiolysis data. The present study is devoted to an examination of the photolysis of solutions of naphthalene and 1,2-benzanthracene by short pulses from a Q-switched laser, to compare the photochemical data with the pulse-radiolysis data. In addition, the experimental technique, which is particularly useful for observing absorption and fluorescence spectra of short-lived species produced by Q-switched lasers, is described in detail.

## Experimental Section

Cyclohexane and benzene were purified by passing these solvents through a 3-ft column of activated alumina. Naphthalene was supplied by J. T. Baker and was twice recrystallized from ethanol before use; 1,2-benzanthracene (1,2-BA) was supplied by the Aldrich Chemical Co; xenon, helium, and argon were supplied by the Matheson Scientific Co. Solutions were prepared and deaerated by the syringe technique which has already been described.<sup>13</sup>

(1) Work performed under the auspices of the U. S. Atomic Energy Commission.

(2) G. Porter, *Proc. Roy. Soc.*, **A200**, 284 (1950).

(3) I. Beriman, "Handbook of Fluorescence Spectra of Aromatic Molecules," Academic Press, New York, N. Y., 1965.

(4) M. Burton and H. Dreeskamp, *Phys. Rev. Lett.*, **2**, 45 (1959).

(5) J. R. Novak and M. W. Windsor, *Science*, **161**, 1342 (1968).

(6) G. Porter and M. R. Topp, *Nature*, **220**, 1228 (1968).

(7) R. Bonneau, J. Faune, and J. Jousot-Dubien, *Chem. Phys. Lett.*, **2**, 65 (1968).

(8) J. W. Hunt and J. K. Thomas, *J. Chem. Phys.*, **46**, 2954 (1967).

(9) J. K. Thomas, *ibid.*, **51**, 770 (1969).

(10) R. Cooper and J. K. Thomas, *ibid.*, **48**, 5097 (1968).

(11) S. K. Ho and S. Siegel, *ibid.*, **50**, 1142 (1969).

(12) D. S. Kliger and A. C. Albrecht, *ibid.*, **50**, 4109 (1969).

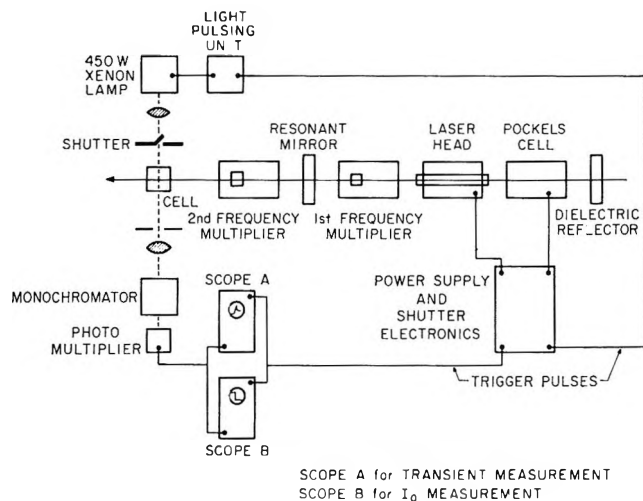


Figure 1. Diagrammatic representation of laser flash photolysis apparatus.

A diagrammatic representation of the laser flash photolysis lay-out using a Korad KIQP laser is shown in Figure 1. A 30-nsec, 2.5-J pulse of light of wavelength  $\lambda = 10,6000 \text{ \AA}$  is produced in the laser cavity, and about 5% of this light is frequency doubled to  $5300 \text{ \AA}$ , by the first potassium dihydrogen phosphate (KDP) crystal doubler. The  $5300\text{-\AA}$  light exits the laser cavity (while the red light is retained within the cavity by the exit mirror which is 100% reflecting at  $10,600 \text{ \AA}$ ) and passes through the second external KDP doubler giving a mixed output beam of  $5300\text{-}$  and  $2650\text{-\AA}$  light. The final ultraviolet output of the laser system was measured by means of a malachite green leucocyanide actinometer developed by Johns, *et al.*,<sup>14</sup> and was found to be about  $10^{-3} \text{ J}$ . The flash duration of the  $2650\text{-\AA}$  light was 15 nsec (half-width) as measured by observation of the fluorescence from a solution of *p*-terphenyl in cyclohexane. The beam cross section was roughly circular, with a radius of 2 mm, and impinged onto a cylindrical quartz irradiation cell of 5-mm length and 5-mm diameter.

A light beam from a 450-W xenon lamp (Osram XBO450) was focused through the cell and onto a diaphragm at the cell window farther away from the lamp. The light is refocused onto the entry slit of a Bausch and Lomb monochromator, which is operated with a band width of  $13 \text{ \AA}$ , while the intensity of the light emerging from the exit slit of the monochromator was monitored by an RCA IP28 photomultiplier. The output of the photomultiplier was displayed on a Tektronix 585A oscilloscope (A), where the signals were photographed on Polaroid 410 film. The rise-time of the optical and electronic system was faster than 5 nsec. To achieve large output signals from the photomultiplier, the 450-W xenon lamp was pulsed to 50 times the normal power for a few milliseconds,<sup>15</sup> thus enabling a current of 20 mA to be drawn from the photomultiplier.<sup>16</sup> This light pulse was recorded

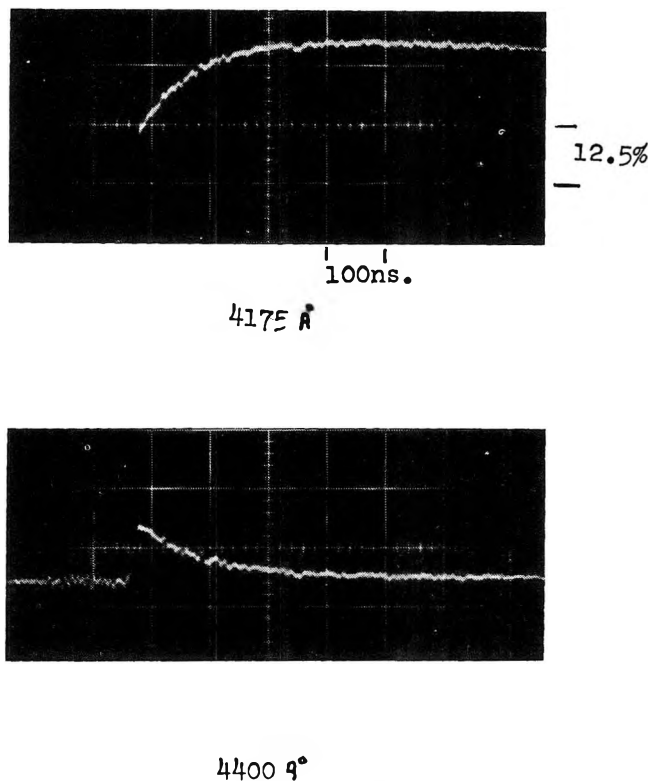


Figure 2. Laser photolysis of  $5 \times 10^{-4} \text{ M}$  naphthalene in  $\text{C}_6\text{H}_{12}$ .

on oscilloscope B and measured the  $I_0$  of the light passing through the irradiation cell. The oscilloscope (A) records the emission of light from the cell and the transitory changes in the level of the light passing through the cell, due to absorption by transitory species. A typical picture of the oscilloscope trace recording such an event is shown in Figure 2.

### Results and Discussion

*Naphthalene in  $\text{C}_6\text{H}_{12}$ .* Figure 2 shows typical pictures of oscilloscope traces taken at  $\lambda = 4175 \text{ \AA}$  and  $\lambda = 4400 \text{ \AA}$  in the laser photolysis of deaerated solutions of  $5 \times 10^{-4} \text{ M}$  naphthalene in cyclohexane. When the laser pulse occurs, transitory species are produced which absorb some of the analyzing light passing through the cell, causing a decrease in the light intensity,  $I_0$ , which in turn is recorded as a deflection of the oscilloscope trace toward the top of the picture. The optical density of the solution at any time may be calculated from the percentage decrease in  $I_0$ . Figure 2 illustrates that following the laser pulse the intensity of the analyzing light may continue to decrease as shown in the top picture of Figure 2, or it

(13) J. K. Thomas, S. Gordon and E. J. Hart, *J. Phys. Chem.*, **68**, 1525 (1964).

(14) G. J. Fisher, J. C. LeBlanc, and H. E. Johns, *Photochem. Photobiol.*, **6**, 757 (1967).

(15) B. Michael, unpublished work.

(16) J. W. Hunt and J. K. Thomas, *Radiation Res.*, **32**, 149 (1967).

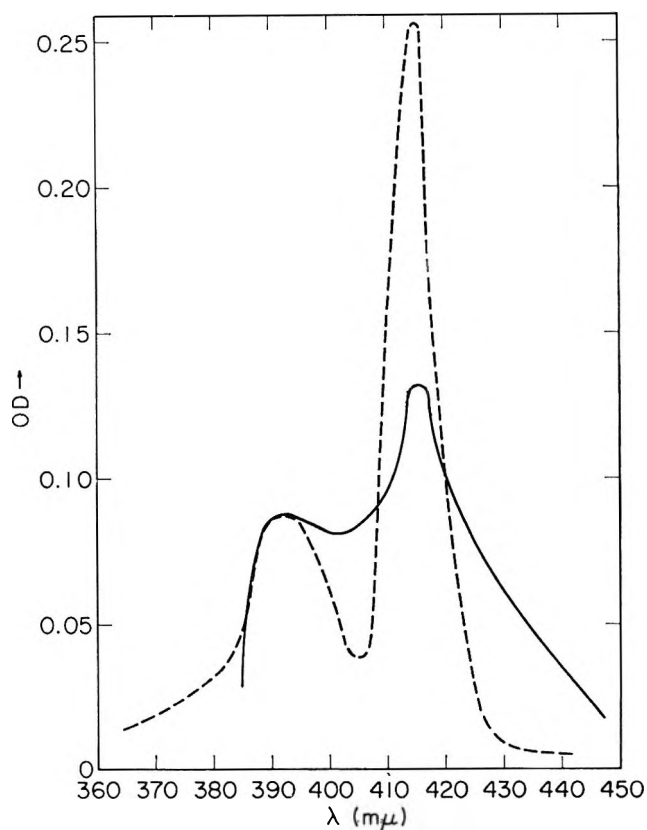


Figure 3. Absorption spectrum of transients in  $5 \times 10^{-4} M$  naphthalene in  $C_6H_{12}$  taken at the end of the pulse (solid line), 400 nsec after the pulse (dotted line).

may increase as illustrated by the bottom picture. These two conditions correspond to an increase and decrease in the concentration of the absorbing species, respectively. Hence it is convenient to express the data as spectra at various time intervals following the laser pulse. Spectra such as those shown in Figure 3 are obtained by plotting the optical density (OD) obtained from pictures such as Figure 2 at the end of the laser pulse and at some specified time interval following the pulse. The accuracy of the data depends mainly on the pulse reproducibility which is  $\pm 5\%$ ; the accuracy of reading the optical density from pictures such as Figure 2 is better than  $2\%$ .

A further feature of the time dependence of the data is that the growth of the absorption at  $\lambda = 4175 \text{ \AA}$  and the decay of the absorption at  $\lambda = 4400 \text{ \AA}$  both follow first-order kinetics with half-lives  $t_{1/2} = 72 \pm 4$  and  $69 \pm 4$  nsec, respectively, while the fluorescence measured at  $3400 \text{ \AA}$  also shows first-order kinetics with  $t_{1/2} = 72 \pm 4$  nsec. Dissolved xenon gas increases the rate of decay of the fluorescence at  $3400 \text{ \AA}$ , the rate of decay of the absorption at  $4400 \text{ \AA}$ , and the rate of growth of the absorption at  $4175 \text{ \AA}$ . At the latter wavelength the long-lived absorption is increased by  $20\%$  on saturating the solution with xenon. The first-order kinetic plots of the data are shown in Figure 4.

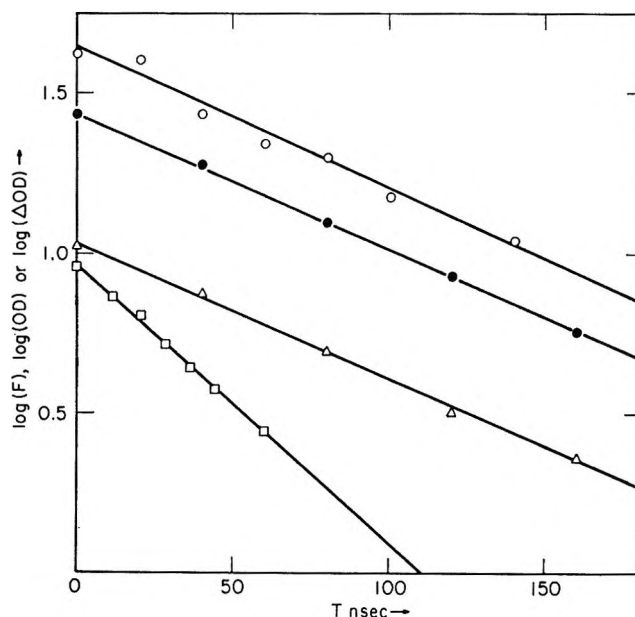
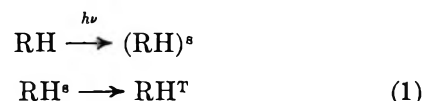


Figure 4. Decay data in  $5 \times 10^{-4} M$  naphthalene- $C_6H_{12}$  solutions:  $\circ$ , decay at  $\lambda = 4400 \text{ \AA}$ ;  $\Delta$ , growth at  $\lambda = 4175 \text{ \AA}$ ;  $\bullet$ , fluorescence at  $3400 \text{ \AA}$ ;  $\square$ ,  $0.1 M$  Xe at  $\lambda = 4400 \text{ \AA}$ .

The spectra illustrated in Figure 3 are best described in terms of excited singlet-singlet and triplet-triplet electronic transitions. The long-lived spectra taken at times greater than 400 nsec following a laser pulse are precisely those attributed to triplet-triplet absorptions in flash photolysis<sup>17</sup> or in steady-state photolysis in rigid media.<sup>18</sup> The rapidly growing and decaying portions of the spectra exhibit first-order kinetics with half-lives in agreement with the fluorescence half-life and show enhanced decay rates in the presence of dissolved xenon gas. This is the predicted behavior of excited singlet states  $(RH)^s$  which was discussed in the Introduction. The mechanism describing the system may be written as



where the overall decay of the singlet state in the absence of Xe is  $k_1 + k_2 = 10^7 \text{ sec}^{-1}$  and the overall rate of decay of the singlet in the presence of Xe is  $k_1 + k_2 + k_3 [Xe]$ . In a solution containing  $[Xe] = 10^{-2} M$ , the half-life of the decay is  $0.7/(k_1 + k_2 + k_3 [10^{-2}])$  and is measured as  $3.4 \times 10^{-8} \text{ sec}$ , giving  $k_3 = 1.06 \times 10^9 M^{-1} \text{ sec}^{-1}$ . This value for  $k_3$  compares well with the literature value of  $k_3 = 1.1 \times 10^9 M^{-1} \text{ sec}^{-1}$  for this reac-

(17) G. Porter and M. Windsor, *Proc. Roy. Soc.*, **A245**, 238 (1958).

(18) M. W. Windsor, W. R. Dawson, R. S. Moore, and D. Weber, TRW Systems Report No. 4162-6004-RU000.

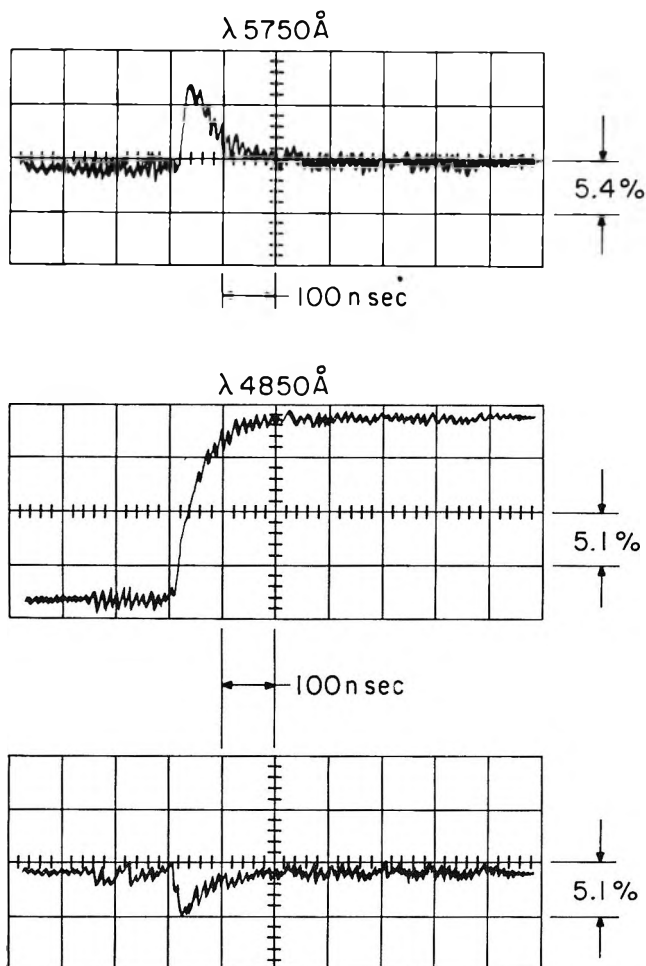


Figure 5. Laser photolysis of  $2 \times 10^{-4} M$  1,2-benzanthracene in  $C_6H_{12}$ : top curve absorption at  $\lambda = 5750 \text{ \AA}$ ; middle curve absorption at  $\lambda = 4850 \text{ \AA}$ ; lower curve fluorescence at  $\lambda = 4850 \text{ \AA}$ .

tion.<sup>19</sup> The experimental evidence is in agreement with the assignment of the spectrum observed at the end of the pulse to the excited singlet state of naphthalene. The data also show that while this spectrum decays, the spectrum of the triplet state of naphthalene is simultaneously produced. The similarity between the two spectra is quite remarkable and is in agreement with previous pulse-radiolysis data.<sup>9</sup> Earlier calculations by Pariser<sup>20</sup> indicate that the transitions responsible for the singlet-singlet spectra are  ${}^1A_{1g} \leftarrow {}^1B_{3u}$  with  $\Delta E = 3.08$  and  $3.40 \text{ eV}$  and  ${}^1B_{1g} \leftarrow {}^1B_{3u}$  with  $\Delta E = 3.54 \text{ eV}$ . These transitions correspond to absorption maxima at 4100, 3700, and  $3560 \text{ \AA}$  corresponding to the observed maxima at 4175 and  $3925 \text{ \AA}$ . It is possible that the observed maximum at  $3925 \text{ \AA}$  is a transition from the  ${}^1B_{3u}$  to a higher vibrational level of the  ${}^1A_{1g}$  state.

In the pulse radiolysis data there was even greater similarity between the spectra of the excited singlet and triplet state. It is not possible to excite naphthalene in liquid benzene with  $\lambda = 2650\text{-}\text{\AA}$  light due to the much larger absorption of the benzene. However, it is possible to excite 1,2-benzanthracene in benzene with

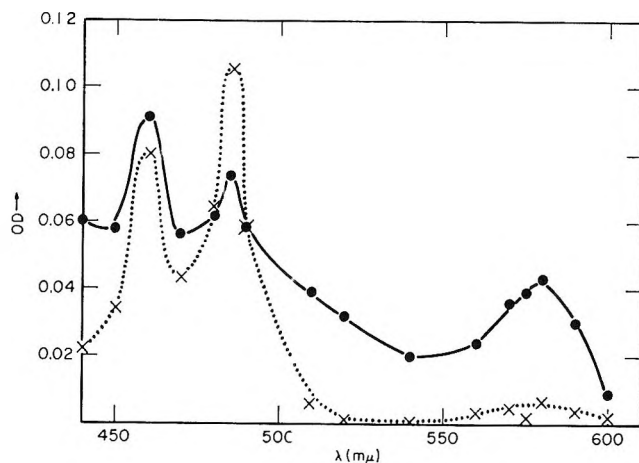


Figure 6. Absorption spectra of transients in 1,2-BA- $C_6H_{12}$  solutions taken at end of pulse (solid line), 400 nsec after the pulse (dotted line).

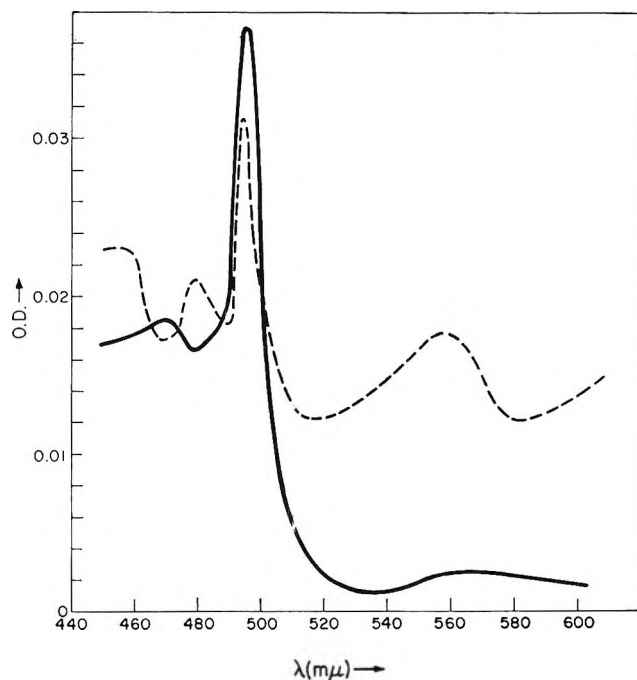


Figure 7. Absorption spectra of transients in 1,2-BA-benzene solution taken at end of pulse (dotted line), 400 nsec after the pulse (solid line).

$3472\text{-}\text{\AA}$  laser light from  $\epsilon$  doubled ruby laser and compare the data to that obtained using cyclohexane as a solvent.

*1,2-Benzanthracene in  $C_6H_{12}$  and  $C_6H_6$ .* Typical oscilloscope pictures for the  $2650\text{-}\text{\AA}$  laser excitation of  $2 \times 10^{-4} M$  1,2-benzanthracene in  $C_6H_{12}$  are shown in Figure 5. The analysis of the data is similar to that used for the naphthalene solutions, apart from one detail. With 1,2-BA the intensity of the fluorescence of

(19) A. R. Horrocks, A. Keavell, K. Tickle, and F. Wilkinson, *Trans. Faraday Soc.*, **62**, 3393 (1966).

(20) R. Pariser, *J. Chem. Phys.*, **24**, 250 (1956).

the excited singlet state at  $\lambda = 4850 \text{ \AA}$  is comparable to analyzing light. The bottom picture in Figure 5 shows the emission from the cell as a downward deflection with no analyzing light passing through the solution. The middle picture taken with the same sensitivity shows the upward deflection due to absorption of the analyzing light which passes through the cell. To obtain the true absorption curve, the emission deflection in the bottom picture is added to the absorption deflection in the middle picture. The optical density immediately after the pulse and at 400 nsec after the pulse are plotted vs. wavelength to give the spectra shown in Figure 6. Similar data are shown for the excitation of 1,2-BA with 3472- $\text{\AA}$  laser light in benzene in Figure 7. The time dependence of the data and the effect of dissolved xenon gas<sup>9</sup> shows that again the spectrum at the end of the laser pulse is due to the excited singlet and that at 400 nsec after the pulse corresponds to the triplet state of 1,2-BA. It is noteworthy that the spectra of excited singlet and triplet are very similar in both solvents, and in particular at the main triplet peak in the 4900- $\text{\AA}$

region, that the change in absorption due to intersystem crossing is 43% in  $\text{C}_6\text{H}_{12}$  and 16% in  $\text{C}_6\text{H}_6$ . This solvent effect is in agreement with pulse radiolysis data on these systems<sup>9</sup> and with that observed for naphthalene in solid solution.<sup>11</sup>

The present photochemical data confirm the conclusions reached in pulse radiolysis, namely that the absorption spectra of the excited singlet and triplet states of naphthalene and 1,2-benzanthracene are strikingly similar with regard to the positions and intensities of the absorption maxima. Similar conclusions with anthracene<sup>12</sup> and biphenyl<sup>11</sup> suggest that this may be a general phenomenon which awaits experimental confirmation.

*Acknowledgment.* We would like to thank Dr. H. Johns for a gift of malachite green leucocyanide, and Dr. J. Kastner for the use of certain components of his laser. J. T. Richards would like to thank Argonne National Laboratory for a postdoctoral fellowship, and R. McNeil recognizes the award of an ANL studentship.

## Line Width Effects on the Lower Field Electron Spin Resonance

### Signal in the Titanium(III)-Hydrogen Peroxide System

by R. E. James and F. Sicilio

*Department of Chemistry, Texas A & M University, College Station, Texas 77843 (Received December 28, 1969)*

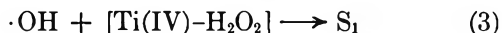
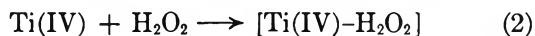
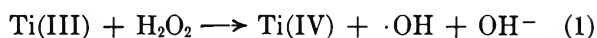
Esr-flow studies on the low-field paramagnetic intermediate,  $S_1$ , in the Ti(III)- $\text{H}_2\text{O}_2$  reaction system show that the previously reported marked enhancement of signal intensities for  $S_1$  upon addition of traces of alcohol is not accompanied by the same relative increase in  $[S_1]$ . Small enhancement of  $[S_1]$ , to the extent of approximately 15%, does occur with  $10^{-3} M$  methanol. This enhancement is probably the result of competition of alcohol with Ti(III) for  $\cdot\text{OH}$  in the early stages ( $t < 15$  msec) of the reaction sequence and subsequent production of  $S_1$  by the substrate radical- $\text{H}_2\text{O}_2$  reaction. Line narrowing of the signal for  $S_1$  upon addition of alcohol is indicative of a rapid reversible formation of an alcohol- $S_1$  complex. Line broadening of the signal for  $S_1$  occurs with an increase in acid concentration, giving evidence for a relatively slow reversible protonation of  $S_1$ .

#### Introduction

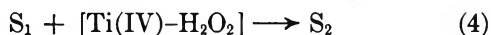
In the Ti(III)- $\text{H}_2\text{O}_2$  reaction system, two paramagnetic intermediates are formed: a species with a low-field peak,  $S_1$  ( $g = 2.0132$ ), and one with a high-field peak,  $S_2$  ( $g = 2.0118$ ).<sup>1-3</sup>  $S_1$  and  $S_2$  have not been directly identified. Takakura and Rånby<sup>4</sup> propose that  $S_1$  is  $\cdot\text{O}_2\text{H}$  and  $S_2$  is  $\cdot\text{OH}$ , both, respectively, complexed with Ti(IV). This is in general agreement with other investigators listed in ref 3. Fischer<sup>5</sup> proposes

the following reaction mechanism for the formation of  $S_1$

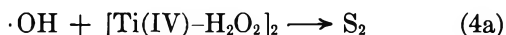
- (1) L. H. Piette, G. Bulow, and K. Loeffler, Preprint, Division of Petroleum Chemistry, American Chemical Society, Washington, D. C., April 1964.
- (2) F. Sicilio, R. E. Florin, and L. A. Wall, *J. Phys. Chem.*, **70**, 47 (1966).
- (3) R. E. James and F. Sicilio, *ibid.*, **74**, 1166 (1970).
- (4) K. Takakura and B. Rånby, *ibid.*, **72**, 164 (1968).
- (5) H. Fischer, *Ber. Bunsenges. Phys. Chem.*, **71**, 685 (1967).



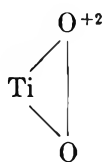
and, with less certainty, the formation of  $\text{S}_2$



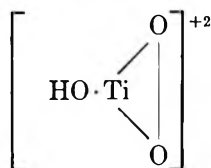
or



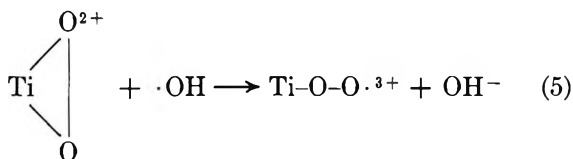
In these reactions, the  $[\text{Ti(IV)-H}_2\text{O}_2]$  species is probably the



yellow complex, and  $\text{S}_1$  could be



or  $\text{HO}^-\text{[Ti-O-O}\cdot\text{]}^{3+}$ . Fischer<sup>5</sup> also proposes the structure  $\text{HO}^-\text{[Ti-O-O-Ti-O-O}\cdot\text{]}^{5+}$  as a possibility for  $\text{S}_2$ . Formation of  $\text{S}_1$  could also occur by<sup>6</sup>



Inclusion of a substrate such as *t*-butanol leads to the reaction

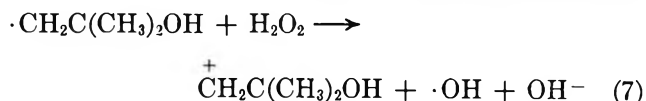


The hydroxyl radical in (6) is either free  $\cdot\text{OH}$ , initially produced in (1), or is a primary reactive species derived therefrom. Reaction 6 is highly competitive with reactions 3 or 4a for nominal concentrations of  $[\text{Ti(III)}]_0 \approx 0.01 \text{ M}$  and  $[\text{H}_2\text{O}_2]_0 \approx 0.1 \text{ M}$ .

Turkevich, *et al.*,<sup>7</sup> report that a twofold or greater enhancement of the "signal intensity" for  $\text{S}_1$  results from the addition of small quantities ( $3.0\text{--}4.0 \times 10^{-2} \text{ M}$ ) of alcohols ( $\text{CH}_3\text{OH}$ ,  $\text{C}_2\text{H}_5\text{OH}$ , *i*- $\text{C}_3\text{H}_7\text{OH}$ , and *t*- $\text{C}_4\text{H}_9\text{OH}$ ) to the  $\text{Ti(III)-H}_2\text{O}_2$  reaction system. The intensity of the signal for  $\text{S}_1$  reaches a maximum and then diminishes with increasing concentration of alcohol substrate. The effects on intensity, or signal height, upon addition of a substrate have been corroborated,<sup>6</sup> and the results of Norman and West for methyl and isopropyl alcohols are in broad agreement.<sup>8</sup>

The enhancement of signal intensity upon addition of traces of substrate appears to be anomalous, since

$\text{S}_1$  is most likely derived from  $\cdot\text{OH}$ , and  $\cdot\text{OH}$  is the most likely candidate for abstracting hydrogen from substrate to form substrate radicals.<sup>3</sup> One explanation offered<sup>8</sup> is that small quantities of alcohol, through reactions such as (6) and (7), release  $\cdot\text{OH}$  at a later time



after mixing, allowing time for buildup of  $\text{Ti(IV)}$  and its complexes. Titanium(IV) can then form  $\text{S}_1$  via (3) provided  $[\text{ROH}]$  is not too high.

During the course of work herein reported, it was noticed that the peaks for  $\text{S}_1$  and  $\text{S}_2$  were better resolved in the presence of a substrate. The improved resolution was traced to line narrowing effects, and the apparent anomalous behavior on the basis of peak intensity can thus be readily explained.

### Experimental Section

**Reagents.**  $\text{Ti(III)}$  solutions were prepared from W. H. Curtin & Co. technical grade 20%  $\text{TiCl}_3$  (analyzed with standardized  $\text{KMnO}_4$  to be 1.43–1.49 *M*) in which no paramagnetic impurities could be detected.  $\text{H}_2\text{O}_2$  solutions were prepared from Baker Analyzed Reagent (30% solution, analyzed to be 9.2–9.7 *M*). The alcohols were Baker Analyzed Reagent or Fisher Certified, none of which gave evidence of interfering impurities by gc analysis.

**Apparatus.** The esr spectrometer and flow system have been described previously.<sup>3,9</sup>

**Procedure.** Two aqueous reactant solutions,  $\text{Ti(III)}$  vs.  $\text{H}_2\text{O}_2$ -alcohol, were mixed immediately before entering the quartz cell in the resonant cavity of the esr spectrometer. Times after mixing were calculated from the ratio hold-up volume (ml):flow rate (ml/sec).<sup>2</sup> For a series of runs in which only one component was varied, 10 l. of one solution with definite composition was prepared, and solutions of different concentrations of reactants were made up in 2-l. quantities. This minimized changes in sensitivity since the complete series could be run with minimal adjustments in tuning.

For line width measurements, the scan rates were optimized at 1.00 G/cm to reduce the uncertainty in measuring maxima and minima for  $\Delta H$  values without undue broadening of the first derivative peaks. In cases of appreciable overlap,  $\Delta H$  of the  $\text{S}_1$  peak was taken as twice the horizontal distance from the maxima to the zero point on the base line, and the peak height as twice the height of the first half of the derivative curve. Standard deviations for  $\Delta H$  ranged from 2.0 to 10%.

(6) R. E. Florin, F. Sicilio, and L. A. Wall, *J. Phys. Chem.*, **72**, 3154 (1968).

(7) Y. S. Chiang, J. Craddock, D. Mickewich, and J. Turkevich, *ibid.*, **70**, 3509 (1966).

(8) R. O. C. Norman and P. R. West, *J. Chem. Soc., B*, 389 (1969).

(9) E. L. Lewis and F. Sicilio, *J. Phys. Chem.*, **73**, 2590 (1969).

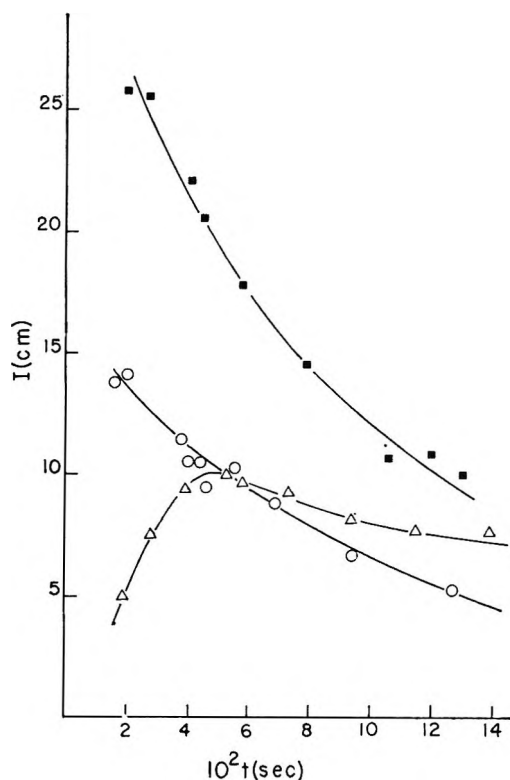


Figure 1. Zero-order plots for  $S_1$ . Peak height,  $I$ , vs. time after mixing,  $t$ .  $T = 25 \pm 0.5^\circ$ . Solution of  $0.010 M \text{TiCl}_3$ - $0.10 M \text{H}_2\text{SO}_4$  mixed with:  $\circ$ ,  $0.10 M \text{H}_2\text{O}_2$ , no  $t\text{-C}_4\text{H}_9\text{OH}$ ;  $\blacksquare$ ,  $0.10 M \text{H}_2\text{O}_2$ ,  $0.020 M t\text{-C}_4\text{H}_9\text{OH}$ ;  $\Delta$ ,  $0.10 M \text{H}_2\text{O}_2$ ,  $0.020 M i\text{-C}_3\text{H}_7\text{OH}$ .

The possibility of an increase in instrument sensitivity due to decrease in dielectric constant upon inclusion of an alcohol was investigated. With the same instrument tuning, spectra of  $0.001 M \text{Mn(II)}$ , with and without alcohol were run, using the same cell as for kinetic runs. Four or five scans were made for each solution and the average area taken. With inclusion of  $0.010 M$  methanol or  $t$ -butanol, the area was decreased by approximately 5%. Thus any sensitivity change due to decrease in dielectric constant is slight.

## Results and Discussion

**Peak Height Enhancement.** The plots in Figure 1 show that peak heights,  $I$ , for the low-field species,  $S_1$ , are enhanced nearly twofold by the addition of  $0.02 M t$ -butanol to the  $\text{Ti(III)}\text{-H}_2\text{O}_2$  system, the degree of enhancement depending on the time after mixing. These results are in general agreement with reports of enhancement of "signal intensity".<sup>7,8</sup> However, as shown in Figure 2, the peak areas for  $S_1$  signals are only slightly greater for the run with  $0.02 M t$ -butanol. The difference in the two sets of plots is a direct result of line narrowing. Results for  $0.02 M$  2-propanol are demonstrably different, but in accord with its greater reactivity toward  $\cdot\text{OH}$ .<sup>8</sup> Line narrowing occurs for  $S_1$  signals with 2-propanol (Table I) but the reduction in  $[S_1]$  results in the absence of peak height enhance-

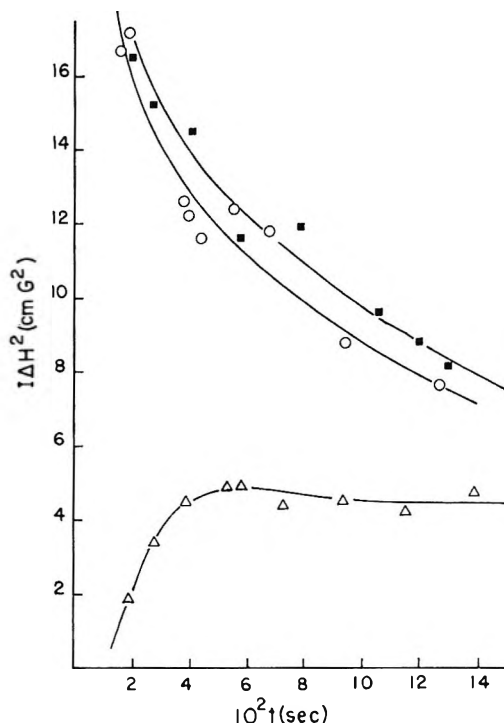


Figure 2. Zero order plots for  $S_1$ . Peak area,  $I\Delta H^2$ , vs. time after mixing,  $t$ . Same runs and peak heights as for Figure 1.

Table I: Line Width Data<sup>a</sup>

$[\text{TiCl}_3]_0$	$[\text{H}_2\text{O}_2]_0$	$[\text{ROH}]_0$	$[\text{H}_2\text{SO}_4]_0$	ROH	$\Delta H, S_1,^b$ G
0.010	0.10	0.0	0.10	...	$1.11 \pm 0.05$
0.010	0.10	0.020	0.10	$t$ -Butanol	$0.84 \pm 0.04$
0.010	0.10	0.030	0.10	$t$ -Butanol	$0.65 \pm 0.03$
0.010	0.10	0.050	0.10	$t$ -Butanol	$0.66 \pm 0.05$
0.010	0.10	0.0	0.25	...	$1.21 \pm 0.07$
0.010	0.10	0.010	0.25	$t$ -Butanol	$1.15 \pm 0.05$
0.010	0.10	0.020	0.25	$t$ -Butanol	$1.04 \pm 0.05$
0.010	0.10	0.020	0.020	$t$ -Butanol	$0.79 \pm 0.04$
0.010	0.10	0.020	0.10	2-Propanol	$0.71 \pm 0.04$
0.0050	0.050	0.0	0.10	...	$0.83 \pm 0.03$
0.0050	0.050	0.0050	0.10	Methanol	$0.79 \pm 0.02$
0.010	0.050	0.010	0.10	Methanol	$0.74 \pm 0.02$
0.010	0.10	0.0	0.050 <sup>c</sup>	...	$0.97 \pm 0.04$

<sup>a</sup>  $T = 24$  to  $26^\circ$ ; variation,  $\pm 0.5^\circ$  for any run. <sup>b</sup> Averages of line widths taken for signals at 20–120 msec (time after mixing). <sup>c</sup>  $[\text{N}_2\text{SO}_4]_0 = 0.20$ ; therefore  $[\text{SO}_4^{2-}] = 0.25$ , for comparison with similar run with  $[\text{H}_2\text{SO}_4]_0 = 0.25$ .

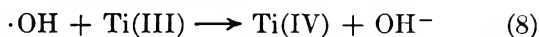
ment. As a check on the method of determination of area, graphical integration was performed on two of the peaks. The resulting areas were 1520 and 1308 (arbitrary units) for peaks with  $I\Delta H^2$  values of 14.5 and 12.3, respectively. Since  $1520/1308 = 1.16$  and  $14.5/12.3 = 1.18$ , the two methods give essentially the same results.

In general, as shown in Table I, increasing  $[t\text{-butanol}]$  causes line narrowing for  $S_1$  signals. An accompanying



decrease in peak area occurs. For 0.05 *M* *t*-butanol, with 0.01 *M* TiCl<sub>3</sub>, 0.1 *M* H<sub>2</sub>SO<sub>4</sub>, and 0.1 *M* H<sub>2</sub>O<sub>2</sub>, the signal from  $\cdot\text{CH}_2\text{C}(\text{CH}_3)_2\text{OH}$  is faintly observable. It should also be noted that line broadening occurs with an increase in [H<sub>2</sub>SO<sub>4</sub>].

For the data in Table I, the actual concentration of *t*-butanol after mixing is  $[\textit{t}\text{-butanol}]_0/2$ . This is valid because a relatively small quantity is consumed *via* (6). The Ti(III):H<sub>2</sub>O<sub>2</sub> consumption ratio was measured as a function of  $[\textit{t}\text{-butanol}]_0$ . For no alcohol present the stoichiometry is 2:1 and can be explained by reactions 1 and 8. With substrate, changes in the stoichiometry



come about by reactions 6 and 7.<sup>3</sup> Solutions of 0.01 *M* TiCl<sub>3</sub> containing alcohol were titrated with 0.1 *M* H<sub>2</sub>O<sub>2</sub>. The results in Table II show that with 0.05 *M* *t*-butanol,

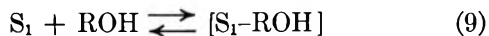
Table II: Stoichiometry Studies<sup>a</sup>

Ti(III), mmol	H <sub>2</sub> O <sub>2</sub> , mmol	ROH, mmol	[ROH] <sub>0</sub>
1.07	0.54	0.0	0.0
1.07	0.57	1.00	0.010
1.07	0.60	1.50	0.015
1.07	0.62	2.50	0.025
1.07	0.65	5.00	0.050

<sup>a</sup> ROH *t*-butanol.

0.11 mmol of H<sub>2</sub>O<sub>2</sub> is consumed in excess of that needed in the absence of alcohol. Thus, 0.11 mmol may be considered to be the maximum possible quantity of alcohol consumed in this case, since the alcohol radical reacts predominantly with H<sub>2</sub>O<sub>2</sub>. The resulting [ROH] = (5.00 - 0.11)/100 = 0.049, only 2% less than [ROH]<sub>0</sub>.

**Exchange Mechanism.** ESR line shapes of paramagnetic species in solution are well known to be affected by exchange reactions involving the paramagnetic species and other species in the solution.<sup>10</sup> Since  $\Delta H$  for the S<sub>1</sub> signal is an inverse function of alcohol concentration, apparently a rapid reversible reaction such as (9) oc-



curs, with a rate in the fast exchange region. In this case, the ESR relaxation of the unpaired electron of S<sub>1</sub> is perturbed by a magnetic nuclear dipole on ROH (*e.g.*, a proton) and the motion is so fast that the electron experiences an average environment that becomes a smaller effective perturbation as the rate increases. Proton transfer probably does not occur, nor could ROH in (9) be protonated, in view of the results for addition of acid (Table I). Apparently, there is an exchange of alcohol for water at the paramagnetic site of S<sub>1</sub>, giving an S<sub>1</sub>-alcohol complex that is stable compared to the aquated form of S<sub>1</sub>. This is somewhat

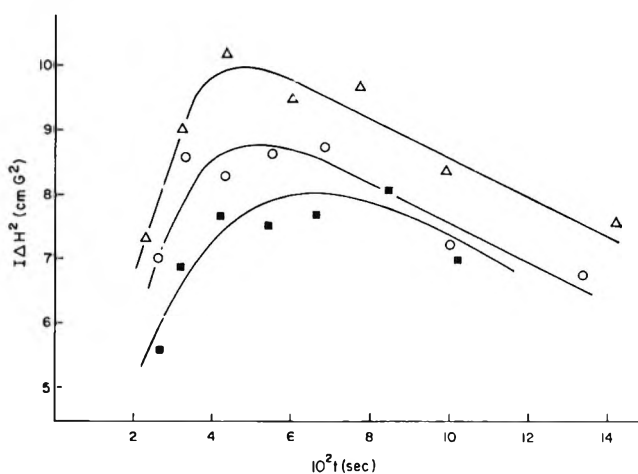


Figure 3. Zero-order plots for S<sub>1</sub>. Peak area,  $I\Delta H^2$ , vs. time after mixing,  $t$ .  $T = 2 \pm 0.5^\circ$ . Solution of 0.0050 *M* TiCl<sub>3</sub>-0.10 *M* H<sub>2</sub>SO<sub>4</sub> mixed with: O, 0.050 *M* H<sub>2</sub>O<sub>2</sub>, no CH<sub>3</sub>OH; Δ, 0.050 *M* H<sub>2</sub>O<sub>2</sub>, 0.0050 *M* CH<sub>3</sub>OH; ■, 0.050 *M* H<sub>2</sub>O<sub>2</sub>, 0.010 *M* CH<sub>3</sub>OH.

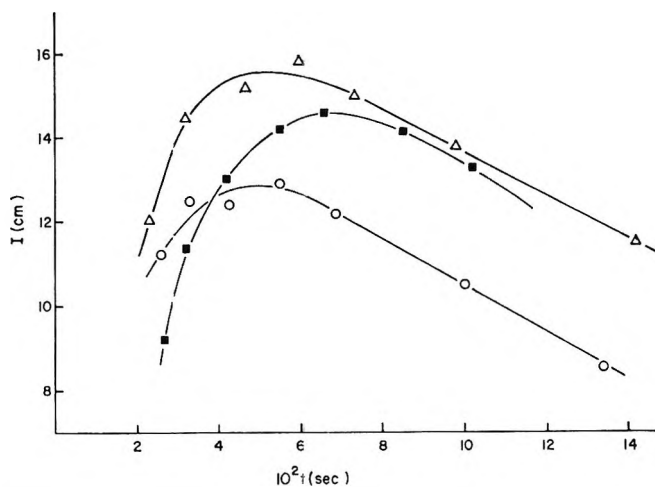
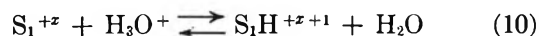


Figure 4. Zero-order plots for S<sub>1</sub>. Peak height,  $I$ , vs. time after mixing,  $t$ . Same runs and peak heights as for Figure 3.

analogous to the reversible reaction for complex formation in the case of phenoxy radicals.<sup>11</sup> Provided  $k_{9f}[\text{ROH}] \approx 10^6 \text{ sec}^{-1}$ , reaction 9 accounts for line narrowing of S<sub>1</sub> as observed.

Line broadening with increased acid concentration seems to be best explained by invoking a protonation equilibrium



provided three conditions hold: (1) the  $g$  factors of S<sub>1</sub><sup>+z</sup> and S<sub>1</sub>H<sup>+z+1</sup> are essentially the same, (2) both species contribute to the observed spectrum, and (3) proton hyperfine splitting in S<sub>1</sub>H<sup>+z+1</sup> is too small to be resolved but is sufficient to cause line broadening. Apparently the exchange in (10) is too slow to modulate

(10) A. Hudson and G. R. Luekhurst, *Chem. Rev.*, **69**, 191 (1969).

(11) R. W. Kreilick and S. I. Weissman, *J. Amer. Chem. Soc.*, **88**, 2645 (1966).

the esr relaxation time of  $S_1$ . This is a reasonable proposition since (10) involves the combination of ions of like charge. Increasing  $[H_2SO_4]_0$  shifts (10) to the right, augmenting the contribution to the spectrum by  $S_1H^{+z+1}$  and broadening the line. This is in accord with the data in Table I. The effect of  $H_2SO_4$  on the line width was demonstrated as being primarily due to the proton rather than the sulfate ion by making comparative runs (see footnote *c* in Table I).

We are indebted to a reviewer for pointing out that spin exchange interactions could be the dominant relaxation mechanism for  $S_1$  in the absence of alcohol, since  $\Delta H$  changes from 0.83 to 1.11 G when  $[TiCl_3]_0$  and  $[H_2O_2]_0$  are doubled (Table I). Since  $[S_1]$  is very low ( $\leq 10^{-6} M$ ), such an interaction could occur if a dimeric species of  $S_1$  were formed. In the latter, spin exchange could readily be effected.

*Kinetics.* Florin, *et al.*,<sup>6</sup> also investigated the effects of low concentrations of alcohol and found a slight increase of  $[S_1]$  upon inclusion of 0.005 *M* methanol. A decrease of  $[S_1]$  occurs with 0.01 *M* methanol, in apparent disagreement with results of Turkevich, *et al.*,<sup>7</sup> and Norman and West.<sup>8</sup> Figure 3 gives plots of peak areas for our runs at these concentrations. The results are in good agreement with those of Florin, *et al.*<sup>6</sup> Figure 4 for the same runs demonstrates the

anomaly that can result from using peak height as a direct measure of radical concentration, in that the curve for 0.01 *M* alcohol is above that for no alcohol. The relative positions of the kinetic curves utilizing peak heights are considerably different from those utilizing peak areas, for the same data, due to the occurrence of line width changes.

The increase in  $[S_1]$  with 0.005 *M* methanol can be rationalized by a scheme similar to that proposed by Norman and West.<sup>8</sup> Instead of the production of a reactive  $\cdot OH$  in the reaction for methanol analogous to (7),<sup>8</sup> evidently  $S_1$  or an unreactive precursor is produced.<sup>3</sup> The argument is as follows. Without substrate, some of the  $\cdot OH$  from (1) reacts immediately with  $Ti(III)$ ,<sup>3</sup> rather than with  $Ti(IV)$  or  $[Ti(IV)-H_2O_2]$  to form  $S_1$ . With the presence of even small quantities of alcohol, (6) competes with (8) and additional  $S_1$  can be produced from reaction of  $\cdot CH_2OH$  with hydrogen peroxide. Norman and West did not consider the involvement of reaction 8. Evidently, small quantities of alcohol (0.005 *M*) do not compete effectively with  $Ti(III)$  for  $\cdot OH$ , reaction 8, and larger quantities of alcohol ( $10^{-2} M$  range) scavenge quantities of  $\cdot OH$  such that  $[S_1]$  is reduced.

*Acknowledgment.* This research was supported by the Robert A. Welch Foundation, Grant A-177.

# Fluorescence Study of 2-(N,N-Dimethylamino)pyridine

## and Related Molecules

by A. Weisstuch and A. C. Testa

Department of Chemistry, St. John's University, Jamaica, New York 11432 (Received February 9, 1970)

Relative fluorescence quantum yields for the title compound in a variety of solvents suggest that the lowest excited singlet state is  $\pi, \pi^*$ . The low fluorescence quantum yields in acid ( $\phi_f = 0.01$ ) is attributed to a quenching process involving intramolecular electron transfer. The assignment was based on two fluorescence properties of this molecule: (a) the high fluorescence yield in nonpolar, polar, and hydrogen bonding solvents, and (b) the fluorescence polarization which is positive with respect to the first two absorption bands. Fluorescence data are also presented for 2-(N-phenylamino)pyridine and 2-benzylaminopyridine. 4-(N,N-Dimethylamino)pyridine was nonfluorescent in all the solvents investigated. The results confirm the proton transfer from the amine group in basic solutions as the fluorescence quenching process which occurs in the excited singlet state of aminopyridines. 2-(N,N-Dimethylamino)pyridine which has both amine hydrogens replaced shows no hydroxide ion quenching.

### Introduction

Recently, we reported that the fluorescence of 2-, 3-, and 4-aminopyridines exhibit pronounced effects dependent upon the polarity and hydrogen bonding properties of the solvent.<sup>1</sup> The fluorescence yield increases in polar and hydrogen bonding solvents and exhibits its highest value in acidic solutions. Similar effects were also observed for the diaminopyridines.<sup>2</sup> In all cases the excited state  $pK_a$  relative to its value in the ground state resembled heterocyclic molecules in which the excited singlet state is more basic.<sup>3,4</sup> Consequently, our results were compatible with excitation occurring at the pyridine nitrogen and interaction between close-lying  $n, \pi^*$  and  $\pi, \pi^*$  states depending upon the polarity of the solvents. Förster, *et al.*,<sup>5</sup> have shown that in the fluorescence of some aromatic aldehydes, *e.g.*, pyrene-3-aldehyde, the energy separation of the two states,  $n, \pi^*$  and  $\pi, \pi^*$ , determines the fluorescence ability of the molecule. Aromatic amines, on the other hand, have been classified by Kasha<sup>6,7</sup> to exhibit a  $1 \rightarrow a_\pi$  transition which is the result of lone-pair excitation to an antibonding  $\pi$  orbital which is not necessarily the same as the phenyl ring. Since it has been shown that substitution of aniline at the amine group with alkyl groups lowers the energy of the first excited singlet,<sup>8</sup> the distinct possibility exists that replacement of the amine hydrogens in 2-aminopyridine may result in some sharp differences in its fluorescence behavior, which may be indicative of excitation occurring at the amine group rather than at the heteroatom. If this effect occurs, the fluorescence may resemble N,N-dimethylaniline more than it would a heterocyclic molecule. With this aim the present investigation was initiated to measure the fluorescence spectra as a function of solvent for the following molecules: 2-(N,N-dimethylamino)pyridine, 4-(N,N-dime-

thylamino)pyridine, 2-(N-phenylamino)pyridine, and 2-(N-benzylamino)pyridine. The last two compounds provide examples of amines with replaceable hydrogen atoms in the amine group to test the hydroxide ion quenching previously reported for 2-aminopyridine.<sup>1</sup>

### Experimental Section

**Materials.** 2-(N,N-Dimethylamino)pyridine, 4-(N,N-dimethylamino)pyridine, 2-(N-phenylamino)pyridine, and 2-(N-benzylamino)pyridine were obtained from Aldrich Chemical Co. 2-(N,N-Dimethylamino)pyridine was vacuum distilled to a clear liquid with a boiling point of 90° (33 mm) which agrees with the literature value.<sup>9</sup> The  $pK_a$  for the pyridine site of the molecule was determined by potentiometric titration using a pH meter in the present study to be 7.50. 4-(N,N-Dimethylamino)pyridine was purified by recrystallization from *n*-hexane and decolorizing carbon. The melting point of 112.5° is in agreement

(1) A. Weisstuch and A. C. Testa, *J. Phys. Chem.*, **72**, 1982 (1968).

(2) A. C. Testa, A. Weisstuch, and J. Hennessy in "Molecular Luminescence," E. C. Lim, Ed., W. A. Benjamin, Inc., New York, N. Y., 1969, p 833.

(3) A. Weller, *Z. Elektrochem.*, **61**, 956 (1957).

(4) R. S. Becker, "Theory and Interpretation of Fluorescence and Phosphorescence," John Wiley and Sons, New York, N. Y., 1969, Chapter 17.

(5) K. Brederick, T. Förster, and H. G. Oesterlin, "Luminescence of Organic and Inorganic Materials," H. P. Kallmann and G. M. Spruch, Ed., John Wiley and Sons, New York, N. Y., 1962, p 161.

(6) M. Kasha in "Fluorescence—Theory, Instrumentation and Practice," G. G. Guilbault, Ed., Marcel Dekker Inc., New York, N. Y., 1967, p 201.

(7) M. Kasha and H. R. Rawls, *Photochem. Photobiol.*, **7**, 561 (1968).

(8) K. Kimura, H. Tsubomura, and S. Nagakura, *Bull. Chem. Soc. Jap.*, **37**, 1336 (1964).

(9) L. C. Anderson and N. V. Seeger, *J. Amer. Chem. Soc.*, **71**, 340 (1949).

with the literature value.<sup>10,11</sup> The  $pK_a$  of this compound has been reported to be 9.71.<sup>10</sup> 2-(N-Phenylamino)pyridine recrystallized from *n*-hexane and decolorizing carbon had a melting point of 107°, which agrees with the literature.<sup>12</sup> The  $pK_a$  of this compound was determined in the present study to be 5.40. 2-(N-Benzylamino)pyridine recrystallized from *n*-hexane and decolorizing carbon had a melting point of 94° agreeing with the literature value.<sup>12</sup> The  $pK_a$  value at the pyridine site was determined in the present study to be 8.90. Matheson Coleman and Bell Spectrograde solvents were used in absorption and emission work and Harelco fluorimetric grade HCl and NaOH were used for preparing acid and base solutions. Quartz-distilled water was used for preparing aqueous solutions.

**Apparatus.** Experiments were performed at room temperature with 285-nm excitation using equipment described elsewhere.<sup>1</sup> Relative fluorescence yields in this study were determined using the value of 0.09 for *dl*-tryptophan in water as a standard;<sup>13</sup> however, Chen<sup>14</sup> has recently determined a more accurate value of  $0.13 \pm 0.01$ . No precautions were taken to exclude oxygen from solutions, since in several instances it was determined to be unimportant. The accuracy of the fluorescence yields is estimated to be  $\pm 50\%$ ; however, relative yields are reliable to  $\pm 10\%$ .

## Results

The fluorescence data for 2-(N,N-dimethylamino)pyridine indicate high fluorescence yields in nonpolar, polar, and hydrogen bonding solvents. In general the bands of this compound are shifted to higher wavelengths relative to 2-aminopyridine. This effect is also observed in the absorption spectra of aniline and dimethylaniline.<sup>8</sup> A summary of the absorption and fluorescence data for this molecule is presented in Table I. The data show that the fluorescence wavelength

maximum in hydrogen bonding solvents such as methanol and ethanol remains the same in acetonitrile, *e.g.*, 370 nm, which differs from the observed red shift in the fluorescence peak of 2-aminopyridine under the same conditions. This observation suggests that hydrogen bonding is not enhanced in the excited state. In 0.1 *N* acid solutions it is seen that the fluorescence yield shows an unexpected large decrease to a value of 0.01. This result contrasts sharply with those for 2- and 3-aminopyridine where the fluorescence yield is largest in acidic solutions.<sup>1</sup> Evidence that the first protonation of aminopyridines occurs at the pyridine nitrogen has been presented by Essery and Schofield<sup>10</sup> and also by Katritzky and Reavill;<sup>15</sup> consequently, in 0.1 *N* acid the absorbing species is protonated at the ring nitrogen.

The low fluorescence yield of 2-(N,N-dimethylamino)pyridine in acid coupled with the fact that the 0-0 bands in acid and base are essentially identical suggests no large difference in acidity between the ground state and the first excited singlet state; consequently, some reorganization process, possibly electron transfer from the amine group to the phenyl ring, during the lifetime of the excited singlet, may be responsible for the fluorescence quenching. It is known that the ionization potentials of N-alkyl substituted aromatic amines are lower than those of the parent molecule, and thus they are better electron donors.<sup>8</sup> Fluorescence quenching by electron transfer has been reported by Leonhardt and Weller<sup>16</sup> in the study of perylene as an acceptor and various amines as donors. They observed that the electron transfer process is enhanced in polar solvents and that dimethylaniline is a more effective quencher than aniline. Their results indicate that an amine is more efficient as a quencher as its ionization potential decreases. In the current study 2-(N,N-dimethylamino)pyridine may be considered as an example of an intramolecular donor-acceptor pair with the dimethylamine part of the molecule as the electron donor. In the presence of 0.1 *N* NaOH the fluorescence of 2-(N,N-dimethylamino)pyridine exhibits no significant quenching. Evidently, the lack of replaceable hydrogen in the amine group prevents the quenching process involving proton transfer in the excited state observed for the 2- and 3-aminopyridine.<sup>1</sup>

**Table I:** Absorption and Fluorescence Data for 2-(N,N-Dimethylamino)pyridine<sup>a</sup>

Solvent	$\lambda_{\max}$ (absorb), nm	$\epsilon_{\max}$	$\lambda_{\max}$ (fl), nm	$\phi_f^b$	0-0 band, $\text{cm}^{-1}$
Cyclohexane	310	3120	348	0.36	30,500
Ethyl ether	310	3200	355	0.42	30,150
Acetonitrile	310	3830	370	0.49	29,500
Ethanol	313	3780	369	0.66	29,600
Water	315	4270	384	0.61	28,800
0.1 <i>N</i> H <sub>2</sub> SO <sub>4</sub> (monocation)	319	6000	370	0.01	28,900
10 <i>N</i> H <sub>2</sub> SO <sub>4</sub>	319	6380	376	0.03	28,800
0.1 <i>N</i> NaOH (neutral molecule)	310	3550	384	0.63	28,900

<sup>a</sup>  $pK_a$  for pyridine nitrogen is 7.50; determined in this study.

<sup>b</sup> Excitation at 285 nm; lowest absorption band listed. Fluorescence yields are normalized to a value of 0.09 for *dl*-tryptophan at pH 6.5.

(10) J. M. Essery and K. Schofield, *J. Chem. Soc.*, 3939 (1961).

(11) J. Barassin and H. Lumbroso, *Bull. Soc. Chim. Fr.*, 3143 (1965).

(12) J. R. A. Pollock and R. Stevens, Ed., "Dictionary of Organic Compounds," Oxford University Press, New York, N. Y., 1965.

(13) V. G. Shore and A. B. Pardee, *Arch. Biochem. Biophys.*, **60**, 100 (1956).

(14) R. Chen, *Anal. Lett.*, **1**, 35 (1967).

(15) A. R. Katritzky and R. E. Reavill, *J. Chem. Soc.*, 3825 (1965).

(16) H. Leonhardt and A. Weller, "Luminescence of Organic and Inorganic Materials," H. P. Kallmann and G. M. Spruch, Ed., John Wiley and Sons, New York, N. Y., 1962, p 74.

4-(N,N-Dimethylamino)pyridine was nonfluorescent in all solvents investigated.

The fluorescence of 2-(N-benzylamino)pyridine was also investigated since this compound has an alkyl group replacing one of the amine hydrogens, and its ionization potential lies between the corresponding property for 2-aminopyridine and 2-(N,N-dimethylamino)pyridine. It is interesting to note that this compound, similar to the behavior of 2-aminopyridine, contains an amine hydrogen and shows significant hydroxide ion quenching. A summary of the absorption and fluorescence data for 2-(N-benzylamino)pyridine is presented in Table II. It can be seen that there is fluorescence

**Table II:** Absorption and Fluorescence Data for 2-(N-Benzylamino)pyridine<sup>a</sup>

Solvent	$\lambda_{\max}$ (absorb), nm	$\epsilon_{\max}$	$\lambda_{\max}$ (fl), nm	$\phi_f^b$	0-0 band, $\text{cm}^{-1}$
Cyclohexane	301	4220	340	0.22	31,500
Ethyl ether	302	4280	350	0.28	30,800
Acetonitrile	302	4015	350	0.36	30,800
Ethanol	305	4330	358	0.42	30,300
Water	307	...	367	0.53	29,650
0.1 N H <sub>2</sub> SO <sub>4</sub> (monocation)	310	7220	385	0.15	29,100
10 N H <sub>2</sub> SO <sub>4</sub>	311	7375	384	0.79	29,250
0.001 N NaOH	300	...	365	0.65	30,200
0.1 N NaOH	301	...	365	0.11	30,300

<sup>a</sup>  $pK_a$  for pyridine nitrogen is 6.35; determined in this study.

<sup>b</sup> Excitation at 285 nm; first absorption band listed. Fluorescence yields are normalized to a value of 0.09 for *dl*-tryptophan at pH 6.5.

yield enhancement in going from a nonpolar to a polar and hydrogen bonding solvent. Similar effects were observed in the simple aminopyridines,<sup>1</sup> while Mataga and Tsuno<sup>17</sup> have reported fluorescence enhancement of quinoline and acridine in hydrogen bonding solvents. It is seen that there are fluorescence wavelength shifts and fluorescence intensity differences from nonpolar to hydrogen bonding solvents. Hydrogen bonding effects on the fluorescence of  $\beta$ -naphthol have also been reported.<sup>18</sup> The low fluorescence ( $\phi_f = 0.15$ ) in 0.1 N acid suggests that charge transfer in the excited state from the amine group may contribute to quenching, since its ionization potential lies between that for 2-aminopyridine and 2-(N,N-dimethylamino)pyridine. It should be pointed out, however, that the cation fluorescence can be enhanced by increasing the acid concentration—see result for 10 N H<sub>2</sub>SO<sub>4</sub>. The shift of 0-0 band to lower wavelengths (29,100 to 30,300  $\text{cm}^{-1}$ ) from acid to base solutions is similar to 2-aminopyridine and typical of aromatic heterocyclic molecules.

The fluorescence of 2-(N-phenylamino)pyridine was also investigated in the solvents listed in Tables I and

II; however, in this case there is observed a very efficient quenching mechanism arising from hydrogen bonding solvents associating with the lone pair electrons on the pyridine ring and/or the amine group. An abbreviated summary of the fluorescence results for this molecule is presented in Table III. The results strongly suggest

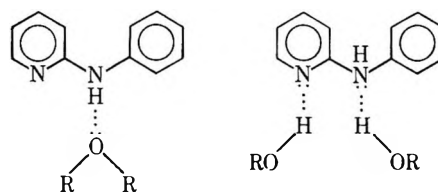
**Table III:** Fluorescence Data for 2-(N-Phenylamino)pyridine<sup>a</sup>

Solvent	$\lambda_{\max}$ (fl), nm	$\phi_f^b$	0-0 band, $\text{cm}^{-1}$
Cyclohexane	346	0.20	30,900
Ethyl ether	364	0.03	30,000
Acetonitrile	385	0.17	29,550
Nonfluorescent in the following solvents: methanol, ethanol, water, 0.1 N H <sub>2</sub> SO <sub>4</sub> , 10 N H <sub>2</sub> SO <sub>4</sub> , 0.1 N NaOH.			

<sup>a</sup>  $pK_a$  for pyridine nitrogen is 5.40; determined in this study.

<sup>b</sup> Excitation at 285 nm; fluorescence yields are relative to *dl*-tryptophan at pH 6.5.

that the following hydrogen bonded species are non-fluorescent



Mataga<sup>19</sup> has reported that in some aromatic heterocyclic molecules where hydrogen bonding is capable of conjugating with the  $\pi$ -electron system of the proton donor, the fluorescence yield decreases as the result of hydrogen bonding formation. It was reported that quenching of fluorescence occurs with phenol but not with benzyl alcohol, which has a hydrogen bond isolated by a  $\sigma$  bond from the  $\pi$ -electron system. Our fluorescence results for 2-(N-phenylamino)pyridine and 2-(N-benzylamino)pyridine show similar hydrogen bonding effects.

## Discussion

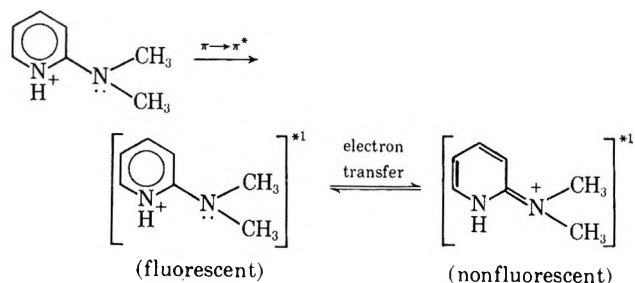
In view of some of the real differences in the fluorescence of the four related molecules: 2-(N,N-dimethylamino)pyridine, 2-(N-benzylamino)pyridine, 2-(N-phenylamino)pyridine, and 2-aminopyridine it becomes necessary to inquire into the character of the lowest excited singlet. In our first study of the aminopyridines it was shown that the lowest singlet exhibited an

(17) N. Mataga and S. Tsuno, *Bull. Chem. Soc. Jap.*, **30**, 368 (1957).

(18) N. Mataga, Y. Kaifu, and M. Koizumi, *ibid.*, **29**, 118 (1956).

(19) N. Mataga, *ibid.*, **31**, 487 (1958).

interplay of  $n, \pi^*$  and  $\pi, \pi^*$  states. In 2-aminopyridine it is predominantly  $\pi, \pi^*$  excitation at the pyridine site with the excited singlet behavior being typically heterocyclic, *i.e.*, more basic in the excited state and the observed fluorescence wavelength maximum being higher in acidic media than in basic media. When we compare the data for 2-(N,N-dimethylamino)pyridine to those for 2-aminopyridine there are two significant differences: (1) the lowest yield occurs in acid for the former, while being the highest for the latter, and (2) fluorescence quenching in NaOH is absent in the former, but very efficient in the latter. Indeed, these two facts appear to characterize aromatic amines more than they do heterocyclics; however, the increased fluorescence quenching in 0.1 *N* acid solutions with substitution of the amine group indicate that electron transfer is probably the cause of radiationless deactivation of the singlet. In addition, fluorescence polarization data support a  $\pi, \pi^*$  assignment for the lowest singlet of these molecules rather than  $1 \rightarrow a_\pi$  as expected for aromatic amines. Weber,<sup>20</sup> Lim, and Chakrabarti<sup>21</sup> have reported the fluorescence polarization of aniline and dimethylaniline to be positive with respect to the first absorption band and negative with respect to the second absorption band. Measurements conducted in our laboratory indicate that the fluorescence polarization of 2-aminopyridine and 2-(N,N-dimethylamino)pyridine measured at room temperature in glycerine and at 77°K in EPA is positive with respect to 285 nm and 254 nm excitation.<sup>22</sup> This result is predicted for a  $C_{1h}$  point group in which the transitions are  $\pi, \pi^*$ , and differs from aromatic amines, *e.g.*, aniline, which are described by point group  $C_{1s}$  (vertical plane of symmetry) arising from the 46° angle between the ring-to-N bond and the  $NH_2$  plane in aniline.<sup>23</sup> It is noteworthy that whereas N,N-dimethylaniline fluoresces, the corresponding anilinium ion does not.<sup>24,25</sup> The fluorescence yield of aniline has been determined to be 0.08 in cyclohexane,<sup>26</sup> while the fluorescence of N,N-dimethylaniline is more than twice as fluorescent as aniline.<sup>24,25</sup> The very weak fluorescence of 2-(N,N-dimethylamino)pyridine when it is protonated at the pyridine nitrogen ( $\phi_f = 0.01$ ) suggests that the following sequence of events may account for its weak fluorescence



The distinct differences in the fluorescence of the molecules studied relative to 2-aminopyridine can be seen

**Table IV:** Relative Fluorescence Yields for Aminopyridines in Different Solvents

	Ethanol	0.1 <i>N</i> H <sub>2</sub> SO <sub>4</sub>	0.1 <i>N</i> NaOH
2-Aminopyridine <sup>a</sup>	0.37	1.20	0.05
2-(N-Benzylamino)pyridine	0.42	0.15	0.11
2-(N,N-Dimethylamino)pyridine	0.66	0.01	0.63

<sup>a</sup> Reference 1.

by a comparison of their quantum yields in different media, which are summarized in Table IV.

The results in Table IV illustrate the necessity of amine hydrogens in order to see fluorescence quenching *via* proton transfer in the excited state. Similar effects have been observed by Förster<sup>27</sup> in the ionization in alkaline solutions in the excited state for  $\beta$ -naphthylamine and N-methyl- $\beta$ -naphthylamine; however, the fluorescence of N-dimethyl- $\beta$ -naphthylamine is not quenched since it has no available proton. In another case White<sup>28</sup> observed that indole and its derivatives exhibit no detectable fluorescence in 0.1 *N* NaOH; however, the fluorescence of N-methylindole remains unchanged even in 5 *N* NaOH.

The absence of fluorescence in 2-(N-phenylamino)pyridine when dissolved in hydrogen bonding solvents is in contrast to the behavior of 2-aminopyridine. In fact Mataga and Tsuno<sup>17</sup> have observed fluorescence enhancement in some heterocyclics, *e.g.*, quinolinium and acridinium ion exhibits more fluorescence than the neutral molecule. In other cases, however, fluorescence quenching of aromatic heterocyclics has been attributed to hydrogen bond formation.<sup>29</sup> They observed that when the hydrogen bond of a donor such as phenol or aniline is intimately related with the  $\pi$ -electron system undergoing absorption a decrease in fluorescence yield was observed. This situation apparently obtains in 2-(N-phenylamino)pyridine. The effective fluorescence quenching observed with ethyl ether relative to cyclohexane and acetonitrile suggests

(20) G. Weber in "Fluorescence and Phosphorescence Analysis," D. M. Hercules, Ed., Interscience Publishers, New York, N. Y., 1966, p 226.

(21) E. C. Lim and S. K. Chakrabarti, *J. Chem. Phys.*, **47**, 4726 (1967).

(22) We thank Mr. Surat Hotchandani of this laboratory for these measurements.

(23) J. C. D. Brand, D. R. Williams, and T. J. Cook, *J. Mol. Spectrosc.*, **20**, 359 (1966).

(24) R. T. Williams, *J. Roy. Inst. Chem.*, **83**, 611 (1959).

(25) R. T. Williams and J. W. Bridges, *J. Clin. Pathol.*, **17**, 371 (1964).

(26) I. Berlmann, "Handbook of Fluorescence Spectra of Aromatic Molecules," Academic Press, Inc., New York, N. Y., 1965.

(27) T. Förster in "Photochemistry in the Liquid and Solid States," L. J. Heidt, R. S. Livingston, E. Rabinowitch, and F. Daniels, Ed., John Wiley and Sons, New York, N. Y., 1960, p 10.

(28) A. White, *Biochem. J.*, **71**, 217 (1959).

(29) N. Mataga and S. Tsuno, *Bull. Chem. Soc. Jap.*, **30**, 711 (1957).

effective quenching by bonding between the lone pair on the oxygen and the amine proton.

In summary, the comparison of the fluorescence behavior of 2-aminopyridine with that for 2-(N,N-dimethylamino)pyridine indicates that the lowest excited state is  $\pi, \pi^*$  in both molecules. The decrease of the fluorescence yield in acid solutions for 2-(N,N-dimethylamino)pyridine and 2-(N-benzylamino)pyridine is due to electron transfer resulting from a lower ionization potential relative to 2-aminopyridine. The shift of the 0-0 band to a higher value for 2-(N-benzylamino)pyridine when going from acidic to basic media, *i.e.*, more basic in the excited state, is expected for an aromatic heterocyclic molecule. The large fluorescence yield for 2-(N-benzylamino)pyridine in 10 *N* H<sub>2</sub>SO<sub>4</sub> may be the result of protonation of the amine lone-pair electrons which would inhibit electron transfer to

the ring and thus lead to an increase of fluorescence yield as observed with 2-aminopyridine.<sup>1</sup> In fact, the largest yield for this molecule is observed in 10 *N* H<sub>2</sub>SO<sub>4</sub>.

In 2-(N-phenylamino)pyridine the fluorescence quenching by ether may be due to bonding between the lone pair electrons of oxygen and the amine proton, which is compatible with increased charge transfer to the heterocyclic ring. The absence of fluorescence in oxygen- and hydrogen-bonding solvents arising from hydrogen-bonding effects is opposite to the observed behavior of simple aminopyridines, but not a generalization for heterocyclic molecules.

The results presented in this study illustrate the difficulty and caution in trying to generalize the behavior of closely related molecules in their electronically excited states.

## Reactions of Adsorbed Organic Molecules. I. Bromination of Diethyl Fumarate on a Silica Surface

by M. J. Rosen and C. Eden<sup>1</sup>

*Department of Chemistry, Brooklyn College of the City University of New York, New York, New York 11210*  
(Received July 9, 1969)

A study has been made of the bromination of diethyl fumarate adsorbed onto Cab-O-Sil, a nonporous hydroxylated silica. The results indicate that the reaction is completely stereospecific and yields exclusively the *trans*-bromination product, *meso*-diethyl 2,3-dibromosuccinate. The kinetics of the reaction indicate first-order dependency on the olefin adsorbed close to the surface and on the bromine adsorbed on the Cab-O-Sil. A mechanism for the reaction is proposed.

Very little is known of the effect of surfaces on the bromination of olefins. For the one reaction studied, the bromination of ethylene on glass,<sup>2</sup> it was shown that the presence of a polar surface is essential for the reaction. Preliminary work in this laboratory<sup>3</sup> showed that silica surfaces exhibit a marked catalytic effect on the bromination of such olefins as oleic and cinnamic acids, both in the presence and absence of a solvent. The rate of bromination, in fact, was so rapid that meaningful kinetic data were difficult to obtain. Since diethyl fumarate is very unreactive to bromine in the absence of a polar solvent or surface and has no allylic hydrogens whose presence might complicate the reaction, this compound was selected for investigating the effect of a polar surface on the bromination reaction. The surface selected for investigation was Cab-O-Sil,<sup>4</sup> a well-defined, nonporous hydroxylated silica.

### Experimental Section

**Materials and Apparatus.** The diethyl fumarate (DEF) and diethyl maleate (DEM) used were both Eastman Kodak Co. White Label grade, redistilled before use. The bromine (Baker Analyzed) was kept over P<sub>2</sub>O<sub>5</sub>.

The Cab-O-Sil used in the experiment was Type M-5. It had a surface area of 200 ± 25 m<sup>2</sup>/g and a surface OH concentration of 0.9 mmol/g.<sup>5</sup> Before use, it was

(1) On leave from the Physical Chemistry Department, The Hebrew University, Jerusalem, Israel.

(2) (a) T. D. Stewart and K. P. Edlund, *J. Amer. Chem. Soc.*, **45**, 1014 (1923); R. G. W. Norrish, *J. Chem. Soc.*, **123**, 3006 (1923); (b) G. Williams, *J. Chem. Soc.*, 1747, 1758 (1932).

(3) M. J. Rosen and A. Silverstein; M. J. Rosen and C. Eden, unpublished results.

(4) Cabot Corp., Boston, Mass.

(5) R. Z. Naar, Cabot Corp., private communication.

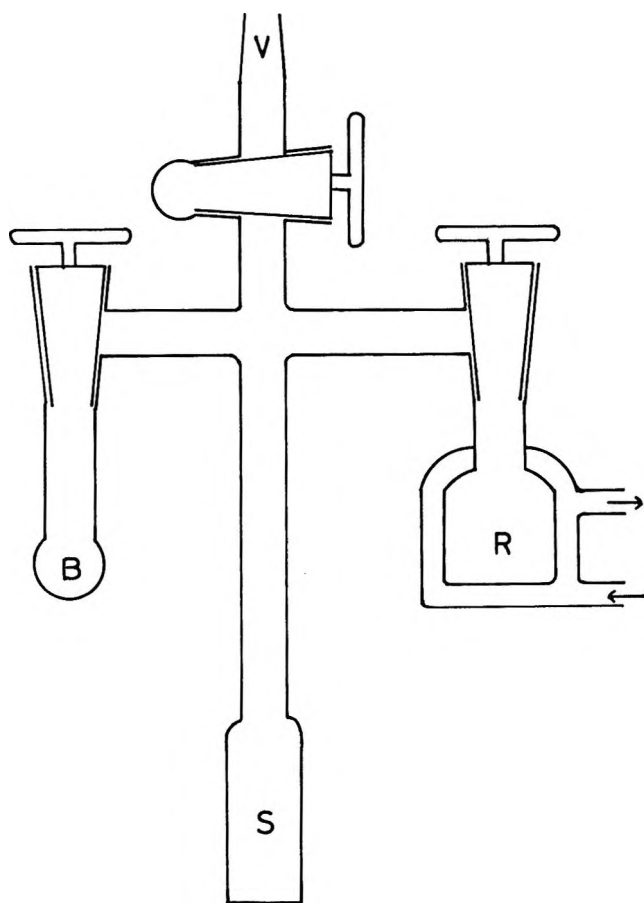


Figure 1. Apparatus for measurements of adsorption isotherms of bromine on Cab-O-Sil.

dried for 3 days at  $110^\circ$  and kept stoppered in a desiccator over  $P_2O_5$ .

The apparatus used (Figure 1) consisted of three parts connected by stopcocks. Arm B is a reservoir for dry, out-gassed liquid bromine. Arm S—the central part—contains at the bottom a 1-cm spectrophotometer cell; arm R is a water-jacketed reaction cell connected to a water bath maintained at  $25 \pm 0.05^\circ$ . The apparatus is of such dimensions that the spectrophotometer cell fits into the cell holder of a Beckman DU spectrophotometer. Measurements were made in a room maintained at  $25 \pm 1^\circ$ .

**Preparation of the Surface.** The desired quantities of diethyl fumarate (DEF) or diethyl maleate (DEM) in Spectral grade  $CCl_4$  solution were added under argon to the Cab-O-Sil in a long-necked Erlenmeyer flask. The  $CCl_4$  was evaporated under reduced pressure in a rotary evaporator and then on a vacuum system to a constant weight. Before removal from the vacuum system, the Erlenmeyer flask containing the treated Cab-O-Sil was filled with dry argon to prevent contact with air or moisture.

**Kinetic Studies.** While argon was flowing into the reaction apparatus through joint V and out the top of arm R, the long neck of the Erlenmeyer flask was in-

serted into R until it was beneath the gas stream and the treated Cab-O-Sil poured into R, the argon again serving as a blanket to prevent contact with water vapor or air. The stoppered empty flask was weighed again and the difference in weight was recorded as the weight of impregnated adsorbent used. The introduction of the sample was done while the barrel of stopcock R was out and no grease present, and only after the sample had been added was the greased barrel inserted. (The vacuum grease used was Kel-F No. 90.) At this stage liquid bromine was introduced into arm B and outgassed by repeated freezings and thawings, using liquid  $N_2$ . The whole apparatus was evacuated to  $10^{-5}$  Torr through joint V. Arm R was covered with opaque black material to exclude light.

The apparatus was put into a Gilford-modified Beckman DU spectrophotometer equipped with a specially constructed light-proof cover and a jacketed spectral cell holder connected to a water bath maintained at  $25 \pm 0.05^\circ$ . With stopcocks V and R closed, bromine vapors were introduced from arm B into arm S. With stopcocks B, V, and R closed, the optical density of the bromine at  $\lambda = 416$  nm was measured, and the initial amount of bromine was calculated, using  $\epsilon = 170$ .<sup>6</sup> Stopcock R was then opened, and the rate of bromination was followed by the change in the optical density of the bromine in the gas phase as a function of time. Initial concentrations of DEF ( $A^\circ/g$ ) used varied from 0.14 mmol/g of Cab-O-Sil to 0.8 mmol/g; initial bromine concentrations ( $B^\circ/g$ ) used varied from 0.21 mmol/g of Cab-O-Sil to 1.26 mmol/g. Concentrations beyond these ranges could not be used because of limitations imposed by the size of the apparatus and the accuracy of optical density measurements.

Measurements of adsorption of bromine on Cab-O-Sil covered with brominated diethyl fumarate (BDEF) showed that 10–40 min, depending on the bromine pressure, was required to reach adsorption equilibrium. As a result, only kinetic data taken after the first 30–40 min were used. Since 5–6 hr was required to complete a kinetic study, the data recorded for the rates of reaction are considered to be at adsorption equilibrium.

The amount of unreacted bromine,  $B^\circ - x$ , in the system at any time (where  $x$  = the amount reacted at that time) was obtained by adding the amount of bromine adsorbed on the surface to that in the gas phase. Thus

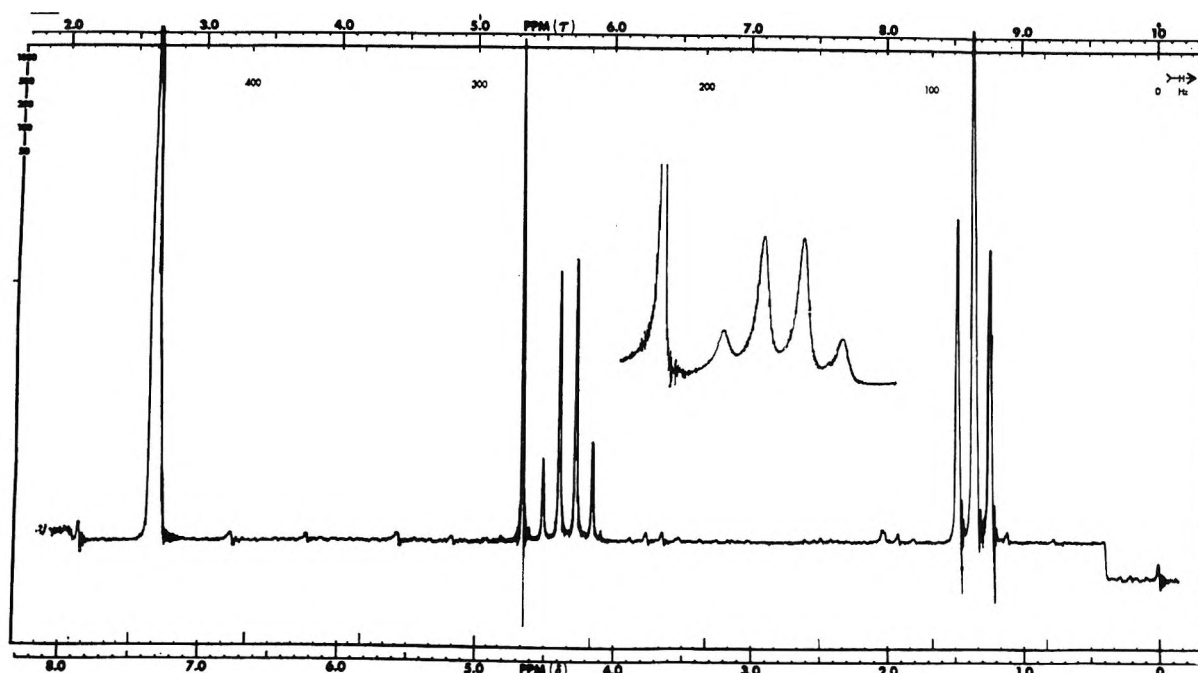
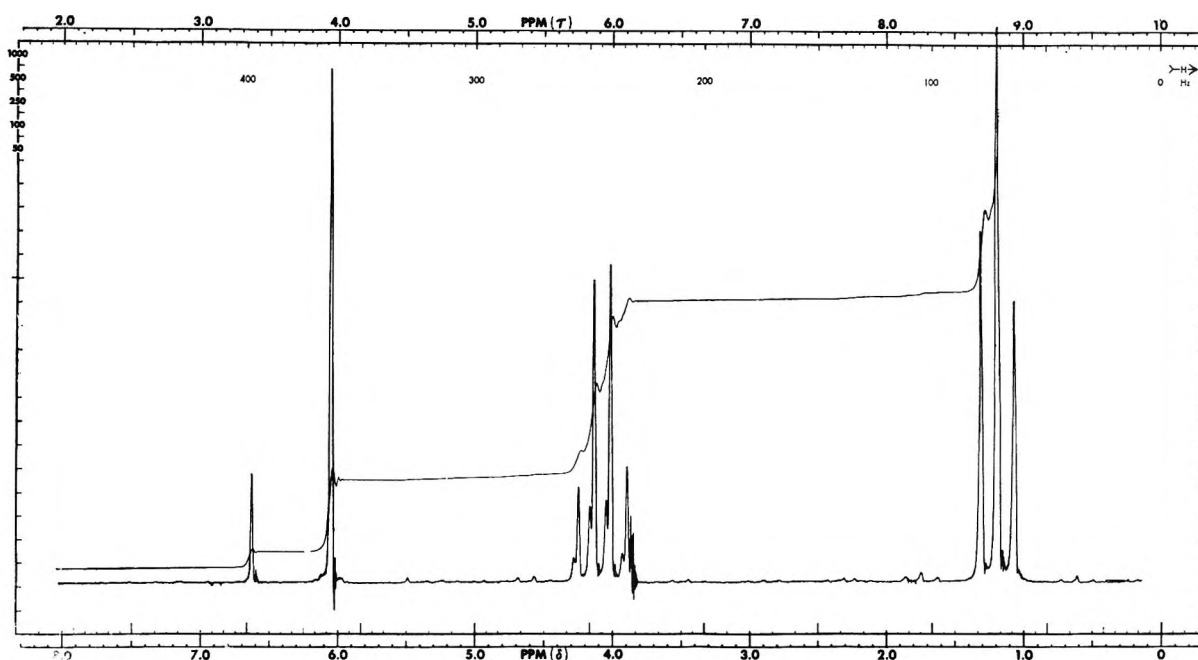
$$B^\circ - x = Ba + [B]V \quad (I)$$

where  $V$  = total free volume of sections R and S of the apparatus. (The experimental error in  $B^\circ - x$ , is estimated at  $\pm 5\%$ .)

The amount of bromine,  $Ba$ , on the surface at any bromine vapor concentration,  $[B]$ , was taken from the

(6) A. A. Passchier, J. D. Christian, and N. W. Gregory, *J. Phys. Chem.*, **71**, 937 (1967).



Figure 2. Nmr spectrum of BDEF in  $\text{CHCl}_3$ .Figure 3. Nmr spectrum of a mixture of DEM and DEF in  $\text{CCl}_4$  solution (19% DEF).

adsorption isotherm of bromine on a BDEF-covered surface with the same coverage (moles/gram) as the DEF used. The error in using the isotherm for a BDEF-covered surface rather than that for a DEF-covered surface (which was impossible to obtain because of the simultaneous bromination reaction) is believed to be insignificant.

Since the DEF is essentially nonvolatile under the conditions of our experiments, its initial concentration on the surface was taken as equal to that originally used in treating the surface.

*Adsorption Isotherms of Bromine on Cab-O-Sil Covered with Brominated Diethyl Fumarate (BDEF).* The same apparatus and procedures for preparation of the surface and introduction of the sample were used in the determination of these adsorption isotherms. However, after measuring the initial optical density of the bromine in arm S, with stopcock R closed, the latter was opened and the bromine vapors were allowed to reach equilibrium with the adsorbent. The optical density was again recorded, and from the predetermined volumes of arms S and R the amount of bromine

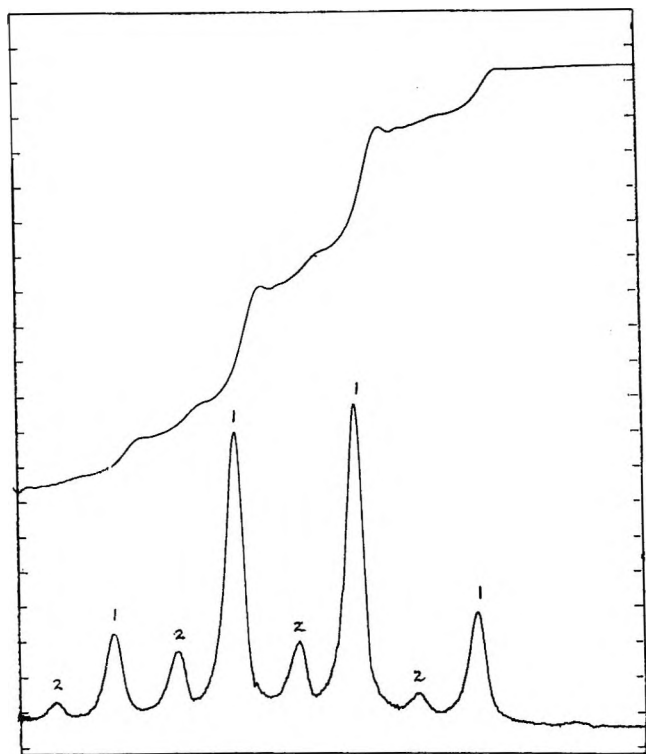


Figure 4. Nmr spectrum of a mixture of BDEM and BDEF in  $\text{CCl}_4$  solution (only methylene quartet part): 1, BDEM; 2, BDEF.

adsorbed per gram of Cab-O-Sil was calculated. Further additions of bromine from arm B permitted the recording of the full adsorption isotherm.

## Results and Discussion

*Nature of the Bromination Product (BDEF).* The nmr spectrum and other physical properties of the bromination product show it to be the product of *trans*-bromination of diethyl fumarate, *meso*-diethyl 2,3-dibromosuccinate.

The nmr spectrum of diethyl fumarate has a peak at 398 cps (6.63 ppm) corresponding to the *trans*-olefinic hydrogens; in the brominated product (Figure 2), extracted directly from the surface by  $\text{CHCl}_3$ , without further purification, these hydrogens are at 280 cps (4.67 ppm). The relative intensity of these hydrogens to the quartet of the methylene group is 1:2, as expected for a completely brominated product. The spectrum in the vicinity of the methylene peaks (inset Figure 2) shows no trace of the isomeric *cis*-bromination product (see below).

To check the stereospecificity of the bromination, a diethyl maleate–diethyl fumarate mixture was adsorbed onto Cab-O-Sil and brominated by the same procedure used for DEF. The original mixture contained approximately 19% DEF, as indicated by the relative intensities of the DEF and DEM olefinic hydrogen peaks at 398 (6.63 ppm) and 364 cps (6.07 ppm), respectively (Figure 3). After bromination, the product contained

approximately 20% BDEF, as indicated by the relative intensities of the peaks in the methylene quartets for BDEF and BDEM (Figure 4).

The bromination product is a solid, crystallizing in needles, mp  $58^\circ$ , in agreement with the literature.<sup>7</sup> By contrast, the *cis*-bromination product, *dl*-diethyl 2,3-dibromosuccinate, is a liquid.<sup>7</sup>

The possibility of isomerization of DEF to DEM on the Cab-O-Sil surface was eliminated by a run in which DEF was adsorbed onto the surface, but no bromine added. Extraction of the DEF from the surface and examination of its nmr spectrum showed it to be identical with the original. No trace of a peak corresponding to *cis*-olefinic hydrogen (at 364 cps) was found.

It is concluded therefore that the bromination of both DEF and DEM on this surface proceeds *via* an exclusively *trans*-bromination mechanism.

*Mobility of the Adsorbed DEF and BDEF.* Bromination experiments using 0.8 mmol DEF/g, equivalent to more than four monolayers (see below), showed that a stoichiometric amount of  $\text{Br}_2$  was consumed in the reaction and that the bromination product had no un-brominated material (as evidenced by the absence of olefinic hydrogen adsorption peaks at 398 cps in the nmr spectrum). Since  $\text{Br}_2$  in the gas phase does not react significantly, under the conditions of our experiments, with DEF which is not adsorbed onto a surface, this implies both lateral and vertical diffusion of the DEF and its bromination product on the surface under these conditions, in the absence of any solvent.

*Adsorption Studies.* Adsorption isotherms of DEF and BDEF from hexane onto Cab-O-Sil are given in Figure 5. From these curves, the monolayer values of DEF and BDEF are 0.183 and 0.150 mmol/g, respectively. These values are in good agreement with the inverse ratio of their molecular cross-sectional areas as determined by models ( $98 \text{ \AA}^2$  for DEF and  $125 \text{ \AA}^2$  for BDEF).

Adsorption isotherms of bromine onto bare Cab-O-Sil and Cab-O-Sil covered with various amounts of BDEF and  $25^\circ$  are illustrated in Figure 6. These isotherms were taken after the termination of the bromination process. Only the uncovered surface of Cab-O-Sil shows a Type II BET isotherm; the other isotherms are of Type III. All isotherms were found to be reversible.

The amounts of adsorbed bromine per gram of Cab-O-Sil are very close to being independent of the coverage of the surface by BDEF at low bromine pressures and low BDEF concentrations. At higher bromine pressures, there is dependency on the extent of coverage by BDEF. Contrary to what one might expect, the amount of bromine on the surface per gram of Cab-O-Sil at high BDEF coverages increases with

(7) "Dictionary of Organic Compounds," Vol. II, 4th ed, Oxford University Press, New York, N. Y., 1965, p 946.

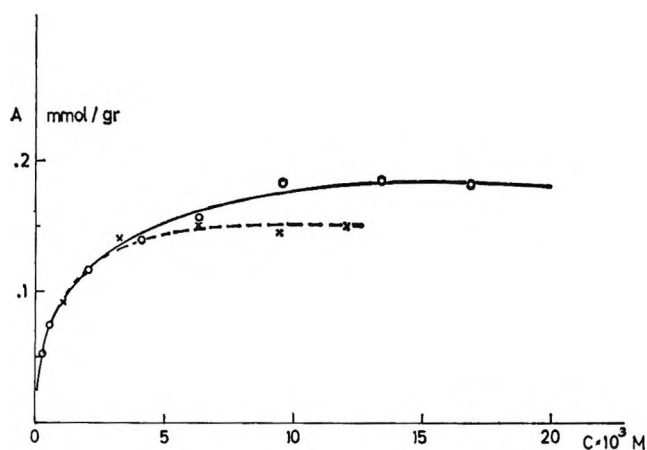


Figure 5. Adsorption isotherm of DEF (O) and BDEF (X) from hexane onto Cab-O-Sil.

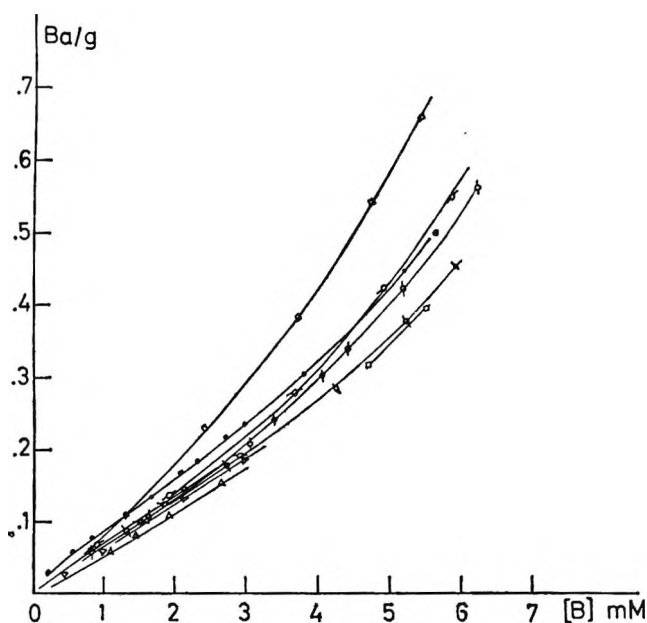


Figure 6. Adsorption isotherms of bromine on Cab-O-Sil at different coverages by BDEF.  $Ba/g$  = millimoles of bromine adsorbed per gram of Cab-O-Sil;  $[B]$  = equilibrium concentration of bromine in the gas phase. Amount of BDEF in moles per gram:  $\bullet$ , 0;  $\circ$ , 0.39;  $\nabla$ , 0.39;  $\Delta$ , 0.086;  $\square$ , 0.088;  $\square$ , 0.183;  $\circ$ , 0.200;  $\phi$ , 0.364;  $\sigma$ , 0.532;  $\diamond$ , 0.736.

coverage instead of decreasing. This effect begins to become apparent at a BDEF coverage of more than 0.2 mmol/g, which is slightly above the monolayer value for BDEF. This increased surface concentration can be explained as solubility of the bromine in the adsorbed multilayer of BDEF. The adsorption isotherms, therefore, illustrate two phenomena: (1) adsorption on Cab-O-Sil, which is linear with  $[B]$  up to a bromine vapor concentration of about  $3 \times 10^{-3} M$ , for low coverages by BDEF (0.2 mmol/g or less), and (2) dissolution in, or adsorption on, BDEF which is dependent on BDEF coverage and becomes significant at a BDEF coverage of more than 0.2 mmol/g

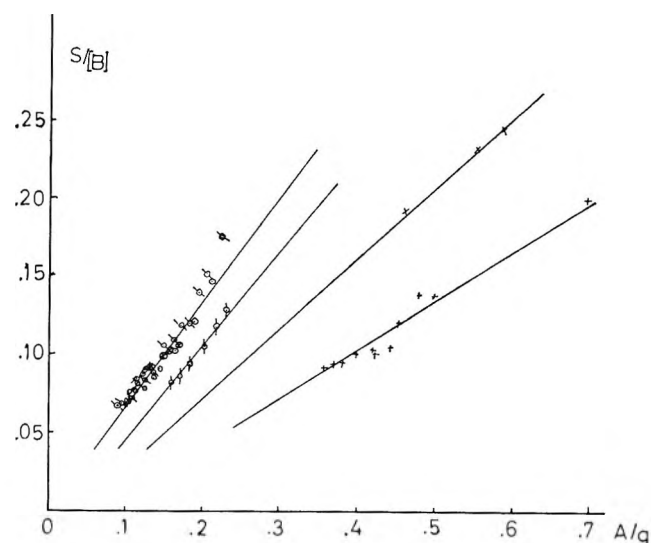


Figure 7. Kinetics of bromination of DEF (notations correspond to run no. in Table I):  $\sigma$ , 1;  $\circ$ , 2;  $\otimes$ , 3;  $\square$ , 4;  $\phi$ , 5;  $\times$ , 6;  $+$ , 7 and 8.

g. For kinetic measurement it is important to distinguish between the two.

*Kinetics of Bromination.* The rate of bromination of DEF was followed by determining the amount of unreacted bromine per gram of Cab-O-Sil,  $B^\circ - x/g$ , as a function of time. During the first 0.5 hr or so a sharp drop in the concentration of bromine in the gas phase was observed, due mainly to the establishment of adsorption equilibrium with the surface. Therefore, only data taken after the first 30–40 min were used for kinetic studies. The rate of bromination at any instant  $[d(B^\circ - x)/g]/dt \equiv S$  was determined from slopes of plots of the above results. Plots of  $S/[B]$  vs.  $A/g$ , where  $A$  is the amount of unreacted diethyl fumarate at time  $t$ , are given in Figure 7. The initial concentrations ( $A^\circ/g$  and  $B^\circ/g$ ) and the rate constants are given in Table I. The data indicate that the bromination is first order with respect to the gaseous bromine and ester on the surface, *i.e.*

Table I

Run no.	$A^\circ/g$ , mmol/g	$B^\circ/g$ , mmol/g	$S$	$S$
			$A/g[B]$ = $k$ , l./mol min	$A^\circ/g[B]$ = $k_c$ , l./mol min
1	0.144	0.212	0.72	0.72
2	0.183	0.629	0.65	0.65
3	0.200	0.396	0.72	0.72
4	0.200	0.617	0.70	0.70
5	0.364	0.658	0.53	0.67
6	0.532	1.045	0.42	0.77
7	0.736	0.568	0.27	0.69
8	0.492	1.260	0.25	0.64
( + 0.244 BDEF )				

$$\frac{d(B^\circ - x)/g}{dt} = k[B]A/g \quad (\text{II})$$

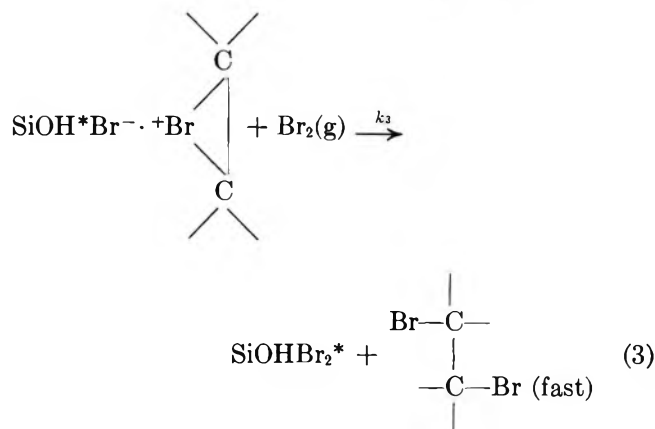
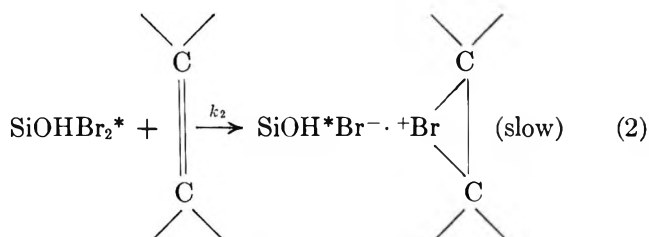
However, the results of previous investigators<sup>2</sup> and the accepted mechanism for bromination of olefins require a polar medium, which in the present case can only be the Cab-O-Sil surface. It must be concluded therefore that only bromine adsorbed on the Cab-O-Sil surface can be activated and react with the olefin. The adsorption studies of bromine on Cab-O-Sil covered with BDEF (Figure 6) show that at low coverages and bromine pressures the amount adsorbed is linear with the pressure in the gas phase. Under these conditions, therefore, the rate of bromination is also proportional to the concentration of adsorbed bromine. At high bromine pressure and/or high BDEF coverages, however, the bromine concentration on the surface is not proportional to the bromine concentration in the gas phase and under these conditions, consequently, the rate of bromination is not proportional to the bromine on the surface. The explanation is that the adsorption of bromine directly on the Cab-O-Sil surface must be distinguished from the second effect causing disappearance of bromine from the gas phase, namely, dissolution of bromine in, or adsorption on, BDEF. This effect, which is superimposed on the adsorption isotherm, becomes significant only at high bromine pressures and at coverages higher than 0.2 mmol of BDEF per gram of Cab-O-Sil. Only the bromine adsorbed onto the Cab-O-Sil surface, not that dissolved in or adsorbed onto BDEF, is "active" bromine and can act as a brominating agent.

For concentrations of  $A^\circ/g$  up to approximately 1.5 monolayers (0.29 mmol/g), the value of the rate constant,  $k$ , in eq II is  $0.69 \pm 0.04$  l./mol min. As  $A^\circ/g$  is increased above this value, the rate constant drops. Since all of the ester used in our experiments was eventually brominated, the drop in rate constant with increase in  $A^\circ/g$  above the value equivalent to about 1.5 monolayers implies that above this concentration only a fraction of the unreacted ester is "active" at any instant. The change in rate constant in the neighborhood of the equivalent of 1.5 monolayers of adsorbed ester may therefore be a reflection of the collision diameter of the "active" bromine, signifying that the DEF in the upper layers can react only after diffusion to the surface of the Cab-O-Sil. Hence, the values of  $k$ , for the experiments where  $A^\circ/g$  is higher than 0.29 mmol/g have to be corrected accordingly. The amount of "active" ester,  $A^*$ , at any instant is  $A(0.29/A^\circ)$  for experiments where  $A^\circ$  exceeds 0.29 mmol/g, and therefore the corrected rate constant,  $k_c$ , equals  $kA^\circ/0.29$ . These corrected values are given in the last column of Table I. When corrected in this manner, the rate constants for all runs fall within the range  $0.69 \pm 0.08$  l./mol min.

The concentration of "active" bromine,  $Ba^*$ , ab-

sorbed directly on the Cab-O-Sil surface can be introduced into the rate equation by using the linear correlation between the concentration of bromine in the gas phase and the adsorbed bromine at low bromine pressure and low coverages. Since the slope of the linear portion of the adsorption isotherm is about 0.065 l./g, this yields a rate constant for the bromination reaction ( $k_2$ ) of about 10 g/mol min.

On the basis of the foregoing, a possible mechanism for the bromination reaction is



where  $\text{SiOH}^*$  represents an active OH group on the Cab-O-Sil surface.

According to this mechanism, the effective brominating agent is a complex formed by adsorption of a molecule of bromine onto an active OH group on the Cab-O-Sil surface. This is consistent with infrared absorption studies on Cab-O-Sil which indicate that there are no Lewis acid sites on this surface<sup>8</sup> and that the hydrogen of the free OH groups on the surface is used to hydrogen bond polar and polarizable molecules to the surface.<sup>9</sup>

This complex reacts with a molecule of olefin adsorbed close to the surface in a rate-determining step which is first order in both adsorbed olefin and bromine adsorbed on active sites on the Cab-O-Sil to yield an ion pair on the surface. Rapid reaction of this ion

(8) N. W. Cant and L. H. Little, *Can. J. Chem.*, **43**, 1252 (1965).

(9) R. S. McDonald, *J. Amer. Chem. Soc.*, **79**, 850 (1957); *J. Phys. Chem.*, **62**, 1168 (1958).

pair with a molecule of gaseous bromine yields the dibromide product and regenerates the active bromine complex.

The rate equations corresponding to the proposed mechanism are

$$K = \frac{k_1}{k_{-1}} = \frac{[Ba^*/g]}{[\text{SiOH}][B]} \quad (\text{adsorption equilibrium}) \quad (4)$$

$$\frac{dA/g}{dt} = k_2[Ba^*/g][A^*/g] = k_2K[\text{SiOH}][B][A^*/g] \quad (5)$$

where  $A^*$  = value of  $A$  corrected for the collision diameter of "active" bromine,  $Ba^*$ .

The calculated corrected rate constant  $k_c = k_2K[\text{SiOH}]$ ; the  $[\text{SiOH}]$  is a constant typical of the silica surface used.

## Confirmation of Spontaneous Spreading by Water on Pure Gold

by Marianne K. Bernett and W. A. Zisman

Laboratory for Chemical Physics, Naval Research Laboratory, Washington, D. C. 20390 (Received October 7, 1969)

A drop of pure water was found to spread spontaneously and remain spread (*i.e.*, contact angle remained zero) on a smooth, clean, pure gold surface provided that strict precautions are observed to avoid any hydrophobic contamination. Throughout these experiments emphasis was placed on the care necessary, even when initially preparing a pure gold surface, to prevent the presence or accidental introduction of trace organics in the atmosphere or in the water from adsorbing on the gold as hydrophobic contaminants. A description is given of the methods used to eliminate possible sources of hydrophilic artifacts on the polished gold surface, such as residual polishing agent or traces of base metal oxides. These experiments confirm the hydrophilic nature of pure gold at ordinary temperatures.

### Introduction

Within the last five years renewed attention has been paid by a small group of investigators to the question whether a clean gold surface is wettable by water. The problem in relation to the wetting properties of high-energy surfaces had been investigated and summarized in more general terms as early as 1955 by Fox, Hare, and Zisman,<sup>1</sup> who concluded then that all pure liquids spread spontaneously on high-energy surfaces unless they are organic liquids which are either autophobic or are hydrolyzed on contact with the solid surface. Renewed interest in the water wettability of gold resulted from a paper by White,<sup>2</sup> who reported experiments with condensed water vapor on gold in a Pyrex and metal system and concluded that water would not spread in the absence of a layer of gold oxide. Erb,<sup>3</sup> subsequently working with a closed cyclic distillation system where pure steam was continuously condensed, reported a steady state and large water contact angles on each metal. In the case of gold, he reported values from 55 to 85° even after several thousand hours of continuous still operation, when he expected the gold would have been thoroughly cleaned from physically or chemically adsorbed contamination; he explained that these results were caused by the presence of an oxide film on the gold. Using a different method, Bewig and

Zisman<sup>4</sup> reported that water on pure gold always exhibited a zero contact angle if the system was maintained free from traces of organic contamination; they came to this conclusion from heating and cooling gold in carefully purified streams of hydrogen, nitrogen, neon, argon, and krypton, and thus were in agreement with the conclusions reached earlier by Fox, Hare, and Zisman.<sup>1</sup> White and Drobek<sup>5</sup> then dropped their claims that a gold oxide caused water wetting of gold and stated that the presence of an inorganic impurity, such as residual alumina polishing agent, made the gold surface more hydrophilic. Therefore, they used diamond paste suspended in kerosene as their polishing agent and followed that by heating the specimen in oxygen at 1000°. By this procedure, they obtained water contact angles on gold of 61°. Erb, whose earlier results were used for theoretical calculations by Thelen,<sup>6</sup> reported more recently<sup>7</sup> that the values of 60–

(1) H. W. Fox, E. F. Hare, and W. A. Zisman, *J. Phys. Chem.*, **59**, 1097 (1955).

(2) M. L. White, *ibid.*, **68**, 3083 (1964).

(3) R. A. Erb, *ibid.*, **69**, 1306 (1965).

(4) K. Bewig and W. A. Zisman, *ibid.*, **69**, 4238 (1965).

(5) M. L. White and J. Drobek, *ibid.*, **70**, 3432 (1966).

(6) E. Thelen, *ibid.*, **71**, 1946 (1967).

(7) R. A. Erb, *ibid.*, **72**, 2412 (1968).

65° were the only reliable contact angles of water on gold. Values of 60–65° are the same as those reported by Bewig and Zisman in an early paper<sup>8</sup> for water on a gold or platinum surface which had been covered with an adsorbed monolayer of a nonpolar organic hydrocarbon, such as hexane or benzene, which points to the possibility that organic contaminants may have been adsorbed on the gold surface in the experiments of Erb and White.

This report demonstrates that pure gold surfaces at 20° can be spontaneously wetted by water (contact angle 0) in the absence of polishing agents or other inorganic contaminants provided that the most scrupulous precautions are taken to remove or to prevent accidental adsorption of traces of organic compounds.

### Experimental Materials and Techniques

The gold specimens of 99.9999% purity were supplied by Handy and Hartmann. Each specimen, in the shape of a disk 1 cm in diameter and 1.6 mm thick, had an integral pin 2.5 mm in diameter and 6 mm long on its back surface in order to facilitate its handling with tweezers. All water used throughout the experiments was obtained by passing the effluent of a Stokes tin still through a double quartz still just prior to use and was always as hot as possible when collected at the still exit in order to boil off dissolved gases. The gold surfaces were polished on AB microcloth (boiled once in Tide solution and three successive times in distilled water to remove gross organic contaminants) with a distilled water slurry of magnesium oxide (Buehler 40-6440 AB Magomet) and then were rinsed copiously until completely water-wetted.

The wet gold specimen was then immersed for 20–25 min in a 6 *N* aqueous solution of HCl to leach out any surface residue of MgO. After this treatment, the disk was flushed thoroughly with distilled water, placed on a freshly flamed gold wire support (carefully avoiding contact with the experimental surface), and was immediately lowered into a cylindrical Pyrex vessel containing 0.5% aqueous NaCl (Baker Analyzed, ACS specification) solution for electrolytic degreasing. The NaCl solution had been previously prepared and was pumped into the electrolysis vessel from the bottom of its storage flask; thus any organic contaminants which originated as the salt dissolved were left behind as a film adsorbed on the solution. A freshly flamed 2 by 2 cm platinum foil (suspended on a platinum wire) was immersed in the electrolytic cell and salt solution to serve as the anode and the gold specimen at the end of a gold wire suspension as the cathode. Electrolysis was carried on in the Pyrex cell for 30–45 sec at 6–7 V and 0.06–0.08 A. Under these conditions the numerous small hydrogen bubbles generated at the gold surface carried away with them any adsorbed organic contaminants and deposited them on the surface of the liquid in the electrolytic cell. Under the electrochemical conditions

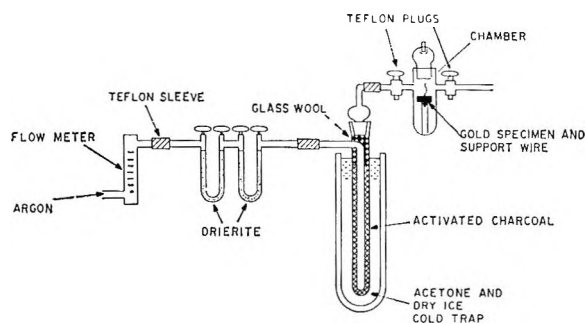


Figure 1. Gas purification assembly and Pyrex chamber.

used, no oxide could form nor could a film of chloride ions be left adsorbed on the gold. The glass electrolysis vessel was then repeatedly overflowed with grease-free distilled water to remove any organic contaminants adsorbed at the water–air interface. The gold electrode supported by the wire then was quickly withdrawn through the surface of the clean water and promptly placed, while still completely coated by water, inside the glass chamber of the system shown in Figure 1.

Prepurified Grade argon, purity 99.998% minimum (Matheson Co.), was led at a flow rate of 350 cm<sup>3</sup>/min through a double 30 cm long U-tube of Drierite followed by a column 40 cm long and 4 cm diameter of Fischer activated coconut charcoal adsorbent (6 to 14 mesh) which was cooled by a Dry Ice–acetone mixture. The charcoal-filled cold trap was essential for removing the traces of organic contaminants in the argon gas stream.<sup>4</sup> Prior to inserting the water-wet gold specimen, the glass chamber had been purged for at least 30 min by the clean argon stream. The complete gas-purification train and viewing chamber were constructed from Pyrex glass components and Teflon sleeves and stopcock plugs for easy disassembly and acid cleaning.

Unless noted otherwise, the gold specimen remained in the gas stream for 35–60 min (which allowed an additional 15–20 min after the gold surface looked dry to the naked eye) before a small sessile drop of water at the end of a freshly flamed platinum wire was touched to its surface. In order to do so, the chamber was opened for 1 sec against the gas current *via* a 6 mm diameter Teflon-plugged opening in the top of the ground-glass cap. If spontaneous spreading of the water drop did not occur over the entire plane surface of the gold disk, the advancing contact angle was measured with an external goniometer telescope<sup>9</sup> which had been modified so that the illuminator and telescope could be moved laterally and independently from the viewing chamber.

All glassware used was cleaned in a hot bath of 1:1 nitric acid and sulfuric acid; the chamber of the experimental train was freshly acid cleaned and mixed with grease-free distilled water before each determination. The gold specimen was manipulated by its stem only

(8) K. Bewig and W. A. Zisman, *J. Phys. Chem.*, **68**, 1804 (1964).

(9) H. W. Fox and W. A. Zisman, *J. Colloid Sci.*, **5**, 514 (1950).

with freshly flamed platinum-tipped tweezers. All experiments were carried out at  $23 \pm 1^\circ$ .

### Experimental Results

Under the carefully controlled conditions described above, 14 out of 19 independent experiments (74%) resulted in complete spontaneous spreading (0 contact angle) of the water drop (Table I), 3 showed contact angles less than  $5^\circ$ , and 2 showed contact angles between 5 and  $10^\circ$ . The causes for each nonzero value could be traced to either delay in the transfer of the gold specimen from electrolyte bath to observation chamber, or to exposure of the specimen in the drying and viewing chamber for times longer than 120 min. Bewig and Zisman<sup>4</sup> showed that even a highly purified gas delivered by such a train usually allows passage of a trace of organic contamination in the gas sufficient to permit its accumulation as a condensed monolayer on the small clean metal disk during runs lasting over several hours. Contact angles larger than  $10^\circ$  occurred only in our preliminary experiments when one or more of the rigid requirements for elimination or prevention of organic contamination had not been recognized and observed.

**Table I:** Spreading Behavior of Water Drop on Gold

Contact angle $\theta$ , deg	First drop		Second drop <sup>a</sup>	
	Total	%	Total	%
0	14	74	5	71
5	3	16	2	29
5-10	2	10	...	...

<sup>a</sup> Drop placed on same area after evaporation of first drop in argon flow.

Several times the original drop, after it spread on the gold surface, was permitted to evaporate undisturbed in the argon gas stream; a second water drop was then placed on the same area. Table I shows that out of 7 such experiments, 5 drops (or 71%) spread spontaneously, and 2 drops (29%) exhibited contact angles of less than  $5^\circ$ . Total exposure of the gold specimen in the chamber was, with one exception, less than 120 min.

### Selection of a Suitable Polishing Agent

White and Drobek<sup>5</sup> and Erb<sup>7</sup> suggested after publication of the paper by Bewig and Zisman<sup>4</sup> that the complete water wettability of gold observed by the latter was caused by residual abrasives retained by the gold surface, and cited examples of low water contact angles, presumably as a result of such hydrophilic contamination. In the experiments described in this report, we decided to eliminate such sources of hydrophilic contamination by leaching out any residual abrasive particles left on the polished gold surface. Polishing

agents suitable for a soft metal, such as gold, are  $\alpha$ -alumina, diamond powder, rouge ( $\text{Fe}_2\text{O}_3$ ), and magnesia ( $\text{MgO}$ ). Alumina was ruled out because it is not easily dissolved in any conventional acid or inorganic solution. Diamond powder was not considered suitable for this investigation for two reasons: first, because it requires kerosene as suspension medium, thus introducing organic contaminants, and second, because any residual diamond particles can be removed only by heating the gold specimen in an oxygen atmosphere; this may introduce contaminants of another nature, as will be discussed later. Rouge could be leached from the surface by immersing the gold specimen, after polishing and rinsing, in concentrated HF for 1 hr. A thorough examination of the polished gold surface with a scanning electron probe X-ray microanalyzer (Applied Research Laboratories) did not detect any  $\text{Fe}_2\text{O}_3$  particles after the HF leaching process, whereas  $\text{Fe}_2\text{O}_3$  particles were found distributed on the surface in fair abundance when the HF leaching was omitted. We did not, however, pursue our studies with  $\text{Fe}_2\text{O}_3$  because the long immersion time in the highly corrosive concentrated HF may cause accidental introduction of impurities from the atmosphere or from the walls of the container, and because an alternate independent technique for the detection of residual particles on the gold surface, as described below, was inapplicable for Fe. Magnesia proved to be the most suitable polishing agent; it could be leached from the surface by a 20-30-min immersion in a 6 N HCl solution in sufficient quantity to remain undetected by the X-ray microanalyzer on preliminary scanning of the entire surface at low magnification (40 $\times$ ) and subsequent detailed examination of twenty randomly selected areas (25  $\mu$  by 20  $\mu$ ) at 4000 $\times$  magnification.

A nuclear activation analysis carried out with a 5-MV Van de Graaf accelerator<sup>10</sup> with the 1.548-MeV resonance in the  $^{26}\text{Mg}(p,\gamma)^{27}\text{Al}$  reaction as the means of detection found less than  $10^{15}$  atoms of magnesium ( $10^{15}$  atoms is the limit of sensitivity of this method for Mg) per  $\text{cm}^2$  of the gold surface after the leaching treatment, compared to  $5 \times 10^{15}$  atoms of magnesium per  $\text{cm}^2$  without such treatment. A convenient way to express such quantities is in terms of the actual distribution of MgO particles over the available surface. If we assume the MgO particles, which have a diameter range from 0.5 to 1.0  $\mu$ , to be spherically shaped, we can compute the number of particles that would contain  $10^{15}$  Mg atoms (or MgO molecules). The average quantity thus calculated is  $10^6$  particles per  $\text{cm}^2$  of gold surface. If these particles were aggregated coherently in one single layer, they would occupy an area of  $3.5 \times 10^{-4} \text{ cm}^2$ . Thus, expressing the presence of less than

(10) J. W. Butler and E. A. Wolicki in "Proceedings of the 1968 International Conference on Modern Trends in Activation Analysis," National Bureau of Standards Special Publication 312, Vol. II, U. S. Govt. Printing Office, Washington, D. C., 1969, p 791.

$10^{15}$  Mg atoms per  $\text{cm}^2$  of gold surface in terms of corresponding coverage of MgO particles, we find that these particles are dispersed over less than 0.035% of the total gold surface area.

No magnesia particles were detected by the X-ray microanalyzer on twenty randomly selected areas of  $5 \times 10^{-6} \text{ cm}^2$  each, which is 0.006% of the total available gold surface. But we can also conclude from the preceding paragraph that activation analysis, which scanned the entire sample area, proved that there were fewer than  $10^{15}$  magnesium atoms present per  $\text{cm}^2$  of the surface. Therefore, our results from the X-ray microanalyzer are more sensitive to the presence of MgO particles for the entire surface by about one order of magnitude. The results of using both activation analysis for the entire surface combined with those of the X-ray microanalyzer at magnifications of  $4000\times$  of 20 random areas may be considered as an indication of essentially zero magnesium oxide particles.

We discontinued the method of electropolishing the gold in a glacial acetic acid, hydrochloric acid, and water solution, which was used by Meakin<sup>11</sup> and Erb,<sup>7</sup> since the inherent sources of organic contamination (possibly in the acetic acid) prevented us from obtaining a gold surface that emerged completely wetted by the solution or by water.

#### Effect of Elevated Temperatures

The experimental procedure in the present work was designed to avoid heating the gold specimen throughout the experiments. There seems to be no doubt that gold neither reacts with air at temperatures up to  $500^\circ$  to form an oxide,<sup>12,13</sup> nor chemisorbs a significant quantity of oxygen.<sup>14-16</sup> It has been suggested, however, that any traces of bulk impurities present in the gold may diffuse to the surface during heating to form base metal oxides<sup>13,17</sup> or segregate at grain boundaries,<sup>18</sup> phenomena which are capable of affecting the wettability of gold. At room temperature no such diffusion could occur, nor is there any likelihood for oxygen to chemisorb onto the surface of gold.<sup>14,15,19,20</sup> Avoidance of high temperatures, incidentally, also eliminated any possible deposition of material from the walls of our glass chamber to the enclosed gold specimen.

The absence of water vapor in the argon atmosphere of the measuring chamber was noted as a possible source of error leading to low water contact angles.<sup>7</sup> In a recent series of papers,<sup>21-23</sup> we demonstrated that water adsorbed on a high-energy surface, such as glass, quartz, sapphire, or a variety of metals, converts such a surface to one of much lower surface energy. In the present work no increase in water contact angle was observed when a second drop of water was added to the first within about 1 hr, provided the first drop had spread spontaneously over the dry gold surface.

#### Conclusion

We conclude from our experimental evidence that pure water spreads spontaneously, *i.e.*, exhibits a zero contact angle, on a smooth, clean, pure gold surface provided the following precautions are rigidly observed to avoid hydrophobic contamination: (1) the water must not contain adsorbed or dissolved organics and gases; (2) the gold surface must be mirror smooth and free of adsorbed organic or inorganic contaminants; and (3) the atmosphere in which the experiments are carried out must be purified of all trace organics to prevent any accidental introduction of hydrophobic adsorbents.

We carefully removed or avoided any hydrophilic artifacts that were proposed by other investigators as contributing to the water wettability of a gold surface, such as residual polishing agent<sup>5,7</sup> or the presence of a gold oxide<sup>2,3,6</sup> or trace base metals.<sup>7</sup> The theoretical concept proposed by Fowkes that dispersion forces across metal surfaces act similarly to those of organic surfaces, and his corollary that water will not spread on many oxide-free metals,<sup>24</sup> is not sustained by the results reported here.

*Acknowledgment.* The authors wish to thank Dr. James W. Butler and Dr. Eligius A. Wolicki of the Nuclear Physics Division for their cooperation in performing and interpreting the nuclear activation analysis; Mr. Edward J. Brooks of the Metallurgy Division for his careful analysis with the X-ray microanalyzer; and Mr. Sigmund Schuldiner of the Chemistry Division for helpful discussions on the electrolysis techniques employed.

- (11) J. D. Meakin, *Rev. Sci. Instrum.*, **35**, 763 (1964).
- (12) D. E. Clark, T. Dickinson, and W. N. Mair, *Trans. Faraday Soc.*, **55**, 1937 (1959).
- (13) D. E. Clark, T. Dickinson, and W. N. Mair, *J. Phys. Chem.*, **65**, 1470 (1961).
- (14) O. D. Gonzales and P. Parravano, *J. Amer. Chem. Soc.*, **78**, 4533 (1956).
- (15) O. Hayward and B. M. W. Trapnell, "Chemisorption," 2nd ed, Butterworth and Co. (Publishers) Ltd., London, 1964.
- (16) M. V. Kul'kova and L. P. Levchenko, *Kinet. Katal.*, **6**, 765 (1965).
- (17) R. C. Plumb and N. Thakkar, *J. Phys. Chem.*, **69**, 439 (1965).
- (18) E. D. Hondras and D. Gladman, *Surface Sci.*, **9**, 471 (1968).
- (19) B. J. Hopkins, C. H. B. Mee, and D. Parker, *Br. J. Appl. Phys.*, **15**, 865 (1964).
- (20) W. M. H. Sachtler, G. J. H. Dorgelo, and A. A. Holscher, *Surface Sci.*, **5**, 221 (1966).
- (21) E. G. Shafrin and W. A. Zisman, *J. Amer. Ceram. Soc.*, **50**, 478 (1967).
- (22) M. K. Bennett and W. A. Zisman, *J. Colloid Interface Sci.*, **28**, 243 (1968).
- (23) M. K. Bennett and W. A. Zisman, *ibid.*, **29**, 413 (1969).
- (24) F. M. Fowkes, *Ind. Eng. Chem.*, **56**, 40 (1964).



# Ultrahigh-Vacuum Techniques in the Measurement of Contact Angles.

## II. Water on Gold<sup>1</sup>

by Malcolm E. Schrader

Naval Applied Science Laboratory, Flushing and Washington Avenues, Brooklyn, New York 11251  
(Received January 5, 1970)

The contact angle of water on gold was measured in ultrahigh-vacuum and conventional vacuum systems by means of the vapor phase transfer technique. Moderate surface activation (heating in oxygen and vacuum) of a polished gold disk resulted in a large contact angle hysteresis, with a gradual decrease in both the receding and advancing angles occurring upon increased activation of the surface. In the conventional vacuum system a limit was reached at which a low receding but relatively high advancing angle was obtained. In the ultraclean (ultrahigh vacuum) system increasing activation resulted in a zero receding angle at first, and ultimately in a zero advancing angle as well. Contact angle measurements in the ultrahigh-vacuum system on gold films evaporated *in situ* yielded zero advancing and receding angles without prior surface activation. The hysteresis on the solid gold surfaces was due to the presence of areas of hydrophobic contamination on the hydrophilic gold surface, with the decrease in contact angle resulting from gradual removal of the contamination during surface activation.

### Introduction

Fox and Zisman<sup>2</sup> have classified solid surfaces into the categories of high and low energy with respect to characteristics affecting their wettability. The high-energy surfaces include metals, metal oxides, and siliceous glasses, while those of low energy consist mainly of organic materials. As a rule, compounds which are liquid at room temperature spread on high energy surfaces, since their surface tensions are considerably less than the surface energies of these solid substrates. An important characteristic of these high energy surfaces from the practical point of view is the tendency they have to lower their surface free energy by picking up hydrophobic organic contamination. It is consequently necessary to subject them to some sort of cleaning procedure before measuring their wettability. In fact, the ability to spread water is widely used as a criterion of the cleanliness of a high-energy surface in this respect.

In 1964 White<sup>3</sup> reported results of observations of the wetting of gold surfaces by water under atmospheric conditions. He obtained dropwise condensation from air saturated with water vapor under conditions of cleanliness during surface preparation and wettability measurement which were adequate to render base metals hydrophilic, *i.e.*, able to spread water. He ultimately reported the contact angle as  $60 \pm 5^\circ$ .<sup>4</sup> In 1965 Erb<sup>5</sup> reported continuous dropwise condensation of water vapor in a gold-plated still at atmospheric pressure. Fused quartz and nonnoble metals were observed to yield filmwise condensation under these same conditions. Shortly thereafter, Bewig and Zisman<sup>6</sup> reported a water contact angle of  $0^\circ$  on a gold disk which had previously been heated to near melting in a flowing

atmosphere of hydrogen (at atmospheric pressure) purified of organic contaminants. When the precautions against contamination of the flowing hydrogen were relaxed, the contact angle was no longer zero. In 1968 Erb<sup>7</sup> reported the results of contact angle measurements at atmospheric pressure on a series of gold surfaces prepared in a variety of ways. There was a very large scatter to the data, with an average contact angle of about  $12^\circ$  under certain conditions and  $63^\circ$  under different conditions. He chose  $63^\circ$  as his best result and attributed lower angles to various types of hydrophilic contamination.

We<sup>8</sup> have previously investigated the contact angle of methylene iodide on glass, using ultrahigh-vacuum techniques in surface preparation followed by *in situ* measurement of the contact angle by means of a vapor phase transfer procedure. The purpose of the ultrahigh-vacuum technique was to eliminate all traces of water in order to obtain and measure contact angles of methylene iodide on truly anhydrous surfaces. In the present work the same technique is utilized, but with the objective of measuring the contact angle of water on a gold surface completely devoid of organic contamination. This is made possible by the complete absence

(1) Presented at the 157th National Meeting of the American Chemical Society, Minneapolis, Minn., April 1969.

(2) H. W. Fox and W. A. Zisman, *J. Colloid Sci.*, **5**, 514 (1950).

(3) M. L. White, *J. Phys. Chem.*, **68**, 3083 (1964).

(4) M. L. White and J. Drobek, *ibid.*, **70**, 3432 (1966).

(5) R. A. Erb, *ibid.*, **69**, 1306 (1965).

(6) K. W. Bewig and W. A. Zisman, *ibid.*, **69**, 4238 (1965).

(7) R. A. Erb, *ibid.*, **72**, 2412 (1968).

(8) M. E. Schrader, *J. Colloid Interface Sci.*, **27**, 743 (1968).

of any organic components in the all metal and glass ultrahigh-vacuum system.

### Experimental Section

*Ultrahigh-Vacuum Runs.* The vapor phase transfer technique for contact angle measurements of true liquids under ultrahigh-vacuum conditions is described elsewhere.<sup>8</sup> Briefly, the method consists of activating the surface in a clean ultrahigh-vacuum system, admitting vapor to the system, condensing the vapor in the sample chamber by means of a cold finger, and depositing a drop on the sample surface through magnetic manipulation. The cold liquid in the finger is removed either immediately after or before deposition of the drop on the sample surface. The contact angle is then read by means of a goniometer eyepiece mounted on a telescope.

The 15 l. per sec ion pump, ion gauge, and bakeable valves were the same as used previously.<sup>8</sup> In this work a quartz sample chamber and manifold were used for the experiments with polished gold disk surfaces. Graded seals joined the manifold to the Pyrex break-seals and adaptor flange on the metal cut-off valve. The graded seals were situated approximately 22, 23, and 30 in., respectively, from the sample. The entire system was capable of attaining a pressure of  $2 \times 10^{-10}$  Torr or lower. The distilled water was thoroughly degassed *in vacuo* before sealing off into the break-seal tubes.

For the experiments on evaporated gold films, a spherical Pyrex sample chamber was utilized. Tungsten electrical leads were spot welded to a tungsten conical basket type heater placed in the chamber between the walls and cold finger. A ball of 99.999+ $\%$  pure gold was placed in the basket and the system given a preliminary bake-out. The tungsten basket was degassed through resistance heating and the entire system baked out until a vacuum pressure reading in the  $10^{-10}$  Torr decade could be obtained at room temperature. The basket was again degassed electrically at red heat for 2 hr before evaporating the gold. The evaporation procedure consisted of raising a polished disk of fused silica or carbon magnetically to the top of the cylindrical portion of the sample chamber, then increasing the heater current until gold evaporated and condensed onto the substrate surface. Towards completion of evaporation the pressure was approximately  $9 \times 10^{-9}$ . Upon cessation of evaporation it dropped rapidly to the  $10^{-10}$  decade. The contact angle was then measured in the usual fashion.

*Conventional High-Vacuum Runs.* In some experiments a manifold with conventional high-vacuum glass stopcocks lubricated with high-vacuum grease was used instead of the bakeable all-glass and metal ultrahigh-vacuum system. This manifold was evacuated with a two-stage oil diffusion pump backed by a mechanical forepump. One liquid nitrogen trap was sealed between

the two pumps and another between the diffusion pump and the Pyrex manifold. A quartz sample chamber, identical in design with that used in the ultrahigh-vacuum system, was connected to the manifold by means of a graded seal.

*Preliminary Preparation of the Gold Disk Surfaces.* The samples consisted of polished gold disks of 99.999+ $\%$  purity. The gold disks were abraded, polished to a mirror finish with an aqueous slurry of diamond powder on clean Gamal cloth, then rinsed in distilled water. Residual diamond powder was then removed with a fresh piece of Gamal cloth wet with distilled water, followed by wiping with wet untreated lens tissue. The surface activation (heating in oxygen and vacuum) performed in the vacuum apparatus will be described separately for each sample in the tables in the Results section. In all runs where heating in air was followed by heating under vacuum (at the same temperature) the temperature was maintained during evacuation.

### Results

*Hysteresis.* A striking feature of the results was the hysteresis of the water contact angle which was observed during the various stages of surface activation of the gold disk. The hysteresis effect was observed in a number of different ways. (a) *Freezing out the water vapor in the vacuum system after the drop was on the gold surface.* As the drop evaporated, a receding angle was observed. Manipulations of the vapor pressure in vacuum eliminated the possibility that this was due to the effect of vapor pressure on the contact angle. (b) *Observing the contact angle change with time.* The drop may continue to spread for many hours. (c) *Agitation of the drop.* This caused immediate partial spreading.

*Experiments with Gold Disks.* Upon raising the temperature and time of heating of gold in air followed by evacuation, the receding angle decreased to zero, while the advancing angle decreased to about 20–30°. With more activation, the advancing angle decreased further, while the receding remained zero. In the conventional vacuum system (Table I), a limit was reached in the decrease of the advancing angle. Further activation either raised the angle or ceased to lower it. In the ultrahigh-vacuum system (Table II) on the other hand, increased activation decreased the advancing angle to zero degrees.

*Experiments on Gold Films Evaporated In Situ.* The contact angle of water on a gold film (Table III) evaporated onto the surface of a polished fused silica disk was zero. The system was evacuated again and another layer of gold deposited on top of the original. The contact angle was zero once more. A few minutes was sometimes required for the drop to reach the equilibrium zero value.

**Table I:** Contact Angles on Gold Disk in Conventional Vacuum System

Surface activation	Drop no.	Advancing angle, deg	Drop history after initial reading: time lapse from previous reading or mechanical agitation	Receding angle, deg
Vacuum, 100°, 3 hr	1	29	...	0
		19	Mechanical agitation	
Air, 570°, 1 hr, followed by vacuum, 580°, 1 hr	1	20	...	14
		18	Mechanical agitation	
Air, 580°, 2 hr	1	28	...	...
		25	...	
	2	14	Mechanical agitation	
		23	...	
	2	11	Mechanical agitation	
		22.5	...	
Vacuum, 600°, 1.5 hr	1	11	Mechanical agitation	0
		35	...	
	2	27	Mechanical agitation	
		20	10 min	
	1	15	30 min	...
		30	...	
Air, 720°, 2 hr	1	28	1 min	...
		19	Mechanical agitation	
	2	48	...	
		37	Mechanical agitation	
Vacuum, 700°, 2 hr	1	28	...	...
		22	3 min	
	2	22	7 min	
		6	Mechanical agitation	
	2	26	...	
		11	Mechanical agitation	

in another experiment the gold was deposited on a polished graphite surface. A zero contact angle was again observed a few minutes after deposition of the water drop. The contact angle of water on the graphite disk surface which was shielded from the gold vapor flux was approximately 22°.

### Discussion

**Hysteresis.** The existence of contact angle hysteresis as a result of contamination or heterogeneity on a smooth surface has been discussed by a number of authors.<sup>9-13</sup> The hysteresis observed in the present work can be attributed to the presence on these surfaces of both hydrophilic and hydrophobic areas, or site clusters. Increased surface activation resulted in an increased ratio of hydrophilic to hydrophobic areas, with an accompanying decrease in both advancing and

**Table II:** Contact Angles on Gold Disk in Ultrahigh-Vacuum System

Surface activation	Drop no.	Advancing angle, deg	Drop history after initial reading: time lapse from previous reading or mechanical agitation	Receding angle, deg
Vacuum, 560°, 2 hr	1	31	...	0
		16	Mechanical agitation	
Air, 1 Torr, 550°, 1.5 hr	1	6	...	...
		2	5	
Air, 710°, 2 hr, followed by vacuum, 710°, 1 hr	1	2	...	...
		0	1 min	
	2	3	...	
		0	5 min	
Air, 715°, 2.5 hr, followed by vacuum, 715°, 2.5 hr	1	5	...	...
		0	5 min	
	2	6.5	...	
		2	1 min	
	2	1	5 min	
		0	30 min	

**Table III:** Contact Angles on Gold Film Evaporated in Ultrahigh-Vacuum System

Run no.	Substrate	Film no.	Drop	Advancing angle, deg	Time after deposition of drop, min
1	Polished silica disk	1	First	Spread with low angle	...
			Subsequent	0	1
		2	First	10	1
			Subsequent	0	6
2	Polished silica disk	1	First	Spreading at low angle	1
			Subsequent	0	2
3	Polished graphite disk	1	First	Spread at <5	...
			Second	8	1
				0	5

receding angles, until a zero receding angle was obtained. At this point the average surface free energy less that of the liquid-solid interface was sufficient to overcome that of the water and keep it spread. The advancing angle was nevertheless still relatively high due to the inability of the drop periphery to advance

(9) F. M. Fowkes and W. D. Harkins, *J. Amer. Chem. Soc.*, **62**, 3377 (1940).

(10) D. C. Pease, *J. Phys. Chem.*, **49**, 107 (1945).

(11) A. B. D. Cassie, *Discuss. Faraday Soc.*, **3**, 11 (1948).

(12) R. J. Good, *J. Amer. Chem. Soc.*, **74**, 5041 (1952).

(13) R. E. Johnson, Jr., and R. H. Dettre, *J. Phys. Chem.*, **68**, 1744 (1964).

across hydrophobic regions. The situation may be pictured on the basis of hydrophilic "islands" in a hydrophobic "sea." As the surface was activated further, the hydrophobic area continued to diminish with an accompanying decrease in the advancing angle until the hysteresis disappeared as the advancing angle reached zero.

*Increase in Surface Hydrophilicity during Activation.* It is clear from a comparison of the conventional high-vacuum and ultrahigh-vacuum experiments that the gradual increase in ratio of hydrophilic to hydrophobic area which occurs upon heating can be interpreted in terms of a gradual removal of hydrophobic organic contamination from the real gold surface. For the case of the measurements in conventional high vacuum, the activation procedure of high temperature oxidation and evacuation gradually cleans the surface, until there are sufficient uncontaminated hydrophilic areas to yield a low or zero receding angle, and an advancing angle of 20–30°. A point is reached at which additional activation is ineffective and may even result in additional contamination. This is due to the fact that the conventional high vacuum is not an ultraclean system. Once the system is evacuated, the residual organic vapors have ready access to the gold surface, unimpeded by the presence of air. When the surface is partially cleaned, a steady state is established at which the rate of contamination equals the rate of vacuum clean up. However, in the ultrahigh-vacuum system which consists solely of metal and glass, there are no organic vapors to recontaminate the gold. The high temperature oxidation–evacuation procedure consequently continues to clean the surface until the hysteresis disappears and the advancing as well as receding contact angle is zero.

The inability of the conventional high-vacuum system to clean the gold surface is not observed for the case of a polished fused-silica surface. In the latter case preliminary heating to 200° is adequate to yield a zero contact angle with water at room temperature. Using water contact angles as a measure of cleanliness, it is apparent that it is far more difficult to remove organic contamination from a gold than from a fused-silica surface. It is clear, then, that a set of conditions which is sufficient to decontaminate one particular surface will not necessarily succeed for a different type.

There is a possible objection to an interpretation of these results in terms of removal of organic contamination. When an impurity in a solid is capable of lowering the surface tension of the clean solid surface, the impurity will tend to migrate to the surface when the temperature is sufficiently high to allow diffusion to take place.<sup>14</sup> Assuming that the surface of real gold is hydrophobic rather than hydrophilic, the ultrahigh vacuum results for the solid gold sample could be explained in terms of hydrophilic impurities diffusing to the surface during the heat cleaning process, causing

hysteresis at first, followed by a zero advancing angle as the surface becomes completely contaminated with the hydrophilic impurities. This explanation is not a very plausible one since the gold is 99.999+ % pure and complete segregation, in a limited time, of impurities from a rather large volume to the surface would be necessary to contaminate a monolayer. Furthermore, for the case of the conventional high-vacuum results it would have to be assumed that the hydrophilic impurities which make their way to the surface subsequently become contaminated by the residual organic vapors, thus preventing the ultimate attainment of a zero advancing angle. Nevertheless, the possibility cannot be completely ruled out on the basis of the solid disk experiments alone. However, the method involving evaporation and condensation of a gold film *in situ* completely bypasses this problem of surface segregation,<sup>15</sup> since the deposited film is very thin and furthermore is not heated.

*Nature of the Uncontaminated Gold Surface.* For the case of any metal other than gold, an uncontaminated real surface would contain chemically combined oxygen, either as a built up surface oxide or as a chemisorbed monolayer. The attainment of a surface which is clean (oxygen free) as well as uncontaminated with organic material, would then entail a procedure such as ion bombardment to remove any chemically combined oxygen already present, followed by maintenance of a suitable ultrahigh vacuum to prevent oxygen from recombining with the surface before the measurement is completed. Of course, for the case of a film evaporated *in situ*, the ion bombardment is not necessary. In the present work, where water vapor is introduced for the measurement, extensive degassing of the water source is not necessarily sufficient to avoid introduction of a sufficient number of oxygen molecules to chemisorb to a few square centimeters of an active metal surface. For the case of metals in general, therefore, a special gettering technique<sup>8</sup> would have to be devised to ensure measurement on an oxygen-free surface.

The surface of gold, however, is unique among all metals in its relative lack of affinity for oxygen. It is the only metal which does not form a bulk oxide which is thermodynamically stable at room temperature. It is consequently not surprising that there is no evidence reported in the literature of the presence of built up (stoichiometric) oxide on the surface of gold.<sup>16</sup> Nevertheless, this does not preclude the existence on the gold surface of a stable chemisorbed monolayer of oxygen at room temperature, since a great deal more energy may be required to dissociate the latter species into a clean gold surface and free oxygen than that required to dis-

(14) L. A. Harris, *J. Appl. Phys.*, **39**, 1428 (1968).

(15) P. W. Palmberg and T. N. Rhodin, *Phys. Rev.*, **161**, 586 (1967).

(16) D. Clark, T. Dickinson, and W. N. Mair, *J. Phys. Chem.*, **65**, 1470 (1961).

sociate the stoichiometric oxide into bulk gold and free oxygen. The energetics of the platinum-oxygen system<sup>17</sup> are a good illustration of this point.

There are, in fact, reports in the literature of the chemisorption of oxygen to gold.<sup>18-20</sup> In these cases, however, the chemisorption is reported to have taken place at elevated temperatures. Attempts to detect chemisorption taking place at room temperature have thus far been unsuccessful.<sup>19,21,22</sup> The effect of temperature seems to be kinetic, with the rate at room temperature, under conditions of pressure thus far investigated, too low to yield significant adsorption even after days of exposure. In short, while the goal of the present work was to report results for the wettability of a gold surface uncontaminated with organic material, it appears, on the basis of presently available information in the literature on the extreme slowness of

oxygen chemisorption to gold, that the conditions of these experiments have resulted in gold surfaces which are oxygen free as well. This is quite likely for the evaporated gold film, of course, and possible also for the gold disk, where the 700° vacuum bake may conceivably have removed chemisorbed oxygen from the surface.

(17) G. Ehrlich, "Metal Surfaces," American Society for Metals, Metals Park, Ohio, 1963, p 221.

(18) N. P. Dobrowolski, V. E. Ostrovski, A. M. Rybushov, and M. E. Temkin, *Dokl. Akad. Nauk SSSR*, **183**, 1120 (1968).

(19) N. V. Kul'kova and L. L. Levchenko, *Kinet. Katal.*, **6**, 765, 688 (1965).

(20) I. S. Sazonova and N. P. Keier, *ibid.*, **6**, 390, 448 (1965).

(21) B. J. Hopkins, C. H. B. Mee, and D. Parker, *Brit. J. Appl. Phys.*, **15**, 865 (1964).

(22) W. M. H. Sachtler, G. J. H. Dorgelo, and A. A. Holscher, *Surface Sci.*, **5**, 221 (1966).

## The Effects of Common Gases on the Flotation of the Water Boule

by Peter J. Harris

Rochester Institute of Technology, Distillation Research Laboratory, Rochester, New York (Received December 8, 1969)

Common gases added to the steam above a floating water boule affect boule behavior in two marked ways, diminution of size and interference with starting. Repeatable quantitative measurements of both effects have been made over the relevant range of 0-7 vol of gas to 1000 vol of supernatant steam. The soluble gases, CO<sub>2</sub>, N<sub>2</sub>O, and C<sub>2</sub>H<sub>2</sub>, caused less alteration of behavior than the insoluble gases, *e.g.*, H<sub>2</sub>, N<sub>2</sub>, A, He, C<sub>2</sub>H<sub>6</sub>, etc. Interference with boule formation is interpreted as evidence that the insoluble gases interacted with the water surface at 100° to provide an adsorbed layer which permits the drop to "wet" and merge with the support water.

### Introduction

This work concerns the interactions of various common gases with the surface of water at the boiling point using a measuring technique centered around the floating liquid boule. The name boule has been applied to those masses of a liquid, larger than individual drops, that can be made to float for periods of minutes or occasionally hours on the surface of the same slightly superheated liquid without mixing. General qualitative and semiquantitative accounts of this phenomenon have been published by Hickman and coworkers.<sup>1-3</sup> They found that injection of N<sub>2</sub>, H<sub>2</sub>, O<sub>2</sub>, and CO<sub>2</sub> into the steam flowing into the boule flask interfered with boule formation and, in general, decreased the size of the boules formed with increasing volume ratio of foreign gas to steam. The effects of the common gases are now studied more fully and it can be shown that these gases, in concentrations of less than 1% by vol-

ume, interact with the water surface and cause: (1) a reduction in boule size and, under highly stylized conditions, (2) prevent the formation of boules—apparently by "wetting" the water surface and the approaching drop allowing them to coalesce. Although boules are chemically nonspecific and can be formed from any liquid, these observations are limited to water.

### Apparatus

The basic apparatus<sup>2,3</sup> generally used for producing boules consisted of a boiler to supply steam to the boule flask and an aerial condenser which returned the condensate at an even rate through a drop counter to the applicator which started and anchored the boule

(1) K. Hickman, *Nature*, **201**, 985 (1964).

(2) K. Hickman, *Ind. Eng. Chem.*, **56**, 18 (1964).

(3) K. Hickman, J. R. Maa, A. Davidhazy, and O. Mady, *Ind. Eng. Chem.*, **59**, 19 (1967).

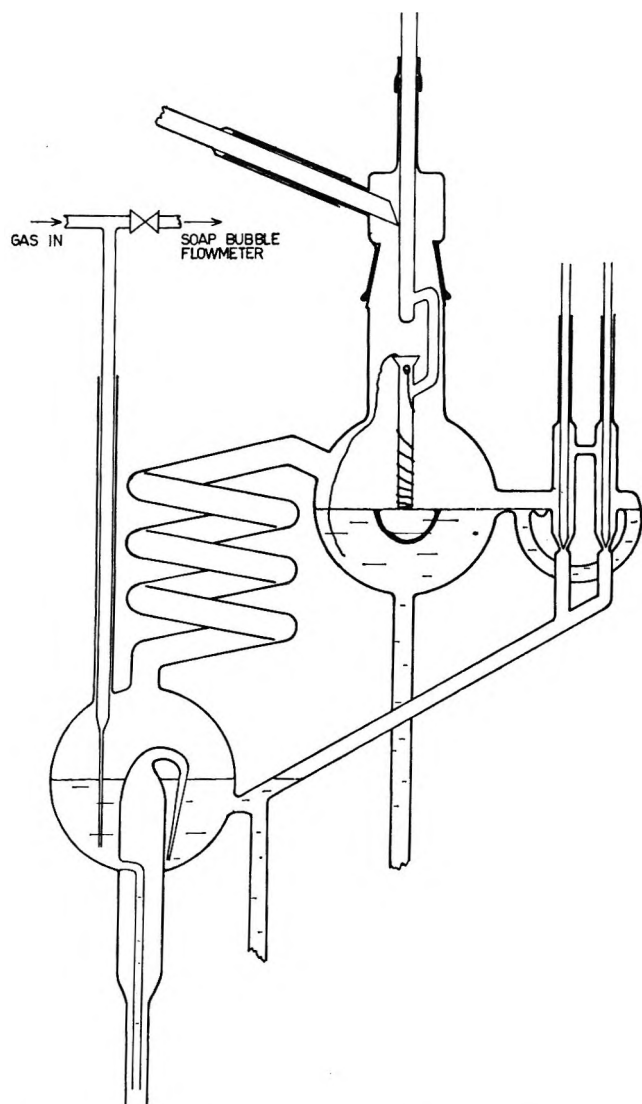


Figure 1. Boulemaker for studying additions of gas to steam.

(Figure 1). In a later design, a constant steam supply was secured by adding a nucleator<sup>4</sup> to the steam boiler. Comparison of illustrations in the references cited will suggest that the "perfect" boulemaker is far from achieved. Modifications for the present research included further steps to exclude air by reducing the diameter of the air-cooled condenser to maintain a very slight back pressure and adjusting the steam supply so that a wisp of steam always issued from the mouth of the condenser. The entrance of the gas-steam mixture to the boule flask was lowered from the neck (as in earlier apparatus) to the body of the flask so that a representative mixture should reach the support water at the position where the new boule is lowered onto the surface. A four-turn glass coil inserted in the steam path served to demist and aid mixing of the gas with the steam. All closures were made by water locks on tight-fitting glass tubing to eliminate contamination from rubber or lubricated seals. The apparatus was employed in an overflow condition,<sup>3</sup> *i.e.*, the surface was

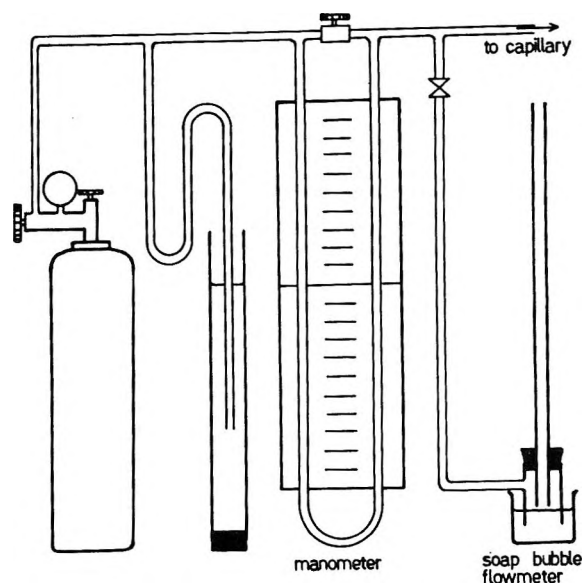


Figure 2. Apparatus for supplying a measured flow of gas to the steam supply flask.

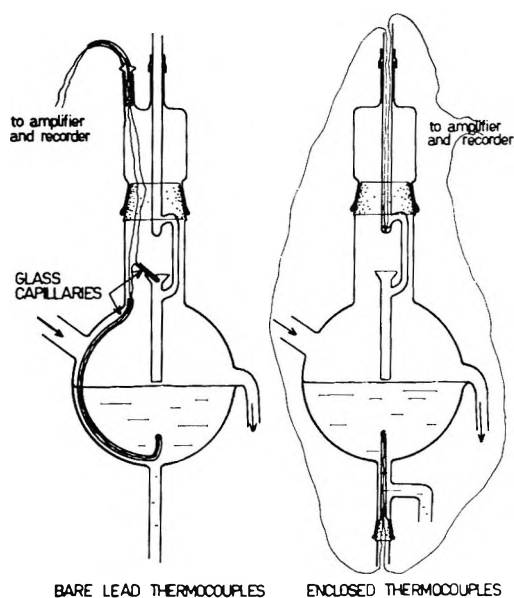


Figure 3. Arrangement of opposed thermocouples in boule flask; left, copper partly shielded; right, copper totally shielded.

allowed to flow away over an escape weir. Thus there was little chance of a contaminating film, *e.g.*, of aluminate-silicate,<sup>4</sup> accumulating on the surface to interfere with gas-water surface interaction. Although not used for this series or experiments, the apparatus was equipped with an alternate device for confining the water surface and allowing the water to escape from beneath, thus establishing the condition of "underflow." All but the condenser and water supply were enclosed in a cabinet held at a temperature of 90°.

(4) K. Hickman, *Separ. Sci.*, **3**, 551 (1968).

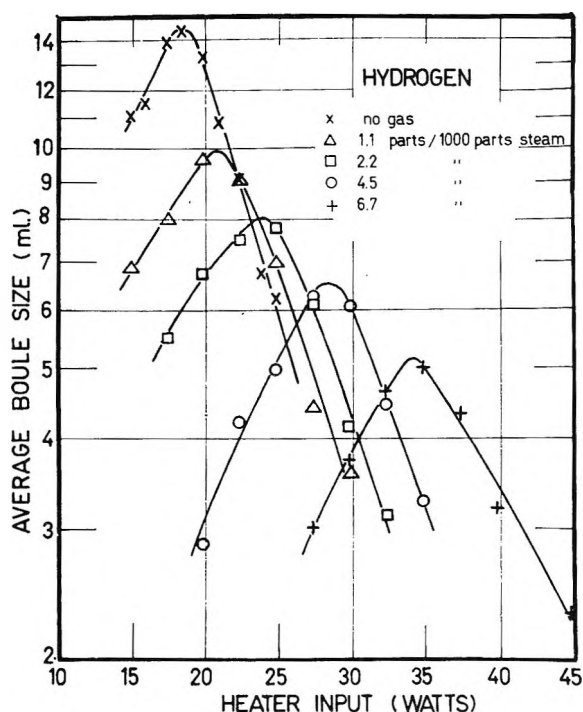


Figure 4. Boule sizes vs. heat input for concentrations of hydrogen in the steam.

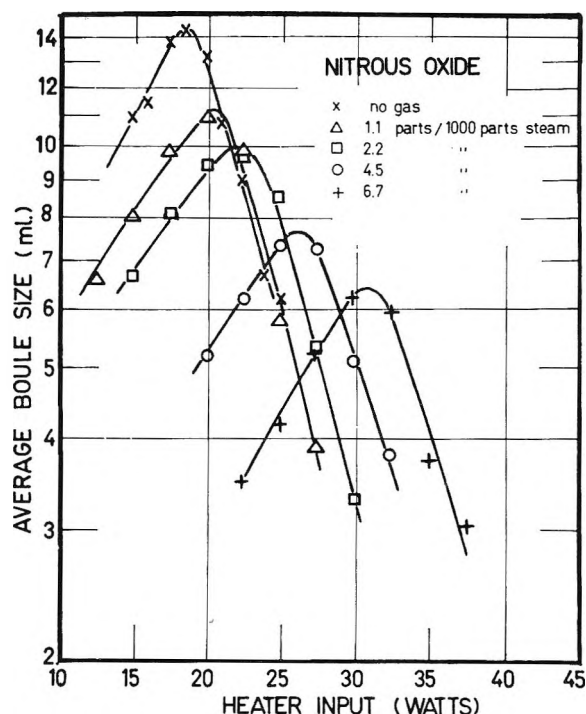


Figure 5. Boule sizes vs. heat input for concentrations of nitrous oxide in the steam.

The test gases used were the highest grade available from the supplier,<sup>5</sup> and in most cases carried a guarantee analysis with a volume purity greater than 99.9%. The individual gases were fed directly from the cylinder through an adjustable hydraulic relief limb and a variable capillary restriction manometer to the steam supply flask through a glass capillary which dipped beneath the boiling water surface (Figure 2). At each setting the manometer was calibrated using a soap bubble flowmeter. Temperature sensors were omitted in the early measurement because knowledge of the degree of superheat,  $\Delta T_s$ , of the support water was not then of primary importance. Later, opposed Cu-Advance thermocouples were inserted to measure the temperature difference between the returning condensate and a point in the support water below the boule, the combination providing a fluctuating history of the superheat (Figure 3). Part of the bare thermocouple leads were exposed to the steam and touched the walls of the flask. When the thermocouples were finally enclosed in glass capillaries, the boule measurements were found to differ slightly from measurements made with the bare wire couples. The discrepancy is discussed below.

**Experimental Section**

Experiments were carried out with volume addition ratios of 0-6.7 vol/1000 vol of steam. Larger concentrations often inhibited boule formation completely.

Inquiry was directed to: (a) change in boule size by

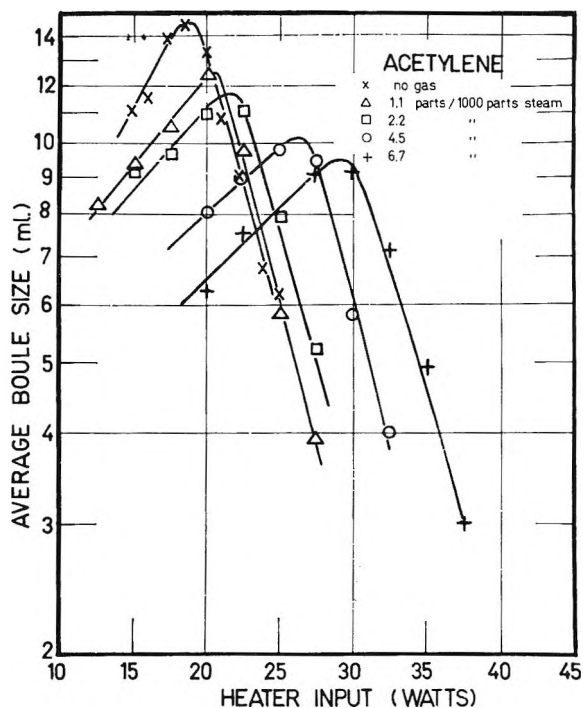


Figure 6. Boule sizes vs. heat input for concentrations of acetylene in the steam.

added gas; and (b) delay in boule formation by added gas.

(a) *Change in Boule Size in Presence of Foreign Gas.* Hickman<sup>3</sup> found that the size of the boule increased

(5) The Matheson Co., Inc.

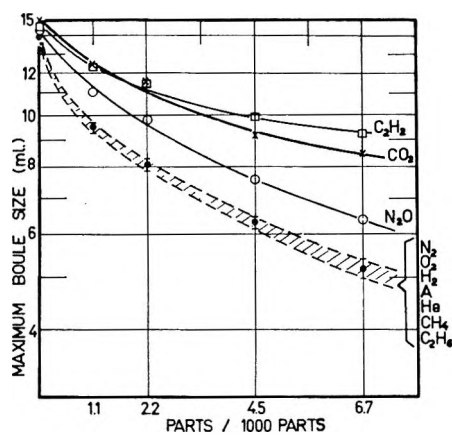


Figure 7. Standard boule size vs. gas concentration in the steam for all gases tested.

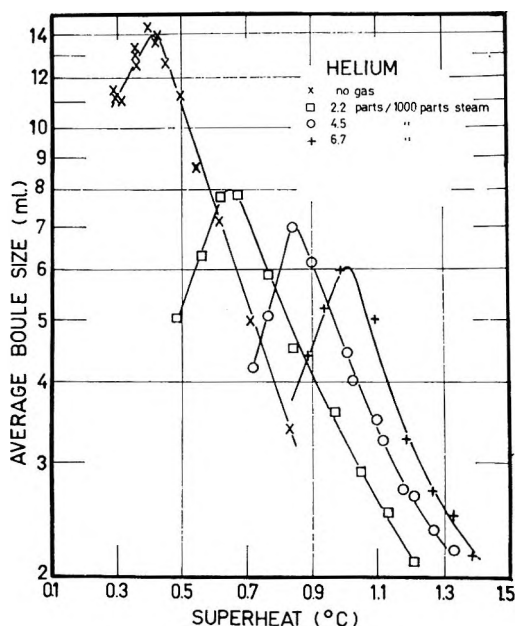


Figure 8. Boule sizes vs. measured superheat for concentrations of helium in the steam.

with increasing pressure of the supporting steam (*i.e.*, superheat) and then decreased when vibrations set in, due to the high velocity of the steam escaping from the shroud. Because of chance factors, the standard size for a boule is taken as the largest boule which can be grown under given conditions. Instead of searching for optimum conditions, it is quicker to determine sizes at ascending inputs of heat energy and adopt the peaks of the size energy curve as the standards of maximum boule size.

The gases under test,  $O_2$ ,  $H_2$ ,  $N_2$ ,  $CO_2$ ,  $N_2O$ ,  $C_2H_2$ ,  $C_2H_6$ ,  $CH_4$ , A, and He were injected into the system at concentrations of 0, 1.1, 2.2, 4.5, and 6.7 vol/1000 vol of steam and the variation of average boule size with the wattage input values of the boule heater were determined for each gas concentration. In this way a family of curves was obtained (*e.g.*,  $H_2$ ,  $N_2O$ ,  $C_2H_2$  in

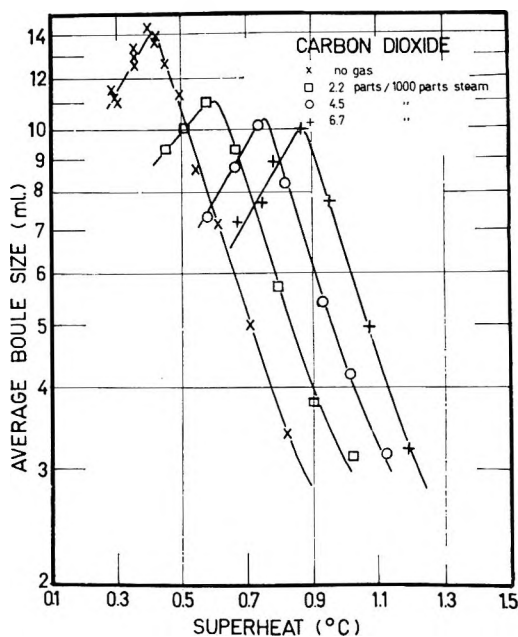


Figure 9. Boule sizes vs. measured superheat for concentrations of carbon dioxide in the steam.

Figures 4, 5, 6, respectively). For each gas a graph can be constructed relating the standard boule size to the proportions of gas added to the steam (Figure 7).

The majority of gases altered boule size to the same degree as hydrogen, within experimental error. A quality common to all these gases is their relative insolubility in water. Soluble gases such as  $N_2O$ ,  $CO_2$ , and  $C_2H_2$  exert *less* effect on boule size roughly in proportion to their solubility.

Since solubility data for gases at  $100^\circ$  are not readily available, Table I<sup>6</sup> lists instead the solubilities at  $30^\circ$  as represented by Henry's law constant  $K_A$  where

$$K_A = \frac{\text{partial pressure of A}}{\text{mole fraction of A in solution}}$$

Table I

Gas	$10^{-4}K_A^a$	Gas	$10^{-4}K_A$
$C_2H_2$	1.11	$CH_2$	34.08
$CO_2$	1.414	$O_2$	36.10
$N_2O$	1.966	$H_2$	55.10
$C_2H_6$	25.98	$N_2$	71.49
A	28.95	He	93.9

<sup>a</sup>  $K_A = p_A/s_A = (\text{partial pressure of A})/(\text{mole fraction of A in solution})$ .

Only stepwise progressions of heat input were required to determine standard maximum boule sizes. When it became necessary to know the corresponding

(6) "International Critical Tables," Vol. III, McGraw-Hill Publications, New York, N. Y., 1928, p 255.



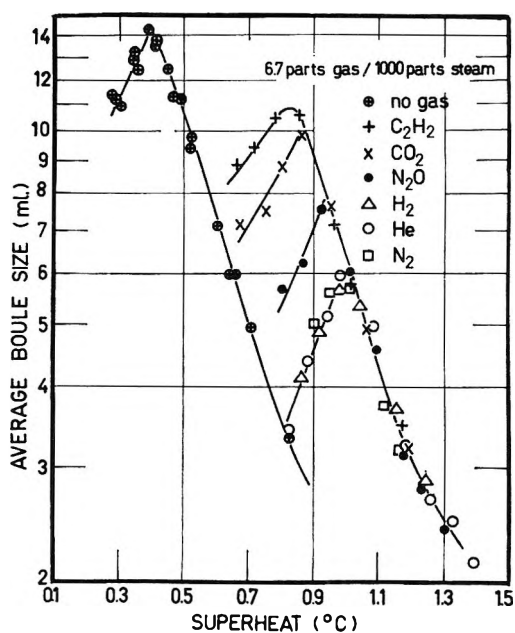


Figure 10. Boule sizes vs. superheat for highest gas-to-steam ratio of 6.7/1000 parts of steam for various gases. Note copper wire present.

degrees of superheat, thermocouples were inserted as mentioned with bare metal in contact with the steam. Boule sizes for some gas-to-steam ratios were determined for some of these gases and data were plotted as superheat vs. boule size. Once again typical families of curves were obtained, e.g., He in Figure 8 and CO<sub>2</sub> in Figure 9.

If these curves for any fixed gas-to-steam ratio are examined, e.g., at highest ratio of 6.7/1000 vol of steam (Figure 10), it is seen that the right-hand sides of all the curves can be superimposed. Also the maximum boule size is again dependent on the solubility of the gas but it should be noted these standard maximum boule sizes recorded in the presence of the bare thermocouples are uniformly larger than they were before the couples were inserted.

To test the possible effect of metal, the thermocouples were completely enclosed in glass and the readings repeated for CO<sub>2</sub>, H<sub>2</sub>, He at the maximum gas-to-steam ratio of 6.7/1000. The apparatus was well cleaned and left running for several weeks before the experiments were carried out to ensure complete removal of metal ions possibly left by the bare wire. The standard maximum boule size values obtained (Figure 11) were now very close to the original values determined in absence of thermocouples. This displacement is tentatively called the "copper effect."

(b) *Effects of Gases on Boule Formation.* Generally when no foreign gas is present and the support liquid is freely overflowing, a boule will begin to form at the first drop after the collapse of the previous one, particularly at high superheat. At low superheats several drops will occasionally merge with the support liquid before

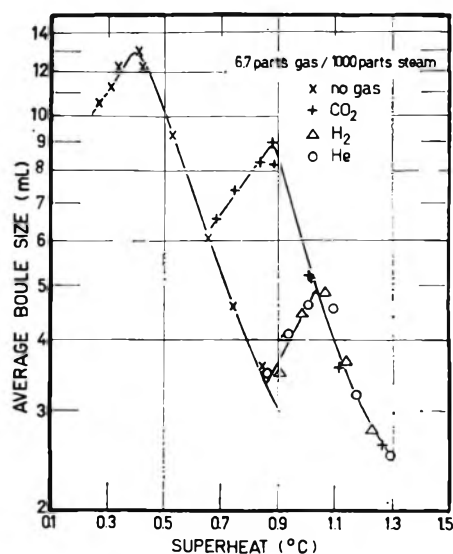


Figure 11. Boule sizes vs. superheat for highest gas-to-steam ratio of 6.7/1000 parts of steam for a selection of gases. Note copper absent.

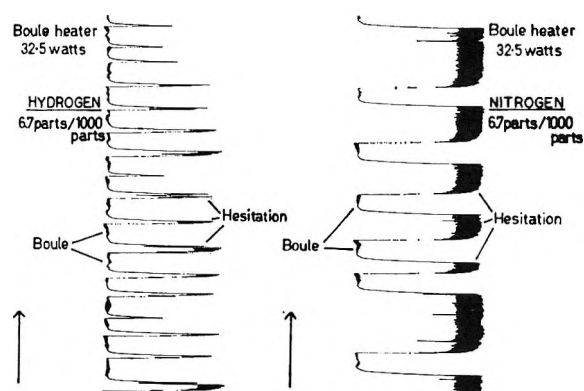


Figure 12. Two typical pen chart records of gas interference on boule formation at the same heat input, left, hydrogen, right, nitrogen. The left-hand side of each record indicates the presence of a boule and the right-hand side the time trace during which drops were merging.

the next boule forms. Upon addition of most gases there was much hesitation at the low superheat values and in the extreme case of C<sub>2</sub>H<sub>6</sub> boules would not form at all if the energy input was below the high value of 32.5 W. For a pure steam system boules would still form with an energy input as low as 7.5 W.

Figure 12 shows two typical chart records of gas interference on boule formation. The energy input of the boule heater is the same in every case. The left-hand side of each record indicates the presence of a boule and the right-hand side the time trace during which drops were merging. For N<sub>2</sub> there is much hesitation, while for H<sub>2</sub> there is very little.

Finding a numerical way to express the degree of hesitation presents difficulties. If each drop were to merge, counting drops would be sufficient. Actually hesitation often comprised sequences of merging drops,

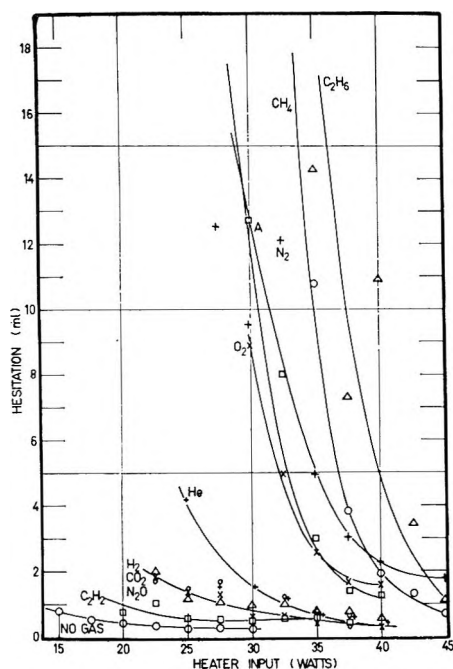


Figure 13. Boule inhibition vs. heat input for all gases examined at the maximum gas-to-steam ratio of 6.7/1000 parts of steam.

then 2 or 3 more drops building to an incipient boule, and then more individual drops. However, when a true boule became established it always grew to a size appropriate for the conditions of superheat and gas-to-steam ratio. Thus for  $N_2$  and  $H_2$  at the same heat input value and gas concentration the average boule size is the same; it is the *hesitations* that differ. The unit for measuring hesitation has been taken as the total volume of water that leaves the applicator before a boule meeting this criterion was formed.

Figure 13 shows hesitation as a function of the energy input of boule heater for each gas. Even so, hesitations are not as regular as the size of the boules, but if the hesitations between a sufficiently large number of boules are measured at each energy input a useful value can be averaged.

It can be seen that the degree of hesitation is not directly connected with the solubility of the gas, although the more soluble gases did not interfere with boule formation as much as the insoluble ones.

During the 18 months occupied in securing the data just reported, the position of the applicator which defined the point on the surface where boules are initiated remained unchanged. Consistent readings of interference were obtained on switching from one gas to another and back again. When, to test the effects of larger and smaller applicators, the position was moved off center, the interference caused by even the most active gases disappeared and boules could be started almost as well in the presence of  $H_2$ , He as  $C_2H_6$ . In the case of  $C_2H_6$ , the sizes of the largest boules increased.

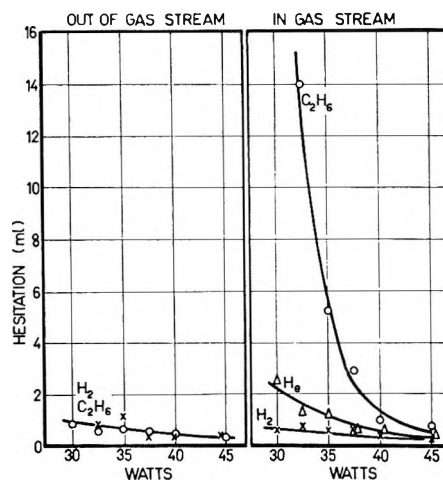


Figure 14. Boule inhibition vs. heat input for a gas-to-steam ratio of 6.7/1000 parts of steam: left, out of gas stream; right, in gas stream.

The reason for the negative results—which in no way disposed of the previous positive findings—was believed to lie in the failure of the gaseous mixture to reach the evaporating surface when the applicator was moved out of line with the incoming stream of gas. To confirm this, an eccentric applicator was inserted which allowed the position to be varied above the surface. Aluminum powder dusted on the water surface showed where the gas-vapor stream impinged. When boules were grown at the point of greatest impingement, hesitations were restored to their full degree. Figure 14 shows hesitations for  $C_2H_6$ ,  $H_2$ , and He in and out of the gas-stream path. The basic factor that influences boule hesitation is evidently the ratio of upward flow of primary steam from the superheated support water to the downward diffusive turbulence of the secondary “doped” steam. Major protection from the secondary steam is afforded by the tip of the applicator and ultimately by the lower side of the drop as it approaches the support water. The larger the area of the applicator and the larger the radius of the drop, the greater the likelihood of an early large boule.

Figure 15 shows that for  $CH_4$  at a ratio of 6.7/1000 vol of steam, the hesitation at lower superheat values is much greater for a small diameter applicator than a large diameter one.

Throughout the paper the gas hesitation measurements were made with a small diameter applicator 0.6 cm diameter without stabilizing attachments.

### Discussion

Boules have been proven sensitive to relatively small proportions, 0.1–1.0%, of gases added to the supernatant steam; two causes are recognized.

First, there is a decrease in the maximum boule size. If the general shape of the curve of boule size vs. superheat is examined, it is noted that the boule size increases with superheat due to an increase in the hy-

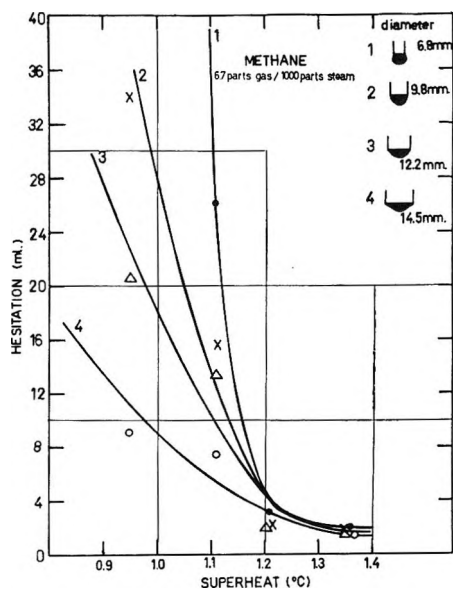


Figure 15. Boule inhibition vs. superheat with methane to steam ratio of 6.7/1000 parts of steam, showing the effect of applicator diameter on hesitation.

draulic support pressure beneath the boule and then decreases with a further increase in superheat. As previously remarked, this reduction in boule size is caused by the vibrations induced by the high velocity of vapor escaping from the shroud which mechanically bursts the boule and overrides any effect of an increase of support pressure. Reduction of partial pressure of the steam by the added gas reduces the size by reducing the support pressure. The gas lowers the boiling point of the exposed surface of the water and the superheat is decreased throughout the contents of the vessel. When the gas is insoluble the steam evolved under the boule remains pure, the true boiling point corresponds to atmospheric pressure plus the hydraulic depth at each point in the shroud, and the boule receives the lesser support corresponding to the lowered boiling point. Soluble gases, on the other hand, are reevaporated with the steam in the shroud and restore effective support pressure. There is also a general displacement of the boule size vs. superheat curve to higher superheat with increase in partial pressure of the foreign gas. The degree of displacement is independent of the solubility of the gas and depends only on the partial pressure because the right-hand limbs of all the curves lie on one line for the maximum gas-to-steam ratio used (Figure 10).

The second action of the foreign gas, namely to cause hesitation or inhibition of boule formation, suggests that the foreign gas has altered in some way the quality of the water surface. Researches<sup>4</sup> in this laboratory have demonstrated that water, even in the very clean borosilicate glassware used in these experiments, can accumulate a diffuse siliceous adsorbate on its surface on which gases could perhaps be further adsorbed. To

prevent this complication the system has been kept in a state of continuous overflow with any siliceous film continuously swept over the weir,<sup>7</sup> the discharge being aided by the momentum of the water that streams outward from the rim of the boule. If, therefore, gas adsorption is occurring, it is most probably on the water itself and at a temperature close to 100°. As mentioned above, the concentration of foreign gas on the water surface is dependent on local conditions and is greatest where the incoming stream is directed downwards. Hesitation experiments with the insoluble gases are repeatable only when the boules are grown in such an impact area. Size experiments, on the contrary, depend on the gas dissolved in the support water, the concentration being the summation of gas dissolved at the surface of the support water from the turbulent diffusive layer of steam above it, and the gas dissolved at supplied concentration in the distillate feeding the boule which later joins the support water. The size measurements are relatively unaffected by the diameter of the applicator or its lateral position over the surface.

Considering the gases that decrease the maximum boule size equally for a given gas-to-steam ratio, *i.e.*, the nonpolar or "insoluble" gases, H<sub>2</sub>, He, N<sub>2</sub>, O<sub>2</sub>, A, CH<sub>4</sub>, and C<sub>2</sub>H<sub>6</sub>, it can be seen (Table II) that the order of interference of these gases increases with increasing molecular diameter; could this be linked to the solubility effect?

Table II

Solute	Molecular diameter $\text{\AA}^{a,c}$	Molecular diameter $\text{\AA}^{b,d}$	Order of interference
H <sub>2</sub>	2.75	2.87	Least ↓ Most
He	2.18	2.63	
O <sub>2</sub>	3.64	3.46	
N <sub>2</sub>	3.74	3.70	
A	3.67	3.40	
CH <sub>4</sub>	4.19	3.82	
C <sub>2</sub> H <sub>6</sub>	5.37	5.63	

<sup>a</sup> Molecular diameter obtained from viscosity calculations which apply strictly at 0°. <sup>b</sup> Molecular diameter calculated from second virial coefficients. <sup>c</sup> S. Dushman, "Scientific Foundations of Vacuum Technique," John Wiley and Sons, New York, N. Y., 1949. <sup>d</sup> J. O. Hirschfelder, C. F. Curtiss, and R. B. Bird, "Molecular Theory of Gases and Liquids," John Wiley and Sons, New York, N. Y., 1945.

The hard-sphere solution theory considers the solution process to take place in two steps: (1) the creation of a cavity in the solvent of a suitable size to accommodate the solute molecule, and (2) introduction into the cavity of the solute molecule which interacts

(7) K. Hickman, presented at the 158th National Meeting of the American Chemical Society, New York, N. Y., Sept 1969; see Abstracts, No. INDE 38.

with the solvent. The results in this paper suggest that the process should be considered to take place in three steps: (1) the creation of an appropriate sized cavity; (2) the entrance of the solute molecule into the cavity; and (3) interaction of the solute with the solvent.

Pierotti<sup>8</sup> determined the hard-sphere diameter of water to be 2.74 Å at 70°, agreeing well with values of other methods.<sup>9,10</sup> This diameter of the water molecule is very close to the diameters of hydrogen and helium, the gases that cause least interference. Insoluble gases with larger molecules will evidently encounter a longer wait before the surface distorts sufficiently to provide a larger cavity and in the interval presumably stays adsorbed to smaller "holes" which they cannot enter. H<sub>2</sub> and He can participate in steps (1) and (2) but only weakly in (3). Large molecules ethane and methane do not readily take any of the three steps. The soluble gases, C<sub>2</sub>H<sub>2</sub>, N<sub>2</sub>O, and CO<sub>2</sub>, have very strong interactions with the water molecules which override the first two steps and cause the molecules to be pulled into the water surface. We advance the *ad*

*hoc* theory that any molecule that can readily be pushed or pulled into the water surface, *e.g.*, by cavitation or true solution, does not cause boule hesitation but that those molecules that "have nowhere to go" do! The generalization carries no suggestion of the mechanics of causing hesitation although two alternatives may be considered. One possible mechanism would be that the temporarily adsorbed molecules block evaporation of the support water and allow the boule to approach within merging distance. The other would be that the gases line both the drop and the support permitting partial wetting. Here we must be content to leave the discussion pending further experiments.

*Acknowledgment.* The author wishes to thank Dr. K. Hickman for his advice and assistance during this work, and also A. Davidhazy and E. Wright for their help in preparing the manuscript.

(8) R. A. Pierotti, *J. Phys. Chem.*, **69**, 281 (1965).

(9) L. Monchick and E. A. Mason, *J. Chem. Phys.*, **35**, 1676 (1961).

(10) J. S. Rowlinson, *Trans. Faraday Soc.*, **45**, 974 (1949).

## On the Ultrasonic Cavitation Intensity of Aqueous Sodium

### Lauryl Sulfate Solutions<sup>1</sup>

by Kenneth Beard,<sup>2a</sup> Michael Rios, Douglas Currell,<sup>2b</sup> and Richard Reis

*Department of Chemistry, California State College at Los Angeles, Los Angeles, California (Received March 10, 1970)*

The ultrasonic cavitation noise intensity as a function of the concentration of aqueous sodium lauryl sulfate solutions has been measured. The cavitation noise decreases with increasing concentration (decreasing surface tension) until a concentration of 0.0128 *M* is reached. Above this concentration a sharp increase in cavitation noise is observed. The possibility that micelles serve as cavitation nuclei is discussed.

#### Introduction

The results of an earlier study<sup>3</sup> showed that the rate of formation of acetylene from the ultrasonic treatment of aqueous solutions of pyridine was not affected by the addition of surfactants. This result was unexpected since the reaction is believed to take place within the cavitation bubbles which form when a liquid is treated with an intense ultrasonic beam.<sup>3,4</sup> Hueter and Bolt<sup>5</sup> have proposed that the higher the surface tension of the liquid the greater the amount of energy released upon collapse (or contraction) of the cavitation bubble since the energy so released should depend on the work required to form a new surface in the expan-

sion of the bubble. Thus, the greater the surface tension of the reaction solution, the faster should be rate of the ultrasonic reaction. To explain the lack of effect of added surfactants on the rate of acetylene formation

(1) This work was supported by a National Science Foundation Institutional Research Grant.

(2) (a) National Science Foundation Undergraduate Research Program Participant. (b) To whom correspondence should be addressed.

(3) D. L. Currell, G. Wilhelm, and S. Nagy, *J. Amer. Chem. Soc.*, **85**, 127 (1963).

(4) V. Griffing, *J. Chem. Phys.*, **20**, 939 (1952); M. E. Fitzgerald, V. Griffing, and J. Sullivan, *ibid.*, **25**, 926 (1956).

(5) T. F. Hueter and R. H. Bolt, "Sonics," John Wiley and Sons, New York, N. Y., 1955, p 238.

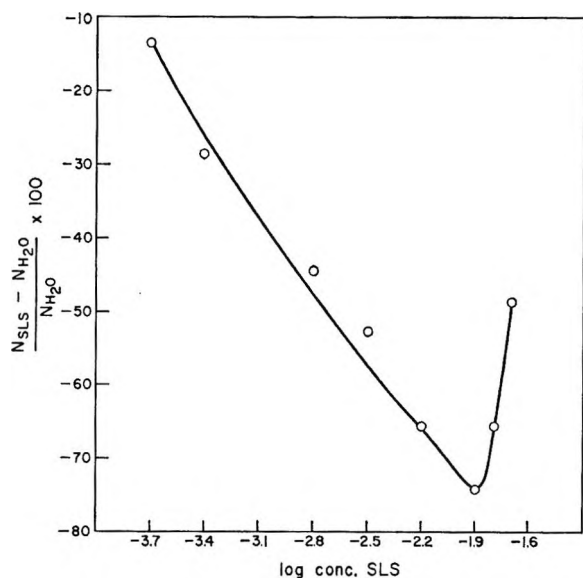


Figure 1. Per cent increase of cavitation noise over water vs. log concentration aqueous sodium lauryl sulfate solutions.

in the ultrasonic treatment of aqueous solutions of pyridine, it was suggested<sup>3</sup> that a greater number of cavitation bubbles formed in the solutions of lower surface tension since a greater number of bubbles leading to a greater production of acetylene per unit time would, perhaps, compensate for the lower yield of acetylene per bubble. To gain insight into the effect of surfactants on the cavitation process, we undertook a study of the ultrasonic cavitation intensity of aqueous sodium lauryl sulfate solutions. Results reported by other laboratories indicate that increased chemical activity can be accompanied by a decrease in cavitation noise.<sup>6</sup>

### Experimental Section

The ultrasonic generator (McKenna Laboratories Model EB240, 1 Mcps) was coupled to a cup-shaped barium titanate-ceramic transducer (9 cm in diameter) which was covered with 350 ml of the sodium lauryl sulfate (Eastman Kodak) solution. The cavitation noise was measured with a barium titanate ceramic hydrophone disk (diameter, 0.750 in., thickness, 0.100 in.) mounted on the side of the flask perpendicular to the plane of the transducer. An electronic 1-Mc shunt was used to filter the driving frequency. The solution was aged for 1 hr at an intensity of 0.2 W/cm<sup>2</sup> (measured by the method of Herrey<sup>7</sup>) at the surface of the transducer after which the intensity was reduced and the cavitation noise measured through small intervals to zero. The results reported are for one intensity, 0.09 W/cm<sup>2</sup>. The average error at this intensity was approximately 5%. Results at three other intensities (0.05, 0.07, 0.10 W/cm<sup>2</sup>) were qualitatively the same. The temperature was maintained constant at 40.0° by circulation of water from a constant-temperature bath through cooling coils surrounding the flask. The determinations of the surfactant solutions were im-

mediately preceded by, and compared with, measurements on distilled water. A minimum of three determinations was made at each concentration and the results were averaged and expressed as per cent increase in cavitation noise over water,  $N$ , where  $N_{H_2O} =$

$$N = \frac{N_{SLS} - N_{H_2O}}{N_{H_2O}} \quad (100)$$

cavitation noise of water in millivolts and  $N_{SLS} =$  cavitation noise of surfactant solution in millivolts.

### Results and Discussion

The results expressed in Figure 1 indicate a decrease in cavitation noise for the surfactant solution relative to water with increasing concentration below a concentration of 0.0128  $M$ . This result can be explained as due to a reduction in surface tension over this range with a resulting lessening of the amount of energy released upon collapse (or contraction) of the cavitation bubble. Above this concentration the cavitation noise increases with an increase in concentration of surfactant. This increase in noise coincides approximately with an increase in surface tension for solutions of sodium lauryl sulfate containing small amounts of lauryl alcohol as an impurity which occurs at 0.0079  $M$ .<sup>8</sup> Above 0.0079  $M$  the situation may be complicated by micelle formation. The critical micelle concentration of sodium lauryl sulfate at 40° is reported to be 0.0089  $M$ .<sup>9</sup> Support for this idea is indicated by the observation that the surface tension is the same for the two highest concentrations measured (0.016 and 0.020  $M$ ) while the cavitation noise continues to increase with increasing concentration.

Pease and Blinks<sup>10</sup> have shown that cavitation occurs relatively easily at a water-glass interface if the glass walls are coated with surfactant. We suggest that an analogous situation may exist in the presence of micelles of surfactant and that the micelles can thereby serve as cavitation nuclei with a resulting increase in cavitation noise above the critical micelle concentration. This suggests that cavitation noise measurements could be used to study the aggregation of association colloids.

These results are not consistent with the previously reported observation that added surfactants had no effect on the rate of production of acetylene in the ultrasonic treatment of aqueous solutions of pyridine. It is

(6) M. Degrois and B. Badilian, *C. R. Acad. Sci.*, **254**, 837 (1962).

(7) E. M. J. Herrey, *J. Acoust. Soc. Amer.*, **27**, 891 (1955).

(8) S. P. Harrold, *J. Colloid Sci.*, **15**, 280 (1960); lauryl alcohol is produced by the hydrolysis of sodium lauryl sulfate.

(9) K. Meguro, T. Kondo, N. Ohba, T. Ino, and O. Yoda, *Bull. Chem. Soc. Jap.*, **30**, 760 (1957).

(10) D. C. Pease and L. R. Blinks, *J. Phys. Colloid Chem.*, **51**, 556 (1947).

(11) B. E. Noltingk and E. A. Neppiras, *Proc. Phys. Soc. London Sect. B.*, **63**, 674 (1950).

conceivable that at the extremely high temperatures possible within the cavitation bubble<sup>11</sup> that the amount of energy available so far exceeds that necessary to

bring about the chemical reaction that any change in the energy available brought about by the addition of surfactants is negligible.

## Sorption Isotherms of Polar–Nonpolar Systems on Liquid-Coated Adsorbents

by Paul Urone, Yoshihiro Takahashi,

*Department of Chemistry, University of Colorado, Boulder, Colorado 80302*

and George H. Kennedy

*Department of Chemistry, Colorado School of Mines, Golden, Colorado 80401 (Received August 5, 1969)*

Experimental studies of polar–nonpolar liquid-coated adsorbent systems at low liquid coatings reveal basic sorption relationships not previously understood. Sorption isotherms were obtained for the bulk liquids, the uncoated adsorbents, and adsorbents coated with 0.1–20% liquid phase. Relative pressures ( $P/P_0$ ) were varied from 0.001 to 0.30, and temperature studies were made for thermodynamic evaluation. Bulk liquid partition coefficients and Henry's law constants at 30° are given. Sorption of polar solutes on squalane-coated adsorbents equal the sum of the contributions of the squalane and the adsorbent, and nonpolar solutes show slight sorption from solution equilibrium effects. Tri-*o*-tolyl phosphate (TOTP) and tris(cyanoethoxypropane) (TCEP) interact with the adsorbent to form a modified surface which gives reduced, and sometimes linear, isotherms. Polar solutes show isotherms that are a sum of the contributions of the liquid-modified surface and the bulk liquid. The isotherms of hexane, as a nonpolar solute, on TOTP-coated adsorbents show the possibility of a small contribution from adsorption on the liquid surface in addition to the contributions of the bulk liquid and the liquid-modified surface. The demonstrated modified surface and the additivity of the sorption terms have long-range potentials for the measurements of thermodynamic properties and the development of specialized surfaces.

An earlier study of sorption isotherms of acetone on liquid-coated adsorbents<sup>1</sup> showed that the amount of solute sorbed at a given partial pressure ( $Q_{\text{total}}$ ) was equal to the sum of: (1) the amount adsorbed by the surface of the adsorbent modified by a thin layer of coating liquid ( $Q_{\text{mod}}$ ) and (2) the amount sorbed by the remainder of the coating liquid ( $Q_{\text{liquid}}$ ).

$$Q_{\text{total}} = Q_{\text{mod}} + Q_{\text{liquid}} \quad (1)$$

The amounts sorbed in each case depended upon the partial pressure of the solute and its isotherm on each of the respective phases; *i.e.*, at constant temperature

$$Q_t = W_m \int_0^P \frac{dQ_{\text{mod}}}{dP} dP + W_L \int_0^P \frac{dQ_L}{dP} dP \quad (2)$$

where  $Q_P$  is the amount of solute sorbed at a given partial pressure,  $P$ ;  $dQ_{\text{mod}}/dP$  and  $dQ_L/dP$  describe the isotherms of the modified surface of the adsorbent and of the bulk liquid, respectively.  $W_m$  is the weight of the modified adsorbent and  $W_L$  is the weight of liquid coating above that needed to modify the surface. When, as is common at low con-

centrations, the isotherm for the solute in the liquid is linear,  $dQ_L/dP$  is constant and eq 2 becomes

$$Q_t = W_m \int_0^P \frac{dQ_{\text{mod}}}{dP} dP + W_L K_L P \quad (3)$$

where  $K_L$ , the partition coefficient, is the ratio of the concentration of the solute in the liquid to that in the gas phase.

When squalane was used as the coating liquid, the adsorbent surface was only slightly modified, and the amount sorbed was essentially the same as that sorbed by the uncoated adsorbent. This report extends the studies to cover in more detail examples of polar–nonpolar solutes, solvents, and modified adsorbent surfaces.

### Experimental Section

The sorption isotherms were determined gravimetrically using the apparatus and techniques described previously<sup>1</sup> except that an electro-torsion Bourdon gauge was added to the vacuum system to measure

(1) P. Urone, Y. Takahashi, and G. H. Kennedy, *Anal. Chem.*, **40**, 1130 (1968).

solute pressures with greater sensitivity and accuracy. The gauge (Ruska Instrument Corp., Houston, Texas) was capable of measuring pressures from 0 to 10 Torr with a sensitivity of  $\pm 10^{-3}$  Torr.

**Materials.** Acid-washed firebrick (AWFB) (60–80 mesh) (Matheson Coleman and Bell), 60–80 mesh Chromosorb W (John Mansville), and 60–80 mesh acid-washed dimethyldichlorosilane-treated firebrick (DMCS) (Varian Aerograph) were used as adsorbents. Before coating with liquid phase, the adsorbents were dried at 110° for more than a day. Tri-*o*-tolyl phosphate (TOTP) (Matheson Coleman and Bell) was used without further purification. 1,2,3-Tris(cyanoethoxy)propane (TCEP) (Wilkins Instrument and Research) was degassed in a vacuum oven at 50° for 6 hr, and squalane, C<sub>30</sub>H<sub>62</sub> (Eastman Organic Chemicals), was purified by passing through a silver nitrate modified silica gel column.<sup>2</sup> When unpurified squalane was used, experimental results were influenced by the impurities present and inconsistent effects were observed.<sup>1</sup> Acetone, methanol, and benzene were all Nanograde (Mallinckrodt Chemical Works); *n*-hexane was reagent grade, boiling range of 0.4° (J. T. Baker Chemical Co.); and 2,2,4-trimethylpentane (isooctane) was also reagent grade (Fisher Scientific). Dissolved oxygen and carbon dioxide were degassed from the water before using.

**Coating of the Supports.** To obtain a uniform liquid coating on the supports, the method developed by Parcher and Urone was used.<sup>3</sup> About 20 g of the solid support was placed in a sintered glass filter funnel which was connected to a suction flask. Approximately 100 ml of the solution of the liquid phase having the desired concentration was poured into the funnel. The solid and the solution were very gently mixed with a glass rod before suction was applied. Care was taken not to break any support particles. The solution was then filtered out with suction until the particles were free flowing, after which dried N<sub>2</sub> was blown through the bottom end of the funnel while heating tape was used to warm the funnel walls. The actual amount of liquid coated on the adsorbent was determined by washing 1 g of the sample several times with a total of 250 ml of the same solvent used for making the solution, and obtaining the loss in weight after drying.

**Measurement of Sorption Isotherms and Solubility Curves.** A sample was hung on one side of the microbalance, carefully counterbalanced with glass weights, and degassed. When the sample was an uncoated solid it was degassed for 6 hr at 10<sup>-5</sup> to 10<sup>-6</sup> Torr. When the sample was a liquid or a liquid-coated solid, it was degassed at room temperature for 3 hr at 10<sup>-2</sup> to 10<sup>-4</sup> Torr, depending upon the vapor pressure of the liquid phase used. Most of the isotherms were taken at 30 ± 0.1°.

A small amount of solute vapor was introduced,

and after equilibrium was reached, the pressure of the vapor and the weight change were recorded. In general it took no more than 2 to 5 min to reach equilibrium for all samples except the pure liquid samples, which took as much as 12 hr. For the coated adsorbents, *Q* was calculated as micromoles sorbed per gram of coated adsorbent.

The above steps were repeated until the relative pressure,  $P/P_0$ , reached approximately 0.1.  $P_0$  is the saturation pressure of the solute at the temperature of the experiment. In order to calculate the surface area of a sample,  $P/P_0$  readings had to be taken to relative pressures of 0.3 or higher. Surface areas were calculated using the well-known BET method.<sup>4</sup>

The solubilities of the solutes in the nonvolatile solvents were measured in the same manner as described for measuring the sorption isotherms. The evaporation rates of the solvents in the presence of comparable helium pressures were determined and applied when necessary.

Buoyancy corrections were obtained by using a nonadsorptive gas (N<sub>2</sub>) at room temperature and were found to be negligibly small. For surface area measurements at liquid nitrogen temperatures, buoyancy corrections were obtained with helium. They were found to be significant, and the proper corrections were made.

## Discussion

**Bulk Liquids.** The isotherms, or solubilities, of the four solutes in the various nonvolatile coating liquids were obtained as described above. In each of the cases studied plots of mole fraction sorbed *vs.* the relative pressure gave straight lines showing adherence to Henry's law for the pressure ranges studied. Table I gives the slopes of the lines expressed as the partition coefficient  $K_L$ , where  $K_L = d\chi/d(P/P_0)$ , and  $\chi$  is the mole fraction of the solute in the solvent. The amounts of *n*-hexane and methanol which may have dissolved in TCEP or squalane, respectively, were so low they could not be observed directly. The

**Table I:** Partition Coefficients at 30.0°:  $K_L = d\chi/d(P/P_0)$

Solute	Solvent		
	Squalane	TOTP	TCEP
<i>n</i> -Hexane	1.55	2.95	<i>a</i>
Isooctane	1.32	...	...
Acetone	0.30	0.94	0.97
Methanol	<i>a</i>	0.60 <sup>b</sup>	...

<sup>a</sup> Below experimental error. See text. <sup>b</sup> Measured at 45.0°.

(2) B. deVries, *J. Amer. Oil Chem. Soc.*, **41**, 403 (1964).

(3) J. F. Parcher and P. Urone, *J. Gas Chromatog.*, **2**, 184 (1964).

(4) S. J. Gregg and K. S. W. Sing, "Adsorption, Surface Area and Porosity," Academic Press, New York, N. Y., 1967.

evaporation of the TCEP or squalane over the many hours required for attaining equilibrium with the bulk liquids at each datum point was of the same order or greater than the amounts sorbed in these two cases. Corrections for evaporation, consequently, gave indeterminate results.

Table II: Henry's Law Constants<sup>a</sup> at 30.0°

Solute	Solvent					
	Squalane		TOTP		TCEP	
	<i>k</i>	<i>k'</i>	<i>k</i>	<i>k'</i>	<i>k</i>	<i>k'</i>
Isooctane	47.3	45.6	...	...	...	...
<i>n</i> -Hexane	120.6	121.6	634.2	639.9	<i>b</i>	<i>b</i>
Methanol	<i>b</i>	<i>b</i>	544 <sup>c</sup>	587 <sup>c</sup>	...	...
Acetone	932.3	946.4	300.5	319.2	290.9	322.1

<sup>a</sup> Where  $k = P/\chi$  and  $k' = f/\chi$ ;  $= \gamma^\infty P_0$ .  $P$  in Torr. <sup>b</sup> Unable to detect amount dissolved. <sup>c</sup> Taken at 45.0°.

Table II gives the Henry's law constants for the same systems. These were calculated using the observed solute pressures for  $k$  and fugacities for  $k'$  where  $P$  was measured in Torr and

$$P = k\chi \quad (4)$$

$$f = k'\chi \quad (5)$$

$$= \gamma^\infty P_0\chi \quad (5a)$$

hence

$$k' = \gamma^\infty P_0 \quad (6)$$

The activity coefficients at infinite dilution were obtained by extrapolation from plots of the natural log of the activity coefficient vs. the mole fraction using<sup>5</sup>

$$\ln \gamma = \ln P/P_0\chi - \frac{(B_{22} - V_2^0)(P_2^0 - P)}{RT} \quad (7)$$

where  $B_{22}$ ,  $V_2^0$  and  $P_2^0$  are the second virial coefficient, the molar volume, and the saturation pressure of the solute, respectively.

**Polar Solute-Polar Coating.** In the earlier paper,<sup>1</sup> the isotherms of acetone on TOTP coated columns were used to develop and confirm eq 2. In extending the studies, several systems representing a wide range of relative polarities were selected. For polar solute-polar coating systems the isotherms of acetone in TCEP and methanol in TOTP coated adsorbents were obtained. Acetone and TOTP are intermediate in polarity while methanol and TCEP are of relatively high polarity.

Figure 1 shows a typical series of isotherms of acetone on the adsorbent (AWFB) coated with increasing amounts of TCEP. As the amount of coating was increased, the adsorbent surface became modified and a

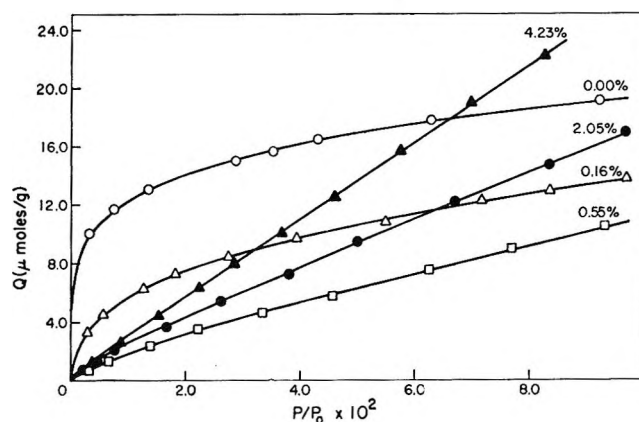


Figure 1. Sorption isotherms for acetone on TCEP-coated AWFB at 30°.

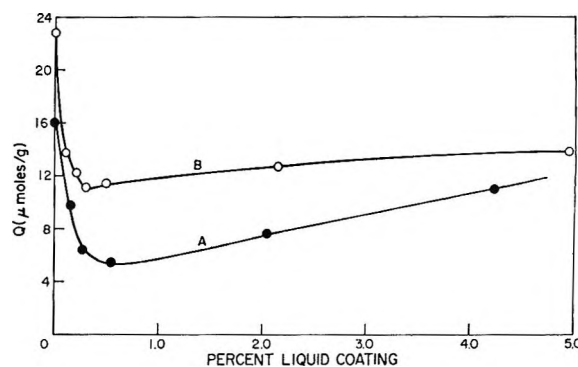


Figure 2. Sorption of acetone on TCEP-coated AWFB at 30° (A) and of methanol on TOTP-coated AWFB at 45° (B) at  $P/P_0 = 0.04$  as a function of per cent liquid coating.

drop in the isotherms was observed. A minimum isotherm developed at an amount of coating roughly equivalent to that necessary for a monomolecular layer covering approximately 0.5% wt/wt for an adsorbent with area of 4 m<sup>2</sup>/g. Beyond the minimum, the sorption isotherms increased in proportion to the amount of TCEP used.

Figure 2 shows the variation of the amount sorbed at a given pressure,  $P/P_0 = 0.04$ , as a function of the per cent of liquid coating for both acetone in TCEP (curve A) and methanol in TOTP (curve B). The data were taken from isotherms similar to those shown in Figure 1. The amount of solute sorbed decreased sharply as the per cent of liquid coating was increased from 0 to approximately 0.5%. After a minimum developed, the amount sorbed increased in proportion to the per cent of liquid coating used (Figure 1). The difference in the slopes beyond the minimum for the two solutes (Figure 2) was caused by the difference in solubilities of the solutes in the respective liquids.

Figure 3 graphically portrays the calculated contributions of the modified surface ( $Q_{mod}$ ) and the bulk

(5) Y. Takahashi, P. Urone, and G. H. Kennedy, *J. Phys. Chem.*, **74**, 2333 (1970).



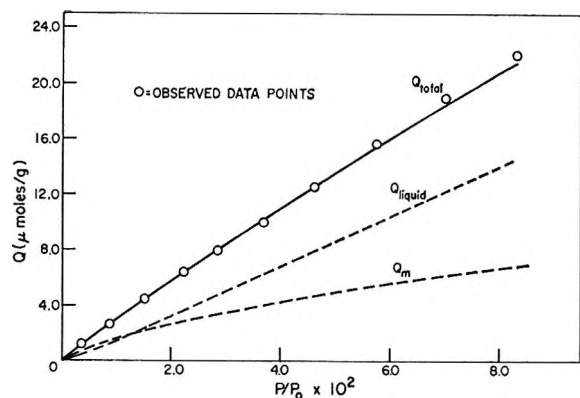


Figure 3. Calculated sorption isotherms and experimental data points at 30° for acetone on 4.23% TCEP-coated AWFB. Dashed lines give the contributions of the modified surface,  $Q_m$ , and the coating liquid in excess of that needed to modify the surface,  $Q_{liquid}$ . The solid line gives the sum of the dashed lines, and the circles are the observed data points.

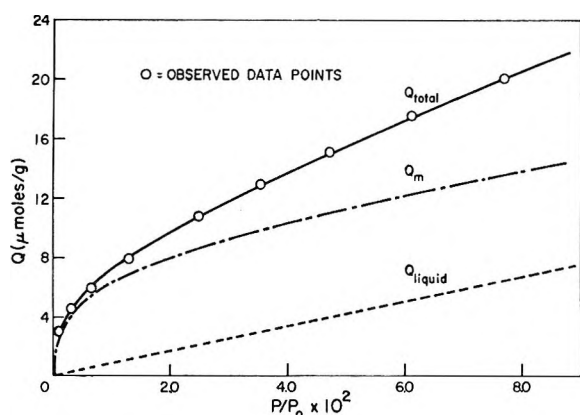


Figure 4. Calculated sorption isotherms and experimental data points for methanol on 4.93% TOTP-coated AWFB at 45°. Curve identities as noted in Figure 3.

liquid ( $Q_{liquid}$ ) to the observed amount sorbed ( $Q_{total}$ ) for acetone on the AWFB adsorbent coated with 4.23% TCEP. The individual contributions (dashed lines, Figure 3) were calculated according to eq 2 using the isotherms obtained from the 0.55% TCEP-coated AWFB and the bulk TCEP, respectively. The solid line represents the sum of the calculated contributions while the small circles indicate the observed data points. There is close agreement between the calculated solid line and the observed data points. Figure 4 represents the same type of data calculated for methanol on 4.93% TOTP-coated AWFB. In this case, the contribution of the modified adsorbent surface ( $Q_{mod}$ ) was greater than that seen in Figure 3, principally because of the differences in the relative polarities and solubilities of the solutes and coating liquids involved. Nevertheless, the calculated isotherm and the observed data points again are in good agreement.

**Polar Solute-Nonpolar Coating.** Although acetone and methanol were only slightly soluble in squalane,

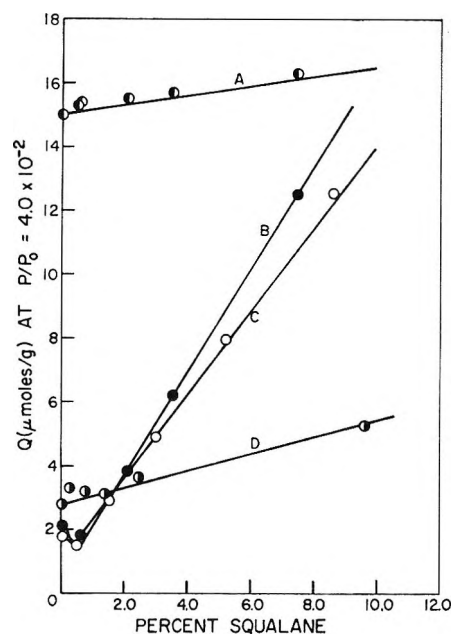


Figure 5. Sorption at 30° and  $P/P_0 = 0.04$  as a function of per cent squalane: A, acetone on AWFB; B, *n*-hexane on AWFB; C, isooctane on AWFB; D, acetone on DMCS-treated AWFB.

the isotherms for these compounds on squalane-coated AWFB showed that both acetone and methanol easily penetrated the nonpolar squalane to interact with the adsorbent surface as if the squalane were not there (Figure 5, curve A). In these cases the total amount sorbed by the liquid-coated adsorbent is more appropriately expressed by

$$Q_{total} = Q_{solid} + Q_{liquid} \quad (8)$$

where  $Q_{solid}$  is the amount sorbed by the adsorbent whose surface is not modified with respect to the solute by the coating liquid.

Figure 5 shows the amounts sorbed at constant relative pressure,  $P/P_0 = 0.04$ , for several solutes on squalane coated adsorbents. Curves A and D are for acetone on two different types of adsorbents: surface active AWFB and deactivated DMCS, respectively. Although the squalane contribution in both cases was identical, curve A is much higher than curve D because the surface activity of the AWFB adsorbent used for curve A was much greater than that of the DMCS adsorbent used for curve D. The DMCS treatment converts the active hydrogen sites on the surface to trimethylsilyl groups imparting a paraffinic character to the surface. Other chemical treatments, a strongly adsorbed compound, or a thin layer of a polar coating liquid can easily modify the adsorbent surface when a nonpolar coating liquid is used. The use of water or steam, for example, to modify the properties of an adsorbent is well known.<sup>6</sup>

(6) H. S. Knight, *Anal. Chem.*, **30**, 2030 (1958).

Both curves A and D (Figure 5) obeyed eq 8 strictly. A curve for methanol on AWFb (not shown) was out of the vertical range of Figure 5, but it also obeyed eq 8. Curve D emphasizes what has been previously observed, that DMCS treatment does not completely deactivate the support surface.<sup>7</sup> Curves B and C are for *n*-hexane and isooctane and will be discussed in the following section on nonpolar solutes.

Figure 6 shows the effect on the isotherm of acetone on squalane-coated AWFb by the addition of 0.6% TCEP to the approximately 3% squalane used. The adsorbent without the TCEP has a high, nonlinear sorption isotherm. The one with the TCEP has a much reduced and essentially linear isotherm. The small amount of TCEP (which was added with the squalane during the coating process) adhered to and modified the surface to give it a more homogeneous and less adsorptive character.

*Nonpolar Solute-Nonpolar Coating.* For a nonpolar system, the isotherms of *n*-hexane and isooctane on squalane (a C<sub>30</sub> saturated hydrocarbon) were studied. Figure 7 shows representative isotherms for isooctane on squalane coated AWFb. As the per cent of squalane was increased, a slight minimum in the sorption isotherms was observed, following which the isotherms continually increased with increasing amounts of squalane. In this case, the squalane competed with the isooctane for the active adsorption sites probably setting up a steady-state adsorption equilibrium such as that proposed by Everett.<sup>8</sup>

$$aL^s + bS^L = aL^L + bS^s \quad (9)$$

where L denotes the coating liquid, S the solute, and the superscripts s and L indicate the sorbed and liquid phases, respectively. The coefficients *a* and *b* are introduced because the size difference in the solute and coating liquid molecules may not allow a 1:1 solute-liquid interchange.

The amount of isooctane sorbed in the modified surface is small compared to its solubility in squalane. Hence, the isotherms of Figure 7 appear to be linear although the modified surface continued to adsorb isooctane irrespective of the amount of squalane present. Such pseudolinear isotherms were observed whenever adsorption by the support was small relative to the amount of solute dissolved by the coating liquid.

Curves B and C in Figure 5 clearly show the variation of the amounts of *n*-hexane and isooctane sorbed with increasing amounts of squalane. A slight minimum is developed after which the curves rise rapidly because of a high solubility in squalane. The difference in the slopes indicates the difference in the solubilities of the two solutes.

*Nonpolar Solute-Polar Coating.* The solubility of a nonpolar solute in a polar solvent will vary considerably depending upon the type and relative polarity of the solvent. Two systems were studied in this respect:

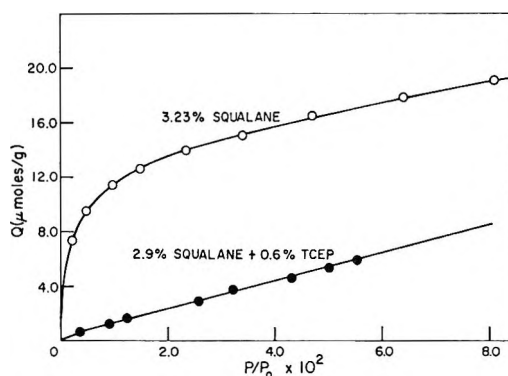


Figure 6. Effect of small amount of TCEP on sorption isotherm of acetone on squalane-coated AWFb.

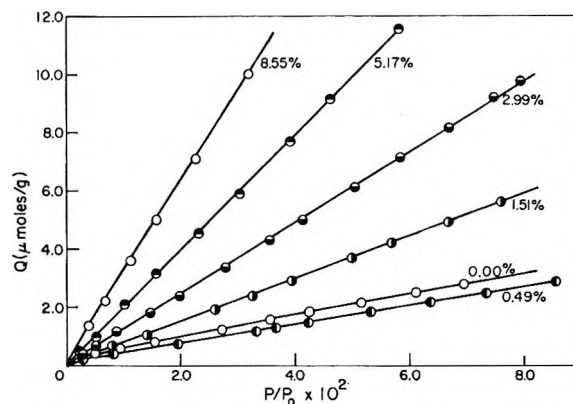


Figure 7. Sorption isotherms of isooctane on squalane-coated AWFb at 30°.

hexane on TOTP and hexane on TCEP-coated adsorbents. Hexane was measurably soluble in TOTP, but it was practically insoluble in TCEP.

The isotherms for *n*-hexane on TOTP-coated AWFb adsorbents showed the typical development of a minimum isotherm at approximately 0.3% TOTP with an increase in the isotherms as the percentage of TOTP coating was increased. When the data were studied for conformance to eq 2, it was found that the calculated total sorbance values matched the experimental data better with a three-component equation. Recognizing the possibility of contributions by all phases present,<sup>9</sup> eq 1 was then expanded to include contributions from the solid-liquid and the liquid-gas interfaces in addition to the modified surface and the bulk coating liquid.

$$Q_{\text{total}} = Q_{\text{solid}} + Q_{\text{mod}} + Q_{\text{liquid}} + Q_{\text{AL}} \quad (10)$$

where  $Q_{\text{mod}}$  is the amount sorbed by the modified adsorbent surface and  $Q_{\text{AL}}$  is the amount sorbed by

(7) J. Bohemen, S. H. Langer, R. H. Perrett, and J. H. Purnell, *J. Chem. Soc.*, 2444 (1960).

(8) D. H. Everett, *Trans. Faraday Soc.*, **60**, 1803 (1964); **61**, 2478 (1965).

(9) R. L. Pecsok and B. H. Gump, *J. Phys. Chem.*, **71**, 2209 (1967).

the coating liquid surface. At constant temperature

$$Q_t = W_s \int_0^P \frac{dQ_s}{dP} dP + W_m \int_0^P \frac{dQ_{mod}}{dP} dP + W_L \int_0^P \frac{dQ_L}{dP} dP + A_L \int_0^P \frac{dQ_{AL}}{dP} dP \quad (11)$$

where  $W_s$  is the weight of the unmodified adsorbent present,  $A_L$  is the surface area of the coating liquid, and  $dQ_s/dP$  and  $dQ_{AL}/dP$  describe the respective isotherms. In general, the  $Q_{solid}$  term disappears when the adsorbent surface is modified, and the  $Q_{AL}$  term is negligibly small except for the special case of a nonpolar solute on a highly polar coating liquid.

At a given pressure and temperature and for liquid coatings above 1%, it can be assumed that the distribution coefficients for the solutes on each of the respective phases remain constant and reasonably independent of the amount of liquid or liquid surface present. Equation 11 simplifies to

$$Q_{(t,P)} = W_m K_{mod} + W_L K_L + A_L K_A \quad (12)$$

where  $K_{mod}$ ,  $K_L$ , and  $K_A$  are distribution coefficients for the modified surface, the bulk liquid, and the liquid surface area, respectively, at the given solute pressure and temperature.<sup>10</sup>

Figure 8 shows the observed sorption as well as the hypothesized contributions of the modified adsorbent surface and the liquid surface as calculated by eq 12 for *n*-hexane on TOTP-coated AWF. The bulk liquid term was obtained from the bulk liquid isotherm, and the other two terms were calculated from eq 12 using simple two-equation, two-unknown techniques. The calculated contribution of the liquid surface was found to be small and possibly within experimental error (Figure 8), but it did help fit the experimental data better, particularly at low per cent liquid coatings.

Figure 9 shows the sorption isotherms of *n*-hexane on TCEP-coated AWF. In this instance *n*-hexane is nearly insoluble in the TCEP. A minimum is developed, but there is a slight increase in the isotherms as the amount of TCEP coating is increased. If the surface area of the liquid TCEP were a major contributor to the sorption isotherms, there would have been a relatively large increase in the isotherms as the liquid surface developed beyond the monolayer covering followed by a drop in the isotherms as the per cent of TCEP became large. This is because the surface area of a liquid on an adsorbent decreases when the micropores and capillaries are filled.<sup>11</sup>

Figure 10 compares the amount of sorption of *n*-hexane and the surface area as a function of the per cent TCEP liquid coating. The surface area curve shows the expected initial rapid drop followed by a more gradual drop as the amount of liquid coating was increased. The amount sorbed followed the same general pattern except that there was a slight increase

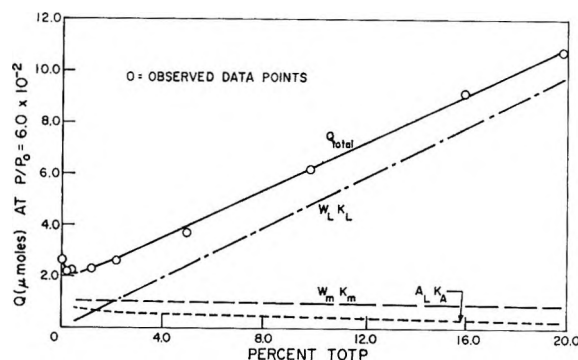


Figure 8. Calculated sorption isotherms and experimental data points for *n*-hexane on TOTP-coated AWF at 30° and  $P/P_0 = 0.04$ . Curve identities as noted in Figure 3.

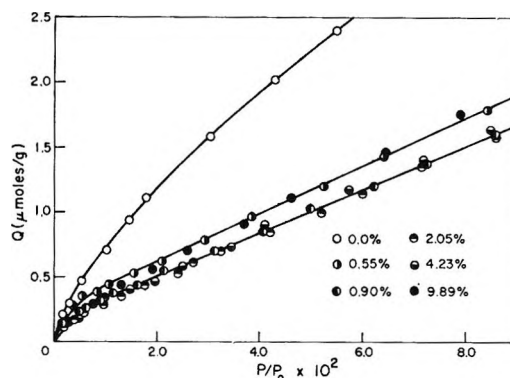


Figure 9. Sorption isotherms for *n*-hexane on TCEP-coated AWF at 30°.

at the higher per cent liquid coating. If adsorption on the liquid surface had been a dominating factor there should have been a noticeable decrease in the amount of *n*-hexane sorbed. Of particular interest is the fact that the amount sorbed at 1–2% TCEP is two to three times the amount of increased sorption that occurs when the liquid coating is increased from 2 to 10%.

Because acetone and the highly polar methanol were easily able to penetrate the nonpolar squalane to interact completely with the sorbent surface and because the chemical potential of a vapor or solute is the same in all phases of a system at equilibrium, it must be assumed that *n*-hexane tends to equilibrate in all phases of a TCEP coated adsorbent—including the modified surface, the bulk liquid, and the liquid surface. Figures 9 and 10 consequently show that sorption by the modified adsorbent surface, as shown by the minimum at about 1%, predominates over the amount of increased sorption beyond the minimum that might be attributed to the sum of the bulk liquid and liquid surface contributions. The possibility of

(10) J. R. Conder, D. C. Locke, and J. H. Purnell, *J. Phys. Chem.*, **73**, 700 (1969).

(11) S. Ross and E. D. Tolles in "The Solid-Gas Interface," Vol. 2, E. A. Flood, Ed., Marcel Dekker, New York, N. Y., 1967, p 652.

continued adsorption by the modified adsorbent surface was not taken into consideration by previous workers.<sup>11-14</sup>

### Summary

Equation 10 is expected to hold for situations involving volatile solutes and adsorbents coated with relatively nonvolatile liquids. Under most conditions one or more of the right-hand terms of eq 10 are negligibly small or nonexistent. The  $Q_{\text{solid}}$  contribution disappears rapidly with per cent coating for highly polar coating liquids on adsorbents of low specific surface areas and persists up to high per cent liquid coatings for adsorbents having high specific areas. The  $Q_{\text{mod}}$  contribution develops at the expense of the  $Q_{\text{solid}}$  term, while the  $Q_{\text{liquid}}$  term develops with the formation of liquid pools. Adsorption by the liquid surface,  $Q_{\text{AL}}$ , cannot become a factor until a liquid surface is developed, and except for nonpolar solutes on polar coating liquids, its magnitude is generally too small to be observed.

Figure 11 helps summarize the contributions of the various phases to the total amount of sorption for the systems studied. Schematically, it shows the expected total amount of sorption with a solid line and the principal contributing sources as areas under dashed lines. A constant temperature and solute pressure is assumed in all cases. It must be emphasized that the relative magnitudes of the respective contributions can change with solute pressure and per cent coating depending upon the linearity of the sorption isotherms and the relative intensities of the sorption forces.

Curve A (Figure 11) shows that a nonpolar coating liquid is not able to compete effectively with a polar solute as the per cent of coating liquid is increased. The contribution of the solid is large and remains constant at constant pressure and temperature. The contribution of the coating liquid rises slowly because the solubility of polar solutes in nonpolar solvents is generally low. For surfaces treated with a silanizing agent or a highly polar compound, the contribution of the surface is significantly reduced but not eliminated (curve D, Figure 5).

Curve B indicates that there is some competition between the nonpolar coating and nonpolar solute for the active sites of an adsorbent. A modified surface is developed at low per cent coatings, but its contribution is small because its interaction with the solute is small. Beyond the minimum, the liquid phase contribution increases rapidly because of the greater solubility of the solute in the liquid.

Polar coatings rapidly develop a modified surface giving a minimum and constant contribution to the total amount of polar solutes sorbed as the per cent coating is increased (curve C, Figure 11). The relative polarities of polar substances cover a wide range, and

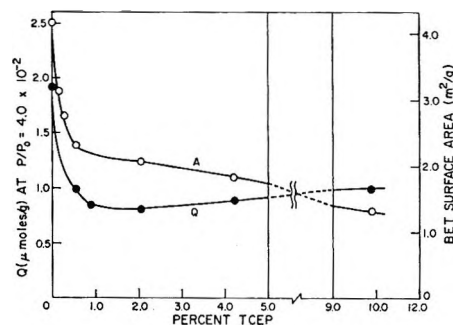


Figure 10. Comparison of amount of *n*-hexane sorbed at 30° and  $P/P_0 = 0.04$  vs. surface area as a function of per cent TCEP coating on AWFb.

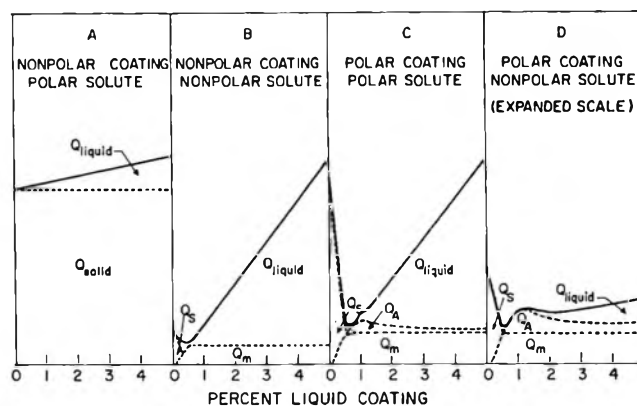


Figure 11. Representative sorption profiles at constant pressure and temperature as a function of per cent coating for various polar-nonpolar systems.

the magnitude of the contributions could vary considerably. A small amount of contribution by the liquid surface is shown to develop after the modified surface is formed. This is not easily seen experimentally, and, if present, may be negligible compared to the contribution of the coating liquid.

Curve D represents those types of systems which have been reported to exhibit liquid surface adsorption.<sup>11-14</sup> Because the interaction of a nonpolar solute with either the adsorbent or the polar coating liquid is small, an expanded vertical scale is used. At low per cent coating a minimum in the sorption isotherm is developed. The increase in sorption beyond the minimum may be attributed to sorption by the bulk liquid or the liquid surface or both. Previous studies have not considered the contribution of the modified surface to the total amount sorbed.<sup>14</sup>

Conder, Locke, and Purnell<sup>10</sup> recently discussed on a qualitative basis the type of chromatographic retention behavior to be expected when the solid-liquid as well as the gas-liquid interfaces contribute to the retention

(12) R. L. Martin, *Anal. Chem.*, **33**, 347 (1961).

(13) D. E. Martire, R. L. Pecsok, and J. H. Purnell, *Trans. Faraday Soc.*, **61**, 2496 (1965).

(14) D. E. Martire, *Anal. Chem.*, **38**, 244 (1966).

of the coating liquid. Their hypothetical curves based on a three-component retention equation and constant solute concentration in the gas phase may be compared to those observed in this study. Although close comparisons cannot be made because of differing emphasis on the relative strengths of the independent retention factors, there is reasonably good agreement. A possible major area of difference is the recognition in this study of the development of a modified adsorbent surface which becomes and remains active as the original solid surface becomes covered; *i.e.*, the total surface area of the adsorbent is at all times active either in its original form ( $Q_s$ ) or a modified form ( $Q_{\text{mod}}$ ). The modified adsorbent surface can be represented by a complicated adsorption-from-solution equilibrium expression, the solution of which would give the  $Q_{\text{mod}}$  curves obtained from data similar to those shown in Figures 1, 7, and 9 and used in Figures 3 and 4.

For those who desire to make adjustments for the

combined modified adsorbent and liquid surface contributions, a correction factor,  $Q'_{\text{adsorbent}}$ , may be obtained from two or three batches of adsorbent coated with amounts of liquid increasing beyond the amount needed for developing a minimum. A plot of the amount sorbed (or in chromatography, the retention time or volume) *vs.* the per cent liquid would give a straight line for a constant solute pressure or gas-phase concentration. Extrapolation to zero per cent coating would give an apparent sorption correction factor for the adsorbent,  $Q'_{\text{adsorbent}}$ , and the slope of the line would give the partition coefficient for the liquid. The apparent  $Q'_{\text{adsorbent}}$  would apply for all coatings beyond the minimum and would make possible study of and allowances for the adsorbent and surface area effects.

*Acknowledgment.* This study was made possible by National Science Foundation Grants No. GP9456, GP5400, and GY4093.

## Some Thermodynamic Properties of Liquid-Coated Adsorbents

by Yoshihiro Takahashi, Paul Urone,

*Department of Chemistry, University of Colorado, Boulder, Colorado 80302*

and George H. Kennedy

*Department of Chemistry, Colorado School of Mines, Golden, Colorado 80401 (Received August 5, 1969)*

The thermodynamic properties of *n*-hexane, isooctane, acetone, and methanol on liquid-coated diatomaceous earth adsorbents show contributions from both the coating liquid and the liquid-modified adsorbent surface. Static equilibrium sorption isotherms were obtained for the solutes in squalane, tri-*o*-tolyl phosphate, tris-(cyanoethoxypropane), and on the adsorbents having 0.1–20% coatings of the liquids. Activity coefficients at infinite dilution of the solutes on the liquid-coated adsorbents are calculated from the respective isotherms after subtraction of the contribution of the isotherm of the liquid-modified support surface. The values agree with those obtained from the bulk liquids and those found in the literature. Observed isosteric heats of sorption are shown to equal the sum of the contributions from adsorption on the liquid-modified surface and solution in the bulk coating liquid. Entropy effects are calculated using the isosteric heats of adsorption and partial molar free energies of adsorption. These show that acetone adsorption on the modified surface conform closely to localized adsorption layer theory.

The thermodynamic properties of liquid-coated adsorbents are of potential interest to workers in a number of fields of science. In the field of gas-liquid chromatography, it has long been realized that partition chromatography is not only a powerful analytical tool but it is also capable of easily and rapidly measuring partition coefficients, activity coefficients, and heats and entropies of solution.<sup>1–4</sup> In the fields of catalysis and surface chemistry, liquid-coated adsorbents give a new dimen-

sion for the development of surfaces with specific chemical and physical properties.<sup>5</sup>

(1) J. R. Conder in "Progress in Gas Chromatography," Vol. 6, J. H. Purnell, Ed., Interscience Publishers, New York, N. Y., 1967, p 209.

(2) Y. Kobayashi, P. S. Chappellar, and H. A. Deans, *Ind. Eng. Chem.*, **59**, 63 (1967).

(3) A. B. Littlewood, C. S. G. Phillips, and D. T. Price, *J. Chem. Soc.*, 1480 (1955).

(4) J. H. Purnell, *Endeavor*, **23**, 142 (1964).

A companion paper<sup>6</sup> has shown that the sorptive properties of liquid-coated diatomaceous earth adsorbents can be described by a four-term equation. At constant temperature the amount of solute sorbed,  $Q$ , for a given solute pressure,  $P$ , is

$$Q_t = W_s \int_0^P \frac{dQ_s}{dP} dP + W_m \int_0^P \frac{dQ_m}{dP} dP + W_L \int_0^P \frac{dQ_L}{dP} dP + A_L \int_0^P \frac{dQ_{AL}}{dP} dP \quad (1)$$

where s, m, L indicate the solid, modified solid, and liquid phases, respectively,  $W$  the weight,  $A_L$  the surface area of the coating liquid, and  $dQ/dP$  the slope of the respective isotherm at the given pressure.

Equation 1 is more simply expressed in descriptive terms

$$Q_{\text{total}} = Q_{\text{solid}} + Q_{\text{modified}} + Q_{\text{liquid}} + Q_{AL} \quad (2)$$

In general, the  $Q_{\text{solid}}$  term disappears when the adsorbent surface is modified, and the  $Q_{AL}$  term is negligibly small except for the special case of a nonpolar solute on a highly polar coating liquid. At a given pressure and temperature, and for liquid coatings greater than those necessary to modify the adsorbent surface, it can be assumed that the distribution coefficient,  $K$ , for the solutes on each of the respective phases remains constant and reasonably independent of the amount of liquid or liquid surface present within a limited range. Equation 1 simplifies to

$$Q_{(t,p)} = K_m W_m + K_L W_L + K_A A_L \quad (3)$$

If the amounts sorbed at a given solute pressure are known, then partition and activity coefficients can be calculated readily. If the same information is obtained over a range of temperatures, then heat and entropy relationships can also be calculated readily.

### Apparatus, Materials, and Procedure

*Apparatus and Materials.* These are the same as those described in ref 6 and 7.

*Procedure.* Activity coefficients were calculated based on the adsorption or sorption isotherms of the sample. In order to calculate the surface area of a sample, the adsorption isotherm should be obtained in the higher range of relative pressure. For surface area measurements at liquid nitrogen temperature, buoyancy corrections were obtained with helium. The corrections were found to be significant, and the proper corrections were made. Surface areas were calculated using the well-known BET method.<sup>8</sup>

Isosteric heats of adsorption were calculated by measuring the adsorption isotherms at various temperatures, mostly between 30 and 75°, and at a given amount adsorbed, pressures were plotted against the inverse of temperatures (Clausius-Clapeyron equation). Heats of solution and heats of sorption were also calculated in the same manner.

The entropy of adsorption was calculated from the heats and the free energy which were experimentally obtained, and by using a proper standard state.

### Activity Coefficients at Infinite Dilution

True activity coefficients at infinite dilution can be obtained from the solubilities of the solutes in the bulk solvents. However, calculation of the activity coefficient from a sorption isotherm of a liquid-coated adsorbent (or retention volume in gas-liquid chromatography) has to be corrected for the fraction contributed from adsorption by the supporting solid. At the same time, fugacity must be used rather than the pressure of solute above the solution to get more accurate activity coefficients.

The activity coefficient at the pressure,  $P$ , and mole fraction of a solute,  $X_2$ , is given by

$$\ln \gamma_2 = \ln \frac{P}{P_0 X_2} - \frac{(B_{22} - V_2^0)(P_0 - P)}{RT} \quad (4)$$

where  $\gamma_2$  is the activity coefficient,  $P_0$  is the saturation pressure of the solute at temperature  $T$ ,  $B_{22}$  is the second virial coefficient of the solute, and  $V_2^0$  is the molar volume of the solute.

Table I: Physical Constants of Adsorbates

Adsorbate	Temp, °C	$V_2^0$ , ml/mol	$P_0$ , mm	$B_{22}$ , ml/mol
Acetone	30.0	74.52 <sup>d</sup>	282.5 <sup>d</sup>	-1860 <sup>e</sup>
Methanol	45.0	41.71 <sup>d</sup>	328 <sup>a</sup>	-1405 <sup>e</sup>
n-Hexane	30.0	132.5 <sup>d</sup>	185.4 <sup>d</sup>	-1600 <sup>f</sup>
Isooctane	30.0	160.1 <sup>d</sup>	62.4 <sup>a</sup>	-2160 <sup>b,g</sup>
Acetone	55.0	77.43 <sup>c</sup>	735 <sup>a</sup>	-1430 <sup>c</sup>

<sup>a</sup> Values calculated using the equation<sup>11</sup>  $\log P = A - B/(C + t)$ , where  $t$  is temperature in degrees centigrade. Acetone:  $A = 7.02447$ ,  $B = 1161.0$ ,  $C = 224$ ; methanol:  $A = 7.87863$ ,  $B = 1473.11$ ,  $C = 230.0$ ; isooctane:  $A = 6.81189$ ,  $B = 1257.84$ ,  $C = 220.74$ . <sup>b</sup> Value calculated using Berthelot's equation,<sup>9</sup>  $B_{22} = 9RT_c/128P_c(1 - 6(T_c^2/T^2))$  where  $P_c$  and  $T_c$  are the critical pressure and temperature, respectively. Isooctane:  $P_c = 25.50$ ,  $T_c = 271.15$ . <sup>c</sup> Obtained by interpolating the values at two temperatures. <sup>d</sup> J. Timmermans, "Physico-Chemical Constants of Pure Organic Compounds," Elsevier Publishing Co., Amsterdam, 1950. <sup>e</sup> See ref 9. <sup>f</sup> See ref 10. <sup>g</sup> G. N. Lewis and M. Randall, "Thermodynamics" 2nd ed, McGraw-Hill Publications, New York, N. Y., 1961, p 187.

(5) S. Ross and E. D. Tolles in "The Solid-Gas Interface," Vol. 2, E. A. Flood, Ed., Marcel Dekker, New York, N. Y., 1967.

(6) P. Urone, Y. Takahashi, and G. H. Kennedy, *J. Phys. Chem.*, **74**, 2326 (1970).

(7) P. Urone, Y. Takahashi, and G. H. Kennedy, *Anal. Chem.*, **40**, 1130 (1968).

(8) S. Brunauer, P. H. Emmett, and E. Teller, *J. Amer. Chem. Soc.*, **60**, 309 (1938).

(9) J. S. Rowlinson, *Trans. Faraday Soc.*, **45**, 974 (1949).

(10) G. A. Lambert, G. A. H. Robert, J. S. Sawlinson, and V. J. Wilkinson, *Proc. Roy. Soc.*, **A196**, 113 (1949).

(11) N. A. Lange, Ed., "Handbook of Chemistry," 10th ed, McGraw-Hill Publications, New York, N. Y., 1961, p 1424.

Table II: Activity Coefficients at Infinite Dilution

Solute	Solvent	Temp, °C	From bulk liquid	From sorption isotherm	From cor isotherm	Lit.
Acetone	TOTP	30.0	1.13			
Acetone	TOTP	55.0	0.95	0.65 <sup>a</sup> (15.87%)	0.92	
Acetone	Squalane	30.0	3.35	1.45 <sup>a</sup> (18.51%) <sup>b</sup>	3.62	1.48 <sup>e</sup>
Acetone	TCEP	30.0	1.14	0.61 <sup>a</sup> (4.23%)	1.12	
Methanol	TOTP	45.0	1.79	0.22 <sup>a</sup> (4.93%)	1.68	
Methanol	Squalane	30.0	<i>c</i>			24.38 <sup>f</sup>
<i>n</i> -Hexane	TOTP	30.0	3.42	2.72 (9.79%)	3.42	
<i>n</i> -Hexane	Squalane	30.0	0.645	0.58 (7.54%)	0.63	<i>d</i>
<i>n</i> -Hexane	TCEP	30.0	<i>c</i>			
Isooctane	Squalane	30.0	0.73	0.63 (5.17%)	0.75	0.721 <sup>g</sup>

<sup>a</sup> Extrapolated from higher mole fraction. Per cent liquid is shown in parentheses. Solid support is AWFb. <sup>b</sup> Solid support is DMCS-treated AWFb. <sup>c</sup> Not determined because of very low solubility. <sup>d</sup> See Table II. <sup>e</sup> See ref 13. <sup>f</sup> See ref 14. <sup>g</sup> See ref 17.

Table I<sup>9-11</sup> lists the physical constants employed in the calculation of activity coefficients. The solubility data for solutes in the bulk liquids were put into eq 4 in order to calculate the true activity coefficients at infinite dilution. Since there were no complications from adsorption, calculations to obtain the mole fraction,  $X_2$ , in the bulk liquid were straightforward. The results are listed in Table II.

In most cases, adsorption at the gas-liquid interface was negligibly small so that eq 2 was approximated as

$$Q_{\text{total}} = Q_{\text{modified}} + Q_{\text{liquid}} \quad (5)$$

when the liquid loading exceeded that needed for a modified layer coverage,  $Q_{\text{modified}}$ . By measuring the sorption isotherms of the solute on the adsorbent coated with just enough liquid to modify its surface ( $\sim 0.3\%$ )<sup>6</sup> and then on a much higher liquid coating, *i.e.*, 10 or 20%, eq 5 can be solved easily. When a polar solute and nonpolar coating liquid are used,  $Q_{\text{modified}}$  should be replaced by  $Q_{\text{solid}}$ .

For liquid-coated adsorbents, eq 4 was slightly modified, and the mole fraction of solute in the solution was expressed as

$$X_2 = \frac{N_{\text{liquid}}}{N_L + N_{\text{liquid}}} \quad (6)$$

or when  $X_2$  is small then

$$X_2 = \frac{N_{\text{liquid}}}{N_L} \quad (6a)$$

An apparent mole fraction of the solute,  $X_2'$ , is obtained when it is assumed that the total amount of the solute sorbed was in the bulk liquid; *i.e.*

$$X_2' = (N_{\text{mod}} + N_{\text{liquid}})/N_L \quad (7)$$

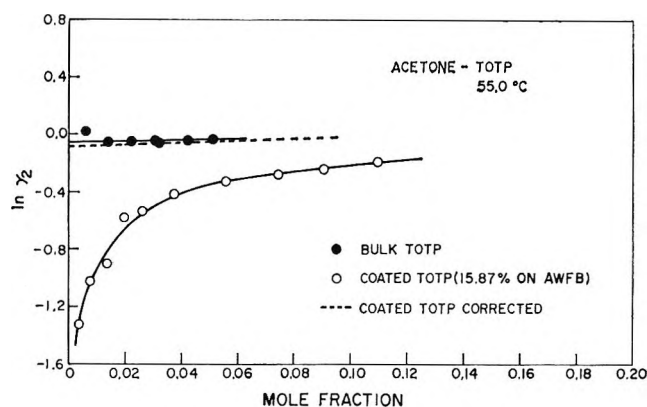


Figure 1. Comparison of uncorrected and corrected activity coefficients obtained from sorption isotherms of acetone on TOTP-coated AWFb adsorbent with that obtained from bulk TOTP liquid.

where  $N_{\text{mod}}$  is the number of moles of the solute adsorbed on the modified surface,  $N_{\text{liquid}}$  is the number of moles of the solute dissolved in the bulk liquid, and  $N_L$  is the number of moles of the liquid coating.

Activity coefficients of acetone on tri-*o*-tolyl phosphate (TOTP) are shown in Figure 1, where  $\ln \gamma_2$  is plotted *vs.* mole fraction. The solid circles were calculated from the solubility of acetone in the bulk TOTP liquid, and the open circles were obtained directly from the sorption isotherm of acetone on 15.8% TOTP-coated acid-washed firebrick (AWFB) without correction. The dashed line shows the corrected values from the sorption isotherm using eq 6. The agreement between the activity coefficient from the bulk liquid solubility data and that from the sorption isotherm of the coated adsorbent with corrections is very good.

Activity coefficients calculated from the uncorrected sorption isotherms were almost impossible to extrapolate to zero concentration with accuracy even though the liquid loading was as much as 16%. If retention volumes were measured by gas chromatography using sample sizes which correspond to mole fractions less than 0.05, then the calculated activity coefficients would be very small because in this range of concentrations, the relative surface adsorption is much greater than at higher concentrations. In such cases the retention volume, and consequently the activity coefficient, depends upon the sample size. If the retention volumes were measured using sample sizes corresponding to the mole fraction range of 0.05 to 0.10, the retention volumes would be almost independent of sample size; however, the activity coefficient still would be significantly lower than the true value.<sup>12</sup>

Figure 2 demonstrates the same type of plot for a nonpolar solute and a nonpolar liquid (*n*-hexane-squalane). In this case, the nonpolar solute interacts with surface sites weakly, and the contribution from the adsorption of the solute on the solid surface is not significant. Thus, the three different plots in Figure 2 are close to each other. It is not surprising that when the liquid loading was more than 15%, the open circles in Figure 2 are on the line traced by the solid circles, and the effect of adsorption on the surface cannot be seen.

Activity coefficient measurements of nonpolar solutes in nonpolar liquids have been reported by many workers. This is the only combination for which gas-liquid chromatographic measurements of activity coefficients at infinite dilution compared well with static measurements. This confirmed the fact that the two methods gave essentially the same results when more than 20% of liquid was used in the gas-liquid chromatographic technique. In particular, the activity coefficient of *n*-hexane in squalane has been studied by a number of investigators by both static and gas-liquid chromatographic techniques. The values are listed in Table III.

The measurement of the activity coefficient of a polar solute in a nonpolar liquid by ordinary gas-liquid chromatographic techniques might be very diffi-

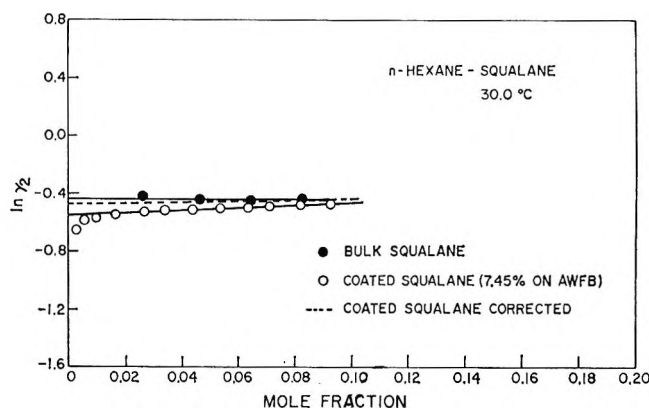


Figure 2. Same as Figure 1 for *n*-hexane on squalane-coated AWF.

cult unless a very inert support and a very high liquid loading were used. However, a very inert support generally has low surface area and if the support is coated with a large amount of liquid phase, the thickness of the liquid may prevent complete equilibration under gas chromatographic conditions.

Figure 3 shows plots of  $\ln \gamma_2$  against mole fraction acetone in bulk squalane and in squalane coated on DMCS-treated AWF. The amount of acetone adsorbed on the adsorbent surface was subtracted from the sorption isotherm in order to obtain the true activity coefficients (dashed line). The line was quite close to the activity coefficients measured with bulk liquid solubility data.

The sorption isotherms of acetone on squalane-coated AWF were also measured. However, AWF was active with respect to acetone. Most of the amount sorbed was due to adsorption on the adsorbent surface giving a large relative error for the liquid term. A plot of  $\ln \gamma_2$  against mole fraction in this case was out of the range of Figure 3; however, the relative adsorptivity of acetone on DMCS-treated AWF and on AWF can be seen in Figure 5 of ref 6.

Bonastre and Grenier<sup>13</sup> reported the activity coefficient of acetone in squalane at 100° relative to *n*-hexane. The substrate material used was Fluoropak 80 coated with 10% squalane. While their sorption studies showed that the activity coefficient of *n*-hexane in squalane was not significantly affected by the support surface under the experimental conditions they used, the relative activity coefficient of acetone was. Using the relative activity coefficient of acetone given by Bonastre and Grenier<sup>13</sup> as 0.351, and 0.66 as the activity coefficient of hexane in squalane,<sup>12</sup> the activity coefficient of acetone in squalane was calculated to be 1.48 from their data. This value does not agree with

Table III: Activity Coefficients of *n*-Hexane in Squalane at Infinite Dilution

Method	$\gamma$ at 30°	Ref
Packed column	0.63	<i>a</i>
Packed column	0.646	<i>b</i>
Tensiometer	0.641	<i>c</i>
Bulk liquid	0.658	<i>d</i>
Bulk liquid	0.645	This work

<sup>a</sup> See ref 17. <sup>b</sup> A. J. B. Cruickshank, D. H. Everett, and M. T. Westaway, *Trans. Faraday Soc.*, **61**, 235 (1965). <sup>c</sup> A. J. Ashworth and D. H. Everett, *ibid.*, **56**, 1609 (1960). <sup>d</sup> D. E. Martire, R. L. Pecsok, and J. H. Purnell, *ibid.*, **61**, 2496 (1965).

(12) K. Kwantes and G. W. A. Rijnders, in "Gas Chromatography—Amsterdam 1958," D. H. Desty, Ed., Academic Press, Inc., New York, N. Y., 1958, p 125.

(13) J. Bonastre and P. Grenier, *Bull. Soc. Chim. France*, 1292 (1968).



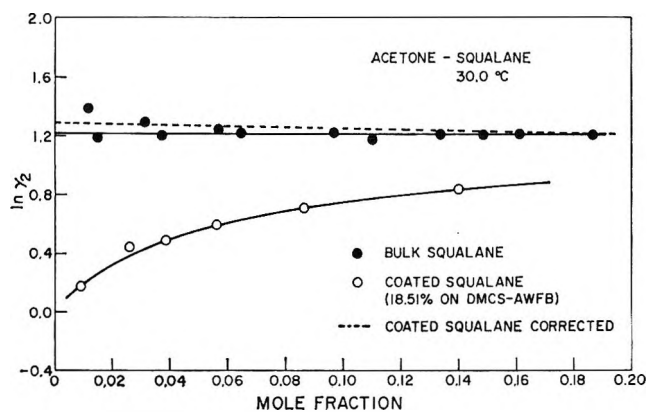


Figure 3. Same as Figure 1 for acetone on squalane-coated AWFb.

our work ( $\gamma = 3.62$ ) nor that of Pecsok and Gump ( $\gamma = 2.85$ ).<sup>14</sup> However, using the sorption isotherm of acetone on 18.51% squalane-coated dimethyldichlorosilane (DMCS)-treated AWFb (Figure 3), the activity coefficient of acetone was calculated to be 1.45 without correction due to adsorption on the support surface. Therefore it is probable that Bonastre and Grenier's activity coefficient measurements had interference from adsorption.

Cadogan, *et al.*,<sup>15</sup> measured activity coefficients of alcohols in squalane at 50° by a gas-liquid chromatographic technique. The retention volume ( $V_R$ ) was assumed to be a result of contributions from three principal terms: solubility in bulk liquid phase ( $K_L V_L$ ), adsorption on the solid surface ( $K_s A_s$ ), and adsorption at the gas-liquid interface ( $K_I A_I$ ).  $V_R/V_L$  was plotted against  $1/V_L$  in order to obtain  $K_L$  which is the intercept when  $1/V_L$  is zero. However, the  $K_L$  value observed was valid only when the concentration of the solute was low enough so that the distribution coefficient,  $K_L$ , was independent of the sample size, and the  $K_s A_s$  term would not hold at low liquid coatings due to the adsorption from solution phenomenon.

When adsorption of a solute at the gas-liquid interface contributes to the total amount sorbed, the treatment gets a bit more complicated. When  $K_m$ ,  $A_L$ , and  $K_A$  in eq 3 are known, the amount of solute dissolved in a liquid phase,  $K_L V_L$ , can be obtained from a sorption isotherm by subtracting from it the amounts adsorbed at the gas-liquid interface,  $K_A A_L$ , and on the modified surface,  $K_m W_m$ . The  $K_L V_L$  can be found and used to calculate the true activity coefficient.

Figure 4 shows the activity coefficients of *n*-hexane in TOTP at 30.0° calculated as in Figures 1-3 from the solubility of *n*-hexane in bulk TOTP, the sorption isotherm on 9.79% TOTP-coated AWFb, and the sorption isotherm corrected by subtracting the amounts adsorbed on the solid surface and the gas-liquid interface. Because of the significant participation of the gas-liquid interface in this case, the latter is not easily performed from a practical point of view. In general, the

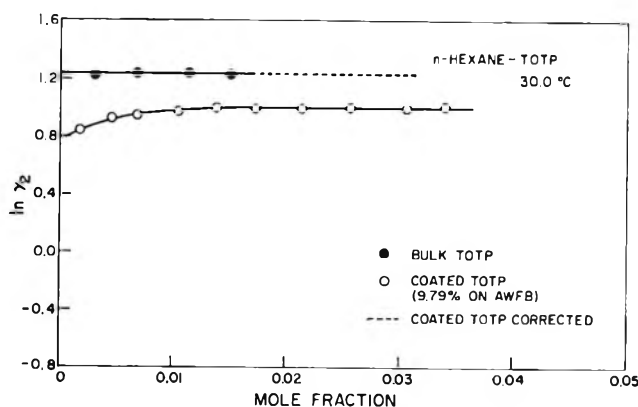


Figure 4. Same as Figure 1 for *n*-hexane on TOTP-coated AWFb.

surface area of a liquid-coated adsorbent is not known and  $K_m$  and  $K_A$  cannot be calculated easily. Thus approximations must be used in order to obtain reasonable activity coefficients at infinite dilution from observed sorption isotherms. The appropriate assumptions are: (1) the difference in the surface areas at, say 10 and 15% liquid loadings is small, and (2) the amounts of the solute adsorbed on the modified solid surface is the same at the different liquid loadings. The first approximation was checked by looking at the surface area measured by Pecsok, *et al.*,<sup>16</sup> and the surface area difference was 12%. Except for a nonpolar solute on a very polar liquid phase surface,  $K_A$  is also small and therefore the difference in  $A_L K_A$  for those two liquid coated adsorbents are much smaller than  $W_L K_L$ . The second approximation was also valid because the adsorption of a nonpolar solute on a modified surface is very small and the solid surface area change in 10 and 15% liquid loadings per gram of the total can be neglected.

Using these two approximations, the calculation of the activity coefficient from the sorption isotherms is simplified. The difference between the total amount sorbed of *n*-hexane on 15% TOTP-coated AWFb,  $Q_{15}$ , and the total amount of *n*-hexane sorbed on 10% TOTP-coated AWFb,  $Q_{10}$ , is equal to the amount of *n*-hexane dissolved in 0.05 g of TOTP, ( $Q_{15} - Q_{10}$ ), for example.

The activity coefficient was calculated using this simplified method with the sorption isotherms of *n*-hexane on 9.79% and 15.87% TOTP-coated AWFb samples. The calculated value was 3.41, and it was close to the activity coefficient, 3.42, measured on the bulk liquid.

The activity coefficients measured from liquid solubilities and using sorption isotherms are summarized in Table II. Methanol in squalane, and *n*-hexane in

(14) R. L. Pecsok and B. H. Gump, *J. Phys. Chem.*, **71**, 2202 (1967).

(15) D. F. Cadogan, J. R. Conder, D. C. Locke, and J. H. Purnell, *ibid.*, **73**, 708 (1969).

(16) R. L. Pecsok, A. Yllana, and A. Abdul-Karim, *Anal. Chem.*, **36**, 452 (1964).

TCEP could not be measured in the relative pressure range up to 0.01 at 30.0° because of their extremely low solubilities in the respective liquids. The sorption isotherm of methanol on squalane-coated AWFb showed that solubility of methanol in squalane was negligibly small.<sup>6</sup> Interestingly, the sorption isotherms of *n*-hexane on TCEP-coated AWFb did show a slight solubility of *n*-hexane in TCEP.<sup>6</sup>

The measurement of activity coefficients at infinite dilution by gas-liquid chromatography<sup>17</sup> is very attractive but the retention volume must be corrected in order to eliminate the fraction of the retention volume contributed from adsorption of a solute on the solid surface and possibly at the gas-liquid interface. Our studies of the adsorption of solutes on liquid-coated adsorbents give a clearer picture of the adsorption phenomena on liquid-coated adsorbents. The additive relationship can separate the total amount sorbed into the amounts present in the respective phases. The recognition of these separate contributions is important for solution and adsorption-from-solution studies. This treatment can be applied to any polar-nonpolar systems.

### Heats of Sorption

The energetic distribution of adsorption sites is another important property of surfaces. Parcher<sup>18</sup> studied the adsorption isotherms of acetone on AWFb. Analysis of the adsorption isotherm showed that its shape agreed with the Temkin better than the Langmuir or Freundlich adsorption models. The Temkin model assumes that the energy of adsorption of an adsorbate decreases linearly with increasing surface coverage rather than remaining constant (Langmuir) or varying exponentially (Freundlich).

However, a real surface has a random energy distribution, and frequently a whole adsorption isotherm does not fit any single adsorption model.<sup>19</sup> Thus it was concluded that the analysis of an adsorption isotherm carried out by a procedure of fitting it to a certain model is not a suitable method to study surface properties. For a better evaluation, the heats of adsorption at different surface coverages should be considered.

Isosteric heats of adsorption of acetone on AWFb were obtained by measuring acetone adsorption isotherms at various temperatures. At constant surface coverage,  $\theta$ , or at a constant amount adsorbed,  $Q$ ,<sup>20</sup>

$$\left[ \frac{d \ln P}{d 1/T} \right]_{n_a} = - \frac{q^{st}}{R} \quad (8)$$

where  $q^{st}$  is the isosteric heat of adsorption;  $n_a$  is the number of moles of adsorbed vapor. Plots of  $\log P$  vs.  $1/T$  for acetone on 0.3% TOTP-modified AWFb are shown in Figure 5, and the isosteric heats of adsorption of acetone on AWFb at varying surface coverage,  $\theta$ , are listed in Table IV.

The isosteric heats of adsorption of acetone on TOTP-modified AWFb surface and on dimethyldichlorosilane

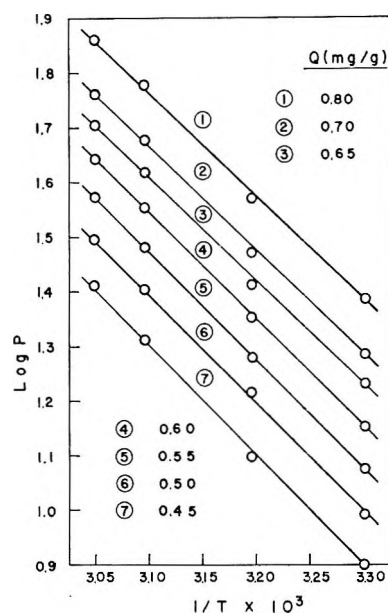


Figure 5. Clausius-Clapeyron plots of  $\log P$  vs.  $1/T$  for heats of adsorption of acetone on a TOTP-modified AWFb surface.

Table IV: Isosteric Heats of Adsorption of Acetone at Various Surface Coverage

AWFB		0.3% TOTP-AWFb		DMCS-AWFb	
$\theta$	$q^{st}$ , kcal/mol	$\theta$	$q^{st}$ , kcal/mol	$\theta$	$q^{st}$ , kcal/mol
0.189	17.39	0.207	9.05	0.113	7.18
0.283	14.49	0.236	9.10	0.151	7.67
0.377	13.12	0.266	9.10	0.189	7.85
0.472	12.81	0.291	9.05	0.226	7.50
0.566	11.74	0.340	9.08	0.264	7.55
0.660	10.68	0.355	9.05		
0.755	9.91	0.450	9.03		
		0.541	9.00		
		0.631	8.72		
		0.721	8.60		

(DMCS)-treated AWFb surface are also listed in Table IV. The isosteric heat of adsorption of acetone on AWFb decreases almost exponentially with increasing surface coverage and it varies from 17.4 to 9.9 kcal/mol. This indicates that the AWFb surface is very heterogeneous with respect to acetone and that acetone is strongly adsorbed on the surface, especially at low surface coverage. The heat of condensation of acetone is  $-7.65$  kcal/mol; thus the excess heat of adsorption varies from  $-9.8$  to  $-2.2$  kcal/mol. Assuming that the isosteric heat of adsorption is the same as the differ-

(17) D. H. Desty and W. T. Swanton, *J. Phys. Chem.*, **65**, 766 (1961).

(18) J. F. Parcher, Ph.D. Thesis, University of Colorado, 1966.

(19) A. W. Adamson, I. Ling, L. Dormant, and M. Orem, *J. Colloid Interface Sci.*, **21**, 445 (1966).

(20) D. M. Young and A. D. Crowell, "Physical Adsorption of Gases," Butterworth and Co. (Publishers) Ltd., London, 1962.

ential heat of adsorption ( $\Delta H_a$ ) but of opposite sign,<sup>21</sup> and the standard state of the adsorbed layer is taken the same as for the pure liquid, the excess heat of adsorption,  $\Delta H_a^{\text{ex}}$ , can be expressed as

$$\Delta H_a^{\text{ex}} = \Delta H_a + \Delta H_c \quad (9)$$

where  $\Delta H_c$  is heat of condensation.

If  $\Delta H_a^{\text{ex}}$  is negative, the adsorption process is more favorable than just a condensation process. The more energetically active are the surface sites, the more negative is the excess heat.

The isosteric heat of adsorption of acetone on a TOTP-modified AWFb surface was almost independent of surface coverage, and was approximately 9.0 kcal/mol. The very active sites on the original surface had interacted with and were modified by TOTP molecules and were not available for acetone molecules. The surface was consequently rendered homogeneous with respect to acetone for the whole range of surface coverage studied. The excess heat of adsorption was approximately  $-1.5$  kcal/mol.

A moderately homogeneous surface with respect to acetone was also established by DMCS treatment. The isosteric heats of adsorption on DMCS-treated firebrick were lower and almost identical with the heat of condensation of acetone. Thus, a monomolecular layer coverage of the solute in the latter case was obtained only at a higher relative pressure.

At a relative pressure of 0.04, the surface of AWFb was about 76% covered with acetone, while only 40% of a TOTP modified surface was covered, and the DMCS-treated AWFb was covered on only 35% of its surface. The adsorption model for acetone on DMCS-treated AWFb was also found to be similar to that for water on dehydrated silica surfaces<sup>22</sup> and of type III in BET classification.<sup>23</sup>

The nature of the adsorbed layer was studied through the thermodynamic data of adsorption. If the adsorbed molecules have perfect two-dimensional movement, the translational entropy of an adsorbed molecule is given by<sup>24</sup>

$$S^2_{\text{trans}} = R \ln MTa + 65.80 \quad (10)$$

where  $M$  is the molecular weight of an adsorbed gas,  $a$  is the area available per molecule ( $22.53T \times 10^{-16}$  cm<sup>2</sup>). For a three-dimensional perfect gas, the translational entropy is given by the Sackur-Tetrode equation

$$S^3_{\text{trans}} = R \ln M^{2/3} T^{5/2} - 2.30 \quad (11)$$

When a perfect unlocalized layer adsorption is assumed, the entropy of adsorption is given by

$$\Delta S = S^2_{\text{trans}} - S^3_{\text{trans}} \quad (12)$$

If the observed entropy loss on adsorption is less than would be expected from eq 11, translational motion perpendicular to the surface is present because of the low potential energy of the surface.

If the observed entropy loss on adsorption is equal to  $-(S^3_{\text{trans}})$  the adsorbed layer is a perfect localized layer. This is a rather extreme case, and only at very low temperatures, where the kinetic energy is small, could this condition be observed.<sup>24</sup>

The free energy and entropy of adsorption were calculated by the method described by Everett<sup>25-28</sup> using the standard state at which the surface is half-covered with an adsorbed gas.

$$\Delta\mu_{\tau}^+ = RT \ln P \quad (13)$$

$$\frac{d \ln P}{d(1/T)} = \frac{\Delta\bar{H}_{\tau}^+}{R} = -\frac{q^{\text{st}}}{R} \quad (14)$$

$$\Delta\mu_{\tau}^+ = \Delta\bar{H}_{\tau}^+ - T\Delta S_{\tau}^+ \quad (15)$$

$$\Delta\bar{S}_{\tau}^{\circ} = \Delta\bar{S}_{\tau}^+ + R \ln \frac{\theta}{1-\theta} \quad (16)$$

where  $\Delta\mu_{\tau}^+$  is the partial molar free energy of adsorption taking the gas state at unit pressure as standard state,  $\Delta\bar{H}_{\tau}^+$  is the partial molar enthalpy of adsorption,  $\Delta\bar{S}_{\tau}^+$  is the entropy of isothermal transfer (per mole) from gas state at 1 mm pressure to adsorbed phase,  $\Delta\bar{S}_{\tau}^{\circ}$  is the excess entropy of transfer when ideal localized monolayer is taken as standard reference system, standard state gas at 1 mm pressure,  $\theta$  is the fractional surface coverage.

Figure 6 shows  $\Delta\bar{H}_{\tau}^+$ ,  $\Delta\bar{S}_{\tau}^+$ , and  $\Delta\bar{S}_{\tau}^{\circ}$  values for acetone adsorption on AWFb at 30.0°. In this case,  $\Delta\bar{H}_{\tau}^+$  varies significantly with surface coverage, and no useful information was obtained from entropy data.

Figure 7 shows  $\Delta\bar{H}_{\tau}^+$ ,  $\Delta\bar{S}_{\tau}^+$ , and  $\Delta\bar{S}_{\tau}^{\circ}$  values for acetone on TOTP-modified AWFb at 30.0°.  $\Delta\bar{H}_{\tau}^+$  values vs. surface coverage show that the heat of adsorption is almost independent of the surface coverage. Not only was the homogeneity of the surface confirmed, but it was also possible to study the surface adsorption model, localized or mobile adsorbed layer, from excess entropy,  $\Delta\bar{S}_{\tau}^{\circ}$ , data.

At half surface coverage ( $\theta = 1/2$ ) the excess entropy of adsorption is  $-34.9$  eu. If the adsorption of acetone on the modified surface forms an ideal localized adsorbed layer, the excess entropy should be equal to  $-S^3_{\text{trans}} - S^3_{\text{trans}}$  was calculated using eq 12, and a value of 38.1 eu was obtained. If the adsorption were an ideal unlocalized adsorbed layer, the excess entropy of adsorption should be equal to  $\Delta S$  in eq 13.  $S^2_{\text{trans}}$  was calculated to be 29.6 eu; thus  $\Delta S = -8.5$  eu.

(21) T. L. Hill, *J. Phys. Chem.*, **17**, 520 (1949).

(22) G. J. Yound, *J. Colloid Sci.*, **13**, 67 (1958).

(23) A. W. Adamson, "Physical Chemistry Surfaces," Interscience Publishers, New York, N. Y., 1960, p 475.

(24) C. Kamball, *Advan. Catal.*, **2**, 233 (1950).

(25) D. H. Everett, *Trans. Faraday Soc.*, **46**, 453 (1950).

(26) D. H. Everett, *ibid.*, **46**, 942 (1950).

(27) D. H. Everett, *ibid.*, **46**, 957 (1950).

(28) D. H. Everett, *Proc. Chem. Soc. London*, **38** (1957).

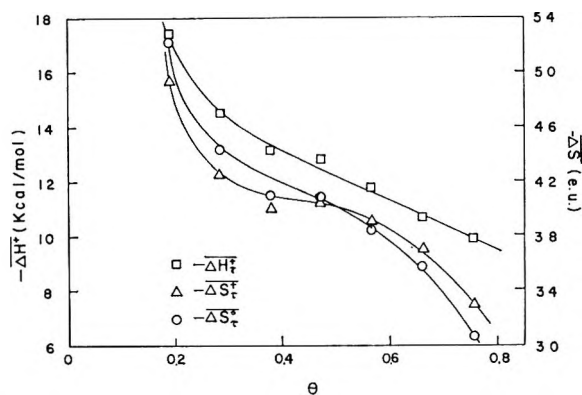


Figure 6. Variation of partial molar free energy of adsorption ( $\Delta\bar{H}_r^+$ ), entropy of isothermal transfer ( $\Delta\bar{S}_r^+$ ), and excess entropy of transfer ( $\Delta\bar{S}_r^0$ ) of acetone on unmodified AWFB adsorbent.

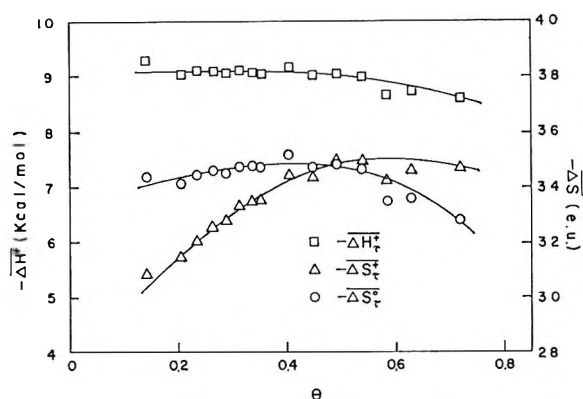


Figure 7. Same as Figure 6 but for acetone on TOTP-modified AWFB surface.

By comparing these values, it was concluded that the adsorption of acetone is strongly localized on a particular site with little movement from one site to another. The slight decrease in magnitude in excess entropy at higher surface coverage might be related to the slightly lower energy of adsorption at higher surface coverage.

Hargrove and Sawyer<sup>29</sup> observed the excess free energy, heat, and entropy of adsorption of hexane, cyclohexane, cyclohexene, and benzene on salt-modified alumina. The results are not easily compared because the standard state of the adsorbed layer was not defined and the measurements involved a variety of surface conditions and coverage.

Heat of solution measurements on coated adsorbents by static or dynamic (*i.e.*, gas-liquid chromatography) techniques should also be corrected for the adsorption of solutes on the support surface. The total heat measured is essentially the sum of two terms

$$\Delta H = \Delta H_a \frac{Q_m}{Q_{\text{total}}} + \Delta H_s \frac{Q_{\text{liquid}}}{Q_{\text{total}}} \quad (17)$$

where  $\Delta H$  is the total heat observed,  $\Delta H_s$  is the heat of solution, and  $\Delta H_a$  is the heat of adsorption on the modi-

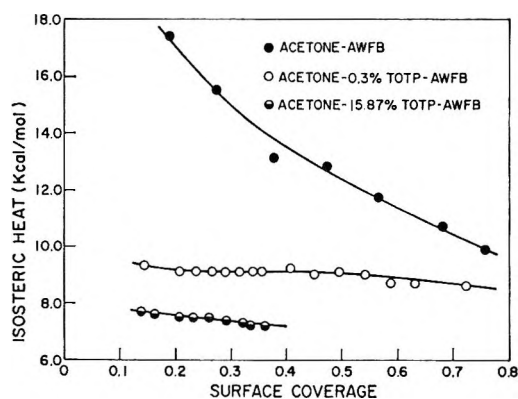


Figure 8. Isosteric heats of adsorption and sorption of acetone as a function of fractional surface coverage,  $\theta$ .

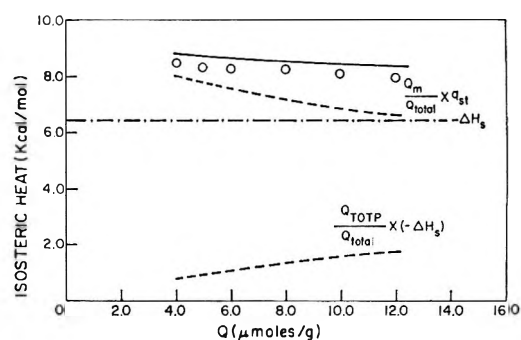


Figure 9. Additivity of the heat of solution,  $-\Delta H_s$ , and the isosteric heat of adsorption on the modified surface,  $q^{st}$ , to give solid line as compared to observed heats of sorption of acetone on 15.87% TOTP-coated AWFB, open circles, as a function of amount sorbed.

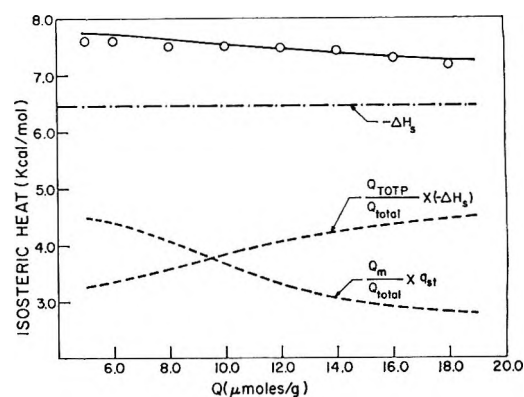


Figure 10. Same as Figure 9 but for 2.15% TOTP-coated AWFB.

fied surface. In general,  $\Delta H_s$  and  $\Delta H_a$  are not the same, hence  $\Delta H$  is usually not equal to  $\Delta H_s$ .

In these studies, the additive relation was demonstrated for the heat of solution of acetone in TOTP. The heat of solution was measured with the bulk TOTP and was found to be  $-6.45$  kcal/mol. Using the sorp-

(29) G. L. Hargrove and D. T. Sawyer, *Anal. Chem.*, **40**, 409 (1968).

tion isotherms of acetone on 15.8% TOTP-coated AWFb obtained at various temperatures, the total heat corresponding to the sorption process was calculated (Figure 8). The heat of adsorption of acetone on TOTP modified AWFb (10.3%) was measured and the value of approximately  $-9.0$  kcal/mol was obtained (Figure 8).

The total heat observed was reproduced from the heat of solution and the heat of adsorption individually measured using eq 17. The results are shown in Figure 9. The agreement of the observed heats and the calculated heats was extremely good. This also helps sup-

port the additive nature of the sorption mechanism of the solute on a liquid-coated adsorbent. Figure 10 shows the same type of plot for the adsorption of acetone on 2.15% TOTP-coated AWFb. The observed and the calculated heats agreed within the experimental error range for all points.

*Acknowledgment.* This study was made possible by National Science Foundation Grants No. GP 9456, GP 5400, and GY 4093. Presented at the 157th National Meeting of the American Chemical Society in Minneapolis, Minn., April 1969.

## The Thermodynamics of Absorption of Xenon by Myoglobin<sup>1</sup>

by Gordon J. Ewing and Sigfredo Maestas<sup>1</sup>

*Department of Chemistry, New Mexico State University, Las Cruces, New Mexico 88001 (Received December 5, 1969)*

The interaction of xenon with solutions of myoglobin, metmyoglobin, and cyanometmyoglobin has been studied at 20, 25, and 30° and at various xenon pressures up to 4.85 atm. Evidence is presented for the formation of  $\text{HpXe}$  for all three myoglobins and  $\text{HpXe}_2$  for myoglobin and metmyoglobin (Hp = hemoprotein). The equilibrium constants for the first step were between 100 and 200  $m^{-1}$  and between 1 and 10  $m^{-1}$  for the second step, depending upon the temperature and the particular myoglobin utilized.

### Introduction

The physiological activity of xenon and other "inert" gases has led to investigations of the interaction of these gases with biological materials.<sup>2</sup> Specifically, the interaction of xenon with hemoglobin and myoglobin has been the subject of several recent investigations.<sup>3-9</sup> The general conclusion to be drawn from the investigations pertaining to hemoglobin-xenon and myoglobin-xenon interactions is that there exists a seeming uncertainty regarding the stoichiometry (or lack of the same) for these "reactions."

Mortimer and Bauer<sup>10</sup> first proposed that a definite stoichiometry involving an inert gas and a heme compound may indeed exist but is difficult to establish for very weak interactions. The interaction is indistinguishable from a "solubility" phenomenon when a small percentage of the protein molecules has combined with the inert gas. Thus far the X-ray studies reported indicate that a specific site for xenon (and perhaps other inert gas molecules) exists in myoglobin and hemoglobin.<sup>5-7</sup> However, the data for absorption studies are generally reported as Henry's law solubilities.

This report concerns the attempt to study the absorption of xenon by myoglobin over a substantial pressure range (0-4.8 atm). The studies were conducted at

various temperatures (20, 25, and 30°) so that the heat of the interaction could be determined.

It was considered of particular importance to determine if a difference existed between the interaction of xenon with ferromyoglobin and with ferrimyoglobin (hereafter referred to as metmyoglobin). The absorption of xenon by myoglobin and metmyoglobin was studied as well as the absorption of the gas by cyanometmyoglobin, in which the coordination sphere of the Fe(III) atom contains a  $\text{CN}^-$  ion. The latter experiments were conducted in order to determine whether the

(1) This work was supported by grants from NASA (NGR 32-003-027) and NSF (GB-7829).

(2) A. P. Rinfret and G. F. Doebbler in G. A. Cook, "Argon, Helium, and the Rare Gases," Vol. II, Interscience Publishers, New York, N. Y., 1961, pp 727-764.

(3) H. L. Conn, Jr., *J. Appl. Physiol.*, **16**, 1065 (1961).

(4) S. Y. Yeh and R. E. Peterson, *ibid.*, **20**, 1041 (1965).

(5) B. P. Schoenborn, H. C. Watson, and J. C. Kendrew, *Nature*, **207**, 28 (1965).

(6) B. P. Schoenborn, *ibid.*, **208**, 760 (1965).

(7) S. P. Schoenborn and C. L. Nobbs, *Mol. Pharmacol.*, **2**, 491 (1966).

(8) J. F. Catchpool, *Fed. Proc.*, **27**, 884 (1968).

(9) M. Keyes and R. Sumry, *ibid.*, **27**, 898 (1968).

(10) R. G. Mortimer and N. Bauer, *J. Phys. Chem.*, **64**, 387 (1960).

formation of a nonlabile compound hindered the absorption of xenon by the hemoprotein.

### Experimental Section

The absorption of xenon by myoglobin, metmyoglobin, and cyanometmyoglobin was studied by measuring amounts of the gas absorbed by 10% aqueous solutions of the hemoproteins by a manometric method. The method involved placing a known quantity of the gas above a solution and then determining the quantity dissolved by measuring the pressure change. This was done in a stainless steel manifold. The pressures of the gas were measured by either of two gauges; one gauge was a 0–3 atm pressure gauge, the other covered the range from 0 to 5 atm. Both were built by the Heise Bourdon Tube Co., Inc. of Newton, Conn. The gauges were sensitive to the nearest 0.5 mm and exhibited maximum hysteresis of 1.5 mm and 3.5 mm, respectively. Both gauges were temperature compensated in the temperature range  $-31.5$  to  $51.5^\circ$ . Since bourdon gauges respond to the difference in pressure between the system and its surroundings, absolute pressures were obtained by adding the barometric pressure to the bourdon gauge reading. This pressure was then corrected for the partial pressure of water. The protein solutions were kept to within  $0.1^\circ$  of the desired temperature while the gauge (not in the constant temperature bath) was regulated to within  $1.0^\circ$  of the desired temperature. The solutions were stirred during the absorption runs by a magnetic bar driven by an immersed stirrer. The length of an absorption run was approximately 6–8 hr.

The amount of xenon absorbed by the solution was determined by measuring the initial pressure and the final pressure to obtain the pressure change,  $\Delta P$ , and applying the ideal gas law

$$\Delta n = \frac{\Delta PV}{RT}$$

To determine the amount of xenon absorbed by the hemoprotein, the amount of xenon calculated to dissolve in water at the temperature and equilibrium pressure of the experiment was subtracted from  $\Delta n$ . This quantity divided by the number of moles of myoglobin in the solution (usually  $\sim 10^{-4}$  mol) yielded the amount of xenon dissolved per mole of myoglobin.

The amounts of xenon attributed to dissolution in water for each run were calculated from the Henry's law constants,  $0.85 \times 10^7$  mm/mole fraction ( $20^\circ$ ),  $0.96 \times 10^7$  mm/mole fraction ( $25^\circ$ ), and  $1.13 \times 10^7$  mm/mole fraction ( $30^\circ$ ), determined in this laboratory. These values are in fair agreement with the data of Wood and Caputi.<sup>11</sup>

The solutions were prepared to contain approximately 10% horse heart myoglobin obtained from Calbiochem. Some of the metmyoglobin solutions included phosphate buffer (pH 8.1), 0.63 mmol/25 ml of solution. The

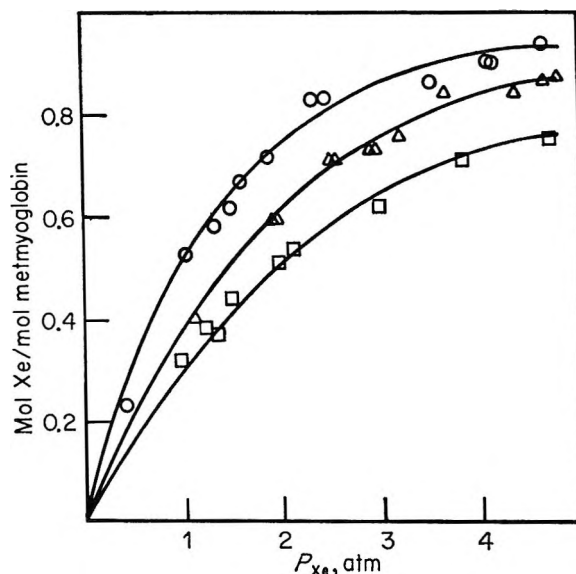


Figure 1. Metmyoglobin adsorption of xenon:  $\circ$ ,  $20^\circ$ ;  $\Delta$ ,  $25^\circ$ ;  $\square$ ,  $30^\circ$ .

unbuffered solutions had a pH of 6.95. No appreciable difference in the absorption of xenon by the buffered and unbuffered solutions was observed.

The myoglobin solutions were prepared by reduction of metmyoglobin with sodium dithionite (approximately 4 mol of dithionite/mol of myoglobin).

The cyanometmyoglobin solutions were prepared by adding to 25 ml of metmyoglobin solution, 0.50 ml of KCN solution (9.6 g of KCN/50 ml), 0.50 ml of  $K_3Fe(CN)_6$  solution (3.0 g/50 ml), and 0.5 ml of  $KH_2PO_4-Na_2HPO_4$  buffer solution (8.5 g of  $KH_2PO_4$ /50 ml and 8.9 g of  $Na_2HPO_4$ /50 ml). All of the solutions were analyzed by the *o*-phenanthroline method for iron or by analyzing cyanometmyoglobin spectrophotometrically.<sup>12</sup>

### Results and Discussion

The xenon absorption data for all three myoglobins show approximately the same characteristics. In the pressure ranges studied, large deviations from Henry's law were observed at the different temperatures. When corrections were made for the solubility of xenon in water, the net interaction with myoglobin produced a curve typical of stoichiometric interactions. Generally, metmyoglobin and cyanometmyoglobin showed slightly larger absorption of xenon than did myoglobin for similar pressures. These differences were small, however.

Figure 1 shows the absorption of xenon by metmyoglobin at 20, 25, and  $30^\circ$ . Figures 2 and 3 show the absorption of xenon by myoglobin and cyanometmyoglobin, respectively, at similar temperatures.

(11) D. Wood and R. Caputi, U. S. Naval Radiological Defense Laboratory Report TR-988, San Francisco, Calif., Feb 1966.

(12) D. Drabkin, *Amer. J. Med. Sci.*, **209**, 268 (1945).

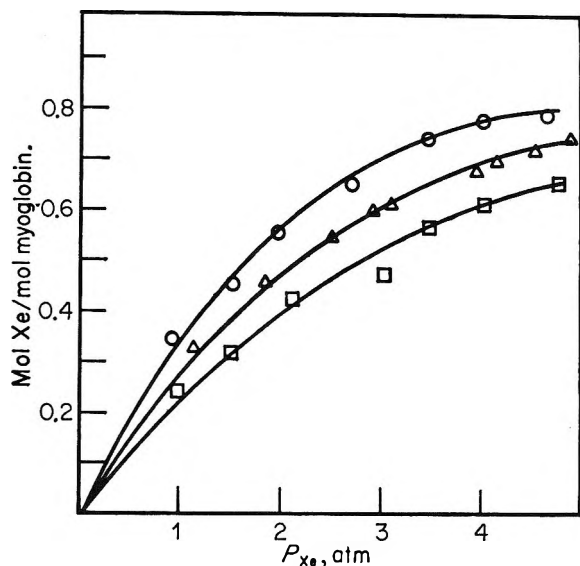


Figure 2. Myoglobin adsorption of xenon:  $\circ$ , 20°;  $\Delta$ , 25°;  $\square$ , 30°.

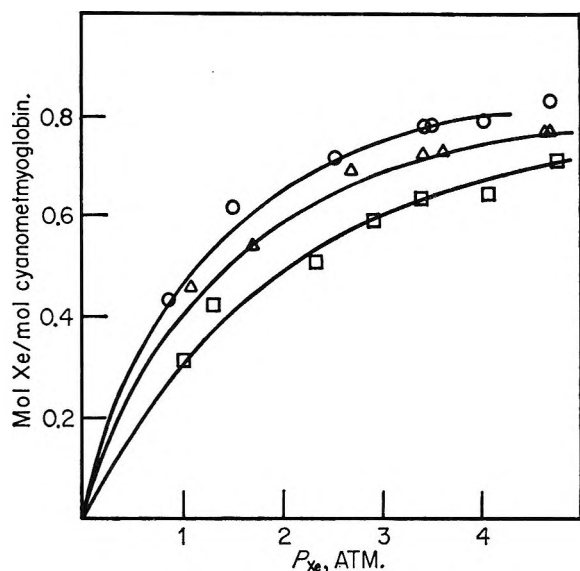
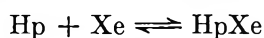


Figure 3. Cyanometmyoglobin adsorption of xenon:  $\circ$ , 20°;  $\Delta$ , 25°;  $\square$ , 30°.

The data for the cyanometmyoglobin-xenon interaction were consistent with a very simple interpretation, so they will be treated first. The data in Figure 3 appear consistent with a single-step equilibrium process



with the corresponding equilibrium expression

$$K_p = \frac{m_{\text{HpXe}}}{m_{\text{Hp}}P_{\text{Xe}}}$$

where  $K_p$  is an equilibrium constant,  $m$ 's are molalities of the species indicated,  $P_{\text{Xe}}$  is the partial pressure of xenon, and Hp is the hemoprotein. This may be written

$$\frac{m_{\text{HpXe}}}{m_{\text{Hp}}} = K_p P_{\text{Xe}}$$

A plot of  $m_{\text{HpXe}}/m_{\text{Hp}}$  vs.  $P_{\text{Xe}}$  should yield a straight line with a slope of  $K_p$  and an intercept of zero.  $K_p$  values can be readily converted to  $K$  values, where

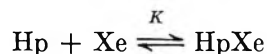
$$K = \frac{m_{\text{HpXe}}}{m_{\text{Hp}}m_{\text{Xe}}}$$

by multiplying  $K_p$  by the Henry's law constant for that particular temperature. Plots of the type described gave the expected straight line with an intercept very near zero. The least-squares method was utilized in determining the slopes. Values of  $K$  for the xenon-cyanometmyoglobin interaction are given in Table I.

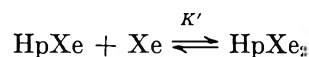
Table I: Equilibrium Constants for Cyanometmyoglobin Absorption of Xenon

Temp, °C	$K_{\text{eq}}$ , $m^{-1}$
20	186
25	145
30	115

The data for the xenon interaction with metmyoglobin and with myoglobin gave some indication of interactions beyond the one to one interaction with cyanometmyoglobin. We were able to obtain a better explanation of our observations by assuming a two-step equilibrium



and



where the equilibrium expressions are

$$K = \frac{m_{\text{HpXe}}}{m_{\text{Hp}}m_{\text{Xe}}}$$

and

$$K' = \frac{m_{\text{HpXe}_2}}{m_{\text{HpXe}}m_{\text{Xe}}}$$

The  $m$ 's correspond to the molal concentrations of the subscripted species in solution. To evaluate the equilibrium constants, two mass balance equations were utilized.

$$f_{\text{Hp}} = m_{\text{Hp}} + m_{\text{HpXe}} + m_{\text{HpXe}_2}$$

$$f_{\text{Xe}} = m_{\text{Xe}} + m_{\text{HpXe}} + 2m_{\text{HpXe}_2}$$

The  $f$ 's correspond to the total (formal) concentration of all forms of the substance indicated. These equations, along with the two equilibrium relationships, can

be utilized to eliminate the concentrations of the various hemoprotein forms ( $m_{\text{Hp}}$ ,  $m_{\text{HpXe}}$ , and  $m_{\text{HpXe}_2}$ ). The appropriate algebraic manipulations<sup>13</sup> yield the following relationship

$$\frac{1}{m^2_{\text{Xe}}} \left( \frac{f_{\text{Xe}} - m_{\text{Xe}}}{2f_{\text{Hp}} - f_{\text{Xe}} + m_{\text{Xe}}} \right) = \frac{1}{2m_{\text{Xe}}} \left( 1 - \frac{f_{\text{Xe}} - m_{\text{Xe}}}{2f_{\text{Hp}} - f_{\text{Xe}} + m_{\text{Xe}}} \right) K + KK'$$

analogous to

$$y = Kx + KK'$$

the equation for a straight line. Plots of  $x$  vs.  $y$  were obtained for each isotherm in Figures 2 and 3, and  $K$  was determined from the slope, and  $K'$  from the slope and the intercept. These values are listed in Tables II and III. The values of  $K'$  are only approximate and merely indicate the possibility for a second site for interaction. Schoenborn and Nobbs<sup>7</sup> also present some evidence for interactions other than the primary one.

**Table II:** Equilibrium Constants for Metmyoglobin Absorption of Xenon

Temp, °C	$K_{\text{eq}}$ , $m^{-1}$	$K'_{\text{eq}}$ , $m^{-1}$
20	200	~8.2
25	146	~7.2
30	130	~2.3

**Table III:** Equilibrium Constants for Myoglobin Absorption of Xenon

Temp, °C	$K_{\text{eq}}$ , $m^{-1}$	$K'_{\text{eq}}$ , $m^{-1}$
20	109	2.3
25	94	2.6
30	85	0.5

The interesting characteristic of the absorption data comparatively is that the equilibrium constants indicate a slightly greater affinity of the Fe(III)-containing myoglobins for xenon whereas the oxygen interaction is with Fe(II)-containing Mb only. The free energies of reaction, enthalpies, and entropies for each of the absorption processes were evaluated from the equilibrium constants and their rate of change with temperature (Table IV).

The most apparent property of the interactions of xenon with the myoglobins is that these are in the "weak-bond" category. The evidence indicates that

**Table IV:** Thermodynamic Functions for Xenon Absorption by Myoglobins

Heme protein	$\Delta G^{\circ}_{25^{\circ}}$ , kcal/mol	$\Delta H^{\circ}$ , kcal/mol	$\Delta S^{\circ}_{25^{\circ}}$ , eu
Metmyoglobin	-2.9 <sup>a</sup>	-7.2 <sup>a</sup>	-14 <sup>a</sup>
Myoglobin	-2.7 <sup>a</sup>	-5.1 <sup>a</sup>	-8.0 <sup>a</sup>
Cyanometmyoglobin	-2.9	-9.0	-20

<sup>a</sup> First equilibrium step.

the binding of xenon to myoglobin is not strong iron-to-ligand bonding as witnessed by (1) the absence of spectral differences in the spectra of xenonated and unxenonated myoglobins, (2) the apparent slow absorption process, and (3) the low heats of reaction. This is an indication that the role of the iron atom in heme proteins is not as prominent in binding "inert" gases as it is in its capacity in binding strong ligands like O<sub>2</sub>, CO, CN<sup>-</sup> ion, etc. This quantitative difference between strong ligand xenon interactions with myoglobin is consistent with the X-ray studies of Schoenborn, *et al.*,<sup>6</sup> which places the xenon on the opposite side of the porphyrin ring from the O<sub>2</sub> absorption site.

In spite of the low enthalpies of absorption, these appear to be the driving forces of the reactions. The large entropies of xenonation of myoglobins are indicative of large conformational changes in the hemoprotein molecules during the absorption process. These have been observed previously in the absorption of other inert gases.<sup>10</sup> Chemisorption may indeed be the phenomenon involved here if one defines the process to include the property of saturation of interaction sites. Clathrate formation is also suggested.

Although the affinities of the myoglobins for xenon are small, these are large in comparison to their affinities for H<sub>2</sub>, N<sub>2</sub>, and Ar.<sup>10</sup>

In conclusion, it is stressed that this simple experimental method allows substantial information to be derived for these processes. Correct values for Xe uptake by myoglobin depend on several factors, namely, (1) the sensitivity of the measuring instrument (gauge), (2) the amount of gas absorbed by the protein, (3) the correctness of the data for the solubility of the gas in the solvent, and (4) temperature control. The latter seems to be the major source of experimental error in this study. A temperature difference of 1° between the reaction vessel and the gauge would result in an error in the calculated quantity of xenon interacting with myoglobin of about 5% when near saturation. This corresponds roughly with the scatter of our measurements.

(13) J. C. Speakman, *J. Chem. Soc.*, 855 (1940).



# Gas-Liquid Partition Chromatographic Determination and Theoretical Interpretation of Activity Coefficients for Hydrocarbon Solutes in Alkane Solvents

by Y. B. Tewari,<sup>1</sup> D. E. Martire, and J. P. Sheridan

Department of Chemistry, Georgetown University, Washington, D. C. 20007 (Received October 20, 1969)

Gas-liquid partition chromatography was used to obtain infinite dilution solute activity coefficients at four temperatures: 76.0, 80.0, 84.0, and 88.0°. Sixty-nine binary systems were studied: 23 hydrocarbon solutes (11 alkanes, 4 alkenes, and 8 aromatics) in three normal alkane solvents ( $n$ -C<sub>24</sub>H<sub>50</sub>,  $n$ -C<sub>30</sub>H<sub>62</sub>, and  $n$ -C<sub>36</sub>H<sub>74</sub>). The probable uncertainty in the determined activity coefficients is estimated to be 0.7%. The temperature-averaged activity coefficients (82.0°) are analyzed in terms of the separability of the configurational or athermal part and the interactional or thermal part. The athermal contributions, due to the size difference between solute and solvent molecules, are determined and subtracted from the logarithm of the measured activity coefficients to yield the thermal contributions. The resulting interaction parameters, arising from disparities in the intermolecular forces, are then examined from the point of view of three existing theories of solution: (1) a contact point lattice treatment, (2) regular solution theory, and (3) a perturbation treatment based on a statistical approach due to Longuet-Higgins. All theories are considered in the limit of random mixing. The lattice theory and perturbation treatment are both shown to be successful in interpreting the free energy of this range of nonpolar mixtures.

## I. Glpc Measurement of Activity Coefficients

Recent experimental developments now make it feasible and desirable to undertake systematic studies on a wide variety of nonelectrolytic solutions. Specifically, gas-liquid partition chromatography (glpc)<sup>2-6</sup> now provides a rapid and reliable method of obtaining a large amount of accurate thermodynamic data in a consistent manner. It has been established<sup>2-6</sup> that sound and meaningful thermodynamic results are obtainable from glpc measurements, provided certain explicit and implicit assumptions are met experimentally and the chromatograms are properly analyzed.

Accordingly, glpc was used here to study 23 hydrocarbon solutes (alkanes, alkenes, and aromatics) in three high-molecular-weight normal alkane solvents. Infinite dilution solute activity coefficients were obtained at four temperatures for these 69 binary systems.

## Experimental Section

**Liquid Phases.** Three stationary liquid phases (the solvents) were used in this work: (1)  $n$ -tetracosane, (2)  $n$ -triacontane, and (3)  $n$ -hexatriacontane.  $n$ -Tetracosane ( $n$ -C<sub>24</sub>H<sub>50</sub>) and  $n$ -hexatriacontane ( $n$ -C<sub>36</sub>H<sub>74</sub>), supplied by Humphrey Chemicals (listed minimum purity of 97%), were each recrystallized three times from ethanol.  $n$ -Triacontane ( $n$ -C<sub>30</sub>H<sub>62</sub>) was synthesized by the Wurtz reaction from  $n$ -pentadecyl bromide (Fisher high-purity grade) and sodium metal. The final product was chromatographed through a 1-in. column packed with alumina using petroleum ether as the eluent. The chromatographed material was then

recrystallized twice from ether. The melting points of the purified paraffins, determined on a Thomas-Hoover capillary melting point apparatus, each agreed with the reported values to within 0.2°. Each of the purified liquid phases was found to have a minimum purity of 99% as determined by high-temperature glpc.

**Preparation of Columns.** The solid support material used was Johns-Manville Chromosorb W, 60-80 mesh, acid washed and DMCS treated. The liquid phase was coated onto the support material in the usual manner.<sup>7</sup> The coated support was packed into 0.25-in. o.d. copper tubing. The amount packed in each column was determined by the difference in weight of the coated supported material before and after packing. The exact liquid phase weight percentage was determined by a combustion or ashing method.<sup>8</sup> Two different

(1) Submitted by Y. B. Tewari to the Department of Chemistry, Georgetown University, in partial fulfillment of the requirements for the Ph.D. degree.

(2) D. E. Martire, "Gas Chromatography," L. Fowler, Ed., Academic Press, New York, N. Y., 1963, p 33.

(3) D. E. Martire and L. Z. Pollara, "Advances in Chromatography," Vol. I, J. C. Giddings and R. A. Keller, Ed., Marcel Dekker, Inc., New York, N. Y., 1966, p 335.

(4) A. J. B. Cruickshank, M. L. Windsor, and C. L. Young, *Proc. Roy. Soc.*, A295, 259, 271 (1966).

(5) (a) D. E. Martire, "Progress in Gas Chromatography," J. H. Purnell, Ed., John Wiley & Sons, Inc., New York, N. Y., 1968, p 93; (b) J. R. Conder, "Progress in Gas Chromatography," J. H. Purnell, Ed., John Wiley & Sons, Inc., New York, N. Y., 1968, p 209.

(6) D. F. Cadogan, J. R. Conder, D. C. Locke, and J. H. Purnell, *J. Phys. Chem.*, 73, 700, 708 (1969).

(7) S. Dal Nogare and R. S. Juvet, Jr., "Gas Chromatography," John Wiley & Sons, Inc., New York, N. Y., 1962, p 45.

**Table I:** Composition of Columns

Liquid phase column	$n\text{-C}_{24}\text{H}_{50}$		$n\text{-C}_{30}\text{H}_{62}$		$n\text{-C}_{36}\text{H}_{74}$	
	A	B	A	B	A	B
Length of column, ft	4	4	4	5	4	4
Liquid phase weight %	11.46	9.89	11.66	8.46	13.01	10.40
Coated support, g	7.2936	6.7721	7.4793	8.6975	6.7573	6.6843
Liquid phase, g	0.836	0.670	0.872	0.736	0.879	0.695

columns were used for each liquid phase. Details of the columns are given in Table I.

**Solutes.** The hydrocarbon solutes selected for this study are listed in Table II. For each of the compounds, the pure component physical properties needed in the calculation of the thermodynamic solution properties are available or can be accurately estimated. Since solute purity is not an important consideration in these glpc studies, all solutes were used without further purification.

**Table II:** Solute Components

Solute number	Compound
1	<i>n</i> -Hexane
2	2-Methylpentane
3	2,2-Dimethylbutane
4	2,3-Dimethylbutane
5	3-Methylpentane
6	<i>n</i> -Heptane
7	3-Methylhexane
8	2,4-Dimethylpentane
9	<i>n</i> -Octane
10	3-Methylheptane
11	<i>n</i> -Nonane
12	1-Hexene
13	1-Heptene
14	1-Octene
15	1-Nonene
16	Benzene
17	Toluene
18	<i>p</i> -Xylene
19	<i>m</i> -Xylene
20	<i>o</i> -Xylene
21	Ethylbenzene
22	Cumene
23	Chlorobenzene

**Apparatus and Procedure.** A dual-column glpc apparatus, utilizing a Perkin-Elmer hot wire thermal conductivity detector (P-E Part No. 008-0686) and a water bath to maintain the column temperature, was employed. The temperature of the bath was controlled to  $\pm 0.05^\circ$  using a Techne Tempunit Model TU-8. Each column was installed and conditioned at  $80^\circ$  for about 12 hr with a gentle flow of carrier gas. Before entering the column, the carrier gas (helium) was passed through a trap containing molecular sieves (Type 5A, 60-70

mesh) to absorb moisture and contaminants. The column inlet pressure was regulated using a Negretti-Zamba precision pressure regulator, Model R/182, and was measured to  $\pm 0.05$  psi with a calibrated pressure gauge (range, 0-15 psig). The outlet pressure, which was determined from barometric readings to  $\pm 0.01$  psi, was always atmospheric. The carrier gas flow rate was measured at room temperature with a soap-film flowmeter placed at the detector outlet. The flow rates (range, 30-160 ml/min) were chosen to give convenient elution times and reasonable column efficiencies.

Samples (the solutes) were injected with a 10- $\mu$ l Hamilton syringe through a Hamilton injection port (Model No. 86800) maintained at about  $150^\circ$ . Keeping the detector on high sensitivity, the smallest detectable sample sizes were used at all times to ensure operation in the Henry's law region of solute concentrations (*i.e.*, the infinite dilution region). This was usually accomplished by injecting solutes in the vapor form. All solute elution peaks were observed to be symmetrical indicating that infinite dilution had been attained.<sup>9</sup> Furthermore, several experiments were conducted to confirm that the peak maximum retention time was independent of sample size.

The operating temperatures chosen were 76.0, 80.0, 84.0, and 88.0. At these temperatures all stationary phases were in the liquid state, and their vapor pressures were negligible<sup>10</sup> (less than  $10^{-4}$  Torr). Three internal standards (*n*-hexane, *n*-heptane, and *n*-octane) were run periodically to check for column bleeding. The constancy of the retention time for each of these standards on a given column indicated that no liquid phase loss occurred during the course of the experiments. Also, the liquid phase weight percentage of each column was redetermined at the end of the experiments, providing additional confirmation of negligible column bleeding.

## Results

**Specific Retention Volumes.** The solute specific retention volumes ( $V_g^\circ$ ) were calculated from the corrected peak retention times and the column operating conditions using the expression derived by Littlewood,

(8) D. E. Martire and P. Riedl, *J. Phys. Chem.*, **72**, 3478 (1968).

(9) J. R. Conder, *J. Chromatogr.*, **39**, 373 (1969).

(10) A. P. Kudchadker and B. J. Zwolinski, *J. Chem. Eng. Data*, **11**, 353 (1966).

*et al.*<sup>11</sup> Each solute was run three times on each column, and the average of these three retention times was used in the calculation of the specific retention volume. For each liquid phase, samples were run on two columns with different liquid weight percentages (see Table I). Thus, each  $V_g^\circ$  value listed in Tables III, IV, and V is the average value of six measurements taken on two different liquid loadings. (Specific retention volumes obtained on different loadings were in agreement to within 0.6% for all systems.)

**Table III:** Solute Specific Retention Volumes (ml/g) on  $n\text{-C}_{24}\text{H}_{50}$  as the Liquid Phase

Solute number	76.0°	80.0°	84.0°	88.0°
1	70.42	63.01	56.49	50.74
2	53.56	48.35	43.53	39.32
3	40.14	36.52	53.24	30.44
4	53.02	47.37	42.78	38.79
5	60.90	55.28	49.55	44.86
6	169.7	149.3	129.5	115.9
7	137.6	121.4	107.0	95.63
8	91.19	81.51	72.13	64.96
9	400.4	345.3	299.1	259.3
10	313.8	271.7	236.7	206.7
11	944.1	797.4	679.3	582.2
12	60.97	54.66	48.70	44.04
13	145.6	128.3	112.5	100.6
14	343.3	295.9	257.4	223.8
15	810.6	686.1	589.5	503.2
16	103.6	92.06	80.97	74.50
17	265.8	233.1	204.4	180.3
18	661.5	569.2	492.6	427.1
19	667.6	575.4	498.3	432.5
20	784.0	673.6	681.9	501.4
21	571.1	493.3	428.2	370.9
22	941.2	807.0	693.9	596.8
23	471.1	411.5	358.3	312.6

A few solutes were run at several different flow rates on a given column and, as expected,<sup>2,4</sup> no dependence of  $V_g^\circ$  on flow rate was found. Experiments were also conducted to establish that solute adsorption was not taking place at the gas-liquid or solid-liquid interface.<sup>5a,6</sup> Hence, the  $V_g^\circ$  values obtained are directly related to true static, bulk solution, thermodynamic quantities independent of all column and operational parameters other than temperature.

The precision in the measurement of  $V_g^\circ$  is estimated to be better than 0.5%. Furthermore, since all the necessary precautions were taken to ensure thermodynamically significant values and to eliminate systematic error, 0.5% should also be a measure of the probable uncertainty in  $V_g^\circ$ . A comparison of some of our values on  $n\text{-C}_{30}\text{H}_{74}$  with published values<sup>12</sup> strengthens the validity of this estimate (see Table VI). Unfortunately, no published  $V_g^\circ$  values are available for comparison on

**Table IV:** Solute Specific Retention Volumes (ml/g) on  $n\text{-C}_{30}\text{H}_{62}$  as the Liquid Phase

Solute number	76.0°	80.0°	84.0°	88.0°
1	64.57	57.26	51.36	46.41
2	48.02	43.76	39.79	36.20
3	35.98	33.01	29.98	27.43
4	47.33	43.37	39.53	35.79
5	55.41	49.81	45.02	41.00
6	154.8	135.3	119.6	105.9
7	125.6	110.2	98.12	87.26
8	81.85	72.52	65.55	58.72
9	369.5	318.9	276.6	236.7
10	288.7	250.7	218.3	189.3
11	859.7	731.4	624.9	531.3
12	54.11	50.10	44.50	40.22
13	133.0	117.1	103.9	91.94
14	314.2	273.1	238.8	206.8
15	735.4	629.2	545.6	462.2
16	98.29	87.50	78.50	71.18
17	255.0	221.2	194.3	172.3
18	634.8	542.5	466.3	404.9
19	640.4	548.6	471.4	408.7
20	756.1	643.7	554.3	478.9
21	546.8	468.7	406.9	352.4
22	881.9	754.0	646.7	560.4
23	454.0	392.2	343.4	301.4

**Table V:** Solute Specific Retention Volumes (ml/g) on  $n\text{-C}_{30}\text{H}_{74}$  as the Liquid Phase

Solute number	76.0°	80.0°	84.0°	88.0°
1	58.23	52.57	46.89	42.64
2	44.85	40.39	36.53	33.03
3	33.35	30.50	27.59	25.40
4	43.61	39.68	35.81	32.86
5	50.61	45.60	41.05	37.27
6	141.6	124.7	107.4	97.59
7	113.9	100.8	89.37	79.42
8	74.42	66.53	59.07	53.17
9	333.6	288.1	249.2	217.7
10	258.4	226.0	196.7	172.6
11	758.1	651.3	553.6	472.0
12	50.29	45.54	41.27	37.42
13	120.8	106.7	94.15	84.79
14	281.3	245.0	213.9	185.4
15	660.0	565.6	485.1	414.0
16	92.95	83.37	72.57	66.36
17	234.5	209.3	183.5	160.4
18	582.2	507.8	442.3	385.0
19	588.8	513.8	446.4	387.9
20	697.7	606.4	522.0	448.4
21	506.6	438.2	379.7	330.3
22	813.3	705.1	604.1	521.7
23	426.1	374.7	326.9	284.4

$n\text{-C}_{24}\text{H}_{50}$  and  $n\text{-C}_{30}\text{H}_{62}$  at the temperatures studied in this work.

(11) A. B. Littlewood, C. S. G. Phillips, and D. T. Price, *J. Chem. Soc.*, 1480 (1955).

(12) E. C. Pease and S. Thorburn, *J. Chromatogr.*, **30**, 344 (1967).

**Table VI:** Comparison of Specific Retention Volumes (ml/g) with Published Values<sup>12</sup> on *n*-C<sub>24</sub>H<sub>74</sub> at 80.0°

Solute number	This work	Reference 12	Difference, %
1	52.57	53.13	-1.06
2	40.39	40.15	+0.59
3	30.50	30.48	+0.07
4	39.68	39.57	+0.28
5	45.60	45.58	+0.04
6	124.7	124.6	+0.10
7	100.8	100.6	+0.21
8	66.53	66.69	-0.24
9	288.1	289.8	-0.61
10	226.0	225.5	+0.23

**Table VII:** Corrected Solute Activity Coefficients ( $\gamma_i^\infty$ ) in *n*-C<sub>24</sub>H<sub>50</sub>

Solute number	76.0°	80.0°	84.0°	88.0°
1	0.794	0.792	0.791	0.791
2	0.822	0.817	0.817	0.817
3	0.831	0.827	0.824	0.819
4	0.784	0.789	0.789	0.788
5	0.788	0.779	0.781	0.778
6	0.818	0.815	0.809	0.816
7	0.817	0.817	0.819	0.811
8	0.874	0.869	0.872	0.869
9	0.850	0.849	0.848	0.850
10	0.855	0.855	0.854	0.855
11	0.875	0.877	0.875	0.872
12	0.785	0.784	0.791	0.788
13	0.818	0.817	0.823	0.816
14	0.849	0.852	0.850	0.853
15	0.875	0.879	0.873	0.877
16	0.752	0.749	0.732	0.733
17	0.763	0.758	0.756	0.752
18	0.767	0.764	0.760	0.757
19	0.788	0.782	0.777	0.772
20	0.801	0.795	0.789	0.789
21	0.828	0.822	0.816	0.815
22	0.878	0.873	0.862	0.859
23	0.847	0.836	0.830	0.826

*Solute Activity Coefficients.* The solute activity coefficients at infinite dilution in the liquid phase ( $\gamma_p^\infty$ ) were determined from the expression<sup>2</sup>

$$\gamma_p^\infty = \frac{1.704 \times 10^7}{Mp^\circ_2 V_g^\circ} \quad (1)$$

where *M* is the solvent molecular weight, and  $p^\circ_2$  is the vapor pressure of the pure saturated solute vapor in Torr. The vapor pressures at each temperature were calculated from the Antoine equation, using the constants from Dreisbach's compilation.<sup>13</sup> To obtain the activity coefficients fully corrected for the nonideality of the vapor phase ( $\gamma_i^\infty$ ), the following expression<sup>3</sup> was used

$$\ln \gamma_i^\infty = \ln \gamma_p^\infty - \frac{p^\circ_2 B_{22}}{RT} \quad (2)$$

where  $B_{22}$  is the second virial coefficient of the pure solute vapor at *T*. The virial coefficients were computed from the modified corresponding states equation of McGlashan and Potter<sup>14-16</sup> using the most recently compiled critical constants.<sup>17</sup> The effective carbon number in their equation<sup>14</sup> was taken to be the actual number of carbon atoms in the molecule (with the Cl in chlorobenzene counted as a carbon atom). By comparison with some measured  $B_{22}$  values where available,<sup>14-16</sup> the computed  $B_{22}$  values are estimated to be accurate to within 5%.

Taking into account the experimental error in  $V_g^\circ$ , the error in the  $B_{22}$  term in eq 2 and the slight error resulting from the approximation implied by eq 2,<sup>3,4</sup> it is estimated that the probable uncertainty in the corrected activity coefficients ( $\gamma_i^\infty$ ) listed in Tables VII, VIII, and IX is about 0.7%. A comparison of the corrected activity coefficients for a few solutes in *n*-C<sub>24</sub>H<sub>50</sub> with literature values<sup>18</sup> is shown in Table X. Since the majority of the published results are reported at 60.0°, the  $\gamma_i^\infty$  values of this work had to be extrapolated to 60.0° for a meaningful comparison. Considering the probable error in the linear extrapolation, the agreement is quite acceptable.

Hence, accurate activity coefficients are obtainable from glpc measurements (through eq 1 and 2), and they represent a true measure of deviations from Raoult's law exhibited by a solute at infinite dilution in a bulk solvent.

## II. Theoretical Interpretation of Activity Coefficients

One of the fundamental problems in physical chemistry is the development of theories of solution which would make it possible to interpret and predict the thermodynamic properties of a wide range of nonelectrolytic mixtures. Despite the vast amount of work carried out in this field over many years, no generalized theory has emerged. However, several relationships, both rigorously exact and empirical in nature, have been developed which are applicable to rather limited classes of solutions.

The more elaborate and sophisticated statistical mechanical theories require much information about the

(13) R. R. Dreisbach, "Physical Properties of Chemical Compounds," *Advances in Chemistry Series*, No. 15, American Chemical Society, Washington, D. C., 1955; *ibid.*, No. 22, 1959; *ibid.*, No. 29, 1961.

(14) M. L. McGlashan and D. J. B. Potter, *Proc. Roy. Soc.*, **A267**, 478 (1962).

(15) M. L. McGlashan and C. J. Wormald, *Trans. Faraday Soc.*, **60**, 646 (1964).

(16) E. A. Guggenheim and C. J. Wormald, *J. Chem. Phys.*, **42**, 3775 (1965).

(17) A. P. Kudchadker, G. H. Alani, and B. J. Zwolinski, *Chem. Rev.*, **68**, 659 (1968).

(18) C. L. Young, *Trans. Faraday Soc.*, **64**, 1537 (1968).

**Table VIII:** Corrected Solute Activity Coefficients ( $\gamma_i^\infty$ ) in  $n\text{-C}_{30}\text{H}_{62}$ 

Solute number	76.0°	80.0°	84.0°	88.0°
1	0.694	0.698	0.697	0.693
2	0.734	0.723	0.716	0.711
3	0.743	0.733	0.732	0.728
4	0.703	0.691	0.684	0.684
5	0.694	0.692	0.688	0.682
6	0.718	0.720	0.701	0.715
7	0.717	0.720	0.716	0.713
8	0.780	0.782	0.769	0.770
9	0.737	0.736	0.734	0.746
10	0.744	0.742	0.742	0.748
11	0.770	0.766	0.762	0.766
12	0.708	0.685	0.693	0.691
13	0.718	0.717	0.714	0.715
14	0.743	0.739	0.734	0.739
15	0.773	0.767	0.755	0.764
16	0.635	0.631	0.605	0.614
17	0.637	0.640	0.637	0.630
18	0.640	0.642	0.643	0.640
19	0.658	0.657	0.658	0.655
20	0.665	0.667	0.664	0.662
21	0.692	0.693	0.688	0.687
22	0.750	0.748	0.741	0.733
23	0.704	0.702	0.694	0.686

**Table IX:** Corrected Solute Activity Coefficients ( $\gamma_i^\infty$ ) in  $n\text{-C}_{36}\text{H}_{74}$ 

Solute Number	76.0°	80.0°	84.0°	88.0°
1	0.640	0.633	0.635	0.628
2	0.654	0.652	0.649	0.648
3	0.667	0.660	0.662	0.654
4	0.635	0.628	0.628	0.620
5	0.632	0.629	0.628	0.624
6	0.653	0.650	0.650	0.646
7	0.658	0.655	0.654	0.652
8	0.714	0.710	0.710	0.708
9	0.680	0.679	0.678	0.675
10	0.692	0.685	0.685	0.682
11	0.727	0.716	0.716	0.717
12	0.634	0.627	0.622	0.618
13	0.657	0.655	0.655	0.645
14	0.691	0.686	0.682	0.686
15	0.717	0.710	0.707	0.710
16	0.559	0.552	0.545	0.549
17	0.577	0.563	0.562	0.564
18	0.581	0.571	0.564	0.560
19	0.595	0.584	0.578	0.574
20	0.600	0.589	0.587	0.588
21	0.622	0.617	0.613	0.610
22	0.677	0.666	0.660	0.655
23	0.625	0.612	0.607	0.605

pure component properties and are usually strictly applicable only to systems involving fairly simple non-polar molecules. At the other extreme are the purely empirical relationships which may describe the prop-

**Table X:** Comparison of Corrected Activity Coefficients ( $\gamma_i^\infty$ ) with Published Values<sup>18</sup> in  $n\text{-C}_{24}\text{H}_{50}$  at 60.0°

Solute	This work <sup>a</sup>	Reference 18	Difference, %
<i>n</i> -Hexane	0.795	0.780	1.88
<i>n</i> -Heptane	0.815	0.813	0.24
<i>n</i> -Octane	0.851	0.832	2.23
1-Heptene	0.818	0.809	1.10
Benzene	0.766	0.757	1.17
Cyclohexane	0.641 <sup>b</sup>	0.640	0.15
		Av	1.12

<sup>a</sup> Linear extrapolation to 60.0°. <sup>b</sup> Y. B. Tewari, Doctoral Dissertation, Georgetown University, 1969, Chapter III.

erties of various classes of solutions well enough, but require many experimental data points to establish the particular class correlation. Furthermore, having no theoretical foundation, they cannot easily be extended into more generalized forms.

There are, however, a number of solution theories which, although they are not highly exact, have a sound theoretical basis, are relatively more flexible than the elaborate theories, and their parameters are in some measure open to physical interpretation. In addition, they require a minimum of experimental data and pure component properties. Three such theories are (1) quasi-lattice theory, (2) regular solution theory, and (3) a recently developed "perturbation approach." To date, the utility and predictive ability of these theories have not been extensively tested over a wide range of systems, with the exception of regular solution theory.

The lack of sufficient and reliable thermodynamic data has impeded the testing of theoretical solution models. Fortunately, gas-liquid partition chromatography (glpc) now provides a definitive method for conducting some of the necessary systematic studies. In this section the glpc results of section I are analyzed to test the applicability of the three solution theories for interpreting the solute activity coefficients for several classes of hydrocarbon mixtures.

#### Determination of the Interaction Parameter

For solutions consisting of molecules differing widely in size, the deviation from Raoult's law is determined by two factors: (a) the difference in size between the solute and solvent molecules, and (b) disparities in the intermolecular forces. In the limit of random mixing, this deviation can be expressed<sup>19</sup> as the sum of two contributions to the logarithm of the solute activity coefficient ( $\ln \gamma_2$ ); *i.e.*

$$\ln \gamma_2 = \ln \gamma_2^{\text{ath}} + \ln \gamma_2^{\text{th}} \quad (3)$$

where  $\ln \gamma_2^{\text{ath}}$  (the athermal part) is associated with the statistical effect arising from the size difference

(19) A. J. Ashworth and D. H. Everett, *Trans. Faraday Soc.*, **56**, 1609 (1960).

between the molecules, and  $\ln \gamma_2^{\text{th}}$  (the thermal part) is associated with the interchange energy arising from interactions between the molecules.

The Flory-Huggins<sup>20,21</sup> equation can be used to evaluate the athermal contribution. Interestingly, Longuet-Higgins<sup>22</sup> derived an identical expression without resorting to any model. Hence, for our systems the statistical contribution to the infinite dilution solute activity coefficient was determined from the expression<sup>19,22</sup>

$$\ln \gamma_2^{\text{ath}} = \ln \frac{1}{r} + \left(1 - \frac{1}{r}\right) \quad (4)$$

where  $r$  is taken as the ratio of the molar volume of the solvent to that of the solute,  $V_1/V_2$ . Rigorously, partial molar volumes should be used in the calculation; however, the lack of such experimental data forces one to assume a zero volume of mixing and to utilize the volumes of the pure substances.

Through eq 4, using available density values<sup>13</sup> for the solvents and solutes (the latter's being given by the law of rectilinear diameters),  $\ln \gamma_2^{\text{ath}}$  values were calculated at 82.0°, the mean temperature of our experiment. The results tabulated in Table XI clearly illustrate the occurrence of appreciable negative contributions to solution nonideality.

**Table XI:** Athermal Contribution to Logarithm of Solute Activity Coefficient ( $-\ln \gamma_2^{\text{ath}}$ ) at 355.2°K

Solute number	<i>n</i> -C <sub>24</sub> H <sub>50</sub>	<i>n</i> -C <sub>30</sub> H <sub>62</sub>	<i>n</i> -C <sub>36</sub> H <sub>74</sub>
1	0.462	0.611	0.743
2	0.455	0.604	0.735
3	0.451	0.599	0.731
4	0.465	0.615	0.747
5	0.468	0.618	0.750
6	0.391	0.534	0.661
7	0.395	0.538	0.666
8	0.379	0.520	0.646
9	0.329	0.464	0.588
10	0.331	0.468	0.590
11	0.276	0.405	0.523
12	0.492	0.644	0.778
13	0.416	0.561	0.689
14	0.351	0.489	0.614
15	0.295	0.425	0.545
16	0.753	0.923	1.067
17	0.623	0.783	0.924
18	0.518	0.671	0.806
19	0.521	0.676	0.810
20	0.535	0.690	0.827
21	0.522	0.677	0.812
22	0.434	0.580	0.710
23	0.659	0.822	0.964

We now write the experimental solute activity coefficient at infinite dilution ( $\gamma_2^\infty$ ) in the form

$$\ln \gamma_2^\infty = \ln \gamma_2^{\text{ath}} + \chi \quad (5)$$

where  $\chi (= \ln \gamma_2^{\text{th}})$ , the so-called interaction parameter, is, strictly, a free-energy term.<sup>23,24</sup> Since the activity coefficients for our systems showed little dependence on temperature, interaction parameters were calculated at 82.0° only. This was done by subtracting the athermal contribution given in Table XI from the logarithm of the mean value of the experimental activity coefficient (*i.e.*, the average of the values listed for 76.0, 80.0, 84.0, and 88.0°). The results, tabulated as  $\chi$  and  $\chi \cdot T$  (where  $T = 355.2^\circ\text{K}$ ), are given in Table XII. Note that the interaction parameters are all positive, indicating that the interchange free energies are positive. Note also that, while the  $\ln \gamma_2^\infty$  values for a given solute varied appreciably from solvent to solvent, once these values are adjusted for the size effect contribution, the resulting values are brought more closely into line. This indicates that the differences in the solute free energies of solution in these three solvents are mainly due to the differences in the athermal contributions.

**Table XII:** Solute Interaction Parameters ( $\chi$ ) at  $T = 355.2^\circ\text{K}$

Solute number	<i>n</i> -C <sub>24</sub> H <sub>50</sub>		<i>n</i> -C <sub>30</sub> H <sub>62</sub>		<i>n</i> -C <sub>36</sub> H <sub>74</sub>	
	$\chi$	$\chi \cdot T$	$\chi$	$\chi \cdot T$	$\chi$	$\chi \cdot T$
1	0.229	81.3	0.248	88.1	0.287	102
2	0.254	90.2	0.276	98.0	0.305	108
3	0.259	92.0	0.289	103	0.317	113
4	0.226	80.3	0.244	86.7	0.281	99.8
5	0.222	78.9	0.245	87.0	0.286	102
6	0.185	65.7	0.196	69.9	0.229	81.3
7	0.192	68.2	0.205	72.8	0.242	86.0
8	0.240	85.2	0.265	94.1	0.304	108
9	0.166	59.0	0.161	57.2	0.199	70.3
10	0.174	61.8	0.171	60.7	0.214	76.0
11	0.143	50.8	0.138	49.0	0.193	68.6
12	0.253	89.9	0.279	99.1	0.309	110
13	0.215	76.4	0.226	80.3	0.263	93.4
14	0.190	67.5	0.187	66.4	0.237	84.2
15	0.162	57.5	0.157	55.8	0.203	72.1
16	0.454	161	0.446	158	0.471	167
17	0.345	123	0.331	118	0.356	127
18	0.246	87.4	0.227	80.6	0.242	86.0
19	0.273	97.0	0.255	90.6	0.270	95.9
20	0.304	108	0.281	99.8	0.301	107
21	0.324	115	0.306	109	0.327	116
22	0.292	104	0.283	101	0.301	107
23	0.478	170	0.460	163	0.473	168

Let us now proceed to the interpretation of the interaction parameters in terms of the three previously mentioned solution theories.

(20) P. J. Flory, *J. Chem. Phys.*, **10**, 51 (1942).

(21) M. L. Huggins, *Ann. N. Y. Acad. Sci.*, **43**, 1 (1942).

(22) H. C. Longuet-Higgins, *Discuss. Faraday Soc.*, **15**, 73 (1953).

(23) E. A. Guggenheim, *Trans. Faraday Soc.*, **44**, 1007 (1948).

(24) D. H. Everett and R. J. Munn, *ibid.*, **60**, 1951 (1964).

### Contact Point Lattice Treatment

*Background.* The particular lattice model being considered here owes its development to Guggenheim<sup>25</sup> and Barker.<sup>26</sup> According to the model, each molecule is divided into a certain number of elements, each of which occupies one site on the lattice. The interaction energies of neighboring molecules are then taken to depend on those parts of the molecular surface which are in contact. An element may contain more than one type of "contact point," the number and type of such points being fixed at the start by considering the geometry and chemistry of the molecules involved.

With a few notable exceptions, little work has yet been done in applying the theory to the general case of nonpolar or weakly polar mixtures. Ott, Goates, and Snow<sup>27</sup> analyzed the heats of mixing of a fairly wide range of hydrocarbon and halogenated hydrocarbon mixtures for which all the interaction energies were small. However, they neglected the effect of the volume change on mixing, which is possibly one reason why they found discrepancies in the same interaction energies calculated from different systems. McClure, *et al.*,<sup>28</sup> studied heats and volumes of mixing of some aromatic-alicyclic systems and recalculated the heats of mixing at constant pressure as energies of mixing at constant volume. However, they also found that the data for all their systems could not be fitted by a single value of the interaction energy. Cruickshank, Gainey, and Young<sup>18,29,30</sup> examined infinite dilution activity coefficients (obtained through glpc) for alkane solutes and benzene in *n*-alkane solvents. Their findings will be discussed in conjunction with ours.

Bhattacharyya and Mukherjee<sup>31</sup> have pointed out that one of the major drawbacks to this type of approach is that the assignment of contact points is often quite arbitrary. The way in which the number of sites can be assigned to different molecules does not always ensure equal volume per segment (element) in different molecules. This arbitrariness can be eliminated by selecting a suitable reference solute and assigning it a number of sites with fixed coordination number, so that the number of contact surfaces obtained is related to its molecular structure. The number of sites for a particular solute can then be fixed unambiguously from the consideration that its volume per segment should be equal to that of the reference molecule as far as is practicable. Fractional numbers of sites may be accepted as long as they give an integral number of contact points for the molecule.

Another limitation lies in the fact that the assignment of interaction energies may also be somewhat arbitrary; different sets may be found which fit the experimental data equally well. Such a situation is encountered principally in those systems where attempts are made to calculate more than one interaction energy from a single set of experimental data on one system only. However, if the systems are well chosen and

systematically analyzed, then more or less consistent values of the interaction energy of various contact pairs should be obtainable.

Specifically now, let us consider the contact point treatment in the "zeroth approximation" according to Guggenheim<sup>23</sup> (*i.e.*, a completely random arrangement of the molecules). From Guggenheim's eq 11.04 and 11.05 it is readily seen that for a binary mixture of molecules of types 1 and 2, with only two kinds of contact points present (a and b), the thermal or interaction contribution to the infinite dilution partial molecular excess free energy of the solute (component 2) is given by

$$\frac{(\bar{g}_2^e)^{th}}{kT} = \ln \gamma_2^{th} = \chi = C_2(f_1^a f_2^b + f_2^a f_1^b - f_1^a f_1^b - f_2^a f_2^b) \frac{\omega^{ab}}{kT} \quad (6)$$

where  $C_2$  is the total number of contact points of the solute molecule,  $f_i^j$  is the fraction of contacts of molecule  $i$  which are of type  $j$ , and  $\omega^{ab}$  is the interchange energy for the formation of an ab contact pair. ( $\omega^{ab}$  is a measure of the deviation of ab interactions from the arithmetic mean of aa and bb interactions; *i.e.*,  $\omega^{ab} = 1/2(\omega_{aa} + \omega_{bb}) - \omega_{ab}$ .)

Equation 6 can be readily generalized to the case where more than two different types of contact are present in molecules 1 and 2

$$\chi = C_2 \sum_{\substack{\alpha, \beta \\ \beta > \alpha}} (f_1^\alpha f_2^\beta + f_2^\alpha f_1^\beta - f_1^\alpha f_1^\beta - f_2^\alpha f_2^\beta) \frac{\omega^{\alpha\beta}}{kT} \quad (7)$$

In the analyses which follow, *n*-hexane is taken as the reference for aliphatic solutes and benzene for aromatic ones in assigning the number of contact points ( $C_2$ ) to the various molecules.<sup>31</sup>

*Alkane Solutes.* Following Cruickshank, *et al.*,<sup>29</sup> each hydrogen atom was assigned one contact point and methyl ( $-\text{CH}_3$ ) and methylene ( $-\text{CH}_2-$ ) hydrogens were treated as being different. Then, for *n*-alkane solutes in *n*-alkane solvents, where there are only methyl and methylene types of contact points, eq 6 reduces to

$$\chi T = C_2(f_1^a - f_2^a)^2 \left( \frac{\omega^{ab}}{k} \right) \quad (8)$$

(25) E. A. Guggenheim, "Mixtures," Oxford University Press, London, 1952, Chapters X and XI.

(26) J. A. Barker, *J. Chem. Phys.*, **20**, 1526 (1952); **21**, 1391 (1953).

(27) J. B. Ott, J. R. Goates, and R. L. Snow, *J. Phys. Chem.*, **67**, 515 (1963).

(28) I. A. McClure, J. E. Bennett, A. E. P. Watson, and G. C. Benson, *ibid.*, **69**, 2759 (1965).

(29) A. J. B. Cruickshank, B. W. Gainey, and C. L. Young, *Trans. Faraday Soc.*, **64**, 337 (1968).

(30) B. W. Gainey and C. L. Young, *ibid.*, **64**, 349 (1968).

(31) S. N. Bhattacharyya and A. Mukherjee, *J. Phys. Chem.*, **72**, 56, 63 (1968).

where  $f_1^a$  and  $f_2^a$  refer to the fraction of hydrogens belonging to methyl groups in the solvent and solute, respectively, and  $\omega^{ab}$  is the methyl-methylene interchange energy. Analysis of the results in Table XII gave the interchange energies listed in Table XIII. The value denoted by the asterisk was rejected in determining the final average value. (This is justified by statistical analysis according to Chauvenet's criterion.<sup>32</sup>) The comparison with the published value is quite favorable. The larger standard deviation found here is a reflection of the greater uncertainty in our experimental values (Cruickshank, *et al.*,<sup>29</sup> claim an error of only  $\pm 0.003$  in  $\ln \gamma_2^\infty$ ).

**Table XIII:** Methyl-Methylene Interchange Energies. Values of  $\omega^{\text{CH}_3\text{-CH}_2}/k$  (in degrees Kelvin) at 355.2°K

Solute	Solvents		
	<i>n</i> -C <sub>24</sub> H <sub>50</sub>	<i>n</i> -C <sub>30</sub> H <sub>62</sub>	<i>n</i> -C <sub>36</sub> H <sub>74</sub>
<i>n</i> -Hexane	61.0	57.2	60.3
<i>n</i> -Heptane	63.3	56.2	58.8
<i>n</i> -Octane	72.3	56.8	61.7
<i>n</i> -Nonane	78.4*	59.3	71.4
Av value	61.6 $\pm$ 5.5		
Lit. value <sup>a</sup>	61.5 $\pm$ 2.6		

<sup>a</sup> Reference 29.

In the application of this treatment to branched chain alkane solutes, methyne ( $>\text{C-H}$ ) hydrogens are not equivalent to methylene hydrogens. However, attempts to treat  $>\text{C-H}$  and  $-\text{CH}_2-$  hydrogens differently yielded results which were quite unrealistic and inconsistent. It would appear that, in view of the extremely small fractions of methyne hydrogens involved, this treatment is incapable of distinguishing between the two types of hydrogens. On the other hand, treating methylene and methyne hydrogens as equivalent yielded interchange energies which were considerably lower than those obtained for the *n*-alkane mixtures. Furthermore, these values decreased with increased degree of branching. This behavior has also been observed by Cruickshank, *et al.*<sup>29</sup>

**Alkene Solutes.** For the 1-alkene solutes each double bond was assigned two contact points. (This assignment was based on comparison of the molar volumes of the alkenes with that of *n*-hexane.) Thus, an ethylenic group ( $-\text{CH}=\text{CH}_2$ ) was assigned a total of five contact points, and all these contacts were treated equivalently without distinguishing  $\pi$  electrons from ethylenic hydrogens. There are then three types of interchange energies:  $\text{CH}_3-\text{CH}_2$ ,  $\text{CH}_3\text{-ene}$ , and  $\text{CH}_2\text{-ene}$ . For *n*-alkane solvent systems containing solute molecules with three types of contact points:  $-\text{CH}_3$  hydrogen,  $-\text{CH}_2-$  hydrogen, and one other type (type c), eq 7 reduces to

$$\chi T = C_2 \left[ (f_1^a f_2^b + f_2^a f_1^b - f_1^a f_1^b - f_2^a f_2^b) \frac{\omega^{a-b}}{k} + (f_1^a f_2^c - f_2^a f_2^c) \frac{\omega^{a-c}}{k} + (f_1^b f_2^c - f_2^b f_2^c) \frac{\omega^{b-c}}{k} \right] \quad (9)$$

where  $f_2^a$  = fraction of methyl type of hydrogens in solute,  $f_2^b$  = fraction of methylene type of hydrogens in solute,  $f_2^c$  = fraction of type c contacts in solute,  $f_1^a$  = fraction of methyl type of hydrogens in solvent,  $f_1^b$  = fraction of methylene type of hydrogens in solvent,  $\omega^{a-b}/k$  = methyl-methylene interchange energy,  $\omega^{a-c}/k$  = methyl-type c interchange energy, and  $\omega^{b-c}/k$  = methylene-type c interchange energy.

Using the average methyl-methylene interchange energy from Table XIII,  $\omega^{\text{CH}_3\text{-ene}}$  and  $\omega^{\text{CH}_2\text{-ene}}$  were determined through eq 9 by employing the least-squares plotting procedure of Gainey and Young.<sup>30</sup> The 12 1-alkene systems were treated as a single group; *i.e.*, values were found for  $\omega^{\text{CH}_3\text{-ene}}$  (the intercept) and  $\omega^{\text{CH}_2\text{-ene}}$  (the slope) which gave the best straight line through all 12 data points. These interchange energies are listed in Table XIV along with the corresponding standard deviations.

**Table XIV:** Interchange Energies (in degrees Kelvin) for 1-Alkenes and Aromatics at 355.2°K

#### 1-Alkenes

$$\omega^{\text{CH}_3\text{-ene}}/k = 77 \pm 12$$

$$\omega^{\text{CH}_2\text{-ene}}/k = 41.2 \pm 2.3$$

Aromatics	Total number of contact points	$\omega^{\text{CH}_3\text{-Bz}}$	$\omega^{\text{CH}_2\text{-Bz}}$
		$k$	$k$
Benzene	12	49.5 $\pm$ 3.0 (36)	15.6 $\pm$ 0.5 (18)
Toluene	14	90 $\pm$ 9	14.8 $\pm$ 1.4
Ethylbenzene	16	97 $\pm$ 8	16.3 $\pm$ 1.1
Cumene	18	126 $\pm$ 7	22.5 $\pm$ 2.5
<i>p</i> -Xylene	16	150 $\pm$ 5	28.0 $\pm$ 1.8
<i>m</i> -Xylene	16	150 $\pm$ 5	29.2 $\pm$ 1.8
<i>o</i> -Xylene	16	153 $\pm$ 5	31.2 $\pm$ 1.5
Average values			
Monosubstituted aromatics		106 $\pm$ 3	17.1 $\pm$ 0.4
Disubstituted aromatics		151	29.4

**Aromatic Solutes.** Following Bhattacharyya and Mukherjee,<sup>31</sup> benzene was assigned 12 contact points: six for the hydrogen atoms and six for the  $\pi$  electrons. These contact points have been considered simply as benzene (Bz) contacts without distinguishing between  $\pi$  electrons and hydrogen atoms. Toluene, ethylbenzene,

(32) H. D. Young, "Statistical Treatment of Experimental Data," McGraw-Hill Book Co., Inc., New York, N. Y., 1962, p 76.



cumene, and the xylenes thus have two types of contact points: benzene type and aliphatic hydrogen types, which are treated as the corresponding aliphatic hydrogens in alkanes (with the methyne hydrogen in cumene, being treated as a methylene hydrogen). The number of Bz-type contacts was taken as 11 in the monosubstituted solutes and 10 in the disubstituted ones. Here, again, there are three types of interchange energies:  $\text{CH}_3\text{-CH}_2$ ,  $\text{CH}_3\text{-Bz}$ , and  $\text{CH}_2\text{-Bz}$ . The values of the two new interchange energies ( $\omega^{\text{CH}_3\text{-Bz}}$  and  $\omega^{\text{CH}_2\text{-Bz}}$ ), determined through eq 9 using the suggested plotting procedure,<sup>30</sup> are listed in Table XIV with the corresponding standard deviations. Listed in parentheses are the reported values<sup>30</sup> for benzene which are somewhat lower than ours.

It was apparent from the results that the aromatic interchange energies fell (roughly) into three classes: (a) benzene, (b) monosubstituted benzenes, and (c) disubstituted benzenes. Accordingly, the data points for all the monosubstituted compounds were considered as a unit and analyzed to give the best single straight line fit. The resulting least-squares "average" interchange energies are given in Table XIV. For the disubstituted benzenes the average value was determined simply by taking the arithmetic mean of the individual interchange energies. The observed trend of increasing positive values in going from benzene to disubstituted benzene is probably due to enhanced solute-solute interaction resulting from an increased electron density in the aromatic  $\pi$ -electron system with substitution.

Using the average interchange energies determined for the various contact pairs considered here, the interaction parameters were retrieved through eq 7. In Table XV the differences between the retrieved value [ $\chi(\text{theor})$ ] and the actual value [ $\chi(\text{exptl})$ ] are listed. For the majority (about 60%) of the systems, the values were recovered to within twice the probable experimental uncertainty.

### Regular Solution Treatment

The Hildebrand-Scatchard treatment of regular solutions<sup>33,34</sup> yields the following expression for the thermal contribution to the infinite dilution solute activity coefficient

$$\ln \gamma_2^{\text{th}} = \chi = \frac{V_2}{RT}(\delta_1 - \delta_2)^2 \quad (10)$$

where  $V_2$  is the solute molar volume and  $\delta_i$  is the solubility parameter of component  $i$ . The solute solubility parameters ( $\delta_2$ ), listed in Tables XVI and XVII, were determined from the equation<sup>33,34</sup>

$$\delta_2 = \left( \frac{\Delta E_2^{\text{V}}}{V_2} \right)^{1/2} = \left( \frac{\Delta H_2^{\text{V}} - RT}{V_2} \right)^{1/2} \quad (11)$$

where  $\Delta E_2^{\text{V}}$  and  $\Delta H_2^{\text{V}}$  are, respectively, the pure solute molar energy and enthalpy of vaporization. Solute

**Table XV:** Comparison of Experimental and Theoretical Interaction Parameters Using Lattice Theory:  $\chi(\text{theor})^a - \chi(\text{exptl})^b$

Solute	Solvent		
	<i>n</i> -C <sub>24</sub> H <sub>50</sub>	<i>n</i> -C <sub>30</sub> H <sub>62</sub>	<i>n</i> -C <sub>36</sub> H <sub>74</sub>
<i>n</i> -Hexane	+0.002	+0.019	+0.006
<i>n</i> -Heptane	-0.005	+0.019	+0.011
<i>n</i> -Octane	-0.024	+0.014	+0.000
<i>n</i> -Nonane	-0.031	+0.005	-0.027
1-Hexene	+0.007	+0.002	-0.010
1-Heptene	+0.005	+0.013	-0.009
1-Octene	-0.007	+0.016	-0.023
1-Nonene	-0.007	+0.017	-0.014
Benzene	-0.011	+0.009	-0.006
Toluene	+0.013	+0.017	-0.009
Ethylbenzene	-0.002	+0.001	-0.024
Cumene	-0.037	-0.011	-0.023
<i>p</i> -Xylene	+0.022	+0.035	+0.016
<i>m</i> -Xylene	-0.005	+0.007	-0.012
<i>o</i> -Xylene	-0.036	-0.019	-0.043

<sup>a</sup> Values calculated through eq 7 using the average interchange energies from Tables XIII and XIV. <sup>b</sup> Values given in Table XII.

**Table XVI:** Comparison of Average Experimental Interaction Parameters ( $\bar{\chi}$ ) with Those Predicted by Regular Solution Theory at 355.2°K (Alkane and Alkene Solutes ( $\delta_1 = 7.730$ ))

Solute	$\delta_2$	$\chi$ (reg soln)	$\bar{\chi}$ (exptl)
<i>n</i> -Hexane	6.738	0.199	0.254
2-Methylpentane	6.536	0.291	0.278
2,2-Dimethylbutane	6.277	0.434	0.288
2,3-Dimethylbutane	6.499	0.305	0.250
3-Methylpentane	6.640	0.238	0.251
<i>n</i> -Heptane	6.855	0.172	0.203
3-Methylhexane	6.738	0.220	0.213
2,4-Dimethylpentane	6.451	0.375	0.269
<i>n</i> -Octane	6.953	0.150	0.175
3-Methylheptane	6.828	0.201	0.186
<i>n</i> -Nonane	7.047	0.126	0.158
1-Hexene	6.789	0.171	0.280
1-Heptane	6.897	0.150	0.234
1-Octene	6.990	0.131	0.204
1-Nonane	7.072	0.114	0.174

molar volumes were calculated from the published densities given by the law of rectilinear diameters.<sup>13</sup> Solute molar enthalpies of vaporization were calculated from published Antoine constants<sup>13</sup> ( $B$  and  $C$ ) through the equation

$$\Delta H_2^{\text{V}} = 2.303RB \left( \frac{t + 273.2}{t + C} \right)^2 \quad (12)$$

where  $t$  is the temperature in degrees Centigrade.

(33) J. H. Hildebrand and R. L. Scott, "Regular Solutions," Prentice-Hall, Englewood Cliffs, N. J., 1962.

(34) J. H. Hildebrand and R. L. Scott, "Solubility of Nonelectrolytes," 3rd ed, Dover Publications, Inc., New York, N. Y., 1964.

**Table XVII:** Comparison of Average Experimental Interaction Parameters ( $\bar{\chi}$ ) with Those Predicted by Regular Solution Theory at 355.2°K. Aromatic Solutes ( $\delta_1 = 6.850$ )

Solute	$\delta_2$	$\chi$ (reg soln)	$\bar{\chi}$ (exptl)
Benzene	8.471	0.358	0.457
Toluene	8.277	0.329	0.344
<i>p</i> -Xylene	8.150	0.316	0.238
<i>m</i> -Xylene	8.177	0.330	0.266
<i>o</i> -Xylene	8.370	0.421	0.295
Ethylbenzene	8.157	0.317	0.319
Cumene	7.910	0.237	0.292
Chlorobenzene	8.822	0.489	0.472

The solubility parameter for the solvent ( $\delta_1$ ) was treated as an adjustable parameter. To fit the experimental data for all the systems studied, two different  $\delta_1$  values were required—one for aliphatic solutes and another for aromatic ones. Comparisons between the experimental solute interaction parameter  $\bar{\chi}$  (which is an average of  $\chi$  in the three solvents) and the best-fit value of  $\chi$  are shown in Tables XVI and XVII. The resulting solvent solubility parameter (chosen such that the sum of the squares of the differences between the experimental  $\bar{\chi}$ 's and those calculated from eq 10 was minimized) may conveniently be regarded as that corresponding to  $n\text{-C}_{30}\text{H}_{62}$ .

### Perturbation Treatment

For statistical solution theories based on a lattice model the necessary assumption of a structured liquid can scarcely be regarded as physically realistic. Longuet-Higgins<sup>22</sup> has suggested that this unrealistic assumption can be removed for solutions of molecules of sufficiently long chain length in which interactions between the different kinds of molecules are not too disparate. He proposed<sup>22,35</sup> a new statistical theory, founded on more general and seemingly more plausible physical assumptions. Based on his treatment, a first-order "perturbation approach" to the free energy of solution has recently been developed by Luckhurst and Martire.<sup>36</sup> It appears potentially useful for interpreting the interaction parameters within a series of geometrically closely related solute molecules in the same solvent.

Consider two solutes, a reference one and a "perturbed" one, in a common solvent, say  $n\text{-C}_{30}\text{H}_{62}$ . These two solutions are assumed to differ only in the strengths of the intermolecular attractions between solute molecules and between such molecules and the common solvent. Under identical conditions of temperature  $T$ , pressure  $P$ , and mole fraction of the solute (here, at infinite dilution), the interaction parameter is then given by the expression<sup>36</sup>

$$\chi = \chi' + \frac{V_2'}{RT} \left[ \frac{E_1}{V_1} - \frac{E_2'}{V_2'} \right] \left[ \frac{T_2^c}{T_2^{c'}} - 1 \right] \quad (13)$$

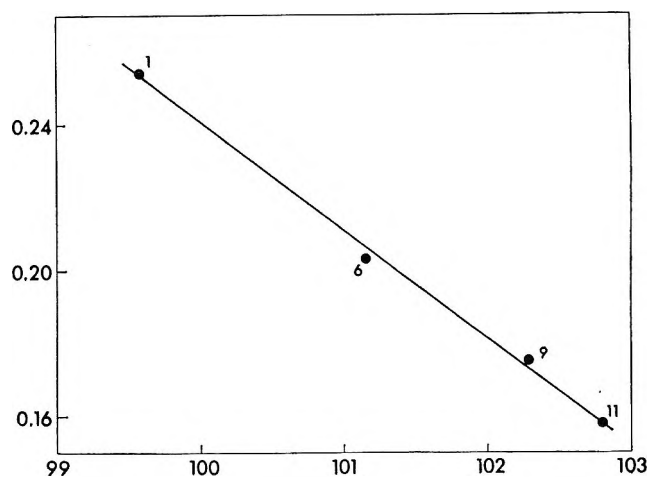


Figure 1. Average solute interaction parameter ( $\bar{\chi}$ ) vs. a measure of the pure solute potential well depth  $[T_2^c/(V_2^*)^{1/3}]$  for normal alkanes. Solutes numbered according to Table II.

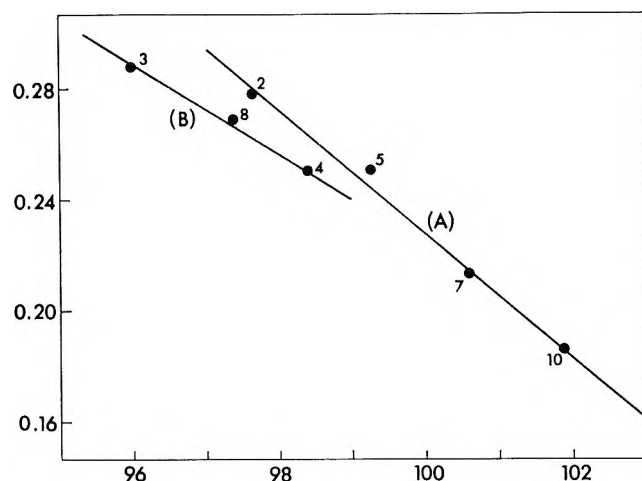


Figure 2. Average solute interaction parameter ( $\bar{\chi}$ ) vs. a measure of the pure solute potential well depth  $[T_2^c/(V_2^*)^{1/3}]$  for monobranched (A) and dibranched (B) alkanes.

where the primed quantities refer to the reference solute and the unprimed quantities to the perturbed one;  $E_i$ ,  $V_i$ , and  $T_2^c$  are, respectively, the molar intermolecular cohesive energy, the molar volume, and the critical temperature of component  $i$ , and the subscripts 1 and 2 refer to the solvent and solute, respectively.

In the derivation of eq 13 the critical temperature of the solute was taken as a measure of the depth of its potential well. Recently, Kreglewski<sup>37</sup> has shown that for large molecules  $T_2^c/(V_2^*)^{1/3}$  is a better measure of the potential well depth, where  $V_2^*$  is defined as the solute molar volume at the temperature  $T_2^* = 0.6T_2^c$ . The modified form of eq 13 would then be

(35) H. C. Longuet-Higgins, *Proc. Roy. Soc.*, **A205**, 247 (1951).

(36) G. R. Luckhurst and D. E. Martire, *Trans. Faraday Soc.*, **65**, 1248 (1969).

(37) A. Kreglewski, *J. Phys. Chem.*, **71**, 2860 (1967); **72**, 1897 (1968).

$$\chi = \chi' + \frac{V_2'}{RT} \left[ \frac{E_1}{V_1} - \frac{E_2'}{V_2'} \right] \left[ \frac{T_2^c/(V_2^*)^{1/3}}{T_2^{c'}/(V_2^{*'})^{1/3}} - 1 \right] \quad (14)$$

Indeed, we observe that if  $\bar{\chi}$  (the average value of the solute interaction parameter in the three solvents) is plotted against  $T_2^c/(V_2^*)^{1/3}$  instead of  $T_2^c$ , much better linear correlations are obtained for our systems. Hence, using this plotting method it was found that the normal alkanes fell on one straight line, whereas the monobranched and dibranched alkanes each fell on different straight lines (see Figures 1 and 2). Thus, as expected from the theory,<sup>36</sup> structurally similar alkanes fell on the same straight line.

These families and the 1-alkene series (Figure 3) exhibit negative slopes, which indicates that the cohesive energy densities ( $-E_t/V_t$  or  $\Delta E_t^V/V_t$ ) of these solutes are less than that of the solvent. On the other hand, positive slopes are observed for the plots of monosubstituted and disubstituted benzenes (Figure 4). For the latter, then, the solute cohesive energy densities are larger than that of the solvent. This behavior is consistent with that found for the regular solution model, as an examination of the relevant solubility parameters will confirm (see Tables XVI and XVIII).

Finally, writing eq 14 in the form

$$\bar{\chi} = \alpha + \beta [T_2^c/(V_2^*)^{1/3}] \quad (15)$$

$\alpha$  (the intercept) and  $\beta$  (the slope) of the plots of  $\bar{\chi}$  against  $T_2^c/(V_2^*)^{1/3}$  were determined for each family by a least-squares fit. These values are listed in Table XVIII along with the corresponding linear correlation coefficients (LCC). The average correlation coefficient for the families studied is 0.984, indicating excellent agreement with the theory. This treatment, therefore, appears to be highly sensitive to the number of substitutions on the solute molecule, *i.e.*, the solute molecular shape.

**Table XVIII:** Values of  $\alpha$  (the Intercept),  $\beta$  (the Slope), and LCC (the Linear Correlation Coefficient) for Family Plots of  $\bar{\chi}$  vs.  $[T_2^c/(V_2^*)^{1/3}]^a$

Solute family	$\alpha$	$\beta$	LCC
<i>n</i> -Alkanes	1.757	-0.0291	0.997
Monosubstituted alkanes	2.732	-0.0222	0.995
Disubstituted alkanes	2.431	-0.0154	0.997
1-Alkenes	1.195	-0.0250	0.999
Monosubstituted benzenes	-1.524	0.0144	0.999
Disubstituted benzenes	-1.432	0.0139	0.919

<sup>a</sup> See Figures 1-4.

## Discussion

The three theories considered here are all based on the assumption of near-random mixing; hence, their application is limited to systems where strong

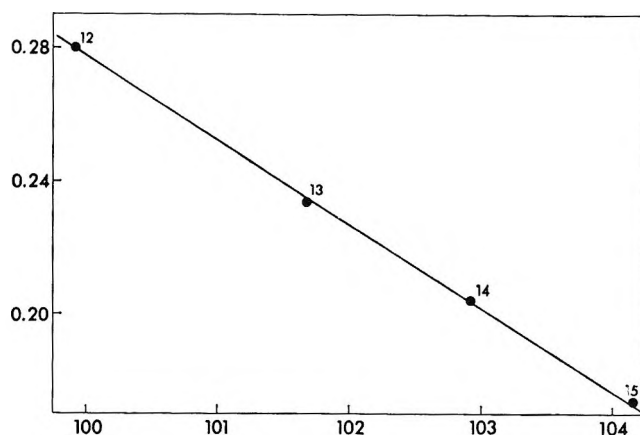


Figure 3. Average solute interaction parameter ( $\bar{\chi}$ ) vs. a measure of the pure solute potential well depth  $[T_2^c/(V_2^*)^{1/3}]$  for 1-alkenes.

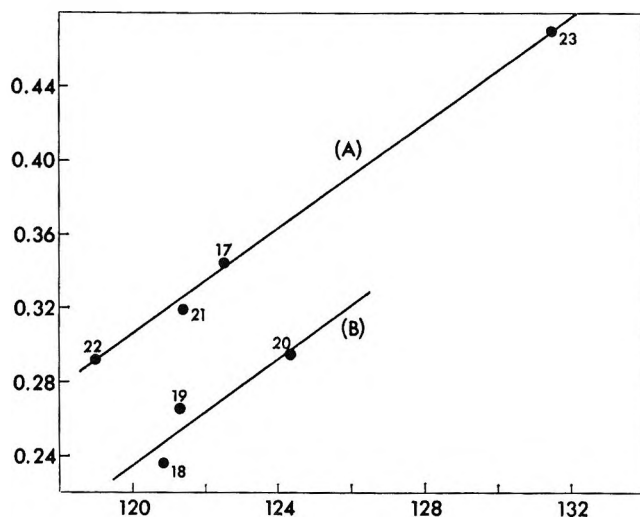


Figure 4. Average solute interaction parameter ( $\bar{\chi}$ ) vs. a measure of the pure solute potential well depth  $[T_2^c/(V_2^*)^{1/3}]$  for monosubstituted (A) and disubstituted (B) benzenes.

dipolar or specific interactions are absent. Although they are used here to analyze infinite dilution excess free energy values (*i.e.*,  $\ln \gamma_2^\infty$ ), our findings permit, in principle, predictions over the entire concentration range. This is possible because no new parameters appear in the concentration-dependent expressions of the three theories. For example, using the appropriate interchange energies given in Tables XIII and XIV, an energy of mixing can be calculated<sup>26</sup> for an equimolar benzene-*n*-hexane mixture which compares favorably with the measured heat of mixing.<sup>27</sup>

With the lattice treatment, once the interchange energies ( $\omega^{\alpha\beta}$ ) have been assigned, they can be used to predict the excess free energy (and, with less confidence, the energy of mixing) of any system containing some combination of the contact pairs studied. Prediction of the thermodynamic properties can now be made for hydrocarbon mixtures whose molecules con-

tain one or more of the following contact pairs: (a)  $\text{CH}_3\text{-CH}_2$ , (b)  $\text{CH}_3\text{-ene}$ ,  $\text{CH}_2\text{-ene}$  (1-alkenes), and (c)  $\text{CH}_3\text{-Bz}$ ,  $\text{CH}_2\text{-Bz}$  (benzene and mono and disubstituted benzenes). A logical extension of this work would be to consider systems which would enable one to evaluate the Bz-ene interchange energies. This could be accomplished through a glpc study of aromatic solutes with a high-molecular-weight 1-alkene solvent. Study of other carefully selected systems can provide additional information and help test the extent of this simple lattice theory. The main drawback, however, is that when more than three different types of contact pairs are involved, the determination of the various interchange energies becomes unwieldy and increasingly inaccurate.

The perturbation approach is as quantitative as and physically more realistic than lattice theory. However, the former requires more experimental data points (at least three points for each family plot) for predictive purposes and knowledge of an additional pure solute property  $[T_2^\circ/(V_2^*)^{1/3}]$ . Both theories were equally successful in treating the mono- and disubstituted aromatics. The advantages of the perturbation ap-

proach are that it can treat systems which cannot readily be handled by lattice theory (*e.g.*, the branched alkanes) and that it is potentially applicable to more complicated systems.<sup>36</sup> It is more quantitative than regular solution theory, which often produces only rough numerical agreement with experiment (see Tables XVI and XVII), and it can treat negative interaction parameters. Studies on more complex, but structurally similar, solute molecules should provide a further test of the perturbation approach.

In summary, simple contact point lattice theory (zeroth approximation) and the present perturbation approach (first-order approximation) show potential for interpreting and predicting the free energy of a range of nonpolar and slightly polar mixtures. Although more sophisticated theories do exist, given the little information needed for predictive purposes, these two seem to strike the middle ground between sophistication and utility.

*Acknowledgment.* This work was supported by basic research grants from the National Science Foundation and the U. S. Army Edgewood Arsenal.

## Solvation Enthalpies of Various Ions in Water and Heavy Water<sup>1</sup>

by C. V. Krishnan and H. L. Friedman

*Department of Chemistry, State University of New York at Stony Brook, Stony Brook, New York 11790*  
(Received December 22, 1969)

New data are reported for enthalpies of transfer of many electrolytes to  $\text{D}_2\text{O}$  from  $\text{H}_2\text{O}$  at 25°. Single ion enthalpies of transfer, based on the convention that the enthalpy of transfer is the same for  $\text{Ph}_4\text{As}^+$  and  $\text{Ph}_4\text{B}^-$ , are derived from these data together with some from the literature. For the tetraalkylammonium ions and the alkali ions the ionic enthalpies of transfer correlate very well with the Walden product ratios reported by Kay and Evans. For these ions and for several oxyanions the enthalpy of transfer seems to be about 5% of the total "structural" contribution to the enthalpy of solvation of the ion, while for the halide ions the enthalpy of transfer seems to be more than 10% of the structural enthalpy. The combination of these data for  $\text{Li}^+$ ,  $\text{Na}^+$ , and  $\text{K}^+$  with data obtained by Feder and Taube for the effect of these ions on the relative fugacities of  $\text{H}_2^{16}\text{O}$  and  $\text{H}_2^{18}\text{O}$  in water supports the interpretation of all of these effects in terms of a model in which one feature is a "structure-broken" region around  $\text{Li}^+$  as well as around the other alkali ions.

### Introduction

Many phenomena associated with solvation in water have been interpreted in terms of structural changes in the solvent in the neighborhood of the solute particles. Models have been proposed for various manifestations of these structural effects and named; iceberg formation,<sup>2</sup> structure-breaking,<sup>2</sup> hydration of the second kind,<sup>3</sup> hydrophobic bonding,<sup>4</sup> flickering clusters,<sup>5</sup> clathrate formation in solution,<sup>6</sup> local proton excess,<sup>7</sup> and

others.<sup>8</sup> While it is widely agreed that the study of aqueous solutions reveals important contributions to

(1) Grateful acknowledgment is made for the support of this work by the National Institutes of Health.

(2) H. S. Frank and M. W. Evans, *J. Chem. Phys.*, **13**, 507 (1945).

(3) H. G. Hertz, *Ber. Bunsenges. Phys. Chem.*, **68**, 907 (1964).

(4) W. Kauzmann, *Advan. Protein Chem.*, **14**, 1 (1959).

(5) H. S. Frank and W. Y. Wen, *Discuss. Faraday Soc.*, **24**, 133 (1957).

the properties from changes in the hydrogen bonding in the solvent in the neighborhood of the solute particles, it is difficult to get evidence which clearly favors one model for these changes over another, and it is still easy to be skeptical about much of the evidence for the importance of these effects.<sup>9</sup>

It is remarkable that the thermodynamic evidence for these structural effects is often compelling while the spectroscopic and diffraction tools which are normally relied on to resolve structural problems have not been decisive here. One reason seems to be the short lifetimes, of the order of picoseconds, characterizing the hydrogen-bond structures in liquid water and its solutions. As a result the spectroscopic<sup>10</sup> and scattering<sup>11</sup> experiments themselves yield structural measures which are averages over the contributions of various structures and which are most often interpreted in terms of chemical models, a process which is no more incisive than the interpretation of thermodynamic data in terms of equilibria among various structures.

The study of transport coefficients of aqueous systems leads to results which are readily interpreted in terms of the same structural effects,<sup>12-14</sup> as was already emphasized by Frank and Evans.<sup>2</sup> But the molecular theory of transport coefficients is so difficult that it seems quite impossible to use such data to distinguish among various models for the structural effects. The interpretation of nmr relaxation data, which yield quantities which may be thought of as local transport coefficients,<sup>15</sup> suffers from the same difficulty.

Under these circumstances it seems useful to attempt to use some of the experimental data to characterize the structural effects in a quantitative way, even though the appropriate description of the structures themselves remains uncertain. An example is the structural entropy  $\Delta S^{\text{st}}$  introduced by Frank and Evans;<sup>2</sup> essentially it is the difference between the experimental standard absolute partial molar entropy of a solute particle in aqueous solution and the value calculated on the basis of a simple theory which neglects the structural effects. Thermodynamic quantities such as this seem to be potentially more useful in distinguishing among alternative structural models than transport quantities like the structural elevation of fluidity<sup>16</sup> which are more easily accessible experimentally but which, as remarked above, are likely to be more difficult to relate quantitatively to models. On the other hand, characterization of the structural effects in terms of shifts of nmr,<sup>17,18</sup> infrared,<sup>19</sup> or Raman spectra<sup>20</sup> seem to be very promising approaches, but are omitted from consideration here. One problem with such studies is that the measurements are often made at solute concentrations which are large enough so that, judging from thermodynamic studies, the interactions between the structural effects around neighboring solute particles are significant.

It has been found<sup>21-24</sup> that the change in solute ther-

modynamic properties when the solvent H<sub>2</sub>O is replaced by D<sub>2</sub>O are particularly useful in characterizing the structural effects in a quantitative way. In this report additional data for the enthalpy change in this process are added to those previously available, single-ion enthalpies of transfer are established in terms of a convention which seems to give close to the real values,<sup>24</sup> and the results are compared quantitatively with  $\Delta S^{\text{st}}$  and with some other manifestations of the structural effects.

## Experimental Section

The instrumental aspects have been described.<sup>23,25,26</sup> Most of the salts used were from earlier preparations. The 99.77% D<sub>2</sub>O obtained from Columbia Organic Chemicals was distilled before use. (Bu<sub>3</sub>N(CH<sub>2</sub>)<sub>4</sub>)<sub>2</sub>Br<sub>2</sub> was a gift from Dr. D. Fennell Evans of Case Western Reserve University.

All the measurements were made at 25°. The results are given in Table I. To minimize the error, heats of solutions in water and D<sub>2</sub>O have been determined for solute samples of the same preparations.

## Enthalpies of Transfer Compared with Mobilities

The new enthalpy of transfer data are presented in the body of Table II. They are augmented by data from other sources to allow the deduction of conventional enthalpies of transfer of single ions which are given on the borders of the table. The convention employed to

- (6) B. Lindman, S. Forsén, and E. Forslind, *J. Phys. Chem.*, **72**, 2805 (1968).
- (7) F. H. Stillinger and A. Ben-Naim, *ibid.*, **73**, 900 (1969).
- (8) A. K. Covington and P. Jones, "Hydrogen-Bonded Solvent Systems," Taylor and Francis Ltd., London, 1968.
- (9) A. Holtzer and M. F. Emerson, *J. Phys. Chem.*, **73**, 26 (1969).
- (10) G. Walrafen, in ref 8.
- (11) G. Safford, P. C. Schaffer, P. S. Leung, G. F. Doebbler, G. W. Brady, and E. F. X. Lyden, *J. Chem. Phys.*, **50**, 2140 (1969).
- (12) R. W. Gurney, "Ionic Processes in Solution," Dover Publications, Inc., New York, N. Y., 1962.
- (13) R. L. Kay and D. F. Evans, *J. Phys. Chem.*, **70**, 2325 (1966).
- (14) R. L. Kay and D. F. Evans, *ibid.*, **69**, 4216 (1965).
- (15) L. Endom, H. G. Hertz, B. Thul, and M. D. Zeidler, *Ber. Bunsenges. Phys. Chem.*, **71**, 1008 (1967).
- (16) E. E. Bingham, *J. Phys. Chem.*, **45**, 885 (1941).
- (17) J. C. Hindman, *J. Chem. Phys.*, **36**, 1000 (1962).
- (18) Z. Luz and G. Yagil, *J. Phys. Chem.*, **70**, 554 (1966).
- (19) K. A. Hartman, Jr., *ibid.*, **70**, 270 (1966).
- (20) G. E. Walrafen, *J. Chem. Phys.*, **40**, 3249 (1964).
- (21) G. C. Krescheck, H. Schneider, and H. A. Scheraga, *J. Phys. Chem.*, **69**, 3123 (1965).
- (22) E. M. Arnett and D. R. McKelvey in "Solute-Solvent Interactions," J. F. Coetzee and C. D. Ritchie, Ed., Interscience Publishers, New York, N. Y., 1969.
- (23) C. V. Krishnan and H. L. Friedman, *J. Phys. Chem.*, **73**, 1572 (1969).
- (24) C. V. Krishnan and H. L. Friedman, *ibid.*, **73**, 3934 (1969).
- (25) Y. C. Wu and H. L. Friedman, *ibid.*, **70**, 2020 (1966).
- (26) Y. C. Wu and H. L. Friedman, *ibid.*, **70**, 501 (1966).

Table I: Enthalpies of Solution of Pure Substances at 25° (kcal/mol)

Solute	Solvent					
	H <sub>2</sub> O			D <sub>2</sub> O		
LiClO <sub>4</sub>	-6.35	-6.345 <sup>a</sup>			-5.95	
LiOCCF <sub>3</sub>	-6.22	-6.33 <sup>b</sup>			-6.19	
NaClO <sub>4</sub>	3.35	3.317 <sup>a</sup>	3.46 <sup>c</sup>		3.95	4.03 <sup>c</sup>
NaOCCF <sub>3</sub>	-1.98	-1.99 <sup>b</sup>			-1.88	
NaBPh <sub>4</sub>	-4.77	-4.79 <sup>b</sup>	-4.77 <sup>d</sup>		-3.99	-4.00 <sup>d</sup>
KCl	4.10	4.115 <sup>a</sup>	4.23 <sup>c</sup>	4.13 <sup>d</sup>	4.71	4.84 <sup>c</sup>
NaClO <sub>3</sub>	5.17	5.19 <sup>a</sup>			5.70	
KNO <sub>3</sub>	8.33	8.34 <sup>a</sup>				8.84
RbCl	4.09	4.04 <sup>b</sup>	4.13 <sup>a</sup>			4.69
RbOCCF <sub>3</sub>	1.88	1.89 <sup>b</sup>				2.05
CsCl	4.14	4.25 <sup>a</sup>	4.155 <sup>b</sup>			4.79
CsOCCF <sub>3</sub>	1.20	1.53 <sup>b</sup>				1.41
NH <sub>4</sub> Cl	3.56	3.53 <sup>a</sup>				3.82
NH <sub>4</sub> OCCF <sub>3</sub>	3.92					3.69
Me <sub>4</sub> NCl	1.06	0.975 <sup>a</sup>	0.94 <sup>d</sup>			1.44
Me <sub>4</sub> NI	10.08	10.06 <sup>a</sup>	10.08 <sup>e</sup>			10.79
Et <sub>4</sub> NCl	-3.10	-3.07 <sup>e</sup>	-3.02 <sup>f</sup>			-2.90
Et <sub>4</sub> NI	6.67	6.67 <sup>e</sup>	6.83 <sup>f</sup>			7.08
Pr <sub>4</sub> NCl						-5.42
Pr <sub>4</sub> NI						2.91
Bu <sub>4</sub> NCl						-7.40
Am <sub>4</sub> NCl						-9.57
Bu <sub>3</sub> N(CH <sub>2</sub> ) <sub>6</sub> NBu <sub>3</sub> Br <sub>2</sub>	-7.90					-7.94

<sup>a</sup> V. B. Parker, "Thermal Properties of Aqueous Uni-Univalent Electrolytes," U. S. National Bureau of Standards NSRDS-NBS2, Washington, D. C., 1965. <sup>b</sup> Y. C. Wu and H. L. Friedman, *J. Phys. Chem.*, **70**, 501 (1966). <sup>c</sup> E. Lange and W. Martin, *Z. Phys. Chem., Abt. A*, **180**, 233 (1937). <sup>d</sup> E. M. Arnett and D. R. McKelvey in "Solute-Solvent Interactions," J. F. Coetzee and C. D. Ritchie, Ed., Interscience Publishers, New York, N. Y., 1969. <sup>e</sup> Y. C. Wu and H. L. Friedman, *J. Phys. Chem.*, **70**, 2020 (1966). <sup>f</sup> E. M. Arnett and D. R. McKelvey, *J. Amer. Chem. Soc.*, **88**, 2598 (1966).

get single-ion values is that Ph<sub>4</sub>As<sup>+</sup> and Ph<sub>4</sub>B<sup>-</sup> have the same enthalpy of transfer.

The dependence of the ionic enthalpy of transfer upon the reciprocal ionic radius is shown for some of these ions in Figure 1. The enthalpy data bear a striking similarity to experimental values for the isotopic Walden product ratio

$$R = (\lambda\eta)_{D_2O}/(\lambda\eta)_{H_2O} \quad (1)$$

reported by Kay and Evans.<sup>14</sup> Here  $\lambda$  is the limiting ionic mobility of the ion and  $\eta$  is the viscosity of the pure solvent. It is remarkable that for  $r_{ion} = 4.5 \text{ \AA}$  both  $R-1$  and the enthalpy of transfer vanish. It is even more remarkable that when the  $R$  scale is adjusted to make the  $R$  curve pass through the enthalpy of transfer datum for Cs<sup>+</sup>, then the entire  $R$  curve fits the cation enthalpy data as well as shown.

The  $R$  values are absolute ionic quantities since they are determined from experimental conductivities and transference numbers. Then the good agreement of the radius dependence for the cations in the two different experiments suggests not only that the two sets of data have a common underlying physical basis but also suggests that the conventional enthalpies of transfer given in Table II are close to the real values.<sup>27</sup>

Kay and Evans<sup>14</sup> show how their  $R$  data are quite consistent with the picture of the structures in the

environment of ions of various sizes in aqueous solution described by Frank and Evans<sup>3</sup> and Frank and Wen.<sup>5</sup> While the reasoning is very qualitative, Kay and Evans<sup>14</sup> also show that this picture provides a consistent interpretation for a variety of other observations of mobilities of alkali, halide, and tetraalkylammonium ions. The same picture also provides an interpretation of the enthalpies of transfer from water to nonhydrogen-bonding solvents.<sup>23,24</sup> It is quite easy to see that it equally well provides an interpretation of the present enthalpy data: it is assumed that about an Li<sup>+</sup> ion in water there are two roughly concentric regions in which the water structure is altered. In the inner one the water molecules are oriented by the electric field of the ion (hydration of the first kind) while in the outer one this orienting influence is negligible except that the stabilization of the water by hydrogen bonds is less than in bulk water (structure-breaking effect) owing to the residual influence of the central ion. As one goes down a series from Li<sup>+</sup> to Cs<sup>+</sup> or from F<sup>-</sup> to I<sup>-</sup>, the hydration of the first kind becomes less important. For still larger singly charged ions, as for nonpolar solutes, a neighboring region of altered water structure of a different kind becomes important, namely some sort of strengthened hydrogen-bonded structure which may be called hydration of the second kind.

(27) J. E. B. Randles, *Trans. Faraday Soc.*, **52**, 1573 (1956).

**Table II:** Enthalpies of Transfer to D<sub>2</sub>O from H<sub>2</sub>O at 25° (kcal/mol)

		F <sup>-</sup>	Cl <sup>-</sup>	Br <sup>-</sup>	I <sup>-</sup>	CF <sub>3</sub> COO <sup>-</sup>	ClO <sub>4</sub> <sup>-</sup>	NO <sub>3</sub> <sup>-</sup>	(C <sub>6</sub> H <sub>5</sub> ) <sub>4</sub> B <sup>-</sup>	CN <sup>-</sup>	ClO <sub>3</sub> <sup>-</sup>	BrO <sub>3</sub> <sup>-</sup>
		Single-ion values										
		-0.61	-0.05	0.09	0.23	-0.51	-0.04	-0.12	0.16	-0.16	-0.08	-0.14
Li <sup>+</sup>	0.45	-0.155 <sup>a,b</sup> (-0.16)	0.40 <sup>a,b</sup> (0.40)	0.535 <sup>a,b</sup> (0.54)	0.675 <sup>a,b</sup> (0.68)	0.03 (-0.06)	0.40 (0.41)					
Na <sup>+</sup>	0.61	0.005 <sup>a,b</sup> 0.00 <sup>c</sup> (0.00)	0.535 <sup>c</sup> 0.59 <sup>d</sup> 0.56 <sup>a,b</sup> (0.56)	0.695 <sup>a,b</sup> (0.70)	0.835 <sup>a,b</sup> (0.84)	0.10 (0.10)	0.60 0.57 <sup>a</sup> (0.57)	0.49 <sup>a</sup> (0.49)	0.78 0.77 <sup>d</sup> (0.76)		0.53 (0.53)	
K <sup>+</sup>	0.66	0.06 <sup>a</sup> (0.05)	0.61 0.615 <sup>a</sup> 0.73 <sup>d</sup> 0.75 <sup>e</sup> (0.61)	0.75 <sup>a,b</sup> (0.75)	0.89 <sup>a,b</sup> (0.89)			0.51 (0.54)		0.50 (0.50)		0.52 (0.52)
Rb <sup>+</sup>	0.68		0.60 (0.63)	0.80 <sup>a</sup> (0.77)		0.17 (0.17)						
Cs <sup>+</sup>	0.71		0.65 0.685 <sup>a</sup> (0.66)	0.81 <sup>a</sup> (0.80)		0.21 (0.20)						
NH <sub>4</sub> <sup>+</sup>	0.30		0.26 (0.25)			-0.23 (-0.21)						
Ag <sup>+</sup>	0.54							0.42 (0.42)				
Me <sub>6</sub> N <sup>+</sup>	0.43		0.38 0.38 <sup>d</sup> (0.38)	0.37 <sup>f</sup> 0.52 <sup>f</sup> (0.52)	0.71 (0.66)							
Et <sub>4</sub> N <sup>+</sup>	0.21		0.20 (0.16)	0.30 <sup>f</sup> (0.30)	0.41 (0.44)							
Pr <sub>4</sub> N <sup>+</sup>	-0.05		-0.12 (-0.10)	0.04 (0.04)	0.15 (0.18)							
Bu <sub>4</sub> N <sup>+</sup>	-0.23		-0.26 (-0.28)	-0.15 <sup>f</sup> (-0.14)								
Am <sub>4</sub> N <sup>+</sup>	-0.38		-0.44 (-0.43)	-0.28 <sup>f</sup> (-0.29)								
Ph <sub>4</sub> As <sup>+</sup>	0.16		0.10 (0.11)	0.24 <sup>f</sup> (0.25)								
Ph <sub>4</sub> P <sup>+</sup>	0.17		0.12 (0.12)	0.26 <sup>f</sup> (0.26) <sup>g</sup>								
diBu <sup>2+</sup>	-0.22			-0.04 (-0.04)								

<sup>a</sup> E. Lange and W. Martin, *Z. Physik. Chem., Abt. A*, **180**, 233 (1937). <sup>b</sup> J. Greyson, *J. Phys. Chem.*, **71**, 2210 (1967). <sup>c</sup> D. H. Davies and G. C. Benson, *Can. J. Chem.*, **43**, 3100 (1965). <sup>d</sup> E. M. Arnett and D. R. McKelvey in "Solute-Solvent Interactions," J. F. Coetzee and C. D. Ritchie, Ed., Interscience Publishers, New York, 1969. <sup>e</sup> V. K. La Mer and E. Noonan, *J. Amer. Chem. Soc.*, **61**, 1487 (1939). <sup>f</sup> C. V. Krishnan and H. L. Friedman, *J. Phys. Chem.*, **73**, 3934 (1969). <sup>g</sup> The data are the plain numbers in the body of the table. Numbers in parentheses are derived by adding the ionic enthalpies along the margins. The latter have been chosen to make the two sets as similar as possible.

The data in Figure 1 can be understood if one makes the additional assumption that hydration of the first and second kind and the structure-breaking effect are all somewhat larger in D<sub>2</sub>O than in H<sub>2</sub>O. Detailed considerations in the following section lead to an estimate of about 5% for the increment in the structure-breaking effect in going from H<sub>2</sub>O to D<sub>2</sub>O.

It seems that the interpretation, even in a qualitative way, of the enthalpy data in Figure 1 is somewhat more definite than the interpretation of the mobility data because of the unsuitably macroscopic nature of the theory leading to the use of the Walden product. However, the same kind of theory leads one to expect that the principal effect on self-diffusion coefficients

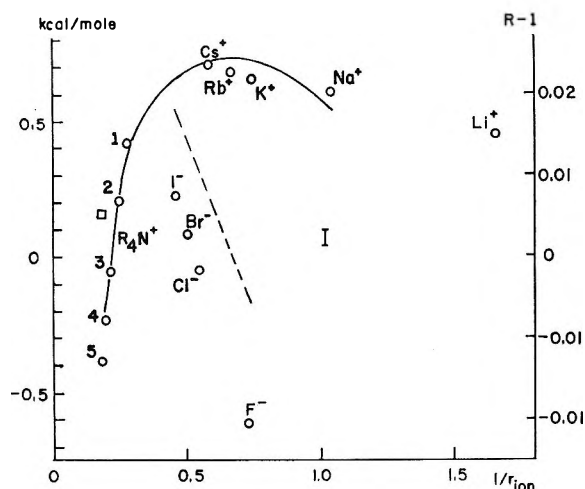


Figure 1. Ionic enthalpies of transfer to  $D_2O$  from  $H_2O$  and solvent isotope effect on the Walden products of these ions. The  $r_{ion}$  is the Pauling crystal radius for the monatomic ions, and is estimated from models for the others (Stokes-Robinson). The  $R_4N^+$  circles are the enthalpy data for these ions, with  $R$  ranging from methyl (1) to  $n$ -pentyl (5). The other circles are the enthalpy data for alkali ions and the halide ions. These single-ion enthalpies are based on the convention that the enthalpies of transfer of  $AsPh_4^+$  and  $BPh_4^-$  are equal; their common value is given by the square data point. The lines are smooth curves through the Walden product ratios  $R$  for the cations (—) and the anions (---) reported by Kay and Evans.<sup>14</sup> The error bar is an estimate of the uncertainty in both the calorimetric and conductivity data.

and nmr and epr relaxation times due to change of medium is accounted for by the change in  $\eta/T$ . These generalized Walden rules are in good agreement with the observations.<sup>28</sup> Also, the Walden products are much more nearly constant in systems in which structural effects are expected to be absent.<sup>13</sup>

It should be noted that the enthalpy changes in Figure 1 are associated with the change of the entire solvent environment of these ions to  $D_2O$  from  $H_2O$ . On the other hand, the ionic mobility, at least for some of these ions, is often pictured in terms of a process in which the ion moves together with the water molecules next to it. If some water moves with the ion, the way in which it is bound can have little effect on the mobility. As an extreme example, in  $Cr^{3+}(aq)$  the inner shell of six water molecules exchanges with the bulk on a time scale of hours. If these molecules were bound a little more or less tightly this could hardly affect the mobility of the ion. Therefore the similarity in the two sets of data for the positive ions in Figure 1 suggests that these ions exchange their solvent water as fast as they move through the solution. In the absence of a quantitative theory this can be no more than a suggestion, but for the tetraalkylammonium ions it is supported by direct observations of solute and solvent self-diffusion coefficients by Hertz, Lindman, and Siepe.<sup>29</sup>

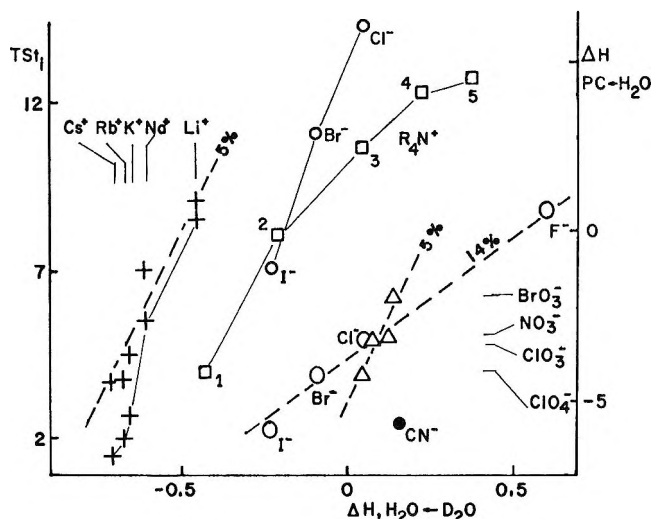


Figure 2. Correlation of other thermodynamic effects with the  $H_2O$  from  $D_2O$  enthalpy of transfer. All energies are in kcal/mol. —, enthalpy of transfer to propylene carbonate from water,<sup>24</sup> right-hand scale. The lines are merely drawn to connect the experimental points. The other data in the figure are  $TS_t1$ , left-hand scale. ---, lines showing the correlation expected in the  $TS_t1$  data if the enthalpy of transfer to  $H_2O$  from  $D_2O$  were a definite percentage of the structural enthalpy effect of the aqueous ion; 5% or 14% as indicated.

### Enthalpies of Transfer and Other Thermodynamic Measures of Ion Hydration

The correlation of the enthalpies of transfer of the tetraalkylammonium ions to  $D_2O$  from  $H_2O$  and to propylene carbonate from  $H_2O$  has already been discussed.<sup>24</sup> The conclusion was that both sets of data reflect the structural effect near hydrocarbon groups (icebergs, clathrates, or hydration of the second kind) in that this effect is about 5% larger in  $D_2O$  than in  $H_2O$ .

It does not seem possible to make as refined a comparison of the  $D_2O$  from  $H_2O$  and propylene carbonate from  $H_2O$  transfers for the other ions but a simple correlation graph is shown in Figure 2. Within a series of ions of similar charge and structure the correlation seems very strong, as good as for the  $R_4N^+$  ions which are also shown, but it seems hard to say much more because of the importance of  $H-O-H \cdots X^-$  hydrogen bonding for the anions in  $H_2O$  and  $D_2O$  and the specific acid-base sort of interaction of the alkali ions with water and propylene carbonate.

It seems of interest to try to get around this by comparing the  $D_2O$  from  $H_2O$  transfer enthalpies with  $\Delta S^{st}$ , the structural contribution to ionic hydration entropies introduced by Frank and Evans.<sup>2</sup> The original table of these quantities<sup>2</sup> is based on rather old

(28) For a spectacular example, see R. Wilson and D. Kivelson, *J. Chem. Phys.*, **44**, 154 (1966).

(29) H. G. Hertz, B. Lindman, and V. Siepe, *Ber. Bunsenges. Phys. Chem.*, **73**, 542 (1969).



data and is not as extensive as required here, so instead we compare with the quantity  $St_i$  defined by the equation

$$-St_i = S_i(\text{aq}) - S_i(\text{g}) + 10 \text{ eu}/(r_i + 2.8)$$

Here  $S_i(\text{aq})$  is the absolute molar entropy of species  $i$  in its hypothetical 1  $M$  standard state in water,  $S_i(\text{g})$  is the same for its hypothetical 1 atm standard state in the gas, and the last term is an estimate, due to Latimer of the electrostriction contribution to  $S_i(\text{aq})$ . The Pauling radius of the ion is  $r_i$  Å. Defined in this way,  $St_i$  differs from  $\Delta S^{\text{st}}$  for the species  $i$  by an amount which does not depend on  $i$ . The electrostriction correction to these quantities is rather uncertain but, fortunately, not very important. It ranges only from 2.0 eu for I<sup>-</sup> to 2.9 eu for Li<sup>+</sup>. The  $St_i$  values are based on<sup>30</sup> -5.3 eu for  $S_i(\text{aq})$  of H<sup>+</sup> while  $S_i(\text{g})$  was computed.

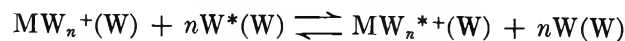
The structural contribution to the ionic entropy differs from  $St_i$  by a constant term, uncertain in magnitude, due to the free volume effect.<sup>2</sup> Also it is remarked that, in the case of structural effects of the kind discussed here, the entropy and enthalpy contributions seem nearly to cancel in the free energy.<sup>31,32</sup> Therefore  $TSt_i$  is approximately equal to the structural effect in the ionic enthalpy plus a constant term and then it is of interest to see whether  $TSt_i$  is linearly correlated with the enthalpy of transfer.

The results are shown in Figure 2. The correlation is quite strong and one finds from the slope that the structural effect measured by the enthalpy of transfer is about 15% of that measured by  $TSt_i$  for the halide ions, about 5% for the alkali metal ions, and about 5% for the oxyanions. Also for the alkaline earth ions, one finds from the enthalpy given by Greyson and Snell<sup>33</sup> that change in enthalpy of transfer to D<sub>2</sub>O from H<sub>2</sub>O is about 5% of the change in  $TSt_i$  as one progresses down the series.

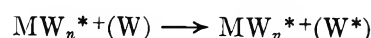
Correlations of similar quality to those shown in Figure 2 are found when the ordinate is the ionic elevation of fluidity<sup>16</sup> or the intrinsic ionic volume.<sup>30</sup> This is not surprising since it is well known that the many qualitative measures of the structural effect in aqueous solutions are correlated in this way except when one inspects a series for which the dominant effect is structure breaking.<sup>34</sup> Unfortunately it seems unlikely that one could elucidate the order in a structure-breaking series by a more extensive study of D<sub>2</sub>O from H<sub>2</sub>O transfers because the strong structure breakers are mostly anions for which there is likely to be a strong solvent isotope effect *via* the H-O-H...X<sup>-</sup> hydrogen bond.

It is interesting to compare the D<sub>2</sub>O from H<sub>2</sub>O transfer of the alkali metal ions with the data for their H<sub>2</sub><sup>18</sup>O from H<sub>2</sub><sup>16</sup>O transfers. The latter have not been measured directly but can be estimated from the H<sub>2</sub><sup>16</sup>O-H<sub>2</sub><sup>18</sup>O fractionation between aqueous solutions of alkali halides and the vapor studies by Feder and

Taube.<sup>35</sup> To demonstrate this without too much complexity of notation let W = H<sub>2</sub><sup>16</sup>O and W\* = H<sub>2</sub><sup>18</sup>O. Then the quantity called either<sup>35a</sup>  $n_A(K_A - 1)$  or<sup>35b</sup>  $n(K - 1)$  is  $K_0 - 1$  (if  $|K_0 - 1| \ll 1$ ) where  $K_0$  is the equilibrium constant of the reaction



where (W) means in solution in normal water. In reducing the data it was assumed<sup>35</sup> that W and W\* form an ideal mixture and that the observed fractionation was due only to the cation component of the salt; the latter assumption is supported by the evidence that the fractionation is insensitive to variation of the anion. If we also assume that there is a vanishingly small free energy change for the process



then the free energy change for the preceding reaction is also the free energy change for  $M^+(\text{W}) \rightarrow M^+(\text{W}^*)$ . For  $M^+ = \text{Li}^+, \text{Na}^+, \text{and K}^+$  there are data<sup>35</sup> at both 4° and 25°, so for these species we can get an estimate of  $\Delta H$  as well as  $\Delta G$ . The results are summarized in Table III.

**Table III:** Thermodynamics for  $M^+(\text{W}) \rightarrow M^+(\text{W}^*)$  at 25°  
Deduced from Data of Feder and Taube

M <sup>+</sup>	$\Delta G^\circ$ , kcal/mol	$\Delta H^\circ$ , kcal/mol
Li <sup>+</sup>	-0.007	-0.11
Na <sup>+</sup>	0.000	0.08
K <sup>+</sup>	0.005	0.04
Cs <sup>+</sup>	0.007 <sup>a</sup>	

<sup>a</sup> This value is at 4°.

As discussed by Feder and Taube,<sup>35</sup> these isotope effects can, in most cases, be understood in terms of the effects on the zero point energy of a vibration in which the motion changes the distance between the metal ion and an inner shell, or coordinated, water molecule. If the force constant for this vibration is much weaker than that for stretching an O-H bond within a water molecule, then each water molecule moves as a whole in its vibration against the central ion and the D<sub>2</sub>O-H<sub>2</sub>O isotope effect ought to include, as one component, the

(30) J. E. Desnoyers and C. Jolicoeur, "Modern Aspects of Electrochemistry," Vol. 5, B. E. Conway and J. O'M. Bockris, Ed., Plenum Publishing Corp., New York, N. Y., 1969, p 23.

(31) R. E. Kerwin, Ph.D. Thesis, University of Pittsburgh, 1964.

(32) J. Greyson, *J. Phys. Chem.*, **66**, 2218 (1962); E. M. Arnett and D. R. McKelvey, *Rec. Chem. Progr.*, **26**, 185 (1965).

(33) J. Greyson and H. Snell, *J. Phys. Chem.*, **73**, 3208 (1969).

(34) M. Eisenstadt and H. L. Friedman, *J. Chem. Phys.*, **46**, 2182 (1967).

(35) (a) H. M. Feder and H. Taube, *ibid.*, **20**, 1335 (1952); (b) H. Taube, *J. Phys. Chem.*, **58**, 523 (1954); (c) H. M. Feder, Ph.D. Thesis, University of Chicago, 1954.

effect measured in Table III. The latter is apparently very much smaller than the observed  $D_2O-H_2O$  effect. It must be concluded that  $D_2O-H_2O$  effect in Figure 1 for the alkali metal ions cannot come from anything except changes in the hydrogen bonding in the neighborhood of the metal ions, *i.e.*, something like what is pictured in the Frank-Evans, Frank-Wen model mentioned above.

It follows that the dominant effect for the alkali metal ions in the  $D_2O$  from  $H_2O$  transfers is a structure-breaking effect which is larger in  $D_2O$  than in  $H_2O$ . It is then interesting to consider whether the structure-breaking effect is also reflected in the data of Table III. In fact, the simplest interpretation of the trend in free energies shown there is that there is a competition between inner shell binding, reflected in the  $M-OH_2$  zero point energy, and a structure-breaking effect in which the first dominates for  $Li^+$  and the second for  $Cs^+$ , with something of a balance for  $Na^+$ . It would be of great interest to have more extensive data of this sort.

### Overlap

The data in Tables I and II are all believed to apply essentially to infinite dilution. As an aqueous solution is concentrated, one may reach a stage at which there is a significant contribution to the solution properties from configurations of the system in which the structurally affected regions of two or more solute particles overlap each other. Gurney<sup>12</sup> and Frank<sup>36</sup> have discussed the effect of such overlap upon activity coefficients and the corresponding entropy functions. For aqueous solutions of molecules with large hydrocarbon groups the overlap effects have been employed to interpret strongly concentration-dependent activity coefficients,<sup>37</sup> apparent molar volumes,<sup>38,39</sup> and heats of dilution<sup>40</sup> even at concentrations as low as a few

tenths molar. The underlying assumption, that in the overlap process the structurally affected regions near hydrocarbon groups interfere with each other, is supported by the following observations.

Evans<sup>41</sup> has proposed that the ion  $(C_4H_9)_3N(CH_2)_8N-(C_4H_9)_3^+$ , which he calls  $diBu^{2+}$ , is of interest as a model for two  $Bu_4N^+$  ions in the act of collision, *i.e.*, in a state of maximum overlap if they are in solution. We see from Table II that the enthalpy of the  $D_2O \leftarrow H_2O$  transfer for  $diBu^{2+}$  is the same as that for one  $Bu_4N^+$ , rather than two as one would expect if the structural effects of two  $Bu_4N^+$  did not interfere in the overlap configuration. A similar but less sharp conclusion is reached on the basis of the propylene carbonate  $\leftarrow H_2O$  transfers, for which  $\Delta H$  is 6.02 kcal/mol for  $diBu^{2+}$  and 4.39 kcal/mol for  $Bu_4N^+$ . By comparison with the systematic study of the enthalpies of transfer for this pair of solvents, it again seems clear that the structural effect for  $diBu^{2+}$  in water is significantly smaller than that for two  $Bu_4N^+$ .

*Acknowledgment.* We are grateful to Dr. D. Fennell Evans of Case-Western Reserve University for providing us with a sample of the salt  $diBuBr_2$  and to Dr. H. M. Feder of Argonne National Laboratory for the use of a copy of his Ph.D. dissertation.

(36) H. S. Frank, "Chemical Physics of Ionic Solutions," John Wiley and Sons, Inc., New York, N. Y., 1966, p 53.

(37) S. Lindenbaum and G. E. Boyd, *J. Phys. Chem.*, **68**, 911 (1964).

(38) F. Franks and D. J. G. Ives, *Quart. Rev. Chem. Soc.*, **20**, 1 (1966).

(39) W. Y. Wen and S. Saito, *J. Phys. Chem.*, **68**, 2639 (1964).

(40) R. H. Wood, H. L. Anderson, J. D. Beck, J. R. France, W. E. de Vry, and L. J. Stoltzberg, *ibid.*, **71**, 2149 (1967). See also Wood and Anderson, *ibid.*, **71**, 1869 (1967).

(41) T. L. Broadwater and D. F. Evans, *ibid.*, **73**, 164 (1969).

# Tunnel Effect, Infrared Continuum, and Solvate Structure in

## Aqueous and Anhydrous Acid Solutions

by Ilse Kampschulte-Scheuing and G. Zundel

*Physikalisch-Chemisches Institut, Universität München, Munich, West Germany (Received October 31, 1969)*

Continuous absorbance occurs in the ir spectrum of hydrous acid solutions, if the acid is dissociated. This indicates that the excess protons tunnel in hydrogen bonds between solvent molecules. A pair of bands shows whether the nondissociated acids are associated. If the solvent molecules have no hydrogen bond acceptors, the *p*-toluenesulfonic acid molecules, nondissociated and associated, are found. If the solvent molecules have acceptor groups, the acid is all the more disassociated and dissociated, the more basic the solvent molecules. The continuous absorbance shows that the tunnel protons have a continuous energy level distribution, *i.e.*, are in energy bands. Two mechanisms which give rise to the energy bands are discussed. The first is the interaction of the tunneling protons by proton dispersion forces and the second, the interaction of the tunneling protons with the Coulomb fields of the neighboring anions. A saturation effect of the intensity of the continuous absorbance in the case of the dimethyl sulfoxide (DMSO) solution is found. With solutions in water and in methanol, the continuous absorbance in the range 2500–650  $\text{cm}^{-1}$  is independent of the wave number. With the DMSO solution, however, the continuous absorbance shows a structure. This is explained by considering the nature of the solvate structure of the DMSO solution.

### Introduction

Continuous absorbance is observed in the ir spectra of hydrous solutions of acids and bases when dissociated<sup>1</sup> and also especially in the spectra of hydrated acidic and basic polyelectrolytes with dissociated groups.<sup>2–7</sup> This indicates that the protons and defect protons exist in energy bands.<sup>3</sup> This continuous absorbance is closely connected with the tunneling of the protons in hydrogen bonds of the hydrate structures. A proton tunneling in a hydrogen bond isolated from its environment leads merely to a splitting up of the energy levels but in no case to a continuity of levels. The continuity results because the tunneling of the proton is connected with a fluctuation of the electromagnetic field near the hydrogen bond. Neighboring tunneling protons are now coupled *via* these fluctuating fields.<sup>8</sup> This coupling *via* the so-called proton dispersion forces leads to a shifting or splitting up, respectively, of the energy levels of the tunneling protons. A second cause of the energy level shift of the tunneling protons is the interaction with the Coulomb fields of the neighboring anions.<sup>9</sup> The magnitude of the shifts and splitting up depend on the distance and orientation of the hydrogen bonds with the tunneling protons as well as on that of the anions and the hydrogen bonds with the tunneling protons. The distances and orientations have random statistical distributions in the solutions and with the polyelectrolytes. The distances of the energy levels thus also have a random statistical distribution, which leads to the continuous ir absorbance observed.

The proton dispersion forces, like the interaction of the tunneling protons with the anions, cause a decrease in the tunneling frequency which, however, does not

fundamentally affect the forces themselves. A more detailed discussion of the interplay of the proton dispersion forces and the anion fields on occurrence of the continuous absorbance is shortly to appear.

If acids such as toluenesulfonic acid, for instance, are not dissociated, a pair of bands is observed when the acid groups are associated. (One band in the range 3000–2700  $\text{cm}^{-1}$  and one in the range 2450–2150  $\text{cm}^{-1}$ .) These bands show that the acid groups are cross-linked *via* extremely strong hydrogen bonds.<sup>10</sup> These bonds are so strong, because on the one hand the hydrogen bond donor property of these OH acid groups is extremely large, and on the other the acceptor property of the two double-bonded O atoms of the  $-\text{SO}_2\text{OH}$  group is quite considerable. The latter ensues from the fact that the bonding electrons in this ion are rearranged when the corresponding excess proton approaches.<sup>11</sup>

(1) T. Ackermann, *Z. Phys. Chem.* (Frankfurt am Main), **27**, 253 (1961).

(2) G. Zundel, H. Noller, and G.-M. Schwab, *Z. Elektrochem.*, **66**, 129 (1962).

(3) G. Zundel and H. Metzger, *Z. Phys. Chem.* (Frankfurt am Main), **58**, 225 (1968).

(4) G. Zundel and H. Metzger, *Z. Naturforsch. A*, **22**, 1412 (1967).

(5) T. Ackermann, G. Zundel, and K. Zwernemann, *Z. Phys. Chem.* (Frankfurt am Main), **49**, 331 (1966).

(6) G. Zundel and H. Metzger, *Z. Phys. Chem.* (Leipzig), **240**, 50 (1969).

(7) G. Zundel, "Hydration and Intermolecular Interaction," Academic Press, Inc., New York, N. Y., 1969.

(8) E. G. Weidemann and G. Zundel, *Z. Phys.*, **198**, 288 (1967).

(9) E. G. Weidemann and G. Zundel, *Z. Naturforsch. A*, in press.

(10) G. Zundel, H. Metzger, and I. Scheuing, *Z. Naturforsch. B*, **22**, 127 (1967).

(11) G. Zundel, *Z. Naturforsch.*, **A**, **22**, 199 (1967).

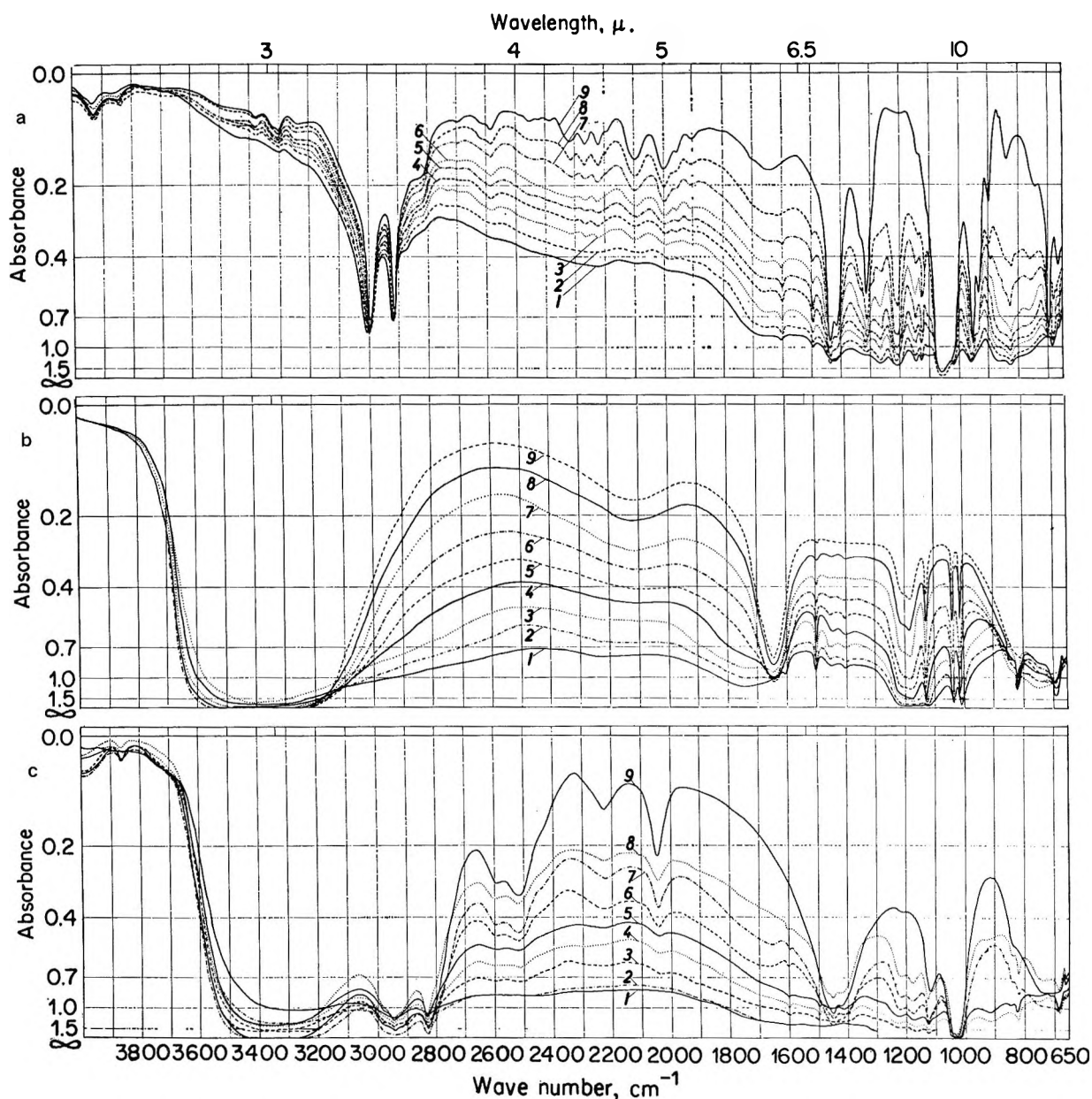


Figure 1. Ir spectra of solutions of *p*-toluenesulfonic acid in dependence on the concentration, at 30°: (a) solution in DMSO, thickness of film 10  $\mu$ , spectrum 1 saturated solution (3.29 *M*); spectra 1 to 8 decreasing concentration; 9 is the spectrum of the pure DMSO; (b) solution in H<sub>2</sub>O, thickness of film 5  $\mu$ , spectrum 1 saturated solution (5.08 *M*), spectra 1 to 9 decreasing concentration; (c) solution in CH<sub>3</sub>OH, thickness of film 10  $\mu$ , spectrum 1 (concentration 1.96 *M*); spectra 1 to 8 decreasing concentration; 9 is the spectrum of pure methanol.

Both bands are caused, according to Hadži, *et al.*,<sup>12,13a</sup> by the stretching vibration and by the overtone of the bending vibration of the OH group. These vibrations are coupled by Fermi resonance (for details see ref 13b).

The present work deals with continuous absorbance, the tunnel effect, the interaction of tunneling protons with their environment, and solvate structure of *p*-toluenesulfonic acid in water and in anhydrous solvents with and without hydrogen bond acceptors.

#### Hydrogen Bond Acceptors of the Solvent and Behavior of the Acids

If anhydrous *p*-toluenesulfonic acid is dissolved in CCl<sub>4</sub>, CHCl<sub>3</sub>, CH<sub>2</sub>Cl<sub>2</sub>, C<sub>6</sub>H<sub>6</sub>, C<sub>7</sub>H<sub>8</sub>, that is, in solvents

without hydrogen bond acceptors, the above-mentioned pair of bands<sup>10</sup> is always observed, thus indicating the association of the -SO<sub>2</sub>OH groups. According to this, the acid groups of the *p*-toluenesulfonic acid molecules are not dissociated in these solvents, but associated *via* extremely strong hydrogen bonds.

The picture is quite different in the case of solvents with hydrogen bond acceptors. A band at 907 cm<sup>-1</sup>, which is ascribed to the stretching vibration of the SO single bond in the nondissociated -SO<sub>2</sub>OH group<sup>11</sup> gives

(12) D. Hadži, *Pure Appl. Chem.*, **11**, 435 (1965).

(13) (a) D. Hadži and N. Kobilarow, *J. Chem. Soc.*, 439 (1966); (b) see ref 7, pp 124-142; (c) see ref 7, p 124 ff.

information on the dissociation. This band disappears with dissociation and thus constitutes a measure of the true degree of dissociation.<sup>7</sup> This band cannot be observed in the spectra of the solutions in dimethyl sulfoxide (DMSO) and water (Figures 1a-1c); accordingly almost all acid protons are removed from the anions also in the saturated solution at 25°. The spectra of the solutions in methanol show this band at 907 cm<sup>-1</sup>. It disappears with increasing dilution; *i.e.*, the acid groups dissociate increasingly. With concentrations greater than 1.96 M acid in methanol, one broad intensive band at about 2935 cm<sup>-1</sup> and one somewhat weaker at 2425 cm<sup>-1</sup> are found in the spectrum. (These spectra are not shown in Figure 1c.) These bands show that some acid groups are associated.<sup>13c</sup> The disassociation and dissociation of the acid in dioxane is even slighter. In general, the acid is the more disassociated and dissociated the more basic the solvent molecules are.

With these solvents the pK<sub>a</sub> values of the removal of the H<sup>+</sup> attached to the solvent molecules are very small and thus difficult to determine. Values of the DMSO are given by Andersen, *et al.*,<sup>14</sup> and Arnett.<sup>15</sup> With regard to the pK<sub>a</sub> value of water data are given in the publication of Arnett.<sup>15</sup> The pK<sub>a</sub> value of methanol was investigated by Weston, *et al.*<sup>16</sup> Unfortunately, the used methods are very different from one another. Consequently, these values are not comparable and can not be used in this work as a quantitative measure for the basicity.

In summary, we can state that the *p*-toluenesulfonic acid dissolves undissociated as an associate in solvents without hydrogen bond acceptors. Disassociation and dissociation occur in solvents with hydrogen bond acceptors. This disassociation and dissociation is larger, the greater the proton acceptor property, that is, the basicity of the solvent.

### Continuous Absorbance and Continuous Energy Level Distribution of Tunneling Protons in the Anhydrous Solutions

In Figures 1a and 1c, spectra 1 are the spectra of the anhydrous solution of *p*-toluenesulfonic acid in DMSO or methanol, respectively. The spectrum in Figure 2 is that of *p*-toluenesulfonic acid-*d*<sub>1</sub> in CH<sub>3</sub>OD. These figures show that the acid protons cause continuous absorbance in the anhydrous solutions, too. This begins, if H<sup>+</sup> is present, at 3200 cm<sup>-1</sup> and, insofar as D<sup>+</sup> is present, at 2400 cm<sup>-1</sup>, and extends to smaller wave numbers.

The acid protons removed from the anion form hydrogen bonds between DMSO or between methanol molecules, respectively. The continuous absorbance shows that the excess protons occur in continuous energy level distribution, *i.e.*, in energy bands. This continuity is caused, as previously discussed, by symmetrical hydrogen bonds with double minimum potential well

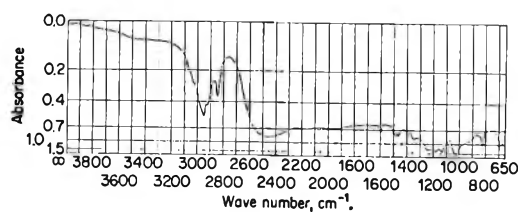


Figure 2. Ir spectrum of *p*-toluenesulfonic acid-*d*<sub>1</sub> in CH<sub>3</sub>OD.

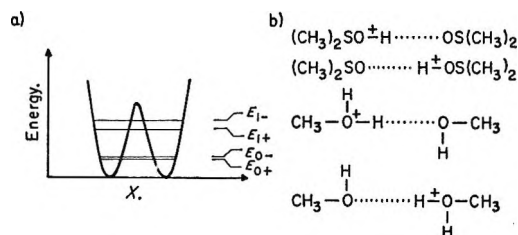


Figure 3. (a) Symmetric potential well with double minimum; (b) proton boundary structures.

(see Figure 3a) in which the proton tunnels. Therefore this hydrogen bond is represented by two proton boundary structures (Figure 3b).<sup>9</sup> Thus, with these systems, too, the fluctuating fields connected with the tunneling may cause proton dispersion forces which act between the groupings. A second cause of the continuity of energy levels is the interaction of the tunneling proton with coulomb fields of neighboring anions.

The result, that the acid proton is bound between the DMSO molecules and does not remain in a hydrogen bond between an oxygen atom of the -SO<sub>3</sub><sup>-</sup> ion and one DMSO molecule, is confirmed by the nature of the band of the antisymmetric stretching vibration of these ions observed at 1200 cm<sup>-1</sup>. In hydrous or hydroxylic solvents this band shows a doublet structure because the degeneracy is removed by varying degrees of interaction of the three oxygen atoms in hydrogen bonds.<sup>17a,b</sup> This band, however, does not show doublet structure in the case of the DMSO solution (Figure 1a). This tells us that the acid proton does not remain in a hydrogen bond between the -SO<sub>3</sub><sup>-</sup> ion and a DMSO molecule. According to the above, it must be bound in a hydrogen bond between the O atoms of two DMSO molecules.

### Concentration Dependence of Continuous Absorbance

Figures 1a-1c show that the absorbance of the continuous spectrum increases with increasing acid concentration. The concentration dependence for

(14) K. K. Andersen, W. H. Edmonds, J. B. Biasotti, and R. A. Strecker, *J. Org. Chem.*, **31**, 2859 (1966).

(15) E. M. Arnett, *Progr. Phys. Org. Chem.*, **1**, 283 (1963).

(16) R. E. Weston, S. Ehrenson, and K. Heinzinger, *J. Amer. Chem. Soc.*, **89**, 481 (1967).

(17) (a) G. Zundel and A. Murr, *Z. Naturforsch.*, **A**, **21**, 1640 (1966); (b) see ref 7, pp 37 ff and p 172; (c) see ref 7, pp 119 ff.

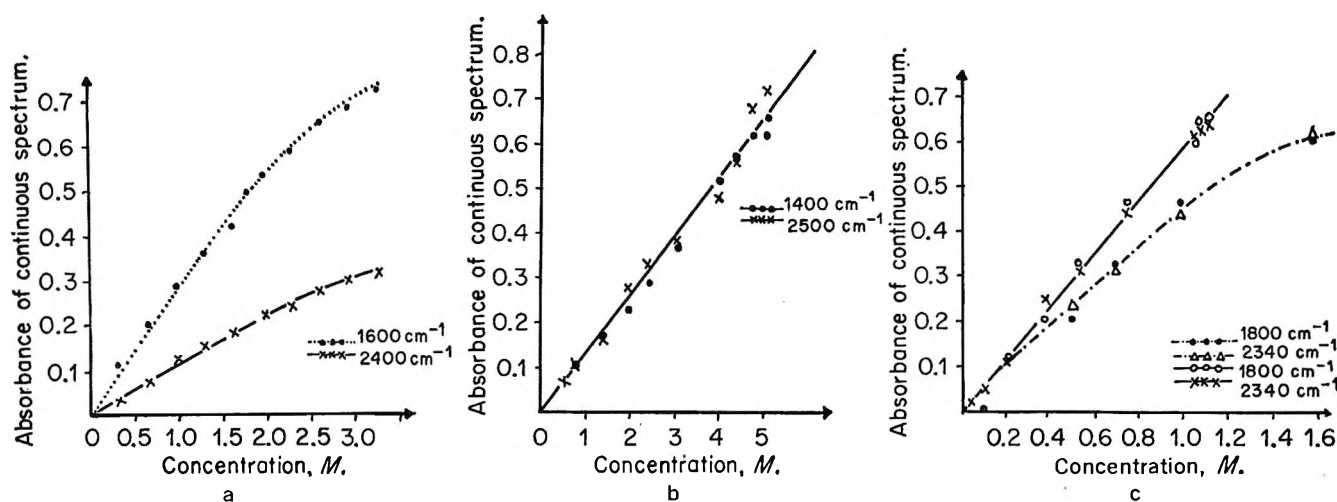


Figure 4. Absorbance of the continuous spectrum of the solution of *p*-toluenesulfonic acid in dependence on the molar concentration: (a) Solution in DMSO; (b) Solution in H<sub>2</sub>O; (c) Solution in CH<sub>3</sub>OH.

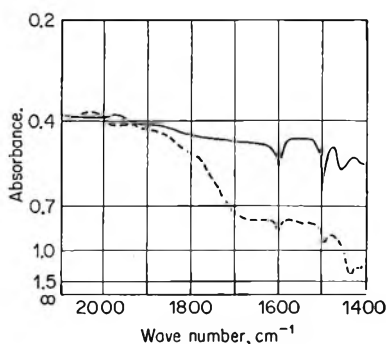


Figure 5. Ir spectra; ---, *p*-toluenesulfonic acid in DMSO; —, *p*-toluenesulfonic acid-*d*<sub>1</sub> in (CD<sub>3</sub>)<sub>2</sub>SO.

various wave numbers is plotted in Figures 4a–4c. The wave numbers used for evaluation were so chosen that a superposition of the continuous absorbance by solvent bands was avoided as far as possible. The absorbance of the continuous spectrum dependent on the concentration of the tunneling protons and not of the acid concentration is of interest. In DMSO and in H<sub>2</sub>O the acid is almost wholly dissociated; thus these two concentrations are equal. In CH<sub>3</sub>OH at higher concentrations the dissociation is incomplete. The concentration of dissociated acid groups and hence the concentration of tunneling protons can be calculated from the integral absorbance of the 907-cm<sup>-1</sup> band.<sup>17c</sup> The absorbance of the continuous spectrum dependent on the calculated tunneling proton concentrations is shown as the points on the straight line in Figure 4c.

Figure 4 demonstrates the following findings: first, with H<sub>2</sub>O and CH<sub>3</sub>OH solutions the absorbance of the continuous spectrum increases in linear proportion to the concentration of the tunneling protons in the concentration range shown in Figure 4 (in the case of H<sub>2</sub>O up to the saturated solution). Second, in the case of the solution in DMSO a linear relationship is found up

to a concentration of the tunneling protons of approximately 2 *M*; then the slope diminishes subsequently.

The linear increase is immediately comprehensible. The absorptivity coefficient of the tunneling protons is independent of the concentration in the concentration range investigated in the case of the H<sub>2</sub>O and methanol solutions. The same holds good for the solution in DMSO with concentrations up to 2 *M*. With larger concentrations, however, the absorbance per tunneling proton decreases as the concentration increases. A saturation effect of the absorbance of the continuous spectrum is observed. A similar saturation effect was studied in detail with polystyrenesulfonic acid.<sup>18a,b</sup>

### Structure of the Continuous Absorbance

With the solution in water or methanol, respectively, the absorbance of the continuous spectrum is independent of the wave numbers in the range 2500–650 cm<sup>-1</sup>; this can be seen from Figures 1b and 1c as well as from Figures 4b and 4c. Contrary to this, in the solution in DMSO the continuous absorbance in the range of large wave numbers is considerably smaller than in the range of smaller wave numbers; thus it shows a distinct structure; this is illustrated by Figures 1a and 4a. The rise in intensity of the continuous absorbance of the DMSO solution at about 1600 cm<sup>-1</sup> with decreasing wave numbers is caused by the tunneling protons since it cannot be observed when, instead of tunneling protons, tunneling deuterons are present (see Figure 5). Then, a rise at about 1200 cm<sup>-1</sup> is found, however, largely masked by the SO bands. The rise observed in the spectra of the solution in methanol results from the extremely widened OH bending vibration of the methanol molecules. This finding, that the continuous spectrum with the DMSO solution has a structure, con-

(18) (a) G. Zundel and H. Metzger, *Z. Phys. Chem. (Leipzig)*, **235**, 33 (1967); (b) see ref 7, pp 187–192.

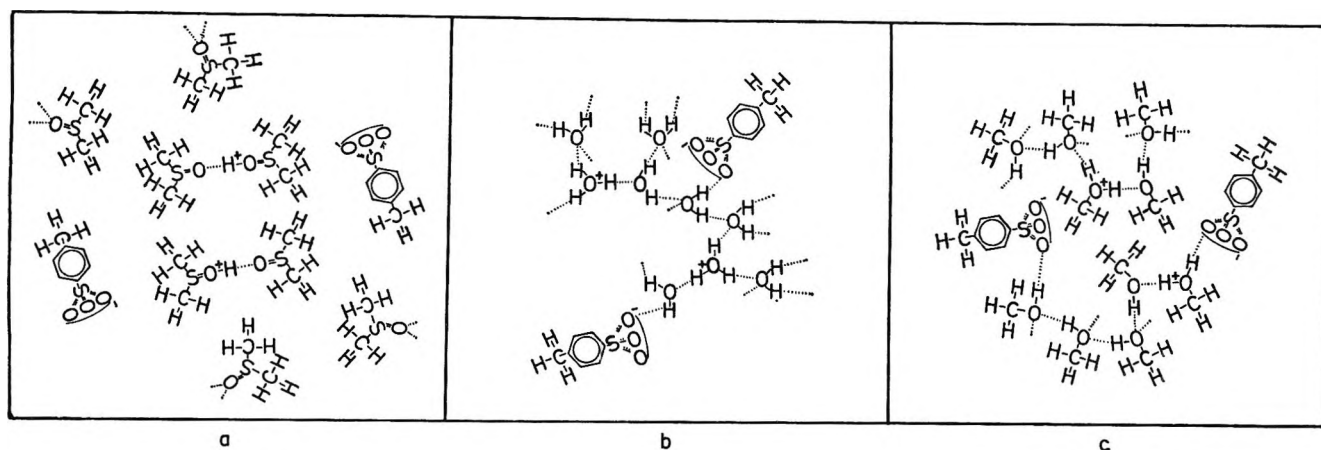


Figure 6. Solvate structures of solutions of *p*-toluenesulfonic acid in: (a) DMSO, (b) H<sub>2</sub>O, (c) CH<sub>3</sub>OH. In considering such schematic representations, we should keep in mind the fact that the solvate structures are continually being rearranged by thermal motions.<sup>19-22</sup> Any attachment position is in dynamic equilibrium with analogous alternative positions. Thus the pictures show temporary equilibrium configurations.

trary to the water and methanol solution, can easily be understood when comparing the nature of the solvate structures in Figure 6.<sup>19-22</sup>

In the hydrous solution, the excess proton tunnels in the hydrogen bond of H<sub>5</sub>O<sub>2</sub><sup>+</sup> or bonds of H<sub>3</sub>O<sub>4</sub><sup>+</sup>, respectively.<sup>23a</sup> The external water molecules of this grouping are linked *via* hydrogen bonds with further water molecules or acceptor groups of anions (Figure 6b).<sup>23b</sup> The network of the solvate structure of the CH<sub>3</sub>OH solution does not differ considerably from that of the hydrous solution, since in the spectra—as shown in Figure 1c—no band of the stretching vibration of free OH groups occurs, *i.e.*, of groups not bound in hydrogen bonds. Thus, as in the case of the hydrous solution, the groupings around the tunneling excess proton are linked with further CH<sub>3</sub>OH molecules or acceptor groups of anions. The linking of the H<sub>2</sub>O and CH<sub>3</sub>OH molecules with the anions is indicated by the doublet structure of the band of the antisymmetric stretching vibration of the anions at 1200 cm<sup>-1</sup> (Figures 1b and 1c); this splitting up—as already mentioned above—is brought about by the elimination of the degeneracy of this vibration. The elimination of the degeneracy, however, results from the varying engagement of the individual O atoms of the -SO<sub>3</sub><sup>-</sup> ions with hydrogen bonds of the solvate structure and thus indicates the linking of anions with the CH<sub>3</sub>OH molecules.

The nature of the solvate structure of the DMSO solution differs considerably from this as indicated by this band too, since in this case the band at 1200 cm<sup>-1</sup> has no doublet structure (Figure 1a). Following this, the DMSO-H<sup>+</sup>-DMSO complexes are not cross-linked (Figure 6a). Contrary to the solution in H<sub>2</sub>O and CH<sub>3</sub>OH in the DMSO solution no steric constraint is exerted by the network of the hydrogen bonds on the groupings with the tunneling excess proton. The groupings with the tunneling protons are therefore

able to orient themselves to one another and to the anions. Therefore, however, more definite distances and orientations occur preferably. A random statistical distribution of distances and orientations is, however, a necessary requisite for the occurrence of a continuity of energy levels. This is seen on examining the equations for the energy level shifts by the proton dispersion forces<sup>24</sup> or by the influence of electric fields<sup>9</sup> of neighboring anions on the bonds with tunneling protons. The magnitude of the shift, for example, of the lowest energy level of a pair of hydrogen bonds with tunneling protons by the proton dispersion forces is according to ref 8 or ref 7, p 205

$$\Delta E = h\nu_0 \left[ 1 - \sqrt{1 + \left( \frac{p^2}{\epsilon h\nu_0 R^3} g \right)^2} \right]$$

where  $\nu_0$  is the tunnel frequency,  $p$  the dipole moment of a proton boundary structure,  $\epsilon$  the dielectric constant of the medium between the tunneling protons (if the tunnel frequencies are high, the optical dielectric constant is decisive).  $g$  is a factor which considers the orientation of the hydrogen bridges to one another. It assumes values at the interval  $2 \geq g \geq -2$ ;  $R$  is the distance of the bridges between the tunneling protons. In Figure 7 the energy levels are plotted as a function of the distance of the bridges for a pair of bridges with tunneling protons.<sup>7,8</sup> If the distance  $R$  and the orientation factor  $g$  has an accumulation value for certain

(19) T. J. Swift and R. E. Connick, *J. Chem. Phys.*, **37**, 307 (1962).

(20) H. G. Hertz and M. D. Zeidler, *Ber. Bunsenges. Phys. Chem.*, **67**, 774 (1963).

(21) H. G. Hertz and M. D. Zeidler, *ibid.*, **68**, 821 (1964).

(22) M. Eigen, *Pure Appl. Chem.*, **6**, 97 (1963).

(23) (a) See ref 7, p 166 and 179; (b) see ref 7, p 180 ff.

(24) See ref 7, pp 203, 205, and 210.

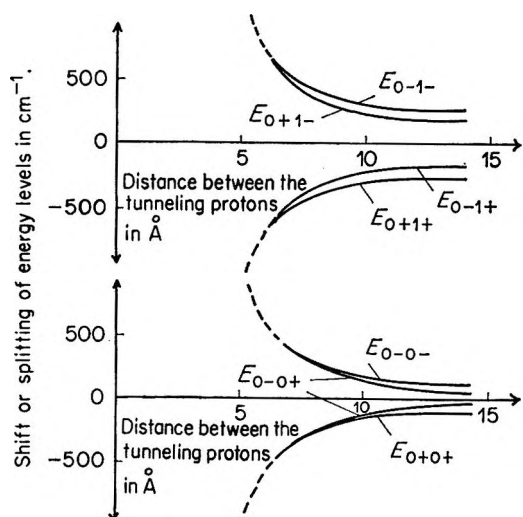


Figure 7. Shift or splitting, respectively, of the energy levels of a pair of tunneling protons in dependence on the distance of the hydrogen bonds (after ref 7).  $o\pm o-$  means, for instance, that one proton is in the state  $\psi_{o+}$  and the other in the state  $\psi_{o-}$ .

distances and orientations, the energies of the individual transitions have accumulation values as well.

Therefore, if—as in the DMSO solution—no steric constraint is exerted on the groupings with the tunneling protons by the solvate structure network, the former can orient themselves more definitely in relation to their environment. Thus more definite distances and orientations are preferred, resulting in accumulation values of certain wave numbers. Thus the continuous absorbance, however, exactly as observed with the DMSO solutions, is given a structure.

### Experimental Procedure

The anhydrous *p*-toluenesulfonic acid was produced from the commercial monohydrate by drying under vacuum at 40°. After approximately 130 hr a constant pressure of  $5 \times 10^{-5}$  Torr sets in. This indicates complete drying.

The *p*-toluenesulfonic acid- $d_1$  was produced by repeated treatment of dry *p*-toluenesulfonic acid with  $D_2O$  and subsequent drying.  $CH_3OH$  and DMSO were dried over a 3-Å molecular sieve. In the case of DMSO, the molecular sieve must be replaced once or twice. Towards the end of the drying process, warming must be undertaken for some hours with the DMSO.

The solutions were examined in an ir cell with variable thickness of the film. This cell was improved as against the usual type in the following way. The cell windows consist of germanium. In order to prevent loss by absorption, this must be *n*-dotted (specific resistance > 50 ohm cm). The cell is completely lined with platinum, thus eliminating any acid corrosion. A vernier with 51 divisions permits a precise adjustment for the thickness of the film. A Teflon O ring with a groove ensures that the cell is well sealed. The cell is fitted outside with a channel all round which allows thermostatisation of the cell by circulating water. All spectra are for 30°.

The measurements were effected with the Perkin-Elmer ir double-beam spectrophotometer Model 221. On account of the high loss of reflection of the germanium slit program 980 was used. Registering speed amounted to one wave number per second. The sensitivity was checked during plotting of the spectra. In order to eliminate loss of energy through absorption of the water vapor in the air, the spectrophotometer was flushed with dry air. The spectra drawings are corrected by a calibration curve plotted with the help of the values given in ref 25.

*Acknowledgment.* We should like to express our thanks to Dr. E. G. Weidemann of the Institute for Theoretical Physics, Munich University, for many valuable discussions. Our thanks are also due to the Deutsche Forschungsgemeinschaft and the Fraunhofer Gesellschaft for providing the facilities for this work, and to the VW-Stiftung for a grant.

(25) "Tables of Wave Numbers for Calibration of Infrared Spectrometers" Butterworth and Co., London, 1961.



# Hydrogen Bonding in Primary Alkylammonium-Vermiculite Complexes

by R. H. Laby and G. F. Walker<sup>1</sup>

*Divisions of Applied Mineralogy and Animal Physiology, Chemical Research Laboratories, Melbourne, Australia  
(Received June 23, 1969)*

X-Ray and infrared data reveal that, in the complexes formed by alkylammonium ions with a vermiculite from Kenya, the ions may adopt two different conformations. In the first, found in the series octylammonium to octadecylammonium, the alkyl chains extend in the *trans-trans* conformation at an angle of  $56^\circ$  to the silicate layer plane, and with the C-N bond perpendicular to it. In the second, found in the ethylammonium to hexylammonium complexes, the *trans-trans* conformation is not preserved, nor is the C-N bond perpendicular to the layer plane. The orientation of the cations is determined by van der Waals interactions between adjacent alkyl chains rather than by hydrogen bonding to the surface. The hydrogen bonds are weak in both series of complexes, but weaker in the second group where the C-N bond is not perpendicular. The reasons for the weak hydrogen bonding observed in these and related systems are examined.

## Introduction

Hydrogen bonding reduces the X-Y distance in X-H...Y below the van der Waals contact distance between X-H and Y, and it is generally accepted that, other things being equal, the strength of the bond is inversely related to the X-Y distance. Inferences regarding the strength of hydrogen bonding between *n*-alkylammonium cations and layer silicates have been made on the basis of X-ray diffraction determinations of N-O bond lengths.<sup>2a,b</sup> However, strong electrostatic attraction between the adsorbed cations and the anionic silicate layers prohibits the unambiguous assignment of a shortened N-O approach distance to hydrogen bonding. Further evidence, particularly related to the energy or spatial environment of the hydrogen, is required. This paper reviews the literature relevant to the subject and reports the results of an infrared study of certain alkylammonium-vermiculite complexes.

## Review

The factors contributing to the formation of hydrogen bonds in ammonium salts were discussed by Chenon and Sandorfy.<sup>3</sup> The major contribution is from an electrostatic component N-H<sup>+</sup>...X<sup>-</sup> and, in general terms, the hydrogen bond is expected to be comparatively weak if the negative charge on X<sup>-</sup> is delocalized among a number of centers as in a complex anion. Waddington<sup>4</sup> studied the hydrogen bonding of a range of ammonium salts, and his results substantiate the above generalization. For example, ammonium fluoride, chloride, bromide, nitrite, and nitrate are hydrogen bonded, while the fluoroborate, NH<sub>4</sub>BF<sub>4</sub>, and fluorophosphate, NH<sub>4</sub>PF<sub>6</sub>, are relatively free. Subsequent work extends the list of ammonium salts for which data on hydrogen bonding, including nmr and neutron scattering, are available (Table I).

In Table I,  $\Delta\nu$  is the depression in  $\nu_3$  below 3332 cm<sup>-1</sup> (taken as the frequency of a "free" ammonium

ion<sup>4</sup>) for the ammonium salts given. The salts are divided into two main groups: the first where the barrier to rotation of the ammonium ion is less than 1.5 kcal/mol and the second where the barrier is near 4.0 kcal/mol, as determined from nmr or neutron scattering data. The references in the first column of Table I after the salt formulas refer to estimations of barrier height. While ammonium perchlorate is here included in the first group of salts, one of the five authorities quoted gives its barrier height as 2.0 kcal/mol.<sup>5</sup> However, this last estimate is questioned by Rush, Taylor, and Havens.<sup>6</sup>

Relatively weakly restricted rotation, as for example in the groups ia and ib salts of Table I, is not a reliable criterion for weak hydrogen bonding, as the close proximity of negative centers could result in the existence of low rotational barriers between nearly equivalent and relatively strongly attracting hydrogen bond acceptors. However, when the data of Table I are considered together, the group i salts are distinguished from the group ii with a consistency that strongly suggests that these groups are, respectively, weakly and strongly hydrogen-bonded salts.

The data of Table I suggest that hydrogen bonding in ammonium salts is weak or absent (1) when single electronic charge of the anion is distributed among 3.5-4 or more centers, (2) when the N-O distance of oxyanion salts is greater than 2.9 Å, and (3) when  $\Delta\nu$  is less than 160-180 cm<sup>-1</sup>. This last value is large when compared with depressions in O-N or N-H stretching frequencies for weak O-H...O or other

(1) Deceased February 17, 1970.

(2) (a) A. Weiss, *Chem. Ber.*, **91**, 487 (1958); (b) D. J. Haase, E. J. Weiss, and H. Steinfink, *Amer. Mineral.*, **48**, 261 (1963).

(3) B. Chenon and C. Sandorfy, *Can. J. Chem.*, **36**, 1181 (1958).

(4) T. C. Waddington, *J. Chem. Soc.*, 4340 (1958).

(5) J. A. Ibers, *J. Chem. Phys.*, **32**, 1448 (1960).

(6) J. J. Rush, T. I. Taylor, and W. W. Havens, Jr., *ibid.*, **37**, 234 (1962).

**Table I:** Depression in  $\nu_3^a$  and N-O Distance in a Range of Ammonium Salts

Salt	$\Delta\nu$ , cm <sup>-1</sup>	N-O, Å
(ia) Salts with NH <sub>4</sub> <sup>+</sup> rotational barrier less than 0.7 kcal/mol		
NH <sub>4</sub> PF <sub>6</sub> <sup>b,c</sup>	2 <sup>a</sup>	
NH <sub>4</sub> ClO <sub>4</sub> <sup>b,d-f,h</sup>	42 <sup>a</sup>	2.89 <sup>d</sup>
(ib) Salts with NH <sub>4</sub> <sup>+</sup> rotational barrier between 0.7 and 1.5 kcal/mol		
(NH <sub>4</sub> ) <sub>2</sub> S <sub>2</sub> O <sub>8</sub> <sup>e,d</sup>	72 <sup>i</sup>	3.18 <sup>d</sup>
(NH <sub>4</sub> ) <sub>2</sub> Cr <sub>2</sub> O <sub>7</sub> <sup>d,h,l</sup>	162 <sup>i</sup>	3.18 <sup>d</sup>
NH <sub>4</sub> SO <sub>3</sub> F <sup>c</sup>	182 <sup>a</sup>	
(ii) Salts with NH <sub>4</sub> <sup>+</sup> rotational barrier near 4.0 kcal/mol		
NH <sub>4</sub> CNS <sup>e,l</sup>	182 <sup>i</sup>	
NH <sub>4</sub> SeO <sub>4</sub> <sup>d</sup>	192 <sup>i</sup>	
NH <sub>4</sub> ClO <sub>4</sub> <sup>d</sup>	202 <sup>j</sup>	
(NH <sub>4</sub> ) <sub>2</sub> CrO <sub>4</sub> <sup>e,e,l</sup>	212 <sup>i</sup>	2.60 <sup>d</sup>
(NH <sub>4</sub> ) <sub>2</sub> SO <sub>4</sub> <sup>h</sup>	232 <sup>k</sup>	2.66 <sup>d</sup>

<sup>a</sup> Following Waddington<sup>4</sup> taking  $\nu_3 = 3332$  cm<sup>-1</sup> for free NH<sub>4</sub><sup>+</sup>. <sup>b</sup> J. A. Janik, J. M. Janik, J. Mellor, and H. Palevsky, *J. Phys. Chem. Solids*, **25**, 1091 (1964). <sup>c</sup> V. Brajovic, H. Boutin, G. J. Safford, and H. Palevsky, *ibid.*, **24**, 617 (1963); also J. J. Rush, G. J. Safford, T. I. Taylor, and W. W. Havens, Jr., *Nucl. Sci. Eng.*, **14**, 339 (1962). <sup>d</sup> R. E. Richards and T. Schaefer, *Trans. Faraday Soc.*, **57**, 210 (1961). <sup>e</sup> Reference 6. <sup>f</sup> Ibers<sup>6</sup> gives the barrier to reorientation as 2.0 kcal/mol. <sup>g</sup> K. Venkatesan, *Proc. Indian Acad. Sci., Section A*, **46**, 134 (1957). <sup>h</sup> P. S. Leung, T. I. Taylor, and W. W. Havens, Jr., *J. Chem. Phys.*, **48**, 4912 (1968). <sup>i</sup> F. A. Miller and C. H. Wilkins, *Anal. Chem.*, **24**, 1253 (1952). <sup>j</sup> H. Siebert, *Z. Anorg. Allg. Chem.*, **303**, 162 (1960). <sup>k</sup> R. Blinc and I. Levstek, *J. Phys. Chem. Solids*, **12**, 295 (1960). <sup>l</sup> J. J. Rush, *Bull. Amer. Phys. Soc.*, **9**, 623 (1964).

N-H...O bonds<sup>7</sup> and suggests that the depression in N-H stretching frequency, when considered alone, is not a reliable criterion of hydrogen bond strength, probably because of the complexity of the band envelope near 3200 cm<sup>-1</sup>, containing  $\nu_3$  and overtone and combination bands.

The electrostatic component N-H<sup>+</sup>...X<sup>-</sup>, which is the major contributor to hydrogen bond formation in ammonium salts,<sup>3</sup> is probably of comparable significance in substituted ammonium salts, and therefore similar relationships are to be expected for alkylammonium salts. Kynaston, Larcombe, and Turner<sup>8</sup> and Nuttall, Sharp, and Waddington<sup>9</sup> reported that methylammonium fluoroborate was not hydrogen bonded. Cabana and Sandorfy<sup>10</sup> discussed the hydrogen bonding in solid methylammonium halides which was of the NH<sup>+</sup>...X<sup>-</sup> type and medium strong to strong in the fluoride salt.

Ammonium ions are not hydrogen bonded to the surface oxygens of layer silicates. The depression in  $\nu_3$  in ammonium rectorite<sup>11</sup> and ammonium montmorillonite<sup>12</sup> is 52 cm<sup>-1</sup>. Also the N-O distance in ammonium vermiculites is 3.26<sup>13</sup> and 3.18 Å.<sup>2a</sup> The negative charge due to isomorphous replacement could

not be associated with less than six oxygens—those surrounding the hexagonal holes into which the ammoniums key. These considerations clearly place the ammonium complexes in the first group of oxyanion salts of Table I.

In the light of the discussion thus far, strong hydrogen bonding of alkylammonium ions in layer silicate complexes to the silicate oxygens would not be expected. Weiss<sup>2a</sup> gives the N-O distance in hexylammonium batavite as not less than 2.85 Å and Haase, Weiss, and Steinfink<sup>2b</sup> report 2.82 Å as the minimum distance in hexamethylenediammonium vermiculite. These distances, when compared with those of Table I, are not consistent with strong hydrogen bonding.

Other recent infrared data for hydrogen bond proton donors adsorbed on a range of silicate adsorbents<sup>14-16</sup> show that hydrogen bonding to the siloxane surface is at best weak. An exception to this appears to be the strong bonding of water molecules (one per cavity) in natrolite revealed by neutron scattering.<sup>17</sup> The same authors contrasted this result with the neutron scattering data for water in the cavities of chabazite, containing some 20 molecules each. In this system, hydrogen bonding was predominantly between the water molecules themselves.

### Experimental Section

Oriented films of a vermiculite from Kenya<sup>18</sup> were prepared by slow evaporation of aqueous dispersions of the butylammonium complex.<sup>19</sup> Films of approximately 8  $\mu$  (2.0 mg/cm<sup>2</sup>) thickness were prepared, and it was found that the infrared spectra of adsorbed alkylammonium ions were of adequate intensity without being masked in the regions of interest by the adsorption bands of the mineral itself.

Alkylammonium halide solutions were prepared, and exchange reactions with the films were performed according to the methods described by Walker.<sup>20</sup>

- (7) K. Nakamoto, M. Margoshes, and R. E. Rundle, *J. Amer. Chem. Soc.*, **77**, 6480 (1955).
- (8) W. Kynaston, B. E. Larcombe, and H. S. Turner, *J. Chem. Soc.*, 1774 (1960).
- (9) R. H. Nuttall, D. W. A. Sharp, and T. C. Waddington, *ibid.*, 4965 (1960).
- (10) A. Cabana and C. Sandorfy, *Spectrochem. Acta*, **18**, 843 (1962).
- (11) J. D. Russell and J. L. White, Proceedings of the 14th National Clays Conference, 1965, p 181 (published 1966).
- (12) M. M. Mortland, J. J. Fripiat, J. Chaussidon, and J. B. Uytterhoeven, *J. Phys. Chem.*, **67**, 248 (1963).
- (13) W. D. Johns and P. K. Sen Gupta, *Amer. Mineral.*, **52**, 1706 (1967).
- (14) K. Wada, *Clay Science*, **2**, 43 (1964).
- (15) H. P. Boehm, *Angew. Chem. Intern. Ed. Engl.*, **5**, 533 (1966).
- (16) A. V. Kiselev, *Zh. Fiz. Khim.*, **41**, 2470 (1967) (transl. p 1338).
- (17) H. Boutin, H. Prask, and R. D. Iyengar, *Advan. Colloid Interface Sci.*, **2**, 1 (1968).
- (18) A. McL. Mathieson and G. F. Walker, *Amer. Mineral.*, **39**, 231 (1954).
- (19) G. F. Walker and W. G. Garrett, *Science*, **156**, 385 (1967).
- (20) G. F. Walker, *Clay Mineral.*, **7**, 129 (1967).

**Table II:** Peak Frequencies and the Mean Frequency in the N-H Stretching Region ( $\nu$  N-H,  $\text{cm}^{-1}$ ), Absorption Frequency for the N-H Symmetric Deformation Mode ( $\delta_s$  N-H,  $\text{cm}^{-1}$ ), and Its Intensity Variation with Film Orientation ( $d(001)$  spacing ( $\text{\AA}$ ) for the Alkylammonium-Vermiculite Complexes Studied)

Exchange cation	$\nu$ N-H absorptions, $\text{cm}^{-1}$	Mean $\nu$ N-H, $\text{cm}^{-1}$	$\delta_s$ N-H, $\text{cm}^{-1}$	Intensity variation	$d(001)$ , $\text{\AA}$	
					Obsd	Calcd <sup>a</sup>
Methylammonium	3065, <i>3175</i> , 3245	3162	1508	Small	12.4	12.3
Ethylammonium	3065, <i>3185</i> , 3245	3165	1500	Small	12.6	13.2
Propylammonium	<i>3065</i> , 3170, 3245	3160	1505	Small	12.8	14.2
Butylammonium	3070, <i>3175</i> , 3250	3165	1504	Small	13.2	15.2
Hexylammonium	3055, <i>3175</i> , 3245	3158	1506	Small	16.3	17.1
Octylammonium	3050, <i>3165</i> , 3230	3148	1540	Large	19.0	19.0
Decylammonium	3050, <i>3160</i> , 3235	3148	1540	Large	21.0	21.0
Dodecylammonium	3040, <i>3160</i> , 3235	3145	1550	Large	23.0	22.9
Octadecylammonium	<i>3055</i> , 3158, 3235	3149	1545	Large	28.5	28.8
Butylammonium <sup>b</sup>	3035, <i>3185</i> , 3255	3158	1535	Large	21.0	21.2

<sup>a</sup> Calculated values obtained by the method of Walker.<sup>20</sup> <sup>b</sup> Expanded to the double-layer complex with butylamine.

Sealed cells were used when studying adsorption of butylamine by butylammonium vermiculite, and the films were dried at 80° overnight prior to study.

Infrared spectra were obtained with a Perkin-Elmer 521 grating spectrometer, with the incident beam set at 90° and at 45° to the plane of the film.

X-Ray data were obtained using a Philips PW 1055 diffractometer and Cu K $\alpha$  radiation.

## Results and Discussion

The results of X-ray diffraction and infrared determinations are summarized in Table II. The infrared data given are the peak frequencies of the three absorption bands in the N-H stretching ( $\nu$  N-H) region and the arithmetic mean of the three frequencies for each complex studied. The italicized frequency is the adsorption band of highest intensity in each group of three. Also given is the peak frequency for the N-H symmetric deformation mode ( $\delta_s$  N-H) and the intensity variation with film orientation in the infrared beam for this absorption. Too much band overlap occurred for a quantitative assessment of intensity variation, and "small" in Table II refers to intensity increases of less than 20% on turning the film from the 90° to the 45° orientation. "Large" refers to intensity increases of greater than 50% or, more usually, to the appearance of a new band. The resultant change in dipole moment for  $\delta_s$  N-H would be closely parallel to the C-N bond, and consequently intensity variation for film orientations of 90° and 45° to the incident beam would be greatest for those complexes where the C-N bond is perpendicular to the aluminosilicate layer. For similar reasons, the symmetric NH stretching mode ( $\nu_s$  N-H) might be expected to show intensity variation with film angle. However, none of the three absorptions in the N-H stretching region showed comparable intensity variation, indicating that the absorption in this region is complex. It is probably made up of  $\nu_{as}$  N-H and  $\nu_s$  N-H, and the first overtones

of  $\delta_s$  N-H and  $\delta_{as}$  N-H. Alternatively,  $\nu_s$  N-H may be partly concealed by the  $\nu$  C-H absorptions which, however, also show no intensity variations with film angle.  $\delta_{as}$  N-H is not included as it is partly obscured by O-H absorption bands near 1630  $\text{cm}^{-1}$ . The spectra of the complexes from octylammonium to octadecylammonium contained weak shoulders near 1500  $\text{cm}^{-1}$  on the stronger 1545- $\text{cm}^{-1}$  absorptions. The shoulders showed no intensity variation with film angle.

The X-ray data of Table II for the octylammonium to octadecylammonium complexes coincide with those given by Walker<sup>20</sup> for the corresponding complexes of a vermiculite from Texas and of batavite and mica. The idealized arrangement of the interlayer alkylammonium ions in these complexes is depicted schematically in Figure 1. The ammonium groups key into the silicate layer surfaces with the C-N bond perpendicular to the layer plane and the alkyl chains at an angle of 56° in the *trans-trans* conformation, thus forming an interpenetrating monolayer in which adjacent chains are in van der Waals contact. In micas, which have a surface charge density of 1 equiv per  $\text{O}_{10}(\text{OH})_2$  formula unit, the idealized arrangement is realized. With vermiculites, however, the surface charge density and hence the interlayer cation population, although variable, is always lower, and the interpenetrating monolayer is consequently less than close packed. With high-charge vermiculites there is still a sufficient population of alkyl chains interacting with one another to maintain the *trans-trans* conformation. Low-charge vermiculites (near 0.55 equiv per formula unit) on the other hand, give X-ray diffraction evidence indicating that rotations of chain segments and/or tilting of chains has occurred.<sup>20</sup> The Kenya vermiculite used in the present work has a moderately low charge density of 0.65 equiv per formula unit, and its ethylammonium to hexylammonium complexes give X-ray spacings lower than the maximum values (Table II, columns 6 and 7). Since van der Waals inter-

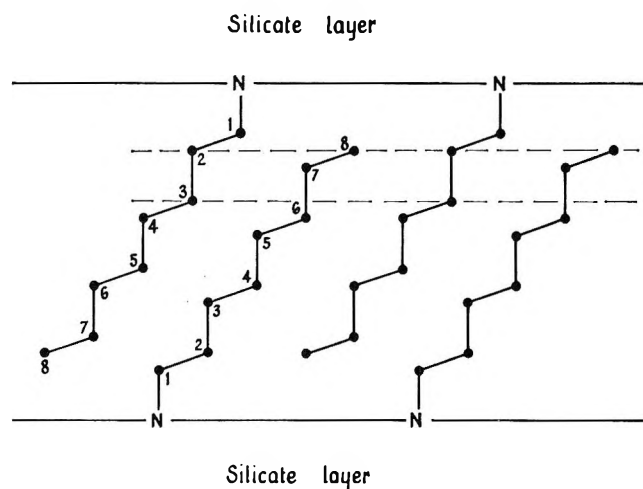


Figure 1. Diagram of the *n*-octylammonium-vermiculite complex (idealized), showing the interpenetrating monolayer of *n*-alkylammonium ions attached to opposite silicate layer surfaces. The C-N bond is perpendicular to the silicate layer plane.  $\text{NH}_3^+$  groups ionically bonded to the surface are indicated by N.

action increases with chain length, the development of the *trans-trans* conformation would be expected to occur in the complexes at some point in the homologous series depending on the charge density of the mineral. For Kenya vermiculite, this point is near hexylammonium (Table II).

When butylammonium vermiculite adsorbed butylamine from the vapor phase, the intercalated material formed a double layer with the spaces between butylammonium ions occupied by butylamine molecules. Comparison of the observed and calculated X-ray spacings (Table II) shows that the *trans-trans* conformation has developed as expected.

The infrared data of Table II reveal that there are two distinct environments in the exchange complexes for the  $\text{NH}_3^+$  group. One (environment I) is present in methylammonium to hexylammonium vermiculite and is characterized by a mean  $\nu$  N-H of  $3162 \pm 4 \text{ cm}^{-1}$ , a mean  $\delta_s$  N-H frequency of  $1505 \pm 5 \text{ cm}^{-1}$ , and the angle of the C-N bond significantly less than  $90^\circ$  to the silicate surface. The other (environment II), present in octylammonium to octadecylammonium vermiculite and in butylammonium vermiculite expanded with butylamine, is characterized by a mean  $\nu$  N-H of  $3150 \pm 8 \text{ cm}^{-1}$ , a mean  $\delta_s$  N-H of  $1545 \pm 5 \text{ cm}^{-1}$  and the C-N bond perpendicular to the silicate surface. It is possible that both environments exist in the latter group of complexes, as the shoulder at  $1500 \text{ cm}^{-1}$  is present in all the relevant spectra. In environment I, the plane of three ammonium hydrogens is not parallel to the silicate layer, while in environment II it is parallel, the  $\text{NH}_3^+$  group being keyed more symmetrically into the "hexagonal hole" (in reality a di-trigonal cavity<sup>21</sup>) of the oxygen surface.

Fripiat, Servais, and Leonard<sup>22</sup> observed that  $\delta_s$  N-H for propylammonium and butylammonium montmorillonite was near  $1504 \text{ cm}^{-1}$ , and for ethylenediammonium and propylenediammonium montmorillonite near  $1535 \text{ cm}^{-1}$ . The  $\text{NH}_3^+$  groups may therefore be in environments I and II in the alkylammonium and alkylenediammonium montmorillonite complexes, respectively.

Hydrogen bonding to the silicate surface is probably weaker in environment I than in II since, in the former, at least one of the three hydrogens must be positioned further from the oxygens of a hexagonal cavity than the remainder. The lower (by  $12 \text{ cm}^{-1}$ ) mean  $\nu$  N-H of environment II as compared with that of environment I may therefore be ascribed to a weak interaction of the hydrogen bonding type. It is probable that the orientation of the C-N bond is not imposed by hydrogen bonding to the silicate surface, but more likely due to interactions of adjacent alkyl chains.

Hydrogen bond strengths of alkylammonium cations in a range of environments may be compared by considering the depression in the mean  $\nu$  N-H below the mean frequency of a "free"  $\text{NH}_3^+$  group, taken as  $3253 \text{ cm}^{-1}$ .<sup>23</sup> However, comparisons cannot be precise because of the complexity of the spectra in the NH stretching region already mentioned. Depressions in  $\nu$  N-H for alkylammonium cations in a range of environments are given in Table III. It

Table III: Depressions ( $\text{cm}^{-1}$ ) in the Mean N-H Stretching Frequency for Methylammonium Ions in Various Salts<sup>10</sup> and the Vermiculite Complexes of the Present Work

Anion	—Vermiculite—		BPh <sub>4</sub> <sup>-a</sup>	I <sup>-</sup>	Br <sup>-</sup>	Cl <sup>-</sup>	F <sup>-</sup>
	Methyl- to hexyl- ammonium	Octyl- to octadecyl- ammonium					
Depression, $\text{cm}^{-1}$	91	103	0	198	193	217	574

<sup>a</sup> Nuttall, Sharp, and Waddington<sup>9</sup> give data which yield a depression of approximately  $155 \text{ cm}^{-1}$ .

is seen that the observed depressions in  $\nu$  N-H are less for the vermiculite complexes than for the halide salts, and the general conclusion may therefore be drawn that hydrogen bonding in alkylammonium vermiculites is weak. This cannot be confirmed in the present work by a consideration of a possible shift in the mean of  $\delta_{as}$  N-H and  $\delta_s$  N-H as  $\delta_{as}$  N-H is partly obscured by absorption bands due to the mineral.

(21) E. W. Radoslovich, *Acta Cryst.*, **13**, 919 (1960).

(22) J. J. Fripiat, A. Servais, and A. Leonard, *Bull. Soc. Chim. Fr.*, 635 (1962).

(23) P. Chevalier and C. Sandorfy, *Can. J. Chem.*, **38**, 2524 (1960).

Hydrogen bonding to siloxanes is usually weak, and it has been proposed that this is due to the influence of the diffuse d orbitals of the silicon on the lone-pair electrons of the oxygen.<sup>24</sup> However, Si-O bond multiplicity arising from  $\pi$  bonding with silicon d orbitals increases the Si-O-Si bond angle and, moreover, restrictions imposed on the increase in this angle, as occurs in some cyclic siloxanes, enhance the ability of the oxygens to accept hydrogen bonds.<sup>24</sup> It is known that the Si-O-Si bond angle in layer silicates is close to the tetrahedral angle  $109^\circ$ ,<sup>21</sup> and consequently delocalization of the lone-pair electrons of the surface oxygens among the d orbitals of the silicon sheet is unlikely to account for the weak bonding observed.

It is known that hydrogen bonds are highly directional and that bending reduces the strength of the bond.<sup>25</sup> There is little likelihood that the orientation of adsorbed molecules, which is determined by the combination of all adsorption interactions, would fortuitously provide the most favorable orientation of the proton donating bond X-H for hydrogen bonding.

When the direction of the lone-pair electrons of the surface atoms is invariable as it is in siloxane groups, the hydrogen bond is likely to be bent. Surface hydrogen bonds of this description would naturally be weaker than in comparable systems in the liquid state.

This explanation for weakened hydrogen bonding in some adsorption systems is compatible with the observation that, in the cavities of chabazite, with some 20 water molecules per cavity, adsorbate-adsorbate interaction is most significant, and hydrogen bonding is essentially between the adsorbed water molecules themselves, and not to the oxygen surface.<sup>17</sup> On the other hand, the single water molecule in each natrolite cavity is strongly hydrogen bonded to the surface.<sup>17</sup> In this system, adsorbate-adsorbate interaction is zero, and the asymmetry of forces determining the orientation of the water molecule would be less than at a planar silicate surface.

(24) C. M. Huggins, *J. Phys. Chem.*, **65**, 1881 (1961).

(25) R. Chidambaram and S. K. Sikka, *Chem. Phys. Lett.*, **2**, 162 (1968).

## The Hindered Rotation of the Cyanide Ion in Its Compounds

by David Smith

*Department of Chemistry, Pennsylvania State University, Hazleton Campus, Hazleton, Pennsylvania 18201*  
(Received October 31, 1969)

The rotational heat capacities of the cyanide ion in NaCN, KCN, RbCN, CsCN, and TlCN have been analyzed using the Devonshire model. By a comparison of the observed and computed rotational heat capacities, the barrier to rotation of the cyanide ion in its compounds is determined.

### Introduction

The cyanide ion in the alkali metal cyanides undergoes hindered rotation.<sup>1</sup> At low temperatures the cyanide ion behaves as a torsional oscillator, so its heat capacity can be represented by an Einstein function. Near room temperature the heat capacity due to the motion of the cyanide ion begins to approach the classical value of a free rotor ( $3/2R$ ). The rotational heat capacity of  $\text{CN}^-$  in KCN has been previously interpreted using the Devonshire model,<sup>2</sup> which permits the computation of the energy levels of a linear ion or molecule in a cubic crystalline environment. In this paper, the rotational heat capacities of a number of cyanide compounds are to be analyzed using the Devonshire model.

The low-temperature heat capacities of NaCN,<sup>3</sup> KCN,<sup>4</sup> RbCN,<sup>5</sup> CsCN,<sup>5</sup> and TlCN<sup>6</sup> have been reported. At room temperature NaCN, KCN, and RbCN are face-centered cubic, while CsCN and TlCN are body-centered cubic.<sup>7</sup> Below room temperature all

(1) D. Smith, *J. Phys. Chem. Solids*, **29**, 525 (1968).

(2) A. F. Devonshire, *Proc. Royal Soc., Ser. A*, **153**, 601 (1936).

(3) T. Matsuo, H. Suga, and S. Seki, *Bull. Chem. Soc. Jap.*, **41**, 583 (1968).

(4) H. Suga, T. Matsuo, and S. Seki, *ibid.*, **38**, 1115 (1965).

(5) M. Sugisaki, T. Matsuo, H. Suga, and S. Seki, *ibid.*, **41**, 1747 (1968).

(6) T. Matsuo, M. Sugisaki, H. Suga, and S. Seki, *ibid.*, **42**, 1271 (1969).

(7) R. W. Wyckoff, "Crystal Structures," Vol. 1, Interscience, New York, N. Y., 1963.

**Table I:** Phase Transitions in Some Cyanide Compounds<sup>a</sup>

Compd	$T_t$	$S_t$	$T_t$	$S_t$	$T_t$	$S_t$
NaCN	171.9	1.21	287.7	2.80		
KCN	82.9	1.32	168.3	2.01		
RbCN	110.3	1.38				
CsCN	193.1	2.60				
TiCN	84.7	0.54	193.2	0.35	266.8	2.74

<sup>a</sup> Data from ref 3-6.  $T_t$  represents transition temperature ( $^{\circ}\text{K}$ ) and  $S_t$  represents the entropy of the transition (cal/deg mol).

these compounds exhibit order-disorder transitions. The temperatures and entropies of these transitions are listed in Table I. The lower transitions of NaCN and KCN and the transition in RbCN are due to the orientational order-disorder rearrangement of the cyanide ion, since the entropy associated with the transitions is approximately equal to  $R \ln 2$  (1.38 cal/mol deg). The upper transitions of NaCN, KCN, and TiCN and the transition in CsCN are due to the number of equivalent positions in the cubic unit cell. Assuming that the cyanide ion in CsCN and RbCN orients itself along one of the four body diagonals in the cubic unit cell, the configurational entropy associated with the order-disorder transition is  $R \ln 4$  (2.76 cal/mol deg). For the fcc compounds, the configurational entropy of the upper transition should be  $R \ln 4$  if the cyanide ions lie along one of the four body diagonals or  $R \ln 3$  (2.18 cal/deg mol) if the cyanide ions lie on one of the three 100 axes. For KCN and NaCN the two anomalous heat capacities correspond to a stepwise reorientational motion of the cyanide ions. The other cyanides, *i.e.*, RbCN, CsCN, and TiCN, appear to have a residual entropy.

### Procedure

The low-temperature heat capacities of KCN, NaCN, RbCN, CsCN, and TiCN may be represented by a sum of Debye and Einstein functions.

$$C_v = 3D(\theta_1/T) + 3E(\theta_2/T) + 2E(\theta_3/T) \quad (1)$$

$$C_p = C_v + (aC_v)^2 T$$

where the Debye and Einstein functions are represented by  $D$  and  $E$ , respectively. The torsional frequency of the cyanide ion is represented by  $\theta_3$ . The internal frequency of the cyanide ion makes no contribution to the heat capacity below room temperature. The value of " $a$ " for the cyanides are estimated from the values of " $a$ " of the alkali halides. The Debye and Einstein characteristic temperatures of the cyanide compounds are listed in Table II. The empirical parameters  $\theta_1$ ,  $\theta_2$ , and  $\theta_3$  are determined from the heat capacity results of the cyanides below about 60 $^{\circ}\text{K}$ .

**Table II:** Debye and Einstein Characteristic Temperatures<sup>a</sup> at Low Temperatures:  $C = 3D(\theta_1/T) + 3E(\theta_2/T) + 2E(\theta_3/T)$ ;  $C_p = C_v + (aC_v)^2 T$ 

Compd	$\theta_1$	$\theta_2$	$\theta_3$	$a$	Torsional freq, $\text{cm}^{-1}$
NaCN	205	217	365	0.0041	254
KCN	138			0.0044	
RbCN	93	155	190	0.0044	132
CsCN	95	150	240	0.0042	167
TiCN	75	165	270	0.0040	188

<sup>a</sup> Characteristic temperatures given in  $^{\circ}\text{K}$ .

At higher temperatures eq 1 will not represent the heat capacity because the order-disorder transitions begin to make a significant contribution to the heat capacity. The values of  $\theta_2$  and  $\theta_3$  for KCN are approximately the same, so it is impossible to determine them individually from the heat capacity results.

Above the order-disorder transitions where the cyanides have a cubic crystal structure, the heat capacity contribution due to the motion of the cyanide ion cannot be represented by an Einstein function, because the motion is no longer harmonic in nature. The contribution to the heat capacity due to the motion of the cyanide ion is calculated by using the equation

$$C(\text{ROT}) = C_v - 3D(\theta_1/T) - 3E(\theta_2/T) \quad (2)$$

$C_v$  is computed from the observed heat capacity,  $C_p$ , by using the relationship previously given. The values of  $\theta_1$  and  $\theta_2$  for NaCN and KCN in the cubic phase are evaluated by considering the values of  $\theta_1$  and  $\theta_2$  for the alkali halides. Assuming that Lindemann's relationship is followed by these compounds, the values of  $\theta_1$  and  $\theta_2$  for KCN and NaCN can be determined.<sup>1</sup> The melting points of the other cyanides have not been reported, so Lindemann's relationship cannot be used for these compounds. For these cyanides the assumption is made that the values of  $\theta_1$  and  $\theta_2$  are the same in both the low-temperature and cubic phases. This is not a good assumption. However, above 150 $^{\circ}\text{K}$  the lattice heat capacity is not a sensitive function of  $\theta_1$  and  $\theta_2$ , because the Debye and Einstein functions are approaching their classical high-temperature values.

The rotational heat capacities of  $\text{CN}^-$  in KCN, RbCN, and CsCN are illustrated in Figure 1. Due to the high transition temperatures of NaCN and TiCN, the rotational heat capacity of the cyanide ion could not be determined over a wide temperature range. The major source of uncertainty in the computation of the rotational heat capacity below 200 $^{\circ}\text{K}$  is the uncertainty in the characteristic temperatures, while above 200 $^{\circ}\text{K}$  it is due to the uncertainty in  $C_p - C_v$ .

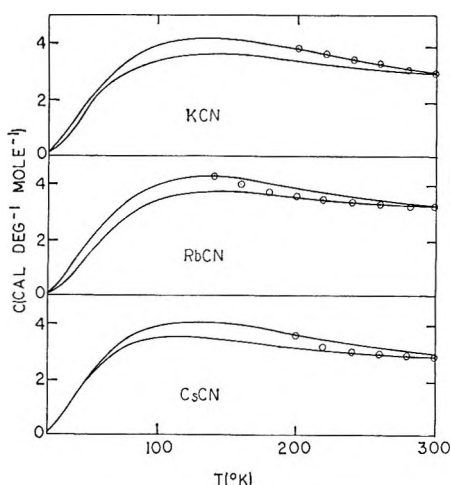


Figure 1. Rotational heat capacities of  $\text{CN}^-$  in KCN, RbCN, and CsCN. The circled points represent the rotational heat capacity of  $\text{CN}^-$  computed from the observed heat capacity. The solid lines represent the heat capacity computed from the Devonshire model. The upper solid lines represent the heat capacities calculated for  $V_0 = 1240$  (KCN), 1260 (RbCN), and 1120 (CsCN) cal and the lower lines for  $V_0 = -1450$  (KCN),  $-1800$  (RbCN), and  $-1270$  (CsCN) cal.

### Discussion

The energy levels of the cyanide ion in a cubic crystalline environment can be computed using the Devonshire model.<sup>2</sup> The potential function for this problem is

$$V = -V_0'/2[3/20 - 3/2 \cos^2 \theta + 7/4 \cos^4 \theta + 1/4 \sin^4 \theta \cos 4\phi]$$

$$V_0 = V_0' \text{ (for } V_0' + \text{)}$$

$$V_0 = 2/3 V_0' \text{ (for } V_0' - \text{)}$$

where  $V_0$  is the barrier to rotation. If  $V_0$  is negative the cyanide ion lies on the 111 axes of the fcc or bcc unit cell. The degeneracy of the ground state would be eight, corresponding to the eight equivalent positions of the cyanide ion in the lattice. If  $V_0$  is positive the cyanide lies along the 100 axes and the degeneracy of the ground state is six. The calculation of the rotational heat capacity using the Devonshire model has been previously outlined.<sup>1</sup>

In Figure 1 the rotational heat capacities calculated from the energy levels computed using the Devonshire model are illustrated for both positive and negative values of  $V_0$ . For CsCN and RbCN the heat capacities computed using a negative value of  $V_0$  represents the rotational heat capacity far better than if  $V_0$  were positive. This is expected, since CsCN has an entropy of transition that is in accordance with the cyanide ion lying along the 111 axes. Both NaCN and TICN have entropies of transition which also indicate that the

cyanide ion lies along the 111 axes, so  $V_0$  is negative. A neutron diffraction investigation of KCN<sup>3</sup> favors a static model having the cyanide ion randomly oriented along the 111 directions. However, a comparison of the rotational heat capacity of  $\text{CN}^-$  in KCN with values computed using the Devonshire model indicates that  $V_0$  is positive (Figure 1). The apparent poor representation of a negative  $V_0$  might be due to the contribution the order-disorder transition makes to the heat capacity of KCN even above 210°K. When the rotational heat capacity is computed using eq 2 it is assumed that the order-disorder transition is making no contribution to the heat capacity. For the cases of RbCN and CsCN the anomalous rise in the value of the rotational heat capacity as the temperature is lowered is undoubtedly due to the order-disorder transition. If the same situation were present for KCN, *i.e.*, the order-disorder transition is making a significant contribution to the heat capacity above 210°K, then the good representation of the rotational heat capacity by a positive  $V_0$  is accidental. The entropy of the upper transition for KCN is in accordance with a model where  $V_0$  is positive. Due to the conflicting evidence, no final determination can be made as to the sign of  $V_0$ .

The torsional frequency can be calculated from  $V_0$ ,<sup>1,2</sup> by using the following equation if  $V_0$  is positive

$$h\nu = 4\sqrt{V_0 B} - 29/6B$$

where  $B$  is the rotational constant. If  $V_0$  is negative

$$h\nu = 4\sqrt{-V_0 B} - 13/2B$$

In Table III the values of the barrier to rotation and torsional frequency are listed for the cyanides. While it is unfortunate that a comparison between the observed and computed rotational heat capacity is not possible over a wider temperature range, the present work does permit the calculation of the potential barrier to rotation.

Table III: Barrier to Rotation for the Cyanides in the Cubic Phase<sup>a</sup>

Compd	$h\nu$ , $\text{cm}^{-1}$	$ V_0 $ , cal
NaCN	200	4150
KCN	105	1240
RbCN	127	1800
CsCN	102	1270
TICN	144	2260

<sup>a</sup> Barrier to rotation is  $V_0$  and torsional frequency is  $h\nu$ .

(8) N. Elliott and J. Hastings, *Acta Crystallogr.*, **14**, 1018 (1961).

# Averaged Potential and the Viscosity of Some Polar Organic Vapors

by I. Crivelli and F. Danon

Department of Chemistry, University of Chile, Santiago, Chile (Received February 16, 1970)

The free energy average potential model, as a representation of molecular interactions in a dilute dipolar gas, is applied to the calculation of the viscosity of several polar organic vapors: chloroform, acetone, and methyl and ethyl alcohols. The agreement between theoretical and experimental values confirms the usefulness of the method. Comparison is made with a recently proposed three-parameter model.

## I. Introduction

The thermodynamic and transport properties of fluids can, in principle, be calculated by means of statistical mechanics once the intermolecular potential function is known. For the case of a dilute dipolar gas, the calculation is complicated by the presence of the orientation-dependent terms of the interaction.<sup>1</sup> Monchick and Mason have presented a solution for the transport properties based on a fixed orientation model<sup>2</sup> using a set of simple assumptions which are physically reasonable. The numerical calculation of the necessary collision integrals remains, however, not simple. Their treatment has also been applied to mixtures of polar gases<sup>3</sup> and to one-component quadrupolar<sup>4</sup> gases.

Danon and Amdur have recently proposed a different method of calculation based on the use of preaveraged free energy potentials.<sup>5</sup> The procedure had previously been applied to the calculation of equilibrium thermodynamic properties of fluids by Cook and Rowlinson<sup>6</sup> and by Rowlinson,<sup>7</sup> following an argument presented by Onsager<sup>8</sup> and Rushbrooke<sup>9</sup> many years ago.

Although there seems to be no similar theoretical basis for using the free-energy average potential in calculating nonequilibrium properties, the empirical evidence indicates, however, this approach as a plausible and much simpler alternative to the more rigorous procedure of Monchick and Mason. Pal and Barua<sup>10</sup> have recently reported on a series of measurements of the viscosity of some polar organic fluids: chloroform, acetone, and methyl and ethyl alcohols on the 30–200° temperature range. They tried to apply the fixed orientation model to their data to determine the molecular parameters of the Stockmayer potential, which can be written as<sup>11</sup>

$$\bar{\Phi}(r, \omega) = 4\epsilon_0 \left[ \left( \frac{\sigma_0}{r} \right)^{12} - \left( \frac{\sigma_0}{r} \right)^6 \right] - \frac{\mu^2}{r^3} g(\omega) \quad (1)$$

where

$$g(\omega) = 2 \cos \theta_1 \cos \theta_2 - \sin \theta_1 \sin \theta_2 \cos \phi \quad (2)$$

and where  $\mu$  is the dipole moment,  $\theta_1$ , and  $\theta_2$ , the angles between the axes of the molecular dipoles and the line joining the molecular centers, and  $\phi$  the azimuthal

angle in the plane perpendicular to this line. As  $\mu \rightarrow 0$ ,  $\bar{\Phi}(r, \omega) \rightarrow \bar{\Phi}(r)$ , the familiar Lennard-Jones (12-6) potential with parameters  $\sigma_0$  and  $\epsilon_0$  so defined that  $\bar{\Phi}(\sigma_0) = 0$  and  $\bar{\Phi}(r_{\min}) = -\epsilon_0$ .

Pal and Barua show it is not possible to obtain a satisfactory fit to their data for a given pair of independent parameters. If a new parameter  $\delta = (1/4) \mu^{*2} g(\omega)$  is defined in terms of a reduced dipole moment  $\mu^* = \mu (\epsilon_0 \sigma_0^3)^{-1/2}$  and it is considered as a third adjustable parameter, then good agreement is obtained between their experimental values of the viscosity and the calculated values obtained from eq 1. The parameter  $\delta$  can be interpreted as an effective value of the angular dependent part  $g(\omega)$  of the potential.

The purpose of the present paper is to show that if an average potential, as defined by Danon and Amdur, with only two independent parameters is used, then the calculated values of the viscosity agree with the experimental measurements of Pal and Barua over the whole temperature range. This confirms the usefulness of the average potential treatment reported earlier.<sup>5</sup>

## II. The Average Potential

The free energy average potential  $\bar{\Phi}$  as derived in ref 5 is given by

$$\bar{\Phi}(r, T) = 4\epsilon_0 \left[ \left( \frac{\sigma_0}{r} \right)^{12} - \left( \frac{\sigma_0}{r} \right)^6 \left( 1 + \frac{\delta_{\max}^2}{3T_0^*} \right) \right] \quad (3a)$$

where

$$\delta_{\max} = (1/2) \mu^2 / (\epsilon_0 \sigma_0^3) \quad (3b)$$

(1) J. O. Hirschfelder, C. F. Curtiss, and R. B. Bird, "Molecular Theory of Gases and Liquids," 2nd ed, John Wiley and Sons, New York, N. Y., 1964.

(2) L. Monchick and E. A. Mason, *J. Chem. Phys.*, **35**, 1676 (1961).

(3) E. A. Mason and L. Monchick, *ibid.*, **36**, 2746 (1962).

(4) F. J. Smith, R. J. Munn, and E. A. Mason, *ibid.*, **46**, 317 (1967).

(5) F. Danon and I. Amdur, *ibid.*, **50**, 4718 (1969).

(6) D. Cook and J. S. Rowlinson, *Proc. Roy. Soc., Ser. A*, **219**, 405 (1953).

(7) J. S. Rowlinson, *Mol. Phys.*, **1**, 414 (1958).

(8) L. Onsager, *Chem. Rev.*, **13**, 73 (1933).

(9) G. S. Rushbrooke, *Trans. Faraday Soc.*, **36**, 1055 (1940).

(10) A. K. Pal and A. K. Barua, *Brit. J. Appl. Phys.*, **1**, 71 (1968).

(11) W. H. Stockmayer, *J. Chem. Phys.*, **9**, 398 (1941).



**Table I:** Comparison of Potential Parameters

Gas	Monchick and Mason			Pal and Barua			This work		
	$\delta_{\max}$	$\sigma_0$ , Å	$\epsilon/k$ , °K	$\delta_{\max}$	$\sigma_0$ , Å	$\epsilon_0/k$ , °K	$\delta_{\max}$	$\sigma_0$ , Å	$\epsilon_0/k$ , °K
CHCl <sub>3</sub>	0.07	5.31	355	0.05	5.678	412.1	0.065	5.35	400
(CH <sub>3</sub> ) <sub>2</sub> CO	0.6	4.50	549	0.43	5.473	421.7	0.55	4.92	450
CH <sub>3</sub> OH	0.5	3.69	417	0.36	4.128	408.3	0.45	3.71	450
C <sub>2</sub> H <sub>5</sub> OH	0.3	4.31	431	0.26	4.872	345.5	0.25	4.35	500

gives the maximum value of  $\delta$ , *i.e.*,  $g(\omega) = 2$  and  $T_0^* = \epsilon_0/kT$  is a reduced temperature; other symbols have the same meaning as in eq 1. Equation 3 can be written in the form of a Lennard-Jones potential applicable to dipolar molecules where  $\epsilon_d$  and  $\sigma_d$  are new parameters which are temperature dependent and

$$\Phi_d = 4\epsilon_d \left[ \left( \frac{\sigma_d}{r} \right)^{12} - \left( \frac{\sigma_d}{r} \right)^6 \right] \quad (4)$$

related to  $\epsilon_0$  and  $\sigma_0$  by

$$\sigma_d = \sigma_0(\epsilon_0/\epsilon_d)^{1/2}$$

$$\epsilon_d = \epsilon_0 \left( 1 + \frac{\delta_{\max}^2}{3T_0^*} \right)^2$$

### III. Determination of Potential Parameters

To calculate the numerical value of the parameters of the free energy average pair potential from the experimental viscosities<sup>10</sup> of the polar gases we use a procedure which is essentially that given by Hirschfelder, Curtiss, and Bird<sup>12</sup> and also by others.<sup>13</sup> Details are given in ref 5 and so are not repeated here. Results are presented in Table I. Values of the parameters from the work of Monchick and Mason, and Pal and Barua are also included for comparison. It should be noted that the values of Pal and Barua are calculated according to eq 3b using their values of  $\sigma$  and  $\epsilon$ . They are clearly not the same as the  $\delta$  values of ref 10 since  $\delta_{\max}$  corresponds to the maximum value of  $g(\omega)$ , *viz.*, 2 whereas Pal and Barua give to  $\delta$  the value corresponding to an "effective"  $g(\omega)$ . This is an average value of  $g(\omega)$  over the orientations at a given temperature,  $T$ , and they consider it to be such a slowly varying function of  $T$  as to be justified to take just one value for the temperature range of interest. By using the equations of the average potential method it can be shown that this is a reasonable assumption. A fixed value of  $\delta$  for a particular substance corresponds to an effective value of  $g(\omega)$ , *i.e.*,  $g_{\text{eff}}$ . From the relationship  $\delta = (1/2) \delta_{\max} g_{\text{eff}}$ , values of  $g_{\text{eff}}$  can easily be obtained. It should be pointed out that these values are, for the molecules considered, larger than the maximum value of 2, which is not physically reasonable.

### IV. Results and Discussion

The parameters of the average pair potential have been used to calculate the viscosities of the molecules considered at the temperatures reported in the measure-

**Table II:** Comparison of the Coefficient of Viscosity  $\eta$  (cgsu  $\times 10^{-7}$ )

Gas	Temp, °C	Calcd		Exptl
		Pal and Barua <sup>10</sup>	This work	
CHCl <sub>3</sub>	30.5	951	963	963.9
	55.2	1038.5	1045	1056.9
	97.9	1181	1183	1195.0
	149.0	1340	1348	1371.7
	200.0	1490	1512	1525.0
(CH <sub>3</sub> ) <sub>2</sub> CO	30.0	683	678	678.1
	54.5	745	739	750.2
	97.8	853	846	865.2
	150.0	997.5	979	998.4
	204.0	1095	1116	1120.0
CH <sub>3</sub> OH	30.3	910	914	913.9
	55.6	928	995	1010.7
	98.5	1136	1136	1158.3
	149.0	1291	1308	1320.2
	204.0	1452	1488	1485.0
C <sub>2</sub> H <sub>5</sub> OH	30.5	789	786	786.3
	56.0	864	855	867.3
	97.8	978.5	969	989.7
	150.5	1126	1115	1135.7
	199.8	1253	1250	1261.0

ments of ref 10. Results of these calculations are shown in Table II together with the values obtained using the method and parameters of Pal and Barua.

Although the purpose of this work is to study the relative "goodness" of Pal and Barua and the average potential methods to correlate experimental viscosity data, some calculations based on the fixed orientation model of Monchick and Mason and using the parameters of ref 2 were also made. Since these parameters were determined, in turn, from a different set of experimental data, they cannot be fairly compared to the values in our Table II. This calculation confirms, however, the general validity of the method of Monchick and Mason.

To test the ability of the three-parameter method of Pal and Barua and that of the average potential to reproduce a different set of experimental data, values of the viscosities at the temperatures reported in a paper

(12) See ref 1, p 562.

(13) E. C. Ytean, A. R. Glueck, and R. S. Svela, NASA Technical Note D-481, NASA, Washington, D. C., 1961.

**Table III:** Comparison of the Coefficient of Viscosity  $\eta$  (cgsu  $\times 10^{-7}$ )

Gas	Temp, °C	Calcd		Exptl
		Pal and Barua <sup>10</sup>	This work	
CHCl <sub>3</sub>	121.3	1254	1265	1357
	218.7	1543	1570	1674
	307.5	1787	1849	1947
(CH <sub>3</sub> ) <sub>2</sub> CO	119.0	903	901	991
	217.3	1123	1167	1253
	306.4	1308	1356	1481
CH <sub>3</sub> OH	111.3	1175	1177	1259
	217.5	1488	1530	1620
	311.5	1757	1836	1921
C <sub>2</sub> H <sub>5</sub> OH	130.2	1070	1083	1173
	217.5	1298	1320	1421
	308.7	1509	1561	1670

published many years ago by Titani<sup>14</sup> were also calculated using the same previously determined set of

parameters. Results are shown in Table III. The average potential model shows a better agreement with experiment than the three-parameter method of Pal and Barua.

Although as discussed earlier,<sup>5</sup> the main limitation of the free energy average potential model lies in the absence of a fundamental justification to apply in the calculation of nonequilibrium properties, the results of this paper indicate, considering the simplicity of the method, the usefulness of this approach.

The average potential procedure could easily be extended to treat different types of molecular interactions that depend both on the distance apart and the relative orientation of a pair of molecules. The validity of the model should, however, be further tested as more experimental data on the viscosity of the polar gases become known.

(14) T. Titani, *Bull. Chem. Soc. Jap.*, **8**, 255 (1933).

## Dielectric Studies. XXVIII. Consideration of Weight Factor

### Anomalies in Hydroxylic Compounds

by M. D. Magee

*Department of Inorganic and Structural Chemistry, University of Bradford, Bradford, England*

and S. Walker

*Department of Chemistry, Lakehead University, Thunder Bay, Ontario, Canada (Received January 4, 1970)*

The dielectric absorption and dispersion of 2,6-di-*t*-butylphenol in *p*-xylene, 4-methylphenol in cyclohexane, carbon tetrachloride, and *p*-xylene, and 4-chlorophenol in *p*-xylene have been measured at four or five microwave frequencies and 2 MHz at 25°. In addition a series of solutions of cholesterol in various solvents and solvent mixtures has been measured at 25° over the same frequency range. The weight factors determined from the experimental data for 2,6-di-*t*-butylphenol in *p*-xylene and for cholesterol in a solution containing 83% of 1,4-dioxane are in agreement with the theoretical values as opposed to those of the other solutions; these latter systems, unlike the current practice in the literature, should not be analyzed into two discrete relaxation contributions but are best described in terms of a distribution of relaxation times. However, analyses of all the systems into two discrete relaxation regions are discussed with special reference to the weight factor values. Self-association of the solute molecules is shown to be a significant factor in the apparent variation of weight factors, and it is also shown that a real variation in the group relaxation time can lead to apparent variation in weight factor for certain methods of analysis.

### Introduction

In general, in molecules containing the OH group two distinct relaxation times are expected. One is due to rotation of the molecule as a whole and the other is due to rotation of the group about the bond connecting it to the bulk of the molecule. In these cases the micro-

wave dielectric data can be analyzed into two contributions<sup>1</sup> each with its characteristic relaxation time and weight (*i.e.*, relative amplitude) factor. However, emphasis is usually placed on the relaxation times values

(1) K. Bergmann, D. M. Roberti, and C. P. Smyth, *J. Phys. Chem.*, **64**, 665 (1960).

and there has been only limited discussion<sup>2</sup> of the solvent dependence of weight factors for these systems.

Fong and Smyth<sup>2</sup> postulated a very pronounced solvent effect for 4-phenylphenol, 1-naphthol, and 2-naphthol in benzene at 20° since the observed weight factors for group relaxation ( $C_2$ ) are 0.23, 0.26, and 0.28, respectively, whereas values nearer to 0.9 are anticipated in the absence of any perturbing influences. Other phenols give weight factors in reasonable agreement with the expected value; for 2,6-dimethylphenol in benzene<sup>2</sup> at 20°,  $C_2$  is 0.83; for 2,6-di-*t*-butyl-4-methylphenol in benzene<sup>3</sup> at 20°,  $C_2$  is estimated from the relative amplitudes of the loss maxima to be 0.89. Fong and Smyth consider that the reduction in  $C_2$  for the first three molecules may be due to hydrogen bonding of the OH group to the  $\pi$  electrons of the solvent and that steric protection by the 2,6-substituents impairs this in the other molecules.<sup>4</sup>

With a view to gaining further information on the solvent dependence of weight factors we have made some microwave measurements on a number of OH-containing molecules in various solvents and solvent mixtures.

### Experimental Section

**Apparatus.** The apparatus and procedure for determining the dielectric constant ( $\epsilon'$ ) and loss factor ( $\epsilon''$ ) have been described previously,<sup>5</sup> and sources of error have been assessed.<sup>6</sup> Measurements were made at four or five microwave frequencies ( $\omega/2\pi$ ): 9.313, 16.20, 23.98, 24.86, and 70.00 GHz. The static dielectric constant was determined at a frequency (2 MHz) by the use of a Dipolmeter DM 01. All measurements were made at  $25 \pm 0.01^\circ$ .

**Evaluation of Data.** The mean relaxation time ( $\tau_0$ ), distribution coefficient ( $\alpha$ ), and high-frequency dielectric constant ( $\epsilon_\infty$ ) were obtained by fitting the experimental data to the Cole-Cole<sup>7</sup> equation

$$\epsilon' - i\epsilon'' = \epsilon_\infty + \frac{(\epsilon_0 - \epsilon_\infty)}{1 + (i\omega\tau_0)^{1-\alpha}} \quad (1)$$

Except in the case of cholesterol solutions the estimate of  $\epsilon_\infty$  from this analysis was then used in the Budó<sup>8</sup> equations

$$\epsilon' - i\epsilon'' = \epsilon_\infty + (\epsilon_0 - \epsilon_\infty) \times \left[ \frac{C_1}{1 + i\omega\tau_1} + \frac{C_2}{1 + i\omega\tau_2} \right] \quad (2)$$

$$C_1 + C_2 = 1 \quad (3)$$

to yield the contributory relaxation times  $\tau_1$ , and  $\tau_2$  and weight factors  $C_1$  and  $C_2$  by a second data fit. In each case an iterative method was used and calculations were performed by an Elliot 803 computer. Further details and the validity of the procedure have been given elsewhere.<sup>6,9</sup> In the special case of the cholesterol solutions a better estimate of  $\epsilon_\infty$  could be obtained

by inspection, owing to the wide separation of the group and molecular loss regions.

The apparent dipole moments of the compounds were obtained from the dispersion of the dielectric constant ( $\epsilon_0 - \epsilon_\infty$ ) using Debye's<sup>10</sup> equation

$$\mu = 0.01281 \left[ \frac{(\epsilon_0 - \epsilon_\infty)}{f_2} \frac{M_1 T}{(\epsilon_1 + 2)^2 d_1} \right]^{1/2} \quad (4)$$

where  $f_2$  is the mole fraction of the solute,  $M_1$  is the molecular weight of the solvent,  $\epsilon_1$  is its static dielectric constant,  $d_1$  is its density, and  $T$  is the absolute temperature. When solvent mixtures are used, the dipole moments are calculated from the mole fraction-weighted values of the dielectric constants, densities, and molecular weights of the components, with the assumption of linear additivity.

**Materials.** The phenols were distilled through a spinning-band column and a small central fraction retained. The 4-methylphenol and 4-chlorophenol existed as metastable liquids at room temperature after distillation. They were stored in dark stoppered bottles in a desiccator over phosphorus pentoxide. The *p*-xylene, cyclohexane, and 1,4-dioxane solvents were distilled from sodium in a spinning-band column and a central fraction stored over sodium in amber Winchester. Carbon tetrachloride was dried over phosphorus pentoxide and similarly distilled through a spinning-band column. The purity of the compounds was checked by gas chromatography or infrared spectroscopy.

### Results

The experimental data are given in Table I together with calculated values of the dielectric constant and loss factor. For 2,6-di-*t*-butylphenol and the cholesterol solutions the calculated values are determined from eq 2 and 3, but the remaining values are calculated from eq 1.

In Table II the mean relaxation times, distribution coefficients, resolved relaxation times, weight factors, static and high-frequency dielectric constants, and apparent dipole moments are listed.

Two series of solvents or solvent mixtures were used for the cholesterol measurements. Each was intended to give an increasing electron donor capacity from A to

(2) F. K. Fong and C. P. Smyth, *J. Amer. Chem. Soc.*, **85**, 1585 (1963).

(3) F. K. Fong, J. P. McTague, S. K. Garg, and C. P. Smyth, *J. Phys. Chem.*, **70**, 2567 (1966).

(4) M. Davies and R. J. Meakins, *J. Chem. Phys.*, **26**, 1584 (1957).

(5) W. F. Hassell, M. D. Magee, S. Tucker, and S. Walker, *Tetrahedron*, **20**, 2137 (1964).

(6) M. D. Magee and S. Walker, *Trans. Faraday Soc.*, **62**, 3093 (1966).

(7) K. S. Cole and R. H. Cole, *J. Chem. Phys.*, **9**, 341 (1941).

(8) A. Budó, *Physik. Z.*, **39**, 706 (1938).

(9) M. D. Magee and S. Walker, *J. Chem. Phys.*, **50**, 2580 (1969).

(10) P. Debye, "Polar Molecules," Chemical Catalog Co., New York, N. Y., 1929.

**Table I:** Experimental and Calculated Dielectric Constants and Losses for Solutions of Hydroxyl Containing Compounds in Various Solvents and Solvent Mixtures at 25°

Freq., GHz	$\epsilon'$ obsd	$\epsilon'$ calcd	$\epsilon''$ obsd	$\epsilon''$ calcd	Freq., GHz	$\epsilon'$ obsd	$\epsilon'$ calcd	$\epsilon''$ obsd	$\epsilon''$ calcd
4-Methylphenol ( $f_2 = 0.0638$ )-Cyclohexane					Cholesterol ( $f_2 = 0.0399$ )- <i>p</i> -Xylene				
34.86	2.081	2.076	0.0264	0.0258	70.00	2.21	2.298	0.0194	0.0190
23.98	2.072	2.083	0.0295	0.0304	34.86	2.310	2.311	0.0251	0.0261
16.20	2.099	2.092	0.0355	0.0349	23.98	2.319	2.319	0.0281	0.0270
9.313	2.106	2.108	0.0392	0.0398	16.20	2.328	2.326	0.0263	0.0265
0.002	2.1920				9.313	2.330	2.333	0.0271	0.0271
4-Methylphenol ( $f_2 = 0.0265$ )-Carbon Tetrachloride					Cholesterol ( $f_2 = 0.0426$ ) + Hexamethylbenzene ( $f_3 = 0.0355$ )- <i>p</i> -Xylene				
34.86	2.251	2.254	0.0219	0.0207	70.00	2.22	2.295	0.0129	0.0130
23.98	2.253	2.261	0.0235	0.0245	34.86	2.298	2.304	0.0186	0.0184
16.20	2.280	2.269	0.0260	0.0275	23.98	2.309	2.309	0.0191	0.0197
9.313	2.284	2.282	0.0291	0.0282	16.20	2.316	2.314	0.0194	0.0202
0.002	2.3143				9.313	2.328	2.319	0.0229	0.0224
4-Methylphenol ( $f_2 = 0.0209$ )- <i>p</i> -Xylene					Cholesterol ( $f_2 = 0.0547$ )-Mesitylene				
34.86	2.269	2.276	0.0156	0.0151	34.86	2.301	2.307	0.0187	0.0177
23.98	2.273	2.280	0.0173	0.0187	23.98	2.307	2.312	0.0200	0.0217
16.20	2.293	2.287	0.0235	0.0220	16.20	2.326	2.318	0.0248	0.0248
9.313	2.302	2.298	0.0219	0.0239	9.313	2.331	2.327	0.0282	0.0279
0.002	0.3260				0.002	2.4392			
4-Methylphenol ( $f_2 = 0.0374$ )- <i>p</i> -Xylene					Cholesterol ( $f_2 = 0.0365$ ) + 1,4-Dioxane ( $f_3 = 0.0831$ )- <i>p</i> -Xylene				
34.86	2.287	2.291	0.0245	0.0245	34.86	2.289	2.293	0.0212	0.0196
23.98	2.289	2.298	0.0305	0.0300	23.98	2.295	2.299	0.0220	0.0217
16.20	2.315	2.308	0.0338	0.0350	16.20	2.308	2.305	0.0203	0.0226
9.313	2.330	2.325	0.0380	0.0380	9.313	2.320	2.312	0.0275	0.0245
0.002	0.3729				0.002	2.4013			
4-Chlorophenol ( $f_2 = 0.0309$ )- <i>p</i> -Xylene					Cholesterol ( $f_2 = 0.0382$ ) + 1,4-Dioxane ( $f_3 = 0.3456$ )- <i>p</i> -Xylene				
34.86	2.286	2.283	0.0303	0.0321	34.86	2.292	2.287	0.0246	0.0250
23.98	2.292	2.291	0.0437	0.0424	23.98	2.295	2.294	0.0268	0.0289
16.20	2.317	2.303	0.0571	0.0546	16.20	2.305	2.303	0.0327	0.0312
9.313	2.309	2.331	0.0673	0.0689	9.313	2.321	2.314	0.0333	0.0335
0.002	2.4376				0.002	2.3959			
2,6-Di- <i>t</i> -butylphenol ( $f_2 = 0.0386$ )- <i>p</i> -Xylene					Cholesterol ( $f_2 = 0.0282$ ) + 1,4-Dioxane ( $f_3 = 0.6404$ )- <i>p</i> -Xylene				
70.00	2.24	2.278	0.0237	0.0233	34.86	2.280	2.272	0.0191	0.0190
34.86	2.294	2.294	0.0327	0.0348	23.98	2.281	2.278	0.0222	0.0244
23.98	2.303	2.307	0.0371	0.0374	16.20	2.291	2.286	0.0325	0.0288
16.20	2.329	2.319	0.0361	0.0361	9.313	2.285	2.300	0.0295	0.0306
9.313	2.345	2.333	0.0315	0.0315	0.002	2.3608			
0.002	2.3642				Cholesterol ( $f_2 = 0.0271$ ) + 1,4-Dioxane ( $f_3 = 0.8320$ )- <i>p</i> -Xylene				
Cholesterol ( $f_2 = 0.0322$ )-Carbon Tetrachloride					Cholesterol ( $f_2 = 0.0271$ ) + 1,4-Dioxane ( $f_3 = 0.8320$ )- <i>p</i> -Xylene				
34.86	2.274	2.275	0.0155	0.0151	34.86	2.263	2.262	0.0178	0.0186
23.98	2.275	2.280	0.0135	0.0145	23.98	2.268	2.267	0.0257	0.0254
16.20	2.288	2.283	0.0138	0.0134	16.20	2.281	2.276	0.0335	0.0325
9.313	2.287	0.286	0.0131	0.0131	9.313	2.290	2.294	0.0319	0.0389
0.002	2.3716				0.002	2.3660			
Cholesterol ( $f_2 = 0.0238$ ) + 1,4-Dioxane ( $f_3 = 0.0380$ )-Cyclohexane					Cholesterol ( $f_2 = 0.0271$ ) + 1,4-Dioxane ( $f_3 = 0.8320$ )- <i>p</i> -Xylene				
34.86	2.054	2.064	0.0088	0.0083	34.86	2.263	2.262	0.0178	0.0186
23.98	2.065	2.067	0.0079	0.0087	23.98	2.268	2.267	0.0257	0.0254
16.20	2.074	2.069	0.0083	0.0090	16.20	2.281	2.276	0.0335	0.0325
9.313	2.078	2.071	0.0109	0.0104	9.313	2.290	2.294	0.0319	0.0389
0.002	2.1183				0.002	2.3660			

E along the series. Solutions containing 1,4-dioxane were corrected for its small loss before analysis.

### Discussion

Measurements on 2,6-di-*t*-butylphenol in *p*-xylene at 25° confirm that OH group relaxation occurs in 2,6-di-

*t*-butyl substituted phenols. The mean relaxation time  $8.6 \times 10^{-12}$  sec is extremely short for a molecule of this size, compared for example with  $20 \times 10^{-12}$  sec for benzotrithloride<sup>11</sup> in *p*-xylene at the same temperature,

(11) J. Crossley and S. Walker, *Can. J. Chem.*, **46**, 841 (1968).

**Table II:** Mean Relaxation Times ( $\tau_0$ ), Discrete Relaxation Times ( $\tau_1$ ,  $\tau_2$ ), Distribution Coefficient ( $\alpha$ ), Weight Factors ( $C_1$ ), High-Frequency Dielectric Constants ( $\epsilon_\infty$ ), and Dipole Moments ( $\mu$ ) for Some Solutions of Hydroxylic Compounds in Various Solvents and Mixed Solvents. Relaxation Times are in Picoseconds and Dipole Moments in Debyes

Solute	Conc, mole fraction	Solvent <sup>a</sup>	$\tau_0$	$\alpha$	$\tau_1^b$	$\tau_2$	$C_1$	$\epsilon_\infty$	$\mu^b$
4-Methylphenol	0.0638	Cyclohexane	28	0.31	56	6.7	0.69	2.054	1.44
	0.0265	(Carbon tetrachloride)	14	0.16	24	4.2	0.66	2.241	1.50
	0.0209	<i>p</i> -Xylene	16.8	0.12	...	...	...	2.268	1.67
	0.0374		17	0.15	32	8.4	0.56	2.276	1.61
4-Chlorophenol	0.0309	<i>p</i> -Xylene	25	0.09	39	12.7	0.61	2.272	2.24
2,6-Di- <i>t</i> -butylphenol	0.0386		8.6	0.14	37	6.0	0.31	2.270	1.56
Cholesterol	0.0332	1A	...	...	198	3.9	0.76	2.260	1.65
	0.0238	1B	...	...	109	4.5	0.79	2.058	1.7
	0.0399	1C	...	...	93	4.8	0.67	2.290	1.82
	0.0426	1D	...	...	104	4.9	0.76	2.290	1.8
	0.0547	1E	...	...	120	8.4	0.77	2.299	1.7
	0.0399	2A	...	...	93	4.8	0.67	2.290	1.82
	0.0365	2B	...	...	100	5.8	0.74	2.300	1.9
	0.0382	2C	...	...	69	6.8	0.65	2.273	1.8
	0.0282	2D	...	...	98	11.5	0.49	2.265	1.8
	0.0271	2E	...	...	178	16.4	0.37	2.257	1.8

<sup>a</sup> Key to the cholesterol solvents: 1A, carbon tetrachloride; 1B, cyclohexane + 1,4-dioxane ( $f_3 = 0.0380$ ); 1C, *p*-xylene; 1D, *p*-xylene + hexamethylbenzene ( $f_3 = 0.0355$ ); 1E, mesitylene; 2A, *p*-xylene; 2B, *p*-xylene + 1,4-dioxane ( $f_3 = 0.0831$ ); 2C, *p*-xylene + 1,4-dioxane ( $f_3 = 0.3456$ ); 2D, *p*-xylene + 1,4-dioxane ( $f_3 = 0.6404$ ); 2E, *p*-xylene + 1,4-dioxane ( $f_3 = 0.8320$ ). <sup>b</sup> For cholesterol solutions  $\tau_1$  relaxation occurs well out of the frequency range of these measurements. Consequently the values quoted, although numerically giving the best fit, in fact are very approximate. Further, the dipole moments of cholesterol in mixed solvents are also approximate.

and benzotrichloride is a smaller molecule. The mean relaxation time obtained by Fong and Smyth<sup>2</sup> for 2,6-dimethylphenol which they found to relax predominantly by OH group relaxation was  $5.3 \times 10^{-12}$  sec in benzene at 20°. This bears comparison with our value on consideration of the greater bulk of the *t*-butyl compound and the consequent longer molecular relaxation time. Analysis for 2,6-di-*t*-butylphenol into discrete relaxation times indicates that group relaxation occurs with a relaxation time of  $6.0 \times 10^{-12}$  sec and weight factor 0.69. The relaxation time is longer than that of OH group relaxation of 2,6-dimethylphenol which has a value of  $3.4 \times 10^{-12}$  sec (possibly showing a slight steric effect of the neighboring *t*-butyl groups), but agrees well with the group relaxation time obtained for 2,4,6-tri-*t*-butylphenol in the solid state of  $6.1 \times 10^{-12}$  sec at 20°. The relaxation time of  $37 \times 10^{-12}$  sec is longer than that of *t*-butylbenzene in cyclohexane<sup>13</sup> at 20° of  $27 \times 10^{-12}$  sec and is in good agreement with the molecular relaxation time for 2,6-dibromophenol in benzene<sup>14</sup> of  $39 \times 10^{-12}$  sec at 20°. The weight factor for group rotation is also in acceptable agreement with the value of 0.74 calculated from the dipole moment of *t*-butylbenzene<sup>15</sup> ( $\sim 0.5$  D), phenol (1.54 D),<sup>16</sup> and the angle of 76° between the O-C bond and the direction of the OH moment in phenol.<sup>17</sup>

For 2,6-di-*t*-butyl substituted phenols molecular interaction of the OH group is prevented by the bulky *ortho* groups, even with strongly electron-donating

molecules such as neighboring phenols. The OH stretching frequency is unaltered for 2,4,6-tri-*t*-butylphenol even in the crystalline state,<sup>4</sup> and no complex formation could be detected between the strong electron donor, diethyl ether, and 2,6-di-*t*-butylphenol.<sup>18</sup> It seems certain, therefore, that OH group relaxation occurs with normal weight factors when the group is sufficiently shielded from environmental perturbations.

To study solvent effects 4-methylphenol would seem especially suitable because the moment of the 4-methyl group is almost equal in magnitude and opposite in direction to the component of the OH group moment along the O-C bond.<sup>15,17</sup> Thus, there should be only a small moment along the molecular axis, and  $C_2$  should be close to unity. In the absence of marked solvent effects the mean relaxation time should tend to that for the typical OH value whereas strong solvent effects

(12) R. J. Meakins, *Trans. Faraday Soc.*, **52**, 320 (1956).

(13) W. F. Hassell and S. Walker, *ibid.*, **62**, 861 (1966).

(14) A. Antony, F. K. Fong, and C. P. Smyth, *J. Phys. Chem.*, **68**, 2035 (1964).

(15) C. P. Smyth, "Dielectric Behaviour and Structure," McGraw-Hill Publications, New York, N. Y., 1955.

(16) J. H. Richards and S. Walker, *Trans. Faraday Soc.*, **57**, 407 (1961).

(17) J. W. Smith, "Electric Dipole Moments," Butterworth and Co., London, 1955.

(18) L. J. Bellamy, G. Eglington, and J. F. Mormon, *J. Chem. Soc.*, 4762 (1961).

should increase the mean relaxation time by lessening  $C_2$ , that is reducing the free relaxation contribution of the OH group.

In this discussion the relaxation time of the OH group in 2,6-dimethylphenol ( $3.4 \times 10^{-12}$  sec)<sup>2</sup> is assumed typical of a phenolic OH group for these reasons: (a) since the much larger *t*-butyl groups do not appreciably hinder the OH group in 2,6-di-*t*-butyl-substituted phenols, the methyl groups in 2,6-dimethylphenol are not expected to interfere in this molecule; (b) the good agreement between the observed and anticipated  $C_2$  values suggests that any OH group interaction with the solvent is insufficient to affect this value significantly.

The mean relaxation time observed for 4-methylphenol in *p*-xylene of  $16.9 \times 10^{-12}$  sec is considerably longer than the typical OH group relaxation time. Thus, there would appear to be an appreciable contribution from overall molecular rotation, and  $C_2$  must be lower than calculated. This is supported by analysis into two discrete relaxation times which yield a  $C_2$  of only 0.44. However, the molecular and group relaxation times of  $32 \times 10^{-12}$  sec and  $8.4 \times 10^{-12}$  sec, respectively, seem anomalously long. If the increased magnitude of these values is to be attributed to hydrogen bonding between the OH groups and the  $\pi$  electrons of the *p*-xylene, then normal values might be expected in carbon tetrachloride and cyclohexane solutions, but the mean relaxation time of 4-methylphenol in carbon tetrachloride was determined as  $14 \times 10^{-12}$  sec, which is still much longer than the typical OH value expected of  $C_2 = 1$ . Analysis again yielded relaxation times rather longer than expected of  $24 \times 10^{-12}$  sec and  $4.2 \times 10^{-12}$  sec, but the group relaxation weight factor of 0.34 was even lower than in *p*-xylene. In cyclohexane, the least electron-donating of the solvents used, the mean relaxation time was as long as  $28 \times 10^{-12}$  sec while analysis gave a very long molecular relaxation time of  $56 \times 10^{-12}$  sec and a long  $\tau_2$  value of  $6.7 \times 10^{-12}$  sec. Again the weight factor  $C_2$  was low and fell to 0.31. In view of the fact that the lowest  $C_2$  value is obtained in the most inert solvent it would seem that the reduction in  $C_2$  cannot be explained by hydrogen bonding of the OH group to the  $\pi$  electrons of the solvent.<sup>2</sup>

The behavior of 4-methylphenol is, in fact, very similar to that of 4-chlorophenol which it resembles in shape and size but for which a large contribution from overall molecular relaxation is anticipated. Analysis of the latter yields a very long molecular relaxation time of about  $40 \times 10^{-12}$  sec in *p*-xylene while the group relaxation time is also longer than the typical value, being  $12.7 \times 10^{-12}$  sec. The weight factor is similar to those of 4-methylphenol, but comparisons with the calculated values in this case are not very fruitful since a good deal of uncertainty arises about this, owing to appreciable mesomeric charge shift across the molecule.<sup>15,17</sup> For 4-methylphenol it may be significant that the distribution coefficient ( $\alpha$ ) increases with decreasing solvent

electron-donor capacity. Both this and the almost doubling of the mean relaxation time of 4-methylphenol in cyclohexane as compared with carbon tetrachloride and *p*-xylene solutions strongly favors the presence of a greater proportion of polymers in the noninteracting cyclohexane solvent. It therefore appears that the apparent reduction in  $C_2$  is due to self-association rather than to solvent effects and that the lowering of  $C_2$  becomes more pronounced as the electron-donating capacity of the solvent decreases and is greatest in cyclohexane solutions in which self-association would be most favored. From infrared evidence, Mecke<sup>19</sup> showed that phenols associate strongly even in dilute solutions and especially in weakly electron-donating solvents. For example, phenol in carbon tetrachloride was found to be about 40% associated even at a concentration of only 0.02 mole fraction—yet this represents virtually the lowest limit of reliable loss measurements for small molecules with a dipole moment of about 1.5 D. Thus, effects of solute interactions are likely to influence the parameters obtained by measurements of phenol solutions by the use of microwave techniques. Naphthols<sup>19</sup> are reported to have greater association constants than phenols and are likely to be even more associated in dilute solutions and thus their  $C_2$  values<sup>2</sup> would accordingly be influenced. Altogether, it seems that although the solvent effect may contribute to the lowering of  $C_2$ , particularly in aromatic solvents,<sup>2</sup> it is probably masked by the effects of solute association.

If this conclusion is valid, the analyses into two discrete relaxation times are thereby rendered incorrect, since additional modes of relaxation, such as rotation of dimers and higher multimers, relaxation by additional internal rotational degrees of freedom present in the multimers are likely to be present, and possibly rate processes related to the formation and destruction of the hydrogen bonds could be involved. It is interesting to note that Fong, McTague, Garg, and Smyth<sup>3</sup> were unable to obtain a good fit to their data on 3,5-dimethylphenol using two discrete relaxation times. It would seem that for such systems Budó analyses can serve only in a diagnostic capacity and have no real physical meaning, and the weight factors obtained should be termed *apparent* weight factors.

In an attempt to gain more information on the solvent effect upon weight factors, cholesterol was chosen as the OH-containing molecule. This was examined for the following reasons: (a) a mesomeric moment is not present to complicate the weight factor calculations; (b) since the molecule is so bulky, and not spherical, the molecular relaxation time is considerably longer than the group relaxation time so that the group relaxation time contributes much the greater proportion to the absorption in the microwave region and should be estimated fairly accurately from such data.

(19) R. Mecke, *Discuss. Faraday Soc.*, 9, 161 (1950).

Meakins<sup>20</sup> has measured  $\Delta^4$ -cholestenone in benzene at 20°, obtaining a relaxation time of  $233 \times 10^{-12}$  sec. Cholestenone is virtually the same size and shape as cholesterol, so this value might be expected to be very similar to the overall relaxation time of cholesterol, but the values of  $\tau_1$  in Table II are in general appreciably shorter, approximating to about  $100 \times 10^{-12}$  sec. A straightforward comparison of the molecular relaxation times of cholesterol and cholestenone, however, is not valid since no consideration has been given to the direction of the dipole moment with respect to the long principal axis.

Cooke and Walker<sup>21</sup> have determined relaxation times of some steroids with moments rigidly held at various angles from the main molecular axes. The molecules are ellipsoidal in shape, and the inclination of the dipole moment from the long axis is critical in determining the relaxation time observed. For  $5\alpha$ -cholestan-3-one, in which the molecular dipole lies virtually on the long principal axis, the relaxation time is  $206 \times 10^{-12}$  sec in *p*-xylene at 25°. A similar steroid  $\Delta^{3,5}$ -cholestadien-7-one which was examined in *p*-xylene at 25° and has a dipole inclination of  $\sim 60^\circ$  to the long axis has a relaxation time of only  $108 \times 10^{-12}$  sec. The angle of the nonrotating component of the OH dipole in cholesterol from the principal molecular axis is of this order so that the molecular relaxation time obtained from the analysis is of the correct order.

The group moment of OH attached to aliphatic hydrocarbon groups is about 1.7 D and is inclined at an angle of  $62^\circ$  to the C–O bond.<sup>15</sup> The observed moment found in *p*-xylene is 1.9 D so that  $C_2$  can be estimated by

$$C_2 = \left( \frac{\mu_{\perp}}{\mu_{\text{mol}}} \right)^2 = \left( \frac{1.7 \sin 62^\circ}{1.9} \right)^2 \quad (5)$$

where  $\mu_{\perp}$  is the component moment perpendicular to the long axis.  $C_2$  so evaluated is 0.62. Alternatively, the aliphatic bond moments of 1.7 D for C–O and 1.5 D for OH<sup>17</sup> acting along bonds inclined<sup>15</sup> at  $115^\circ$  may be used to calculate  $C_2$ . This procedure also yields 0.62, indicating the good agreement between the two approaches when mesomeric factors are absent.

The experimental values of  $C_2$  in Table II are in general lower than this estimate. In series 1, for example, the  $C_2$  value in carbon tetrachloride is practically the same as that in mesitylene, while in series 2, far from decreasing with increasing 1,4-dioxane concentration, the  $C_2$  values tend to increase despite the fact that 1,4-dioxane would be expected to be a better donor than *p*-xylene.

The discrepancy between the observed and calculated weight factors can be due to: (a) an effective concentration of relaxing groups is lower than the concentration of molecules undergoing overall rotation, which implies strong association, or (b) a rotating component of the dipole moment is smaller than calculated,

which requires that either the COH group moment be less than 1.7 D (0.9 D to 1.25 D to account for observed values of  $C_2$ ) or that the angle of inclination of the group moment from the C–O bond be much less than  $62^\circ$  ( $27$ – $37^\circ$ ), or a combination of these. It seems unlikely that the COH group moment or angle is so much in error, and, therefore, the major cause of these anomalies would appear to be due to association.

Infrared spectra were obtained for solutions of cholesterol in carbon tetrachloride and *p*-xylene. At concentrations similar to those necessary for dielectric studies, two OH stretching bands appeared for cholesterol solutions in carbon tetrachloride. A sharp band at  $3635 \text{ cm}^{-1}$  remains even at high dilution, but a very broad band centered at about  $3340 \text{ cm}^{-1}$  disappears at high dilution and is to be identified with an intermolecular hydrogen bond of the type O–H $\cdots$ O.

In *p*-xylene a sharp band appears at  $3585 \text{ cm}^{-1}$  and the broad band at about  $3370 \text{ cm}^{-1}$ . The latter is less intense than the broad band in carbon tetrachloride solutions at similar cholesterol concentrations. If the extinction coefficients of the hydrogen-bonded OH stretching band are substantially the same in the two solvents, then the apparent reduced intensity in *p*-xylene would suggest a lower degree of self-association in that solvent. Thus, there would be fewer OH $\cdots$ O bonds in *p*-xylene solution and the weight factor  $C_2$  should be higher than in carbon tetrachloride. This is, in fact, found. Self-association of the solute, therefore, interferes with direct interpretation of the results in terms of solvent effects.

For cholesterol in the mixed solvents, *p*-xylene–1,4-dioxane, the results in Table II indicate that as the proportion of 1,4-dioxane (the stronger electron donor solvent) increases then so does  $C_2$ . In fact, for the highest concentration of 1,4-dioxane the  $C_2$  value of 0.63 is in excellent agreement with the calculated value of 0.62. It would seem feasible that when the 1,4-dioxane is in such excess the O–H $\cdots$ O bonding is largely between the solute and the solvent, 1,4-dioxane, rather than between solute molecules and that the effective concentration of relaxing groups is virtually the same as the molecules undergoing overall relaxation. For such a case analysis of the results into  $\tau_1$  and  $\tau_2$  contributions would appear justifiable.

It is to be noted that increasing solvent electron-donor capacity is accompanied by a striking increase in the relaxation time  $\tau_2$ . Thus, in the most satisfactory case for analysis, that of solution 2E, the  $\tau_2$  value is  $16.4 \times 10^{-12}$  sec. Such a long relaxation time is understandable in terms of hydrogen bonding with the solvent since the free energy of activation opposing group re-orientation would be increased. Another possibility is

(20) R. J. Meakins, *Trans. Faraday Soc.*, **54**, 1160 (1958).

(21) B. Cooke, M.S. Thesis, Lakehead University, Ontario, Canada, 1969.

that OH group rotation in these systems involves breaking of the hydrogen bond followed by rotation.<sup>22</sup> The lengthening  $\tau_2$  value is then dependent on the increased free energy required to break the hydrogen bond. Obviously specific interactions complicate the relaxation mechanisms and, in fact, the analyzed  $\tau_2$  value would then be a composite value made up of relaxation times of free and hindered OH groups. In solution 2E which has the greatest proportion of 1,4-dioxane (83%)—the strongest donor solvent employed—the OH relaxation time of cholesterol is  $16.4 \times 10^{-12}$  sec compared with  $4.8 \times 10^{-12}$  sec obtained in *p*-xylene. The ratio of these values is 3.4. A comparison can be made with the influence of hydrogen bonding on the relaxation time of monomeric water in benzene and 1,4-dioxane. Crossley and Smyth<sup>23</sup> find that the ratio of the relaxation time of water in 1,4-dioxane at 25° to that in benzene at 25° is 3.5; this ratio is in good agreement with those for the  $\tau_2$  ratios for cholesterol in 1,4-dioxane and *p*-xylene.

If, then, the  $C_2$  values are not markedly altered by solvent effects in the systems discussed, the question remains whether it is possible to obtain appreciable *apparent* reductions. In fact, apparent reductions can easily arise when analyses are performed by crude "trial and error" or graphical methods which begin with some preconceived idea of the values of  $\tau_1$  and  $\tau_2$  and the resulting bias may not permit a sufficient change in  $\tau_2$  if the data fit is not good. Under these circumstances, however, an improved fit (although not the 'best') can be obtained by varying  $C_2$ .

To test this idea for the cholesterol systems studied here,  $\tau_2$  was fixed in the computer program at the value obtained in *p*-xylene solution of  $4.8 \times 10^{-12}$  sec, and the variables  $\tau_1$ ,  $C_2$ ,  $\epsilon_\infty$  were allowed to vary until the "best" fit was found. For series 1A to E the apparent  $C_2$  values were 0.20, 0.21, 0.33, 0.24, and 0.18, respectively, while for series 2A to 2E they were 0.33, 0.25, 0.30, 0.26, and 0.23. In series 1, the weight factors

change little because  $4.8 \times 10^{-12}$  sec is near to the group relaxation time in Table II in each case. The change is more noticeable in series 2. Whereas previously  $C_2$  had tended to increase with greater 1,4-dioxane concentration, the biased estimate of  $\tau_2$  leads to an apparent decrease in  $C_2$ .

### Conclusions

For cholesterol in the mixed solvent, *p*-xylene and 1,4-dioxane, as the proportion of the 1,4-dioxane is increased, the  $C_2$  value deduced from the experimental results tends more to the theoretical value and for a solution containing 83% of 1,4-dioxane virtually coincides with that value. Thus, stronger interaction of the solute with the solvent appears to favor agreement between the calculated and experimental  $C_2$  values. In addition, there does appear to be a definite increase of OH group relaxation time with increasing donor capacity. A bias towards a fixed  $\tau_2$  value in systems in which  $\tau_2$  is really varying can result in an apparent reduction in  $C_2$ . Other cases of lowering of  $C_2$  can be caused by underestimating the effect of self-association. Altogether, it would seem that, except for the cases where approach to the O-H group in phenols is hindered by substituents in the 2 and 6 positions, or where self-association is precluded by fairly strong interaction with excess of the solvent, analysis of the data into a molecular and a hydroxyl relaxation time, which has been the recent practice in the literature, cannot be justified.

In general, when dielectric data are analyzed into contributions from a molecular and an intramolecular relaxation time care has to be taken to ensure that no additional factor is present which leads to an analysis which is meaningless in terms of molecular behavior.

(22) S. K. Garg and C. P. Smyth, *J. Phys. Chem.*, **69**, 1294 (1965).

(23) J. Crossley and C. P. Smyth, *J. Chem. Phys.*, **50**, 2259 (1969).



## Evaluation of Some Interactions in Permselective Membranes

by N. Lakshminarayanaiah

Department of Pharmacology, University of Pennsylvania, Philadelphia, Pennsylvania 19104 (Received August 27, 1969)

The number of moles of water ( $\bar{l}_3$ ) accompanying ion transport, following passage of 1 faraday of current across three cation selective membranes, one of high water content and the other two of low water content, has been measured at 25° using 0.01 *N* solutions of NaCl, RbCl, or CsCl. Also, specific conductance, counterion self-diffusion coefficient, and hydrodynamic permeability of the membranes have been determined. These data and other equilibrium parameters like water content and exchange capacity have been used to derive values for the Stefan–Maxwell diffusivity coefficients,  $\bar{D}_{1*1}$ ,  $\bar{D}_{14}$ ,  $\bar{D}_{13}$ , and  $\bar{D}_{34}$ , from a few relations given by Scattergood and Lightfoot. The diffusivity coefficient  $\bar{D}_{1*1}$  was the lowest (*i.e.*, the interaction between species 1\* and 1 was the highest) in the case of membranes of low water content in which  $\bar{l}_3$  showed little dependence on the current density used in its measurement. In the case of high water content membrane,  $\bar{l}_3$  was dependent on the current density employed during electrolysis. At low current densities,  $\bar{l}_3$  was greater than the quantity of water associated with 1 equivalent of counterion in the membrane phase. With this value of  $\bar{l}_3$ ,  $\bar{D}_{34}$  assumed negative values. On the other hand, when the limiting value of  $\bar{l}_3$  observed at high current densities was used in the equations, values obtained for the diffusivity coefficients increased in the order  $\bar{D}_{14} < \bar{D}_{1*1} < \bar{D}_{13} < \bar{D}_{34}$ . The order of these coefficients for membranes of low water content was  $\bar{D}_{1*1} < \bar{D}_{14} < \bar{D}_{13} < \bar{D}_{34}$ .

### Introduction

A variety of transport phenomena arise across a membrane when it is subject to different driving forces.<sup>1,2</sup> Some of these phenomena such as ion migration, electroosmosis, self-diffusion, hydrodynamic permeability, etc., occurring across ionic membranes have been described by Spiegler<sup>3</sup> applying the principles of nonequilibrium thermodynamics and by Lightfoot and coworkers<sup>4–6</sup> using the generalized Stefan–Maxwell equations. Under simplifying conditions, *viz.*, co-ions absent from the membrane phase ( $\bar{C}_2 = 0$  and counterion transport number  $\bar{l}_1 = 1$ ), Spiegler<sup>3</sup> derived the following set of equations

$$\bar{X}_{13} = (aE - 1)/B \quad (1)$$

$$a = (RT/\bar{D}_1) = \bar{X}_{13} + \bar{X}_{14} \quad (2)$$

$$E = (\bar{k}/\bar{C}_1 F^2) \quad (3)$$

$$B = (\bar{k}\bar{l}_3/\bar{C}_3 F^2)$$

$$= (\bar{C}_1 \bar{X}_{13}) / [\bar{C}_1 \bar{X}_{13} \bar{X}_{14} + \bar{C}_3 \bar{X}_{34} (\bar{X}_{13} + \bar{X}_{14})] \quad (4)$$

where subscripts 1, 3, and 4 represent counterion, water, and membrane including the ionized groups fixed to the membrane matrix, respectively,  $\bar{C}_i$ 's are the concentrations,  $\bar{X}_{ij}$ 's are the friction coefficients between the components *i* and *j*,  $\bar{k}$  is the specific conductance,  $\bar{l}_3$  is the transport number of water, and  $\bar{D}_1$  is the self-diffusion coefficient. *R*, *T*, and *F* have their usual significance. Overbars refer the parameters to the membrane phase.

With the help of these equations values for the friction coefficients could be derived provided reliable measurements of  $\bar{l}_3$ ,  $\bar{D}_1$ , and  $\bar{k}$  are made for the membrane in its proper ionic form. Equations 1–4 do not contain the term  $\bar{X}_{1*1}$  which indicates the interaction of the

radioactive isotope 1\* employed to measure  $\bar{D}_1$  with its abundant species, the counterion itself. The importance of this isotope interaction has been pointed out by Laity,<sup>7</sup> and Caramazza, *et al.*,<sup>8</sup> have questioned the omission of this term and furthermore have given an expression for  $\bar{D}_1$  including this interaction term. The effects of this interaction term on measurements of unidirectional fluxes using radioactive isotopes have been considered by some workers,<sup>9–12</sup> and Curran, *et al.*,<sup>13</sup> have examined the available experimental data and came to the conclusion that the tracer flow could be used to predict the flow of the bulk substance. Recently, Scattergood and Lightfoot,<sup>6</sup> for the first time, have evaluated the diffusivity coefficient  $\bar{D}_{1*1}$ . This followed from the fourth measurement of hydrodynamic permeability ( $L_p$ ) of the membrane under the condition of zero current. They obtained the following relations, again for the condition,  $\bar{C}_2 = 0$  and  $\bar{l}_1 = 1$ .

- (1) N. Lakshminarayanaiah, *Chem. Rev.*, **65**, 493 (1965).
- (2) N. Lakshminarayanaiah, "Transport Phenomena in Membranes," Academic Press, Inc., New York, N. Y., 1969, p 6.
- (3) K. S. Spiegler, *Trans. Faraday Soc.*, **54**, 1408 (1958).
- (4) E. N. Lightfoot, E. L. Cussler, Jr., and R. L. Rettig, *A.I.Ch.E. J.*, **8**, 708 (1962).
- (5) E. N. Lightfoot and E. M. Scattergood, *ibid.*, **11**, 175 (1965).
- (6) E. M. Scattergood and E. N. Lightfoot, *Trans. Faraday Soc.*, **64**, 1135 (1968).
- (7) R. W. Laity, *J. Phys. Chem.*, **63**, 80 (1959).
- (8) R. Caramazza, W. Dorst, A. J. C. Hoeve, and A. J. Staverman, *Trans. Faraday Soc.*, **59**, 2415 (1963).
- (9) L. F. Nims, *Yale J. Biol. Med.*, **31**, 373 (1959).
- (10) L. F. Nims, *Science*, **137**, 130 (1962).
- (11) O. Kedem and A. Essig, *J. Gen. Physiol.*, **48**, 1047 (1965).
- (12) A. Essig, *J. Theor. Biol.*, **13**, 63 (1966).
- (13) P. F. Curran, A. E. Taylor, and A. K. Solomon, *Biophys. J.*, **7**, 879 (1967).

$$\bar{i}_3 = (\bar{x}_3/\bar{D}_{13})/[(\bar{x}_1/\bar{D}_{13}) + (\bar{x}_4/\bar{D}_{34})] \quad (5)$$

$$L_p = (\bar{x}_3\bar{C}\bar{V}_3^2)/\{[(\bar{x}_1/\bar{D}_{13}) + (\bar{x}_4/\bar{D}_{34})]RTd\} \quad (6)$$

$$\bar{k} = (\bar{C}_1F^2/RT)/[(\bar{x}_3/\bar{D}_{13}) + (\bar{x}_4/\bar{D}_{14}) - (\bar{i}_3\bar{x}_1/\bar{D}_{13})] \quad (7)$$

$$(1/\bar{D}_1) = [(\bar{x}_1 + \bar{x}_{1*})/\bar{D}_{1*1}] + [\bar{x}_3/\bar{D}_{13}] + [\bar{x}_4/\bar{D}_{14}] \quad (8)$$

where  $\bar{x}_i$ 's are mole fractions,  $\bar{D}_{ij}$ 's are Stefan–Maxwell diffusivity coefficients,  $\bar{C}$  is the total concentration,  $\bar{V}_3$  is the partial molar volume of water,  $d$  is the thickness of the membrane, and \* indicates the radioactive counterion. The two treatments mentioned above are essentially equivalent in that the friction coefficients of eq 1–4 are related to the diffusivity coefficients of eq 5–8 by the relation<sup>5</sup>

$$\bar{X}_{ij} = (RT/\bar{D}_{ij})\bar{x}_j \quad (9)$$

and

$$\bar{D}_{ij} = \bar{D}_{ji} \quad \bar{x}_i\bar{X}_{ij} = \bar{x}_j\bar{X}_{ji} \quad (10)$$

These relations indicate that small values for the diffusivity coefficients  $\bar{D}_{ij}$ 's mean large values for the interaction between species  $i$  and  $j$ , *i.e.*, the values for the friction coefficients  $\bar{X}_{ij}$ 's are high, and vice versa.

The four measurements ( $\bar{i}_3$ ,  $\bar{D}_1$ ,  $\bar{k}$ , and  $L_p$ ) including the membrane equilibrium data and the results of evaluation of the four diffusivity coefficients,  $\bar{D}_{1*1}$ ,  $\bar{D}_{14}$ ,  $\bar{D}_{13}$ , and  $\bar{D}_{34}$ , for three strong acid cation-exchange membranes and three ions,  $\text{Na}^+$ ,  $\text{Rb}^+$ , and  $\text{Cs}^+$  are presented in this paper.

## Experimental Section

**Cation-Exchange Membranes.** Two membranes, AMF C-103 and AMF C-104, were supplied by the American Machine and Foundry Co. They were polyethylene-styrene graft copolymer type containing sulfonic acid groups. The third was the cross-linked phenolsulfonic acid (PSA) membrane which was prepared following the procedure described elsewhere.<sup>14</sup> The membranes were conditioned in 1 *N* HCl solution, washed thoroughly with deionized water, and equilibrated with the required 0.01 *N* solution ( $\text{NaCl}$ ,  $\text{RbCl}$ , or  $\text{CsCl}$ ) which was changed a number of times for complete conversion of the membrane into the proper ionic form.

**Measurement of Different Equilibrium Properties.** Pieces of equilibrated membrane were blotted with filter paper, placed in a weighing bottle, and weighed. They were then dried to constant weight at 103° to determine their water content which was estimated to have an error of  $\pm 4\%$  in the case of PSA membrane and  $\pm 3\%$  in the case of other membranes.

A piece of equilibrated membrane of accurately known area, surface dried between filter papers, was held in a micrometer caliper for measurement of its thickness (error =  $\pm 2\%$ ). This piece of known volume was weighed for the determination of its density which was accurate to  $\pm 0.3\%$ . Next it was equilibrated with stirring overnight with a known excess of 0.1 *N*  $\text{HNO}_3$

solution. The acid used up by ion exchange only was estimated in the usual way<sup>14</sup> with an error of  $\pm 1\%$ . The chloride ion (co-ion) content of  $\text{HNO}_3$  solution and washings was negligible ( $\ll 0.001 N$ ).

**Electrical Conductance.** The resistance ( $\bar{R}$ ) of the membrane was determined by a method described elsewhere.<sup>15</sup> As the area ( $A$ ) and thickness ( $d$ ) were known by independent measurements, the specific conductance ( $\bar{k}$ ) of the membrane was evaluated with an accuracy of  $\pm 2.5\%$  from the relation

$$\bar{k} = (d/\bar{R}A) \quad (11)$$

**Water Transport Number.** Two methods, one based on weight changes and the other based on volume changes, are available for this measurement.<sup>16</sup> In this work the rate of movement of water through the membrane subject to an electric field was followed by the volume method with an accuracy better than  $\pm 2\%$  in the manner described in an earlier paper.<sup>17</sup> The observed volume change for the passage of 1 faraday of current was corrected for the electrode reactions in the way described by Lakshminarayanaiah.<sup>18,19</sup>  $\bar{i}_3$  is given by

$$\bar{i}_3 = (V_c/\bar{V}_3) \quad (12)$$

where  $V_c$  is the actual increase in volume on the cathode side.  $\bar{i}_3$  values obtained in this study with AMF membranes were independent of current density whereas the results obtained with PSA membrane were dependent on current density displaying the characteristics described elsewhere.<sup>17–19</sup>

**Self-Diffusion Coefficient.** Counterion self-diffusion coefficients were measured using <sup>22</sup>Na, <sup>86</sup>Rb, and <sup>137</sup>Cs by a quasi-steady-state method described by Lakshminarayanaiah.<sup>20</sup> The radioactivity was counted on Packard Tri-Carb liquid scintillation counter. In these studies both bulk solutions and the liquid layers near the membrane–solution interfaces were kept well stirred. Small rotating magnetic bars were used in the cell as close to the membrane faces as possible to displace the stagnant liquid films. Preliminary investigations of this process of diffusion as a function of the rates of stirring of the small bars placed close to the membrane faces showed that the diffusion coefficient was little affected by increasing the rate of stirring but was lowered by about 15% when the stirring was stopped completely even though the bulk solutions were kept

(14) A. Lakshminarayanaiah and V. Subrahmanyam, *J. Polym. Sci., Part A*, **2**, 4491 (1964).

(15) V. Subrahmanyam and N. Lakshminarayanaiah, *J. Phys. Chem.*, **72**, 4314 (1968).

(16) N. Lakshminarayanaiah, *J. Electrochem. Soc.*, **116**, 338 (1969).

(17) N. Lakshminarayanaiah and V. Subrahmanyam, *J. Phys. Chem.*, **72**, 1253 (1968).

(18) N. Lakshminarayanaiah, *Proc. Indian Acad. Sci., Sect. A*, **55**, 200 (1962).

(19) N. Lakshminarayanaiah, *Desalination*, **3**, 97 (1967).

(20) N. Lakshminarayanaiah, *Biophys. J.*, **7**, 511 (1967).

well stirred all the time. The diffusion coefficient was evaluated from the equation<sup>20,21</sup>

$$\bar{D}_1 = \frac{1.15VdC_1}{\Delta t A \bar{C}_1} \log \frac{C^* - 2C^*_{t_0}}{C^* - 2C^*_{t_0 + \Delta t}} \quad (13)$$

where  $V$  is the equal volume of solution (150 ml) used in the two compartments,  $C^*$  is the initial concentration (taken as counting rate per milliliter) on the "hot" side, *i.e.*, at  $t = 0$ , and  $C^*_{t_0}$  and  $C^*_{t_0 + \Delta t}$  are concentrations at  $t = t_0$  and  $t = t_0 + \Delta t$ , respectively.  $\Delta t$  therefore is the time elapsing between samplings in seconds.  $t_0$  is the time at which the initial sample is withdrawn. The errors involved in these measurements were  $\pm 3\%$ .

**Hydrodynamic Permeability Coefficient.** This was determined following the procedures described by Lakshminarayanaiah.<sup>20,22</sup> A membrane without any support was used in these measurements. Although the membrane used this way had been stretched by about 10% due to application of gas pressure to one side, none of its equilibrium properties were affected. Even its electrical resistance and self-diffusion coefficient were not significantly changed. Membrane in the proper ionic form bounded on either side by water only was used. In the case of PSA membranes,  $L_p$  values had an error of  $\pm 6\%$ , while in the other cases the error was  $\pm 5\%$ . In some preliminary experiments, 0.01  $N$  NaCl solution instead of water only was used. The  $L_p$  values obtained were practically the same as the values realized with water on either side of the membrane. So in all experiments, only water was used to measure  $L_p$ . In some experiments with Na-form AMF C-104 membrane, instead of  $N_2$  gas pressure, osmotic force was applied by using 0.5  $M$  sucrose solution on one side and water on the other side. Little sucrose passed through the membrane and a value of  $(9.0 \pm 0.6) \times 10^{-7} \text{ cm}^4 \text{ J}^{-1} \text{ sec}^{-1}$  was realized for  $L_p$ . The method using gas pressure gave a value of  $(9.6 \pm 0.5) \times 10^{-7}$ .

## Results and Discussion

The various values of the equilibrium parameters determined for the different membranes and monovalent ions are given in Table I. The results of other measurements are summarized in Tables II and III. These data for each membrane and the ion concerned have been used in eq 5-7 and solved to derive values for the three unknowns,  $\bar{D}_{13}$ ,  $\bar{D}_{34}$ , and  $\bar{D}_{14}$ . The fourth unknown  $\bar{D}_{1+1}$  has been evaluated from eq 8. The values so derived for the diffusivity coefficients are given in Table IV. In these calculations the hydration of the ion,  $\text{Na}^+$ ,  $\text{Rb}^+$ , or  $\text{Cs}^+$ , and of the fixed groups of the membrane are ignored and so the entries given in Tables II-IV are for the species  $\text{R-SO}_3^-$  cation involved and water.

In the case of PSA membrane and  $\text{Na}^+$  ion,  $\bar{t}_3$  is dependent on the current density used in its measurement (see Table V). At low current density,  $\bar{t}_3$  has a

**Table I:** Different Equilibrium Membrane Parameters

Membrane system	Thickness, $d$ , cm	Density, $g/\text{cm}^3$	Exchange capacity, $C_4$ , $\text{mol}/\text{cm}^3 \times 10^3$	Water content, $g/100 \text{ g wet membrane}$
PSA				
$\text{Na}^+$	0.0292	1.160	0.98	59.00
AMF C-103				
$\text{Na}^+$	0.0134	1.063	0.92	15.99
$\text{Rb}^+$	0.0134	1.091	0.88	11.35
$\text{Cs}^+$	0.0134	1.093	0.79	12.00
AMF C-104				
$\text{Na}^+$	0.0149	1.072	1.10	13.61
$\text{Rb}^+$	0.0149	1.103	0.96	11.47
$\text{Cs}^+$	0.0149	1.105	0.84	11.30

**Table II:** Transport Data for Membranes in Contact with 0.01  $N$  Solution

Parameter	PSA	AMF C-103		
	$\text{Na}^+$	$\text{Na}^+$	$\text{Rb}^+$	$\text{Na}^+$
$\bar{C}_1$ ( $\text{mol}/\text{cm}^3$ ) $\times 10^3$	0.99	0.92	0.88	0.79
$\bar{C}_4$ ( $\text{mol}/\text{cm}^3$ ) $\times 10^3$	0.98	0.92	0.88	0.79
$\bar{C}_3$ ( $\text{mol}/\text{cm}^3$ ) $\times 10^3$	38.60	9.45	6.89	7.30
$\bar{C}$ ( $\text{mol}/\text{cm}^3$ ) $\times 10^3$	40.57	11.29	8.65	8.88
$\bar{x}_1$	0.0244	0.0814	0.102	0.089
$\bar{x}_4$	0.0241	0.0814	0.102	0.089
$\bar{x}_3$	0.95	0.837	0.796	0.822
$\bar{D}_1$ ( $\text{cm}^2/\text{sec}$ ) $\times 10^8$	265	5.74	7.54	11.46
$\bar{k}$ ( $l./\text{ohm cm}$ ) $\times 10^3$	15.24	1.793	2.01	1.38
$\bar{t}_3$ ( $\text{mol}/F$ )	28	7.0	4.7	4.9
$L_p$ ( $\text{cm}^4/\text{J sec}$ ) $\times 10^6$	141	2.1	1.8	1.7

**Table III:** Transport Data for Membranes in Contact with 0.01  $N$  Solution

Parameter	AMF C-104		
	$\text{Na}^+$	$\text{Rb}^+$	$\text{Cs}^+$
$\bar{C}_1$ ( $\text{mol}/\text{cm}^3$ ) $\times 10^3$	1.10	0.96	0.84
$\bar{C}_4$ ( $\text{mol}/\text{cm}^3$ ) $\times 10^3$	1.10	0.96	0.84
$\bar{C}_3$ ( $\text{mol}/\text{cm}^3$ ) $\times 10^3$	8.11	7.03	6.94
$\bar{C}$ ( $\text{mol}/\text{cm}^3$ ) $\times 10^3$	10.31	8.95	8.62
$\bar{x}_1$	0.1067	0.1072	0.0975
$\bar{x}_4$	0.1067	0.1072	0.0975
$\bar{x}_3$	0.7866	0.7856	0.8050
$\bar{D}_1$ ( $\text{cm}^2/\text{sec}$ ) $\times 10^8$	7.33	10.54	17.13
$\bar{k}$ ( $l./\text{ohm cm}$ ) $\times 10^3$	1.396	1.735	1.225
$\bar{t}_3$ ( $\text{mol}/F$ )	6.3	3.9	4.4
$L_p$ ( $\text{cm}^4/\text{J sec}$ ) $\times 10^7$	9.2	7.0	7.0

value of 69 and decreases with increasing current density to a value of 28 in the range 15.8-31.5  $\text{mA}/\text{cm}^2$ . Several factors such as changes in the structure of ion-solvent complex or the distribution of ions and charges

(21) R. Schlögl and F. Helfferich, *Z. Elektrochem.*, **56**, 644 (1952).

(22) N. Lakshminarayanaiah, *J. Appl. Polym. Sci.*, **11**, 1737 (1967).

**Table IV:** Stefan–Maxwell Diffusivity Coefficients

$\bar{D}_{ij}$ × 10 <sup>8</sup> cm <sup>2</sup> / sec	PSA Na <sup>+</sup>	AMF C-103			AMF C-104		
		Na <sup>+</sup>	Rb <sup>+</sup>	Cs <sup>+</sup>	Na <sup>+</sup>	Rb <sup>+</sup>	Cs <sup>+</sup>
$\bar{D}_{1*1}$	23	0.5	0.9	1.4	1.0	1.5	3.2
$\bar{D}_{14}$	10	4.4	6.5	4.3	3.7	5.6	4.1
$\bar{D}_{13}$	2770	270	453	401	161	228	210
$\bar{D}_{34}$	7030	575	680	450	948	290	240

**Table V:** Transport Number of Water  $\bar{i}_3$  in PSA Membrane in Contact with 0.01 *N* NaCl Solution as a Function of Current Density

Current density, mA/cm <sup>2</sup>	$\bar{i}_3$ , mol/F	Current density, mA/cm <sup>2</sup>	$\bar{i}_3$ , mol/F
0.3	69.0	15.8	28.4
1.6	44.7	31.5	27.6
3.2	37.3		

in the membrane, different types of current carriers in the membrane and concentration polarization at the membrane–solution interface (so-called Bethe–Toropoff effect<sup>23</sup>) causing this current dependence of  $\bar{i}_3$  have been considered in our earlier papers.<sup>17–19</sup> It has been shown<sup>18</sup> that  $\bar{i}_3$  is related to other membrane parameters  $\sigma$  (surface charge density of pore liquid) and  $r$  (pore radius) by the relation

$$\bar{i}_3 = (rF)/(36\sigma) \quad (14)$$

In terms of this equation variation of  $\bar{i}_3$  with current density has been explained. It is postulated that low current densities affect ion distribution and water mobilization in the membrane in such a way that the effective  $r$  is large and the effective  $\sigma$  is small. That is, transport takes place through uncharged or slightly charged pores. At high current densities, average values of  $r$  and  $\sigma$  act to give a limiting value for  $\bar{i}_3$ . In view of this and the fact that the values given for different membrane parameters in Tables I–III are all averages, the limiting value of  $\bar{i}_3$  given in Table II has been used to derive values given in Table IV.

The simplified eq 1–4 are derived for membranes of high water content and so must be applicable to PSA membrane system and inapplicable to AMF membrane systems. That is so is confirmed by the present results. In the case of AMF membranes, eq 1–4 give negative values for  $\bar{X}_{14}$ , whereas the following values are obtained for the PSA membrane when the limiting value of  $\bar{i}_3$  is used in eq 4:  $\bar{X}_{13} = 4.6 \times 10^8$ ;  $\bar{X}_{14} = 4.74 \times 10^8$ ;  $\bar{X}_{34} = 4.6 \times 10^6$  J sec cm<sup>-2</sup> mol<sup>-1</sup>. When the value of 69 realized at very low current density is used,  $\bar{X}_{13}$  is lowered to a value of  $1.86 \times 10^8$  and  $\bar{X}_{14}$  is increased to  $7.48 \times 10^8$ , but  $\bar{X}_{34}$  becomes negative. At a value of about 39 for  $\bar{i}_3$ ,  $\bar{X}_{34}$  is zero and  $\bar{X}_{13}$  and

$\bar{X}_{14}$  are about  $3.3 \times 10^8$  and  $6.04 \times 10^8$ , respectively. For this condition, the equation derived by Spiegler<sup>3</sup> to describe electroosmosis, *viz.*

$$(J_3/J_1) = (\bar{C}_3)/[\bar{C}_1 + \bar{C}_3(\bar{X}_{34}/\bar{X}_{13})] \quad (15)$$

where  $J_i$ 's are the fluxes, becomes

$$(J_3/J_1) = (\bar{C}_3/\bar{C}_1) \quad (16)$$

This equation is equivalent to the one derived by Lakshminarayanaiah and Subrahmanyam<sup>17</sup> for a wide pore membrane in which there is no interaction between membrane and water. That is, when  $J_1 = 1$  equiv  $J_3 = \bar{i}_3$  and so

$$\bar{i}_3 \approx (55.56/\bar{m}_1) \approx \bar{m}_3 \quad (17)$$

( $\bar{m}_1$  is the interstitial molality of the counterion and  $\bar{m}_3$  is the moles of water associated with 1 mol of counterion). Analysis of the membrane phase gives a value of 38.5 for  $\bar{m}_3$ . In the case of AMF membranes  $\bar{i}_3$  values are all lower than  $\bar{m}_3$ . In these systems considerable quantity of water is immobile. In order that  $\bar{i}_3$  may exceed  $\bar{m}_3$ , the condition prescribed by the results obtained with the PSA membrane system at low currents, water must be transported from some source existing in the membrane structure. One such source as already mentioned is an uncharged or slightly charged pore or pores. If water transport is confined to these pores, then  $\bar{i}_3 \gg \bar{m}_3$ .

When eq 5 and 6 are solved using the appropriate data for the PSA membrane and a value of 69 for  $\bar{i}_3$  obtained at low current, a negative value for  $\bar{D}_{34}$ , as expected, is obtained. However, when the limiting value of  $\bar{i}_3$  given in Table II is used, values for  $\bar{D}_{13}$ ,  $\bar{D}_{34}$ , and  $\bar{D}_{14}$  given in Table IV are obtained from eq 5–7. These values according to eq 9 are converted to the corresponding values for the friction coefficients given below:  $\bar{X}_{13} = 8.5 \times 10^7$ ;  $\bar{X}_{14} = 5.8 \times 10^8$ ; and  $\bar{X}_{34} = 8.5 \times 10^5$  J sec cm<sup>-2</sup> mol<sup>-1</sup>. Although the value of  $\bar{X}_{14}$  is close to the value given above, the values of  $\bar{X}_{13}$  and  $\bar{X}_{34}$  are *ca.* 18% lower. The  $\bar{X}_{1*1}$  term omitted in the Spiegler's simplified theory has a value of  $2.7 \times 10^8$ , which is nearly half of  $\bar{X}_{14}$  and higher than the values of  $\bar{X}_{13}$  and  $\bar{X}_{34}$ .

The values of  $\bar{D}_{ij}$ 's given in Table IV for the AMF C-103 and Na<sup>+</sup> ion do not agree with similar values derived by Scattergood and Lightfoot<sup>6</sup> for the same system. This disagreement cannot be assigned to any errors of measurement or uncertainty in the estimation of the  $\bar{D}_{ij}$  values as the errors or uncertainty involved in our work were practically the same as those found by Scattergood and Lightfoot. However, one major difference between the two studies, besides variations in the properties of the membrane samples which were high in the case of AMF C-103 membranes, is that a

(23) A. Bethe and T. Toropoff, *Z. Physik. Chem.*, **88**, 686 (1914); **89**, 597 (1915).

dilute solution of NaCl (0.01 *N*) was used in our study and 0.1 *N* solution was used in the other study. This would lead to some difference in the  $\bar{D}_{ij}$  values, since use of a stronger solution would increase electrolyte uptake and decrease water content of the membrane. These in turn would affect  $\bar{l}_3$  and  $L_p$  values. However, the observed large differences in the  $\bar{D}_{ij}$  values derived in the two studies are unlikely to arise from this one factor alone. There is the further possibility that a systematic error in some measurements, particularly of  $\bar{D}_1$ ,  $L_p$ , and  $\bar{l}_3$ , may cause these discrepancies. Extensive measurements made in this direction in our laboratories under a variety of experimental conditions to detect these systematic errors prove this possibility to be highly improbable.

A casual look at the membrane equilibrium parameters like thickness, water content, and exchange capacity reveal that the same type of membrane used in the two studies has different characteristics. This is also evident in the values of  $\bar{D}_1$  and  $\bar{l}$ . Consequently, the observed differences in the  $\bar{D}_{ij}$  values become attributable to the differences in the properties of the membrane, although the same AMF C-103 membrane has been used in the two studies.

From the results given in Table IV, the following conclusions may be drawn. (1) The diffusion parameter  $\bar{D}_{1*1}$  is relatively small, *i.e.*, the interaction between the isotope 1\* and the counterion 1 is relatively high. (2) The PSA membrane (large water content) has high values for all the diffusivity coefficients compared to the AMF membranes (low water content). (3) In all cases, PSA membrane excepted, the diffusivity coefficients are in the order  $\bar{D}_{1*1} < \bar{D}_{14} < \bar{D}_{13} < \bar{D}_{34}$ . (4) In all cases it is seen that  $\bar{D}_{14}$  is small compared to  $\bar{D}_{13}$ . In other words, the interaction of counterion with the membrane is large compared to the interaction between counterion and water. The counterions are more closely associated with the sulfonic acid groups than

they are with water. This is in qualitative agreement with the calculations of Spiegler<sup>3</sup> made for a poly-methacrylic acid membrane and Na<sup>+</sup> ion but is not in agreement with the results of Mackay and Meares,<sup>24</sup> who found counterions to be more associated with water than with Zeokarb 315 membrane, a material similar to PSA membrane used in this study. (5) The values of  $\bar{D}_{1*1}$  are about  $1/10$  the values of  $\bar{D}_1$  in the case of PSA and AMF C-103 membranes and about  $1/6$  in the case of AMF C-104 membrane. The values of  $\bar{D}_{1*1}$  for the different counterions in AMF membranes lie in the increasing order  $\bar{D}_{1*1(\text{Na})} < \bar{D}_{1*1(\text{Rb})} < \bar{D}_{1*1(\text{Cs})}$ . (6) The interactions of different counterions with water in AMF membranes follow practically the same sequence as in aqueous solutions but they are higher in membranes. These interactions increase with decrease in membrane water content. This is reflected in the fact that the interactions of counterions with water in AMF C-104 which has a relatively low water content are greater than the corresponding ones in AMF C-103 membrane. Na has the highest interaction with water in the membrane compared to Rb and Cs ions. This is in accordance with the fact that its hydration energy (*i.e.*, ion-water dipole interaction) in aqueous solution is higher than that of either Rb or Cs ion. (7) The water membrane interaction is the lowest for all the membranes. This seems to increase with decrease in water content of the membrane. Least water-membrane interaction is seen in the PSA membrane system.

*Acknowledgments.* The work was supported in part by U. S. Public Health Service Grant NB-08163. The author thanks the reviewers for their valuable suggestions and for pointing out some errors in the original manuscript.

(24) D. Mackay and P. Meares, *Trans. Faraday Soc.*, **55**, 1221 (1959).

# Correlation of Fluorescence Quenching and Photopolymerizability of N-Vinylcarbazole in the Presence of Electron Acceptors<sup>1</sup>

by Shigeo Tazuke

Department of Polymer Chemistry, Kyoto University, Kyoto, Japan (Received July 11, 1969)

Photoinduced charge-transfer polymerization of N-vinylcarbazole (VCZ) in the presence of electron acceptors was correlated with the quenching action of electron acceptors on the fluorescence of VCZ in benzene. Photopolymerization of VCZ is readily induced in the presence of acrylonitrile, acetonitrile, nitrobenzene, halogenated hydrocarbons, and silver perchlorate. The propagating species of these photopolymerization systems are mostly cationic or mixtures of cation and radical. Since charge-transfer interactions between VCZ and these electron acceptors at the ground state are not observed by electronic spectroscopy in most cases and since the dynamic quenching of fluorescence is observed, it is strongly suggested that the electron-transferring interactions of the singlet excited state of VCZ with electron acceptors are the primary processes of photopolymerization. The fluorescence of N-ethylcarbazole (ECZ) is similarly quenched by electron acceptors, indicating that the excited carbazyl group interacts with electron acceptors. On the other hand, the photopolymerization of VCZ in donor solvents, such as N,N-dimethylformamide (DMF) or dimethyl sulfoxide (DMSO), proceeds *via* radical path and fluorescence is not quenched. Consequently, the polymerization mechanism was concluded as the conventional one which proceeds *via* triplet states.

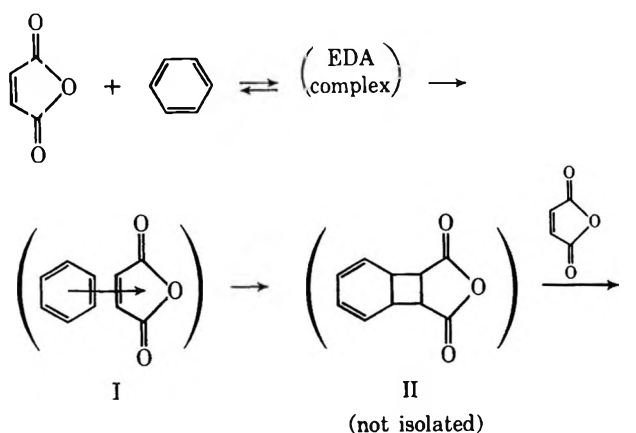
## Introduction

Photoinduced ionic polymerization *via* charge-transfer initiation would be a new branch of unconventional photochemical reactions.<sup>2</sup> The principle of photosensitized charge-transfer excitation has been applied only to a limited number of photochemical reactions<sup>3</sup> although a considerable number of photosensitized charge-transfer phenomena have been investigated by means of electron spin resonance spectroscopy, conductivity measurement, flash photolysis, and absorption and emission spectroscopy.

A well-known example of photoinduced charge-transfer reaction will be the 1,2 cycloaddition of maleic anhydride (MAH) to benzene. The intermediate I was

proposed by Bryce-Smith<sup>5</sup> is to assume a zwitterion as the result of coupling of cation radical with anion radical.

Such charge-transfer processes imply the contribution of extensive polarization and subsequent ionic dissociation, which could induce ionic reactions under appropriate conditions. The ionic processes brought about by charge transfer are a unique feature of photochemistry of charge-transfer complexes. It is, however, not easy to conclude an ionic mechanism in photoinduced reactions of nonchain mechanism. The polymerization technique provides an excellent method of distinguishing between radical and ionic processes since these two mechanisms are characterized by the kinetics, the additive effects on the rate of polymerization, and the copolymerization reactivity. Owing to a large kinetic chain length of polymerization, the incident photochemical events are amplified and memorized by the growing active species. Consequently, polymerization is an extremely sensitive method for detecting photochemical changes providing that the incident events could induce growing polymer chains.



considered as the triplet state of electron donor-acceptor (EDA) complex.<sup>4</sup> An alternate mechanism

(1) This article is part III of "Photo and Thermal Polymerization Sensitized by Donor-Acceptor Interaction." The preceding article is S. Tazuke and S. Okamura, *J. Polym. Sci., A-1*, **7**, 715 (1969).

(2) (a) S. Tazuke, *Advan. Polym. Sci.*, **6**, 321 (1969); (b) S. Tazuke and S. Okamura, SPE Conference on Photopolymers, Ellenville, N. Y., Nov 1967, postprint p 98.

(3) Photosensitized charge-transfer reactions both in organic and inorganic systems were recently reviewed. S. Tazuke, *J. Synth. Org. Chem. Jap.*, **27**, 507 (1969), with 132 references.

(4) W. M. Hardham and G. S. Hammond, *J. Amer. Chem. Soc.*, **89**, 3200 (1967).

(5) D. Bryce-Smith, "Organic Photochemistry," Vol. 2, Butterworths, London, 1967, p 47.

The insight of the initiation process of photosensitized charge-transfer polymerization is not at all clear. The interpretation based on photoexcitation of charge-transfer complexes cannot be justified in all systems since some of the efficient photoinitiators for the polymerization of VCZ such as acrylonitrile and acetonitrile do not form detectable complexes with VCZ at the ground state as measured by electronic absorption spectroscopy. An alternative mechanism is to assume electron transfer between excited VCZ and unexcited acceptor. In this case, preliminary formation of EDA complex at ground state is not essential. A potential method of distinguishing the electron transfer at the excited state from the excitation of EDA complex would be to compare the fluorescence spectra with the results of polymerization and absorption spectroscopy. When the mechanism of excited-state electron transfer involves the singlet excited state of VCZ, the fluorescence of VCZ should be quenched by the dynamic mechanism in accordance with the Stern-Volmer equation. Alternatively, if participation of ground-state complex alone is considered, the effects of electron acceptor on fluorescence of VCZ should be static.

In this article, fluorescence studies were made on VCZ and N-ethylcarbazole in the presence of various additives. The results were interpreted in connection with the photopolymerizability of VCZ.

### Experimental Section

**Materials.** A. *Amines.* N-Vinylcarbazole (VCZ) and N-ethylcarbazole (ECZ), purchased from Koch Light Laboratories Ltd., were purified as already reported.<sup>6</sup>

B. *Acceptors.* Acrylonitrile (AN) was distilled at least twice over calcium hydride after removal of stabilizer by washing. Acetonitrile (G. R. grade) was fractionally distilled over calcium hydride. Carbon tetrachloride (G. R. grade) was washed with water, dried, and distilled. Carbon tetrabromide, hexachloroethane, and *p*-dichlorobenzene were purified by recrystallization from ethanol, ethanol-benzene mixture, and ethanol, respectively. If necessary, activated charcoal was used for decolorizing solutions. Silver perchlorate (G. R. grade) was used as received. The purification of nitrobenzene was already reported.<sup>7</sup>

C. *Solvents.* Benzene (G. R. grade) was distilled through a 40-cm Widmer column. N,N-Dimethylformamide (DMF, G. R. grade) and dimethyl sulfoxide (DMSO, Extra Pure (E. P.) grade) were repeatedly distilled over calcium hydride under a reduced pressure.

D. *Other Materials.* Styrene was purified by washing and distillation in a stream of nitrogen as generally practiced. Azobisisobutyronitrile (AIBN) was recrystallized twice from methanol-acetone mixture.

**Spectroscopic Measurements.** Absorption spectra were measured by a Shimadzu MPS-50L spectrometer. For the measurement of emission spectra, Fluorometry

Attachment Type II was added to the spectrometer. The excitation light source was a 100-W high-pressure mercury lamp, and the light of appropriate wavelength was selected by means of optical filters. Since the fluorescence spectra of carbazole derivatives were not influenced by the wavelength of excitation light, unfiltered, multichromatic light was later used. The emitted light was measured from the position perpendicular to the direction of excitation light with a slit width of 0.7 mm. All measurements were made in the presence of air.

**Polymerization and Analysis of Copolymers.** The method of polymerization was conventional and similar to those already reported<sup>6</sup> except the  $\text{AgClO}_4$ -VCZ system. The glass tubes used as polymerization vessels absorbed 98.0-99.9% of light at 290  $m\mu$  and less than 25% of light at 310  $m\mu$ . Consequently, the effective irradiation absorbed by the polymerization was conducted at wavelengths longer than 300  $m\mu$ .

The VCZ- $\text{AgClO}_4$  system was irradiated by monochromatic light at 365  $m\mu$ . The reaction apparatus was the same as that used for the photopolymerization of VCZ-sodium chloroaurate system.<sup>8</sup> Photopolymerization of VCZ in DMF or in DMSO was carried out in a dilatometer of ca. 20-ml capacity with the irradiation by a 300-W high-pressure mercury lamp in a thermostated water bath. Copolymerization of VCZ with styrene was made in a sealed ampoule. The polymeric products were precipitated in methanol, and the copolymer composition was determined by elemental analysis.

### Results and Discussion

**VCZ-AN System.** Photopolymerization of this system was reported previously.<sup>6,9</sup> The results indicate that radical and cationic propagation reactions occur simultaneously as judged by additive effects and copolymerization. The most plausible explanation for the initiation process was presented by considering the photoinduced electron-transfer interaction between electron-donating VCZ and electron-accepting AN. Both components are stable under photoirradiation at wavelengths longer than 300  $m\mu$  if independently irradiated. Consequently, a certain kind of interaction between VCZ and AN must exist. All spectroscopic attempts, however, could not provide evidence of complex formation between these two monomers. For instance, the data of continuous variation method in *n*-hexane ( $[\text{VCZ}] + [\text{AN}] = 0.3 M$ ) fall on a straight line indicating the absence of electronic interaction between these two components.<sup>6</sup> Although one may consider the possibility of intermolecular interactions which do not influence the orbital energy levels, such interactions

(6) S. Tazuke and S. Okamura, *J. Polym. Sci., A-1*, **6**, 2907 (1968).

(7) S. Tazuke, M. Asai, and S. Okamura, *ibid.*, **6**, 1809 (1968).

(8) S. Tazuke, M. Asai, and S. Okamura, *Kogyo Kagaku Zasshi*, **72**, 1841 (1969).

(9) S. Tazuke and S. Okamura, *Polym. Lett.*, **6**, 173 (1968).

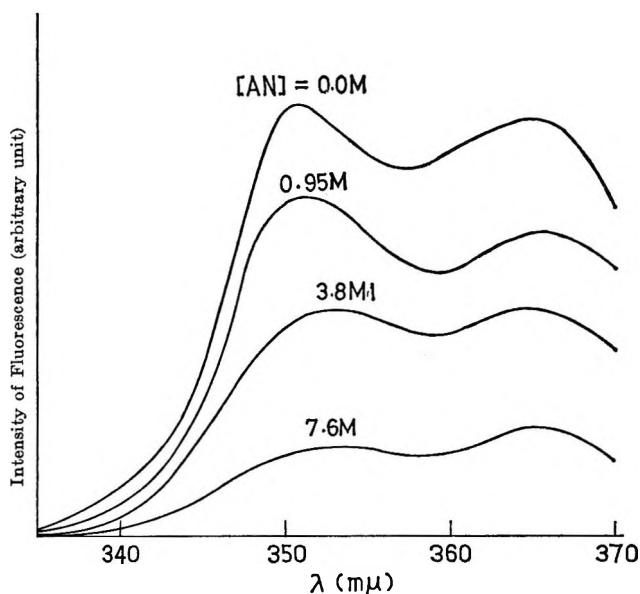
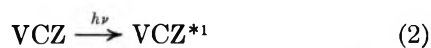


Figure 1. Fluorescence of VCZ ( $10^{-4} M$ ) in the presence of acrylonitrile; solvent, benzene.

should not participate in the initial process of photochemistry. The absence of a charge-transfer band does not necessarily mean the absence of charge-transfer interaction since the intense absorption of VCZ below  $360 m\mu$  might overlap with the charge transfer band if any. While this author considered formerly<sup>6</sup> that the last possibility might explain the present photochemical system, the results of fluorescence spectroscopy suggest an alternative and more acceptable mechanism involving excited-state electron transfer. Fluorescence of VCZ is quenched by AN as shown in Figure 1, whereas no change is observed in absorption spectra. Considering the nature of propagating species being cation and radical and the photoabsorbing species being VCZ, the initiation process must proceed *via* interactions of the singlet excited state of VCZ with the ground state of AN.



A similar mechanism may be suggested for the photopolymerization of AN in the presence of N-ethylcarbazole. As judged by the fluorescence quenching experiments of ECZ by AN, the charge-transfer interaction of AN with excited ECZ will be the reason for photoinitiation. This photosensitization depends on the electron-accepting properties of vinyl compounds since the combination of ECZ with styrene which is neutral or even donor in the light of donor-acceptor concept is an inefficient photoinitiation system. The Stern-Volmer plots are depicted in Figure 2. If reactions 2 and 3 alone occurred, the quenching process should be dynamic. The nonlinear relation of  $f_0/f$  vs. AN would indicate either the participation of static

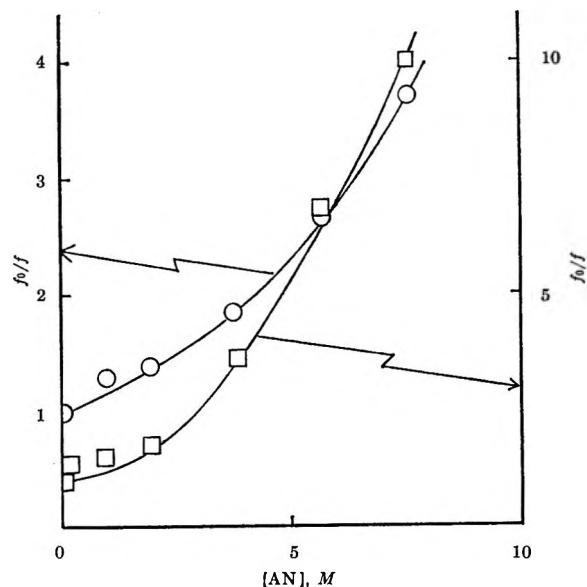


Figure 2. Stern-Volmer plots of VCZ-AN and ECZ-AN systems:  $\circ$ ,  $[VCZ] = 10^{-4} M$ ;  $\square$ ,  $[ECZ] = 10^{-4} M$ .

quenching which causes an additional decrease in fluorescence intensity or the presence of solvent effects. The quenching effect of AN is rather small so that the fraction of quencher is comparable or even more than solvent. The change in dielectric constant and viscosity of medium in the presence of AN might in part be responsible for the nonlinearity of Figure 2.

Acetonitrile is even a weaker quencher for the fluorescence of VCZ and ECZ (Table I), since the de-

Table I: Fluorescence of VCZ and ECZ in the Presence of Acetonitrile ( $[Amine] = 1.0 \times 10^{-4} M$ )

Fluorescer	Solvent	$f_1$ ( $\lambda$ , $m\mu$ )	$f_2$ ( $\lambda$ , $m\mu$ )
VCZ	Benzene	52.0 (350)	55.0 (365)
	Bz-CH <sub>3</sub> CN =	44.2 (352)	49.1 (365)
	1/1 (v/v)		
ECZ	Benzene	67.0 (352)	75.0 (368)
	Bz-CH <sub>3</sub> CN =	60.0 (353)	67.2 (368)
	1/1 (v/v)		

crease in fluorescence intensity in the presence of acetonitrile is so small that it is not possible to decide as to whether acetonitrile acts as a mere solvent or a quencher. Photopolymerization of a VCZ-acetonitrile system was, however, suggested to proceed by ion-radical mechanism.<sup>6</sup>

*VCZ-Halogenated Hydrocarbon Systems.* Halogenated hydrocarbons have been claimed to be efficient photosensitizers for the polymerization of N-vinyl compounds.<sup>10</sup> The polymerization of VCZ initiated by

(10) E. Wainer, U. S. Patent 3,042,517 (1962).



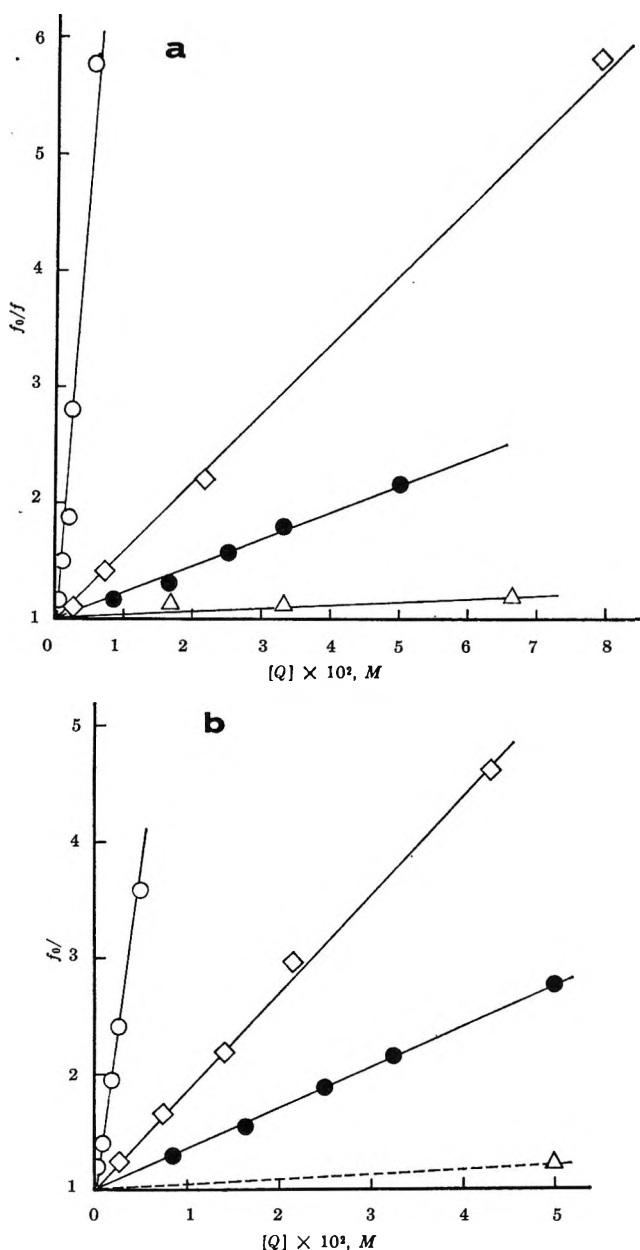


Figure 3. Stern-Volmer plots of (a) VCZ-halogenated hydrocarbon and (b) ECZ-halogenated hydrocarbon systems:  $[VCZ]$  (or  $[ECZ]$ ) =  $10^{-4}$  M;  $f$  at 351 m $\mu$  for VCZ, at 368 m $\mu$  for ECZ;  $Q$ :  $CBr_4$  (O),  $CCl_4$  ( $\diamond$ ),  $C_2Cl_6$  ( $\bullet$ ),  $p\text{-Cl}_2C_6H_4$  ( $\Delta$ ).

carbon tetrachloride had been a point of disputation.<sup>11</sup> Ellinger showed that the polymerization proceeded only under the influence of light.<sup>11c</sup> He did not observe definite complex formation between VCZ and  $CCl_4$ , and the VCZ- $CCl_4$  mixture remained colorless over a period of several days in the dark. The mixture kept in the light remained colorless over 2 days, but gradually changed to orange-red after exposure to light for 5 days.

Although it is not possible at this moment to explain the total initiation process, the incident event of photochemistry of VCZ- $CCl_4$  system is very likely to be the excitation of uncomplexed VCZ molecule. The con-

cept of charge-transfer excitation would contradict the finding that the ground-state interaction of VCZ with  $CCl_4$  could not be detected. The example of interaction of excited tertiary amine with  $CCl_4$  demonstrated by flash photolysis study of Leuco Ethyl Crystal Violet (tris(*p*-N,N'-diethylaminophenyl)methane) in the presence of  $CCl_4$ <sup>12</sup> provides support for the exciplex mechanism for VCZ- $CCl_4$  system. Interaction of the singlet excited state of VCZ with halogenated hydrocarbon was confirmed by fluorescence quenching of VCZ, shown in Figure 3. Furthermore, the Stern-Volmer plots fall on straight lines with the exception of the VCZ-carbon tetrabromide system.<sup>13</sup>

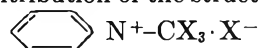
The sequence of quencher strength is the same for VCZ and ECZ. The quenching constants shown in Table II

Table II: Quenching Constant ( $k_q$ ) and Acceptor Strength of Halogenated Hydrocarbons

$Q$	$k_q, M^{-1}$		Acceptor strength <sup>a</sup>
	Fluorescer VCZ	Fluorescer ECZ	
$CBr_4$	$\sim 600^b$	540	170
$CCl_4$	59	83	15
$C_2Cl_6$	22	35	12
<chem>Clc1ccc(Cl)cc1</chem>	<2.9	<4.4	4.3

<sup>a</sup> Reference 13. <sup>b</sup> The Stern-Volmer plot is concaved upward.

are approximately in the order of acceptor strengths which were determined from the total molar polarization of pyridine in the presence of halogenated hydrocarbons.<sup>14</sup> The polarization thus determined expresses the extent of contribution of the structure



which is taken as the relative index of acceptor strength based on the affinity to hybridized lone-pair electrons.

These results of quenching study do not directly provide evidence in support of ion-radical initiation of polymerization. However, the parallelism between  $k_q$  and acceptor strength would imply that the initial event of photopolymerization is the excitation of VCZ leading to exciplex formation.

*VCZ-Nitrobenzene System.* A nitrobenzene solution of VCZ is thermally stable but photochemically active. The photopolymerization of a VCZ-nitrobenzene system

(11) (a) A. Chapiro and G. Hardy, *J. Chim. Phys.*, **59**, 993 (1962); (b) J. W. Breitenbach and Ch. Srna, *Polym. Lett.*, **1**, 263 (1963); (c) L. P. Ellinger, *Polymer*, **5**, 559 (1964); (d) J. W. Breitenbach and O. F. Olaj, *Polym. Lett.*, **2**, 685 (1964); (e) H. Scott, T. P. Konen, and M. M. Labes, *ibid.*, **2**, 689 (1964).

(12) A. McLachlan, *J. Phys. Chem.*, **71**, 718 (1967).

(13) Preliminary experiment of photoirradiation of VCZ in the presence of  $CBr_4$  in air indicates that the development of green color is very rapid, which might influence the fluorescence measurement.

(14) A. N. Sharpe and S. Walker, *J. Chem. Soc.*, 157 (1962).

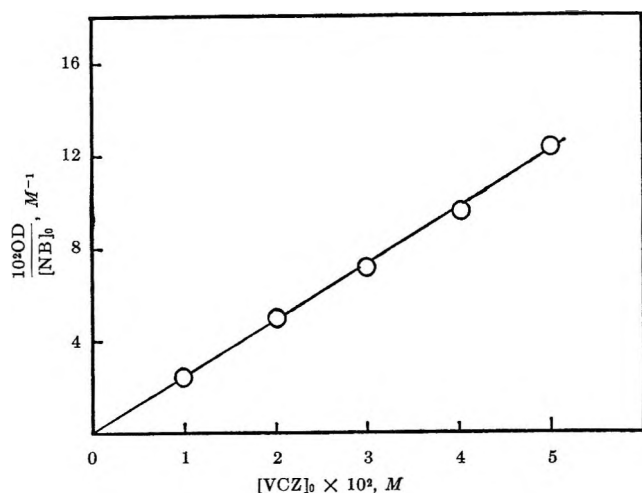


Figure 4. Contact charge-transfer complex between VCZ and nitrobenzene: OD at  $437\text{ m}\mu$ ; optical length, 10 mm; measurement in benzene at room temperature.

was confirmed to be cationic by examining additive effects.<sup>15</sup> Ammonia inhibits the polymerization whereas DPPH does not. A difference of this system from preceding systems is the formation of a charge-transfer complex at the ground state. The pale yellow color of nitrobenzene is greatly intensified by addition of VCZ or ECZ. While a new absorption band is not observed, the absorption spectrum tails to nearly  $500\text{ m}\mu$ , which means a red shift of  $\sim 40\text{ m}\mu$  in comparison with the spectrum of nitrobenzene itself. The complex seems to be of contact charge-transfer type. As shown in Figure 4, the plots of  $\text{OD}/[\text{NB}]$  vs.  $[\text{VCZ}]$  fall on a straight line crossing the origin.

Under the conditions of fluorescence measurement, the absorptions by nitrobenzene and its complex are not serious disturbances. Although the quencher itself has absorptions in the wavelength region of excitation and emission light, the internal filter effects of quencher and its complex are negligible if the emission peak intensity at longer wavelength ( $365\text{ m}\mu$  for VCZ and  $368\text{ m}\mu$  for ECZ) is used for determination. Linearity of the Stern-Volmer plots is satisfactory as shown in Figure 5. The value of  $k_q$  is  $1450\text{ M}^{-1}$  both for VCZ and ECZ.

The most plausible mechanism of photochemical initial process which interprets both fluorescence quenching and cationic propagation would be the excited-state electron transfer producing ion radicals.

**VCZ-Silver Perchlorate System.**<sup>16</sup> Silver perchlorate was reported to induce explosive polymerization of VCZ at elevated temperature<sup>17</sup> supposedly by cationic mechanism. Under much milder conditions of solution polymerization ( $[\text{VCZ}] = 0.125\text{--}1.0\text{ M}$ ,  $[\text{Ag}^+] < 10^{-3}\text{ M}$ , polymerization at  $30^\circ$  in benzene), photoirradiation at  $365\text{ m}\mu$  greatly enhances the rate of cationic polymerization. In this polymerization system, the interaction between solvent and monomer is unimportant. Although silver perchlorate may also interact with ben-

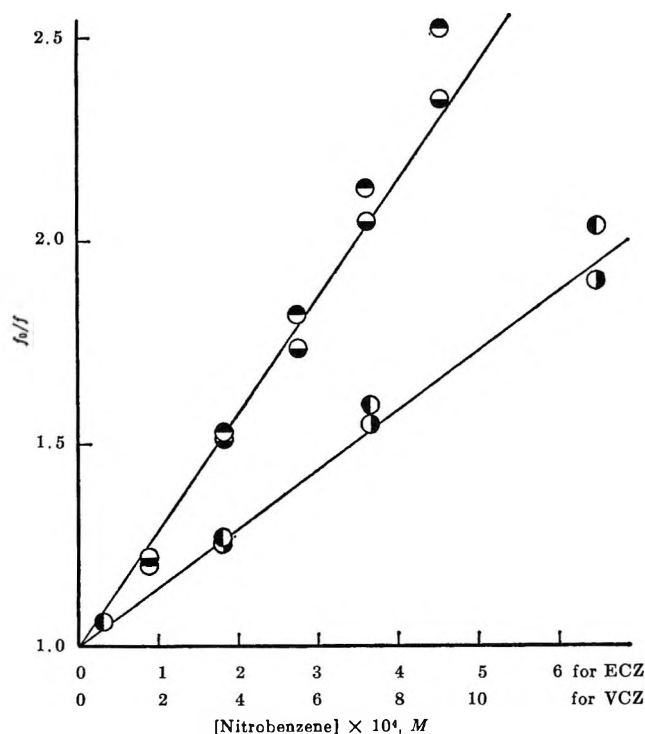


Figure 5. Stern-Volmer plots of VCZ and ECZ-nitrobenzene systems:  $[\text{fluorescer}] = 10^{-4}\text{ M}$  in benzene. VCZ:  $f$  at  $351$  (●) and  $365\text{ m}\mu$  (○); ECZ:  $f$  at  $353$  (○) and  $368\text{ m}\mu$  (●).

zene, the interaction with VCZ seems to be much stronger. Figure 6 shows the spectral change of VCZ in the presence of silver perchlorate measured at more dilute concentration of VCZ than the polymerization system. Since the spectral change of Figure 6 is entirely reversible, there is no reason for suspecting permanent chemical changes. Furthermore, the presence of a distinct isosbestic point in Figure 6 means that only a single complexed species exists. On the other hand, the silver salt does not form a complex with ECZ, suggesting the importance of vinyl group.

Fluorescence spectra of a VCZ-silver perchlorate system are of interest. Figure 7 clearly indicates emission from complexed VCZ. The mirror image relation of absorption and emission spectra is held for these complexed systems. By addition of silver perchlorate both absorption and emission maxima show a blue shift of about  $7\text{ m}\mu$  whereas the shape and position of fluorescence spectra of ECZ is unaffected in the presence of the silver salt. Further increase in the concentration of silver salt brings about a decrease in fluorescence intensity of both VCZ and ECZ. Since a vinyl group is not essential in the course of fluorescence quenching, it would be concluded that silver perchlorate interacts

(15) S. Tazuke, M. Asai, M. Ikeda, and S. Okamura, *Polym. Lett.*, **5**, 453 (1967).

(16) S. Tazuke, Y. Takeda, M. Asai, and S. Okamura, presented to the 18th Annual Meeting of the Polymer Society of Japan, May 1969, Kyoto.

(17) O. F. Solomon, N. Cobianu, D. S. Vasilescu, and C. Boghina, *Polym. Lett.*, **6**, 551 (1968).

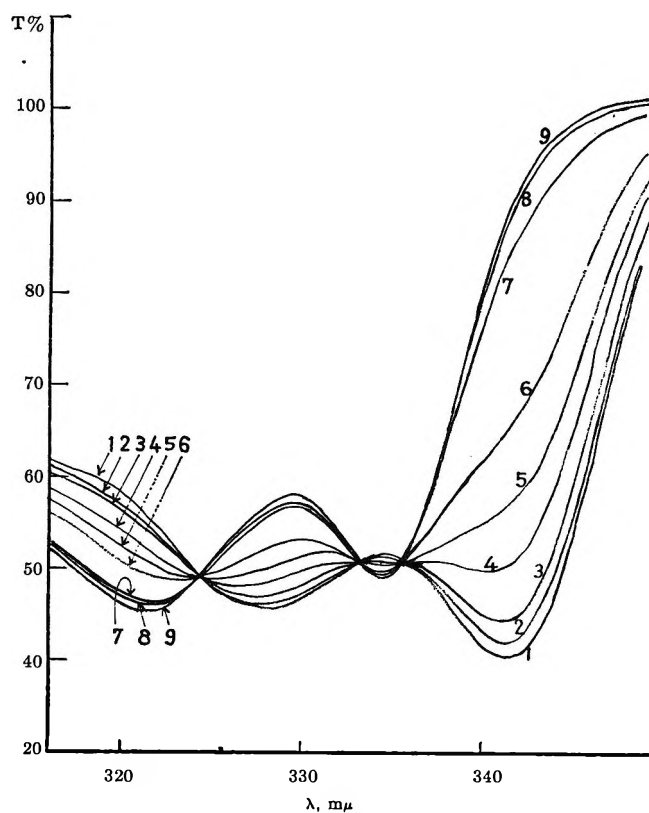
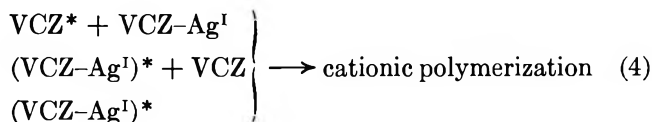


Figure 6. Absorption spectra of VCZ ( $10^{-4} M$ ) in the presence of silver perchlorate: 1, VCZ alone;  $[Ag^I] (M)$ ; 2,  $4 \times 10^{-7}$ ; 3,  $6 \times 10^{-7}$ ; 4,  $8 \times 10^{-7}$ ; 5,  $10^{-6}$ ; 6,  $1.5 \times 10^{-6}$ ; 7,  $2 \times 10^{-6}$ ; 8,  $4 \times 10^{-6}$ ; 9,  $6 \times 10^{-6}$ .

with the singlet excited state of carbazole derivatives at the carbazyl group whereas the ground-state interaction requires the presence of a vinyl group attached to the nitrogen atom of a carbazole ring.

The Stern-Volmer plots shown in Figure 8 fall approximately on a linear line. The maximum emission of complex (*i.e.*  $[AgClO_4] \approx 10^{-5} M$ ) was taken as  $f_0$ . Under the irradiation at  $365 m\mu$ , photoenergy is absorbed mostly by VCZ.<sup>18</sup> Although the VCZ- $AgClO_4$  complex might participate in photoabsorption, the amount would be very much less than that by VCZ. The initiation process will be one of the three reactions in (4). Although spectroscopic data do not provide information for distinguishing these possible initiation mechanisms, the importance of the singlet excited state is suggested.



**VCZ-DMF and -DMSO Systems.** Photopolymerizations of VCZ hitherto mentioned are most likely to be initiated by charge-transfer mechanisms. VCZ can also be polymerized by simple photoirradiation in DMF or in DMSO. These solvents are electron donating and are not expected to conduct charge-transfer processes in

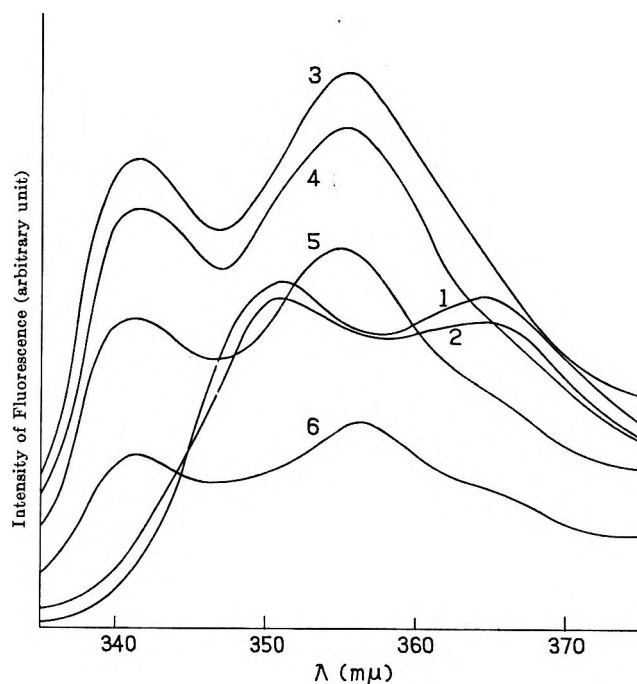


Figure 7. Fluorescence of VCZ-silver perchlorate system:  $[VCZ] = 10^{-4} M$  in benzene;  $[Ag^I] (M)$ : 1, 0.0; 2,  $3.4 \times 10^{-7}$ ; 3,  $3.0 \times 10^{-6}$ ; 4,  $1.5 \times 10^{-4}$ ; 5,  $6.3 \times 10^{-3}$ ; 6,  $2.5 \times 10^{-2}$ .

the presence of VCZ. Additive effects shown in Table III and copolymerization composition curves shown in Figure 9 provide confirmatory evidence in support of radical propagation. The copolymerization reactivity ratios tabulated in Table IV are slightly affected by the kind of solvent, but the fluctuation of data does not contradict the conclusion of radical propagation. If cationic propagation occurred, the copolymer composition should be very rich in VCZ units.<sup>19</sup>

Table III: Photopolymerization of VCZ in DMF and DMSO ( $[VCZ] = 0.75 M$ ,  $30^\circ$  in air; irradiation at a distance of 10 cm from a 300-W high-pressure mercury lamp)

	$R_p \times 10^6,$ $mol l^{-1} sec^{-1}$
VCZ-DMF	5.92
VCZ-DMF	5.97
$[H_2O] = 0.01 M$	
VCZ-DMF	5.52
$[NH_4OH] = 0.01 M$	
VCZ-DMSO	10.9
VCZ-DMSO	10.6
$[H_2O] = 0.01 M$	
VCZ-DMSO	11.0
$[NH_4OH] = 0.01 M$	

(18) Under the conditions of spectroscopy (Figure 6), there seems to be no absorption band of VCZ at  $365 m\mu$ . However, under the conditions of photopolymerization in which the monomer concentration is over  $0.125 M$ , VCZ is a good photoabsorber at  $365 m\mu$ . S. Tazuke, *Advan. Polym. Sci.*, **7**, 321 (1969).

(19) R. Hart, *Makromol. Chem.*, **47**, 143 (1961).

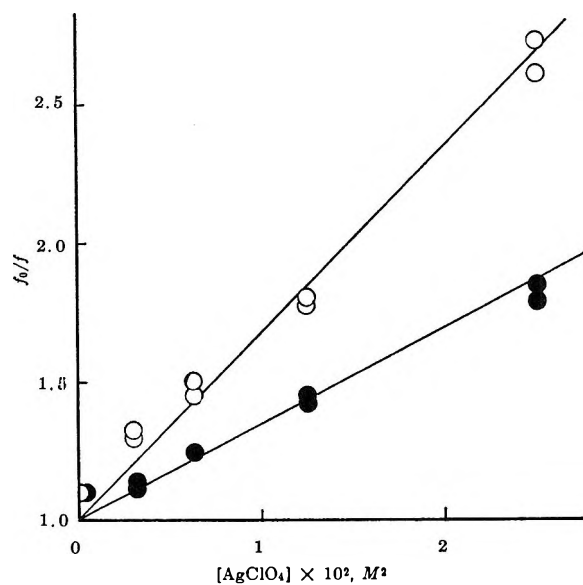


Figure 8. Stern-Volmer plots of VCZ-AgClO<sub>4</sub> (O) and ECZ-AgClO<sub>4</sub> (●) systems: [fluorescer] = 10<sup>-4</sup> M in benzene; *f* at 351 and 365 mμ for VCZ; *f* at 353 and 368 mμ for ECZ.

Table IV: Reactivity of VCZ (*M*<sub>1</sub>)-Styrene System

Photopolymerization in DMF	0.05 ± 0.015	15 ± 2
Photopolymerization in DMSO	0.15 ± 0.1	5 ± 1
Radical polymerization <sup>a</sup>	0.012	5.5
<sup>a</sup> Reference 19.		

Fluorescence intensities of VCZ and ECZ in the presence of DMF and DMSO are tabulated in Table V. The intensity of emission from the solution containing DMF or DMSO is even stronger than that from pure benzene solution of carbazoles. This is a totally different observation from any previously discussed systems. Higher viscosity of DMF or DMSO in comparison with benzene would cause an increase in the lifetime of excited carbazoles and consequently an increase in the fluorescence intensity as well. The slight red shift of emission maxima would be due to the high dielectric constant of DMF and DMSO as expected from the equation of Mataga and his coworkers.<sup>20</sup>

Table V: Fluorescence of VCZ and ECZ in the Presence of DMF and DMSO

Fluorescer	Solvent	<i>f</i> <sub>1</sub> (λ, mμ)	<i>f</i> <sub>2</sub> (λ, mμ)
VCZ	Benzene	37.5 (350)	40.0 (365)
	Bz-DMF = 1/1 (v/v)	41.0 (354)	44.0 (366)
	Bz-DMSO = 1/1 (v/v)	42.3 (356)	45.0 (366)
ECZ	Benzene	55.7 (352)	62.0 (368)
	Bz-DMF = 1/1 (v/v)	61.3 (354)	68.9 (370)
	Bz-DMSO = 1/1 (v/v)	67.0 (355)	71.8 (371)

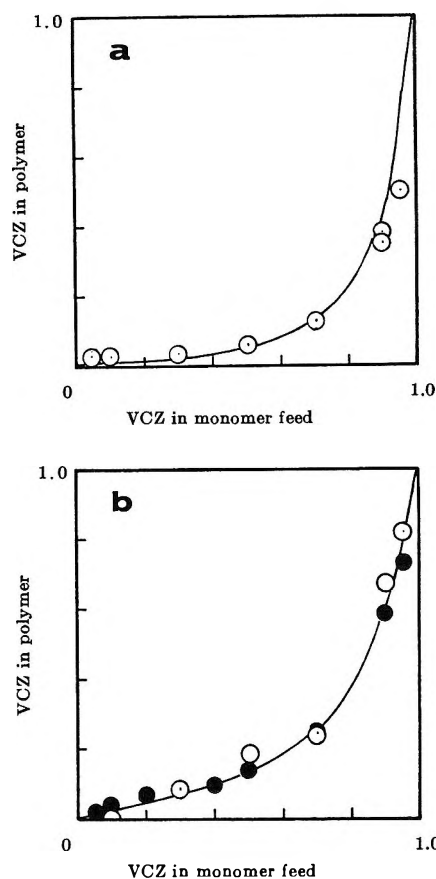


Figure 9. Photoinduced copolymerization of VCZ (*M*<sub>1</sub>) with styrene in DMF (a) and DMSO (b) at 30°: O, polymerization in air; ●, polymerization *in vacuo*.

In any case, the singlet excited state of VCZ is not an active species. Probably, the triplet state of VCZ, the excited carbonyl group or the excited sulfoxide group would be responsible for initiating polymerization. In other words, these photopolymerizations are nothing different from conventional systems.

## Conclusion

From the comparison of spectroscopic data with polymerization study, a distinct classification of photosensitized charge-transfer polymerization from "conventional" (*i.e.*, noncharge-transfer initiation) photopolymerization became possible. The following conclusions were derived by correlating photopolymerization and spectroscopic behavior of VCZ. Firstly, any extent of cationic propagation is always accompanied by fluorescence quenching of VCZ. This is the case of AN, acetonitrile, nitrobenzene, carbon tetrachloride, or silver perchlorate. However, the quenching of fluorescence does not necessarily mean that the propagation reaction is cationic. Secondly, when the fluores-

(20) N. Mataga, Y. Kaifu, and M. Koizumi, *Bull. Chem. Soc. Jap.*, **29**, 465 (1956).

cence of VCZ is not quenched, the polymerization proceeds *via* radical intermediates. Thirdly, charge-transfer interaction at the ground state is not an essential condition of photoinduced charge-transfer polymerization.

There is no positive or negative evidence to discuss the contribution of triplet excited states to charge-transfer processes. The role of triplet states may be ex-

amined by studying the effect of triplet sensitizers on photosensitized charge-transfer reactions.

*Acknowledgment.* The author is greatly indebted to Professor Seizo Okamura for his continuous encouragement and expresses his thanks to Mr. M. Asai and Mr. Y. Takeda for their help in measuring absorption spectra of VCZ-nitrobenzene and VCZ-silver perchlorate systems.

## Stretching Vibration of Nitro and N-Oxide Groups of the Anion Radicals of 4-Nitropyridine N-Oxide and Related Nitro Compounds

by Kiyoshi Ezumi, Hiroshi Miyazaki, and Tanekazu Kubota

*Shionogi Research Laboratory, Shionogi and Co., Ltd., Fukushima-ku, Osaka, Japan (Received October 27, 1969)*

Infrared spectra of the anion radicals of 4-nitropyridine N-oxide, 4-nitropyridine-nitro-N<sup>16</sup> N-oxide, 4-nitropyridine, nitrobenzene, and *p*-nitrotoluene were examined in the region of 1600 cm<sup>-1</sup> to 1100 cm<sup>-1</sup>. The radicals were prepared by the technique of controlled-potential electrolysis in CH<sub>3</sub>CN and CD<sub>3</sub>CN. It was characteristically observed that the stretching vibration of nitro and N-oxide groups in the anion radicals occurs at a considerably lower frequency (see Table I) than in the free molecules. This kind of shift was reasonably attributed to the change in the electronic state of the free molecule on anion radical formation. Theoretical considerations based on the assumption that the formation of anion radicals is due to the putting of an electron in the lowest vacant molecular orbital of free molecules support this conclusion. It is now safe to say that the valence bond state in the anion radicals is sacrificial in comparison with that in the free molecules.

Although there are some reports<sup>1</sup> on the infrared (ir) spectra of small free radicals such as ·CH<sub>3</sub>, ·CF<sub>3</sub>, ·ClOO etc., which were studied by low-temperature matrix methods, reports on the ir spectra of usual organic free radicals are few because of experimental difficulties; however, the ir study of organic anion or cation free radicals seems to be especially interesting from the viewpoint of charge-transfer complexes. Mulliken<sup>2</sup> said that the valence bond of, for example, a  $\pi$ -type acceptor molecule in a charge-transfer complex itself turns out to be sacrificial in comparison with that of the free molecule, since the electron transferred to the lowest vacant anti-bonding molecular orbital (LVMO) of an acceptor molecule brings about a necessarily sacrificial valence bond state of the acceptor molecule. In addition, anion or cation free radicals are considered to be extreme cases of charge-transfer complexes, D<sup>δ+</sup>-A<sup>δ-</sup>, *i.e.*, the free radicals correspond to completely dissociated forms of the complex: namely D<sup>+</sup> and A<sup>-</sup>. Thus the spectroscopic study of free radicals may yield important information about the mechanism of molec-

ular interaction and also on the molecular structure of the free radical itself. In this paper, the change in the stretching vibration of nitro and N-oxide groups in 4-nitropyridine N-oxide (4NPO) and related nitro compounds upon anion radical formation has been particularly discussed in relation to their valence bond strength.

### Experimental Section

In a foregoing paper<sup>3</sup> we reported, on the basis of the electron spin resonance spectral measurements, that the anion radicals of 4NPO and related compounds are formed by the technique of controlled potential electrolysis and that the former radical is relatively stable.

(1) (a) L. Andrews and G. C. Pimentel, *J. Chem. Phys.*, **47**, 3637 (1967); (b) D. E. Milligan and M. E. Jacox, *ibid.*, **47**, 5146 (1967); (c) D. E. Milligan, M. E. Jacox, and J. J. Comeford, *ibid.*, **44**, 4053 (1966); (d) A. Arkell and I. Schwager, *J. Amer. Chem. Soc.*, **89**, 5999 (1967).

(2) R. S. Mulliken, *J. Chim. Phys.*, **61**, 20 (1964).

(3) T. Kubota, K. Nishikida, H. Miyazaki, K. Iwatani, and Y. Oishi, *J. Amer. Chem. Soc.*, **90**, 5080 (1968).

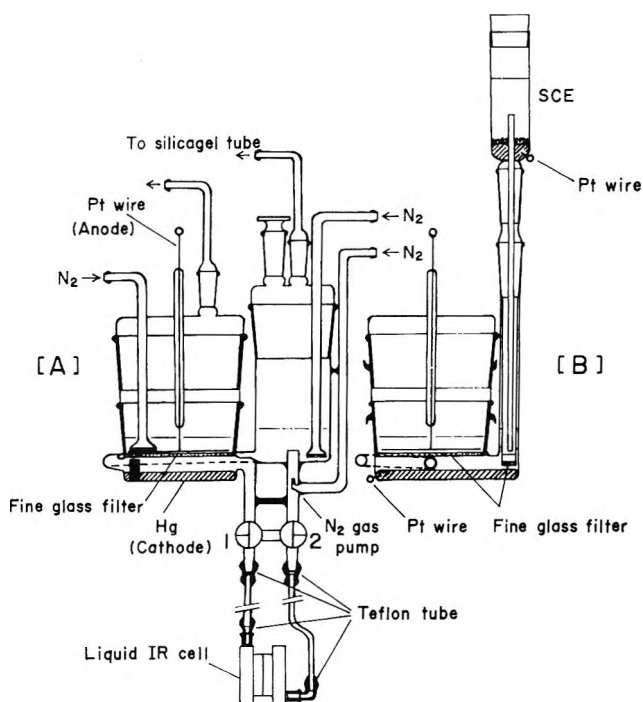


Figure 1. Controlled-potential electrolysis cell for measurement of infrared spectra of anion radicals. Front and side views are shown in [A] and [B], respectively. In the side view, however, only the parts of sce, cathode, and anode are illustrated to make the apparatus clear, the other parts being omitted. The anode is a Pt wire ring in the shape of swirl. The cathode area (Hg) is designed to be quite wide so that the radical anion is generated speedily. A fine sintered glass filter separating the cathode and the anode solutions is selected to satisfy the experimental conditions that the permeation of anode electrolyte solution with no sample to the cathode solution comes out minimum (see also text), but the electric resistance between the cathode and the anode is not so large as the operation of a constant-potential electrolyzer (a Yanagimoto VE-3 type) becomes impossible. The black rectangle at left side and below glass filter in part [A] is a baffle which is placed at the inlet of cathode solution to produce a more efficient liquid movement in all the space between cathode and fine glass filter. Teflon tubing connections to the ir cell were suitable for the present purpose. Because of the good potential stability a saturated calomel electrode (sce) cell has been frequently employed as a standard electrode cell even in the case of nonaqueous medium (See references in the experimental section of ref 3 in this text.) The detailed explanation of the sce cell was already given.<sup>3</sup> This was designed to be suitable for nonaqueous electrochemical experiment.

Here, the anion radicals have been produced using an apparatus for controlled potential electrolysis shown in Figure 1, designed to enable the recording of ir spectra. The explanation of each part of the apparatus is given in Figure 1 and the figure caption. For recording the ir spectra, first about 40 cm<sup>3</sup> of sample solutions ( $\sim 0.05 M$ ), dissolved in solvent containing tetra-*n*-propylammonium perchlorate (TNPAP: 0.1 M) as a supporting electrolyte, is put into a cathode chamber, then the same electrolyte solution ( $\sim 10$  cm<sup>3</sup>) as the above but having no sample is put into an anode chamber. It is noted

that for minimizing the contamination of cathode solution due to the permeation of the anode solution to the cathode chamber, the level of cathode solution is kept a little higher than that of anode solution, as is shown in the Figure 1 [A]. Pure dry N<sub>2</sub> gas is next bubbled through cathode and anode solutions to remove the dissolved oxygen. Here note that by bubbling N<sub>2</sub> gas from an N<sub>2</sub> gas pump (see Figure 1 [A]) at a suitable speed the cathode solution can circulate through ir cell or stopcocks 1 and 2. After the first recording of the ir spectra of neutral species, an appropriate minus set potential (reduction potential:  $-1.30$ ,  $-1.20$ ,  $-1.30$ , and  $-1.45$  V vs. sce for 4NPO, 4NP, nitrobenzene, and 4-nitrotoluene, respectively) that we can determine by recording the polarogram using the same sample solution<sup>3</sup> is applied between cathode and sce terminals, and circulate the cathode solution through the stopcocks 1 and 2 to produce the anion radicals as speedily as possible. Usually, maximum radical concentrations were obtained after 5–10 min, these being suitable for ir spectra measurement. Now, operating the three-way stopcocks 1 and 2, the pathway of the circulation of radical solutions (cathode solutions) is changed to go to the ir cell, the ir spectra being recorded with the lapse of time under continuing electrolysis. The dry air is finally passed through the cathode and anode chambers and the ir spectra of the decomposition products (partial conversion to the neutral molecule also occurs) of anion radicals are recorded for comparison. The formed radical species were also frequently checked by recording the esr spectra<sup>3</sup> by the method of capillary tube in which the cathode solution was taken, suitably diluted, and sealed. Solvents used were CH<sub>3</sub>CN and CD<sub>3</sub>CN. These solvents containing a supporting electrolyte (0.1 M of TNPAP) make the recording of ir spectra impossible in the wave number regions: higher region than 2000 cm<sup>-1</sup>, 1550  $\sim$  1350, 1125  $\sim$  1025, and 930  $\sim$  918 cm<sup>-1</sup> for the system of CH<sub>3</sub>CN + TNPAP; higher region than 2000 cm<sup>-1</sup>, 1125  $\sim$  1000, and 857  $\sim$  825 cm<sup>-1</sup> for CD<sub>3</sub>CN + TNPAP system. The spectrograde acetonitrile was dried with CaH<sub>2</sub> and carefully rectified. CD<sub>3</sub>CN purchased from E. Merck AG (Darmstadt) was used with no further treatment. The ir spectra were recorded with a Nihon-Bunko DS-402G grating spectrometer. Liquid NaCl cells of 0.25 mm thickness were used and the reference cell was filled with the electrolyte solution with no sample to compensate for blank absorption. Samples employed were 4NPO, 4-nitropyridine-nitro-N<sup>15</sup> N-oxide (4N<sup>15</sup>PO), 4-nitropyridine, nitrobenzene, and 4-nitrotoluene, the latter two commercially available being purified by the usual methods. 4N<sup>15</sup>PO was synthesized by the nitration of pyridine N-oxide with KN<sup>15</sup>O<sub>3</sub> in a concentrated H<sub>2</sub>SO<sub>4</sub>-fuming H<sub>2</sub>SO<sub>4</sub> mixture,<sup>4</sup> then recrystallized

(4) M. Itoh, T. Okamoto, and S. Nagakura, *Bull. Chem. Soc. Jap.*, **36**, 1665 (1963).

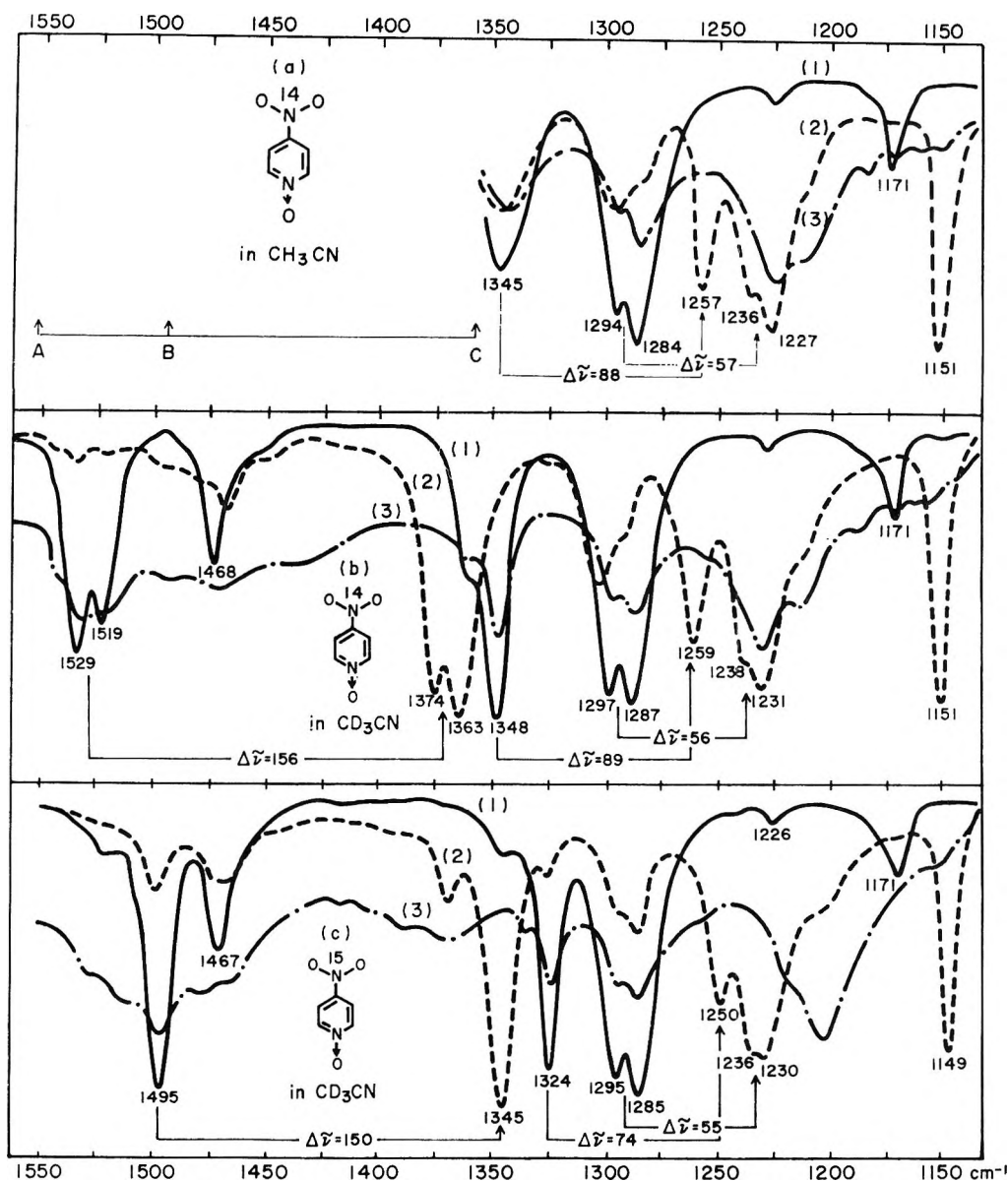


Figure 2. Infrared spectra of 4-nitropyridine N-oxide and its nitro- $\text{N}^{15}$ -labeled compound. Curves 1, 2, and 3 are, respectively, for the neutral molecule, anion radical, and the decomposition product of the anion radical with air. Solvents used are designated in each figure. In figure (a) are shown the wave number regions where the ir measurement of samples is impossible because of the solvent ( $\text{CH}_3\text{CN}$ ) absorption: A  $\sim$  C and B  $\sim$  C regions are for cell lengths 0.25 mm and 0.1 mm, respectively. The spectra appearing in the regions, however, can be easily recorded by using the  $\text{CD}_3\text{CN}$  solvent. See text for the other explanations.

twice from acetone, and subjected to elementary analyses. 4-Nitropyridine, obtained by the deoxygenation of the N-oxide group oxygen atom of 4NPO by the well-known method,<sup>5</sup> was repeatedly recrystallized from petroleum ether.

### Results and Discussion

As examples, in Figures 2 and 3 are shown the ir spectra of 4NPO, 4N<sup>15</sup>PO, and nitrobenzene for the three species: neutral molecule, anion radical, and the decomposition product of the anion radical, formed by passing air through the electrolyte solution (the last species is abbreviated henceforth to DPA). It will be noted that the spectral intensity of the radicals is not so accurate;

this is because the radical concentration changes more or less with time. Moreover, suitable solvents for the present ir study are limited by the experimental technique to  $\text{CH}_3\text{CN}$  or  $\text{CD}_3\text{CN}$ . Figures 2 and 3 show the spectral changes of neutral species with the anion radical formation as well as the spectra of DPA, where we can see that the ir spectra of anion radicals are quite different from those of neutral molecules and also vary greatly with the formation of DPA. Therefore, the absorption bands of radical species are easily identified. Except for the wave number region seen in Figures 2

(5) M. Hamana and H. Yoshimura, *J. Pharm. Soc. Jap.*, **72**, 1051 (1952).

**Table I:** Frequencies of the Stretching Band of Nitro and N-Oxide Groups in the Neutral (N) and Anion Radical (AR) Species of 4-Nitropyridine N-Oxide and Related Nitro Compounds, and Hyperfine Coupling Constant  $|a_N|$  Due to the Nitrogen Atoms in the Anion Radicals

Comps and solvs	$\bar{\nu}_{\text{NO}_2^{\text{as}}}$			$\bar{\nu}_{\text{NO}_2^{\text{s}}}$			$\bar{\nu}_{\text{NO}_2^{\text{m}}}$			$\bar{\nu}_{\text{N}\rightarrow\text{O}}$			$ a_N $ , <sup>a</sup> G	
	N	AR	$\Delta\bar{\nu}_{\text{NO}_2^{\text{as}}}$	N	AR	$\Delta\bar{\nu}_{\text{NO}_2^{\text{s}}}$	N	AR	$\Delta\bar{\nu}_{\text{NO}_2^{\text{m}}}$	N	AR	$\Delta\bar{\nu}_{\text{N}\rightarrow\text{O}}$		
Nitrobenzene														
CH <sub>3</sub> CN	...	...	...	1345	1231	114	...	...	...	...	...	...	...	
CD <sub>3</sub> CN	1530	1357	173	1352	1236	116	1441	1297	144	...	...	...	9.70 (NO <sub>2</sub> ) <sup>b</sup>	
<i>p</i> -Nitrotoluene														
CH <sub>3</sub> CN	...	...	...	1347	1225	122	...	...	...	...	...	...	...	
CD <sub>3</sub> CN	1523	1356	167	1350	1231	119	1437	1294	143	...	...	...	10.40 (NO <sub>2</sub> ) <sup>b</sup>	
<i>p</i> -Nitropyridine														
CD <sub>3</sub> CN	1538	1375	163	1358	1265	93	1448	1320	128	...	...	...	{ 7.26 (NO <sub>2</sub> ) <sup>c</sup> 2.62 (ring N) <sup>c</sup>	
4N <sup>14</sup> PO														
CH <sub>3</sub> CN	...	...	...	1345	1257	88	...	...	...	1294	1237	...	...	
CD <sub>3</sub> CN	{ 1529 1519	{ 1374 1363	155	1348	1259	89	1436	1314	122	{ 1284 1297 1287	{ 1227 1238 1231	57 56	{ 6.04 (NO <sub>2</sub> ) <sup>d</sup> 4.73 (ring N) <sup>d</sup>	
4N <sup>15</sup> PO														
CH <sub>3</sub> CN	...	...	...	1323	1246	77	...	...	...	{ 1291 1284	{ 1233 1226	58	8.39 (NO <sub>2</sub> ) <sup>d</sup>	
CD <sub>3</sub> CN	1495	1345	150	1324	1250	74	1410	1298	112	{ 1295 1285	{ 1236 1230	55	4.69 (ring N) <sup>d</sup>	

<sup>a</sup> All of the values were obtained on the anion radical generated electrochemically in dimethylformamide solvent. <sup>b</sup> P. H. Rieger and G. K. Fraenkel, *J. Chem. Phys.*, **39**, 609 (1963); T. M. McKinney and D. H. Geske, *J. Amer. Chem. Soc.*, **89**, 2806 (1967). <sup>c</sup> Y. Oishi, T. Kubota, H. Miyazaki, and K. Nishikida, *Bull. Chem. Soc. Jap.*, in press. <sup>d</sup> Reference 3 in text.

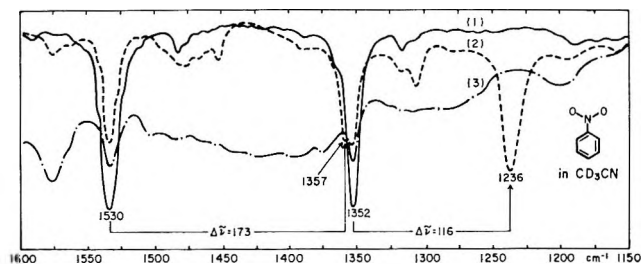


**Figure 3.** Infrared spectra of nitrobenzene in CD<sub>3</sub>CN. Curves 1, 2, and 3 are, respectively, for the neutral molecule, anion radical, and the decomposition product of the anion radical with air. Note that curve 2 mainly consists of the spectra of neutral molecule and anion radical.

and 3, examination of the ir spectra of anion radicals is not so straightforward because of the solvent absorption, etc., but some spectral recordings indicated that the spectral change caused by anion radical formation may not be *apparently* very large (see later discussions). Therefore, our special attention would be put on the wave number regions shown in Figures 2 and 3, where, however, the stretching vibration of nitro and N-oxide groups<sup>6</sup> occurs in both the neutral and anion radical species of 4NPO, etc., so discussions will be made on the behavior of the stretching vibrations caused by anion radical formation. Asymmetric ( $\bar{\nu}_{\text{NO}_2^{\text{as}}}$ ) and symmetric ( $\bar{\nu}_{\text{NO}_2^{\text{s}}}$ ) vibrations pertinent to nitro groups, and the N-oxide stretching ( $\bar{\nu}_{\text{N}\rightarrow\text{O}}$ ) vibration of 4NPO and 4N<sup>15</sup>PO, are doubtlessly assigned as follows<sup>6</sup>: 1529 and 1519 ( $\bar{\nu}_{\text{NO}_2^{\text{as}}}$ ), 1348 ( $\bar{\nu}_{\text{NO}_2^{\text{s}}}$ ), 1297 and 1287 ( $\bar{\nu}_{\text{N}\rightarrow\text{O}}$ ) for

4NPO; 1495 ( $\bar{\nu}_{\text{NO}_2^{\text{as}}}$ ), 1324 ( $\bar{\nu}_{\text{NO}_2^{\text{s}}}$ ), 1295 and 1285 ( $\bar{\nu}_{\text{N}\rightarrow\text{O}}$ ) for 4N<sup>15</sup>PO. Note that some stretching vibrations appear apparently in doublet structures, but the acceptable explanations for this phenomenon are not completely clear. We therefore assume that the doublet structures correspond to stretching vibrations whose average values were tentatively adopted here as the position of the stretching vibrations (see Table I). It is a very reasonable result that the  $\bar{\nu}_{\text{NO}_2^{\text{as}}}$  and  $\bar{\nu}_{\text{NO}_2^{\text{s}}}$  of 4N<sup>15</sup>PO are at lower frequency than those of 4NPO,<sup>7</sup> but  $\bar{\nu}_{\text{N}\rightarrow\text{O}}$  occurs at almost the same wave number for both the compounds, 4NPO and 4N<sup>15</sup>PO. Inspection of Figure 2 also leads to the conclusion that the  $\bar{\nu}_{\text{NO}_2^{\text{as}}}$ ,  $\bar{\nu}_{\text{NO}_2^{\text{s}}}$ , and  $\bar{\nu}_{\text{N}\rightarrow\text{O}}$  of the anion radicals of 4NPO and 4N<sup>15</sup>PO are, respectively, in that order: 1374 and 1363, 1259, 1238 and 1231 for the radical of 4NPO; and 1345, 1250, 1236 and 1230 for 4N<sup>15</sup>PO radical. Again note that although the frequencies of  $\bar{\nu}_{\text{NO}_2^{\text{as}}}$  and  $\bar{\nu}_{\text{NO}_2^{\text{s}}}$  for 4N<sup>15</sup>PO anion radical are lower than those of 4NPO anion radical, there is almost no difference in the  $\bar{\nu}_{\text{N}\rightarrow\text{O}}$  of the two species. These facts as well as the succeeding discussions may suggest that the above said assignments of  $\bar{\nu}_{\text{NO}_2^{\text{as}}}$ ,  $\bar{\nu}_{\text{NO}_2^{\text{s}}}$ , and  $\bar{\nu}_{\text{N}\rightarrow\text{O}}$  in the anion radicals are reasonable. The  $\bar{\nu}_{\text{NO}_2^{\text{as}}}$  and  $\bar{\nu}_{\text{NO}_2^{\text{s}}}$  of the anion

(6) (a) G. Costa and P. Blasina, *Z. Phys. Chem. (Frankfurt)*, **4**, 24 (1955). (b) A. R. Katritzky, "Physical Methods in Heterocyclic Chemistry," Vol. 2, Academic Press, New York, N. Y., 1963, p 283.

(7) Assumption of three-atom molecule for NO<sub>2</sub> group indicates that the observed frequency shift due to the isotope replacement from N<sup>14</sup> to N<sup>15</sup> is reasonably ascribable to the change of atomic mass. See text on the equation used.



radicals of nitrobenzene (see Figure 3) etc. are also in almost the same wave number region as in the case of 4NPO anion radical. All of these data are included in Table I, together with some esr data on the hyperfine coupling (hfc) constants due to the nitrogen atom of  $\text{NO}_2$  and  $\text{N}\rightarrow\text{O}$  groups.

Thus, the frequency shifts of  $\bar{\nu}_{\text{NO}_2^{\text{as}}}$ ,  $\bar{\nu}_{\text{NO}^{\text{s}}}$ , and  $\bar{\nu}_{\text{N}\rightarrow\text{O}}$  caused by anion radical formation are very large, as is seen in Table I. This order of large frequency shift resulting from free radical formation was also reported by Kosower and Poziomek<sup>8</sup> for the 1-methyl-4-carbomethoxypyridine neutral radical whose  $\text{C}=\text{O}$  stretching vibration suffers a lower frequency shift<sup>9,10</sup> of more than  $90\text{ cm}^{-1}$ . The conspicuous frequency shifts of the ir bands given in Table I can be attributed to the change in the electronic state of neutral molecules with anion radical formation. To produce an anion radical the LVMO of neutral molecules will be occupied by an electron, which brings about a sacrificial valence bond state.<sup>11,12</sup>

Let us now examine how the degree of the lower frequency shifts of nitro and N-oxide stretching vibrations can be expected from the change in electronic state on anion radical formation. In the previous paper<sup>3</sup> we already reported in detail the results of molecular orbital calculations concerning the anion radicals of 4NPO and many related compounds, and succeeded in explaining the observed hfc constants by applying the McLachlan modification method.<sup>13</sup> Using the HMO parameters<sup>3</sup> given therein, the molecular diagrams of the anion radicals of 4NPO, 4-nitropyridine, and nitrobenzene were easily calculated, and for the last anion radical the open shell SCF-MO calculation<sup>14</sup> was also reported. The results calculated here and also obtained using the MO's reported by other workers<sup>15</sup> are listed in Table II for the bond order of the nitrogen-oxygen bond in neutral and anion radical molecules. It is understood that the values of bond order mentioned above decrease remarkably with the formation of anion radicals. Jonathan<sup>16</sup> pointed out that there is a good correlation between force constant and bond order, or between force constant and stretching frequency for the  $\text{N}=\text{O}$  bond. Use of these smooth curves leads to the conclusion that the difference of the  $\text{N}=\text{O}$  bond order between a neutral molecule and an anion radical should correspond to the lower frequency shift of the stretching vibration, the values of which are also included in Table II. We can now say that the experimental values of  $\Delta\bar{\nu}_{\text{N}\rightarrow\text{O}}$  and  $\Delta\bar{\nu}_{\text{NO}_2^{\text{m}}} = (1/2)(\Delta\bar{\nu}_{\text{NO}_2^{\text{as}}} + \Delta\bar{\nu}_{\text{NO}_2^{\text{s}}})$  are in the same order in magnitude as those assessed from Jonathan's curves.<sup>16</sup> In addition, the observed value of  $\Delta\bar{\nu}_{\text{NO}_2^{\text{m}}}$  means that a decrease ( $\Delta k_{\text{N-O}^{\text{NO}_2}}$ ) of the  $\text{N}=\text{O}$  stretching force constant ( $k_{\text{N-O}^{\text{NO}_2}}$ ) is engendered by becoming anion radicals. The values of  $\Delta k_{\text{N-O}^{\text{NO}_2}}$  can be also estimated from Jonathan's curves using either the observed frequency or calculated bond order. Results listed in Table II show that  $k_{\text{N-O}^{\text{NO}_2}}$  obtained by both the treat-

ments mentioned above are in quite good agreement, and that a decrease of about 20% in the force constant occurs in the anion radicals.

Assuming the model of a three-atom molecule, it is also possible to calculate the  $k_{\text{N-O}^{\text{NO}_2}}$  roughly from

$$\bar{\nu}_{\text{NO}_2^{\text{as}}} = \left(\frac{1}{2\pi c}\right) \left[ \left\{ \left(\frac{1}{M_{\text{O}}}\right) + \left(\frac{1}{M_{\text{N}}}\right) (1 - \cos \phi) \right\} k_{\text{N-O}^{\text{NO}_2}} \right]^{1/2} \quad (1)$$

eq 1<sup>17</sup> where  $M_{\text{O}}$  and  $M_{\text{N}}$  are the atomic weight of oxygen and nitrogen atoms, respectively, and  $\phi$  is the angle between the two  $\text{N}-\text{O}$  bonds. Putting  $\phi = 120^\circ$  and assuming no change of  $\phi$  between neutral molecule and anion radical, the values of  $k_{\text{N-O}^{\text{NO}_2}}$  have been calculated by using the observed  $\bar{\nu}_{\text{NO}_2^{\text{as}}}$ . The results in units of  $\text{mdyn}/\text{\AA}$  are: 8.14, 6.40; 8.06, 6.39; 8.22, 6.57; 8.07, 6.51; 8.11, 6.56 for nitrobenzene, 4-nitrotoluene, 4-nitropyridine, 4NPO, and 4N<sup>15</sup>PO, respectively, the first and the second numbers in each set being for neutral molecule and anion radical, respectively. Again,  $k_{\text{N-O}^{\text{NO}_2}}$  values for the anion radicals are about 20% smaller than those of neutral molecules, although the absolute values of  $k_{\text{N-O}^{\text{NO}_2}}$  derived above are somewhat smaller than those given in Table II. One of the reasons for his result may be due to a disregard for the interaction term ( $k_{\text{int}}^{\text{NO}_2}$ ) between the force constants pertinent to the two  $\text{N}-\text{O}$  bonds in nitro group. If  $k_{\text{int}}^{\text{NO}_2}$  is taken into account, the  $k_{\text{N-O}^{\text{NO}_2}}$  appearing in the right-hand side of eq 1 should be replaced by the term  $(k_{\text{N-O}^{\text{NO}_2}} - k_{\text{int}}^{\text{NO}_2})$ .<sup>17</sup> Thus, if we adopt the value of  $\sim 2\text{ mdyn}/\text{\AA}$ <sup>18</sup> for  $k_{\text{int}}^{\text{NO}_2}$  it is easily understood that the calculated  $k_{\text{N-O}^{\text{NO}_2}}$  values for both the neutral molecules and the anion radicals become almost equal to those given in Table II. However, the above mentioned calculations may be due to the model being too

(8) E. M. Kosower and E. J. Poziomek, *J. Amer. Chem. Soc.*, **86**, 5515 (1964).

(9) Very recently, Iida<sup>10</sup> also reported that the carbonyl stretching vibration,  $\bar{\nu}_{\text{C}=\text{O}}$ , of *p*-chloranil and *p*-bromanil shifts considerably to lower frequency with the anion radical formation.

(10) Y. Iida, *Bull. Chem. Soc. Jap.*, **43**, 345 (1970).

(11) Circumstances similar to these may also obtain in the case of the cation radical which is produced by removing an electron from the highest occupied MO. It is, however, worthwhile to note that the spin (free electron) orbital of, for example, 1-methyl-4-carbomethoxypyridine neutral  $\pi$  radical,<sup>8</sup> mono (neutral) or di-(cation)-protonated (to N atom) pyrazine  $\pi$  radical,<sup>12</sup> etc. is, of course, LVMO.

(12) B. L. Barton and G. K. Fraenkel, *J. Chem. Phys.*, **41**, 1455 (1964).

(13) A. D. McLachlan, *Mol. Phys.*, **3**, 233 (1960).

(14) D. H. Geske, J. L. Ragle, M. A. Bambenek, and A. L. Balch, *J. Amer. Chem. Soc.*, **86**, 987 (1964).

(15) T. E. Peacock, *Proc. Phys. Soc.*, **78**, 460 (1961).

(16) N. B. H. Jonathan, *J. Mol. Spectrosc.*, **4**, 75 (1960).

(17) G. Herzberg, "Molecular Spectra and Molecular Structure (II)," Infrared and Raman Spectra of Polyatomic Molecules, D. Van Nostrand Company, Inc., New York, N. Y., 1949, p 160, 187.

(18) It is worthwhile to note that the values of  $k_{\text{N-O}^{\text{NO}_2}} = 7.50$  and  $k_{\text{int}}^{\text{NO}_2} = 1.66\text{ mdyn}/\text{\AA}$  were reported for  $\text{NO}_2^-$  ion in KBr crystals. R. Kato and J. Rolfe, *J. Chem. Phys.*, **47**, 1901 (1967).

**Table II:** The Values of Nitrogen-Oxygen Bond Order ( $P$ ) of Neutral (N) and Anion Radical (AR) Species of Nitrobenzene, *p*-Nitropyridine, and 4NPO, and the  $\Delta\bar{\nu}_{\text{NO}_2^{\text{m}}}$  and  $k_{\text{NO}^{\text{NO}_2}}$  (Force Constant) Values Estimated from the Relationship<sup>a</sup> of  $P - \bar{\nu}_{\text{NO}_2^{\text{m}}}$ ,  $P - k_{\text{NO}^{\text{NO}_2}}$ , and  $\bar{\nu}_{\text{NO}_2^{\text{m}}} - k_{\text{NO}^{\text{NO}_2}}$

Compd	Bond order, $P$				$\Delta\bar{\nu}_{\text{NO}_2^{\text{m}}}$ ( $\text{cm}^{-1}$ ) from the relation of $P - \bar{\nu}_{\text{NO}_2^{\text{m}}}$	$k_{\text{N-O}^{\text{NO}_2}}$ (mdyn/Å) from the relations of		$\bar{\nu}_{\text{NO}_2^{\text{m}}} - k_{\text{NO}^{\text{NO}_2}}$	
	NO <sub>2</sub> group		N → O group			$P - k_{\text{N-O}^{\text{NO}_2}}$		$\bar{\nu}_{\text{NO}_2^{\text{m}}} - k_{\text{NO}^{\text{NO}_2}}$	
	N	AR	N	AR		N	AR	N	AR
Nitrobenzene	0.627 <sup>b</sup>	0.444 <sup>b</sup>	...	...	115	10.02	8.48	...	...
	...	0.414 <sup>c</sup>	...	...	...	...	8.23	...	...
	0.639 <sup>d</sup>	0.429 <sup>d</sup>	...	...	122	9.98	8.37	9.99 <sup>e</sup>	8.07 <sup>e</sup>
<i>p</i> -Nitropyridine	0.644 <sup>d</sup>	0.458 <sup>d</sup>	...	...	111	10.10	8.60	10.10 <sup>e</sup>	8.37 <sup>e</sup>
4NPO	0.627 <sup>d</sup>	0.449 <sup>d</sup>	0.440	0.335	112	10.02	8.51	9.90 <sup>e</sup>	8.33 <sup>e</sup>

<sup>a</sup> Reference 16 in text. <sup>b</sup> Reference 15 in text. <sup>c</sup> Reference 14 in text. <sup>d</sup> Calculated by HMO method using the parameters given in ref 3 in text. Unpaired electron occupies LUMO. <sup>e</sup> These values were yielded using the mutual relation<sup>a</sup> between  $\bar{\nu}_{\text{NO}_2^{\text{m}}}$  and  $k_{\text{NO}^{\text{NO}_2}}$ , and also using the observed  $\bar{\nu}_{\text{NO}_2^{\text{m}}}$  (see Table I) value.

simplified, so that the results seem to be qualitative in nature. Nevertheless, the results obtained from all the above discussions may support the assignments of  $\bar{\nu}_{\text{NO}_2^{\text{as}}}$ ,  $\bar{\nu}_{\text{NO}_2^{\text{s}}}$ , and  $\bar{\nu}_{\text{N} \rightarrow \text{O}}$  for the radical species listed in Table I. It is also reasonable that the values of  $\Delta\bar{\nu}_{\text{NO}_2^{\text{m}}}$  are in quite good parallelism with those of hfc constant  $|a_{\text{N}^{\text{NO}_2}}|$  due to the nitro group nitrogen atom as is seen in Table I. The  $|a_{\text{N}^{\text{NO}_2}}|$  value may be a measure<sup>3</sup> of free (spin) electron density at the nitrogen atom.

Aside from the discussions pertinent to the stretching bands of NO<sub>2</sub> and  $\text{N} \rightarrow \text{O}$  groups, we would like to make some remarks on the other bands, particularly of 4NPO anion radical. As is seen in Figure 2 the radical anion of 4NPO shows a quite strong band at 1151  $\text{cm}^{-1}$  which, however, we could not find in the spectrum of nitrobenzene anion radical (see Figure 3). At the present time the assignment of the 1151- $\text{cm}^{-1}$  band of 4NPO anion radical is not clear. Two possibilities are: the shift to lower frequency and the intensification of the 1171- $\text{cm}^{-1}$  band of neutral species or the higher frequency shift of strong 1117- $\text{cm}^{-1}$  band of neutral species. In any way ir bands in this region may be attributed to the ring C-H in-plane bending vibrations

and skeletal vibrations. It was also observed that the 4NPO anion radical has a relatively strong band<sup>19</sup> at 753  $\text{cm}^{-1}$ , from the wave number region of which it may be thought that the 753- $\text{cm}^{-1}$  band might originate from the ring C-H out-of-plane bending vibration or bending vibration of nitro group. In the regions of these wave numbers, however, there are some difficulties for spectral measurement, as was already written. Additional discussions will not be given here, and will be postponed to future studies from the experimental and theoretical viewpoints.

In conclusion, we would say that the valence bond of usual organic molecules should be altered more or less by becoming an anion radical (and also perhaps a cation radical or a neutral free radical). In the case of the compounds reported herein, however, the variation for the nitrogen-oxygen bonds in nitro and N-oxide groups seems to be especially large.

*Acknowledgments.* The authors wish to express their thanks to Dr. Yoshiki Matsui in our laboratory for his advice.

(19) This band position agrees almost with the one (751  $\text{cm}^{-1}$ ) of a medium intensity band appearing in the neutral molecule.

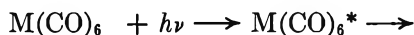
# NOTES

## Photochromism of Metal Carbonyls

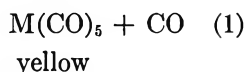
by James A. McIntyre

*Chemical Physics Research Laboratory, The Dow Chemical Company, Midland, Michigan 48640 (Received December 29, 1969)*

Photochromism of metal carbonyls has been observed both in solution<sup>1-3</sup> and in polymer films.<sup>4</sup> For the group VIb metal hexacarbonyls, the suggested<sup>1,3</sup> mechanism of the photochromic reaction is



colorless



where D represents a charge donor. For many donors the substituted carbonyl ( $\text{M}(\text{CO})_5\text{D}$ ) is yellow, as is a cyclohexane solution of the pentacarbonyl. In the absence of a donor, and upon removal of the uv source, a degassed solution appears colorless, suggesting that reaction 3 is quite fast. No quantitative measurements of the rate of this reaction have been reported. In this communication we report rate constants (for  $\text{M} = \text{Cr}$ ) for reaction 3 in cyclohexane and in polystyrene.

Experiments with both degassed and nondegassed solutions demonstrated the sensitivity of the rate to traces of oxygen, which increases the apparent rate. Several freeze-pump-thaw cycles were sufficient for thorough degassing, as evidenced by the reproducibility of fading rate for successive flashes. The cyclohexane used was checked by vpc and mass spectrometry for impurities which could interfere in the reaction. The polymer films, about 0.5 mm thick and containing 1 wt %  $\text{Cr}(\text{CO})_6$  in polystyrene (Dow QX4500) were prepared by evaporating a methyl ethyl ketone solution of the two onto quartz plates in the dark.

The colored species was produced using a flash lamp, and the rate of fading at room temperature, 21–22°, was determined by following the decrease in absorbance at 450 m $\mu$ . This wavelength was chosen from the absorption band obtained using the following technique. A solution of  $\text{Cr}(\text{CO})_6$  in cyclohexane was flushed for about 10 min with nitrogen, then exposed to the full output of a 200-W Hg lamp while flushing

continued. Since the photochemical reaction is 1 above, flushing during exposure removes CO. The pentacarbonyl is sufficiently stable in the absence of a donor (including CO in this category) to allow an absorption spectrum to be obtained over small wavelength intervals by standard techniques (in this case using a Cary Model 11 spectrophotometer). The absorption band of  $\text{Cr}(\text{CO})_5$  in the visible region was found to be very similar in shape and energy to that for  $\text{Cr}(\text{CO})_5(\text{Et}_2\text{O})$ .

If the fading proceeds by reaction 3, then, using the stoichiometry of the photodissociation ( $[\text{M}(\text{CO})_5] = [\text{CO}]$ ), the rate expression is

$$-\frac{d[\text{M}(\text{CO})_5]}{dt} = k[\text{M}(\text{CO})_5]^2 \quad (4)$$

Application of Beer's law and integration yields

$$\frac{1}{A_t} = \frac{kt}{\epsilon l} + \frac{1}{A_0} \quad (5)$$

where  $A$  = absorbance,  $\epsilon$  = molar extinction coefficient,  $l$  = sample pathlength,  $c$  = concentration of absorbing species,  $k$  = second-order rate constant. That the fading reaction follows a second-order rate law is evidenced by the good linear plots of  $1/A_t$  vs.  $t$  that were obtained (Figure 1). The slope of such lines is  $k/\epsilon l$ . The path length is readily obtained. In the case of polystyrene, care was taken to ensure that the sample was sufficiently thin so that it could be assumed that the concentration of colored species was uniform throughout the thickness of the sample. However, the extinction coefficient is not easily determined. The common method of using the decrease in concentration of starting material (obtained by absorbance measurements) as the concentration of transient cannot be applied here due to the extensive overlap of all absorption bands of  $\text{Cr}(\text{CO})_6$  and  $\text{Cr}(\text{CO})_5$  except the one at 450 m $\mu$ . For this reason we report results in terms of  $k/\epsilon$ . It is possible to place a lower limit on  $\epsilon$  from measurements of the maximum absorbance attained and the assumption of complete conversion of  $\text{Cr}(\text{CO})_6$  to  $\text{Cr}(\text{CO})_5$ . Our results for cyclohexane solutions just above the melting point (where the reaction is relatively slow) suggest that the minimum value of  $\epsilon$  is 1000 l./mol cm; a value of 200 has also been suggested.<sup>2</sup> The values of  $k/\epsilon$  that we observed are

(1) W. Strohmeier and D. von Hobe, *Chem. Ber.*, **94**, 2031 (1931).

(2) M. A. El-Sayed, *J. Phys. Chem.*, **68**, 433 (1964).

(3) G. R. Dobson, *ibid.*, **69**, 677 (1965).

(4) A. G. Massey and L. E. Orgel, *Nature*, **191**, 1387 (1961).

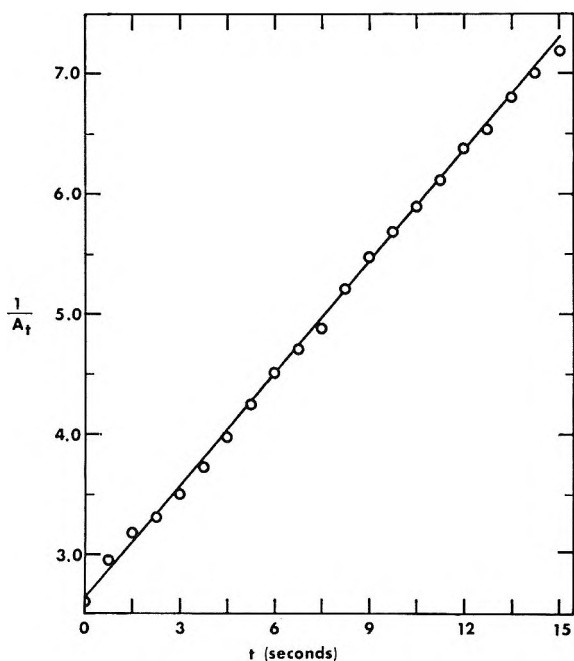


Figure 1. Representative plot of kinetic data for cyclohexane solutions, including a least-squares fit.

0.317 and 0.00025 cm/sec (with average deviation 3% and 5%) for cyclohexane and polystyrene as solvent, respectively. We attribute this large difference to the greatly decreased mobility of CO in polystyrene relative to cyclohexane. If this is the correct interpretation, one can visualize the use of polymer films as "solvents" for other similar reactions which would require fast reaction techniques for study in normal solvents.

*Acknowledgment.* Helpful discussions with P. J. Hart are gratefully acknowledged. I thank G. J. Kallos and E. J. Strojny for analysis of the solvents.

### Fluorescence of Liquid Benzene under Proton and Electron Impact<sup>1a</sup>

by M. L. West and L. L. Nichols

Battelle Memorial Institute, Pacific Northwest Laboratory, Richland, Washington 99362 (Received November 13, 1969)

Extensive studies have been conducted in recent years on the radiation physics and chemistry of aromatic molecules and because it is the simplest of the aromatics, benzene has perhaps received the most attention. The reported optical emission spectra of benzene obtained under various modes and conditions of excitation have led to several theories of reaction kinetics. The reported emission<sup>1b</sup> from dilute solutions of benzene at

room temperature under uv excitation was identified as fluorescence from the lowest excited singlet state of the monomer. At higher concentrations, a broad structureless emission band peaked at 320 nm has been attributed<sup>2</sup> to excimers formed from the interaction of excited singlet and ground-state benzene molecules. Under electron bombardment<sup>3,4</sup> of liquid benzene, the monomer emission was reported to be absent and the observed fluorescence was assigned to excimers formed directly *via* ion recombination. Cooper and Thomas<sup>5</sup> observed short-lived species *via* fluorescence at wavelengths below 400 nm and *via* absorption in the 500-nm region in the electron pulse radiolysis of liquid benzene and this emission and absorption was attributed<sup>5,6</sup> to the lowest singlet state ( $B_{1g}$ ) of the benzene excimer. Phillips and Schug<sup>7</sup> observed both singlet monomer and singlet excimer emission in the electron radiolysis of frozen benzene. That the observed emission was not totally excimeric as was that reported by Carter, Christophorou, and Abu-Zeid<sup>3,4</sup> was explained by the fact that the benzene molecule was bound by the crystalline form and not free to assume the excimer geometry.

This note reports an experimental study of the luminescence from benzene at room temperature upon excitation by electrons and protons. In addition to the singlet monomer fluorescence previously unobserved under electron and proton bombardment in liquid benzene, we observed several fluorescing radiolysis products. By use of a flowing target cell, we are able to eliminate most of the radiolysis product emission and thus obtain spectra consistent with those reported for uv excitation.

The experimental setup has been previously described.<sup>8</sup> A Van de Graaff accelerator provided 1.7-MeV protons and beam currents up to 50 nA. An electron accelerator provided 80-keV electrons and beam currents up to 10  $\mu$ A. Protons (or electrons) entered the front of the cell through a  $2.8 \times 10^{-4}$  cm thick nickel foil and were totally absorbed in less than 40  $\mu$  (100  $\mu$ ) of liquid. Estimates of beam heating based on calculations of heat conductivity give temperature changes of less than 1° for the data presented in this note. Fluorescence was observed through a quartz

(1) (a) This paper is based on work performed under United States Atomic Energy Commission Contract AT(45-1)-1830; (b) I. B. Beriman, "Handbook of Fluorescence Spectra of Aromatic Molecules," Academic Press, Inc., New York, N. Y., 1967.

(2) J. B. Birks, C. L. Braga, and M. D. Lumb, *Proc. Roy. Soc., Ser. A*, **283**, 83 (1965).

(3) J. G. Carter, L. G. Christophorou, and M-E. M. Abu-Zeid, *J. Chem. Phys.*, **47**, 3879 (1967).

(4) L. G. Christophorou, M-E. M. Abu-Zeid, and J. G. Carter, *ibid.*, **49**, 3775 (1968).

(5) R. Cooper and J. K. Thomas, *ibid.*, **48**, 5097 (1968).

(6) J. B. Birks, *Chem. Phys. Lett.*, **1**, 625 (1968).

(7) D. H. Phillips and J. C. Schug, *J. Chem. Phys.*, **50**, 3297 (1969).

(8) L. L. Nichols and W. E. Wilson, *Appl. Opt.*, **7**, 167 (1968).

window at the rear of the cell. All measurements were made with a scanning spectrometer (grating of 1180 lines/mm, blazed at 250 nm; reciprocal dispersion of approximately 2 nm/mm; a typical slit width was 400  $\mu$ ). Maximum dose rates were  $10^6$  rads/sec and  $10^7$  rads/sec for protons and electrons, respectively.

The irradiation cell had a relatively small volume (1.0 cm<sup>2</sup>  $\times$  0.14 cm thick) to reduce self-absorption in the liquid and was also designed to operate under static or flowing conditions. Static conditions refer to a closed system of benzene in which radiolysis products are allowed to accumulate. In the flowing mode, a reservoir of deaerated benzene continuously replaced irradiated liquid in the target volume.

"Nanograde" (Trademark of Mallinckrodt Chemical Corp.) benzene was used without further purification. Nitrogen gas from a liquid nitrogen dewar flask was bubbled through the samples to remove dissolved oxygen.

Emission spectra of benzene excited by electrons or protons are shown in Figure 1. Emission from dilute solutions of benzene in cyclohexane (Figure 1a) is identical with that observed under uv excitation<sup>1</sup> and corresponds to monomer emission from the first excited singlet state. Figure 1b shows a typical emission spectrum of liquid benzene for proton or electron bombardment under static conditions where radiolysis products are allowed to accumulate in the microcell. The two less intense peaks (279 and 286 nm) are attributed to monomer emission as they agree in wavelength with the two most intense peaks of monomer fluorescence. The 272-nm peak was not observed because of its lower intensity and because of increased absorption in the sample at this wavelength. The intense band near 320 nm is at the proper wavelength for excimer fluorescence but a large portion was found to be stable radiolysis product emission.

Figure 1c illustrates the time behavior of fluorescence following steady-state proton or electron irradiation ( $1 \times 10^6$  rads/sec) of liquid benzene in the static cell. If monomer (curve I) and excimer (curve II) fluorescence were the only sources of emission at 279 nm and 370 nm, respectively, then curves I and II would rise to the maximum intensity in approximately 0.04 sec as determined by the time constant of the phototube. The emission at 279 nm (curve I) reaches maximum intensity in about 0.04 sec. The emission at 320 nm (curve II) shows an initial rapid rise followed by a slow buildup to maximum intensity. The slower rising portion of curve II indicates a buildup of an emission from a stable radiolysis product. This build-up emission can be reduced by flowing the liquid through the target cell. This is illustrated in Figure 1d which shows a typical spectrum of benzene emission under proton or electron impact when liquid benzene was allowed to flow through the microcell at a rate of 2 cm<sup>3</sup> min<sup>-1</sup>. Assuming a uniform flow, the average dose

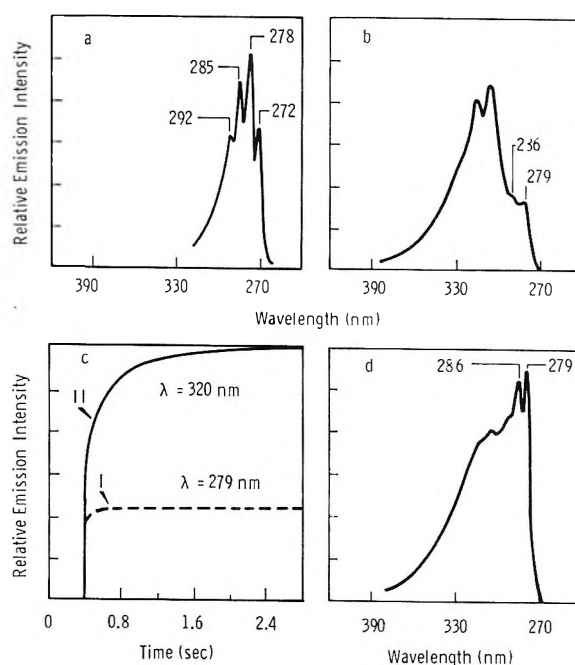


Figure 1. Optical spectra of benzene under proton and electron impact: (a) benzene (5%) in cyclohexane; (b) emission of liquid benzene when radiolysis products are allowed to accumulate in the microcell (static system); (c) time variation of liquid benzene emission under proton or electron impact (dose rate  $\sim 1 \times 10^6$  rads/sec; static system); (d) emission of liquid benzene under proton or electron impact (average dose  $\sim 10^6$  rads; flowed system).

was  $10^6$  rads. Under these conditions, the emission at 279 nm and 320 nm reaches maximum intensity in about 0.04 sec following exposure to a steady-state irradiation.

Radiolysis products contribute a significant portion of the emitted light in the proton and electron bombardment of liquid benzene. The intense emission spectrum near 320 nm (Figure 1b) from the static sample is similar to the reported<sup>1</sup> emission of biphenyl. A C<sub>12</sub>H<sub>10</sub> fraction has been found<sup>9</sup> in the complex polymer products of irradiated benzene and one of the proposed mechanisms of hydrogen formation in irradiated benzene involves biphenyl as a by-product.<sup>10,11</sup> We have conclusively shown that emission spectra from liquid benzene under proton and electron bombardment includes monomer fluorescence. We have not conclusively established that the enhanced emission in the long wavelength portion of benzene emission in the flowing cell is excimer fluorescence. However, the similarity of this emission to the reported emission under uv excitation<sup>2</sup> and the observed rapid rise to maximum intensity following steady-state irradiation suggest that

(9) S. Gordon, A. R. Van Dyken, and T. F. Doumani, *J. Phys. Chem.*, **62**, 20 (1958).

(10) W. G. Burns, *Trans. Faraday Soc.*, **58**, 961 (1962).

(11) W. G. Burns and C. R. V. Reed, *ibid.*, **59**, 101 (1963).

the primary emission before the accumulation of radiolysis products is the same from the various modes of excitation (*i.e.*, *via* proton, electron, and photon irradiation). The reaction mechanism of direct excimer formation *via* ion recombination is not needed to explain the presently reported emission of liquid benzene under electron and proton bombardment.

## Mutual Diffusion Coefficients of Aqueous Copper(II) Sulfate Solutions at 25°

by L. A. Woolf<sup>1</sup> and A. W. Hoveling

Department of Chemistry, University College of Townsville, Townsville, Queensland, Australia (Received December 29, 1969)

This work was undertaken to obtain accurate values of the mutual diffusion coefficient of copper sulfate over the concentration range 0.05–1.4 *M*. Emanuel and Olander<sup>2</sup> had reported an accuracy of about 5% in their measurements for the range 0.35–1.4 *M*, but these results did not agree well with earlier data<sup>3</sup> which extended to lower concentrations. The diffusion coefficients reported here are thought to be accurate to about 1–2%. These results enable a test to be made of the suitability for 2:2 electrolytes of a method used previously to predict diffusion coefficients in concentrated solutions of 1:1 electrolytes. In addition, viscosity results are presented for the range 0.005–1.4 *M*.

### Experimental Section

All solid chemicals used were of analytical reagent quality and were not further purified; before use once-distilled water was passed through an ion-exchange column. The diffusion measurements were made by allowing copper sulfate solutions to diffuse into water using the magnetically stirred diaphragm cell method of Stokes.<sup>4</sup> All copper sulfate solutions were analyzed by determination of copper to  $\pm 0.1\%$  by standard electrogravimetric methods. The several diffusion cells used were calibrated at frequent intervals by allowing 0.5 *M* potassium chloride solutions to diffuse into water at 25°; analyses of the resulting solutions generally were made by precise (*ca.* 0.05%) conductance measurements although some concentrations were determined by potentiometric titration. The overall reproducibility of successive cell constant determinations was 0.1–0.2%.

The viscosity measurements were made with an Ubbelohde-type viscometer incorporating flared capillaries<sup>5</sup> which eliminated kinetic energy corrections. Experimental flow times agreed to  $\pm 0.01\%$ . The densities measured for the viscosity determinations agreed well with the data reported by Pearce and Pumpin<sup>6</sup> but were of lower precision (*ca.* 0.001%).

### Results

The 26 diffusion measurements which were made used solutions which varied in initial concentration from 0.07 to 1.4 *M*. The resulting integral diffusion coefficients were converted to differential coefficients by the method of Stokes.<sup>7</sup> Derivatives necessary for this conversion were obtained numerically by a standard five-point Lagrange method at intervals of 0.01 in  $c^{1/2}$ . Smoothed values of these derivatives were obtained by plotting them against  $c^{1/2}$  and reading the required values from a curve drawn through the points. For convenience the diffusion coefficients are reported in Table I at equal intervals of  $c^{1/2}$ ; the values at 0.01 *M* and 1.440 *M* (saturation) may be subject to extrapolation errors since they lie outside the range of the experimental measurements.

The viscosity measurements covered the range of concentration from 0.005 to 1.42 *M* and are reported in Table I relative to water at 25° having an absolute viscosity of 0.8903 cP. At the lower concentrations these results were in excellent agreement with the equation given by Stokes and Mills<sup>8</sup> and at higher concentrations generally agreed within 0.1% with other literature values.<sup>9</sup> The results reported in Table I were read from a smooth curve drawn through the experimental points.

### Discussion

The present diffusion coefficients are shown in Figure 1. While slightly lower (except at saturation) than those of Emanuel and Olander,<sup>2</sup> they generally agree within the estimated error of either set of measurements. On the other hand, the present results coincide with those of Eversole, *et al.*,<sup>3</sup> only near 0.16 *M*. Above that concentration our results are lower (in agreement with the data of ref 1) and below 0.16 *M* they are higher.

The diffusion of associated electrolytes has been the subject of papers by Harned and Hudson<sup>10</sup> on two 2:2 electrolytes and for some 1:1 electrolytes and a

(1) Address inquiries to Diffusion Research Unit, Research School of Physical Sciences, Australian National University, Canberra, A.C.T., Australia.

(2) A. Emanuel and D. R. Olander, *J. Chem. Eng. Data*, **8**, 31 (1962).

(3) W. G. Eversole, H. M. Kindswater, and J. D. Peterson, *J. Phys. Chem.*, **46**, 370 (1942).

(4) R. H. Stokes, *J. Amer. Chem. Soc.*, **72**, 763 (1950); **73**, 3527 (1951).

(5) B. J. Steel, *J. Sci. Instrum.*, **42**, 751 (1965).

(6) J. N. Pearce and G. G. Pumpin, *J. Amer. Chem. Soc.*, **59**, 1221 (1937).

(7) R. H. Stokes, *ibid.*, **72**, 2243 (1950).

(8) R. H. Stokes and R. Mills, "Viscosity of Electrolytes and Related Properties," Pergamon Press, London, 1965, p 88.

(9) See, for example, "International Critical Tables," Vol. 5, 1st ed, McGraw-Hill Publication, New York, N. Y., 1926, p 14.

(10) H. S. Harned and R. M. Hudson, *J. Amer. Chem. Soc.*, **73**, 3781, 5880 (1951).

**Table I:** Experimental and Calculated Diffusion Coefficients for Copper Sulfate<sup>a</sup>

$c, M$	$D \times 10^6,$ $\text{cm}^2 \text{sec}^{-1}$	$D^+ \times 10^6, \text{cm}^2 \text{sec}^{-1}$		$\eta/\eta_0$	$c, M$	$D \times 10^6,$ $\text{cm}^2 \text{sec}^{-1}$	$\eta/\eta_0$
0	0.858 <sup>a</sup>			1.000	0.360	0.484	1.241
0.01	0.713	0.721 <sup>b</sup>	0.705 <sup>c</sup>	1.006	0.490	0.456	1.347
0.04	0.632	0.652	0.626	1.026	0.640	0.432	1.486
0.09	0.587	0.606	0.577	1.058	0.810	0.413	1.665
0.16	0.547	0.579	0.552	1.102	1.000	0.399	1.875
0.25	0.513	0.563	0.534	1.162	1.210	0.391	2.144
					1.440	0.390	2.520

<sup>a</sup> Calculated from literature data.<sup>14</sup> <sup>b</sup>  $a = 3.64 \text{ \AA}$ . <sup>c</sup>  $a = 6.0 \text{ \AA}$ .

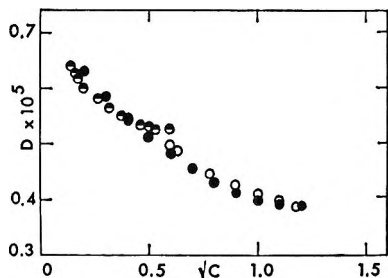


Figure 1. Diffusion in copper sulfate solutions. Filled circles, this work; open circles, ref 2; half-filled circles, ref 3.

2:1 electrolyte by Stokes and others.<sup>11,12</sup> The interpretation of the diffusion process in associated systems described by Wishaw and Stokes<sup>11</sup> has been applied by Robinson and Stokes<sup>13</sup> with considerable success in the calculation of the mutual diffusion coefficients of several 1:1 electrolytes up to several molar in concentration but with poor results for a 2:1 electrolyte. We have endeavored to use the same methods as Harned and Hudson<sup>10</sup> and Wishaw and Stokes to calculate the diffusion coefficients of  $\text{CuSO}_4$  solutions; we are unaware of any previous attempt to use the method of ref 11 for higher order symmetrical valence-type electrolytes.

Equation 4 of ref 11 which gives an expression for calculating  $D$  the mutual diffusion coefficient was rearranged in the form

$$D = D^+ \{1 + 0.036m[(D^*/D^0) - h]\} (\eta_0/\eta) \quad (1)$$

where

$$D^+ = \{[\alpha(D^0 + \Delta_1 + \Delta_2) + 2(1 - \alpha)D_{12}] \times [1 + m(d \ln \gamma_{\pm}/dm)]\} \quad (2)$$

Here  $\alpha$  is the degree of dissociation,  $D^*$  the self-diffusion coefficient of water,  $D^0$  the limiting diffusion coefficient of  $\text{CuSO}_4$ ,  $D_{12}$  the diffusion coefficient of the ion pair,  $m$  the stoichiometric molality,  $\gamma_{\pm}$  the mean molal ionic activity coefficient,  $h$  the hydration number, and  $\eta/\eta_0$  the relative viscosity. An expression equivalent to eq 2 was derived by Harned and Hudson<sup>10</sup> and used by them to calculate diffusion coefficients for  $\text{ZnSO}_4$  solutions. By comparison with experimental measurements over the range 0.001–0.005  $M$  those authors were

able to show that  $D_{12}$  was largely concentration independent. For the present system the mobility of the ion pair was estimated as  $D_{12} = 0.67 \times 10^{-5} \text{ cm}^2 \text{sec}^{-1}$  by a method similar to that described in ref 11 with the exception that instead of using the arithmetic mean to calculate the radius of the minor axis of the ion pair the geometric mean was preferred. This was thought to make some allowance for the different shapes of the  $\text{CuSO}_4$  and  $\text{NH}_4\text{NO}_3$  (ref 11) ion pairs. The necessary limiting equivalent conductances were obtained from the literature.<sup>14</sup> The electrophoretic corrections  $\Delta_1$  and  $\Delta_2$  were calculated for two values of  $a$ , the ion size parameter. The first value of  $3.64 \text{ \AA}$  was chosen because Owen and Gurry<sup>15</sup> had used it for interpreting conductance data for  $\text{CuSO}_4$  solutions. The second choice of  $6.0 \text{ \AA}$  was used because it is close to the figure of  $6.2 \text{ \AA}$  which has been estimated for a similar salt,  $\text{ZnSO}_4$ .<sup>16a</sup> Activity coefficient derivatives and the degree of dissociation were obtained from the literature.<sup>6,13</sup> To obtain values of  $\alpha$  above 0.1  $M$  the data from ref 16b, were plotted against concentration and extrapolated graphically obtaining  $\alpha = 0.38$  at 0.16  $M$  and  $\alpha = 0.35$  at 0.25  $M$ .

Values of  $D^+$  obtained from the calculations are given in Table I. For  $a = 6.0 \text{ \AA}$  the agreement between  $D^+$  and the experimental values is within the anticipated error of the calculations. For  $a = 3.64 \text{ \AA}$  the agreement is not as good and decreases with increasing concentration.

Robinson and Stokes<sup>13</sup> have used equations similar to eq 1 to determine values of  $h$ . According to them the use of the relative viscosity in eq 1 is rather arbitrary and it may be omitted. When  $(\eta/\eta_0)$  is omitted from

(11) B. F. Wishaw and R. H. Stokes, *J. Amer. Chem. Soc.*, **76**, 2665 (1954).

(12) J. R. Hall, B. F. Wishaw, and R. H. Stokes, *ibid.*, **75**, 1556 (1953).

(13) R. A. Robinson and R. H. Stokes, "Electrolyte Solutions," 1st ed, Butterworth and Co., Ltd., London, 1955.

(14) H. S. Harned and B. B. Owen, "Physical Chemistry of Electrolytic Solutions," 3rd ed, Reinhold Publishing Corp., New York, N. Y., 1958, p 697; ref 13, p 452.

(15) B. B. Owen and R. W. Gurry, *J. Amer. Chem. Soc.*, **60**, 3074 (1938).

(16) (a) See ref 13, p 120; (b) see ref 13 p 402; (c) see ref 13 p 317; (d) A. Giacomini and B. Pesce, *Chem. Abstr.*, **35**, 1292 (1941).

eq 1 then a plot of  $D/D^+$  against molality should yield a straight line of unit intercept and slope 0.036 [ $(D^+/D^0 - h)$ ]. Using the values of  $D$  and  $D^+$  from Table I there results when  $a = 3.6 \text{ \AA}$  a value of  $h = 12.8$  (using  $D^* = 2.44 \times 10^{-5}$  (ref 16c)). This value of  $h$  is in good agreement with the value of 12 determined for a similar salt, cadmium sulfate, from compressibility measurements.<sup>16d</sup> It is difficult, however, to reconcile such a large hydration number with the small ion-size parameter  $3.64 \text{ \AA}$ . Using the same procedure with  $a = 6.0 \text{ \AA}$  yields values of  $D/D^+$  which are so scattered as to render meaningless any value of  $h$  determined from them. With the inclusion of the relative viscosity term the calculations give  $h = 3.8$  when  $a = 3.64 \text{ \AA}$ ; with  $a = 6.0 \text{ \AA}$  the  $D/D^+$  values are again considerably scattered and also suggest a negative value of  $h$ .

It is therefore difficult to justify the use of eq 1 for  $\text{CuSO}_4$  solutions. Equation 1 was derived from Hartley-Crank's<sup>17</sup> description of diffusion by regarding  $D^+$  (eq 2) as an intrinsic diffusion coefficient. Bearman<sup>18</sup> and Mills<sup>19</sup> have pointed out that the usual assumptions involved in applying that description to diffusion measurements makes it strictly applicable only to regular solutions. Equation 2 has a sounder theoretical basis although it has been suggested (ref 13, p 323) that it omits a correction for an electrophoretic-type effect operating between the diffusing ion pairs and water molecules and their neighbors. The hydration model of diffusion used by Stokes and coworkers has recently been criticized by Rasaiah and Friedman,<sup>20</sup> who have used a theoretical model which does not rely on hydration to predict thermodynamic (but not transport) properties of 1:1 electrolyte solutions.

(17) G. S. Hartley and J. Crank, *Trans. Faraday Soc.*, **45**, 801 (1949).

(18) R. J. Bearman, *J. Phys. Chem.*, **65**, 1961 (1961).

(19) R. Mills, *ibid.*, **67**, 600 (1963).

(20) J. C. Rasaiah and H. L. Friedman, *J. Chem. Phys.*, **48**, 2742 (1968); **50**, 3965 (1969).

### Thin Layer Direct Current Conductivity of Benzene Solutions of Quaternary Ammonium Salts<sup>1a</sup>

by Alfred Prock and William A. LaVallee

Chemistry Department, Boston University,  
Boston, Massachusetts 02215 (Received October 21, 1969)

This note describes measurements of dc conductivity of solutions of quaternary ammonium salts in benzene at room temperature, where electrode spacing lies within the range 0.002–0.060 cm. Electrolyte concentration was sufficiently low to produce specific conductances in a decade wide range with center around

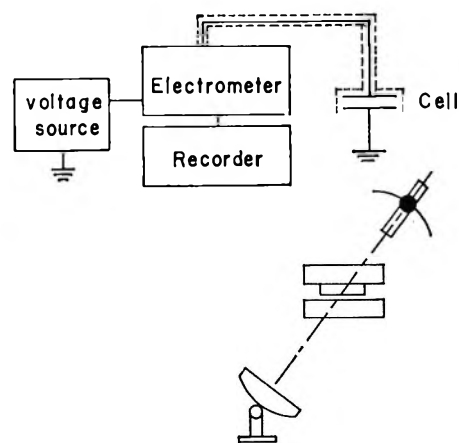


Figure 1. Diagram of apparatus. Cell alignment and spacing are determined through interferometry.

$10^{-12} \text{ ohm}^{-1} \text{ cm}^{-1}$ . The electrolytes used were tetraisoamylammonium picrate and tetraisoamylammonium tetraisoamyl boride. The latter is useful because anion and cation radii in solution can be assumed equal within a small error.<sup>1b</sup> A great simplification is afforded in the mathematical treatment of conduction in this case. The interfacial double layer thicknesses of such solutions span a range around  $10^{-3} \text{ cm}$ ,<sup>2</sup> which is within the lower range of electrode half-spacing. Under these conditions it was possible to test the theory proposed by Gavis,<sup>3</sup> which predicts that apparent specific conductance should increase without limit as electrode spacing decreases. The relationship derived by Gavis is  $\kappa_{\text{app}} = \kappa_0 \coth L/2\delta$ , where  $L/2$  is the half-spacing distance and  $\delta$  is diffuse double layer thickness. In some cases our results can be fitted reasonably well to the Gavis theory, but the conductivity increase at small spacing is shown to be a result of metal ion injection at the anode.

### Apparatus

Figure 1 outlines the apparatus. The electrometer is a Keithley Model 610B and the recorder is a Texas Instruments Model Servowriter II, and the voltage source is Zener diode regulated. The solution cell contains a pair of optical flats with evaporated metal films (Au or Ag) over a base layer of stannous oxide. The reflection of the films at the wavelength of Na D is high enough to provide sharp interference fringes which are then employed to align electrodes and to measure spacing through the angular variation of the fringes. The method used for electrode support and alignment is similar to that shown in ref 2, Figure 3, except that both electrodes are optical flats and both are immersed into the solution. The measurement cell is supported on an

(1) (a) Research supported by NSF Grant GP 7094; (b) J. F. Coetzee and G. P. Cunningham, *J. Amer. Chem. Soc.*, **86**, 3403 (1964); *ibid.*, **87**, 2529 (1965); TIATIB was prepared by John Reardon of this department.

(2) A. Prock, *Rev. Sci. Instrum.*, **36**, 949 (1965).

(3) J. Gavis, *J. Chem. Phys.*, **41**, 3787 (1964).



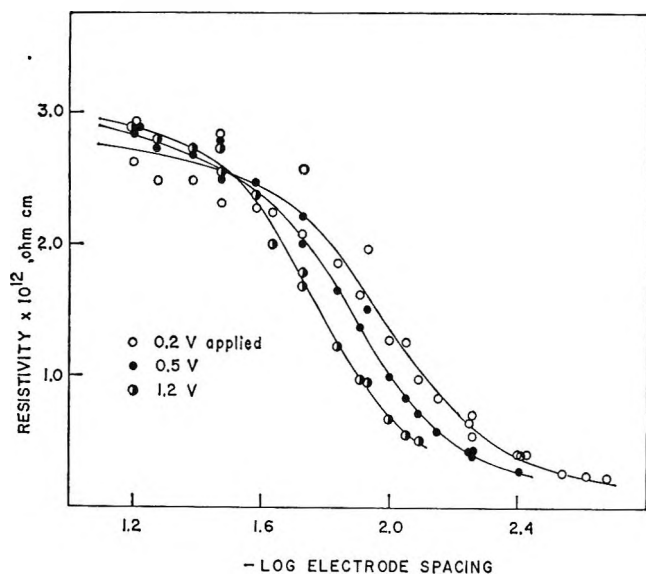


Figure 2. Apparent specific resistivity of TIAP ( $6 \pm 2$ )  $\times 10^{-7} M$  in benzene as a function of electrode spacing. Electrodes are evaporated gold. Spacing is expressed in centimeters. Temperature is  $25^\circ$ .

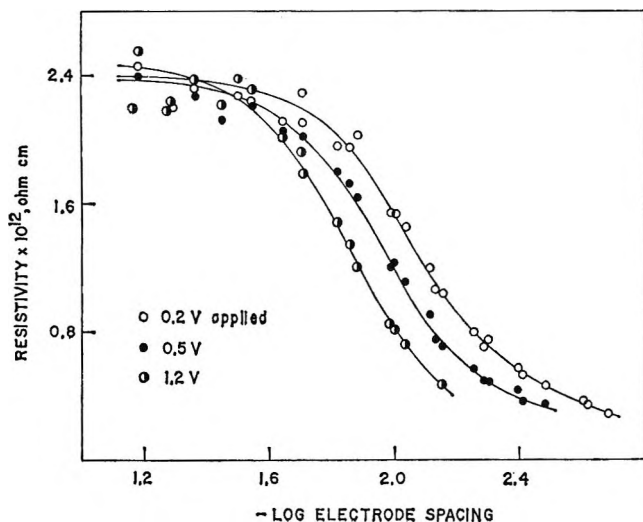


Figure 3. Same conditions as in Figure 2, but electrodes are evaporated silver.

aluminum base weighted with lead and held by extensions springs, and solution is led in and out through Teflon tubing. This mounting has a natural frequency of only 2–3 Hz, well below the usual building noise frequencies. Interference patterns are thereby stabilized, and electrical noise is kept very low. Benzene was prepared by distillation of spectroquality material over  $\text{LiAlH}_4$  in a nitrogen atmosphere. Tetraisoamylammonium picrate (TIAP) was prepared by a standard method,<sup>2</sup> and tetraisoamylammonium tetraisoamylboride (TIATIB)<sup>1</sup> was purified by chromatography over silica gel with benzene as eluent, after the method of Sangster and Ervine,<sup>4</sup> and melted at  $242\text{--}244^\circ$ . This is higher than that given in the literature<sup>1</sup> but its

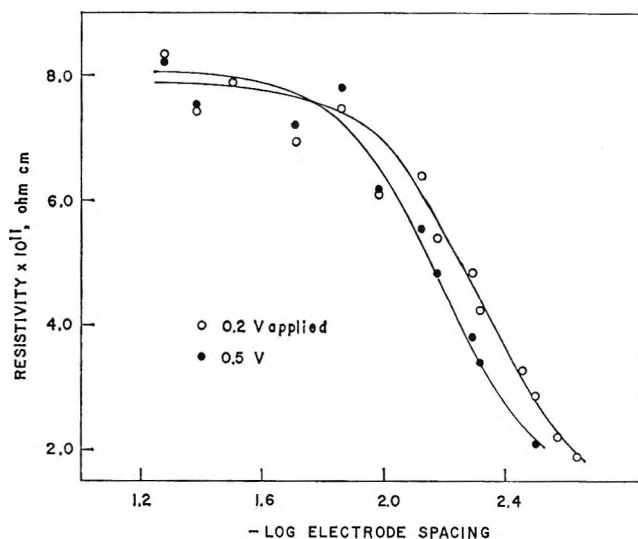


Figure 4. Apparent specific resistivity of TIATIB ( $1 \pm 0.3$ )  $\times 10^{-7} M$  in benzene as a function of electrode spacing with evaporated gold electrodes. Temperature is  $25^\circ$ .

analysis is in reasonable agreement with expectation. *Anal.* Calcd for TIATIB: C, 80.88; O, 14.94, N, 2.36. Found: C, 81.08; O, 15.00; N, 2.52. Stock solutions were diluted on the rack by distillation of fresh benzene.

## Results and Discussion

Figures 2, 3, and 4 show typical results of specific resistance *vs.* electrode spacing for TIAP in benzene with Au and Ag electrodes, and for TIATIB in benzene with Au electrodes, respectively, under conditions of different applied voltages. The points were fit to Gavis' equation by least squares and show a reasonable fit, particularly at small electrode spacing. However, two discrepancies exist between experiment and theory. First, the dependence on applied voltage is opposite to what is expected. As shown by accounting for the missing term in the Gavis theory,<sup>5</sup> the diffuse double layer thickness,  $\delta$ , decreases with increasing applied voltage according to the expression

$$\delta_1 = \frac{\delta}{\left(1 + \left(\frac{e\delta}{kT} \frac{dV}{dx}\right)^2\right)^{1/2}}$$

where  $\delta$  is the limiting low voltage value. As an example, if the large spacing specific resistance is  $10^{12}$  ohm cm, electrode spacing is 0.010 cm, and applied voltage is 0.20 V, then  $\delta$  is  $1.5 \times 10^{-3}$  cm, and  $\delta_1$  is  $0.7\delta$ . This leads one to expect to observe a decrease in specific resistance at smaller spacing when higher voltage is applied. Experimentally, the opposite effect is observed. Second, the values of  $\delta$  as determined by the fit to Gavis'

(4) R. C. Sangster and J. S. Ervine, Jr., *J. Phys. Chem.*, **24**, 670 (1956).

(5) A. Prock and M. Djibelian, *ibid.*, **73**, 4398 (1969).

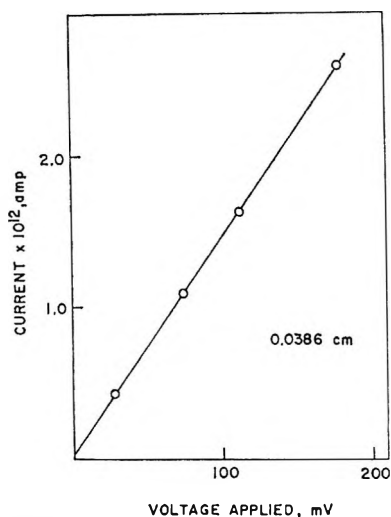


Figure 5. Ohm's law behavior shown extended to low values of applied voltage for TIAP ( $(6 \pm 2) \times 10^{-7} M$ ) in benzene with evaporated gold electrodes. Temperature is  $25^\circ$ .

equation are too large. For example, the data of graph 3 yield for 0.5 V applied a value of  $\delta$  of  $11.7 \times 10^{-3}$  cm, whereas measurement<sup>2</sup> indicates a value of  $2.7 \times 10^{-3}$  cm.

On the basis of the results shown in Figure 5, which illustrates Ohm's law behavior of TIAP in benzene at large spacing down to 20 mV applied potential, it was suggested<sup>6</sup> that a reaction involving an injection of ions from the metallic anode might be involved. Figure 6 shows experimental results for TIAP in benzene obtained using a cell of different design in which both electrodes were stannous oxide coated optical flats. The cell diagram is given as Figure 3, ref 7. The result is to be contrasted with Figure 3 of this paper. In the present case there is no corresponding decrease in resistance as electrode spacing decreases, actually some rise is evident in harmony with the predictions of Silver's theory.<sup>8,9</sup> It would appear that a metal film at the electrode is required in order that the enhancement of apparent conductance be observed. In an attempt to obtain a visual proof of migration of metal ions, experiments were performed with Ag and Au evaporated films of about  $100 \text{ \AA}$  on a base of evaporated stannous oxide, with use of solutions of much higher salt concentration so that currents of  $10^{-7}$ – $10^{-8}$  A could be made to flow under voltages of less than half a volt. After several days of current passage it was clearly seen that metal had been stripped from the anode and deposited on the cathode. In one case, a silver film was totally stripped from the anode under applied voltage of 0.2 V after several days of passage of  $10^{-7}$ – $10^{-8}$  A. Although only qualitative, these experiments clearly corroborate the theory that metal ions are injected into the solution.

It can be shown theoretically that metal ion injection is able to account qualitatively for all of the features observed in this conductivity study. If, for the present, bulk conductance is disregarded and if diffusion is neglected, the equations to be satisfied for injection at

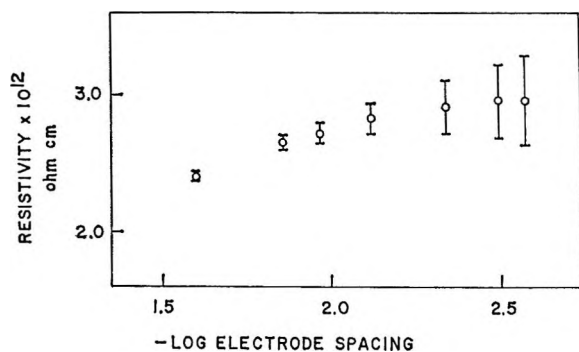


Figure 6. Apparent specific resistivity of TIAP in benzene as a function of electrode spacing. Electrodes are stannous oxide coated flats without evaporated metal films.

the anode in the case of plane parallel electrodes are

$$J_+ = n_+ e \mu_+ E \quad (1)$$

$$\text{Div } J_+ = 0 \quad (2)$$

$$\text{Div } E = 4 \frac{\pi}{\epsilon} \rho \quad (3)$$

$$-\int E dx = V \quad (4)$$

where symbols have the usual meaning. At the injecting electrode the boundary condition is that the ratio of real field to geometric field is  $f$ . The result is

$$J_+ = \frac{9\mu_+\epsilon}{32\pi} \left[ \frac{1}{2} - \frac{2}{3}f^2 + \left( \frac{1}{4} - \frac{4}{27}f^2 \left( f^2 - 4f + \frac{9}{2} \right) \right)^{1/2} \right] \frac{V^2}{L^3}$$

As a check it is noted that when  $f = 0$ , the expression reduces to the familiar space charge limited (SCL) form

$$J_+ = \frac{9}{32\pi} \mu_+ \epsilon \frac{V^2}{L^3}$$

and when  $f = 1$ ,  $J_+$  vanishes. This corresponds to an unperturbed field with no injection. It is not possible at this stage to evaluate the ratio,  $f$ , which is determined by the rate of oxidation of metal at the electrode, but for purposes of discussion it is assumed to be close to unity, so that the total field is only slightly perturbed. Under this assumption, the bulk current can be added without modification to  $J_+$  in order to give the total current. The result of such a calculation is shown in Figure 7 for two different large-spacing specific resistances. Mobilities of all ions were assumed to be equal and were obtained from a Stokes' law calculation with the ionic radius taken as being  $3 \text{ \AA}$ . The ratio,  $f$ , was chosen to be the constant, 0.90, at all electrode spacings. The result is qualitatively similar to those of

(6) Professor J. J. Lingane, Harvard University, private communication.

(7) A. Prock and R. Zahradnik, *J. Chem. Phys.*, **49**, 3204 (1968).

(8) M. Silver, *J. Chem. Phys.*, **42**, 1011 (1965).

(9) G. Briere, *Chem. Phys. Lett.*, **1**, 706 (1968).

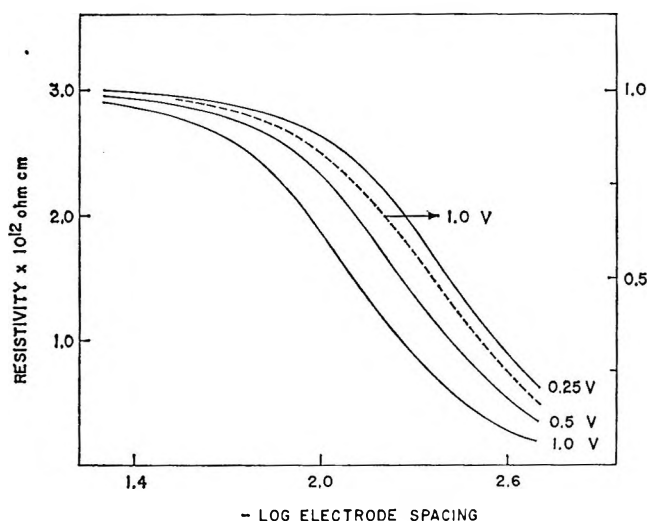


Figure 7. Calculated apparent specific resistivity vs. electrode spacing. See text for details.

graphs 2, 3, and 4. For fixed applied voltage the curve shape at small spacings is a result of the enhancement of current through the  $L^{-3}$  dependence of injected cur-

rent, and at large spacing as a result of the disappearance of injection. The apparent double layer thickness,  $\delta$ , increases with increasing voltage owing also to the  $V^2/L^3$  dependence of the injected current component. This means that for  $f$  close to unity, the ratio of injected current to bulk current is  $V/L^2$  and an increase in applied voltage requires an increase in spacing in order to keep the ratio, hence apparent resistivity, constant, e.g., at 50% of its large spacing (bulk) value. The graph also indicates the proper dependence of the effect on the bulk resistivity. For lower values of bulk resistivity, then at fixed applied voltage a closer spacing is required to produce an injected current which matches bulk current and thereby reduces apparent resistivity to 50% of its large spacing value. This behavior is found experimentally, as was also anticipated by the Gavis theory on the basis that  $\delta$  decreases as ionic concentration increases.

In conclusion, the systems studied do indeed show an increase in apparent conductivity with decrease in electrode spacing, but not as described by the Gavis theory. Rather it is due to the augmenting effect of ion injection from the anode.

## COMMUNICATIONS TO THE EDITOR

### Fluorescence of *p*-Dioxane

*Sir:* Fluorescence has recently been reported from a wide variety of saturated hydrocarbons implying the existence of at least one excited electronic state in these systems which is either bound or at least sufficiently stable to permit the development of an observable emission.<sup>1,2</sup> In this communication we report a fluorescence from the saturated cyclic ether, *p*-dioxane. However, as will be demonstrated in what follows, its emission characteristics differ importantly from those of the saturated hydrocarbons.

For excitation of *p*-dioxane as neat liquid (at 25°) in its first absorption system at 1849 Å, a structureless fluorescence is observed with  $\lambda_{\text{max}} = 2470$  Å and quantum yield  $\phi_f = 0.029$ .<sup>3,4</sup> Upon dilution with isooctane,<sup>5</sup> the emission yield is strongly reduced and the emission spectrum blue-shifted, as shown in Figure 1. It will be noted that both  $\phi_f$  and  $\lambda_{\text{max}}$  continue to decrease strongly even in solutions which are already predominantly isooctane. An effect of the solvent to

simply perturb the emitting species appears inadequate to explain this behavior. No fluorescence ( $\phi_f < 10^{-5}$ ) has been observed from the vapor (at 25 Torr) when excited at 1849 Å. Since this excitation is only 1340  $\text{cm}^{-1}$  above what has been assigned as the first 0-0

(1) F. Hirayama and S. Lipsky, *J. Chem. Phys.*, **51**, 3616 (1969).

(2) F. Hirayama, W. Rothman, and S. Lipsky, *Chem. Phys. Lett.*, in press.

(3) Matheson Coleman and Bell *p*-dioxane (Spectroquality) was purified immediately before use by refluxing for 24 hr over sodium and then distilling under nitrogen atmosphere. The experimental technique for fluorescence measurements has been previously described (see ref 11). All quantum yields have been determined ultimately relative to a fluorescence quantum yield of 1.0 for 2537 Å excitation of 9,10-diphenylanthracene ( $2 \times 10^{-3} M$  in cyclohexane; degassed). Comparison of 1849-Å and 2537-Å excitation was achieved through the use of oxygenated *p*-xylene whose internal conversion efficiency has been determined to be unity (ref 11).

(4) During the course of this work, a similar fluorescence has been reported following high-energy pulsed electron irradiation of *p*-dioxane liquid. [J. H. Baxendale, D. Beaumont, and M. A. J. Rodgers, *Chem. Phys. Lett.*, **4**, 3 (1969)].

(5) Isooctane (Matheson Coleman and Bell, Spectroquality) was chosen as diluent since, unlike most other saturated hydrocarbons, it is negligibly fluorescent (see ref 2).

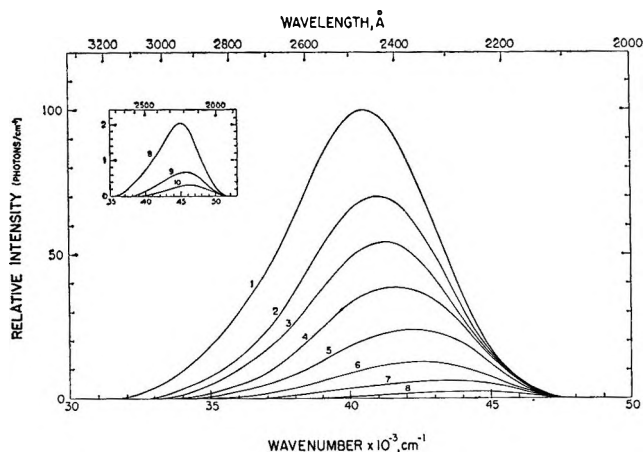


Figure 1. Fluorescence spectra (photons/cm<sup>-1</sup>) of *p*-dioxane in isooctane (deoxygenated) corrected for spectral response of the analyzing system. 1, neat *p*-dioxane; 2, 10 *M*; 3, 8 *M*; 4, 6 *M*; 5, 4 *M*; 6, 3 *M*; 7, 2 *M*; 8, 1 *M*; 9, 0.5 *M*; 10, 0.2 *M*.

transition at 1896 Å in the vapor phase,<sup>6,7</sup> it is concluded that "monomeric" dioxane does not fluoresce. The liquid fluorescence is therefore postulated to arise from some form of excited aggregate whose composition varies with dilution. Further evidence for an aggregate emission is obtained from calculation of an unusually large encounter radius for oxygen quenching. For neat dioxane, at an oxygen concentration of  $3 \times 10^{-3}$  *M*, the fluorescence intensity is reduced by a factor of 0.69 without change in spectrum. From this, Halpern and Ware,<sup>8</sup> using a measured lifetime of 2.15 nsec and appropriate diffusion coefficients, have calculated an encounter radius for quenching of at least 13 Å. Additionally, they observed a monotonic decrease in radiative lifetime on dilution with isooctane, consistent with a change in nature of the emitting species.

If the aggregate responsible for emission is formed subsequent to light absorption, increasing the viscosity of the diluent solvent should reduce  $\phi_f$ . This was indeed observed in a 1 *M* solution of *p*-dioxane in hexadecane.<sup>9</sup> The intensity was reduced by about half as compared to that in isooctane while the viscosity increased by a factor of ca. 4.<sup>10</sup> Additionally, we have studied the absorption spectrum of *p*-dioxane from 0.002 *M* to 0.32 *M* in perfluorinated hexane (which has adequate transmission to 1670 Å). An absorption spectrum of neat dioxane was also determined using a thin film of the liquid compressed between Suprasil windows. All samples exhibited the same structureless spectrum with maximum absorptivity at ca. 1720 Å. Also for the fluorocarbon solutions the optical density was found to be linear over the concentration range studied. Thus the liquid absorption spectrum gives no evidence for extensive ground-state aggregation. Nevertheless, the liquid and vapor spectra are markedly different. The vapor spectrum exhibits a pronounced vibrational structure on the long wave-

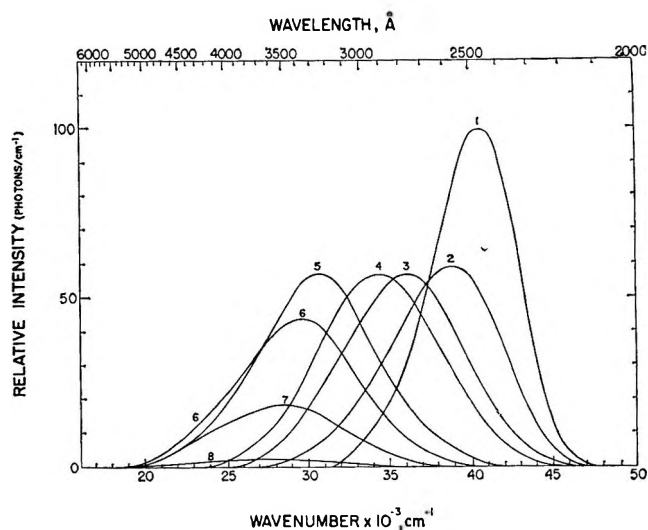


Figure 2. Fluorescence spectra (photons/cm<sup>-1</sup>) of *p*-dioxane with added water. 1, neat *p*-dioxane; 2, 0.056 *M* (0.1 vol %) H<sub>2</sub>O in *p*-dioxane; 3, 0.278 *M* (0.5%); 4, 0.556 *M* (1%); 5, 2.78 *M* (5%); 6, 5.56 *M* (10%); 7, 11.1 *M* (20%); 8, 27.8 *M* (50%). The spectra are corrected for spectral response of the analyzing system.

length side of the first absorption system which is superimposed on a continuum peaking at 1810 Å, ca. 2890 cm<sup>-1</sup> red-shifted from the liquid. Since the liquid spectrum remains invariant to dilution even with the very weakly perturbing fluorocarbon solvent,<sup>11</sup> these differences between vapor and liquid spectra suggest a profound modification in the relative nuclear configurations of ground and excited states on condensation.

The fluorescence of *p*-dioxane is found to be extremely sensitive to the presence of water as shown in Figure 2. Traces of water noticeably reduce  $\phi_f$  and red-shift the fluorescence. Further addition of water continues to strongly red-shift the spectrum.<sup>12</sup> The origin of these effects is still unknown, although the participation of a fluorescent dioxane-water complex is indicated. From dilute solutions of *p*-dioxane and water in isooctane, we have found, in preliminary experiments, a very broad fluorescence which appears to consist of a superposition of two emission spectra—one possibly from water-dioxane complex and the other from uncomplexed dioxane.

(6) L. W. Pickett, N. J. Hoefflich, and T. C. Liu, *J. Amer. Chem. Soc.*, **73**, 4865 (1951).

(7) G. J. Hernandez and A. B. F. Duncan, *J. Chem. Phys.*, **36**, 1504 (1962).

(8) A. Halpern and W. R. Ware, *J. Phys. Chem.*, **74**, 2413 (1970).

(9) Although hexadecane is slightly fluorescent (see ref 1), it absorbs a negligible fraction of the exciting light in the 1 *M* solution of dioxane.

(10) The viscosity of the mixture was estimated by assuming each component's contribution is proportional to its mole fraction.

(11) C. W. Lawson, F. Hirayama, and S. Lipsky, *J. Chem. Phys.*, **51**, 1590 (1969).

(12) Similar effects have been noted on addition of methanol.

No fluorescence has been observed from either *m*-dioxane or tetrahydrofuran, whereas a weak fluorescence has been detected from tetrahydropyran and oxepane. A systematic study of the fluorescence from these and other saturated cyclic ethers will be presented elsewhere.

It is to be emphasized that all fluorescence quantum yields and spectra reported in this communication were determined at 25°. On cooling *p*-dioxane, a marked increase in  $\phi_f$  has been noted accompanied by a slight red shift (*e.g.*, at 12°,  $\phi_f = 0.040$  and  $\lambda_{\max} = 2500 \text{ \AA}$ ). However, no fluorescence has been detected from solid *p*-dioxane (at -78°). A study of these temperature effects is currently in progress.<sup>13</sup>

(13) This work was supported by the U. S. Atomic Energy Commission, Document No. COO-913-34.

*Acknowledgment.* The authors wish to thank Mr. William Rothman for his assistance in obtaining some of the experimental data.

DEPARTMENT OF CHEMISTRY  
UNIVERSITY OF MINNESOTA  
MINNEAPOLIS, MINNESOTA 55455

FUMIO HIRAYAMA  
CRAIG W. LAWSON  
SANFORD LIPSKY

RECEIVED MARCH 6, 1970

## Fluorescence of *p*-Dioxane.

### Lifetime and Oxygen Quenching<sup>1</sup>

*Sir:* Using the time-correlated single photon technique,<sup>2a,b</sup> we have been successful in obtaining the fluorescence decay of the saturated cyclic ether *p*-dioxane excited at 1850 Å. The instrument incorporated a gated (20 kHz) nanosecond flashlamp fitted with a Suprasil window and filled with 38 cm of deuterium.

Radiation of this energy was isolated by a Bausch and Lomb high-intensity grating monochromator, and the entire optical system was purged with dry nitrogen. The lamp decay was less than 1 nsec (1/e); lamp tailing was unimportant. Excited at this wavelength, neat *p*-dioxane has a fluorescence quantum yield of 0.029 at 25°. This note reports the lifetimes of *p*-dioxane systems in condensed media. All decay curves were deconvoluted with respect to the exciting light and were observed to follow a single exponential. The results are listed in Table I. Concerning oxygen quenching at 25°, Hirayama, Lawson, and Lipsky<sup>3</sup> obtain a diminution in the fluorescence yield of 0.69 relative to deaerated *p*-dioxane. Incorporating this value with the unquenched lifetime of 2.15 nsec, and

using a diffusion coefficient<sup>4,5</sup> for the *p*-dioxane-oxygen system of  $5 \times 10^{-5} \text{ cm}^2 \text{ sec}^{-1}$  and an oxygen concentration of  $3 \times 10^{-3} M$  at 25°, we calculate an effective encounter radius for quenching of at least 13 Å. This distance is obtained from the steady-state form of the solution to the diffusion equation (see eq 15 of ref 6). Since this value is considerably larger than the sum of the molecular radii of *p*-dioxane and oxygen, it is postulated that the excited species being quenched is an aggregate. This hypothesis is supported not only by the decrease in fluorescence yield with increasing dilution with isooctane,<sup>3</sup> but also by the concomitant change observed in the radiative rate constant (see Table I).

**Table I:** Fluorescence Lifetimes and Rate Constants for *p*-Dioxane under Various Experimental Conditions

System	Temp, °C	$\tau$ , nsec	$\phi_f^c$	$k_F \times 10^{-7}$ , sec <sup>-1</sup>	$k_{NR} \times 10^{-8}$ , sec <sup>-1</sup>
Neat <sup>a</sup>	25	2.15	0.029	1.35	4.5
Neat <sup>b</sup>	25	1.70	0.020		
Neat <sup>a</sup>	12	3.2	1.040	1.25	3.0
Neat <sup>b</sup>	12	2.3	0.025		
10 M in isooctane <sup>a</sup>	25	1.75	0.020	1.14	5.6
8 M in isooctane <sup>a</sup>	25	1.5	0.016	1.07	6.6

<sup>a</sup> Deaerated. <sup>b</sup> Oxygen saturated. <sup>c</sup> See ref 3.

As a check, a decay curve was synthetically generated from the time-dependent fluorescence intensity function, including the transient term,<sup>6</sup> using appropriate values for the encounter radius, diffusion coefficients, oxygen concentration, and the unquenched lifetime. This plot showed only minute nonexponentiality at very short times (<0.4 nsec) and had a lifetime of 1.65 nsec. To check our deconvolution method for any error that may have arisen due to the slight nonexponentiality, the time-dependent decay function was convoluted with the lamp function and then deconvoluted according to the procedure used for actual data. The result was entirely consistent with our measured lifetime of 1.7 nsec for *p*-dioxane quenched by oxygen at 25°. The rather large temperature coef-

(1) Supported by a grant from the National Science Foundation GP 7813.

(2) (a) J. B. Birks, *Progr. React. Kinet.*, **4**, 239 (1967); (b) W. R. Ware in "Creation and Detection of the Excited State," Marcel Dekker, New York, N. Y., in press.

(3) F. Hirayama, C. W. Lawson, and S. Lipsky, *J. Phys. Chem.*, **74**, 2411 (1970).

(4) W. R. Ware, *ibid.*, **66**, 455 (1962).

(5) C. J. Clemett, *J. Chem. Soc., A*, 458 (1969).

(6) W. R. Ware and J. S. Novros, *J. Phys. Chem.*, **70**, 3246 (1966).

ficient governing the nonradiative rate constant of *p*-dioxane is to be noted.

The value of the observed lifetime in neat *p*-dioxane is not inconsistent with that observed with pulsed 12-Mev electron excitation by Baxendale, Beaumont, and Rodgers.<sup>7</sup> The transient measurements described above, when considered together with the steady-state results of Hirayama, Lawson, and Lipsky,<sup>3</sup> provide strong evidence for aggregate emission of *p*-dioxane.

Measurements on other saturated molecules are in progress.

(7) J. H. Baxendale, D. Beaumont, and M. A. J. Rodgers, *Chem. Phys. Lett.*, **4**, 3 (1969).

DEPARTMENT OF CHEMISTRY  
UNIVERSITY OF MINNESOTA  
MINNEAPOLIS, MINNESOTA 55455

ARTHUR M. HALPERN  
WILLIAM R. WARE

RECEIVED MARCH 6, 1970